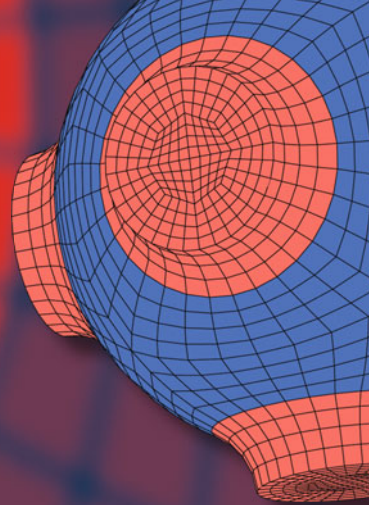


Advanced Structured Materials

Shobhit K. Patel  
Sofyan A. Taya  
Sudipta Das  
K. Vasu Babu *Editors*



# Recent Advances in Graphene Nanophotonics

 Springer


# Advanced Structured Materials

Volume 190

## Series Editors

Andreas Öchsner, Faculty of Mechanical Engineering, Esslingen University of Applied Sciences, Esslingen, Germany

Lucas F. M. da Silva, Department of Mechanical Engineering, Faculty of Engineering, University of Porto, Porto, Portugal

Holm Altenbach , Faculty of Mechanical Engineering, Otto von Guericke University Magdeburg, Magdeburg, Sachsen-Anhalt, Germany

Common engineering materials are reaching their limits in many applications, and new developments are required to meet the increasing demands on engineering materials. The performance of materials can be improved by combining different materials to achieve better properties than with a single constituent, or by shaping the material or constituents into a specific structure. The interaction between material and structure can occur at different length scales, such as the micro, meso, or macro scale, and offers potential applications in very different fields.

This book series addresses the fundamental relationships between materials and their structure on overall properties (e.g., mechanical, thermal, chemical, electrical, or magnetic properties, etc.). Experimental data and procedures are presented, as well as methods for modeling structures and materials using numerical and analytical approaches. In addition, the series shows how these materials engineering and design processes are implemented and how new technologies can be used to optimize materials and processes.

Advanced Structured Materials is indexed in Google Scholar and Scopus.

Shobhit K. Patel · Sofyan A. Taya · Sudipta Das ·  
K. Vasu Babu  
Editors

# Recent Advances in Graphene Nanophotonics

 Springer



*Editors*

Shobhit K. Patel  
Department of Computer Engineering  
Marwadi University  
Rajkot, Gujarat, India

Sofyan A. Taya  
Department of Physics  
Islamic University of Gaza  
Gaza, Palestine

Sudipta Das  
Department of Electronics  
and Communication Engineering  
IMPS College of Engineering  
and Technology  
Malda, West Bengal, India

K. Vasu Babu  
BVRIT Hyderabad College of Engineering  
for Women  
Bachupally, Hyderabad, India

ISSN 1869-8433

ISSN 1869-8441 (electronic)

Advanced Structured Materials

ISBN 978-3-031-28941-5

ISBN 978-3-031-28942-2 (eBook)

<https://doi.org/10.1007/978-3-031-28942-2>

© The Editor(s) (if applicable) and The Author(s), under exclusive license to Springer Nature Switzerland AG 2023

This work is subject to copyright. All rights are solely and exclusively licensed by the Publisher, whether the whole or part of the material is concerned, specifically the rights of translation, reprinting, reuse of illustrations, recitation, broadcasting, reproduction on microfilms or in any other physical way, and transmission or information storage and retrieval, electronic adaptation, computer software, or by similar or dissimilar methodology now known or hereafter developed.

The use of general descriptive names, registered names, trademarks, service marks, etc. in this publication does not imply, even in the absence of a specific statement, that such names are exempt from the relevant protective laws and regulations and therefore free for general use.

The publisher, the authors, and the editors are safe to assume that the advice and information in this book are believed to be true and accurate at the date of publication. Neither the publisher nor the authors or the editors give a warranty, expressed or implied, with respect to the material contained herein or for any errors or omissions that may have been made. The publisher remains neutral with regard to jurisdictional claims in published maps and institutional affiliations.

This Springer imprint is published by the registered company Springer Nature Switzerland AG  
The registered company address is: Gewerbestrasse 11, 6330 Cham, Switzerland

# Preface

In these modern times, the graphene due to its exceptional properties has been identified as a futuristic material with applications in every single field with higher performance, and the growing applications of graphene, its oxides and nanocomposites in communication, sensing, security, safety, spectroscopy, manufacturing, bio-medical, agriculture, imaging, etc., are still an undergoing research area. Thanks to graphene nanophotonics that makes it possible due to its enormous advantages like extraordinary mechanical and electrical properties, it advances the latest scale of field.

This book is aimed to bring the emerging application aspects of graphene nanophotonics and various modules used for its successful realization. It gathers scientific technological novelties and advancements already developed or under development in the academic and research communities. This work focuses on recent advances, different research issues in terahertz technology and would also seek out theoretical, methodological, well-established and validated empirical work dealing with these different topics. The book chapters cover a very vast audience from basic science to engineering, technology experts and learners. This could eventually work as a textbook for material, mechanical, electrical, chemical engineering and communication technology students or science master's programs and for researchers as well. This book chapters also serve the common public interest by presenting new methods for application areas of technology, its working and its effect on the environment and human health, etc.

In particular, this textbook covers the latest trends in graphene nanomaterials and its prospects with various fabrication processes and its challenges as well as the potential applications. In addition to this, graphene's role and applications in several optoelectronics devices, high speed communication, selective sensing of VLC systems in 6G networks, flexible electronics and energy storing, nanophotonic biosensors for near-patient testing purposes, photonic crystal fiber-based graphene biosensor are also demonstrated. Graphene nanoribbons as the futuristic materials for transistors and interconnect have been observed for potential THz applications. Graphene material for different types of sensing including gas, chemical, temperature, SPR, pressure and blood sensing with future challenges has been discussed. Effective approaches of

synthesized methods and their recent development of various catalytic applications of graphene and its oxides nanocomposites have been discussed. Recent development of flexible, compact, and effective THz antennas using graphene, their applications and challenges have been highlighted. Uniqueness and universality of graphene oxide—ferrite nanocomposites versus other unconventional materials in terms of materials chemistry and physics, electronic, magnetic characteristics, synthesis strategies and selected applications in an electromagnetic interference shielding and microwave absorbing field have been validated.

Once the readers finish study of this book, then they will learn about the importance of graphene and its oxides, advancement in the field, applications, graphene-based devices like energy storage applications, biosensors; photonic crystal fibers; antennas; synthesized methods and challenges for fabrication techniques, etc., and future scope. It also leads to enhancement in their knowledge in graphene nanophotonics and gives a platform to future technology and novel applications realization.

Rajkot, Gujarat, India  
Gaza, Palestine  
Malda, West Bengal, India  
Bachupally, Hyderabad, India

Shobhit K. Patel  
Sofyan A. Taya  
Sudipta Das  
K. Vasu Babu

# Contents

<b>Graphene-Based Nanomaterials</b> .....	1
Ila Jogesh Ramala Sarkar, Ankit Devenbhai Badiyani, Labharth Bharatkumar Sonagara, Jenius Jayesh Keralaia, Nityarajsinh Chudasama, and Sanjay Kumar	
<b>High-Performance Metric of Graphene-Based Heterojunction LEDs and PDs in Visible Light Communication Systems</b> .....	31
Mohamed El Jbari and Mohamed Moussaoui	
<b>Variants of Graphene Nanoribbon (GNR) Interconnects for THz Applications</b> .....	55
S. Kanthamani	
<b>A Study on Graphene-Based Sensor Devices</b> .....	69
Jahid Tanvir, Kawsar Ahmed, Francis M. Bui, and Shobhit K. Patel	
<b>Graphene: A Promising Material for Flexible Electronic Devices</b> .....	83
Yogesh Chendake, Harshada Mhetre, Supriya Khatavkar, Vishal Mhetre, Swapnil Namekar, Vikas Kaduskar, and Prashant Chougule	
<b>Catalytic Performance of Graphene-Based Nanocomposites</b> .....	119
Prasenjit Mandal and Hari Shankar Biswas	
<b>Graphene-Based Nanophotonic Biosensors</b> .....	145
Alma Mejri, Ahmed Hichem Hamzaoui, Hamza Elfil, and Abdelmoneim Mars	
<b>An Investigation on Unique Graphene-Based THz Antenna</b> .....	163
Rachit Jain, P. K. Singhal, and Vandana Vikas Thakare	
<b>Two-Dimensional Carbon Nanomaterial-Based Biosensors: Micromachines for Advancing the Medical Diagnosis</b> .....	181
Shalini Bhatt, Vinay Deep Punetha, Rakshit Pathak, and Mayank Punetha	

<b>Micro-sized Graphene-Based UWB Annular Ring Patch Antenna for Short-Range High-Speed Terahertz Wireless Systems</b> .....	227
Asma Khabba, Jamal Amadid, Zakaria El Ouadi, Layla Wakrim, Saida Ibnyaich, Ahmed Jamal Abdullah Al-Gburi, and Abdelouhab Zeroual	
<b>Surrogate Optimization-Assisted Dual-Band THz Inverted-F Coplanar Graphene Antenna</b> .....	249
K. C. Rajarajeshwari, T. Sathiyapriya, and E. L. Dhivya Priya	
<b>Recent Advances in Graphene Oxide-Ferrite Hybrid Framework as Radar Absorbing Material</b> .....	263
Ajay Singh, Sunil Sambyal, and Vishal Singh	
<b>Graphene-Based THz Antenna: Rudiments, Fabrication, and Forthcoming Opportunity</b> .....	287
Sunil Lavadiya, Vishal Sorathiya, Kumutha Duraisamy, Delshi Howsalya Devi, and Sudipta Das	
<b>Design of Monopole Ground Graphene Disc-Inserted THz Antenna for Future Wireless Systems</b> .....	305
K. Vasu Babu, Gorre Naga Jyothi Sree, Kumutha Duraisamy, M. Jeyabharathi, and Sudipta Das	
<b>Graphene-Based D-Shaped Gold-Coated Photonic Crystal Fiber for Transformer Oil Moisture Sensing</b> .....	313
M. S. Mani Rajan and N. Ayyanar	
<b>Recent Advances in Graphene-Based Adsorbents for Fluoride Removal from Groundwater</b> .....	333
Swati Dubey, Avanish Kumar, and Abhishek Gupta	
<b>Design and Analysis of Fractal-Based THz Antenna with Co-Axial Feeding Technique for Wireless Applications</b> .....	351
K. Vasu Babu, Gorre Naga Jyothi Sree, Kumutha Duraisamy, Devi Priya Vanarajan, and Sudipta Das	
<b>Application of Graphene, Its Derivatives, and Their Nanocomposites</b> ...	359
Rahul Kumar Sinha and Navjot Kaur Kanwal	

# Graphene-Based Nanomaterials



Ila Jogesh Ramala Sarkar, Ankit Devenbhai Badiyani,  
Labharth Bharatkumar Sonagara, Jenius Jayesh Keralaia,  
Nityarajsinh Chudasama, and Sanjay Kumar

**Abstract** Graphene, the wonder carbon-material is a lone-atom-wide two-dimensional nanostructure having large surface area of modifiable interest for fabricate composites. Graphene-based nanostructure has fascinated enthusiasm among research groups for its exclusive physico-chemical properties and utilization in numerous fields such as energy-storage devices, fuel cells, bioengineering, sensors, and analysis. Graphene nanomaterials with various utilizations are estimated to transform many other fields like optical, electronic, thermo-, and mechanic. During hybridization, these nanomaterials are usually treated with chemicals for functionalization and material reduction, together doping with foreign atoms, oxidation, which introduce functional groups. A number of techniques have been followed for developing graphene nanomaterials (both “top down” and “bottom up”) having its unique advantages and disadvantages. This book chapter will lay down the prospects and consequences of new progress graphene nanoparticles, manufacturing processes, challenges, and its potential value-added applications in assorted fields.

**Keywords** Graphene nanomaterials · Top down · Bottom up · Utilization · Value-added applications · Challenges

## 1 Introduction

Till now (2022), there are almost as many patent applications as there are scholarly articles published each year about graphene, its properties, and applications. Since the carbon allotrope in graphite contains a lot of double bonds, the name is derived from “graphite” and the suffix -ene [1]. The term “graphene” was first used in 1986 by the chemists Hanns-Peter Boehm, Ralph Setton, and Eberhard Stump. The compounds graphite and -ene, which stands for polycyclic aromatic hydrocarbons, are combined

---

I. J. R. Sarkar (✉) · A. Devenbhai Badiyani · L. Bharatkumar Sonagara · J. Jayesh Keralaia · N. Chudasama · S. Kumar  
Department of Chemical Engineering, Faculty of Technology, Marwadi University,  
Rajkot 360003, India  
e-mail: [sarkarila@gmail.com](mailto:sarkarila@gmail.com)

to form this term [1–3]. Researchers continually discover and develop new, superior materials in every field of engineering, pharmacology, biotechnology, etc., leading to believe that graphene is the substance of the future for all of the aforementioned fields. In 2004, Andre Geim and Konstantin Novoselov made initial discovery of graphene. The layers of 2D graphene that make up 3D graphite are confined collectively with substantially weaker Van der Waals bonds rather than by molecular bonds [1–5]. The graphene layers have a weak connection that allows them to slide over one another easily, giving the material appropriate to be utilized as a lubricant because it has a soft and slippery feel. Geim and Novoselov separated monolayer graphene sheets for the first time off the plane of an extremely aligned pyrolytic graphite flake in 2003 using several peels of ordinary adhesive tape.

A plane sheet of carbon atoms only single atom wide makes up the two-dimensional allotrope of carbon known as graphene (G). One atom acts as the vertex of each hexagon in the hexagonal, honeycomb lattice that holds these atoms together and resembles “chicken wire”. Out of six electrons, two and four electrons are arranged in inner and valence shells. Every electron has confined with another three electrons via extremely tough covalent bonds which are really hard to split, the last electron of outer shell accessible for conduction or relate with other atoms or molecules [2, 3]. Both sides of graphene layer have p-orbitals and “pi” electrons, also referred to as the highly mobile electrons. The overlap of the pi orbitals in graphene strengthens carbon-to-carbon bonds. The bonding of these orbitals controls the electric characteristics of graphene. This 2D carbon graphene lattice is often found as platelets or flakes that are around 0.3 nm thick [3]. Although it is typically thinner than this, the layer can stretch up to roughly 0.5 mm in the lateral direction.

Through an extremely crystalline arrangement and exceptional, distinctive physical properties, monolayer graphene is produced via this so-called mechanical exfoliation technique [3, 5]. They transferred the graphene layers from the graphite to thin silicon dioxide ( $\text{SiO}_2$ ) on a silicon wafer using either the scotch tape method or micromechanical cleavage.  $\text{SiO}_2$  provided almost charge-neutral graphene layers by electrically isolating it from the graphene and barely interacting with it. Serving as a “back gate” electrode, the silicon underlying the  $\text{SiO}_2$  might be utilized to change the charge density in the graphene across a wide range.

Recently, there is a significant increase in attention for graphene-based nanomaterials for use in nanocomposites, energy-storage systems, electronics, chemical sensors, opto-electronics, and health applications including osteogenic [1, 4, 6]. Applications for graphene include energy-storage devices like supercapacitors and lithium-ion batteries, conducting electrodes, and gas detection. The internal structure of graphene is, each atom in a graphene sheet forms a strong bond with its three closest neighbors, adding one electron to the sheet’s overall valence band. The key advantages of graphene include its near-perfect heat and electrical conductivity, lightness, strength, thinness, and other properties. The use of graphene in a composite precludes the production of additional nano-sized active materials, improves non-Faradic capacitive behavior, boosts conductivity, and stops disintegration. Numerous extraordinary electronic features of graphene have fascinated a lot of interest, including Dirac energy dispersion, relativistic effects, the half-integer

quantum Hall effect, and Klein tunneling. Additionally, in its Van der Waals heterostructures with other two-dimensional materials, it hosts a number of single particle and emergent correlated states that are topologically non-trivial [5–8].

## 2 Physico-Chemical Properties of Graphene Nanomaterials

After the year 2004, it was established that 2D complex can subsist due to monolayer graphene which was isolated. However, the scientists were looking for more details about it. After suspended graphene layers were analyzed by high-resolution transmission electron microscopy (TEM), researchers considered that can be established the cause to be minor rippling in graphene, altering arrangement of layers. Though, by lately they suggested that the carbon-to-carbon bonds in graphene are very tiny and robust that they resist thermal disturbance from unsettling it.

### 2.1 *Electronic Properties*

Conjugating both holes and electrons as charge carriers, zero-overlap semi-metal graphene is established as highly electrical conductor. Then, 2, 4 electrons are arranged in inner and outer shells, respectively, in graphene. Out of four valence electrons, three electrons are bonded to other atoms to form 2D plane, whereas one electron is always free for electronic conduction [9]. Those strongly mobile electrons (“pi” electrons) are occupying below and above the graphene layer. The overlapped pi orbital increases the strength of carbon–carbon bonds. Basically, the valence and conduction bands or bonding and anti-bonding of “pi” orbital of graphene are termed as electronic properties.

Over through last decade, it was studied that electrons and holes have zero effective mass at the Dirac point in graphene. This happens due to the spectrum for excitations or energy-movement association, which behaves linear for less energy beside the six separate bends of Brillouin zone. The electrons and holes are termed as Dirac fermions, and six turns of the Brillouin zone are called as Dirac points [10]. Electric conduction is actually very low because of zero-density status at Dirac points. Although Fermi level can be adjusted with doping holes or electrons for material, electronic conductivity can be improved by that.

Graphene has extremely high electron mobility of more than  $15,000 \text{ cm}^2 \text{ V}^{-1} \text{ s}^{-1}$  and tentative potential of  $200,000 \text{ cm}^2 \text{ V}^{-1} \text{ s}^{-1}$  [11]. Due to lack of mass, the electrons behave alike of photons during their mobility. Those charge carrier electrons are capable to move sub-micrometer path with no spreading, a trend called as ballistic transport [11]. Although the limiting factor may be the substrate or the quality of graphene. As an example, the substrate silicon dioxide has the mobility of  $40,000 \text{ cm}^2 \text{ V}^{-1} \text{ s}^{-1}$ .



## 2.2 Mechanical Strength

Graphenes' prominent physical property is its intrinsic strength (ultimate tensile strength 130 GPa) because of 0.142 Nm extended carbon bonds, which made graphene as the strongest material ever explored [12]. Compared to strength, graphene is also very light in weight (0.77 mg/m<sup>2</sup>) [12]. It is frequently mentioned that a solitary layer of graphene (simply one atomic wide) is adequate in dimension that can cover a complete football ground and would weigh less than one gram.

As elastic property, graphene is capable to preserve its own shape and size after strain, which makes it special. Atomic force microscope (AFM) analysis of graphene was conducted in 2007, where graphene layers were suspended over silicone dioxide cavities. Those results provided that between 2 and 8 Nm thick of graphene layer had spring constants in the range of 1–5 N/m and a Young's modulus (unlike 3D graphite) of 0.5 TPa [15]. Those exceptional results were based on theoretical prediction assuming graphene as flawless containing no deficiency and therefore costly and tricky to synthetically reproduce, although manufacturing processes are gradually improving, ultimately reducing expenses and difficulty [13].

## 2.3 Optical Properties

Graphene has the capacity to absorb around 2.3% of white light, which is an exceptional and attractive property, particularly taking into account that it is merely lone atomic wide. Owing to its aforesaid electronic properties, the electrons act like massless charge carriers with extremely high mobility [14]. The amount of white light absorbed depends on the fine structure constant, rather than being dictated by material specifics. Addition of one more sheet of graphene enhances the quantity of white light absorbed by roughly similar value (2.3%). Graphenes' opacity of  $\pi\alpha \approx 2.3\%$  connects to a universal dynamic conductivity value of  $G = e^{2/4} \hbar (\pm 2-3\%)$  more than the noticeable frequency series [14].

The following characteristics apply to this amazing nanomaterial:

- Owing to its dense arrangement and tough covalent bonds among atoms, graphene is 200 times stronger than steel while also being exceedingly light.
- Really thin but incredibly durable.
- Flexible; it can be folded or bent.
- Due to its small structure, it can function as a perfect barrier. Helium cannot even get through it.
- Because of its little thickness, transparent, graphene is practically invisible since it only absorbs 2.3% of the light that passes through it.
- Tiniest substance presently known to exist.
- Chemically inactive.
- Conduction band does not have any band gap due to fourth electron, the pi-electron and the valence shell are not normally elevated toward an upper plane.

- Because of the highly mobile free pi-electrons, more conductive than copper both electrically and thermally.
- While carbon is the fourth large prevalent component on earth, graphene is honestly affordable.
- Flexibility alters the resistance of the sheet and able to be extended up to 20% without causing faults.
- Researchers from the University of Maryland and the Lawrence Berkeley National Laboratory have also noted that the flexibility pattern of graphene layer could change the magnetic characteristics. Corresponding result in pi-electrons moving in rounds in graphene layer, like a tough magnetic field, had been applied perpendicular to the sheet even though there was no actual external magnetic field (up to 300 T or 107 times the earth's magnetic field). This might make it possible to manipulate the conductivity, optical, and microwave properties of graphene. Currently, any alternative feasible is not available to produce magnetic fields of that size.
- Another peculiar behavior that was noticed in two-dimensional graphene structures under strong magnetic fields and low temperatures is the quantum Hall effect. This is a quantum-mechanical interpretation of the Hall effect, in which electrons enter quantized energy levels and the Hall conductance undergoes quantum Hall transitions to take on quantized values.
- By using doping or other techniques, graphene can be given semiconducting features, such as an adjustable band gap, even if the lack of a band gap prevents graphene conduction from being switched off like a transistor.
- Graphene oxide (GO) is graphene derivatives whose large array of physico-chemical properties is modified and used for specific utilizations.

### 3 Synthesis of Graphene Nanomaterials

A number of techniques, including ball milling, exfoliation, chemical vapor deposition, and physical vapor deposition, can be used to create graphene nanomaterials. Several techniques for the exfoliation of graphite have been documented as a result of the long-standing interest in graphene and the numerous researchers that have been working on its creation. They fall into two categories like top-down strategy and the bottom-up strategy.

Processes of synthesizing graphene depend on preferred purity, size, and efflorescence. Many techniques for producing thin graphitic films have been discovered at the early stage. In the late 1970s, carbon precipitated as thin graphitic coatings on the surfaces of transition metals [15]. In 1975, few-layer graphite was produced using chemical breakdown procedures on a single platinum crystal, but owing to lack of characterization tools or possibly because of its restricted prospective uses, this material was not recognized as graphene.

Their electronic properties were not investigated at that time since it was difficult to isolate and transfer on resisting supports. At the end of nineteenth century, Ruoff

and associates sought to separate fine graphitic flakes on silicon dioxide support using mechanically friction decorative islands on extremely organized pyrolytic graphite [16]. On the characterization of their electrical properties, there was, however, no information. Later, in 2005, Kim and associates used a similar procedure to do this, and the electrical properties were published [17]. However, graphene research proceeded quite swiftly when Geim and others declared their effort of separating graphene over silicon dioxide support, analyzing all electrical properties. Following the material's discovery, numerous methods were discovered to manufacture slim graphitic layers and few sheets of graphene. Thin graphene flakes exfoliation from their bulk counterparts and additional substances including molybdenum disulphide, niobium diselenide, and boron nitride led to the primary experimental demonstration of two-dimensional crystals in 2004 and 2005. However, graphite was first mechanically exfoliated with scotch tape to produce tiny flakes of a few microns, which were then used to make graphene [17]. Although the graphene produced by this procedure is of the highest quality, mass manufacturing of graphene requires a fabrication technique that can manufacture wafer-scale graphene.

A wide range of techniques has recently been discovered for the manufacturing of graphene. But currently, mechanical cleaving, chemical exfoliation, chemical synthesis, and thermal chemical vapor deposition synthesis are the methods most often used. Other techniques, such as producing microwaves and unzipping nanotubes, have also been reported [18]. Although it was shown that mechanical exfoliation using an atomic force microscopy cantilever could manufacture graphene with a few layers, the method was constrained by the graphene's thickness, which ranged to 10 nm, or roughly equivalent to 30-layer graphene.

Chemical exfoliation of solution dispersed graphite is accomplished by injecting large alkali ions between the graphite layers. Creating graphite oxide, spreading it in a solution, and then reducing it using hydrazine are similar processes. Chemical synthesis is the term for this. The most crucial process for producing graphene on a big scale, much like carbon nanotubes, has shown to be catalytic thermal chemical vapor deposition. The phrase "thermal chemical vapor deposition" refers to the thermal chemical vapor deposition procedure that makes use of a resistive heating furnace. The term for the thermal chemical vapor deposition method that makes use of plasma-assisted growth is plasma-enhanced chemical vapor deposition. Every aspect of our environment has drawbacks, so the final application of graphene will determine which synthesis method is best. As an example, the mechanical exfoliation technique can produce monolayer to few-layer graphene, but there is little chance of successfully producing a structure similar to that structure.

Additionally, chemical synthesis techniques are less-range temperature methods, by which it is possible graphene synthesis at room temperature on a range of substrate types, particularly polymeric ones. However, the large-area synthetic graphene produced by this technique is scattered and not homogeneous. Again, depending on the degree of reduction, the partial decrease of graphite oxide which effect from creation of graphene from reduced graphene oxides usually deteriorates the electrical properties of graphite oxide over time. Contrarily, by substituting Si, thermal chemical vapor deposition technique is most suited in favor of creating bigger-space

devices that are helpful for upcoming corresponding metal oxide semiconductor skill [19]. Another technique to generate graphene is by thermally graphitizing a silicon carbide surface; however, this method has two drawbacks: a high process temperature, and it cannot be transferred to other substrates. The unique feature of the thermal chemical vapor deposition technique is its capacity to deposit a uniform layer of carbon atoms that have been chemically and thermally catalyzed onto metal surfaces.

### ***3.1 Top-Down Technique***

Graphene or modified graphene sheets are produced using a top-down technique by exfoliating or separating graphite and its derived including graphite fluoride and graphite oxide.

#### **Chemical Exfoliation**

Chemical synthesis represents the finest ways to make graphene. Modifying graphite and a graphite intercalation component chemically to create colloidal suspension, this is then converted into graphene. Numerous paper-like materials, polymer composites, energy-storage materials, and transparent conductive electrodes have already incorporated graphene produced chemically into them. The Brodie, Hummers, and Staudenmaier processes were first used to create graphene oxide in 1860 [23].

Chemical exfoliation is a two-continued method. By initial lowering the Van der Waals forces between two layers, one can enhance the interlayer separation. Consequently, it produces chemicals that intercalate graphene. Then, a single sheet or a few layers of graphene are exfoliated using rapid heating or sonication. To produce various layer thicknesses for single-layer graphene oxide, density gradient ultracentrifugation is combined with ultrasonication. It is simple to create graphene oxide using the Hummers process, which includes oxidizing graphite with strong oxidizing chemicals like potassium permanganate and sodium nitrate in sulfuric acid/phosphoric acid. In a dimethyl formide/water combination, single-layer graphene was produced via ultrasonication. As a result, interlayer spacing rises from 3.7 to 9.5 Å. High functional group densities call for oxidation, and graphene-like properties call for reduction. The sheets are spread by chemically reducing single-layer graphene sheets with hydrazine monohydrate. Polycyclic aromatic hydrocarbons have been used in the production of graphene using a cyclodehydrogenated and planarized dendritic precursor. Make a couple small graphene domains. Larger flakes of poly-dispersed, hyper-branched polyphenylene are produced by the precursor. The initial ones were produced through oxidative cyclodehydrogenation and  $\text{FeCl}_3$ . Graphene is dispersed using orthodichlorobenzene, perfluorinated aromatic, chloroform, isopropanol solvents. An electrostatic force draws graphene on silicon dioxide

substrates to the Si substrate. Reduced graphene oxide is first-class graphene obtained via exfoliation by heating or reduction of graphite oxide.

### 3.2 *Bottom-Up Techniques*

The typical graphene dimensions as well as its layers depth are generated through various bottom-up techniques, and perks and drawbacks of every technique will be discussed.

#### **Mechanical Exfoliation**

The much more typical and important method for producing single-layered graphene flakes on chosen substrates may be mechanical exfoliation. It is the initial known technique for producing graphene. This top-down nanotechnology method stresses the materials that make up the layered structure's surface longitudinally or transversely. Weak Van der Waals forces allow mono-atomic graphene sheets as stack one on top of the other to create graphite. The space and bond energy between sheets are 3.34 Å and 2 eV/nm<sup>2</sup>, respectively. To split mechanically single atomic sheet from graphite, ~ 300 N/mm<sup>2</sup> external force is needed [20]. In graphite, stacking of sheets is caused by the crossover of a half-filled p-orbital that is orthogonal toward the sheet's plane and involves Van der Waals forces. Exfoliation means inverse from assembling together since there is weaker bonding and a larger average crystallite size in the direction parallel than there is in the hexagonal lattice plane and vice versa. In fact, layers of graphitic materials like highly ordered pyrolytic graphite, single-crystal graphite, or natural graphite can be peeled off to produce graphene sheets of various thicknesses. The many tools that can be employed to carry out this peeling or exfoliation include Scotch tape, ultrasonication, electric fields, transfer printing methods, etc. The highly oriented pyrolytic graphite has occasionally been connected to the substrate using traditional adhesives like epoxy resin or even S-adenosyl methionine for advancing the production of individual or more layers graphene sheets.

A latest research reveals the use of gold films to manufacture macroscopic graphene patterns from patterned highly oriented pyrolytic graphite. The typical methods used to characterize graphene flakes that are made using mechanical exfoliation processes include optical microscopy, Raman spectroscopy, and atomic force microscopy. An atomic force microscopy analysis is performed for exfoliated graphene to measure the width and amount of sheets. There is low chance of finding a single-layer flake, and this technique produces poorer yields for mono- and several sheets of graphene with smaller flakes. Optical microscopy is a conventional way for discovering single-sheet graphene. Graphene peels above the surface offer a significant color contrast in respect to thickness. The silicon dioxide layer on silicon wafers is 300 nm thick and produced thermally [21]. This is one of the fastest, finest specific processes for gauging crystallinity and width of graphene sheets. This

is because, depending on the number of sheets present, graphene exhibits various Raman spectra. For micromechanical process, graphene is peeled off single graphite crystal via sticky ribbon. Flaking off graphite leaves multilayer graphene above ribbon. Through frequent flaking, multi-sheet graphene is divided within countless sheets of some-layer graphene.

In order to remove, ribbon is then secured onto acetone support. Unopened ribbon is used for the final peeling. With diameters in support of mono-sheet graphene (wafer spanning) from nanometers to many tens of micrometers, the generated flakes have a wide range in size and thickness. Absorption speed of monolayer graphene is approximately 2%, yet due to interference effects, it can still be seen under a light microscope on silicon dioxide/silicon [22]. Despite the fact that this procedure poses very few challenges, it is labor-intensive to locate the graphene flakes on the substrate surface. The prepared graphene is of extremely high quality and has almost no defects. Mechanical exfoliation still requires improvement based on industrial-scale, flaw-free, more-purity graphene wholesome manufacturing for area of nanotech.

### Pyrolysis of Graphene

Using the solvothermal process, graphene was chemically created in a bottom-up manner. During this heat reaction, salt and ethanol were mixed in a closed vessel at a 1:1 molar ratio. Sheets of graphene can be smoothly separated by pyrolyzing sodium ethoxide with sonication. Up to 10 nm thick graphene sheets were produced as a result. In order to look at crystalline arrangement, various layers, graphitic character, and band configuration, three different techniques have been used: selected area of electron diffraction, transmission electron microscopy, and Raman spectroscopy [24]. Raman spectroscopy of graphene layers indicated large *D*-band and *G*-band, and an intensity ratio of  $I_G/I_D$  was 1.16, which is suggestive of flawed graphene. This technique had the benefit of producing highly pure, functionalized graphene with ease at low temperatures.

## 4 Functionalization of Graphene

Low-cost graphene functionalizations by conventional ways are well known. By changing exterior-plane chemistry of graphene oxide for modification of its properties in a variety of ways, such as by replacing the oxygen atoms through other atoms/molecules or by connecting molecules to oxygen atom for generate variants known as nanocomposite materials. This can be possible because graphene oxide has an abundance of oxygen-containing groups. Functionalization is a key chemical process that significantly affects the material's reactivity and enables the addition of new functions, features, capabilities, or attributes [25]. This customization of graphene has been used in support of specific purposes like biosensors, drug delivery, catalysts, semiconductors, or for improving material characteristics of

complex supplies. Both covalent and non-covalent bonds can be used to combine the exclusive properties of *G* and graphene oxide amid different molecules and nanomaterials, like metals, metal oxides, magnetic nanoparticles, and quantum dots (extremely tiny semiconductor elements along special characteristics), to permit all variety of utilizations.

#### ***4.1 Immobilization***

In order to immobilize molecules like enzymes on graphene support structures, bonding is also used to attach the molecules to the supports. In medication delivery applications, the graphene serves as a carrier for the enzymes, which serve as catalysts for biochemical reactions [26]. Because of their immobilization, the enzymes are less susceptible to environmental influences, they are more stable and do not readily mix with the surroundings, and they can therefore be reused while still maintaining their integrity and effectiveness.

#### ***4.2 Covalent Bonding***

When employed for attaching location for covalent interactions along various molecules and nanoparticles, the oxygen-containing functional groups on the GO lattice's surface or along the margins of the GO sheets can change the surface functionality and enable a range of functions [27]. Thus, graphene is a potential first step in the immobilization of numerous substances, such as a variety of metals, proteins, fluorescent compounds, medications, and inorganic nanoparticles. However, by accommodating the extra molecules, covalent functionalization can damage the structure of *G* lattices, leading to flaws and the deterioration of the lattice's electrical characteristics.

#### ***4.3 Non-covalent Bonding***

The non-covalent functionalizations for graphene or graphene oxide are made possible by the reduced Van der Waals and electrostatic forces or interactions between graphene and desired element [28]. The structure or electrical properties of the graphene lattice are unaffected even while additional chemical groups are simultaneously added to facade. Non-covalent functionalization could improve graphene's dispersion ability, biocompatibility, reactivity, binding power, and sensing effects.

Van der Waals forces often govern bonds between *G* and organic molecules. Pure *G* cannot form ionic connections because it lacks oxygen atoms, which are necessary

for such interactions [28]. However, GO derivatives are capable of ionic interactions, and hydrogen bonding due to GO's edges and surface both has oxygen groups.

Non-covalent pi–pi bonds are created when two overlapping regions of atomic orbitals come into contact with one another. In addition, aromatic hexagonal rings, which contain one free electron each and are cyclic atomic structures, interact with molecules via molecular pi–pi interactions. Such rings are frequently found in organic compounds and polymers, and graphene also possesses a ring structure. However, the unbound electrons would tend to resist one another if the hexagonal nucleus was in direct opposition or parallel to one another, lowering the strength of the bond and lessening the impact of non-covalent contact among aromatic rings [28]. However, distance between electrons of two layers that are straight across from one another is less negative than the distance between the atoms composing an individual ring's periphery rings that are equalized across one another via short path among closest peripheral atoms that make up the nucleus that will have a stronger non-covalent pi–pi interaction. The electrons will instead fall into the somewhat fewer negative areas on each face of opposing couples of atom as a result, preventing them from being in direct opposition to one another. Electromagnetic interactions work inside or between molecules rather than the sharing of electrons. The same interactions still take place even if the rings are in ordered differently, like perpendicular with one another in a *T*-formed arrangement.

Any metal, an anion, a different particle, or yet other system can interact with an electron-rich system like graphene. Biological relationships depend on non-covalent interactions across systems, featuring the stacking of DNA's and RNA's double-ringed nucleotides [29]. Non-covalent bonding has the significant advantage that, in the majority of appliances, graphene and graphene oxide pattern are not interrupted, preserving critical characteristics like electrical conductivity, mechanical strength, and solubility. The many “-” contacts among graphene-derived polymers, for instance, polymers with duplicating aromatic rings, can tightly bind monolayers in bigger or extended systems, producing very uniform polymer compounds with improved mechanical, electrical, and thermal properties. GO has specific promise for usage in nano-medicine, as do several other functional groups that enable further surface functionalization and improve biocompatibility [30].

#### ***4.4 Graphene Conjugation with Organic Molecules***

Through the processes of amination, esterification, and halogenation, organic compounds could be utilized for covalently or non-covalently functionalized graphene arrangement. In studies on covalent functionalization methods for graphene quantum dots, the graphene plane was functionalized with organic compounds, for example, alcohols and diamines for bioimaging applications [29]. It demonstrates that graphene and the two dipoles (*T*, *P*) have fewer interactions compared to non-ionic particles.



#### ***4.5 Graphene Functionalization with Polymers***

Graphene and GO can be functionalized with a variety of polymers through chemical and non-covalent interactions. The created nanoparticles can be used in catalysis, medicine, and power generation [30]. Researchers proved that it is feasible to covalently functionalize GO with polyvinyl alcohol (PVA) in order to enhance PVA's physical merits. Compared to non-modified PVA, the authors found a 400% increase in mechanical parameters and a 60% rise in Young's modulus. It is known that adding GO to PVC increases contact angle values, hence reducing surface roughness.

#### ***4.6 Graphene Establishment in Anti-cancer Drugs***

The non-covalent interactions between drug and graphene layer allowed for the combination of graphene-based nanomaterial (GBN) by anti-cancer treatments. As reported by scientists, covalent functionalization of graphene oxide along sulfonic acid groups and folic acid enhanced its selectivity for MCF7 cells (human breast cancer cell line) [31]. The incorporation of anti-cancer drugs through non-covalent alteration significantly boosts therapeutic effectiveness in comparison with separate medications. The covalent alteration of graphene oxide along chlorotoxin (CTX) increases the release of medication to glioma cells.

#### ***4.7 Graphene Alteration with Biomolecules***

Chain-length proteins, catalysts, and polymers all have graphene and GO bonded to them either covalently or non-covalently. The substance could be used to build detectors that are extremely sensitive to small molecules like antigens [32]. In order to act as a cationic vector for gene transport, GO may be chemically linked with poly-ethyleneimine, according to research. The compound was used as a bioimaging material because of its potent photoluminescence properties.

The scientists achieved covalent and non-covalent conjugation of GBN with biomolecules such as enzymes, sugars, and pathogens for a number of pharmaceutical uses, cancer treatment, synthetic biology, bioimaging, and the advancement of biomaterials in order to identify extremely small portion of biological molecules such as nucleic acids, peptides, or proteins, particularly for disease detection. The usage of GBN as nano-modifiers has received considerable attention in scholarly papers [31, 32]. Data on the nature of the produced nanomaterial are similarly scarce. The lack of knowledge about GBN's biosynthetic pathways for biomedical applications is another disadvantage. However, this study would open the door for later applications.

## 5 Advantages and Disadvantages of Graphene Synthesis Methods

### 5.1 Advantages

- The exfoliation process produces graphene that is extremely pure and of high grade. The exfoliation method's simplicity and lack of complexity make it ideal for laboratory testing. The size of the getting flakes and their controllability are bad for industrial formation [33].
- If we allow graphene to expand on layers, it will have great controllability and a low infinity size of its layers that can pass more. Due to the low clarity of the material obtained, these procedures are not appropriate for laboratory analyses of graphene [33].
- The structure is not only harmed when we compare the electrochemical approach with the reduction of oxidized graphene into graphene oxide, but the material also exhibits strong electrical conductivity without incurring any loss in the treatment. Compared to alternative chemical exfoliation methods like liquid-phase exfoliation of graphite by substantial intercalation and expansion of graphene, the electrochemical technique produces sheets of graphene that are more robust, clean, and huge in size [34].
- To create a liquid-phase solution, the prepared sheet of graphene can be dispersed in an organic solvent. At 150 °C, an organic solvent like dimethyl formamide (DMF) can evaporate.

### 5.2 Disadvantages

- The output from the liquid exfoliation process was decreased.
- The newly produced graphene has some structural and manufacturing flaws. Thus, it is impossible to guarantee the quality of newly produced graphene.
- The contaminants in different types of unclean salt may be fixed between layers of graphene in the electrochemical procedure, which has an impact on the physical phenomena of graphene [33].
- Additionally, because the thickness parameter is managed by the chemical vapor deposition (CVD) process, one cannot control it [34].
- To allow for a comprehensive benchmark of this material and an analysis of its prospective performance, a deeper understanding of factors including breakdown voltage, electron rate, and corresponding saturation current is necessary.

## 6 Applications of Graphene Nanomaterials

### 6.1 Graphene in Fuel Cells

Graphene is impermeable to even hydrogen atoms, which are thought to be the tiniest atoms. In a different study, Sir Andre Geim and his group investigated the possibility of graphene's ability to block protons. Surprisingly, protons may move across graphene. The characteristic definitely increases fuel cell results by minimizing fuel transfer, and this issue significantly decreases fuel cell lifetime and efficiency. Fuel cell is a power generation device that converts the chemical energy of hydrogen and oxygen directly into electricity and can achieve an efficiency of more than 50% [35].

### 6.2 Graphene Batteries

Since graphene-reinforced lithium-ion batteries have amazing qualities including increased flexibility and weight, longer life, higher capacity, and quicker charging times, they could be employed in portable electronics.

Graphene lithium-ion batteries are anticipated to be developed within the next one to three years, solid-state batteries over the next four to eight years, and graphene supercapacitors within the next ten years. Lithium-ion batteries may eventually be replaced with graphene sodium-ion and graphene aluminum-ion batteries because they are less expensive, easier to recycle, and more prevalent in nature than lithium.

Future electric vehicles may use graphene aluminum-ion batteries as their main power source since they can charge 60 times quicker than lithium-ion batteries and store a lot more energy than pure aluminum cells. For instance, AA batteries can be recharged in a minute and coin-cell battery in 10 s using graphene aluminum-ion cells.

### 6.3 Graphene in Solar Cells

In 2017, scientists from Massachusetts Institute of Technology (MIT) successfully used *G* into solar cell. For current density and energy conversion efficiency, the researchers established that the *G*-solar cell was equivalent to other cells completed with aluminum and indium tin oxide, though slightly less efficient than cells made of aluminum. An apparent cell is expected to achieve worse against an opaque aluminum-based cell [35]. A bendable, clear solar cell, which attached to some area (transport, clothing, document, electric items, and many more) has unremarkable electrical characteristics, has been designed. In addition, other researchers are investigating the theoretically feasible ability of graphene solar cells to produce electricity from raindrops.

## ***6.4 Graphene in Thermoelastic***

The Seebeck effect occurs after energy is pushed to any electrical conductors/semiconductors that are incompatible with one another. Electrons move from the hot part to the cooler section as a result of the thermoelectric effect, creating electricity. Though, heat produced through the process is very little and is frequently measured in microvolts. Although it essentially lost heat from the motors, it is believed that it can be utilized to capture it. When coupled with graphene, the strontium titanate-produced Seebeck effect can almost be doubled by five.

## ***6.5 Graphene in Alcohol Distillation***

Big water molecules can travel through glass thanks to the interesting and unique physical properties of graphene, but helium molecules cannot. Andre Geim, one of the originators of graphene, and Rahul Nair of the College of Manchester demonstrated that graphene can successfully distill ethanol by normal temperature with no vacuum required in this processes by attempting to seal a vodka bottle with a graphene membrane they developed. This space can be used to filter alcohol, water, and other chemicals.

## ***6.6 Drug Delivery Using Graphene***

For cancer patients, graphene that has been functionalized is utilized to deliver chemotherapy medications directly to tumors [36]. Delivery methods based on graphene are more effective against cancer cells and less harmful to healthy cells. Anti-inflammatory medications are conceded using mixtures of graphene and chitosan, with promising results. Drug delivery is not just for the treatment of cancer.

## ***6.7 Graphene in Cancer Treatment***

The early stages of cancer can also be detected via graphene. Furthermore, it can stop the growth of many cancer types by impeding normal tumor development or inducing autophagy, which results in the death of cancer cells [37].

## **6.8 *Graphs for Gene Delivery***

By transferring foreign DNA into cells, gene transfer is a technique for treating various genetic illnesses. As has been the case with medication delivery, it is anticipated that GO customized with poly-ethyleneimine also be utilized for those applications and has low cytotoxicity.

## **6.9 *Graphene in Photo-Thermal Therapy***

In photo-thermal therapy (PTT), aberrant cells are removed from the target area of the body by being exposed to a particular substance that produces heat that can kill the cells. Graphene oxide improves PTT's efficiency in many conducts. This will be utilized for concurrently delivering chemotherapeutic medicines and PTT radiation to tumor cells [38]. Chemotherapy and PTT used in this manner are more efficient than either treatment alone. For cancer cell bioimaging during PTT, a reduced graphene oxide nanocomposite (QD-CRGO) will be utilized. The use of graphene oxide functionalized with biocompatible porphyrin for photo-thermal therapy killed more those cells in skull tumors than PTT alone, without harming healthy cells, according to a team of researchers from Texas Tech and Texas A&M University [36].

## **6.10 *Monitoring Diabetes with Graphene***

Researchers at the Bath University have created unique blood sugar investigation method, for that skin pricking not required, dissimilar to the pricking technique now in use. With at least one hair follicle, this patch, which has a graphene sensor, can operate on a limited area. By removing glucose from the intercellular fluid, it may detect glucose. With this, blood glucose measurements are no longer uncomfortable, and the accuracy of the results should also improve.

## **6.11 *Graphene in Dialysis***

Graphene-based membranes have applications outside the energy, nuclear, and food industries. The use of graphene to purge blood of waste, medicines, and chemicals has been shown by MIT researchers [35]. Because it is 20 times thinner than conventional membranes, graphene has an advantage in this case because it shortens the amount of time patients that must undergo dialysis.

## ***6.12 Graphene in the Implantation of Bones and Teeth***

A calcium apatite compound called hydroxyapatite is available for an artificial bone alternative as the regeneration of bone and dental tissues. The inclusion of graphene, hydroxyapatite, and chitosan has improved the alternative material's mechanical and osteogenic properties as well as its strength, corrosion resistance, flexibility, and other properties as contrast with only Hap.

## ***6.13 Graphene for Cell Treatment and Tissue Engineering***

Graphene can heal tissue other than bones as well. It has been demonstrated that specific types of graphene are compatible with human mesenchymal cells and osteoblasts and that they share characteristics with the physiological milieu of the cells. This technique improved cell growth, proliferation, and differentiation while leaving unaffected cell viability [39]. For tissue re-engineering to enhance the lives of persons with neurological illnesses or neurodegenerative diseases, stem cells are very crucial.

## ***6.14 Graphene for UV Sensors***

UV sensors are utilized to sense dangerous UV radiation which leads to skin problems or even cancer. UV sensors be utilized for a variety of applications, including environmental monitoring, optical communications, and the military. While graphene by itself does not have a high photosensitivity, when coupled with other materials, it produces flexible, transparent, and cheap UV sensors that are ecologically benign and will soon be used in wearable electronics.

## ***6.15 Graphene for the Brain***

There is still much to learn about the brain's secrets. By observing the electrical activity of the brain, a graphene-based device might enable researchers to learn a lot about these unanswered questions. This new technology does not impair brain function and can hear frequencies that are below the threshold of earlier technologies [37]. The technology may aid researchers in understanding the causes of epilepsy episodes and creating patient treatments, in addition to helping them better understand how the brain functions [40]. Additionally, as more is learned about the brain, new brain-computer interfaces that can be used to operate prosthetic limbs and other devices may be developed.

### **6.16 Graphs in HIV Diagnosis**

Even with all the advancements, there are still numerous problems with existing HIV detection techniques. Although these methods take longer to develop and are more expensive than the antibody method, almost a month after the patient has the infection, they can either identify the antibodies in the body or find the virus itself. The Spanish National Research Council has developed a silicon- or graphene-based biosensor that detects the HIV p24 antigen and incorporates gold nanoparticles. When compared to current testing, the new technique can detect the virus 100,000 times earlier, up to one week after infection. Additionally, test results are accessible five hours after the test [40].

### **6.17 Graphene Biosensors**

The capacity of graphene to detect minuscule amounts of chemicals is one of its advantages. In a very large volume, it can find even a single molecule. Biosensors prepared by G, GO, and rGO can detect DNA, ATP, dopamine, oligonucleotides, thrombin, or other molecules with incredibly high sensitivity [41]. Numerous medical businesses already sell graphene-based medical sensors.

### **6.18 Bactericidal Graphene**

Because it damages the cell membranes of microorganisms including bacteria, viruses, and fungi in between its outer layers, graphene is a good antibacterial substance. The best antibacterial activity among graphene derivatives is demonstrated by graphene oxide and reduced graphene oxide. To further boost its antibacterial effects, GO can also be combined with silver nanoparticles.

### **6.19 Body Scans with Graphene**

In contrast to X-rays and  $T$ -waves works for scans, this is safe for individual use. Though, sometimes  $T$ -waves, referred to as THZ radiation, are difficult to both make and detect [39, 42]. The good news is that CVD graphene can identify THZ radiation with a few adjustments and other materials. This will eventually lead to both safer body scanning and highly speedy Internet.

## 6.20 Graphene in Nuclear Power Plants

In addition to being expensive to make the production of profound water for nuclear power plants of cooling reactor produces one million tons of CO<sub>2</sub>. A more cost-effective and ecologically friendly method of producing heavy water has been found by researchers at the College of Manchester: graphene membranes. The team's leader, Dr. Lozada-Hidalgo, believes that despite the nuclear industry's usual reluctance to new technology, this discovery is significant and will soon be adopted by that industry.

## 7 Nanocomposite of Graphene and its Application

Electrochemical sensors, aircraft, solar cells, supercapacitors, biomedical, and environmental applications all use graphene-based nanocomposites as special materials. Due to its uniform functionalization and functional repeatability, graphene is chosen over carbon nanotubes (CNTs) or fullerenes in sensing applications [43]. Due to the amazing material characteristics of elasticity limit, strengths, electronic conduction, thermal conduction, optical properties of polymer nanocomposites (PNC), research on PNC has increased over the past ten years, and their applications are expanding significantly. Conventional complex arrangements typically include major quantity filler (50 vol. %) bound in polymer matrix, as well as a modest number of inorganic particles with sizes smaller than 100 nm and relatively greater surface region scattered throughout polymer template. Although, micron-sized graphene may be scaled up for mass production. This makes composite materials based on graphene interesting for a wide range of applications [28].

Large strength, elasticity, higher electronic, thermal conduction and stability, more aspect ratio, huge gas permeability, and better geometric firmness are just a few of the many attractive qualities of graphene [6–12]. By incorporating graphene at a modest volume fraction, the characteristics of polymers can be significantly enhanced. Additionally, graphene is being employed for less volume percentage and more surface-to-volume ratio compared to CNT. It is more effective for enhancing a variety of polymer matrices' characteristics. From a precursor of graphite, graphene can be created in vast quantities through oxidation. As a result, graphene-based polymer nanocomposites have piqued significant global scientific interest. Epoxy [40], PMMA [21], HDPE [11], polystyrene [13, 14], and nylon [12, 15–18] are only a few of the polymers that have been employed as matrices in the creation of graphene polymer nanocomposites. Special overviews for creation of graphene-based nanocompounds are given by Malucelli et al. (2016) [43]. It is important to know about effectiveness of graphene spreading on polymer matrix in enhancing the properties of nanocomposites that is closely correlated with this quality [44]. The aspect ratio of graphene filler has a direct impact on the characteristics of a composite.

In order to create fresh resources for alternative energy supply, graphene-based nanocompounds are more and more being used. As instance, (i) graphene-based



nanocomposites perform better in lithium-ion batteries because of large power and energy density as well as quick charging rush for H<sub>2</sub> fuel cells; (ii) graphene electrode for enhancing electro-catalytic performance; and (iii) graphene-based compounds already in use for photo-volatilization in solar. Understanding the fundamental of physico-chemical properties of nanocompound requires their characterization. Different businesses use various methods to create the many types of graphene materials that are sold on the market. These graphene are anticipated to differ greatly from one another in terms of flakes width, thickness, and imperfection. In order to obtain knowledge for a variety of components disturbing the nanocompounds microstructure and various methods for altering filler area in addition to synthesizing polymer nanocompounds require strong analysis of those methods and properties.

The dispersion, supply, and arrangement of nanocomposites inside polymer matrix have all been studied using various methodologies. The measurement of nanocomposites has been demonstrated to benefit greatly from a variety of techniques, including optical microscopy, X-ray diffraction, Raman spectroscopy, scanning electron microscopy, high transmission electron microscopy, and atomic force microscopy [44]. Additionally, it is frequently required to use more than one characterization method to completely describe the nanocomposite material. Mechanical Characteristics of Nanocomposites Based on Graphene: When compared to conventional composites, graphene-based nanocomposite materials show a considerable improvement in mechanical characteristics. Many nanocomposites have been strengthened mechanically with the help of graphene. When compared to conventional composites, graphene-based nanocomposite materials show a considerable improvement in mechanical characteristics. Many nanocomposites have been strengthened mechanically with the help of graphene. For instance, adding up relatively few weight percentage of graphene increased the tensile strength of baseline epoxy by almost 40%. The crosslinking density of the nanocomposites is increased by the presence of nanoparticles within the matrix, which significantly improves the mechanical properties. Those characteristics are mostly connected to number of sheets and internal flaws in arrangement of the graphene. Monolayer graphene sheets, for instance, have outstanding mechanical characteristics.

As a result of high surface area that can interact through polymer matrix, graphene-related materials have the potential to deliver relevant performance increases at modest loadings, which is supported by this information. For mechanical performance, an ideal loading was found to be around 0.4 wt% for both materials [43, 44]. Epoxy nanocomposites were created by King et al. by adding 1–6 wt% GNP to the epoxy. Typical macroscopic measurements were used to test the tensile characteristics of these composite materials. Modulus and creep compliance were also measured using nanoindentation. These macroscopic findings demonstrated that adding 6 wt% of GNP to an epoxy composite enhanced the tensile modulus from plain epoxy's 2.72–3.36 GPa. The modulus outcomes of nanoindentation exhibited the same pattern. Polyvinyl alcohol (PVA) composite fibers reinforced with graphene reduced from graphene oxide were created by Li et al. Following reduction, the majority of oxygen-containing group can be taken out of graphene oxide, creating rGO. In particular, the tensile strength and Young's modulus of the 2.0 wt% rGO and PVA composite

fiber improved to 244% and 294%, respectively, in comparison with neat PVA fibers. The PVA/rGO composite fibers showed a considerable improvement in mechanical parameters at low rGO loadings.

For biomedical applications like tissue engineering, medication delivery, and cellular treatments, a variety of polymeric nanocomposites are used. A variety of property combinations can be produced to imitate the structure and qualities of natural tissue because of the special interactions between polymer and nanoparticles.

### ***7.1 Applications of Nanomaterials-Based Graphene (GN) in Neural Tissue Engineering***

An incredibly appealing method for treating neuronal injuries and disorders involves using graphene distinctive plane, electronic effects to imitate intrinsic stimuli and promote difference of stem cells through neurons [45]. GN-based products have been proven to encourage stem cells to develop into neurons and increase their pace of proliferating. However, the precise mechanism underlying graphene's impact on brain stem cell development is still understood. In this article, we cover various strategies that scientists have employed to encourage neuron discrimination from stem cells in addition to potential prospect of connected research.

Neural stem cells (NSCs) were grown on ginseng-reduced graphene oxide nanosheet in an effort to increase its biocompatibility and electron transfer capacity [25]. Ginseng extract was used for support and Fe foil served as catalyst in the reduction of GO sheets, resulting in addition of ginsenosides, flavanones, starch on exterior, and formation of denser layers. Additional compounds were shown to promote neuronal development and proliferation. In general, cell density of ginseng-rGO is about ten times more than purified graphene oxide after three weeks of incubation. When compared to glial cells, ginseng-rGO also showed more number of neurons, despite the fact that the cell displayed same percentage of pure graphene oxide [46, 47]. Those findings demonstrated that biomolecule functionalization on graphene-based nanomaterial might produce helpful chemical indications, enhancing graphene capacity for promoting NSC dissimilarities in neurons.

GO was chosen over pure graphene because it can assemble laminin more efficiently. The test sets included positively charged glass with graphene coating, laminin, monolayer of nanoparticles, nanoparticles, and graphene. It was demonstrated that GO with NPs had much higher levels of neural marker expression than naked GO. Maintaining stem cells requires communication between the cell's surroundings and 3D vibrant network of macromolecules. For interconnected 3D neural networks, 3D GNs offer good electrical interaction between the material and neurons, resulting in greater conductivity and electroactivity. They also enable cells to grow in 3D milieu for steer to particular lineage. For instance, Shah et al. looked at how differentiation of NSCs into oligodendrocytes was affected by GO density on 3D nanofibrous arrangements [45, 47].

Polycaprolactone (PCL) was used to create 200–300 nm electro-spun fibers that were subsequently composed on glass support and covered with GO at various quantities (0.1, 0.5, and 1.0 mg/mL). All supports were covered by graphene oxide with no nanofibers, and it was discovered that less GO clung to them because of their smaller surface areas, which indicates a strong similarity between PCL and GO. The analysis concluded that supported nanomaterials showed much oligodendrocyte separation even as lesser glial cell and neuron isolation [49]. Additionally, at higher GO concentrations, there was a much distinct appearance of myelin vital protein, which is advantageous for neural regeneration. Interdependent result for nanomaterial scaffold and GO conduction on NSCs was capable for balancing in neural tissue manufacturing as evidenced by PCL-GO, which demonstrated more than twice the quantity of oligodendrocyte marker Oligo version compared to PCL/GO alone [48, 49].

## 7.2 *Drug Delivery Software*

An optimized drug delivery systems (DDS) principal objective depends on transport healing mediators within the sick section in manageable way with less negative results on strong tissues. Some chemotherapy medications may not dissolve well in water, and their localization into tumors is not always precise, resulting in severe adverse effects on tissues that are not the intended target. Owing toward their suitable large surface region, biocompatibility, ease of functionalization, G and its derived, mainly graphene oxide, have received the most attention among other nanocarriers within area of nano-medicine as bacterial inhibitors, imaging distinct agents, and drug/gene release structures [50, 51].

Furthermore, the ability of graphene nanostructures to absorb a significant amount of near-infrared (NIR) light makes it possible to use those for photo-thermal treatment purpose. Thus, graphene-based nanomaterial has interdependent impact to exist like heat-reactive nano-sized drug carriers in healing purposes such as cancer by fusing together all potentials of transport pharmaceuticals and increased photo-heat alteration. Other kinds of therapeutic agent-loaded modified graphene-based nanoplateforms, on the other hand, might be identified as stimuli-responsive arrangements in support of effective drug release [50]. According to the various forms of environmental stimuli, a variety of documents based on stimuli-responsive graphene-based nanoparticles are reassessed based on following parameters (like, pH, light, redox, magnetic field, and temperature).

## 7.3 *Specific Drug Delivery*

Currently, a wide range of investigations has been presented us with a number of drug release processes in addition to specific techniques.

Graphene-based materials could be used to create tailored DDSs, just like other nanosystems that have been used for drug delivery. Histidine (His) was used in a unique way by Zhang et al. to mediate hydrothermal extension of the unstructured zinc oxide (a-ZnO) shells on gold nanomaterial (Au-His@a-ZnO). They inserted Au-His@a-ZnO NPs on the surface of PEGylated graphene oxide using carbodiimide crosslinker chemistry (PEG-GO). This work involved the creation of Apt@GO@Au-His@a-ZnO@DOX (Apt stands aptamer) nanocompounds, which demonstrated high doxorubicin (DOX) carrying capacity together through near-infrared/pH-sensitive drug delivery, allowing metal-drug composite for dissociate to release anti-cancer ions of  $Zn^{2+}$  in less pH surroundings (endosome/lysosome of tumor cell). Those also showed excellent biostability and aptamer-enhanced lung carcinoma cell attachment [52]. Compared to untargeted controls, the precise binding facilitated cellular absorption into the epidermal growth factor receptor (EGFR)-mutated tumor location. This study used Apt@GO@Au-His@a-ZnO nanocompounds in vivo to demonstrate significant focused drug release and strong anti-cancer efficiency using A549 cells (human lung adenocarcinoma cells) in turmeric mice. The research's use of mixed-use nanocompounds (Apt@GO@Au-His@a-ZnO@DOX) produced highly effective focused photo-/chemotherapy for lung cancers.

One more trial showed, sound nanocarrier capable of effectively delivering a medicine during cancer treatment was created using quantum dot-based GO nanomaterial. An effective nano-cargo was created by conjugating GOQD with chitosan-functionalized folic acid in order to use this DDS in cancer therapy (FA-CH). That revealed the synthesized FA-CH-GOQD is an effective, adaptable nanocarrier toward release of DOX [50].

For MRI and DOX delivery, a folic acid besieged method established on graphene oxide-covered  $Fe_3O_4$  nanocompounds is adopted. The FA- $Fe_3O_4$ @nGO-DOX system may be a useful and reliable substance for targeted medication delivery. Investigations into FA- $Fe_3O_4$ @nGO-DOX nanoplatfoms' potential to support cell survival revealed Callisaurus cell line/MGC-803 preferential perception. The careful nanomaterial intake into MGC-803 cells with folic acid receptor and pH-mediated drug release were used to demonstrate the selective death of tumor cells.

Additionally, it has been suggested that G quantum dots and  $Fe_3O_4$  nanocompounds bound among the lectin protein Concanavalin-As may be a promising contender for identification of tumor cells and the focused delivery of DOX targeting HeLa cells [53]. GQD-ConA@ $Fe_3O_4$  was the abbreviation for the entire system. It has been demonstrated that the incorporation of  $Fe_3O_4$  into the nanocarriers causes drug concentrations in HeLa cells to enhance by greater than double in the presence of an external magnetic field. In addition, the targeting function of Concanavalin-A in nanomaterials was confirmed after demonstrating HeLa cells' 13% increased susceptibility toward drug in comparison to natural cells.

Enhanced fluorinated graphene oxide (FGO) possesses the following qualities as a hugely significant drug carrier: The following characteristics of the drug delivery system were prepared: high drug loading capacity, switchable fluorescence, water solubility, regulated and pH-sensitive drug delivery, large NIR absorption, improved photo-thermal effects, and desired drug release, nano-configuration. FGOs were

initially adjusted in folic acid acting like desired material by purging  $O_2$  through nanosheets. Additionally, the photo-thermal performance was improved by modifying fluorinated G into a nanoscale arrangement using  $sp^2$  carbon. Notably, endocytosis into cells is facilitated by the FGO's microscopic size. Quickly, DOX was installed on FGO-FA. FA ensures that the nanoparticle is delivered to cancer cells that have FA receptors on them, and the remaining portion of the particle causes the release of DOX when there is intracellular acidity [53, 54].

Energy transport among GO, FITC, and ATP was noted within a three-part system known as GONsFITCATP (GONs: graphene oxide nanosheets, FITC: fluoresce in isothiocyanate, ATP: adenosine-5'-triphosphate). In order to deliver DOX to tumor cells, a focused drug release scheme build on graphene quantum dots (GQDs) connected to biotin as a selecting unit was developed. GQD was biocompatible, and biotin-linked GQDs burdened among DOX in the A549 cell line demonstrated more absorption against free DOX or GQDs-DOX.

For the delivery of camptothecin (CPT), methods related by decorated magnetic nanomaterials on graphene oxide covered in mesoporous silica were created. The carriers demonstrated a regulated and pH-responsive drug release and have a 20% capacity for drug loading. It was discovered in this investigation that the synthetic structures had a significant amount of success against HeLa cells. Additionally, with appropriate magnetic characteristics and more adsorption capacity, the adaptable nanosurface can be used for tumor chemotherapy [55].

#### ***7.4 Graphene in Smart Gene Delivery System***

A foreign DNA is effortlessly sent to a cell using a smart gene delivery system (SGDS) on behalf of gene therapy or investigation. SGDS is categorized the same as chemicals (such as lipids or nanomaterial carriers), biologicals (such as viral or bacterial vectors), and mechanicals (such as electroporation, microinjection, and biolistics) depending on the mode of the gene's entry into the cytosol [54, 56]. Gene delivery through chemical means is more typical and uses organic nucleic acid complexes including lipid, cationic polymer, and calcium phosphate. Although biological approaches rely upon creating viral gene discharge system, for that a particular gene is infected into the target cells (s). However, using electroporation, microinjection, and photo-transfection, exposed nucleic acid is delivered into cells using mechanical methods. The successful outcomes of a smart gene delivery system primarily found scheduled transfer of DNA for chosen organs in terms of system's effectiveness. Various parts considering scientific or research emphasis are experiencing a growth due to the development of nanotechnology in the twenty-first century [56].

## 8 Challenges to Produce Value-Added Graphene Nanomaterial Products

Producing graphene on a large scale has its own difficulties. While graphene has received recent attention, it is important to remember that other materials face similar difficulties. Do not disregard the challenges posed by the dispersion and alignment of graphene, which have recently started to be utilized in products. Commercial-scale 3D printing has faced several difficulties in the past. In reality, no matter the material or industry, there are always production obstacles [57]. So why is graphene receiving so much attention? The so-called wonder material is often portrayed as the substance that can solve all application problems and be used to increase productivity in virtually every field of science and technology [58]. Graphene is nevertheless aware of the numerous difficulties that many manufacturing sectors encounter.

There are several different types of graphene (even though this is disputed, the general consensus within the industry is now that there are a family of graphene). Secondly, different processes for making graphene result in extremely varied results. Thirdly, the graphene that can be used in products is not the same as the raw material used to make it. There are many distinct varieties of graphene, and each is beneficial in its own way. Single-layer graphene is preferable for electronics, while some of the larger layer counts (but less than 10) are more affordable and better as additives. Unfortunately, neither end-user markets nor large organizations in general have received adequate information about graphene, and the majority of those looking to use it are unaware of what they are purchasing [58]. Because of this, even if a good form of graphene is available for someone's application, they could not always select the right variety, leading to poor results and a drop in market trust. As more research is being done to better inform decision-makers and more end-user products are now becoming a reality, confidence in graphene is starting to return.

Chemical vapor deposition (CVD) and exfoliation from graphite are the two main methods used in commercial manufacture of G. A solitary sheet of G is deposited using the bottom-up CVD technique on a substrate. Due to its single layer, this graphene is undoubtedly the "highest quality", but it is also often more expensive and can only be produced (at the moment) in smaller amounts [59]. Due to challenges in extracting graphene from the substrate on which it originates, it must frequently be deposited on a customer's substrate of interest in-house.

As a result, it is not the most scalable, yet it works perfectly for specific uses, like electronics. You also have exfoliation techniques, though. These processes convert graphite to graphene. Graphite's intermolecular connections are broken down by strong chemicals, mechanical stress, sun radiation, or high temperatures, but this makes the process much more unpredictable. This typically results in products with inconsistent layer distributions between batches. Even though this type of graphene is typically regarded as being of lower quality, it is significantly more inexpensive, can be produced in considerably larger quantities, and is nonetheless acceptable as an additive in a range of composites and applications [59, 60].

The second aspect to consider is how graphene is used in a product. Before being used as an additive, it must first be functionalized in order to be stable within the composite matrix. The so-called quality is frequently meaningless (since the properties change nonetheless) because the properties of the usable graphene differ from those of the raw material, which is why exfoliated graphene has lately become more usable. The same is true for further graphene derivatives, like rGO and partly functionalized GO [60].

Overall, there are a few issues to resolve, but they are no more significant than those that face any other industrial sector. Because everyone is aware of graphene and is aware of its potential, there is a difference in that everyone is so eager for things to work the first time. Additionally, many mention a lack of standards. Though no physical or measurement standards are currently in existence, they are being developed and will take time, just like they do for any other substance. Again, because it is graphene, researcher anticipates everything to happen right away, but every material must go through a protracted process until all standards are met. In conclusion, neither the manufacturing difficulties associated with making graphene nor its fundamental differences from other materials are particularly noteworthy.

The adoption of graphene may be slowed by a few problems. The restricted manufacturing volume is one such element. Although a variety of ways to produce different kinds of graphene are growing, their combined volume production remains limited. The graphene industry's major challenge will be to achieve volume manufacturing within the next two to five years. The uniformity of the materials and the cost of production must be the main concerns [59, 60]. Since graphene's debut on the market, costs have decreased significantly. The cost of sheet graphene has decreased to a third over the last two years, while the cost of powdered graphene (including liquid graphene) has decreased to a quarter of its initial cost. However, the high initial material cost encourages the development of high-margin applications and applications that make use of a variety of graphene's features.

Chemical vapor deposition (CVD), a time-consuming, expensive method which made use of dangerous chemicals to develop graphene as a single-layered with heating platinum, nickel, or titanium carbide in the presence of ethylene or benzene, was until recently the only way to produce large areas of graphene. There was just one substrate available for crystalline epitaxy, and that was metal. Due to those manufacturing problems, graphene was originally not available for commercial use or advanced research. It was challenging to employ CVD graphene in electronics because it was challenging to remove the graphene sheets from the metallic support exclusive of hurting the graphene [59].

Graphene can be successfully separated from the metallic board on which it is formed, and the metallic board can theoretically be used an endless number of times for subsequent applications, according to research from 2012. As a result, less harmful waste is being generated throughout this process. Additionally, the graphene that was extracted using this method was of a quality that could be applied to molecular electronics. Since that time, research on the synthesis of CVD graphene has improved quickly, rendering the material's quality unimportant to scientific recognition that at present based on the cost of metal support used as a foundation [60].

However, researchers are working towards developing reliable methods for producing graphene on specific supports with organize more than flaws like ripples, doping levels, and domain size, as well as the number and comparative crystallographic arrangement of the graphene sheets.

## 9 Conclusions

A detailed study concerning graphene nanomaterials, its manufacturing processes, numerous potential value-added applications, and challenges in assorted fields has been discussed in this chapter. The physico-electrical properties of graphene which led to its relevant uses in various fields have made graphene the supermaterial of this century. A number of techniques, including ball milling, exfoliation, chemical vapor deposition, and physical vapor deposition, can be used to create graphene nanomaterials. Electrochemical sensors, aircraft, solar cells, supercapacitors, biomedical, and environmental applications all use graphene-based nanocomposites as special materials. Due to its uniform functionalization and functional repeatability, graphene is chosen over other carbon materials in sensing applications.

## References

1. Tiwari, S.K., Kumar, V., Huczko, A., Oraon, R., Adhikari, A.D., Nayak, G.: Magical allotropes of carbon: prospects and applications. *Crit. Rev. Solid State Mater. Sci.* **41**(4), 257–317 (2016)
2. Yang, Y., Liu, R., Wu, J., Jiang, X., Cao, P., Hu, X., Pan, T., Qiu, C., Yang, J., Song, Y., Wu, D., Su, Y.: Bottom-up fabrication of graphene on silicon/silica substrate via a facile soft-hard template approach. *Sci. Rep.* **5**, 13480 (2015)
3. Tiwari, S.K., Mishra, R.K., Ha, S.K., Huczko, A.: Evolution of graphene oxide and graphene: from imagination to industrialization. *Chem. Nano. Mat.* **4**(7), 598–620 (2018)
4. Liao, L., Peng, H., Liu, Z.: Chemistry makes graphene beyond graphene. *J. Am. Chem. Soc.* **136**(35), 12194–12200 (2014)
5. Hughes, Z.E., Walsh, T.R.: Computational chemistry for graphene-based energy applications: progress and challenges. *Nanoscale* **7**(16), 6883–6908 (2015)
6. Flynn, G.W.: *Atomic Scale Imaging of the Electronic Structure and Chemistry of Graphene and Its Precursors on Metal Surfaces*. Columbia Univ, New York, NY (United States) (2015)
7. Peng, Y., Wang, Z., Zou, K.: Friction and wear properties of different types of graphene nanosheets as effective solid lubricants. *Langmuir* **31**(28), 7782–7791 (2015)
8. Zhang, J., Li, S., Tang, B., Wang, Z., Ji, G., Huang, W., Wang, J.: High photocatalytic performance of two types of graphene modified TiO<sub>2</sub> composite photocatalysts. *Nanoscale Res. Lett.* **12**(1), 457 (2017)
9. Katsnelson, M.I.: Graphene: carbon in two dimensions. *Mater. Today* **10**, 20–27 (2007)
10. Lagendijk, A., Tiggelen, B.V., Wiersma, D.S.: Fifty years of Anderson localization. *Phys. Today* **62**, 2429 (2009)
11. Geim, A.K., Grigorieva, I.V., Der, V.: Waals heterostructures. *Nature* **499**, 419–425 (2013)
12. Xu, Z., Buehler, M.J.: Geometry controls conformation of graphene sheets: membranes, ribbons, and scrolls. *ACS Nano* **4**, 386–387 (2010)



13. Nair, R.R., Blake, P., Grigorenko, A.N., Novoselov, K.S., Booth, T.J., Stauber, T., Peres, N.M.R., Geim, A.K.: Fine structure constant defines visual transparency of graphene. *Science* **320**, 1308 (2008)
14. Kelly, B.T.: *Physics of Graphite*. Applied Science Publishers, London (1981)
15. Park, S., Ruoff, R.S.: Chemical methods for the production of graphenes. *Nat. Nanotechnol.* **4**, 217–224 (2009)
16. Lu, X., Yu, M., Huang, H., Ruoff, R.S.: Tailoring graphite with the goal of achieving single sheets. *Nanotechnology* **10**(3), 269–272 (1999)
17. Boehm, H.P., Setton, R., Stumpp, E.: Nomenclature and terminology of graphite intercalation compounds (IUPAC Recommendations 1994). *Pure Appl. Chem.* **66**(9), 1893–1901 (1994)
18. Xin, G.Q., Hwang, W., Kim, N., Cho, S.M., Chae, H.: A graphene sheet exfoliated with microwave irradiation and interlinked by carbon nanotubes for high-performance transparent flexible electrodes. *Nanotechnology* **21**(40), 405201 (2010)
19. Sutter, P.: Epitaxial graphene: how silicon leaves the scene. *Nat. Mater.* **8**(3), 171–172 (2009)
20. Zhang, Y.B., Small, J.P., Pontius, W.V., Kim, P.: Fabrication and electric-field dependent transport measurements of mesoscopic graphite devices. *Appl. Phys. Lett.* **86**, 73–104 (2005)
21. Ni, Z.H., Wang, H.M., Kasim, J., Fan, H.M., Yu, T., Wu, Y.H., Feng, Y.P., Shen, Z.X.: Graphene thickness determination using reflection and contrast spectroscopy. *Nano Lett.* **7**(9), 2758–2763 (2007)
22. Casiraghi, C., Hartschuh, A., Lidorikis, E., Qian, H., Harutyunyan, H., Gokus, T., Novoselov, K.S., Ferrari, A.C.: Rayleigh imaging of graphene and graphene layers. *Nano Lett.* **7**(9), 2711–2717 (2007)
23. Brodie, B.C.: Sur le poidsatomique du graphite. *Ann. Chim. Phys.* **59**, 466–472 (1860)
24. Choucair, M., Thordarson, P., Stride, J.A.: Gram-scale production of graphene based on solvothermal synthesis and sonication. *Nat. Nanotechnol.* **4**(1), 30–33 (2009)
25. Berger, C., Song, Z.M., Li, X.B., Wu, X.S., Brown, N., Naud, C., Mayou, D., Li, T.B., Hass, J., Marchenkov, A.N., Conrad, E.H., First, P.N., de Heer, W.A.: Electronic confinement and coherence in patterned epitaxial graphene. *Science* **312**, 1191–1196 (2006)
26. Seselj, N., Engelbrekt, C., Zhang, J.: Graphene-supported platinum catalysts for fuel cells. *Sci. Bull.* **60**(9), 864–876 (2015)
27. Bourlinos, A.B., Gournis, D., Petridis, D., Szabo, T., Szeri, A., Dekany, I.: Graphite oxide: chemical reduction to graphite and surface modification with primary aliphatic amines and amino acids. *Langmuir* **19**, 6050–6055 (2003)
28. Soo, L.T., Loh, K.S., Mohamad, A.B., Daud, W.R.W., Wong, W.Y.: An overview of the electrochemical performance of modified graphene used as an electrocatalyst and as a catalyst support in fuel cells. *Appl. Catal. A* **497**, 198–210 (2015)
29. Min, S.K., Cho, Y., Mason, D.R., Lee, J.Y., Kim, K.S.: Theoretical design of nanomaterials and nanodevices: nanolensing, supermagnetoresistance, and ultrafast DNA sequencing. *J. Phys. Chem. C* **115**, 16247–16257 (2011)
30. Su´arez, M.Q., Rurali, R., Gammaitoni, L., Abadal, G.: Nanostructured graphene for energy harvesting. *Phys. Rev. B* **84**, 161401 (2011)
31. Wehling, T.O., Novoselov, K.S., Morozov, S.V., Vdovin, E.E., Katsnelson, M.I., Geim, A.K., Lichtenstein, A.I.: Molecular doping of graphene. *Nano Lett.* **8**, 173–177 (2008)
32. Das, A., Pisana, S., Chakraborty, B., Piscanec, S., Saha, S.K., Waghmare, U.V., Novoselov, K.S., Krishnamurthy, H.R., Geim, A.K., Ferrari, A.C., Sood, A.K.: Monitoring dopants by Raman scattering in an electrochemically top-gated graphene transistor. *Nat. Nanotechnol.* **3**(4), 210–215 (2008)
33. Novoselov, K.S., Geim, A.K., Morozov, S.V., Jiang, D., Zhang, Y., Dubonos, S.V., Grigorieva, I.V., Firsov, A.A.: Electric field effect in atomically thin carbon films. *Science* **306**(5696), 666–669 (2004)
34. Sharma, V.: *Advantages and Disadvantages of Different Approaches of Graphene Synthesis* (2017)
35. Durbin, D.J., Malardier-Jugroot, C.: Theoretical investigation of the use of doped graphene as a membrane support for effective CO removal in hydrogen fuel cells. *Mol. Simulat.* **38**, 1061–1071 (2012)

36. Shen, H., Zhang, L., Liu, M., Zhang, Z.: Biomedical applications of graphene. *Theranostics* **2**(3), 283 (2012)
37. Song, E., Han, W., Li, C., Cheng, D., Li, L., Liu, L., Zhu, G., Song, Y., Tan, W.: Hyaluronic acid-decorated graphene oxide nanohybrids as nanocarriers for targeted and pH-responsive anticancer drug delivery. *ACS Appl. Mater. Interfaces* **6**, 11882–11890 (2014)
38. Richards, P.L.: Bolometers for infrared and millimeter waves. *J. Appl. Phys.* **76**, 1–24 (1994)
39. Daneshmandi, L., Barajaa, M., Rad, A.T., Sydlik, S.A., Laurencin, C.T.: Graphene-based biomaterials for bone regenerative engineering: a comprehensive review of the field and considerations regarding biocompatibility and biodegradation. *Adv. Health Mater.* **10**, 2001414 (2021)
40. Li, N., Zhang, Q., Gao, S., Song, Q., Huang, R., Wang, L., Liu, L., Dai, J., Tang, M., Cheng, G.: Three-dimensional graphene foam as a biocompatible and conductive scaffold for neural stem cells. *Sci. Rep.* **3**, 1604 (2013)
41. Xie, L., Ling, X., Fang, Y., Zhang, J., Liu, Z.: Graphene as a substrate to suppress fluorescence in resonance Raman spectroscopy. *J. Am. Chem. Soc.* **131**, 9890–9891 (2009)
42. Wang, J., Mi, P., Lin, G., Wang, Y.X., Liu, G., Chen, X.: Imaging-guided delivery of RNAi for anticancer treatment. *Adv. Drug Deliv. Rev.* **104**, 44–60 (2016)
43. Akhavan, O., Ghaderi, E., Abouei, E., Hatamie, S., Ghasemi, E.: Accelerated differentiation of neural stem cells into neurons on ginseng-reduced graphene oxide sheets. *Carbon* **66**, 395–406 (2014)
44. Campbell, E., Hasan, M.T., Pho, C., Callaghan, K., Akkaraju, G., Naumov, A.: Graphene oxide as a multifunctional platform for intracellular delivery, imaging, and cancer sensing. *Sci. Rep.* **9**(1), 1–9 (2019)
45. Hosseini, M., Farjadian, F., Makhlof, A.S.H.: Smart stimuli-responsive nano-sized hosts for drug delivery. In: *Industrial Applications for Intelligent Polymers and Coatings*, pp. 1–26. Springer (2016)
46. Lu, C.H., Yang, H.H., Zhu, C.L., Chen, X., Chen, G.N.: A graphene platform for sensing biomolecules. *Angewandte Chemie*. **121**(26), 4879–4881 (2009)
47. Singh, N., Kushwaha, P., Gupta, A., Prakash, O.: Recent advances of novel therapeutic agents from botanicals for prevention and therapy of breast cancer: an updated review. *Curr. Cancer Ther. Rev.* **16**(1), 5–18 (2020)
48. Yang, K., Wan, J., Zhang, S., Tian, B., Zhang, Y., Liu, Z.: The influence of surface chemistry and size of nanoscale graphene oxide on photothermal therapy of cancer using ultra-low laser power. *Biomaterials* **33**(7), 2206–2214 (2012)
49. Yang, K., Feng, L., Liu, Z.: Stimuli responsive drug delivery systems based on nano-graphene for cancer therapy. *Adv. Drug Deliv. Rev. B* **105**, 228–241 (2016)
50. Yang, Y., Zhang, Y.M., Chen, Y., Zhao, D., Chen, J.T., Liu, Y.: Construction of a graphene oxide based noncovalent multiple nanosupramolecular assembly as a scaffold for drug delivery. *Chem. Eur. J.* **18**(14), 4208–4215 (2012)
51. Zhang, L., Xia, J., Zhao, Q., Liu, L., Zhang, Z.: Functional graphene oxide as a nanocarrier for controlled loading and targeted delivery of mixed anticancer drugs. *Small* **6**(4), 537–544 (2010)
52. De, S., Patra, K., Ghosh, D., Dutta, K., Dey, A., Sarkar, G., Maiti, J., Basu, A., Rana, D., Chattopadhyay, D.: Tailoring the efficacy of multifunctional biopolymeric graphene oxide quantum dot-based nanomaterial as nanocargo in cancer therapeutic application. *ACS Biomater. Sci. Eng.* **4**(2), 514–531 (2018)
53. Li, D., Deng, M., Yu, Z., Liu, W., Zhou, G., Li, W., Wang, X., Yang, D.P., Zhang, W.: Biocompatible and stable GO-coated Fe<sub>3</sub>O<sub>4</sub> nanocomposite: a robust drug delivery carrier for simultaneous tumor MR imaging and targeted therapy. *ACS Biomater. Sci. Eng.* **4**(6), 2143–2154 (2018)
54. Ratajczak, K., Stobiecka, M.: Ternary interactions and energy transfer between fluorescein isothiocyanate, adenosine triphosphate, and graphene oxide nanocarriers. *J. Phys. Chem. B.* **121**(28), 6822–6830 (2017)

55. Itatahine, A., Mehdi, Y.A., Fizir, M., Qi, M., Dramou, P., He, H.: Multifunctional carbon nanomaterials for camptothecin low-water soluble anticancer drug delivery. *N J Chem.* **42**(2), 1326–1336 (2018)
56. Avouris, P., Chem, Z., Perebeinos, V.: Carbon-based electronics. *Nature Nanotech.* **2**, 605–615 (2007)
57. Geim, A.K., Novoselov, K.S.: The rise of graphene. *Nature Mater.* **6**, 183–191 (2007)
58. Zhi, L., Mullen, K.: A bottom-up approach from molecular nanographenes to unconventional carbon materials. *J. Mater. Chem.* **18**, 1472–1484 (2008)
59. Ruoff, R.: Calling all chemists. *Nature Nanotech.* **3**, 10–11 (2008)
60. Li, D., Muller, M.B., Gilje, S., Kaner, R.B., Wallace, G.G.: Processable aqueous dispersions of graphene nanosheets. *Nature Nanotech.* **3**, 101–105 (2008)

# High-Performance Metric of Graphene-Based Heterojunction LEDs and PDs in Visible Light Communication Systems



Mohamed El Jbari and Mohamed Moussaoui

**Abstract** Due to the considerable attention in GaN-based semiconductor materials such as large-size, low-cost amorphous SiO<sub>2</sub> substrate, high-frequency, and efficient energy design with a low level of light sources, there are more applications in optoelectronics components, such as light-emitting diodes (LEDs), laser diodes (LDs), and indium gallium nitride (InGaN)-based photodetectors (PDs). The high bandwidth of LED transmitters and the high signal-to-noise ratio (SNR) of PDs receivers have great advantages in visible light communication (VLC) systems. Nevertheless, the low data rate speed influences the application of GaN-based LEDs and InGaN-based PDs which have a traditional structure in VLC systems. Given its excellent physical and chemical characteristics, graphene is an attractive material for LEDs and PDs technologies. Combining graphene (Gr) with other materials such as InGaN or GaN can further eliminate the shortcomings of graphene and lead to high-performance Gr/InGaN-based LEDs and Gr/GaN-based PD heterojunctions. It finds that the application of metal nanorods with graphene gap layers by metal-organic chemical vapor deposition (MOCVD) as monolayer Gr (M-Gr) or three-layer Gr (T-Gr) can make a perfect optoelectrical property. The T-Gr/GaN LEDs and T-Gr/InGaN PDs exhibit high responsivity. Furthermore, nanophotonics is a significant field in which a VLC modulator provides various optical device applications employing single-photon devices, quantum communications, advanced plasmonics, and electro-optic modulator architectures. This is due to the use of high-quality GaN or InGaN growth layers and the limited density of T-Gr states. The T-Gr/GaN LEDs and T-Gr/InGaN PDs have a rapid response time and an excellent responsivity, respectively, and high-speed modulation capability (i.e., electro-optic modulator structures) with considerable potential for selective sensing of the VLC system in 6G networks.

**Keywords** Visible light communication (VLC) · Graphene · Light-emitting diodes (LEDs) · Photodetectors (PDs) · Heterojunction · Optical modulator

---

M. El Jbari (✉) · M. Moussaoui  
LabTIC Laboratory, National School of Applied Sciences of Tangier, Abdelmalek Essaadi University, Tetuan, Morocco  
e-mail: [mohamed.eljbari2@etu.uae.ac.ma](mailto:mohamed.eljbari2@etu.uae.ac.ma)

M. Moussaoui  
e-mail: [m.moussaoui@uae.ac.ma](mailto:m.moussaoui@uae.ac.ma)

## 1 Introduction

Two-dimensional (2D) materials have generated a lot of regard in efficient optoelectronic applications due to their unique exceptional characteristics, including ultrathinness, lightness, flexibility, ease vertical heterojunction fabrications by van der Waals, compatibility to conventional microfabrication techniques, and a regulated energy band. The most well-known 2D material is graphene. Zero band gap with very high carrier mobility has validated their use in optoelectronics, such as LEDs and PDs. The constant absorbance ( $\approx 2.31\%$  per layer) throughout a very large range of the electromagnetic spectrum is useful for wide illumination detection of visible light [1]. Moreover, the electronic and optical properties, the anisotropic structure of graphene, and the chemical stability of material make it promising for the easy use of multilayers in heterojunction-based LEDs and PDs [2]. All these 2D materials mentioned in the rest of this chapter are appealing for optoelectronics applications. Graphene has previously been used to detect radiation using visible light which is a wide wavelength range of 370–800 nm, as shown in Fig. 1 (visible light band). Broadband detection of visible light has been realized with InGaN-based photodetectors.

GaN or InGaN/graphene-based materials show numerous attractive optoelectronic properties that make 2D materials advantageous candidates for optoelectronics instead of traditional optical communications. In particular, the extraordinary electric-optical combination in visible light communication (VLC) systems with high performance metrics such as high-frequency communication and great security in different environments [4].

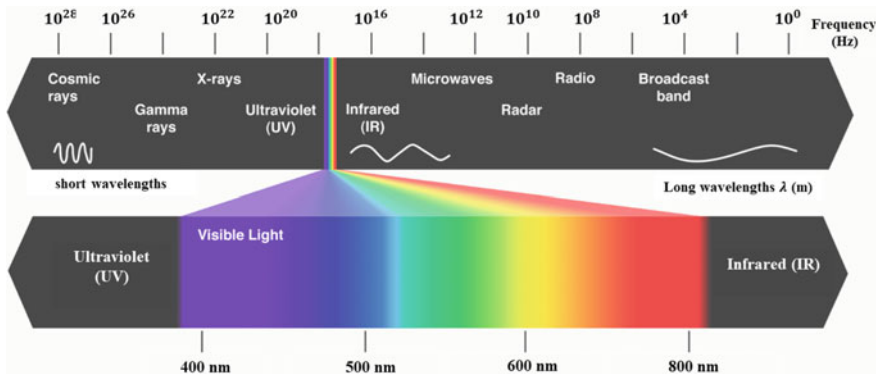


**Fig. 1** The visible light band in electromagnetic spectrum

### 1.1 Motivation

With rapidly increasing radio frequency (RF) spectrum saturation and the deployment of most RF bands in wireless communication systems in fifth-generation (5G) mobile networks, identifying suitable green and environmentally friendly technologies for 6G networks is important [3, 4]. VLC is an optical wireless communication that has attracted the attention as a complementary solution to RF waves owing to its very high information rate, large electromagnetic spectrum (EM) bandwidth from 428THz to 750THz, anti-interference robustness, low cost in commercial, network energy efficiency, and greater data security [5, 6].

In order to successfully achieve optoelectronic signal conversion, the VLC transceiver composites, as illustrated in Fig. 2, include the laser diodes (LDs), light-emitting diodes (LEDs) at the transmitter, and photodetectors (PDs) at the receiver [4]. Currently, the most common LEDs are blue LEDs based on silicon dioxide (SiO<sub>2</sub>) substrates, which offer the advantages of wide wavelength conversion and ultrahigh-speed response. The low bandwidth and high bit error rate (BER) limitations, however, reduce the latency and reliability of the VLC systems. The most effective way to achieve rapid-speed communication, high efficiency, and high channel capacity is through modulation of the LED’s bandwidth, which is possible with GaN-based LED semiconductor materials [7]. High modulation bandwidth is accomplished by GaN LEDs, which also improve BER and spectral response. Although it is possible to bend active components like diodes (such as LEDs and LDs), highly flexible interconnections and electrodes are still difficult to use because of their high current densities, heat dissipation, and low power. Additionally, enhanced resonance is not effective for wireless VLC system transmitters.

As they are highly effective in VLC systems, flexible InGaN PDs are widely used in a variety of areas, including wireless optical communication. The traditional PD material is very rigid, which significantly restricts how well it performs when bent or stretched, diminishes its photosensitive surface, and lowers its responsiveness due to metal electrode shielding [7]. On the other hand, the low response speed of broadband light sources can decrease the signal-to-noise ratio (SNR) [8]. Consequently, the design of novel flexible photonic devices such as InGaN-heterojunction PDs with bending and folding functionalities is very important and is of considerable interest to wearable optoelectronic devices in VLC. Due to the difficulty of directly growing

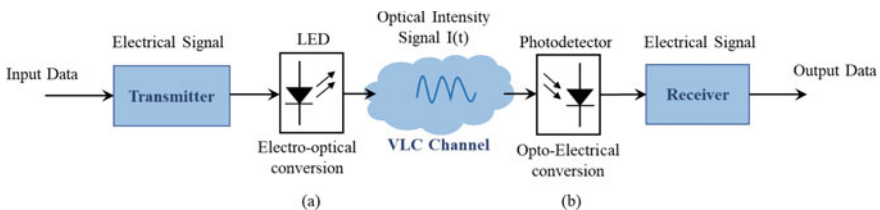


**Fig. 2** Flowchart of VLC system: **a** LED at transmitter end; **b** PD at receiver end

nitride materials on the amorphous substrate and the absence of an epitaxial growth connection between the amorphous substrate and nitrides, these traditional epitaxy procedures are no longer appropriate.

Due to its larger benefits such as high conductivity, transparency from the visible to infrared spectral range, excellent chemical stability, and optical-electrical performance, two-dimensional (2D) planar graphene has a significant potential for use in GaN LEDs and InGaN-LDs [9]. Graphene (Gr) 2D layer material has been used in the construction of high responsivity heterojunction-based LEDs or PDs using GaN or AlN grown on a substrate [10], AlGaIn nanowire grown on the SiO<sub>2</sub>/Si (100), Ga<sub>2</sub>O<sub>3</sub> films [11], and Gr/MoS<sub>2</sub>/Gr lateral heterostructure [12]. In recent years, graphene's ability to act as a buffer layer has been getting a great deal of attention, such as the preparation of GaN-based LEDs on graphene-covered sapphire [13]. As a result, previous 2D graphene-based LDs and LEDs focused on high-performance metrics like modulation bandwidth and photoresponsivity, not to mention the influence mechanism of graphene materials layers, which is a challenge in VLC system speed [14–16].

## 1.2 Graphene's Electronic and Optical Properties

A significant portion of the scientific community has become interested in graphene and 2D materials since the initial experiment conducted by the Nobel Prize winners Novoselov and Geim back in 2010 [17]. These 2D material structures of carbon atoms provide fresh insights in a variety of scientific areas, especially optoelectronic devices [18–21].

### Gr-Based Structure

The single sheet of  $sp^2$ -hybridized carbon atoms bound together in a honeycomb lattice constitutes graphene. The many electron wave functions of atoms overlap, excluding the  $p_z(\pi)$  orbital and the others,  $p_x$  and  $p_y$  atomic orbitals. This  $p_z$  electrons which form  $\pi$  orbitals can relate independently the  $\pi$ -band approximation. The dispersion expressions  $E(k_x, k_y)$  can be easily derived [20]:

$$E^{\pm(k_x, k_y)} = \pm\gamma_0 \sqrt{1 + 4 \cos^2\left(\frac{a}{2}k_y\right) + 4 \cos\left(\frac{\sqrt{3}}{2}k_x\right) \cos\left(\frac{a}{2}k_y\right)} \quad (1)$$

where  $a = 1.44\sqrt{3}$  Å is the lattice carbon–carbon distance and  $\gamma_0$  is the first and second neighbors' coulomb integral  $\pi$ -orbitals. A couple of electronic momentums are usable in the 1st Brillouin zone  $k = (k_x, k_y)$ , manufacturing graphene based on

semimetal or zero-gap semiconductors. Figure 3 shows the real-space honeycomb graphene lattice in (a) and (b).

The following linear dispersion formula is obtained by developing Eq. (1) for low energy close to the  $K$  points:

$$E(k) = \pm \hbar V_F |k - K| \tag{2}$$

where  $\hbar = 1.05 \times 10^{-34}$  J.s and  $V_F$  is the Fermi velocity ( $\sim 0.91 \times 10^6$  m/s). Figure 4 shows the graphene band structure and first Brillouin zone with the demonstration of the energy band of one Dirac point.

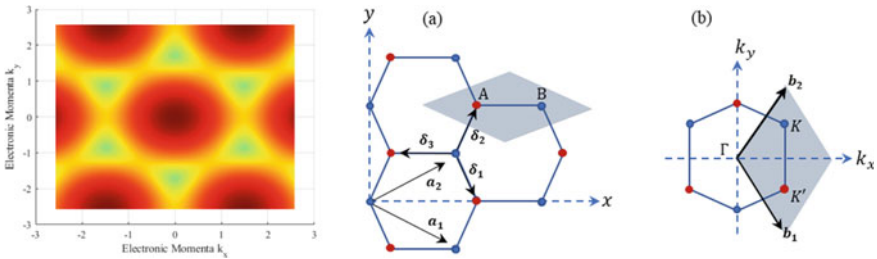


**Fig. 3** The cross section of hexagonal shape of Dirac point of graphene, and the honeycomb graphene lattice presented in **a** and **b** as function of the momentum

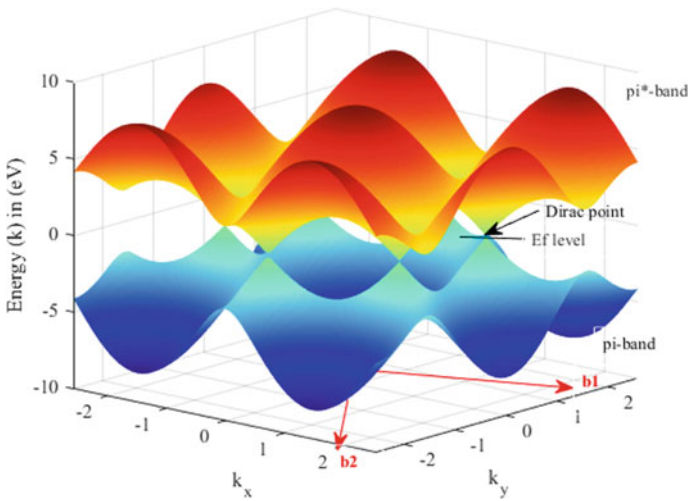


**Fig. 4** Graphene three-dimensional (3D) band structure and first Brillouin zone in momentum space



## Graphene Optoelectronic Characteristics

Graphene conductivity is temperature and Fermi level location dependent (the doping density). Extensive doping can be accomplished in practice by graphene rinsing in nitric acid [2], which has guided to a resistivity at room temperature in a 4-layer graphene sheet assembled. The neutral conductivity of graphene was found to be perplexing, with Fermi energy just at Dirac point and zero density of state, but of no practical significance since devices would always be developed with improved conductivity doping. While the previous literature reported a minimal conductivity for sheer neutral graphene and at room temperature, found the theoretical values Mott-Anderson metal—semiconductor transition for neutral graphene [2]. In practical situations, observing the insulator transition is difficult because the stray electric fields created by the substrate induce “puddles of charge” which render adjacent regions of the supposedly neutral substance conductive so that the real Dirac-point behavior of brocade. By using the random phase approximation [22] and the Kubo formula [23], the total conductivity can be expressed as follows:

$$\sigma_T = \sigma_{\text{intra}} + \sigma'_{\text{inter}} + i\sigma''_{\text{inter}} \quad (3)$$

where

$$\sigma_{\text{intra}}(\omega) = \sigma_0 \frac{4\mu}{\hbar\pi(\tau_1 - i\omega)} \quad (4)$$

$$\sigma'_{\text{inter}}(\omega) = \sigma_0 \left( 1 + \frac{1}{\pi} \left( \arctan \frac{\hbar\omega - 2\mu}{\hbar\tau_2} - \arctan \frac{\hbar\omega + 2\mu}{\hbar\tau_2} \right) \right) \quad (5)$$

And

$$\sigma''_{\text{inter}}(\omega) = \frac{-\sigma_0}{2\pi} \ln \frac{(2\mu + \hbar\omega)^2 + \hbar^2\tau_2^2}{(2\mu - \hbar\omega)^2 + \hbar^2\tau_2^2} \quad (6)$$

where  $\sigma_0 = \pi e^2/(2\hbar)$ ,  $\tau_1$  and  $\tau_2$  denote the relaxing rate of intraband and interband transitions, respectively, and  $\mu > 0$  is the chemical potential. Since there is zero bandgap, the interband and the intraband contributors compete that the interband transition only arises above the photon Fermi energy threshold. Figures 5 and 6 show the interband contribution in Dirac fermions with a large band from the visible band for weakly doped graphene and high-frequency dynamic conductivity.

The nonlinear optical properties are the original from the optical signal resonates and the electric field ( $E$ ) with the carbon atoms, especially the electronic polarization (i.e., displace the electron cloud to the nucleus). The linear relationship between the applied electric field and electronic polarization [24]:

$$P = \varepsilon_0 \sum_{n=1}^N \chi^n E^n; \quad n = 1, 2, 3, \dots, N \quad (7)$$

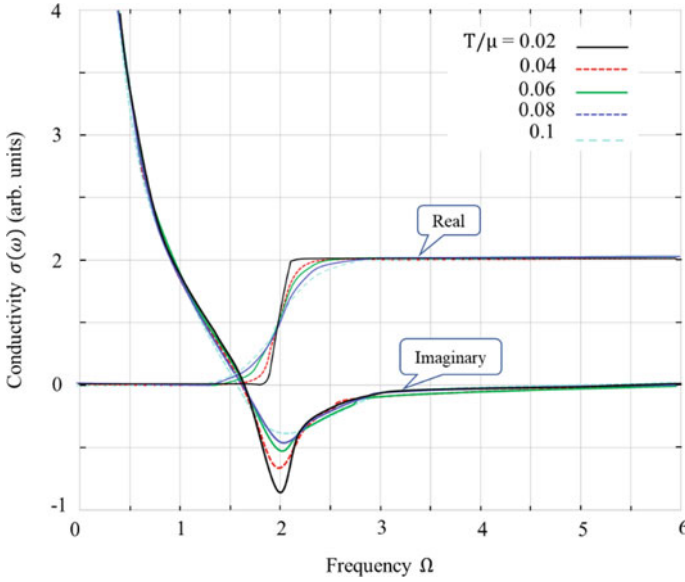


**Fig. 5** Optical conductivity rate versus of frequency ( $\Omega = \hbar\omega)/\mu$ , the real and imaginary parts of the dynamic graphene conductivity (under zero temperature condition with ignoring the effect of collision)

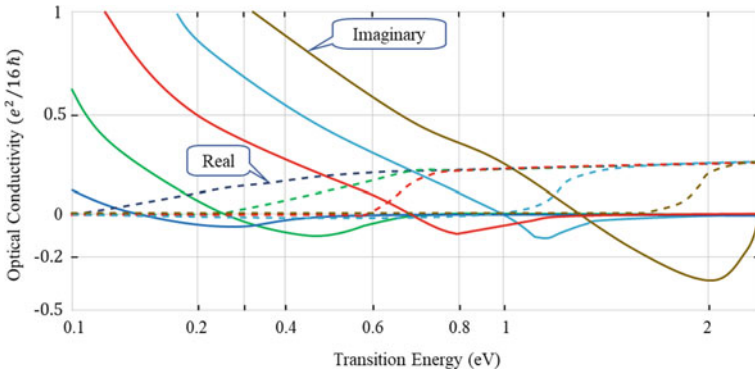


**Fig. 6** Optical conductivity as function of a different Fermi energy ( $E_F$ ) in real and imaginary parts

where  $\chi^n$  is the  $n$ -order nonlinear susceptibility and  $\epsilon_0$  is the electric permittivity in free space. The most nonlinear optical graphene corresponds to the 3rd-order susceptibility  $\chi^3$ , then it is associated with the electric field's polarization per unit volume to the 3rd power, and the graphene is a tiny fine and isotropic conductivity surface. Since the classical approach cannot adequately explain the optical nonlinearities in graphene which the nonlinear response is better described in term of  $n$ th-order

complete control layer current [25]:

$$J_n = \frac{1}{4\pi^2} \iint dP_J N(\varepsilon) \quad (8)$$

where  $N(\varepsilon)$  is the thermal factor and  $J_n$  is the n-order current. The third-order current associates can be expressed as:

$$J_3 = \sigma_1 \left( \frac{eV_F E_0}{\hbar\omega^2} \right)^2 [N_1(\omega)e^{j\omega t} + N_3(\omega)e^{3j\omega t}] \quad (9)$$

This 3rd-order current is associated with three-photon processes in which the superposition of two 3rd-order currents creates a single and 3rd-harmonic generation frequency. The 3rd-order current proportionality to the frequency and the electric field power are due to a large range of nonlinear optical phenomena in graphene, such as self-focusing and nonlinear change in refractive index that the visible spectrum of graphene just reflects 0.1% [26], saturable absorption of layer 2.3% over the visible light band [27], optical bistability, and switching [25].

The visible light radiated from the graphene surface interacts with the light ray's source from Si surface. If we exclude the little proportion of the light reflected or absorbed by graphene, the intensity of interference modulated is  $I(\omega; d_t)$  calculated by

$$I(\omega; d_t) = I_0(\omega) \left( \frac{1 + (r(\omega))^2}{2} + \text{Re} \left( r(\omega) e^{\frac{2i\omega d_t}{c}} \right) \right) \quad (10)$$

where  $I_0(\omega) \approx \varepsilon\omega^3 / \left( e^{\frac{\hbar\omega}{k_B T}} - 1 \right)$  is the thermal radiation intensity from the graphene,  $r(\omega) \sim 0.5$  is the reflection index of Si for the VL band,  $k$  is the wave vector of the photon,  $d_t$  is the trench depth, and  $c$  are the speed of light (see Fig. 7a and b). Figure 8 demonstrates the enhancement of thermal radiation for a particular wavelength from suspended electrically biased graphene devices by properly designing their trench depth  $d_t$  with interference effects. However, any irregularity in the trench depth caused by the Si and graphene surfaces' tilt or roughness, as well as the thermal vibration of the graphene, partially obscures washes out the interference pattern.

## 2 GaN/Graphene-Based Heterojunction LEDs

The high response frequency ( $\sim 85 - 405$  MHz) and the high optical output power could apply to VLC systems. In general, GaN-based visible light LEDs can be applied for overall illumination, automobile headlights, traffic signals, LCD backlight units, and in more VLC applications. The  $(V_{\text{bias}} - I)$  curve and nonlinear characteristic current-incident optical power are shown in Fig. 9a and b, respectively. Metal-GaN

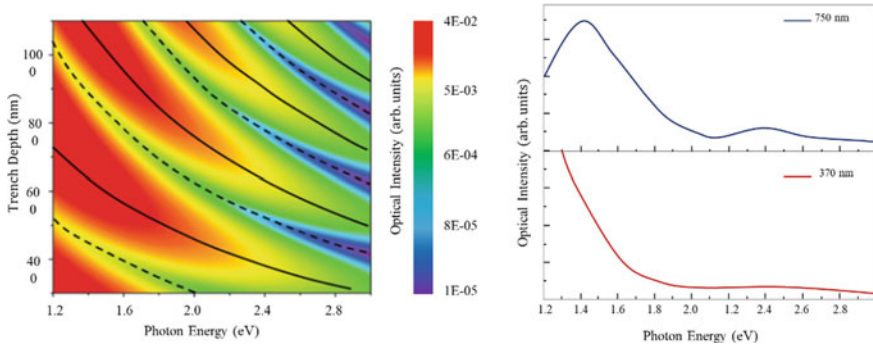
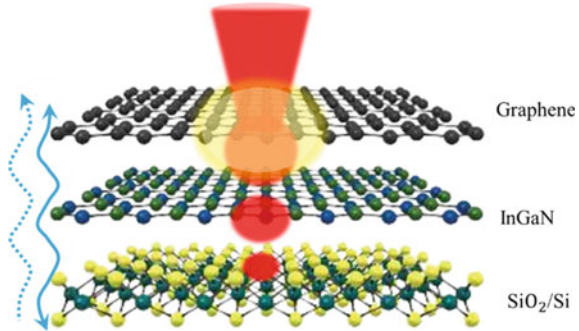


**Fig. 7** Electrically biased suspended graphene’s simulated radiation spectrum VLC

**Fig. 8** Schematic hypothetical three-layer structure with vertical charge separation for graphene/InGaN growth on with transition electron-hole pairs



nanorods (AlGaIn) were used to create GaN films directly on monolayer graphene buffer layers on amorphous SiO<sub>2</sub>/Si (100) substrates. In [28], controlled nanorods (NRs) coalescence methods were used to produce continuous metal-organic chemical vapor deposition (MOCVD) GaN films. However, the Gr/AgGaIn nanoparticles-polymethyl methacrylate (NPs-PMMA) applying in LEDs can produce blue LEDs at a wavelength of 400 nm because of the surface plasmon resonance (SPR) of the Ag-NPs. They exhibit increased light emission. They can also be efficiently gate-tunable by inserting a graphene layer into the electroluminescence (EL) structure of Gr/AgGaIn and the static voltage applied between the top and bottom layers of graphene [29]. Figures 11 and 13 show the two different heterostructure LED’s schematic of the carrier kinetics process.

Figure 12 represents the intensity as function Raman spectra of M-Gr and T-Gr layers with the Ag NRs. In [30], the single layer of graphene is elaborated on the high resistivity of Si by atmospheric-pressure chemical vapor deposition (APCVD). Carrier localization in ternary InGaIn – NPs grown by MOCVD was saturated in the Gr/GaN/Si heterojunction itself because the size and composition fluctuation in steady state versus temperature were measured using photoluminescence (PL).

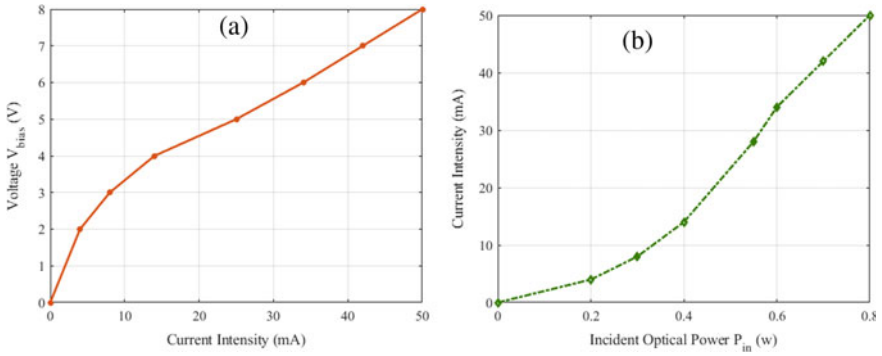


**Fig. 9** **a** Voltage–current ( $V-I$ ) curve and **b** the current incident as function of the optical power of GaN-based LEDs

The PL pulse energy generation of the InGaN-NRs is accurately recreated by the localized state group model.

More results demonstrated the high optical sensitivity of GaN-based LEDs that grow by the adding of M-Gr and a high-quality metal/GaN NRs or NPs buffer layer. Other CVD techniques for high transparent LEDs on Gr-Cu nanowire combinations of transparent electrode materials are demonstrated in [31]. The encapsulation of Gr-layer on Cu nanowire GaN-based LEDs is achieved by the better optoelectronic device performance of 95% transmittance at the sheet resistance.

Figure 10 presents the room temperature Raman spectra of the InGaN films, with the peak sharpening at  $566\text{ cm}^{-1}$  make to Si substrates. Only research has merited finding large field applications in recent years. However, as shown in Fig. 17, there has been a significant increase in Gr – GaN LED integrations as well as the number of publications and patent applications on graphene (Figs. 9, 10, 11, and 12).

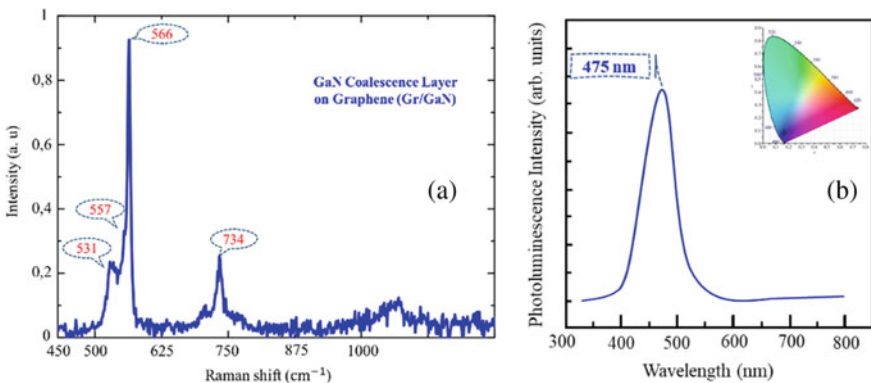


**Fig. 10** Detailed graph of GaN Raman response. **a** GaN coalescence layer on graphene devices. **b** Room temperature of photoluminescence (PL) spectra by GaN-based rise on substrate with the NRs interlayer

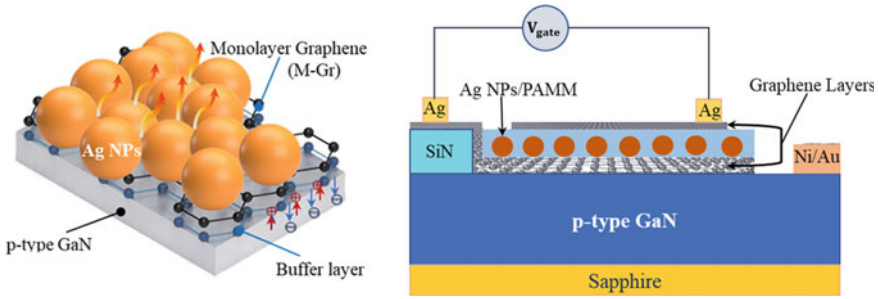


**Fig. 11** Ag nanoparticles (NPs) and schematic carrier kinematics process in Ag-NPs/Gr/p-GaN heterostructure of LEDs

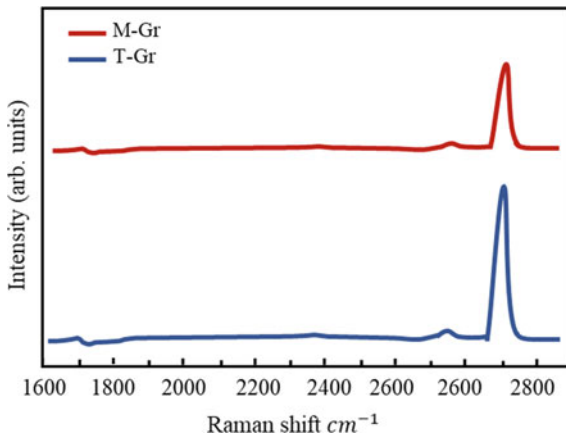


**Fig. 12** Raman spectra of monolayer and three layers with the Ag nanoparticles (NPs)

The electro-optic modulation depth with highly doped graphene gives a considerable advantage for optical communication development and the deployment of high-speed VLC systems. Additionally, recent optical modulators use traditional optical components such as pulse-based modulation, lens, and spectroscopes [32].

The Gr-metasurface plasmonic structures have the capacity to enable a high light modulator and high response when we use the nanoscale devices and 2D nanomaterials in the OWC and especially in VLC. This modulation performance is obtained by using the Pauli blocking effect and Kubo formula (i.e., Eq. (3)) and disabling the interband transition carriers with the high Fermi level [20, 33]. Figure 14 represents the energy band diagram heterojunction of Gr-GaN-based LEDs.

The research describes an efficient approach for growing GaN-based LEDs on amorphous substrates by including graphene as a buffer layer NRS-AlGaIn nanorods and AgGaIn nanoparticles, which is useful for large-area GaN-based optoelectronic contributions of technology. MOCVD is used to develop GaN-based LEDs grown on an amorphous SiO<sub>2</sub> substrate using NRs and graphene buffer layers.

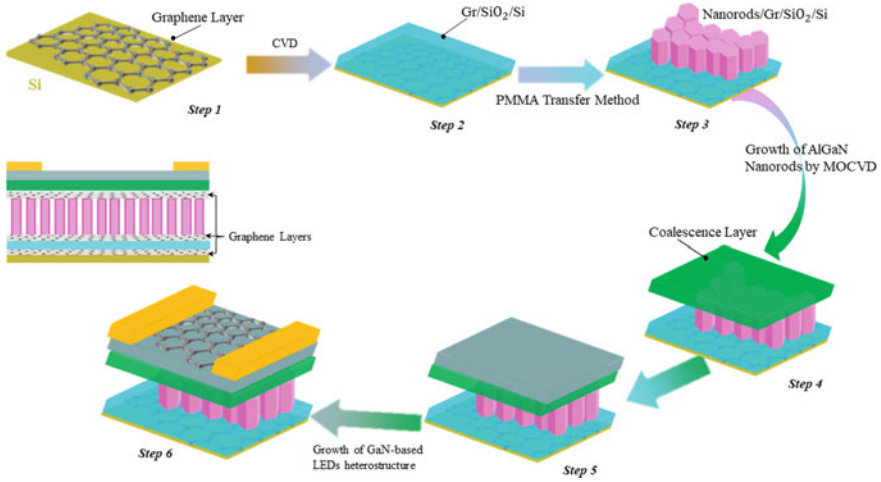


**Fig. 13** Design for the production process by integrated hybrid Gr/AlGaIn NRs/Gr visible light (VL)-based LEDs heterostructure in six steps

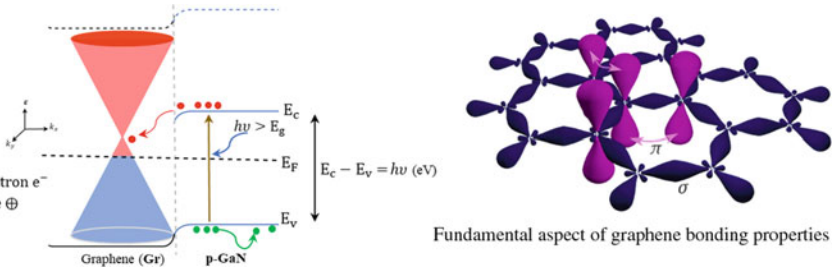


**Fig. 14** Photo-generated energy band diagram, and the carrier diffusion scenario a Fermi–Dirac distribution of the Gr-GaN LED, which the generated electron–hole pairs are separated causing the band bending at the Gr/InGaIn plane. And the process of saturable absorption in Gr, where the interband transition is excited by incident light

The multilayer graphene one with good quality can effectively screen the lattice potential field from the SiO<sub>2</sub> (SiC) substrate. Analyzing growth kinetics, the influence of varied growth factors on nanorod shape and vertical-to-lateral aspect ratio was investigated. Graphene-based organic LEDs (OLEDs) have been made without the usage of metal catalysts or a graphene transfer process by utilizing high-quality monolayer graphene directly grown on a transparent substrate by applying a commercially available MOCVD process. The transparency of graphene materials in the visible spectral range is similar, indicating a high potential for its usage in optoelectronic devices such as LEDs (Figs. 13 and 14).



### 2.1 Optical Modulators

The modulation of visible light accomplished by tunable semi-metallic graphene 2D materials with Dirac fermions represents an important prospect for the implementation of VLC communication [34, 35]. In [35], the TiO<sub>2</sub> Metasurface designs for visible modulation (600–800 nm) have a highly efficient transmission modulation of 65% under the small voltage range of 3–5 V, and it is grounded on TiO<sub>2</sub> nano-disks implanted in a lean liquid crystal layer. In [36, 37], graphene-based optical modulation is demonstrated with low energy consumption, modulation depth, response time, and modulation speed based on M-Gr on Germanium (Ge) (Fig. 15).

The electro-optical Gr-optical modulation speed is related to graphene position and the number of Gr layers. In [33], the modulation speed and depth for optical modulator mode with 1 GHz and RC constant limit are given. The optical nonlinearity of 2D materials is stably decreased at high intensity, as shown by the saturation absorption of GaAs semiconductors (see Fig. 16).

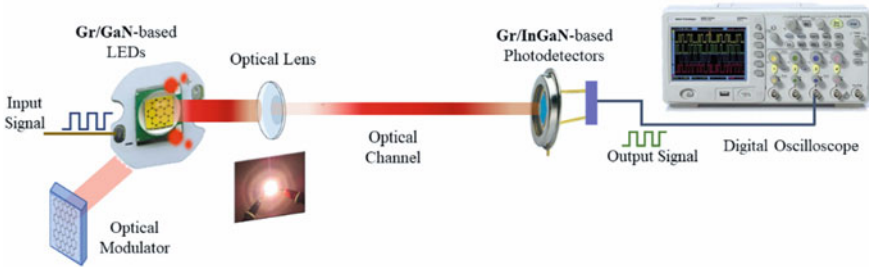


**Fig. 15** Schematic of the experimental configuration used for the modulation measurements of the graphene on germanium (Gr-o-Ge) all optic modulation

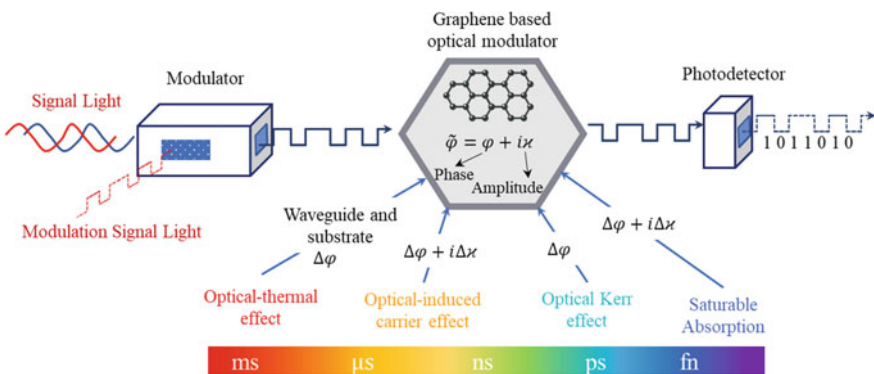


**Fig. 16** Optical communication system consisting of a modulator and photodetector. Solid and dashed curves represent optical and electrical signals, respectively



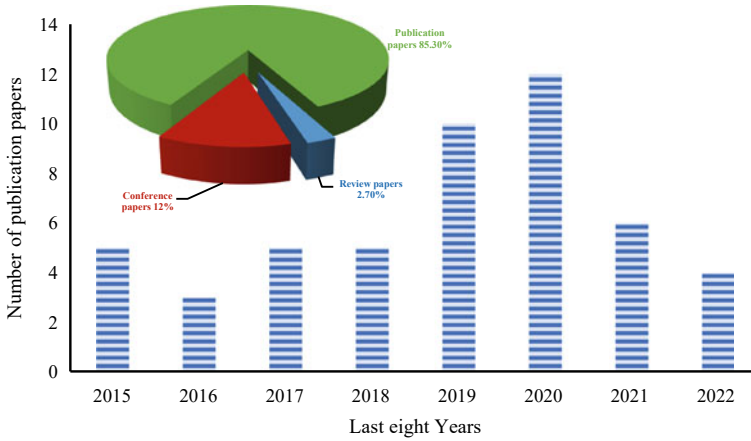


**Fig. 17** The number of the publication papers of the world “graphene-based LEDs” occurring in the titles, abstracts, and full text from 2015 today

According to [37], the modulation efficiency can be improved by optimizing the gap width of diagonal graphene optical modulation, affecting the edge plasmonic with a modulation bandwidth of 0.61 THz and a low energy consumption of 137 femtoJoule per bit as a benefit wedge of the intrinsic surface plasmon polariton enhancement. As a result, the design challenge in this case is the polarization shift Gr-light region.

The high efficiency of Gr-optical modulators can improve the modulation capacity, and their technology may give a more efficient technique for developing nanophotonics and optoelectronic devices using 2D-Gr materials.

For transmission electron microscopy, optical modulation provides considerable benefits in terms of low power dissipation. As shown in Fig. 16, the graphene-based mechanisms reference all optical modulations and their response time. Complex refractive index modulation  $\sim \varphi$  can be divided into two parts: the first real part of the refractive index (for phase modulation) and the second imaginary part of the refractive coefficient (for amplitude modulation) (Fig. 17).

### 3 InGaN/Graphene Heterojunction PDs Performances

Using graphene Gr-metal junctions or Gr/p-n junctions, ultrafast photodetection from visible light regions  $\sim 370 - 800$  nm is possible. The two primary criteria for the development of high-quality graphene photodetectors using the Gr/InGaN heterojunction PDs are higher optical absorption within the effective junction regions and better graphene photocarrier lifetime ( $\sim 1 \mu s$ ), which is determined by interband transitions in graphene (as seen in Fig. 14). Available commercially CVD-grown

graphene is great shifted to a high resistivity silicon chip coated with such as 130 nm heavy generate thermal SiO<sub>2</sub> layer.

The heterostructure of Gr-InGaN PDs films on Si substrates is dependent on the number of Gr layers. In T-Gr/InGaN, carrier transfer improves photoelectric conversion using a simple Schottky junction design as compared to M-Gr/InGaN. However, in visible light communication systems, it produces a high responsivity of 60/200 μs fast rise and fall [38].

The superb performance of InGaN-based PDs films on Si is achieved with high temperature MOCVD combined with low temperature pulsed laser deposition. The InGaN surface is covered with many metal layers, and the PMMA-Gr micro sheets are transferred to the remaining InGaN by rapid thermal annealing for 30 s at 750–800 °C. The schematic structural of Gr/InGaN heterostructure for PDs is followed in Fig. 18.

The photoresponsivity of PDs (R) is determined by dividing the photocurrent by the incident optical power, as shown in Eq. (11) [4, 39].

$$R = \frac{\Delta I}{P_{\text{diff}} \cdot S_d} \quad (11)$$

where  $\Delta I = I_{\text{ph}} - I_{\text{dark}}$  the measured output current,  $I_{\text{ph}}$ , and  $I_{\text{dark}}$  denotes the photo and the dark currents, respectively,  $P_{\text{diff}}$  represent the diffraction-limited beam of power is given by Eq. (12), and  $S_d$  is the in-plane surface of the device (nm).

$$P_{\text{diff}} = \frac{S_d}{S_F} P_{\text{in}} \quad (12)$$

where the  $S_d/S_F$  ratio is calculated by  $\omega_{0,x}$ ,  $\omega_{0,y}$  the spot size is controlled by the linear photoresponse in laser power and the measured photocurrent of the imaging device in X- and Y-direction (13).

$$S_d = \pi_i \omega_{0,\text{diff}}^2 = \frac{\lambda^2}{T} \quad (13)$$

where  $\lambda$  is the terahertz laser wavelength in nm. As shown in Figs. 19 and 20, the responding speed at 400 nm wavelength when the fast response of integrated

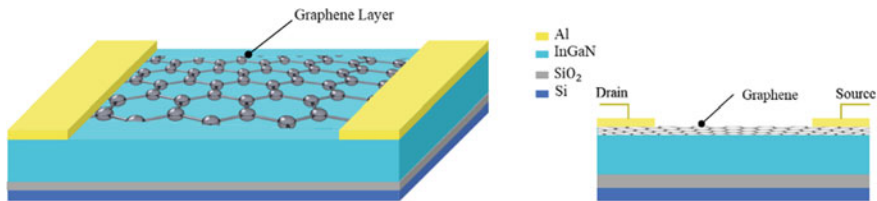


**Fig. 18** The Gr-InGaN heterostructure and the optical microscope image of PDs

graphene/InGaN NRAs/Gr Gr-Semiconductor-based PDs have been discovered, the rise ( $\tau_r$ )/fall times ( $\tau_f$ ) is observed to have a positive bias.

Another efficiency metric is the detectivity ( $D$ ) of the PDs, which shows how much of the minimal signal can be detected. It is calculated using the following equation [40, 41]:

$$D = R \times \sqrt{\frac{S}{2qI_{\text{dark}}}} \quad (14)$$

where  $S$  is the junction of the plane interface and  $q$  is the electron elementary charge of  $1.602 \times 10^{-19}$  Coulombs. The photoresponsivity peak is moved to lower wavelengths, and the metal–semiconductor–meta-PDs have the detectivity of  $1.6 \times 10^{11} - 3.9 \times 10^{12} \text{ cmHz}^{\frac{1}{2}}\text{W}^{-1}$  with the different metal mole fractions. The noise-equivalent optical power (NEP) defines the sensitivity of the photodetection. It is calculated as:

$$\text{NEP} = \frac{I_{\text{noise}}}{R} = \frac{\sqrt{S}}{D} \quad (15)$$

where the noise spectral density is given by:

$$I_{\text{noise}} = \sqrt{\frac{4K_B T}{R_P}} \quad (16)$$

$T = 300 \text{ K}$  is the standard temperature of PDs,  $K_B$  denotes the Boltzmann constant, and  $R_P$  is the PD resistance. The external quantum efficiency (EQE) is widely considered as one of the important parameters to determine the photodetection

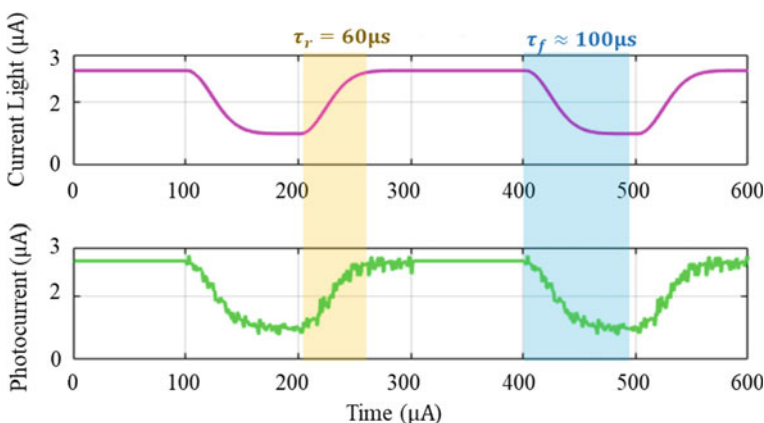
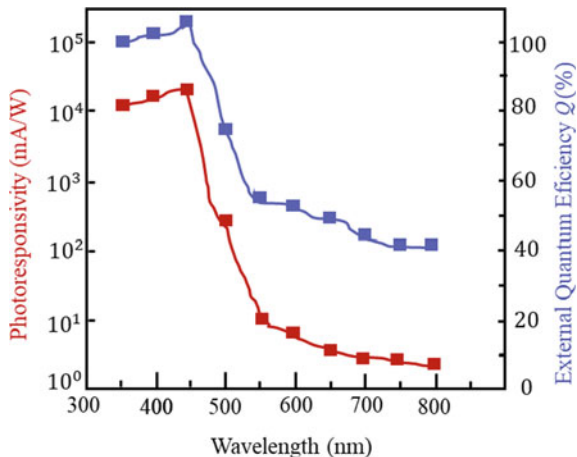


**Fig. 19** Time-seated photocurrent response of integrating Gr/InGaN NRAs/Gr Gr-Semiconductor Schottky junction visible PDs under 10 kHz shaped visible light at a positive bias voltage

**Fig. 20** Photon-response spectra of the photoresponsivity and external quantum efficiency of the device as the illumination of visible light near the UV range (350–500 nm) at a positive bias



efficiency and optoelectronic conversion performance of the device [40]. The EQE can be calculated using Eq. (17) as follows:

$$Q_E = \frac{h\nu}{e} R \quad (17)$$

where  $h\nu$  is the electron–volt energy of the excitation. The EQE spectral response as curve for the device is measured in the wavelength range from  $\sim 370$  to 500 nm at a bias voltage of  $V_b > 0$  in the VL band as shown in Fig. 20.

The responsiveness of many InGaN-based PDs is shown in Table 1. The improved photoresponsivity and significant rise/fall time demonstrate graphene integration on InGaN.

Table 1 contains an overview of the key parameters acquired in this analysis. The graphene integration work involves the first demonstration of a VLC network with record high modulation bandwidth exploiting Gr-InGaN-based PDs as the receiver. Secondly, in comparison with previous results, the graphene sensor was operated at short rising and falling periods for high-speed modulation optimized further to minimize carrier lifetime for high speed ( $\sim 1 \mu s$ ). The PD array device configurations can also be investigated to increase the bandwidth and photoresponsivity of Gr-InGaN-based PDs for varied bias voltage levels. Aside from device optimization, the orthogonal frequency division-multiplexing (OFDM) or the orthogonal time frequency space modulation (OTFS)-based VLC-link system may be enhanced further by applying pre-equalization [46] or bit/power packing approaches.

In Fig. 21, the high response rate in VLC where the maximal generated photocurrent reaches the milliampere (mA) near when the wavelength is  $\sim 700$  nm, the efficient response rate is as much as photoresponsivity allow  $\sim 10$  A/W, the detectivity is  $\approx 1.3 \times 10^{11}$ , and the maximal photoconductivity gain is of 30 using the Eq. (19). Because high graphene mobility allows for high-speed operation, the metal-graphene-metal (MGrM) structure-based PDs is regularly used. However, this limits

**Table 1** Progress in research on the performance of InGaN-based LDs in visible light onto the (370–800 nm) wavelength band

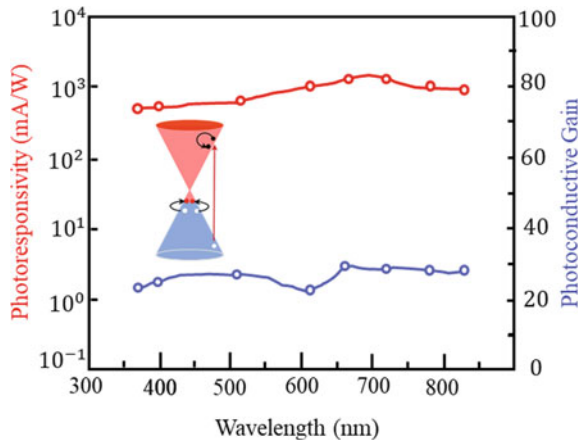
PD heterojunction	Photoresponsivity ( $R$ )	Rise/fall time ( $\tau_r/\tau_f$ )	Bandwidth $B_w$ (3 dB)	Refs.
Gr-InGaN	1.39 A/W	60/200 $\mu s$	–	[38]
InGaN/GaN (MQW)	70.7 mA/W	2.13/1.70 ns	71.5 MHz	[42]
InGaN/GaN (PIN)	0.31 A/W	22/23.7 ns	41.2 MHz (–3 dB)	[43]
InGaN/Si (PIN)	94.2 mA/W	20/33 ms	13.56 MHz	[44]
InGaN/GaN (MQW Semipolar)	191 mA/W	–	347 MHz	[45]
Gr-Au/SiO <sub>2</sub> /Si (MGrM)	0.6 A/W	–	1 GHz	[46]
Gr-Sic (PIN-MOS)	254.1 A/W	–	–	[47]

the responsiveness at lower bias voltages, and in the elimination of photoconductive gain  $G$ , the dark current  $I_{\text{dark}}$  is relatively low.

Notably, the graphene mobility  $\mu_n$  could be used to estimate the optical absorption in graphene and the electron lifetime  $\tau_{\text{lifetime}}$  of the graphene in PDs by using  $G$  calculated from the following equation:

$$G = \frac{\tau_{\text{lifetime}}}{\tau_{\text{transit}}} = \frac{\tau_{\text{lifetime}} \times \mu_n V_{\text{DS}}}{L^2} \tag{19}$$

**Fig. 21** Photoresponsivity density and photoconductive gain versus the nano-wavelength of PDs with the optical interband transitions



where  $L$  is the channel length,  $V_{DS}$  is the source-drain voltage of  $10 \mu m$  and  $2 V$ , respectively, the mobility is  $1298.4 \text{ cm}^2\text{V}^{-1}\text{s}^{-1}$ , and then the photoconductive gain is  $304.7$  [48]. The long lifetime of the graphene contributed to the high gain. In addition, the linear dynamic range (LDR) is a critical factor to achieve the high photoelectric performance that is measured in the Gr-heterojunction-based PDs, where the LDR of PDs can be expressed by Eq. (20):

$$\text{LDR} = 20\log_{10}\left(\frac{P_{LC}}{P_{low}}\right) \tag{20}$$

where  $P_{LC}$  is the light current intensity at which the current density starts to distort the linear area (i.e., the photon current) and  $P_{low}$  is the low light intensity measured in relation to the PD's dark current. At the maximum light current intensity, the LDR for InGaN/GaN-based PDs could exceed  $64.41 \text{ dB}$  [44], whereas the linear dynamic range for InGaN, M-Gr/InGaN, and T-Gr/InGaN-based PDs equal to  $8.81$ ,  $5.3$ , and  $19.5 \text{ dB}$ , respectively. Hence, the T-Gr/InGaN considered the best candidate to LDR improved in InGaN-based photodetectors compared to M-Gr/InGaN, the InGaN, and InGaN/GaN with the encouraged photoresponsivity in short rise/fall time belong. Considering the evolution of photoresponsivity values and its relationship between the bandwidth  $B_w$  using Gr-heterostructure-based PDs, we summarize the result research as shown in Fig. 22.

Although the fact that graphene-based hybrid devices are better standard PDs regarding performance, they are not yet utilized in large-scale commercial applications. In [49], the Gr/InGaN NR arrays/Gr structure is demonstrated to use the M-Gr and T-Gr layers growth on *Si* with the photoresponsivity of PDs and the rise/fall time as a critical parameter. This integration of 2D materials-based PDs at the beginning of the visible light spectrum  $\lambda \approx 380 \text{ nm}$ .

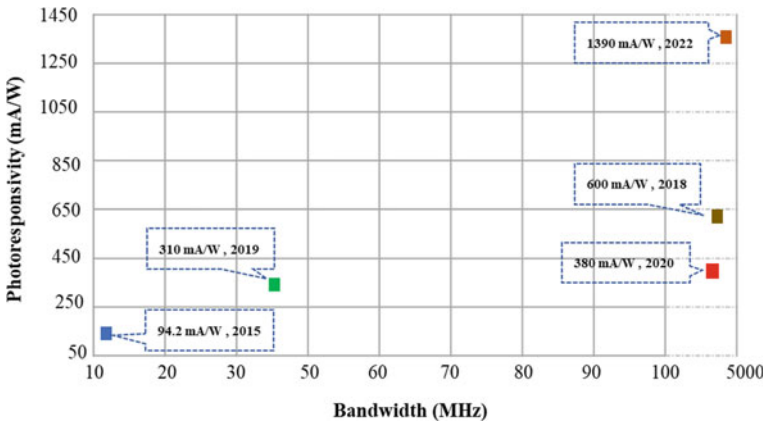


**Fig. 22** Benchmark comparison of previous photoresponsivity versus bandwidth for graphene-based photodetectors at 3 dB in the last five years applied in the visible light band

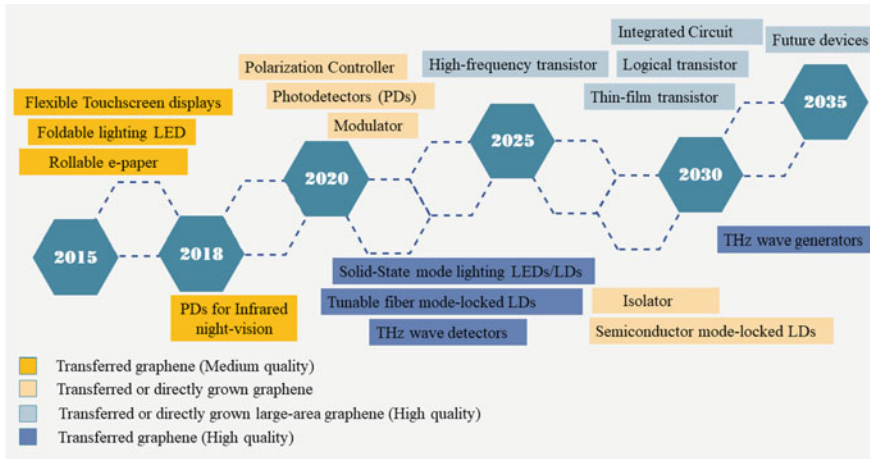


**Fig. 23** Over the next 20 years, graphene applications and research are expected to show promise in electronic, photonic, optical, and interconnect devices. This will provide a good indicator of when a practical device prototype will be available. For each kind of application, the graphene's properties and production techniques are shown [50]

Therefore, developing novel materials in multilayers with appropriate band gaps and efficient light absorption rests challenging. Figure 23 illustrates the rapid evolution of the graphene application in optoelectronic devices and emerging technology of semiconductor LEDs, the LDs as transmitter optical-electrical end, and PDs as receiver end for VLC applications in future wireless communication networks. The graphene detector's bandwidth can exceed 40 GHz without attenuation and in future can be increased to 500 GHz.

Further graphene advancements and research are essential to achieving the potential smart uses of Gr-based optoelectronics devices such as LEDs, LDs, and PDs in the next 20 years for UV–Visible light to THz band in the next generation.

## 4 Conclusion

In this chapter, we have introduced graphene photonics properties, followed by presenting several graphene nanostructures for optoelectronic and photonic applications. The great potential of graphene 2D materials is a best candidate to integrate in optoelectronic devices such as GaN-based LEDs and InGaN-based PDs in visible light communication systems; this integration can improve the high-speed response of LEDs and increase the bandwidth modulation. This research work demonstrates the better photoresponsivity and detectivity of Gr-InGaN heterojunction of PDs in visible light band of  $\sim 10$  A/W and  $\sim 10^{12}$ , respectively, with short rise/fall time for VLC devices. The contribution of high time of the graphene channel increases

the photoconductive gain. The ability to successfully integrate graphene directly into devices and ongoing achievements could not just enhance electronic, photonic, and/or optical qualities, but they also allow for the implementation of a large range of smart applications. More functionalities are expected to emerge, such as energy efficiency of the VLC channel, and to develop the nanodevices with the InGaN or GaN/Gr 2D materials using Schottky junction. This work can provide a detailed knowledge to implement high-speed LED/PD heterojunction for the smart application in VLC systems.

## References

1. Wang, J.L., Fang, H.H., Wang, X.D., Chen, X.S., Lu, W., Hu, W.D.: Recent progress on localized field enhanced two-dimensional material photodetectors from ultraviolet—visible to infrared. *Small* **13**, 894 (2017)
2. Bonaccorso, F., Sun, Z., Hasan, T., Ferrari, A.C.: Graphene photonics and optoelectronics. *Nat. Photonics* **4**, 611 (2010)
3. Porambage, P., Gür, G., Osorio, D.P.M., Liyanage, M., Gurtov, A., Ylianttila, M.: The roadmap to 6G security and privacy. *IEEE Open J. Commun. Soc.* **2**, 1094–1122 (2021). <https://doi.org/10.1109/OJCOMS.2021.3078081>
4. El Jbari, M., Moussaoui, M., Chahboun, N.: A review on visible light communication system for 5G. In: *International Conference on Advanced Technologies for Humanity*. Springer, Cham (2021). [https://doi.org/10.1007/978-3-030-94188-8\\_9](https://doi.org/10.1007/978-3-030-94188-8_9)
5. Zhang, Y., Wang, L., Wang, K., Wong, K.S., Wu, K.: Recent advances in the hardware of visible light communication. *IEEE Access* **7**, 91093–91104 (2019)
6. Chi, N., Zhou, Y., Wei, Y., Hu, F.: Visible light communication in 6G: advances, challenges, and prospects. *IEEE Veh. Technol. Mag.* **15**(4), 93–102 (2020)
7. Li, B., Zhang, Z., Zhang, X., Wang, H., Wang, H., Wu, Z., Wang, G., Jiang, H.: InGaN-based MSM visible light photodiodes with recessed anode. *IEEE Photonics Technol. Lett.* **31**(17), 1469–1472 (2019)
8. Gao, X., Yuan, J., Yang, Y., Li, Y., Yuan, W., Zhu, G., Zhu, H., Feng, M., Sun, Q., Liu, Y., Wang, Y.: A 30 mbps in-plane full-duplex light communication using a monolithic GaN photonic circuit. *Semicond. Sci. Technol.* **32**(7), 075002 (2017)
9. Sun, H., Tian, W., Cao, F., Xiong, J., Li, L.: Ultrahigh-performance self-powered flexible double-twisted fibrous broadband perovskite photodetector. *Adv. Mater.* **30**, 1706986 (2018)
10. Liu, Y., Xu, Y., Cao, B., Li, Z., Zhao, E., Yang, S., Wang, C., Wang, J., Xu, K.: Transferable GaN films on graphene/SiC by van der Waals epitaxy for flexible devices. *Phys. Status Solidi* **216**, 1801027 (2019)
11. Kong, W.Y., Wu, G.A., Wang, K.Y., Zhang, T.F., Zou, Y.F., Wang, D.D., Luo, L.B.: Graphene-beta-Ga<sub>2</sub>O<sub>3</sub> heterojunction for highly sensitive deep UV photodetector application. *Adv. Mater.* **28**(48), 10725–10731 (2016)
12. Gao, S., Wang, Z., Wang, H., Meng, F.: Graphene/MoS<sub>2</sub>/graphene vertical heterostructure-based broadband photodetector with high performance. *Adv. Mater. Interfaces* **8**, 2001730 (2020)
13. Chen, Z., Chang, H., Cheng, T., Wei, T., Wang, R., Yang, S., Dou, Z., Liu, B., Zhang, S., Xie, Y., et al.: Direct growth of nanopatterned graphene on sapphire and its application in light emitting diodes. *Adv. Funct. Mater.* **30**, 2001483 (2020)
14. Song, W., Ren, F., Wang, Y., Yin, Y., Zhang, S., Shi, B., Feng, T., Wang, J., Liang, M., Zhang, Y., Wei, T., Yan, J., Wang, J., Li, J., Yi, X., Liu, Z.: GaN-based LEDs grown on graphene-covered SiO<sub>2</sub>/Si (100) substrate. *Curr. Comput.-Aided Drug Des.* **10**, 787 (2020). <https://doi.org/10.3390/cryst10090787>



15. Chai, J., Kong, D., Chen, S., Chen, L., Wang, W., Li, G.: High responsivity and high speed InGaN-based blue-light photodetectors on Si substrates. *RSC Adv.* **11**(40), 25079–25083 (2021)
16. Singh, A.K., Ahn, K., Yoo, D., et al.: van der Waals integration of GaN light-emitting diode arrays on foreign graphene films using semiconductor/graphene heterostructures. *NPG Asia Mater.* **14**, 57 (2022). <https://doi.org/10.1038/s41427-022-00403-6>
17. Geim, A.K., Novoselov, K.S.: The rise of graphene. *Nat. Mater.* **6**, 183–191 (2007)
18. Castro Neto, A.H., Guinea, F., Peres, N.M.R., Novoselov, K.S., Geim, A.K.: The electronic properties of graphene. *Rev. Mod. Phys.* **81**, 109–162 (2009)
19. Liu, M., Yin, X., Ulin-Avila, E., Geng, B., Zentgraf, T., Ju, L., Wang, F., Zhang, X.: A graphene-based broadband optical modulator. *Nature* **474**, 64 (2011)
20. Sun, Z., Zheng, Y., Fu, Y.: Graphene-based spatial light modulator using metal hot spots. *Materials* **12**, 3082 (2019). <https://doi.org/10.3390/ma12193082>
21. Yusoff, A.R.b.M.: Graphene Optoelectronics Synthesis, Characterization, Properties, and Applications. Weinheim, Bergstr Wiley-VCH (2014)
22. Gusynin, V., Sharapov, S., Carbotte, J.: Unusual microwave response of Dirac quasiparticles in graphene. *Phys. Rev. Lett.* **96**, 256–802 (2006)
23. Gusynin, V., Sharapov, S.: Transport of Dirac quasiparticles in graphene: hall and optical conductivities. *Phys. Rev. B* **73**, 245–411 (2006)
24. Banerjee, P.P.: Nonlinear Optics: Theory, Numerical Modeling, and Applications. CRC Press (2003)
25. Ishikawa, K.L.: Nonlinear optical response of graphene in time domain. *Phys. Rev. B* **82**, 201402 (2010)
26. Zhang, H., Virally, S., Bao, Q., Kian Ping, L., Massar, S., Godbout, N., Kockaert, P.: Z-scan measurement of the nonlinear refractive index of graphene. *Opt. Lett.* **37**, 1856–1858 (2012)
27. Bao, Q., Zhang, H., Wang, Y., Ni, Z., Yan, Y., Shen, Z.X., Loh, K.P., Tang, D.Y.: Atomic-layer graphene as a saturable absorber for ultrafast pulsed lasers. *Adv. Funct. Mat.* **19**, 3077–3083 (2009)
28. Wang, Y., Dheeraj, D., Liu, Z., Liang, M., Li, Y., Yi, X., Wang, J., Li, J., Weman, H.: AlGaIn nanowires grown on SiO<sub>2</sub>/Si (100) using graphene as a buffer layer. *Cryst. Growth Des.* **19**(10), 5516–5522 (2019)
29. Hao, Z., Feng, S., Lu, Y., Lin, S.: Gate tunable surface plasmon resonance enhanced graphene/Ag nanoparticles-polymethyl methacrylate/graphene/p-GaN heterostructure light-emitting diodes. *Opt. Express* **26**(19), 25257–25264 (2018)
30. Hidouri, T., Nasr, S.: Graphene induced weak carrier localization in InGaN nanorods directly grown on graphene-covered Si. *Diam. Relat. Mater.* (2020). <https://doi.org/10.1016/j.diamond.2020.107841>
31. Huang, Y., Huang, Z., Zhong, Z., et al.: Highly transparent light emitting diodes on graphene encapsulated Cu nanowires network. *Sci. Rep.* **8**, 13721 (2018). <https://doi.org/10.1038/s41598-018-31903-7>
32. El Jbari, M., Moussaoui, M.: Efficient nM-PAWM hybrid modulation scheme for high data transmission in visible light communication system. *e-Prime-Adv. Electr. Eng. Electron. Energy* **2**, 100061 (2022). <https://doi.org/10.1016/j.prime.2022.100061>
33. Luo, S., Wang, Y., Tong, X., Wang, Z.: Graphene-based optical modulators. *Nanoscale Res. Lett.* **10**(1), 1–11 (2015)
34. Gan, X., Englund, D., Van Thourhout, D., Zhao, J.: 2D materials-enabled optical modulators: from visible to terahertz spectral range. *Appl. Phys. Rev.* **9**(2), 021302 (2022)
35. Sun, M., Xu, X., Sun, X. W., Liang, X.A., Valuckas, V., Zheng, Y., Paniagua-Domínguez, R., Kuznetsov, A.I.: Efficient visible light modulation based on electrically tunable all dielectric metasurfaces embedded in thin-layer nematic liquid crystals. *Sci. Rep.* **9**(1), 1–9 (2019)
36. Zhong, C., Li, J., Lin, H.: Graphene-based all-optical modulators. *Front. Optoelectron.* **13**(2), 114–128 (2020)
37. Hao, R., Ye, Z., Peng, X., Gu, Y., Jiao, J., Zhu, H., Sha, W.E.I., Li, E.: Highly efficient graphene-based optical modulator with edge plasmonic effect. *IEEE Photonics J.* **10**(3), 1–7 (2018)

38. Chai, J., Chen, L., Cao, B., Kong, D., Chen, S., Lin, T., Wang, W., Liu, Y., Li, G.: High-speed graphene/InGaN heterojunction photodetectors for potential application in visible light communication. *Opt. Express* **30**(3), 3903–3912 (2022)
39. Ravikiran, L., Radhakrishnan, K., Dharmarasu, N., Agrawal, M., Wang, Z., Bruno, A., Soci, C., Lihuang, T., Ang, K.S.: GaN schottky metal–semiconductor–metal UV photodetectors on Si (111) grown by ammonia-MBE. *IEEE Sens. J.* **17**, 72–77 (2017)
40. Xu, K., Xu, C., Xie, Y., Deng, J., Zhu, Y., Guo, W., Xun, M., Teo, K.B.K., Chen, H., Sun, J.: Graphene GaN-based schottky ultraviolet detectors. *IEEE Trans. Electron. Devices* **62**, 2802–2808 (2015)
41. Journot, T., Bouchiat, V., Gayral, B., Dijon, J., Hyot, B.: Self assembled UV photodetector made by direct epitaxial GaN growth on graphene. *ACS Appl. Mater. Interfaces* **10**, 18857–18862 (2018)
42. Ho, K.-T., Chen, R., Liu, G., Shen, C., Holguin-Lerma, J., Al-Saggaf, A.A., Ng, T.K., Alouini, M.-S., He, J.-H., Ooi, B.S.: 3.2 Gigabit-per-second visible light communication link with InGaN/GaN MQW micro-photodetector. *Opt. Express* **26**, 3037–3045 (2018)
43. Liu, X., Lin, R., Chen, H., Zhang, S., Qian, Z., Zhou, G., Chen, X., Zhou, X., Zheng, L., Liu, R., Tian, P.: High-bandwidth InGaN self-powered detector arrays toward MIMO visible light communication based on micro-LED arrays. *ACS Photonics* **6**(12), 3186–3195 (2019). <https://doi.org/10.1021/acsp Photonics.9b00799>
44. Chandan, G., Mukundan, S., Mohan, L., Roul, B., Krupanidhi, S.B.: Trap modulated photore-sponse of InGaN/Si isotype heterojunction at zero-bias. *J. Appl. Phys.* **118**(2), 024503 (2015)
45. Kang, C.H., Liu, G., Lee, C., Alkhazragi, O., Wagstaff, J.M., Li, K.H., Alhawaj, F., Ng, T., Speck, J., Nakamura, S., Denbaars, S., Ooi, B.S.: Semipolar (20 $\bar{1}$ ) InGaN/GaN micro-photodetector for gigabit-per-second visible light communication. *Appl. Phys. Express* **13**(1), 014001 (2019)
46. Cakmakyapan, S., Lu, P.K., Navabi, A., et al.: Gold-patched graphene nano-strips for high-responsivity and ultrafast photodetection from the visible to infrared regime. *Light Sci. Appl.* **7**, 20 (2018). <https://doi.org/10.1038/s41377-018-0020-2>
47. Li, Y., Chen, P., Chen, X., Xu, R., Liu, M., Zhou, J., Ge, C., Peng, H., Mao, X., Feng, J., Hu, X., Peng, Y., Xu, X., Xie, Z., Xiu, X., Chen, D., Liu, B., Han, P., Shi, Y., Zhang, R., Zheng, Y.: High-responsivity graphene/4H-SiC ultraviolet photodetector based on a planar junction formed by the dual modulation of electric and light fields. *Adv. Opt. Mater.* **8**(19), 2000559 (2020)
48. Chen, C., Zhong, W.D., Wu, D.: Indoor OFDM visible light communications employing adaptive digital prefrequency domain equalization. In: 2016 Conference on Lasers and Electro-Optics, pp. 1–2 (2016)
49. Zheng, Y., et al.: Self-integrated hybrid ultraviolet photodetectors based on the vertically aligned InGaN nanorod array assembly on graphene. *ACS Appl. Mater. Interfaces* **11**(14), 13589–13597 (2019)
50. Novoselov, K.S., Fal, V., Colombo, L., Gellert, P., Schwab, M., Kim, K.: A roadmap for graphene. *Nature* **490**, 192–200 (2012)

# Variants of Graphene Nanoribbon (GNR) Interconnects for THz Applications



S. Kanthamani

**Abstract** As a potential future candidate material for both transistors and interconnect, graphene nanoribbons (GNRs) have been suggested. Single-layer GNR (SLGNR) interconnect has favored compact physics-based circuit model, since GNRs possess low resistivity than Cu and carbon nanotube (CNT). The intrinsic resistance of SLGNR is considered to be high so that multi-layer graphene nanoribbon (MGLNR) interconnect has been proposed. Equivalent lumped modeling was used to study the performance attributes of MLGNR interconnects. In this chapter, the radio frequency (RF) performances of SLGNR and MLGNR interconnects are studied using proposed equivalent circuit model. The performance characteristics of SLGNR and MLGNR interconnects are compared for 21 and 13.4 nm technology nodes with Agilent Advanced Design System (ADS). ADS simulation shows a return loss ( $S_{11}$ ) of  $-50.966$  dB and transmission loss ( $S_{12}$ ) of  $-0.203$  dB for SLGNR, and for MLGNR, return loss is about  $-89.69$  dB at a frequency of 1THz. From the return loss, the power loss calculated is very less, and the result shows that the MLGNR interconnect performs well beyond the THz frequency range which will be suitable as an interconnect for RF applications.

**Keywords** Metallic CNT · Graphene nanoribbon · Radio frequency · Electromagnetic simulation · Lumped model

## 1 Introduction

Nanotechnology is considered to be a versatile area of science that has the power of evoking interest in the study of structures at nanoscopic dimensions. Circuits approaching 10 nm length scale have led to the budding research related to electronic properties of nano-scale devices [1]. For developing miniaturized RF components, copper (Cu) is considered as a base material for a longer period [2]. In a

---

S. Kanthamani (✉)

Electronics and Communication Engineering Department, Thiagarajar College of Engineering, Madurai, India

e-mail: [skmece@tce.edu](mailto:skmece@tce.edu)

nanometer system, interconnects formulated using Cu have grain boundary scattering and surface roughness problems [3]. Carbon nanotubes (CNTs) are well known in the field of interconnects, because of high mechanical and thermal stability, high thermal conductivity and large current-carrying capacity [4, 5].

CNTs which are molecular-scale tubes made up of graphitic carbon with excellent properties are considered as a class of nanotube/nanowire [5]. CNTs can be either single walled or multi-walled. Depending on the direction in which CNTs are rolled up, they demonstrate either metallic or semiconducting properties [6]. Single-walled carbon nanotubes (SWCNTs) as well as multi-walled carbon nanotubes (MWCNTs) are being inquired for performance and scalability. Metallic carbon nanotubes are identified as a possible interconnect material and could be the inheritor to Al and Cu interconnects [7]. In MWCNTs, it is difficult to achieve ballistic movement over long lengths [6], whereas in SWCNTs, electron mean free path is in the order of micron and could be suitable for interconnect designs. The possible use of CNTs as interconnects and their equivalent circuit modeling and performance comparison in terms of switching delay have been recently proposed [6–8]

In CNTs, there exists impedance mismatch problem and crosstalk because of EMC/EMI evaluation. Hence, graphene nanoribbon (GNR) was proposed as a hopeful interconnect material. GNRs are arranged in classes as single-layer GNR (SLGNR) and multi-layer GNR (MLGNR). The SLGNR has been modeled as interconnect using compact physics-based circuit model [9]. Conventional lithography process makes SLGNR for building up horizontal interconnects than Cu and CNT. To overcome the high intrinsic resistance issues present in SLGNR, MLGNR interconnect has been put forward in [10] to intensify the action of interconnection. MLGNR interconnects [11] using equivalent lumped element modeling is characterized, and performance was compared with Cu and CNT interconnects.

This chapter discusses modeling the CNT using equivalent lumped elements such as distributed kinetic and magnetic inductances along with distributed quantum capacitance and electrostatic capacitances. This chapter also discusses the modeling of graphene nanoribbon using single layer and multi-layer to determine the RF performance of the graphene nanoribbon. The model is simulated using electromagnetic simulator Agilent's ADS1.1C with the effective equivalent circuit model proposed by Burke [8]. The radio frequency performance and simulation results are discussed with respect to power loss and the interconnect operation.

## 2 Equivalent Circuit Models

### 2.1 Equivalent Circuit Model for a Single SWCNT

Single CNT as can be seen in Fig. 1a along with the lumped equivalent circuit model as in Fig. 1b [8] describes the interconnect behavior as proposed in [9]. The equivalent circuit has magnetic inductance ( $L_{\text{magnetic}}$ ), kinetic inductance ( $L_{\text{Kinetic}}$ ), electrostatic

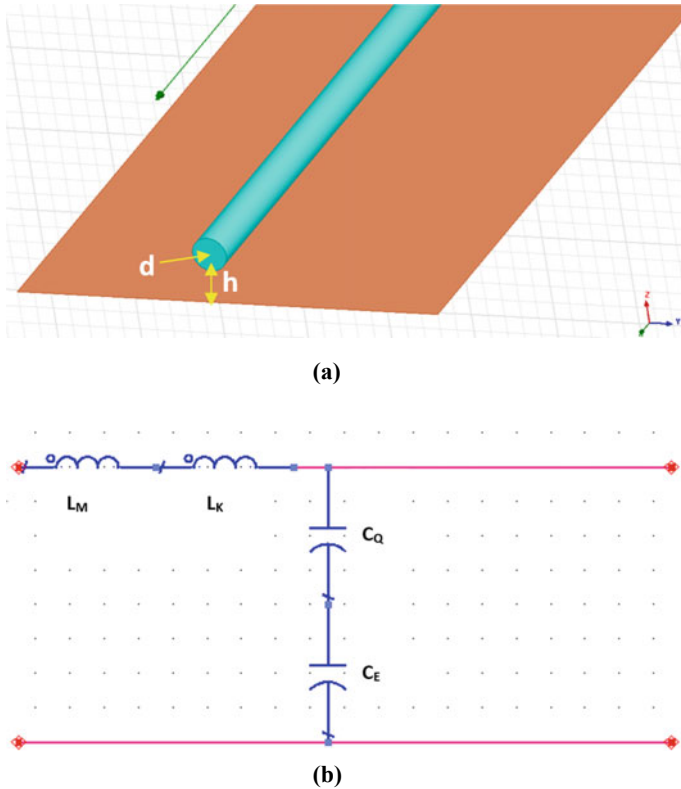


**Fig. 1** **a** Single CNT geometry. **b** Equivalent circuit model for a CNT

capacitance ( $C_E$ ) and quantum capacitance ( $C_Q$ ). The influence of each parameter and the formulas to calculate are present in [9]

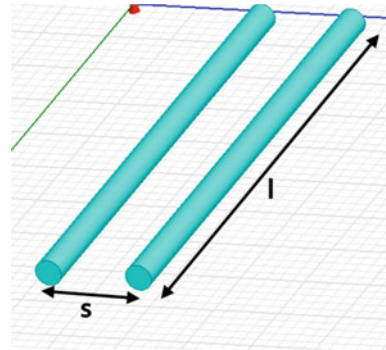
### 2.2 Equivalent Circuit for Single-Walled CNTs in Parallel

CNTs arranged in parallel, as in Fig. 2a, have an impact on the coupling capacitance between two CNTs in addition to kinetic inductance, quantum and electrostatic capacitance [1].

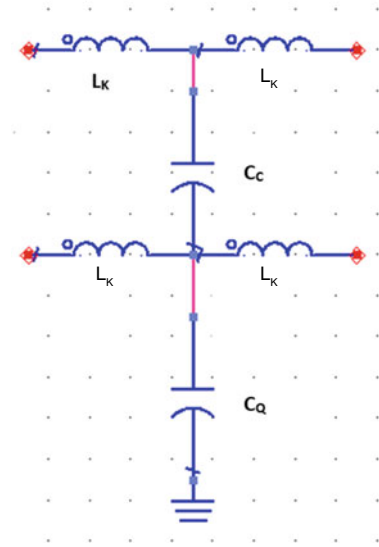
### 2.3 Graphene Nanoribbon

Carbon atoms are arranged in a honeycomb lattice to form the single atomic layer of graphene, which is a flat, two-dimensional (2D) sheet. Excellent electrical and

**Fig. 2** **a** Arrangement of CNTs in parallel. **b** Equivalent lumped model



(a)



(b)

thermal properties of graphene are comparable to those of CNT. It has been proposed that GNRs could take the place of conventional Cu-based interconnect systems [12]. The physics-based circuit model for GNR interconnect is proposed and characterized in [13–16]. Considering as a candidate for future interconnection, it requires to investigate the performance of high frequency performance of GNR. In this section using circuit models, the radio frequency performances such as return loss and transmission loss are studied. The performance comparison of SLGNR and MLGNR is done in ADS. Figures 3a and b show the geometries of single- and  $N$ -layer GNR interconnects along with RLC equivalent circuit model. The per unit-length resistance ( $R$ ), kinetic inductance ( $l_K$ ), magnetic inductance ( $L_m$ ), quantum capacitance ( $C_q$ ) and electrostatic capacitances ( $C_e$ ) are calculated by using formulas available in [9].

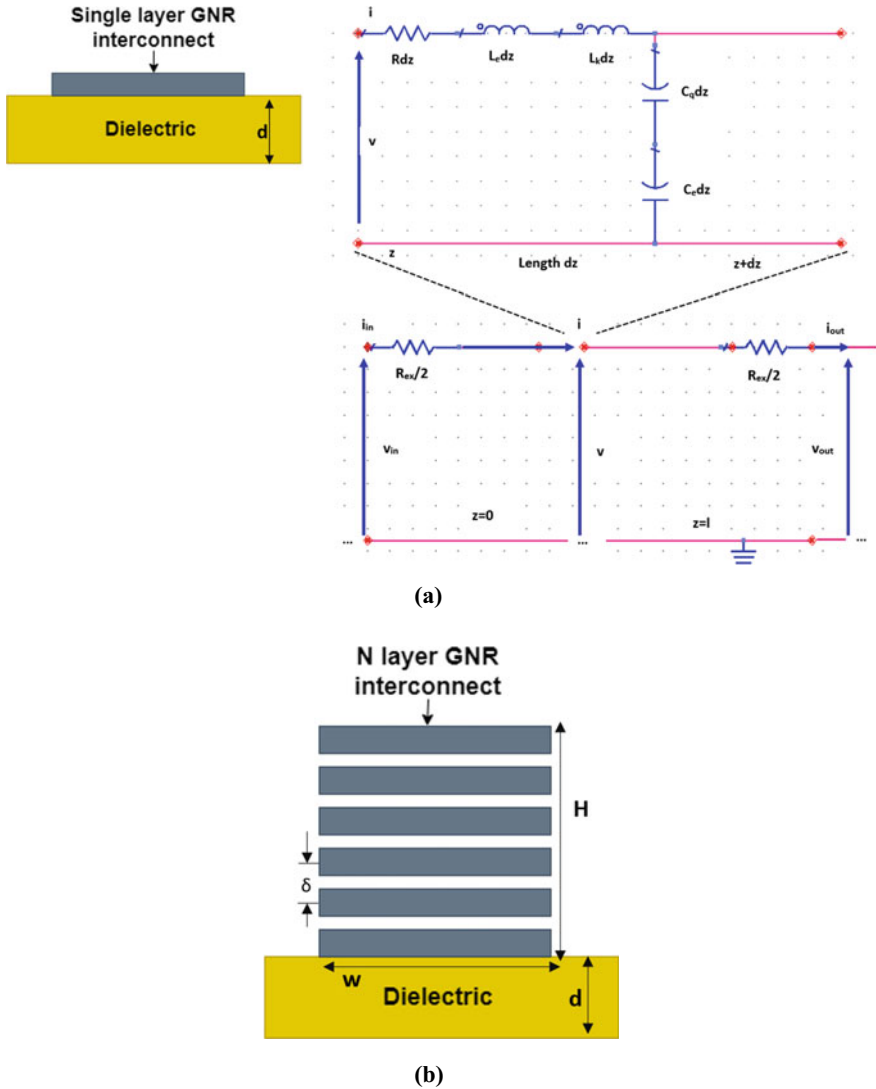


Fig. 3 a Single-layer GNR. b N-layer GNR

### 3 Radio Frequency Performance

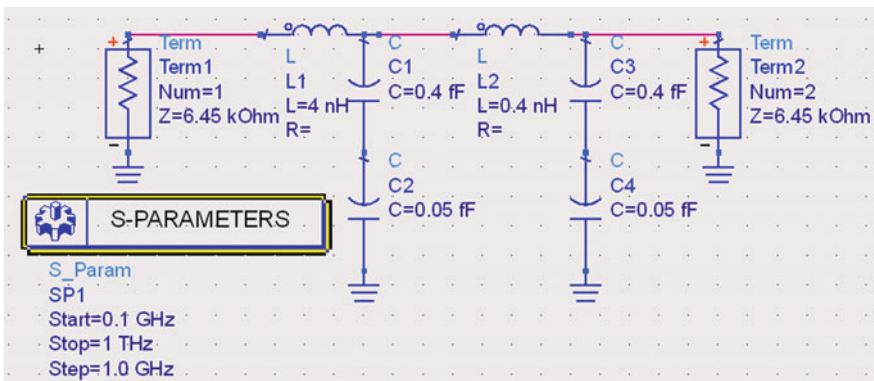
#### a. Single CNT interconnect

CNT-based interconnect modeled using L and C is simulated in Agilent ADS to understand the high frequency performance. To characterize as an interconnect, the equivalent capacitance and the inductances are calculated using the formulas [9].

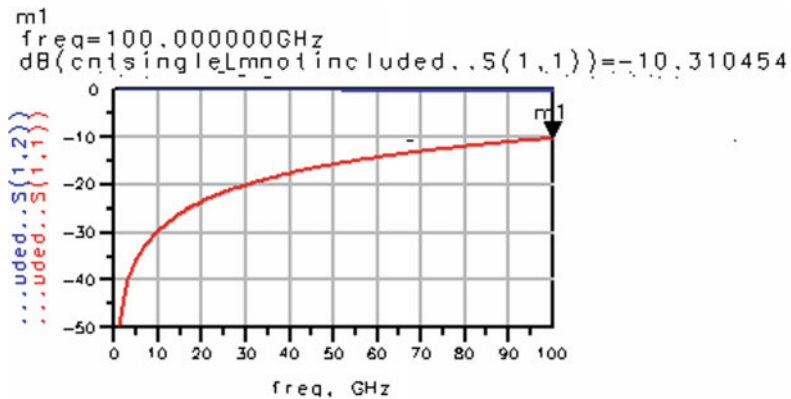
The values are  $L_K = 16 \text{ nH}/\mu\text{m}$ ,  $L_M = 1 \text{ pH}/\mu\text{m}$ ,  $C_C = 31 \text{ aF}/\mu\text{m}$ ,  $C_E = 50 \text{ aF}/\mu\text{m}$  and  $C_Q = 100 \text{ aF}/\mu\text{m}$  with the physical dimensions of the CNT as  $r = 1 \text{ nm}$   $l = 1 \mu\text{m}$ . Figure 4a shows the lumped circuit model of a single CNT used as an interconnect simulated in ADS. The outcome of the simulation gives a return loss ( $S_{11}$ ) of  $-10.310 \text{ dB}$  at a frequency of  $100 \text{ GHz}$  as shown in Fig. 4b, which proves the applicability of CNT for terahertz region. From the return loss curves, the calculated power lost in this case is about  $9.38\%$ .

**b. Parallel CNT interconnects:**

To reduce the losses in single CNT, CNTs are arranged in parallel to transmit a single signal. The schematic layout for four CNTs placed in parallel is demonstrated in Fig. 5a. A coupling capacitor  $C_c$  present in Fig. 5a shows the difference between



(a)



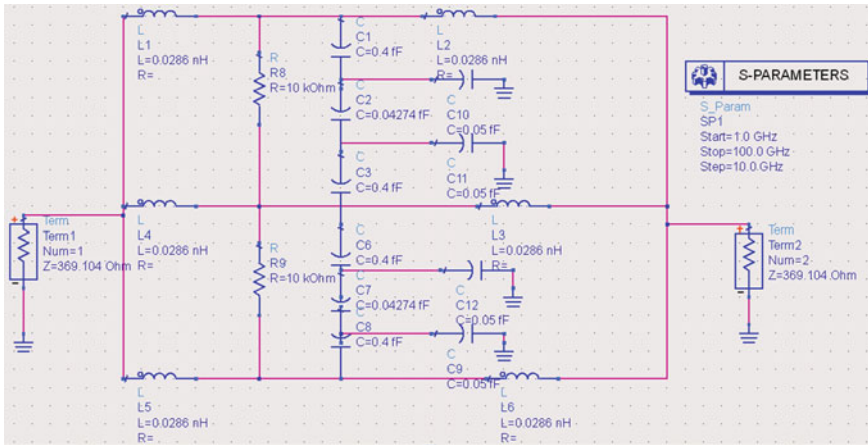
(b)

**Fig. 4 a** Effective equivalent model simulated using ADS. **b** EM simulated value of return loss ( $S_{11}$ ) and  $S_{21}$  of single CNT over the frequency range 1 to 100 GHz

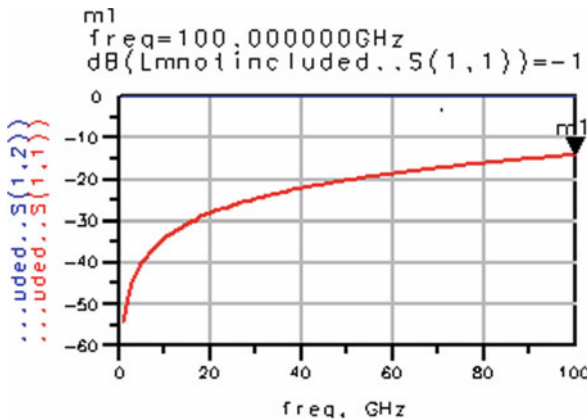


single and parallel CNTs. Figure 5b gives the corresponding scattering parameter variations obtained using ADS.

The simulation provides a return loss ( $S_{11}$ ) of  $-14.1245$  dB which means the amount of power lost is only 3.8%. The transmission loss is also negligible for the same configuration at a frequency of 100 GHz, with a length of CNT as  $10^{-6}$  m as Fig. 5b. Figure 6 shows the comparison of power lost between single and parallel CNTs and reveals that the power lost in parallel CNT is 6% less than the single CNT.



(a)



(b)

**Fig. 5** a Effective equivalent model for parallel CNTs simulated using ADS. b ADS simulated  $S_{11}$  and  $S_{12}$  of parallel CNTs over the frequency range 1–100 GHz

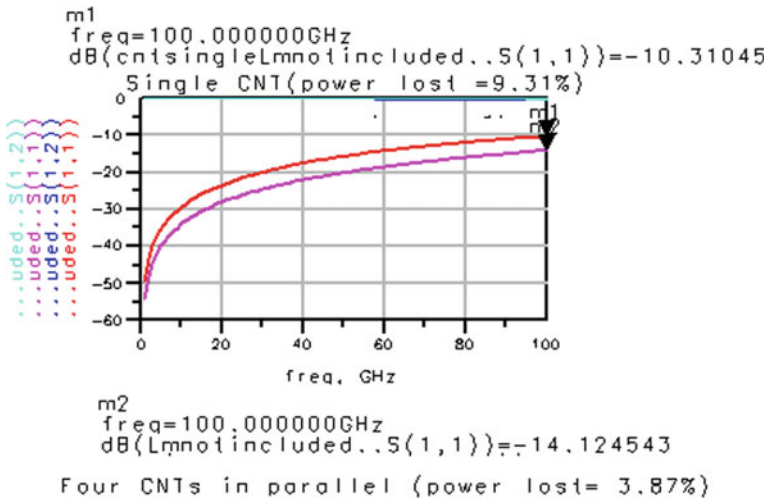


**Fig. 6** Performance comparison of  $S_{11}$  and  $S_{12}$  of single and parallel interconnects over the frequency range 1–100 GHz

Since  $C_c$  is a function of length of CNT as in Eq. (6), variation of coupling capacitor causing a corresponding change in scattering parameter has been plotted in Fig. 7.

**c. Single-Layer GNR and Multi-Layer GNR**

To study the radio frequency performance of SLG NR- and MLG NR-based interconnects, the ESC model shown in Fig. 3 is simulated using Agilent ADS. To characterize an interconnect, its p. u. l. parameters are calculated using the above formula with

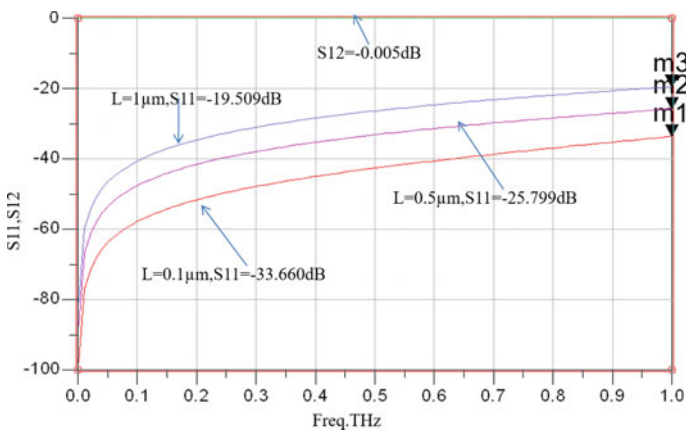


**Fig. 7** Comparison of return loss of the parallel CNT with respect to various lengths of nanotube

**Table 1** Performance comparison of GNR and MLGNR up to THz frequency for different technology nodes

		L- $\mu\text{m}$	21nm node S11-dB	13.4 nm node S11-dB
Multi-layer GNR	Intermediate level	0.1	-80.490	-68.237
		0.5	-66.514	-54.271
		1	-60.498	-48.268
	Global level	0.1	-89.690	-78.331
		0.5	-75.712	-63.995
		1	-69.693	-58.340
Single-layer GNR	Intermediate level	0.1	-46.888	-41.685
		0.5	-32.910	-27.713
		1	-26.896	-21.714
	Global level	0.1	-50.966	-45.283
		0.5	-36.999	-31.307
		1	-30.981	-25.296

physical dimensions  $L = 0.5\text{--}1\ \mu\text{m}$  and  $w = 24\text{--}36\ \text{nm}$  for 21 nm technology node and  $15\text{--}22.5\ \text{nm}$  for 13.4 nm technology node according to Table 1.

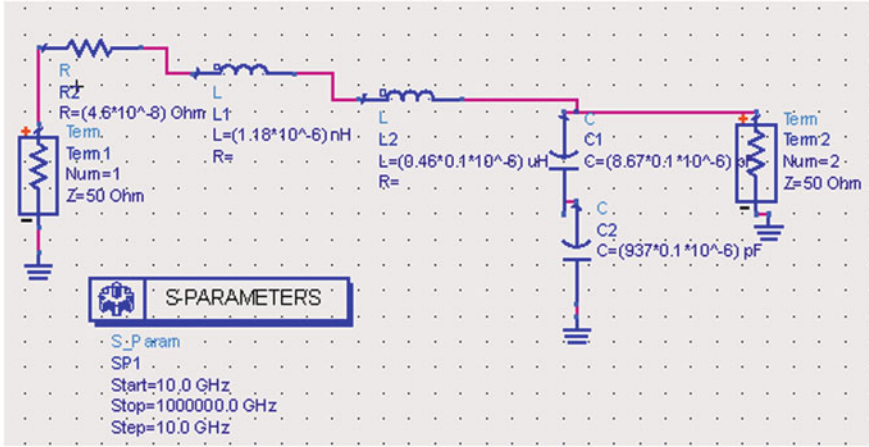
Figure 8a shows the equivalent model of single GNR simulated using ADS. Figure 8b shows the return loss and insertion loss for different lengths ranging from 0.1 to  $1\ \mu\text{m}$  at intermediate and global levels using 21 and 13.4 nm technology nodes.

The analogous circuit model of the MLGNR, as simulated by ADS, is displayed in Fig. 9a. Using technology nodes at 21 and 13.4 nm, Fig. 9b displays the return loss and insertion loss for various lengths ranging from 0.1 to 1 m at intermediate and global levels.

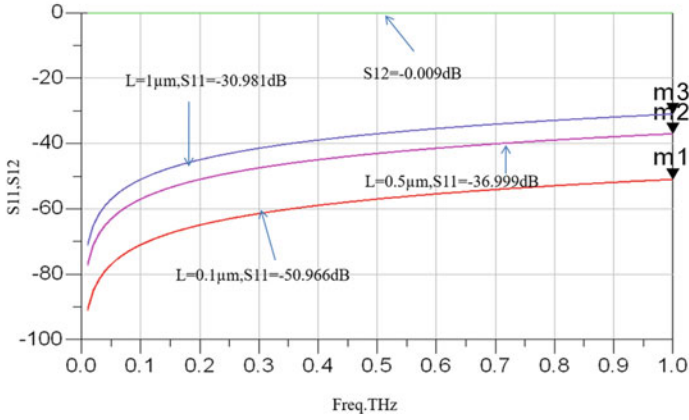
Figure 9b presents a return loss of  $-30.98\ \text{dB}$  for length of  $1\ \mu\text{m}$ , and calculated power loss is about  $2.04 \times 10^{-3}\%$  for SLGNR. Since the power loss increases with increase in length of interconnect, it is not suitable for high-speed applications. To reduce the power loss, GNRs are arranged one over the other and simulated. The return loss obtained is  $-58.34\ \text{dB}$  for MLGNR which means amount of power loss is only  $1.07 \times 10^{-7}\%$  making it suitable for high-speed application.

#### d. Performance Comparison of GNR and CNT at THz Frequency

With the help of equivalent circuit model, the radio frequency performances of single-walled CNT and single-walled graphene nanoribbon are also compared. Figure 10 displays the return loss ( $S_{11}$ ) of  $-0.203\ \text{dB}$  for SWCNT and  $-51.05\ \text{dB}$  for SLGNR. The transmission coefficient is almost negligible for SLGNR. For the same model, the simulation at a frequency of 1THz results in a return loss of  $-33.80\ \text{dB}$  for MWCNT and  $-89.69\ \text{dB}$  for MLGNR as shown in Fig. 11.

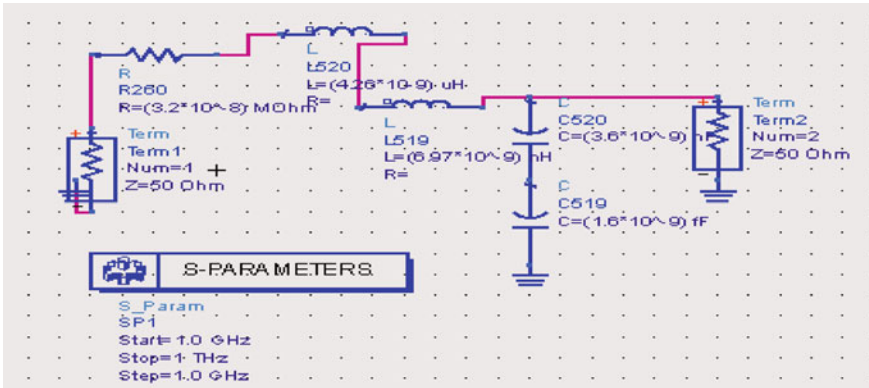


(a)

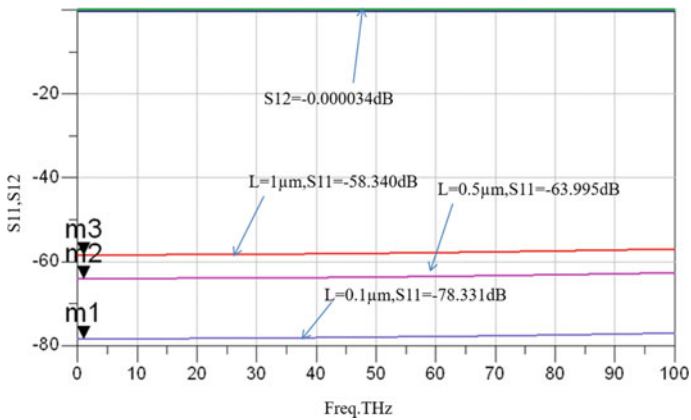


(b)

**Fig. 8** a ADS simulation of the intermediate-level lumped equivalent model SLG NR, b Simulated magnitude of scattering parameters for SLG NR



(a)



(b)

**Fig. 9** a MLGNR (global level) schematic model simulated with ADS. b Simulated scattering parameter magnitude for MLGNR

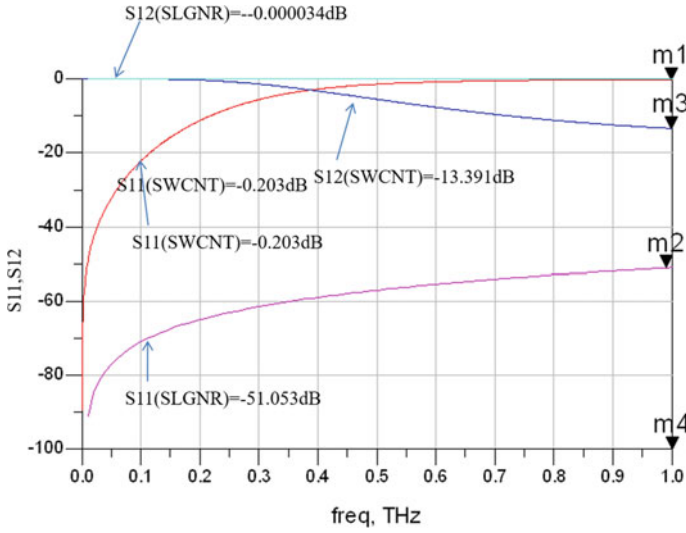


Fig. 10 Simulated magnitude of scattering parameters for SWCNT and SLGNR

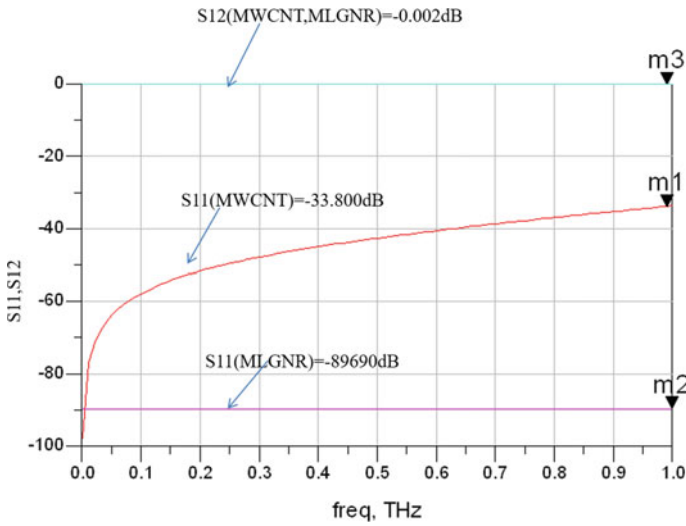


Fig. 11 Comparison of return loss and insertion loss for MWCNT and MLGNR

## 4 Conclusion

Performance comparison of scattering parameter responses of SLGNR and MLGNR is presented. Comparison is done using electromagnetic simulator—Advanced Design System (ADS). The result reveals that MLGNR has low power loss compared to SLGNR, making it as a suitable candidate for RF interconnects applications.

## References

1. 2003 International Technology Roadmap for Semiconductors (ITRS)—Semiconductor Industry Association. <https://www.semiconductors.org/resources/2003-international-technology-roadmap-for-semiconductors-itrns/>
2. Sarto, M.S., Tamburrano, A., D'Amore, M.: New electron-waveguide-based modeling for carbon nanotube interconnects. *IEEE Trans. Nanotechnol.* **8**, 214–225 (2009). <https://doi.org/10.1109/TNANO.2008.2010253>
3. Srivastava, N., Banerjee, K.: A comparative scaling analysis of metallic and carbon nanotube interconnections for nanometer scale VLSI technologies. In: Proceedings 21st International VLSI Multilevel Interconnect Conference, pp. 393–398. (2004)
4. Kreupl, F., Graham, A.P., Duesberg, G.S., Steinhögl, W., Liebau, M., Unger, E., Hönlein, W.: Carbon nanotubes in interconnect applications. *Microelectron. Eng.* **64**, 399–408 (2002). [https://doi.org/10.1016/S0167-9317\(02\)00814-6](https://doi.org/10.1016/S0167-9317(02)00814-6)
5. Srivastava, N., Joshi, R.V., Banerjee, K.: Carbon nanotube interconnects: implications for performance, power dissipation and thermal management. In: Technical Digest—International Electron Devices Meeting, IEDM. pp. 249–252. (2005). <https://doi.org/10.1109/iedm.2005.1609320>
6. Raychowdhury, A., Roy, K.: Modeling of metallic carbon-nanotube interconnects for circuit simulations and a comparison with Cu interconnects for scaled technologies. *IEEE Trans. Comput. Des. Integr. Circuits Syst.* **25**, 58–65 (2006). <https://doi.org/10.1109/TCAD.2005.853702>
7. Li, J., Ye, Q., Cassell, A., Ng, H.T., Stevens, R., Han, J., Meyyappan, M.: Bottom-up approach for carbon nanotube interconnects. *Appl. Phys. Lett.* **82**, 2491–2493 (2003). <https://doi.org/10.1063/1.1566791>
8. Burke, P.J.: Luttinger liquid theory as a model of the gigahertz electrical properties of carbon nanotubes. *IEEE Trans. Nanotechnol.* **1**, 129–145 (2002)
9. Burke, P.J.: An RF circuit model for carbon nanotubes. *IEEE Trans. Nanotechnol.* **2**, 55–58 (2003). <https://doi.org/10.1109/TNANO.2003.808503>
10. Xu, C., Li, H., Banerjee, K.: Modeling, analysis, and design of graphene nano-ribbon interconnects. *IEEE Trans. Electron Devices.* **56**, 1567–1578 (2009). <https://doi.org/10.1109/TED.2009.2024254>
11. Naeemi, A., Meindl, J.D.: Compact physics-based circuit models for graphene nanoribbon interconnects. *IEEE Trans. Electron Devices.* **56**, 1822–1833 (2009). <https://doi.org/10.1109/TED.2009.2026122>
12. Zhao, W.S., Yin, W.Y.: Signal integrity analysis of graphene nano-ribbon (GNR) interconnects. In: 2012 IEEE Electrical Design of Advanced Packaging and Systems Symposium, EDAPS 2012. pp. 227–230. (2012). <https://doi.org/10.1109/EDAPS.2012.6469382>
13. Sarto, M.S., Tamburrano, A.: Comparative analysis of TL models for multilayer graphene nanoribbon and multiwall carbon nanotube interconnects. In: IEEE International Symposium on Electromagnetic Compatibility. pp. 212–217. (2010). <https://doi.org/10.1109/IEMC.2010.5711274>

14. Zhao, W.S., Yin, W.Y.: Comparative study on multilayer graphene nanoribbon (MLGNR) interconnects. *IEEE Trans. Electromagn. Compat.* **56**, 638–645 (2014). <https://doi.org/10.1109/TEMC.2014.2301196>
15. Das, S., Bhattacharya, S., Das, D., Rahaman, H.: RF performance analysis of graphene nanoribbon interconnect. In: *IEEE TechSym 2014—2014 IEEE Student's Technology Symposium*. pp. 105–110. IEEE Computer Society (2014). <https://doi.org/10.1109/TechSym.2014.6807923>
16. Kanthamani, S., Srujana Vahini, N., Raju, S., Abhaikumar, V.: Quasi-static modelling of carbon nanotube interconnects for gigahertz applications. *Micro Nano Lett.* **5**, 328–332 (2010). <https://doi.org/10.1049/mnl.2010.0073>



# A Study on Graphene-Based Sensor Devices



Jahid Tanvir, Kawsar Ahmed, Francis M. Bui, and Shobhit K. Patel

**Abstract** A hexagonal-shaped structure of carbon atoms organized in a 2D single-layer manner is defined as graphene which has extraordinary physical as well as electrochemical properties that may lead to the utilization of graphene in several crucial fields. Graphene has great potential in optoelectronic and photoelectric applications as it supports a very wideband of spectral regions, surface plasmon polaritons (SPP), superfast optical responding and thermoelectric and large carrier conduction. In this graphene-based plasmonics era, it can be synthesized with other nanomaterials. Graphene-infused materials have found their way into various sensing areas notably optical and electrochemical sensors, chemical and gas sensors, strain and temperature sensors, biosensors and health monitoring devices with high sensitivity responses, cheaper cost and compact sizes. Furthermore, the transmittance and absorption rate of light can be controlled by stacking additional monolayers of graphene. Herein, several optoelectronic properties of graphene, for instance, optical absorption, transmission mechanisms, photo-thermionic effect, etc. along with novel materials synthesis, structural developments and overall feasibility will be discussed from recent significant research works. The overview of recent advancements in

---

J. Tanvir

Department of Information and Communication Technology, Mawlana Bhashani Science and Technology University, Santosh Tangail-1902, Bangladesh  
e-mail: [jahidtanvir.ict@gmail.com](mailto:jahidtanvir.ict@gmail.com)

K. Ahmed (✉) · F. M. Bui

Department of Electrical and Computer Engineering, University of Saskatchewan, 57 Campus Drive, Saskatoon, SK S7N 5A9, Canada  
e-mail: [kawsar.ict@mbstu.ac.bd](mailto:kawsar.ict@mbstu.ac.bd); [k.ahmed@usask.ca](mailto:k.ahmed@usask.ca)

F. M. Bui

e-mail: [francis.bui@usask.ca](mailto:francis.bui@usask.ca)

J. Tanvir · K. Ahmed

Group of Bio-photomatiχ, Department of Information and Communication Technology, Mawlana Bhashani Science and Technology University, Santosh Tangail-1902, Bangladesh

S. K. Patel

Department of Computer Engineering, Faculty of Technology, Marwadi University, Rajkot, Gujarat 360003, India  
e-mail: [shobhitkumar.patel@marwadieducation.edu.in](mailto:shobhitkumar.patel@marwadieducation.edu.in)

graphene-based sensor devices, a roadmap of future research insights and the challenges to be overcome for day-to-day implementation of graphene-inspired sensors are also provided in this chapter.

**Keywords** Graphene · Sensors · Surface plasmon polaritons · Gas sensor · Biosensor · Optoelectronics

## 1 Introduction

Human has been searching for a more sustainable substance to enhance development. A substance with suitable properties can be used in all fields of science and technology. Graphene has raised attention among researchers around the globe since its first discovery from bulk graphite [1, 2]. Graphene is a special orientation of carbon atoms where a single layer of atoms is arranged in honeycomb-like hexagonal lattices in a two-dimensional plane. Graphene has extraordinary properties like ultra-wide carrier mobility, super-high-thermal conductivity, massive physical strength, compatibility with other materials, etc. [3, 4]. Graphene is an allotrope of carbon atoms—carbon nanotube (CNT). Before graphene, researchers have tried many other nanomaterials such as quantum dots (QDs), nanoparticles, CNTs, nanowires and many other zero- or one-dimensional (0D or 1D) nanomaterials [5]. But because of graphene's rich properties, it has been used in many types of research such as photodetectors and photovoltaic devices [6, 7], LEDs and lasers [8, 9] and optical limiters and frequency converters [10, 11]. But graphene-based sensors can truly draw the proper utilization of graphene. In recent years, with the help of artificially manipulated Van der Waals (vdWs) atomic bonding, graphene has shown tremendous development of coexisting (stacking) with other 2D materials, namely phosphorene, silicone and hexagonal-shaped boron nitride (h-BN) which enables the easy manipulation of atomic properties [12–14]. These materials are being used in various sensors because of the proper synthesis of graphene with other materials [15]. These syntheses are possible by hybridizing quantum dots (0D dots), 1D nanomaterials and 3D bulk structures with heterostructured 2D graphene sheets [16].

To ensure the high quality of graphene and to reduce the production cost, researches are being conducted still today. Pristine graphene is only made by the “scotch tape” method where graphene sheets are placed onto any material's surface by physical means. This type of process is not suitable to tune and proper use for sensor devices [17]. It is still needed to mass produce high-quality graphene with minimum expenses. Some methods are promising enough to produce graphene with reasonable quality at the industrial level such as the chemical vapor deposition (CVD) method, silicon carbide (SiC) decomposition, graphene oxide (GO) and reduced graphene oxide (rGO) method [18–20]. CVD method-driven graphene offers a large area of sensing film, multi-layers structures and low noise. GO and rGO methods introduce high defect regions by the  $sp^3$  bond of C–C and  $sp^2$  bond of C–O, respectively, which enable to develop ultra-sensitive biochemical and electrochemical sensors

[21]. Graphene also shows higher optical damage magnitude and higher mobility compared to Si, GaAs materials which brings hope to researchers for photonics-based applications [22–24]. But mere monolayer of graphene comes with its own limitations such as low-light absorption, faster recombination and no-gain mechanism. These limit the usages of mere graphene in real-life nanophotonics applications [25]. So, hybridization and synthesis of graphene with other materials (1D, 2D and bulk 3D) may provide a solution to these problems and may utilize the unprecedented properties of graphene to its full extent.

In this chapter, we will look into some important properties of graphene which are very crucial to achieve highly sensitive sensor devices. Some recent development in graphene-based optical sensors, chemical sensors, physical sensors and biosensors will also be discussed later in this chapter.

## 2 Opto-Electronic Properties of Graphene

Graphene has shown many extraordinary properties which enable it to be properly utilized in many sensing areas. Some properties of graphene which are crucial to developing good sensor devices are discussed below.

### 2.1 Transmission and Absorption

It is reported that 2D graphene semi-metal with zero energy bandgap property had shown  $10^{13}$  magnitude of electron–hole concentration per square centimeter and approximately 10,000 square centimeters magnitude of carrier mobility per Volt-second [1]. This high carrier conductivity is possible at gate voltage,  $V_G = \pm 60$  V, and it is possible by zero bandgap property and sudden resistivity drop at gate voltage [26]. The charge density of the graphene surface is defined by Novoselov et al. [1],

$$n = \frac{\varepsilon_0 \varepsilon V_G}{t \times e} \quad (1)$$

where  $\varepsilon_0$ ,  $\varepsilon$ ,  $t$ ,  $e$  are the permittivity of free space, permittivity of SiO<sub>2</sub>, layer thickness of SiO<sub>2</sub> and electron charge, respectively. This surface charge density helps to vary the Fermi energy level to 0-doping in the annealed condition in the complete vacuum. But Fermi energy level ( $E_F$ ) goes to n-type or p-type doping by exposing the graphene surface to NH<sub>3</sub> gas or H<sub>2</sub>O molecules, respectively. Thus graphene can change from a pre-dielectric material to a super-metallic material. This optoelectronic property or biochemical doping mechanism is the core idea of biochemical sensors [1].

This biochemical doping mechanism also changes graphene's refractive index (RI) as positive and negative charge carrier density is altered. The RI change of graphene is calculated by Shivananju et al. [21],

$$n_g = \left( -\frac{\sigma_{g,i}}{\omega\Delta} + \frac{i\sigma_{g,r}}{\omega\Delta} \right)^{\frac{1}{2}} \quad (2)$$

where  $\sigma_{g,r}$  and  $\sigma_{g,i}$ , are real and imaginary parts of graphene's conductivity constant, respectively, and  $\omega$ ,  $\Delta$  are angular frequency of light and graphene layer thickness, respectively. This refractive index changes ( $n_g$ ) of graphene are used to determine the effective refractive index ( $n_{eff}$ ) of graphene-based sensor devices.

Graphene absorbs a significant amount of applied light because of its no bandgap property. The light absorption rate of each graphene layer is defined by a structure constant,  $\alpha$  which is [27],

$$\alpha = \frac{e^2}{\hbar \times c} \approx \frac{1}{137} \quad (3)$$

$$1 - T \approx \pi \times \alpha = 2.3\% \quad (4)$$

where  $T$ ,  $\hbar$ ,  $c$  are transmittance of light (97.7%), Planck constant ( $6.626 \times 10^{-34}$  m<sup>2</sup>kg/s) and speed of light ( $3 \times 10^8$  ms<sup>-1</sup>), respectively. This transmittance ratio indicates the transparent nature of the single graphene sheet. But absorption can be increased by 2.3% if additional graphene layers are stacked together.

Another important formula related to graphene's optical properties is the Kubo formula. It predicts dynamic optical response from intraband and interband conductivities. The formula is [24],

$$\sigma = \sigma_{\text{intra}} + \sigma_{\text{inter}} + i\sigma'_{\text{inter}} \quad (5)$$

And intraband conductivity,  $\sigma_{\text{intra}}$ , interband conductivities,  $\sigma_{\text{inter}}$  and  $\sigma'_{\text{inter}}$ , are defined as [24],

$$\sigma_{\text{intra}} = \sigma_0 \frac{4\mu}{\pi(\hbar\tau_1 - i\hbar\omega)} \quad (6)$$

$$\sigma_{\text{inter}} = \sigma_0 \left( 1 + \frac{1}{\pi} \arctan \frac{\hbar\omega - 2\mu}{\hbar\tau_2} - \frac{1}{\pi} \arctan \frac{\hbar\omega + 2\mu}{\hbar\tau_2} \right) \quad (7)$$

$$\sigma'_{\text{inter}} = -\sigma_0 \frac{1}{2\pi} \ln \frac{(2\mu + \hbar\omega)^2 + \hbar^2\tau_2^2}{(2\mu - \hbar\omega)^2 + \hbar^2\tau_2^2} \quad (8)$$

where  $\sigma_0 = \frac{\pi e^2}{2\hbar}$ ,  $\mu$  is the chemical potential of graphene ( $\mu > 0$ ) and  $\tau_1$  and  $\tau_2$  are the relaxation rate of intraband and interband transitions, respectively. Chemical potential,  $\mu$ , is calculated from carrier concentration,  $n_0 = \left(\frac{\mu}{\hbar v}\right)^2/\pi$ , and carrier concentration is controlled by doping and gate voltage [24].

## 2.2 *Surface Plasmon Resonance Operation*

Graphene has an absorption rate of 2.3% for a single-layer sheet and very low photo-carrier concentrations. Due to the zero bandgap property, the recombination of electron–hole pairs generated by photons is superfast. This also leads to a high “dark current”. These properties may lead to non-ideal conditions for sensor devices. Researchers have been trying to overcome these limitations by combining several other operations with graphene-based devices.

Plasmonic materials with the combination of graphene can excite the surface plasmon polaritons (SPPs) resulting in strong surface plasmon resonance (SPR) [28]. So graphene can be used to make waveguides with higher refractive indices which lead to higher light cache time signals as a result of deceleration of the propagating light in those mediums [29–31]. As metallic nanoparticles scatter the incident light in various directions, it helps the near-stacking absorbing materials (analytes) to effectively absorb the localized light beams. Therefore, graphene is a light-absorbent material, and it can co-exist with metallic plasmonic nanoparticles to improve surface plasmon effects.

In 2016, Lin et al. increased the efficiency of power conversion of a solar cell model from 8.83 to 11.8% by stacking 80 nm thick gold (Au) nanoparticles layer onto heterostructured graphene and gallium arsenide (GaAs) sheets [32]. In recent years, Tian et al. have designed a D-shaped PCF biosensor with indium tin oxide (ITO) and graphene combination which has shown a staggering wavelength sensitivity of 12,000 nm/RIU [33]. Many more kinds of research have shown graphene as a good choice for SPR-generating material [34–36].

## 2.3 *Photo-Thermionic Effect*

Materials absorbing incident light generate heat energy. Photoelectricity is generated by the freely moving electrons inside the materials. The main concept of the photo-thermionic (PTI) effect is that high-energy selective wideband absorbing materials absorb the heat energy from excited electrons as well. The carrying capacities of the internal materials must be higher than the photon interactions [28].

A heterostructure model of a tungsten diselenide ( $\text{WSe}_2$ ) single layer sandwiched between h-BN and graphene layers was designed by Massicotte et al. [37]. When graphene absorbs the incident photons, an additional photo-current was discovered as thermal carriers cause high-energy electrons to push through the barrier. Thermal carriers between  $\text{WSe}_2$  and graphene layers carry more energy than Schottky barriers [37]. This PTI incident is helpful to detect the photons of sub-bandgap levels.

### 3 Sensor Devices

Sensor devices are those which convert external or environmental stimulations such as heat, motion, light, sound, pressure and stain into mechanical, electrical or optical outputs [20]. Having some extraordinary physical properties, graphene has shown promising growth in sensor field areas. Some graphene-based sensor devices (details in Fig. 1) of various aspects are discussed below.

#### 3.1 Chemical and Gas Sensors

All forms of graphene such as pristine graphene (PG), graphene oxide (GO) and reduced graphene oxide (rGO) have their own electrical conductivity level and surface activity. Due to the 2D structure of graphene, the electron mobility in graphene is drastically affected by the gas molecule's absorption [38]. The gas molecule adsorbates act as electron acceptors or donors. So the electron conductivity and the local

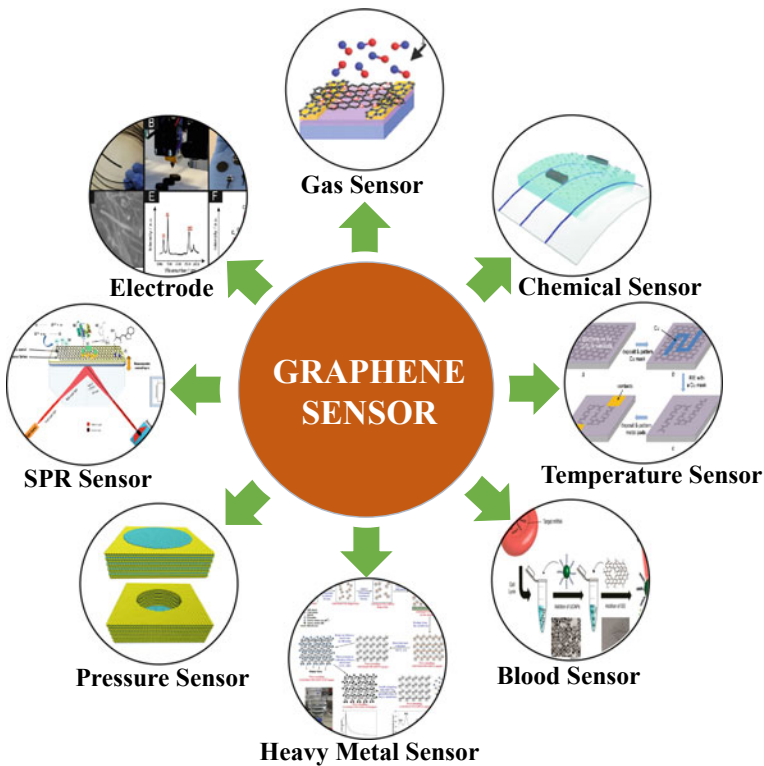


Fig. 1 Graphene-based sensors and devices

carrier distribution are changed as graphene's surface absorbs gas molecules [39]. As a result, the notable change in carrier concentration near the Dirac point or electrical conductivity due to the absorption of gas molecules leads to the successful detection of gases by graphene-based sensors.

In the early stages of graphene-based gas sensors development, Novoselov et al. sense extremely diluted nitrogen dioxide ( $\text{NO}_2$ ) gas by the mechanically exfoliated pristine graphene [39]. But their research has still been used as a standard for gas sensing purposes since it can detect gas parts per billion (ppb). They are the first ones to define the limit of detection (LOD) parameter for graphene-based gas sensors. They also refine the sensor by implementing Hall geometry. This operation was conducted by leaking 1 ppm  $\text{NO}_2$  gas at a rate of  $10^{-3}$  mbar/s to the optimized sensing device. Some other researchers in the following years successfully detected  $\text{NO}_2$ ,  $\text{NH}_3$ ,  $\text{CO}_2$  and other gases by also using pristine graphene-based sensors [40–43]. The sensing performance is affected by the room temperature, leaking rate and shape of the graphene sheet.

Apart from fundamental graphene substrates, many other procedures are also followed to improve sensitivity responses such as graphene-based defective and functionalized materials (nitrogen (N) and silica ( $\text{SiO}_2$ ) co-doped graphene sensors [44], boron (B) and nitrogen (N)-doped graphene nanosheets [45], aluminum (Al)-doped graphene materials [46]); graphene-polymer compositions polymethyl methacrylate (PMMA) and graphene composites [47], polypyrene (PPr) and graphene oxide (GO) composites [48], polypyrrole (PPy) and GO composites [49]); graphene-metal or graphene-metal oxide nanoparticles (zinc oxide (ZnO) and graphene hybrid [50], copper-I oxide ( $\text{Cu}_2\text{O}$ ) and rGO hybrid [51]); graphene-organic materials [52], etc.

In recent years, much research are conducted to develop graphene-based gas sensor devices. Ghazi et al. developed GO-coated microfluidic gas sensors to detect environmental pollutants, volatile organic compounds (VOCs) [53]. They achieved an average of 64.4% improvement for microfeatures and 120.9% improvement for nano-microfeatures sensors. M Yang et al. designed an ammonia ( $\text{NH}_3$ ) sensor by employing holey graphene oxide (HGO) with Fenton reagents ( $\text{Fe}_2/\text{Fe}_3/\text{H}_2\text{O}_2$ ) [54]. In 2021, a rubidium (Rb-G)-doped graphene-based sensor is designed for hydrogen ( $\text{H}_2$ ) gas detection [55]. This sensor offers a higher percentage sensitivity response of 482 at a relatively lower temperature (348 K  $\approx$  74.5 °C). An acetone sensor is proposed by using Co-MOF-74-derived  $\text{Co}_3\text{O}_4$ /graphene heterostructured nanoscrolls ( $\text{Co}_3\text{O}_4$ /GNS) structure which offers a high response with a short recovery time, and it can even detect 50 ppb acetone [56].

### 3.2 Temperature Sensors

General temperature sensors with lack of flexibility and transparency are made of ceramic-based thermistors or transition metal oxides (TMOs) [57, 58]. As graphene has excellent thermal properties along with unique photo-electronic properties, it can be used to design flexible temperature sensor devices.

Graphene has both semiconductor and metallic-like behaviors regarding the temperature effects on resistivity [59]. Like a semiconductor material, graphene generates thermal electron–hole pairs as temperature rises, resulting in a decrease in resistivity, whereas resistivity increases whenever the temperature rises as graphene generates more charge carriers. These behaviors can be affected by graphene layer number, the crystallinity of graphene and the field-effect transistor's (FET) gate voltage [60]. Yan et al. designed a graphene thermistor using silver nanowires (AgNWs)-made electrodes [61]. Polydimethylsiloxane (PDMS) was used to embed the whole graphene sensing channel and electrodes which were later peeled off. This thermometer showed 12.63 and 7.45 M $\Omega$  resistivities at 30 °C and 100 °C, respectively, which can be applied to calculate the temperature at any measured resistivity. This design allows the sensor to be twisted or stretched without any fracture.

Using rGO/P (VDF-TrFE) composition as the primary sensing material, Trung et al. also developed a FET temperature sensor that provides great flexibility [62]. One of the major features of this model is that it can detect even a 0.1 °C change in temperature. Another notable development of graphene-based temperature sensors is the implementation of wearable temperature sensors by Yang et al. [63].

### 3.3 *Biosensors and Health Monitoring Devices*

Development of various graphene-based electro-optical sensors, chemical and gas sensors, temperature sensors, flow and strain sensors and very other sensor devices is enriching the wide field of biomedical graphene-based sensors (details in Fig. 2). It is becoming more convenient to use graphene-doped materials for efficient and successful medical testing and monitoring applications.

Human body cells or tissues exchange ions between themselves through the cell membranes. These transmembrane ion's exchange can create resting potential and action potential which are marked as bio-electrical signals. This potential is generated by the imbalance of sodium and potassium ions ( $\text{Na}^+/\text{K}^+$ ) on the inner and outer sides of cell membranes [64]. Every specific cell generates a unique amount of voltages. Generally, these bio-electric signals are recorded by some forms of electrodes such as electroencephalogram (EEG), electrocardiogram (ECG) and electroretinogram (EOG) after proper filtering and amplification processes [65]. The importance of graphene lies in manufacturing these bio-electric signal capturing electrodes. Graphene offers a wide dynamic range, high SNR with low impedance, accuracy, robustness and overall flexibility for biological electrodes. In 2017, an extra thin (about  $463 \pm 30$  nm thin) graphene electronic tattoo (GET) was fabricated through the “wet transfer, dry patterning” method [66]. The fabrication process of GET is also polished over the year [67]. These GET sensors can be integrated with EEG, ECG and EOG to fetch bio-electrical signals. The 3D graphene shows piezoresistive properties which can be utilized in pressure sensors. Yogeswaran et al. designed a pressure sensor by implementing a graphene field-effect transistor (GFET) which has an operating voltage of 50 mV and sensitivity responses of  $2.70 \times 10^{-4}$  kPa $^{-1}$



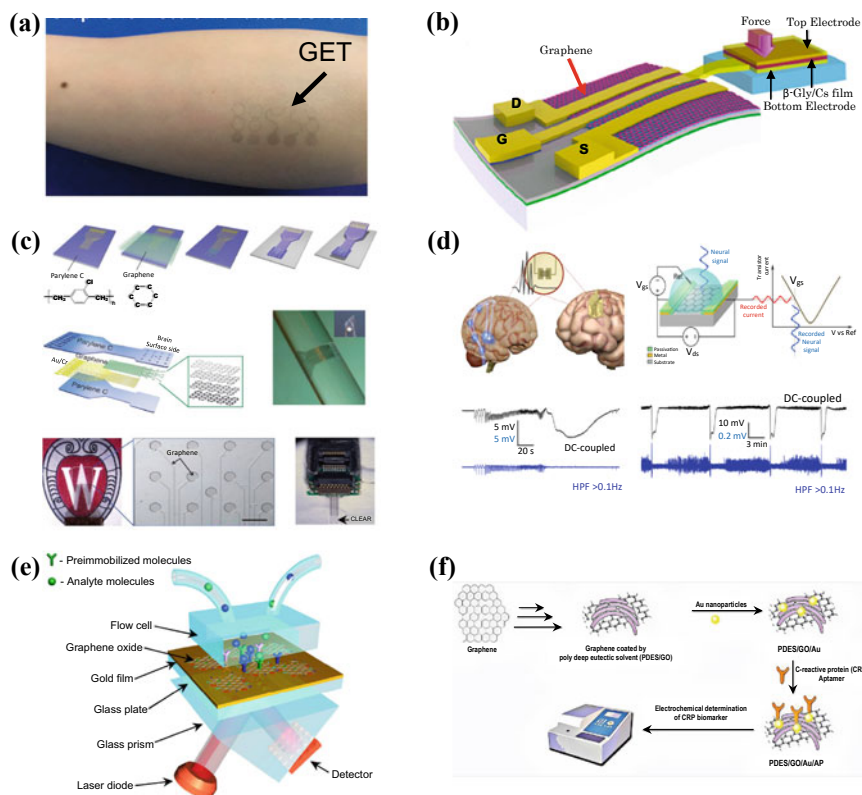


**Fig. 2** Several graphene-based biosensors and health monitoring devices. **a** GET sensor [66], **b** pressure sensors [68], **c** CLEAR sensor [69], **d** gSGFETs sensor [70], **e** Go-coated SPR-based DNA sensor [71] and **f** Au-Ir NPs tagged PDES-GOCPR sensor [73]

and  $7.56 \times 10^{-4} \text{ kPa}^{-1}$  with a wide dynamic range of  $5 \sim 20 \text{ kPa}$  and  $20 \sim 35 \text{ kPa}$ , respectively [68].

For neural imaging, graphene sheets can be combined with micro-electrocorticography (micro-ECoG) devices. DW Park et al. designed an invasive device using a graphene-based carbon-layered electrode array (CLEAR) which has four layers of graphene [69]. It has minimum  $76\Omega$  sheet resistance with 90% broadband transmission of  $300 \sim 1500 \text{ nm}$  wavelength. Solution-gated field-effect graphene micro-transistors (gSGFETs) were developed in 2022 as an implant to detect neural signal transduction which has direct brain cells contacting a 2D graphene sheet [70]. It can detect a varied range of frequencies of brain signals and can create high-density mapping as graphene has higher electrochemical stability. These types of invasive sensors can be attached to the target organs or tissues for accurate sensing and curative application's performance.

Bio-molecules like DNA and protein analysis have also leaped forward with the introduction of graphene-based sensors. In 2015, YV Stebunov et al. designed a

graphene oxide (GO)-layered SPR biological sensor with three times higher sensitivity than commercial responses. This device utilizes the interaction between streptavidin molecules and bio-molecules having biotin residues. The absorption rates of D<sub>1</sub>, D<sub>2</sub> oligonucleotide sequences confirm the capability of DNA interaction sensing of the GO-layered SPR-based optical prism microfluidic sensor chip [71]. C-reactive protein (CRP) found in blood plasma is utilized as a bio-marker for the early detection of cardiovascular diseases and body infections. Gold-Iridium nanoparticles with GO and gold-poly deep eutectic solvent with GO sensor are designed with an extreme CPR antigen sensitivity range of 0.01 ~ 100 ng mL<sup>-1</sup> and 0.0003 ~ 50 ng mL<sup>-1</sup>, respectively [72, 73].

## 4 Future Challenges

Despite showing extraordinary properties such as biocompatibility, large interactive area, high electrical carrier conductivity and fast transfer rate, it is still challenging to produce graphene and graphene-based materials for industrial-level applications. More researches are required to solve this graphene synthesis problem and make graphene more usable in our day-to-day life and as many fields of applications as possible.

Another challenge of graphene-based sensors is the fabrication expenses. To produce a good sensor, it needs graphene of the best quality. But it is still very expensive to produce high-quality graphene. So fabrication processes should be studied to make them more accessible but more refined.

It is hoped that graphene will replace silicon-based electronics in the near future. It will not hurt to say that, graphene still needs to go a long way to entirely take place of silicon-driven industries despite its excellent properties. More research should be conducted to open up more fields of graphene-based devices. A single layer of graphene sheet does not provide many options, so the synthesis of graphene-based materials should be examined thoroughly. These studies may open up feasible solutions to unlock all these extraordinary properties of graphene.

**Acknowledgements** The study was supported by funding from the Natural Sciences and Engineering Research Council of Canada (NSERC).

## References

1. Novoselov, K.S., Geim, A.K., Morozov, S.V., Jiang, D.E., Zhang, Y., Dubonos, S.V., Grigorieva, I.V., Firsov, A.A.: Electric field effect in atomically thin carbon films. *Science* **306**(5696), 666–669 (2004)
2. Zhang, Y., Tan, Y.W., Stormer, H.L., Kim, P.: Experimental observation of the quantum Hall effect and Berry's phase in graphene. *Nature* **438**(7065), 201–204 (2005)

3. Chang, H., Wu, H.: Graphene-based nanomaterials: synthesis, properties, and optical and optoelectronic applications. *Adv. Func. Mater.* **23**(16), 1984–1997 (2013)
4. Nguyen, B.H., Nguyen, V.H.: Advances in graphene-based optoelectronics, plasmonics and photonics. *Adv. Natur. Sci.: Nanosci. Nanotechnol.* **7**(1), 013002 (2016)
5. Zeng, S., Baillargeat, D., Ho, H.P., Yong, K.T.: Nanomaterials enhanced surface plasmon resonance for biological and chemical sensing applications. *Chem. Soc. Rev.* **43**(10), 3426–3452 (2014)
6. Ferreira, A., Peres, N.M.R., Ribeiro, R.M., Stauber, T.: Graphene-based photodetector with two cavities. *Phys. Rev. B* **85**(11), 115438 (2012)
7. Stratakis, E., Stylianakis, M.M., Koudoumas, E., Kymakis, E.: Plasmonic organic photovoltaic devices with graphene based buffer layers for stability and efficiency enhancement. *Nanoscale* **5**(10), 4144–4150 (2013)
8. Tchernycheva, M., Lavenus, P., Zhang, H., Babichev, A.V., Jacopin, G., Shahmohammadi, M., Julien, F.H., Ciecchonski, R., Vescovi, G., Kryliouk, O.: InGaN/GaN core-shell single nanowire light emitting diodes with graphene-based p-contact. *Nano Lett.* **14**(5), 2456–2465 (2014)
9. Luo, Z., Zhou, M., Weng, J., Huang, G., Xu, H., Ye, C., Cai, Z.: Graphene-based passively Q-switched dual-wavelength erbium-doped fiber laser. *Opt. Lett.* **35**(21), 3709–3711 (2010)
10. Zheng, C., Chen, W., Huang, Y., Xiao, X., Ye, X.: Graphene oxide-noble metal (Au, Pt, and Pd) nanoparticle composites as optical limiters. *RSC Adv.* **4**(75), 39697–39703 (2014)
11. Ding, J., Arigong, B., Ren, H., Shao, J., Zhou, M., Lin, Y., Zhang, H.: Mid-infrared tunable dual-frequency cross polarization converters using graphene-based L-shaped nanoslot array. *Plasmonics* **10**(2), 351–356 (2015)
12. Geim, A.K., Grigorieva, I.V.: Van der Waals heterostructures. *Nature* **499**(7459), 419–425 (2013)
13. Frisenda, R., Molina-Mendoza, A.J., Mueller, T., Castellanos-Gomez, A., Van Der Zant, H.S.: Atomically thin p–n junctions based on two-dimensional materials. *Chem. Soc. Rev.* **47**(9), 3339–3358 (2018)
14. Zhang, Z., Lin, P., Liao, Q., Kang, Z., Si, H., Zhang, Y.: Graphene-based mixed-dimensional van der Waals heterostructures for advanced optoelectronics. *Adv. Mater.* **31**(37), 1806411 (2019)
15. Brisebois, P.P., Siaj, M.: Harvesting graphene oxide—years 1859 to 2019: a review of its structure, synthesis, properties and exfoliation. *J. Mater. Chem. C* **8**(5), 1517–1547 (2020)
16. Ryder, C.R., Wood, J.D., Wells, S.A., Yang, Y., Jariwala, D., Marks, T.J., Schatz, G.C., Hersam, M.C.: Covalent functionalization and passivation of exfoliated black phosphorus via aryl diazonium chemistry. *Nat. Chem.* **8**(6), 597–602 (2016)
17. He, Q., Wu, S., Yin, Z., Zhang, H.: Graphene-based electronic sensors. *Chem. Sci.* **3**(6), 1764–1772 (2012)
18. Berger, C., Song, Z., Li, X., Wu, X., Brown, N., Naud, C., Mayou, D., Li, T., Hass, J., Marchenkov, A.N., Conrad, E.H.: Electronic confinement and coherence in patterned epitaxial graphene. *Science* **312**(5777), 1191–1196 (2006)
19. Li, X., Cai, W., An, J., Kim, S., Nah, J., Yang, D., Piner, R., Velamakanni, A., Jung, I., Tutuc, E., Banerjee, S.K.: Large-area synthesis of high-quality and uniform graphene films on copper foils. *Science* **324**(5932), 1312–1314 (2009)
20. Dreyer, D.R., Park, S., Bielawski, C.W., Ruoff, R.S.: The chemistry of graphene oxide. *Chem. Soc. Rev.* **39**(1), 228–240 (2010)
21. Shivnanjanu, B.N., Yu, W., Liu, Y., Zhang, Y., Lin, B., Li, S., Bao, Q.: The roadmap of graphene-based optical biochemical sensors. *Adv. Func. Mater.* **27**(19), 1603918 (2017)
22. Roberts, A., Cormode, D., Reynolds, C., Newhouse-Ilidge, T., LeRoy, B.J., Sandhu, A.S.: Response of graphene to femtosecond high-intensity laser irradiation. *Appl. Phys. Lett.* **99**(5), 051912 (2011)
23. Wang, X., Shen, Z.H., Lu, J., Ni, X.W.: Laser-induced damage threshold of silicon in millisecond, nanosecond, and picosecond regimes. *J. Appl. Phys.* **108**(3), 033103 (2010)
24. Bao, Q., Loh, K.P.: Graphene photonics, plasmonics, and broadband optoelectronic devices. *ACS Nano* **6**(5), 3677–3694 (2012)

25. Konstantatos, G., Badioli, M., Gaudreau, L., Osmond, J., Bernechea, M., De Arquer, F., Gatti, F., Koppens, F.H.: Hybrid graphene–quantum dot phototransistors with ultrahigh gain. *Nat. Nanotechnol.* **7**(6), 363–368 (2012)
26. Geim, A.K., Novoselov, K.S.: The rise of graphene. *Nat. Mater.* **6**(3), 183–191 (2007)
27. Nair, R.R., Blake, P., Grigorenko, A.N., Novoselov, K.S., Booth, T.J., Stauber, T., Peres, N.M., Geim, A.K.: Fine structure constant defines visual transparency of graphene. *Science* **320**(5881), 1308–1308 (2008)
28. Wang, J., Song, J., Mu, X., Sun, M.: Optoelectronic and photoelectric properties and applications of graphene-based nanostructures. *Mater. Today Phys.* **13**, 100196 (2020)
29. Link, S., El-Sayed, M.A.: Spectral properties and relaxation dynamics of surface plasmon electronic oscillations in gold and silver nanodots and nanorods. *J. Phys. Chem. B* **103**(40), 8410–8426 (1999)
30. Barnes, W.L., Dereux, A., Ebbesen, T.W.: Surface plasmon subwavelength optics. *Nature* **424**(6950), 824–830 (2003)
31. Yang, J.L., Xu, J., Ren, H., Sun, L., Xu, Q.C., Zhang, H., Li, J.F., Tian, Z.Q.: In situ SERS study of surface plasmon resonance enhanced photocatalytic reactions using bifunctional Au@ CdS core–shell nanocomposites. *Nanoscale* **9**(19), 6254–6258 (2017)
32. Lin, S.S., Wu, Z.Q., Li, X.Q., Zhang, Y.J., Zhang, S.J., Wang, P., Panneerselvam, R., Li, J.F.: Stable 16.2% efficient surface plasmon-enhanced graphene/GaAs heterostructure solar cell. *Adv. Energy Mater.* **6**(21), 1600822 (2016)
33. Tian, J., Xu, C., Cui, S., Ma, L., Fu, Y.: A photonic crystal fiber-based biosensor with quasi-D-shaped layout and ITO-graphene combination. *Plasmonics* **16**(5), 1451–1460 (2021)
34. Yang, H., Liu, M., Chen, Y., Guo, L., Xiao, G., Liu, H., Li, J., Yuan, L.: Highly sensitive graphene-Au coated plasmon resonance PCF sensor. *Sensors* **21**(3), 818 (2021)
35. Esfahani Monfared, Y., Qasymeh, M.: Plasmonic biosensor for low-index liquid analyte detection using graphene-assisted photonic crystal fiber. *Plasmonics* **16**(3), 881–889 (2021)
36. Sorathiya, V., Lavadiya, S., Faragallah, O.S., Eid, M., Rashed, A.N.Z.: D shaped dual core photonics crystal based refractive index sensor using graphene–titanium–silver materials for infrared frequency spectrum. *Opt. Quant. Electron.* **54**(5), 1–13 (2022)
37. Massicotte, M., Schmidt, P., Violla, F., Watanabe, K., Taniguchi, T., Tielrooij, K.J., Koppens, F.H.: Photo-thermionic effect in vertical graphene heterostructures. *Nat. Commun.* **7**(1), 1–7 (2016)
38. Lu, G., Ocola, L.E., Chen, J.: Reduced graphene oxide for room-temperature gas sensors. *Nanotechnology* **20**(44), 445502 (2009)
39. Schedin, F., Geim, A.K., Morozov, S.V., Hill, E.W., Blake, P., Katsnelson, M.I., Novoselov, K.S.: Detection of individual gas molecules adsorbed on graphene. *Nat. Mater.* **6**(9), 652–655 (2007)
40. Leenaerts, O., Partoens, B., Peeters, F.M.: Adsorption of H<sub>2</sub>O, NH<sub>3</sub>, CO, NO<sub>2</sub>, and NO on graphene: a first-principles study. *Phys. Rev. B* **77**(12), 125416 (2008)
41. Romero, H.E., Joshi, P., Gupta, A.K., Gutierrez, H.R., Cole, M.W., Tadigadapa, S.A., Eklund, P.C.: Adsorption of ammonia on graphene. *Nanotechnology* **20**(24), 245501 (2009)
42. Ko, G., Kim, H.Y., Ahn, J., Park, Y.M., Lee, K.Y., Kim, J.: Graphene-based nitrogen dioxide gas sensors. *Curr. Appl. Phys.* **10**(4), 1002–1004 (2010)
43. Yoon, H.J., Yang, J.H., Zhou, Z., Yang, S.S., Cheng, M.M.C.: Carbon dioxide gas sensor using a graphene sheet. *Sens. Actuators, B Chem.* **157**(1), 310–313 (2011)
44. Niu, F., Liu, J.M., Tao, L.M., Wang, W., Song, W.G.: Nitrogen and silica co-doped graphene nanosheets for NO<sub>2</sub> gas sensing. *J. Mater. Chem. A* **1**(20), 6130–6133 (2013)
45. Zhang, Y.H., Chen, Y.B., Zhou, K.G., Liu, C.H., Zeng, J., Zhang, H.L., Peng, Y.: Improving gas sensing properties of graphene by introducing dopants and defects: a first-principles study. *Nanotechnology* **20**(18), 185504 (2009)
46. Ao, Z.M., Yang, J., Li, S., Jiang, Q.: Enhancement of CO detection in Al doped graphene. *Chem. Phys. Lett.* **461**(4–6), 276–279 (2008)
47. Dan, Y., Lu, Y., Kybert, N.J., Luo, Z., Johnson, A.C.: Intrinsic response of graphene vapor sensors. *Nano Lett.* **9**(4), 1472–1475 (2009)

48. Zhang, L., Li, C., Liu, A., Shi, G.: Electrosynthesis of graphene oxide/polypyrrole composite films and their applications for sensing organic vapors. *J. Mater. Chem.* **22**(17), 8438–8443 (2012)
49. Bai, H., Sheng, K., Zhang, P., Li, C., Shi, G.: Graphene oxide/conducting polymer composite hydrogels. *J. Mater. Chem.* **21**(46), 18653–18658 (2011)
50. Cuong, T.V., Pham, V.H., Chung, J.S., Shin, E.W., Yoo, D.H., Hahn, S.H., Huh, J.S., Rue, G.H., Kim, E.J., Hur, S.H., Kohl, P.A.: Solution-processed ZnO-chemically converted graphene gas sensor. *Mater. Lett.* **64**(22), 2479–2482 (2010)
51. Deng, S., Tjoa, V., Fan, H.M., Tan, H.R., Sayle, D.C., Olivo, M., Mhaisalkar, S., Wei, J., Sow, C.H.: Reduced graphene oxide conjugated Cu<sub>2</sub>O nanowire mesocrystals for high-performance NO<sub>2</sub> gas sensor. *J. Am. Chem. Soc.* **134**(10), 4905–4917 (2012)
52. Zhang, Y.H., Zhou, K.G., Xie, K.F., Zeng, J., Zhang, H.L., Peng, Y.: Tuning the electronic structure and transport properties of graphene by noncovalent functionalization: effects of organic donor, acceptor and metal atoms. *Nanotechnology* **21**(6), 065201 (2010)
53. Ghazi, M., Janfaza, S., Tahmooressi, H., Tasnim, N., Hoorfar, M.: Selective detection of VOCs using microfluidic gas sensor with embedded cylindrical microfeatures coated with graphene oxide. *J. Hazardous Mater.* **424**, 127566 (2022)
54. Yang, M., Wang, Y., Dong, L., Xu, Z., Liu, Y., Hu, N., Kong, E.S.W., Zhao, J., Peng, C.: Gas sensors based on chemically reduced holey graphene oxide thin films. *Nanoscale Res. Lett.* **14**(1), 1–8 (2019)
55. Singh, S.A., More, P.S., Kholam, Y.B., Kondawar, S.B.: Enhanced hydrogen gas sensing characteristics of graphene modified with rubidium (Rb). *Mater. Chem. Phys.* **260**, 124105 (2021)
56. Xiong, Y., Chang, X., Qiao, X., Li, K., Zhu, L., Xia, F., Li, X., Zheng, Q., Xing, W., Xue, Q.: Co-MOF-74 derived Co<sub>3</sub>O<sub>4</sub>/graphene heterojunction nanoscrolls for ppb-level acetone detection. *Sens. Actuators B: Chem.* **300**, 127011 (2019)
57. Feteira, A.: Negative temperature coefficient resistance (NTCR) ceramic thermistors: an industrial perspective. *J. Am. Ceram. Soc.* **92**(5), 967–983 (2009)
58. Park, K., Bang, D.Y.: Electrical properties of Ni–Mn–Co–(Fe) oxide thick-film NTC thermistors prepared by screen printing. *J. Mater. Sci.: Mater. Electron.* **14**(2), 81–87 (2003)
59. Yang, T., Zhao, X., He, Y., Zhu, H.: Graphene-based sensors. In: *Graphene*, pp. 157–174. Academic Press (2018)
60. Skákalová, V., Kaiser, A.B., Yoo, J.S., Obergfell, D., Rost, S.: Correlation between resistance fluctuations and temperature dependence of conductivity in graphene. *Phys. Rev. B* **80**(15), 153404 (2009)
61. Yan, C., Wang, J., Lee, P.S.: Stretchable graphene thermistor with tunable thermal index. *ACS Nano* **9**(2), 2130–2137 (2015)
62. Trung, T.Q., Ramasundaram, S., Hong, S.W., Lee, N.E.: Flexible and transparent nanocomposite of reduced graphene oxide and P (VDF-TrFE) copolymer for high thermal responsivity in a field-effect transistor. *Adv. Func. Mater.* **24**(22), 3438–3445 (2014)
63. Yang, J., Wei, D., Tang, L., Song, X., Luo, W., Chu, J., Gao, T., Shi, H., Du, C.: Wearable temperature sensor based on graphene nanowalls. *RSC Adv.* **5**(32), 25609–25615 (2015)
64. Huang, H., Su, S., Wu, N., Wan, H., Wan, S., Bi, H., Sun, L.: Graphene-based sensors for human health monitoring. *Front. Chem.* 399 (2019)
65. Reilly, R.B., Lee, T.C.: Electrograms (ecg, eeg, emg, eog). *Technol. Health Care* **18**(6), 443–458 (2010)
66. Kabiri Ameri, S., Ho, R., Jang, H., Tao, L., Wang, Y., Wang, L., Schnyer, D.M., Akinwande, D., Lu, N.: Graphene electronic tattoo sensors. *ACS Nano* **11**(8), 7634–7641 (2017)
67. Kireev, D., Ameri, S.K., Nederveld, A., Kampfe, J., Jang, H., Lu, N., Akinwande, D.: Fabrication, characterization and applications of graphene electronic tattoos. *Nat. Protoc.* **16**(5), 2395–2417 (2021)
68. Yogeswaran, N., Hosseini, E.S., Dahiya, R.: Graphene based low voltage field effect transistor coupled with biodegradable piezoelectric material based dynamic pressure sensor. *ACS Appl. Mater. Interfaces.* **12**(48), 54035–54040 (2020)

69. Park, D.W., Schendel, A.A., Mikael, S., Brodnick, S.K., Richner, T.J., Ness, J.P., Hayat, M.R., Atry, F., Frye, S.T., Pashaie, R., Thongpang, S.: Graphene-based carbon-layered electrode array technology for neural imaging and optogenetic applications. *Nat. Commun.* **5**(1), 1–11 (2014)
70. Wykes, R.: The advantages of mapping slow brain potentials using DC-coupled graphene micro-transistors: clinical and translational applications. *Clin. Translat. Med.* **12**(7) (2022)
71. Stebunov, Y.V., Aftenieva, O.A., Arsenin, A.V., Volkov, V.S.: Highly sensitive and selective sensor chips with graphene-oxide linking layer. *ACS Appl. Mater. Interfaces.* **7**(39), 21727–21734 (2015)
72. Ma, Y., Yang, J., Yang, T., Deng, Y., Gu, M., Wang, M., Hu, R., Yang, Y.: Electrochemical detection of C-reactive protein using functionalized iridium nanoparticles/graphene oxide as a tag. *RSC Adv.* **10**(16), 9723–9729 (2020)
73. Mahyari, M., Hooshmand, S.E., Sepahvand, H., Gholami, S., Rezayan, A.H., Zarei, M.A.: Gold nanoparticles anchored onto covalent poly deep eutectic solvent functionalized graphene: an electrochemical aptasensor for the detection of C-reactive protein. *Mater Chem Phys* **269**, 124730 (2021)

# Graphene: A Promising Material for Flexible Electronic Devices



Yogesh Chendake, Harshada Mhetre, Supriya Khatavkar, Vishal Mehtre, Swapnil Namekar, Vikas Kaduskar, and Prashant Chougule

**Abstract** Today, the world is looking for ease of use, application materials, and carrying options. This is extended towards all material and electronic devices. Large applications and requirements are there for ease to use and flexible displays in the computational and telecommunication industry, and considerable work is targeted towards the same. Similarly, if solar cell applications are considered, a flexible solar cell would be elementary to install and use compared to their rigid equivalence. This results in a lookout towards polymeric counterparts for current rigid materials. Though some of these polymeric materials have shown excellent potential, their property tuning needs to be addressed to a greater extent to obtain the desired outcome and properties. These materials need to match the properties and applicability of materials like indium tin oxide (ITO) electrodes, which are weak, get more expensive, and are chemically unstable. As a promising material, graphene stands out due to its unique electrical and mechanical characteristics and excellent optical transmittance. This makes graphene a viable material for flexible transparent conductive electrodes. This has led to graphene's widespread adoption in bendable electrical components like LEDs, PV cells, and field-effect transistors (FETs). However, some limitations must also be addressed for graphene to be used in flexible electronics. This chapter aims to overview graphene applications for energy storage devices, flexible solar cells, integrated circuits, etc. It would also shed light on the methods for overcoming the limitations of graphene to create flexible electronics that are both highly effective and reliable. Finally, the possible future developments will be outlined, providing a lookout towards further research opportunities for flexible electrical devices based on graphene.

---

Y. Chendake

Department of Chemical Engineering, Bharati Vidyapeeth (Deemed to be University) College of Engineering, Pune 411043, India

H. Mhetre (✉) · S. Khatavkar · V. Kaduskar · P. Chougule

Department of Electronics and Communication Engineering, Bharati Vidyapeeth (Deemed to be University) College of Engineering, Pune 411043, India

e-mail: [hvmhetre@bvucoep.edu.in](mailto:hvmhetre@bvucoep.edu.in)

V. Mehtre · S. Namekar

Department of Electrical Engineering, Bharati Vidyapeeth (Deemed to be University) College of Engineering, Pune 411043, India

**Keywords** Graphene · Flexible electronic devices · Energy storage devices · Flexible solar cells · integrated circuits

## 1 Introduction

The development of flexible electronics has indeed been an exciting area of research and development in recent years. The ability to create electronic devices that can bend, twist, and even stretch opens up a wide range of new possibilities for how we use and interact with technology. Flexible electronics are electronic devices that are built on thin, bendable substrates, such as plastic or paper, rather than on rigid materials like silicon. The use of flexible substrates allows for electronics to be made into new form factors, such as wearable devices, roll-up displays, and curved surfaces. These flexible electronics are more comfortable, lighter, and compact than rigid ones [1]. Such devices and their every component, including a base material, must possess a high degree of mechanical toughness upon bending, to make these flexible electronics useful in the real world. Most of the primary parts of today's electronic gadgets are prepared from brittle inorganic materials, incompatible with flexibility. These components should be replaced by pieces made of alternative materials. However, electrical devices made from organic materials hold great promise for the delivery of stretchability or flexibility [2].

Various materials are extensively investigated to obtain the properties required for flexible electronic device formation whilst providing stability and functional properties. During the last decade, graphene has been the most talked about substance in the flexible and wearable technology development field. Extreme tensile strength of over 130 GPa, Young's modulus of roughly 0.5–1 TPa, spring constant of around 1–5 N/m, and the capacity to stretch to many times its original length are only a few of its extraordinary mechanical features result in a material that is perfect for use in wearable and flexible electronics (elasticity) [1–5].

Moreover, graphene's outstanding material features, such as its excellent chemical and thermal resilience [3], a sizeable two-dimensional surface area enabling conformal adherence to other surfaces and materials [6] high spectral width (300–1400 nm) for optical absorption, [7, 8] transparency of 97% or more in the visible spectrum [9], thermo-resistance and piezoelectricity [10], and undoubtedly, this is one of the promising multifunctional substrates for bendable electronics because of its electrical sensitivity towards biochemical. In contrast to other electronic materials, graphene's ultra-ultra-high electronic mobility (15,000–200,000 cm<sup>2</sup>/Vs) stands out as a notable distinction (Vs) [11] caused by ballistic carrier transfer. It has excellent conductivity and ambipolar behaviour similar to commercially available indium tin oxide. Monolayer graphene's resistivity changes when bias voltages are applied due to the ballistic motion of carriers; this material has an extremely high electrical mobility [15,000–200,000 cm<sup>2</sup>/(Vs)]. It indicates the material's ambipolar behaviour, with the charge neutrality point at zerovolts (Fig. 1).



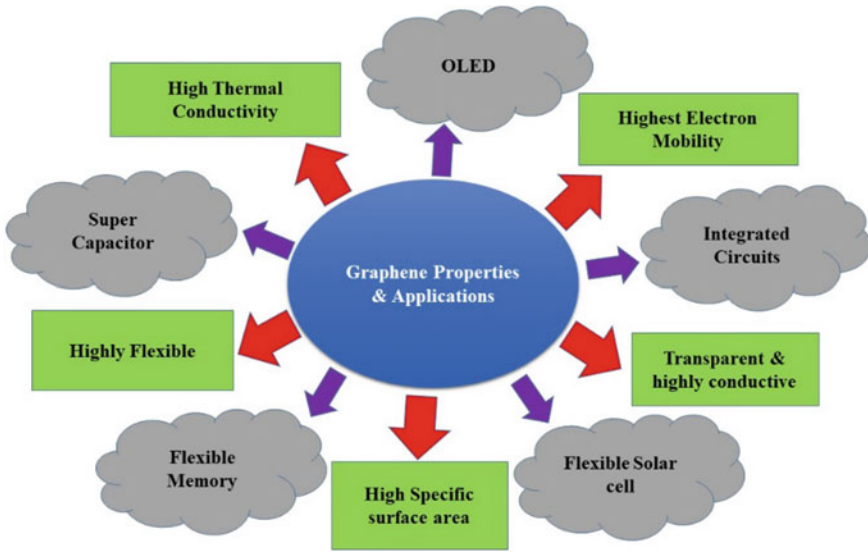


Fig. 1 Graphene as a material for property application correlation

## 2 Use of Graphene in Highly Flexible Electronics

### 2.1 Graphene-Based Supercapacitors

Graphene-based materials have unique characteristics, such as excellent electrical conductivity on a highly-tunable surface, a high resistance to chemical breakdown, and high-quality mechanical behaviour, which make them an attractive candidate for supercapacitors and other energy storage devices. Extensive studies are being conducted to rationalise their structures across several sizes and dimensions. Future research should concentrate on battery life, energy efficiency, and industrial scale at low cost for future use in transportation, wearable electronics, and portable electronics use in transportation, wearable electronics, and portable electronics, battery-powered, and hybrid automobiles. Supercapacitors and ultracapacitors have been widely used due to their high power density, quick charge/discharge speeds, and long cycle life. They have the potential to replace or ultimately replace batteries used in energy storage uses, including wearables and handheld electronics, electric and hybrid automobiles, and so on.

Two graphene-based supercapacitors are primarily electric double-layer capacitors (EDLCs) and pseudo-capacitors. Since the multi-electron redox faradaic processes in EDLCs may be reversed, energy can be stored by moving the faradic charges back and forth between the electrodes. Since the multi-electron redox faradaic processes in EDLCs may be changed, energy can be stored by moving the faradic amounts back and forth between the electrodes.

Higher capacitance and energy density are typical in pseudo-accommodations, but poor electrical conductivity reduces their performance and shortens their lifespans. Because of their exceptional physical, chemical, mechanical, and energy storage electrochemical capabilities, graphene-based materials are becoming increasingly popular. Graphene is a famous mineral with a highly anisotropic structure and behaviour. The electrical and thermal conductivities are one thousand times higher in the in-plane direction than in the out-of-plane order. Several methods exist for preparing graphene, the monolayer of graphite. Energy storage is another common usage for this material.

Graphene-based materials of several dimensionalities, 0D, 1D, 2D, and 3D, have shown materials with great potential for use as electrodes for devices that can store energy electrochemically. However, improvements in the quality and repeatable amount of electrode materials are needed to achieve the desired large-scale practical use. The best structures may be adjusted on any of the length scales from nano to macro. Energy storage performance is affected by the behaviour categorised as physical, mechanical, or chemical of electrode materials based on graphene with varied topologies [12]. To maximise interior area and ionic/electric charge routes and prevent collapse and lack of volume, focussing on the tunable 3D graphene networks inside a porous structure is essential. Deformable and flexible energy storage devices are required to expand flexible electronics rapidly.

When compared to regular capacitors, supercapacitors can discharge enormous amounts of current. Since graphene has a vast interior surface area ( $2630 \text{ m}^2/\text{g}$ ), it is a natural candidate for supercapacitor technologies that rely on this energy storage [13].

Energy is stored in a supercapacitor at the junction of an electrolyte and an electrode material, which might be either liquid or solid. The second layer of ions adsorbs at the electrode during charging to counteract the buildup of electronic charge in the electrode. These characteristics make SCs ideal for use as fast charging and fast discharging battery devices [14]. Electrode materials of SCs benefit from the high conductivity and massive gravimetric surface areas of carbon-based foams, activated carbon, and graphene. The extent to which an SC may boost an electric car's top speed depends on its particular power. However, the distance it can go on a single charge depends on its specific energy.

Most research into the electrode performance of supercapacitors has focussed on graphene, metal oxides, non-native elements, and carbon nanotubes. KOH, NaOH, and  $\text{H}_2\text{SO}_4$  are examples of liquid or gel-like electrolytes employed to conduct the analysis. Researchers found that particular capacitance at the GA/TiO<sub>2</sub> electrode was relatively high in simulated water that contains dissolved salts (0.1 M NaCl solution), values from fifty to one hundred fifty faraday grammes<sup>-1</sup> over a broad spectrum of scanning velocities (between 5 and 1000 mV/s). Most research into the electrode performance of supercapacitors has focussed on graphene, metal oxides, non-native elements, and carbon nanotubes. KOH, NaOH, and  $\text{H}_2\text{SO}_4$  are examples of liquid or gel-like electrolytes employed to conduct the analysis [15].

Because of its enormous surface area, graphene is commonly employed in batteries, and supercapacitors are examples of devices that can store energy for

later use. For this study, pillared graphene was produced @ 750 degrees on 20 m of copper foil using the chemical vapour deposition technique employing ethylene and hydrogen gas as carbon sources. Li-ion batteries with an anode made from synthetic graphene showed enhanced cycling stability of over 250 cycles [16].

As an alternative to batteries, supercapacitors might be manufactured in vast quantities. Electrode preparation relies heavily on nano-structured materials, which are pivotal in improving the device's electrochemical characteristics. A viable method to enhance a few electrons in host systems by harmonising the behaviour of electron donors and acceptors includes hetero-atoms (N, B, or F), either surface- or bulk-level of reduced graphene oxide (RGO). Consequently, reduced graphene oxide that has been N-doped (RGO) may be helpful as a supercapacitor. The supplementary materials included material characterisation methods, electrode preparation, and device construction [17].

The results of the (XPS) X-ray photoelectron spectroscopy experiment demonstrate narrow spectra of C1s and O1s (at 284.3 eV) (399.37 eV) and N1s (at 396.37 eV). In addition, the outcomes of GCD cycling and voltage holding tests conducted on the SSC device for 16 h are provided. Self-discharge charts confirm GCD cycle findings for stability.

The unusual substance graphene and composites made from it have shown significant growth in several manufacturing sectors. The areas of catalysis, energy storage, electrode batteries, and biomedicine have recently attracted researchers' attention. Graphene's adaptability has made it a top choice amongst researchers developing new methods for storing and transporting energy. Graphene is an excellent sustaining electrical materials medium to lessen the powered stress brought on by volumetric fluctuations whilst the cycle is running. Substances that are actively engaged also carry electricity more efficiently. Supercapacitors and batteries made of lithium-ion and sodium-ion are covered in depth, as is the use of graphene composites in each. Some of the applications have increased the combined hybrid graphene capacitor-battery storage system to enhance charge density by 3–10 times (up to 6,00,000 mAh), with fast charging (charge time less than 10 min) and a high number of cycles 1,00,00 cycles against 10,000 compared to conventional supercapacitor or battery storage system [17].

Since the encased and injected hetero-atoms increase the density of active spots in graphene's structure, graphene-doped composites play a more critical role in integrating functional elements to store energy. The SIB anode is a hybrid structure made of graphene-containing alloy. Red phosphorous nanoparticles are dispersed evenly in a 3D graphene lattice using a vapour-repellent distribution method. Metal-air batteries and metal-O<sub>2</sub> batteries are two further applications for graphene alloys. Aerosols modified with ruthenium (Ru) particles are employed directly as the cathode material for Li-O<sub>2</sub> batteries (lithium superoxide), which boosts their effectiveness to 12,000 mAhg<sup>-1</sup> [18]. Cathode improvements over Se are achieved using a composite aerogel made of 3D graphene CNTs and Se. Electrolyte infiltration and gas diffusion were aided by the composite's hierarchical porous structure, whilst the 3D consistency of the structures enhanced electron transmission. Numerous businesses use graphene and graphene composites, such as those that produce energy storage

devices like batteries, fuel cells, and supercapacitors. Graphene may be used as an electrode, leading to a vast infrastructure of energy storage devices. This means graphene may be useful in enhancing device reliability, capacity, efficiency, and rate performance for storing energy.

The fast charging and discharging, excellent power density, extended cycle life, and safe operating conditions of supercapacitors (electrochemical capacitors) have garnered considerable interest. Graphene aggregates because of the high-interaction between sheets, resulting in a substantially lower specific extent of the surface ( $13.4\text{--}35.8\text{ m}^2\text{g}^{-1}$ ) than theoretically expected [19]. Researchers are working on creating pseudo-capacitive active materials/graphene hybrid fibres and surface-porous graphene fibres.

### **Holey Graphene-Based Materials for Supercapacitors**

Conductive skeletons in holey graphene serve as pathways for electron transport, whilst many mesopores facilitate the long-distance movement of ions. This design guarantees high-rate and high-capacity energy storage by efficiently delivering charges over a thick electrode and making the most of electrode use. Because of its large surface area and high ionic penetrability, holey graphene is an appealing gigbet for dynamic materials with high mass loading.

Large surface areas and active sites in holey graphene-based nano-materials may boost electrochemical processes and, in turn, energy density. Additionally, even in a severely compressed shape, the pores formed in graphene sheets offer adequate cross-plane pathways for ionic transport. That is because it would boost ion kinetics and energy density in volume [20] (Table 1).

## ***2.2 Graphene Used in Fuel Cell (FCs)***

When it comes to storing energy and generation, graphene has enormous potential uses in energy storage devices, including batteries, supercapacitors, and solar panels. Graphene is often used as catalyst support on the fuel cell membrane, notably PEM fuel cells. Dye sensitizers and nitrogen-coordinated metal catalysts are additionally used in fuel cells. Several alternatives to platinum catalysts are cheaper and widely used in various industrial applications such as Palladium (Pd) Catalysts, Rhodium (Rh) Catalysts, Nickel (Ni) Catalysts, and Cobalt (Co) Catalysts. Graphene serves primarily two functions: (i) reducing the catalytic loading of Pt and Pt alloy and (ii) increasing the stability of the catalyst. Fuel cells' anode and cathode catalyst loadings have been reported to be lowered in several ways, with several strategies being proposed to replace the Pt catalyst with less expensive alternatives [4].

Graphene's application in Pt catalysts has boosted activity by enhancing electrical conductivity and Pt dispersion. Additionally, Ni, those most often mentioned in the non-precious catalyst used in the anode of low-temperature fuel cells, including fuel

**Table 1** Comparison of graphene materials used in supercapacitors

Material	Electrolyte	Capacitance value	References
Holey graphene	6 M KOH	102 F/g at 0.1 A/g	[21]
Holey graphene	6 M KOH	698 mF/cm <sup>2</sup> at 2 mA/cm <sup>2</sup>	[22]
Holey graphene	6 M KOH	295 F/g at 1 A/g	[23]
Holey graphene film	EMIMBF <sub>4</sub> /aceto-nitrile	298 F/g at 1 A/g	[24]
Holey graphene film	6 M KOH	216 F/cm <sup>3</sup> at 1 A/g	[25]
Holey graphene film	PVA-H <sub>2</sub> SO <sub>4</sub>	56 mF/cm <sup>2</sup> at 0.1 mA/cm <sup>2</sup> (cell)	[26]
Holey graphene film	EMI: TFSI	53 F/cm <sup>3</sup> at 3 A/g (cell)	[27]
Holey graphene film	TEABF <sub>4</sub> with aceto-nitrile	45 F/g at 0.25 A/g (cell)	[28]
Porous holey graphene film	PVA-H <sub>2</sub> SO <sub>4</sub>	304 F/g at 0.1 mA/cm	[29]
CNT/holey graphene film	0.5M H <sub>2</sub> SO <sub>4</sub>	268 F/g at 0.25 A/g	[30]
Holey graphene oxide	6 M KOH	240 F/g at 1 A/g	[31]
r-holey graphene oxide	6 M KOH	224 F/g at 1 A/g	[32]
r-holey graphene oxide film	20 mM [Fe(CN) <sub>6</sub> ] <sup>3-/4-</sup> in 1 M Na <sub>2</sub> SO <sub>4</sub>	31.1 mF/cm <sup>2</sup> at 1 mA/cm <sup>2</sup>	[33]
Holey graphene nanosheets	BMP-DCA	330 F/g <sup>1</sup> at 0.2 mA	[34]
Holey graphene aerogel	6 M KOH	178 F/g at 0.2 A/g	[35]
N-doped holey grapheme	6 M KOH	439 F/cm at 0.1 A/g	[36]
N-doped holey graphene	2 M H <sub>2</sub> SO <sub>4</sub>	343 F/g at 0.3 A/g	[37]
N-holey graphene aerogel	6 M KOH	318 F/g at 0.5 A/g	[38]
S-doped holey grapheme	1 M Na <sub>2</sub> SO <sub>4</sub>	257 F/g at 0.25 A/g	[39]
N,F-holey graphene hydrogel	6 M KOH	345.4 F/g at 1 A/g	[40]
N,S,P-holey graphene	2 M KOH	295 F/g at 1 A/g	[41]
N-C/holey graphene	6 M KOH	316 F/g at 1 A/g	[42]
CNTs/holey graphene	6 M KOH	557 F/g at 0.5 A/g	[30]
C sphere/holey graphene film	6 M KOH	207 F/g at 1 A/g	[43]
MnO <sub>2</sub> /holey graphene aerogel	1 M Na <sub>2</sub> SO <sub>4</sub>	192.2 F/g at 0.5 A/g	[44]
MnO <sub>2</sub> nanorods/holey graphene	1 M Na <sub>2</sub> SO <sub>4</sub>	117 F/g at 5 mV/s	[45]

(continued)

**Table 1** (continued)

Material	Electrolyte	Capacitance value	References
Fe <sub>3</sub> O <sub>4</sub> /holey graphene	PVA-H <sub>2</sub> SO <sub>4</sub>	63.5 F/g at 1 A/g (cell)	[46]
MoO <sub>2</sub> /holey graphene aerogel	1 M KOH	473 F/g at 10 mV/s	[47]
RuO <sub>2</sub> /holey graphene/CNTs nanofiber	1 M H <sub>2</sub> SO <sub>4</sub>	199 F cm <sup>-3</sup> at 2 mV/s	[48]
r-Holey graphene oxide/NiCo <sub>2</sub> O <sub>4</sub> @CF	3 M KOH	1178 F/g at 1 A/g	[49]
MoS <sub>2</sub> /holey graphene/C fibres	1 M H <sub>2</sub> SO <sub>4</sub>	421 F/g at 5 mV/s	[50]
NiCo <sub>2</sub> S <sub>4</sub> /holey graphene	3 M KOH	1000 F/g at 0.5 A/g	[51]
N-hole graphene /PANI	1 M H <sub>2</sub> SO <sub>4</sub>	1058 F/g at 0.5 A/g	[52]
N-r-hole graphene oxide/PANI	1 M H <sub>2</sub> SO <sub>4</sub>	746 F/g at 1 A/g	[53]
r-hole graphene oxide-PPD	1 M H <sub>2</sub> SO <sub>4</sub>	375.5 F/g at 0.5 A/g	[54]
Holey graphene/G-caffeic acid	3 M H <sub>2</sub> SO <sub>4</sub>	389 F/g at 1 A/g	[55]
Mxene/holey graphene film	3 M H <sub>2</sub> SO <sub>4</sub>	1445 F/cm <sup>2</sup> at 2 mV/s <sup>2</sup>	[56]

cells using methanol, ethanol, or urea, is supported on graphene. Pt's activity rose after being combined with graphene, and it rose even more after being doped with boron [4].

## Graphene in Green Energy Research

Graphene nanostructure and its material loading can be easily enhanced and optimised by its physico-chemical modification by a suitable method. This provides new arenas for its property optimisation for applicability in fuel cells and other applications as an electro-catalyst. Developing electro-catalytic fuel cells and batteries is a very active research field in green energy. These fuel cells reduce reliance on nonrenewable fossil fuels by producing electricity via the electrochemical oxidation of renewable alcoholic fuels such as methanol, ethanol, and glucose. 2D and 3D graphene-based electro-catalysts are considered distinct subsets of the graphene-based electro-catalyst field.

## Direct Alcohol Fuel Cells

Graphene-based catalysts demonstrated much higher electrochemical activity than commercial Pt/C, Pt/carbon black, or pure Pt catalysts; they work better during half-cell electro-oxidation. Because of this, the most excellent anodic sweep current density (Jf) has been achieved at 2540 A/g (unit mass) or 30 mA cm<sup>2</sup> (unit area), with exceptional tolerance against CO as high as 6.6%. To prevent carbon monoxide (CO) poisoning during the methanol oxidation reaction (MOR) and the ethanol electro-oxidation process, these graphene-based electro-catalysts may be used instead of conventional, non-platinum monometallic, or bimetallic catalysts (EOR). Electro-catalysts based on two-dimensional graphene doped with metals (M/rGO) or a graphene aerogel doped with metals (M/GA) showed significantly increased activity of oxidation reaction (highest possible Jf: 15.59 mA cm<sup>-2</sup>, or 105.98 mA mg<sup>-1</sup>) and glucose oxidation reaction (GOR) than platinum-based and non-platinum-based catalysts [15]. The structure of graphene nanosheets is destroyed, however, by this method. In the case of three-dimensional graphene nanostructures, this is strikingly clear. Graphene electrodes that do not need binders have several advantages over their more conventional counterparts.

When stacked or linked, graphene nanosheets provide a conductive solid and sturdy network that may be used to reinforce electrodes. Considering a large amount of available surface area, the electrolyte can make good contact with the electrode interface, lowering the diffusion resistance. A binder-free pure GA/NF could synthesise the exact chemical pathway and create a supercapacitor electrode. One hundred fifty cycles were maintained. There was remarkable consistency between the 100–500 cycle range spanning 1456 cycles in the enlarged EOR and 1248 cycles in the extended GOR. [15] Higher power and current density were achieved compared to conventional direct ethanol fuel cells (DEFCs) and direct glucose fuel cells (DGFCs) systems that do not use graphene catalysts.

## 2.3 Oxygen Reduction Reactions (ORR) for Metal Batteries

Both acidic (HClO<sub>4</sub> and H<sub>2</sub>SO<sub>4</sub>) and primary (NaOH, KOH) environments were used to investigate the activity of graphene-based compounds. These catalysts maintained a constant activity rate in the oxygen reduction reaction (ORR), significantly increasing output current density. Also, compared to conventional Pt/C cathodes, the findings demonstrated that tolerance for methanol at the cathode was surprisingly high in ORR catalysts based on graphene.

## Lithium–Ion and Lithium–Ion Metal Batteries

Graphene has many potential applications in the field of energy storage and conversion due to its unique combination of excellent mechanical, electrical, and thermal

properties. It is been hypothesised that its large specific surface area accounts for its strong conductivity to electricity. As a result, it aids in charge transfer in lithium-ion (LIB) and Li-air (Li-air) batteries. The most reliable anodic substance for LIBs was an active grapheme. With a discharge activity of two to three times that of pure graphene aero gel and a current density of  $500 \text{ mAhg}^{-1}$ , its discharge-specific capacity can be kept steady for 400 cycles. In addition, the  $\text{Nb}_2\text{O}_5/\text{HGF}$  and N-doped graphene aerogel (GA) anodes do not need a binder or conductive additives to be built into conventional CR2016 and CR2025 coin cells for electrochemical research [15]. So, the ability of graphene products to be used as anodic materials was a crucial signal for device-scale LIBs of how they could be used. Bulk cylinder-shaped 3D GAs products fit into standard coin cells without extra work.

The lithium-ion battery is anticipated to have an energy density per unit volume of more than  $700 \text{ W-h}$  [57]. Regrettably, it is still inadequate to meet the rising need for space anxiety and rapidly emerging electric gadgets. Materials with a high cathode and anode capacity are the most straightforward technique to boost volumetric energy density. High-capacity anodes for storing  $\text{Li}^+$ , such as those made of Si, Sn, and P, through alloying processes may give much greater theoretical capacity for volume and gravity.

Because they have a high energy density and operating voltage, apricot lithium-ion batteries (LIBs) have grown to be amongst the most extensively used commercial sources of electricity for a wide range of portable electronic items. Flexible, highly conductive, tensile, and structurally-tunable graphenes are only one kind of conductive fibre that has shown promise in the fibre-shaped LIB. The anode was constructed of  $\text{SnO}_2$  quantum dots@ rGO fibre, whilst the cathode was composed of  $\text{LiCoO}_2$  nano particles@ rGO fibre, which has a flexible structure. This LIB was presented by one of the researchers and is based on GF. After being bent, knotted, and subjected to 5 different healing methods, the LIB maintained its remarkable flexibility, cyclic stability, and excellent retention capability ( $82.6 \text{ mAhg}^{-1}$ ) [19] (Table 2).

## 2.4 GF-Based Electric Double-Layer Capacitors (ELDCs)

Graphene fibres (GF) are commonly used as electrodes in electric double-layer capacitors (EDLCs). There is a plethora of methods for expanding GFs' particular surface area. For instance, a 3D porous graphene framework may be deposited on top of the GF fibres to create an all-graphene core-shell graphene fibre. This would significantly enhance their electrochemical performance. Incorporating holey graphene with graphene can dramatically raise GF's inherent capacitance to  $220.1 \text{ Fcm}^{-3}$ , which is 2.9 times more than unadulterated GF. The electrochemical performance was enhanced in core-shell GFs made from carbonised phenol formaldehyde and small-size graphene. The surface area and other properties can be modified by suitable fabrication and formation enhancements. The micro-fluidic spinning technique controls the GFs' structure and creates porous GFs [82]. Nitrogen-doped porous



**Table 2** Comparison of graphene materials used in LIBs

Material	Reversible capacity	Rate capacity	Cycling performance	References
sr-holey graphene oxide	430 mAh/g for 50 mA/g	100 mAh/g for 2 A/g	–	[58]
Holey graphene	423 mAh/g for 0.1 A/g	85 mAhg <sup>-1</sup> for 0.4 A/g	400 mAh/g for 0.1 A/g at 100 cycles	[59]
Stacked holey graphene	889 mAh/g for 0.05 C	200 mAh/g for 5 C	672 mAh/g for 0.5 C at 70 cycles	[60]
Holey graphene paper	403 mAh/g for 0.14 C	178 mAh/g for 5.4 C	250 mAh/g for 0.67 C at 400 cycles	[61]
3D holey graphene framework	1,174 mAh/g for 0.2 A/g	800 mAh/g for 5 A/g	5 mAh/cm <sup>2</sup> for 8 mA/cm <sup>2</sup> at 2000 cycles	[62]
N-holey graphene	989.5 mAh/g for 0.1 A/g	310 mAh/g for 5 A/g	553.5 mAh/g for 5 A/g at 6000 cycles	[63]
N-r-holey graphene oxide	1,354 mAh/g for 0.2 A/g	570 mAh/g for 5 A/g	800 mA/g for 3 A/g at 1,500 cycles	[64]
N-holey graphene monolith	1,052 mAh/cm <sup>3</sup> for 0.1 mA/cm <sup>2</sup>	808 mAh/cm <sup>3</sup> for 3.2 mA/cm <sup>2</sup>	800 mAh/cm <sup>3</sup> for 0.1 mA/cm <sup>2</sup> at 1,200 cycles	[65]
N-holey graphene foam	1194 mAh/g for 0.25 C	420 mAh/g for 5 C	450 mAh/g for 5 C at 1,000 cycles	[66]
N-holey graphene hollow sphere	1,563 mAh/g for 0.5 C	254 mAh/g for 20 C	1,643 mAh/g for 100 mA/g	[67]
Fe <sub>2</sub> O <sub>3</sub> -nano-particle/holey graphene	1692 mAh/g for 50 mA/g	555 mAh/g for 1 A/g	883 mAh/g at 1 A/g at 1000 cycles	[68]
H-Fe <sub>2</sub> O <sub>3</sub> /holey graphene oxide	1,473 mAh/g for 0.2 A/g	487 mAh/g for 30 A/g	990 mAh/g for 5 A/g at 1,600 cycles	[69]
g-Fe <sub>2</sub> O <sub>3</sub> /r-holey graphene oxide	680 mAh/g for 0.1 A/g	530 mAh/g for 2 A/g	1141 mAh/g for 0.5 A/g at 230 cycles	[70]
Fe <sub>2</sub> O <sub>3</sub> -nanorods/holey graphene fluoride	1050 mAh/g for 0.1 A/g	473.5 mAh/g for 4 A/g	805.6 mAh/g for 1 A/g at 500 cycles	[71]
Fe <sub>3</sub> O <sub>4</sub> /holey graphene	1516 mAh/g for 0.2 A/g	761 mAh/g for 5 A/g	554 mAh/g for 5 A/g at 2,500 cycles	[72]

(continued)

**Table 2** (continued)

Material	Reversible capacity	Rate capacity	Cycling performance	References
MnO/holey graphene aerogel	876 mAh/g for 0.05 A/g	493.6 mAh/g for 2 A/g	979.6 mAh/g for 0.5 A/g at 300 cycles	[73]
MoO <sub>2</sub> nano-dots/holey grapheme	1021 mAh/g for 0.2 A/g	425 mAh/g for 5 A g <sup>-1</sup>	750 mAh/g for 1 A/g at 450 cycles	[74]
NiO/holey graphene	940 mAh/g for 0.1 A/g	228 mAh/g for 10 A/g	722 mAh/g for 0.2 A/g at 200 cycles	[75]
Co <sub>3</sub> O <sub>4</sub> /holey graphene	1,543 mAh/g for 0.15 A/g	1,075 mAh/g for 1 A/g	760 mAh/g for 1 A/g at 100 cycles	[76]
SnO <sub>2</sub> /holey graphene	1001 mAh/g for 0.5 A/g	792 mAh/g for 2 A/g	570 mAh/g for 2 A/g at 2,000 cycles	[77]
3D SnO <sub>2</sub> /holey graphene	1220 mAh/g for 0.02 A/g	850 mAh/g for 2 A/g	791 mAh/g for 0.5 A/g at 400 cycles	[78]
MoS <sub>2</sub> /holey graphene	240 mAh/g for 0.1 A/g	140 mAh/g for 1 A/g	–	[79]
LiFePO <sub>4</sub> /holey graphene	156 mAh/g for 0.1 C	59 mAh/g for 5 C	128 mAh/g at 1 C at 50 cycles	[80]
Li <sub>4</sub> Ti <sub>5</sub> O <sub>12</sub> /holey graphene	161 mAh/cm <sup>3</sup> for 0.035 A/g	103 mAh/cm <sup>3</sup> for 14 A/g	102 mAh/cm <sup>3</sup> at 7 A/g at 1,000 cycles	[81]

GFs supercapacitors (NMGFs) may be woven into textiles and worn to store electricity for use with other electrical gadgets on the go. By intercalating carbon black into graphene sheets and then spinning the resultant material, it is feasible to make absorbent graphene fibres. Hybrid fibres made of nitrogen-doped graphene (N-RGO) and carbon nanotubes (CNTs) have been manufactured by certain researchers using a hydrothermal process [19]. All these efforts have resulted in the enhanced surface and its related power density.

### GF-Based Pseudo-Capacitors

Several initiatives have been made to enhance energy storage capacity and other features of hybrid fibres by incorporating pseudo-capacitive materials with graphene during fabrication; e.g. GFs' specific capacitance increased from 24.0 to 314.5 mFcm<sup>-2</sup> by grafting graphene onto the existing structure. The high energy density (7.93 Wh/cm<sup>2</sup>, 5.7 mWhcm<sup>3</sup>) and ultra-long cycle life were shown by the core-shell polyaniline nanorods/graphene hybrid fibre (GF@PANI). The maximum energy density of the GF/MoS<sub>2</sub> hybrid fibre supercapacitor was 14.665 μWhcm<sup>2</sup>

(6.5 mWhcm<sup>-3</sup>) [19]. Electrochemically, the GF tungsten nitride core-shell demonstrated improvement over GF, with higher specific capacitance and energy density.

### Graphene Oxide Reduction for Energy Storage

An innovative porous hierarchical anode structure was created in three dimensions. According to reports, lithium-ion batteries' energy and power density are pretty high. The capacitive Li | Na ion storage architecture was established by producing CO<sub>3</sub>O<sub>4</sub> nano-pore arrays from Co(OH)<sub>2</sub> nanosheet. With a loss of just 6%, the composite electrode demonstrated exceptional rate efficiency (1490–1399 mAhg<sup>-1</sup> at 0.1–2 Ag<sup>-1</sup>). Graphite is chemically treated to induce exfoliation into GO sheets, as shown by XPS data, as a result of being surrounded by various carbon and O<sub>2</sub> functional groups. It was found that the GO sample had two significant peaks, each of which could be further functional groupings converged into four distinct peaks containing carbon and oxygen. As the laser intensity increased, the carbon-to-oxygen ratio dropped from 3.85 at 80% to 6.50 at 100%, suggesting photothermal ruffling of the GO sheets or a higher spot temperature. Oxygen levels would inevitably drop [83].

## 2.5 Graphene in Flexible Solar Cells

A solar cell is a solar cell that uses electrochemistry to convert energy directly into usable hole-and-electron pairings. Subsequently, these ionised particles may be effectively isolated and flushed away using electrodes at the device's ends. One problem that requires fixing is that photoactive materials need very transparent and conductive electrodes that are also chemically stable. Other topics include the function of the electrode, the incorporation of a highly effective electron/hole-blocking layer, and others. Recent years have seen a surge in the use of flexible solar cells, which emerged as a bright spot for PV technology benefits because of their superiority to rigid solar cells, such as their light weight, resistance to complex deformations, ability to be incorporated into rounded areas, compatibility with production in a continuous rolling process, and ease of transport and storage [84]. Flexible solar cells offer intriguing uses in various new domains; conformal solar cells have several applications, including powering portable or wearable devices, synthetic skin, and architectural integration [85]. Hence, primary research is targeted towards the definition of alternative material for these applications. Graphene is one of the leading contenders in this case due to its many favourable properties.

Graphene may readily find a home in any electrical system that requires electrodes with high conductivity, transparency, and exceptional flexibility. This is because graphene possesses all of these desirable characteristics. For this apparent reason, graphene was a viable candidate to incorporate as a TCE in solar cell systems. Graphene, a material having a single-layer atomic structure, is the world's most

lightweight, thin, complex, and flexible material. Due to superior thermal and electrical characteristics, electrons flow more freely than silicon. Graphene is flexible and can be used in various settings, including ecologically friendly installations. This has resulted in its applications in energy storage systems. Economic and industrial development systems have resulted in the production of many graphene energy storages and conversion devices. They play a crucial role in developing flexing, folding, and stretching machinery to fabricate battery, fuel cell, supercapacitor, and nanogenerator components [86].

Flexible graphene, graphene foam, graphene fibre, and graphene paper are the four main types of graphene, and they each have their applications. Due to its flexibility and foldability, mobile devices are an ideal use case for flexible graphene paper. The graphene film is used when higher strength is required as it is thicker than graphene paper by a certain amount. Graphene foam has average qualities that may be enhanced because of the flexibility and improved form provided by the graphene fibres. Also, it is simple to set up [87].

Whilst various thin-film photovoltaic devices and amorphous silicon solar cells have been made malleable, their bending radius is inadequate and too pricey. To achieve this, new types of solar cells, such as organic solar cells (OSCs) [85], dye-sensitised solar cells (DSCs) [88], and perovskite solar cells (PSCs) [89], have proven to be reasonably attractive due to their fabrications at low temperatures (below 150 °C), thin layers, and tuneable colours [84].

## 2.6 *Some Important Properties of Graphene*

1. Graphene/carbon nano-nano-thiophene devices offer superior bending stability and PCE than ITO devices. Graphene is an effective environmental barrier that blocks oxygen, hydrogen, and water vapour in photovoltaic systems. In graphene, the space between layers is typically 0.54 nm, making air and water impermeable. It may generate optoelectrodes (OPVs) without packaging, increasing flexibility, and reducing cost [90].
2. Graphene is carbon-rich and mechanically resilient, making it the ideal PSC electrode material. Graphene has more excellent morphology and transparency than SWNTs; hence, it provides higher PCE in inverted PSCs [91].
3. Electrodes for organic solar cells made from graphene have low sheet resistance, excellent transparency, with high surface roughness [92].
4. GQDs can potentially lessen the number of interface trap states whilst simultaneously improving the quality and stability of PSCs [93].
5. Graphene is a potentially transparent and flexible electrode material [2].
6. The properties of graphene sheets include flexibility and transmit light consistently (Tr) through high chemical stability and a large optical window [85].
7. The electrical industry has shown a lot of enthusiasm for three-dimensional graphene-based materials, semiconductors, and the energy storage sectors

because of graphene's unique features, such as its large specific surface area, low density, excellent mechanical properties, and electrical conductivity [94].

8. The graphene electrode has more excellent physical and thermal stability than the ITO electrode, extending the device's lifetime and photo conversion efficiency [9].
9. Graphene-based solar cells are low-cost, high-performing, and stable compared to ITO-based ones [95].

### Flexible Organic Solar Cell

Researchers from HPU and MRCC in China are developing flexible organic solar cells utilising graphene for applications in wearable electronics devices and synthetic skin. Graphene/carbon nano-nano-thiophene devices offer superior bending stability and PCE than ITO devices. The graphene electrodes have a maximum PCE of 2.7%, compared to P<sub>3</sub>HT: PCBM and ITO electrodes at 4.5%. Low O<sub>2</sub> permeability makes polystyrene-graphene nanocomposites good packaging—bottom-doped graphene using PEDOT: PSS and Au, top with PMMA. It is an effective environmental barrier to block water vapour, hydrogen, helium, and oxygen in photovoltaic systems. The typical space between two graphene layers is 0.54 nm, making air and water impenetrable. It may generate optoelectrodes (OPVs) without packaging, increasing flexibility, and reducing cost [90].

Exfoliated graphene is the basis for a bendable organic solar cell nano anode which has a 4.23% conversion efficiency. Transparency, roughness, and low sheet resistance characterise graphene-based organic solar cell electrodes. According to researchers at Wuhan University in China, this is the first solution-processed transparent EG electrode. The graphite sheets were centrifuged twice at 6000 rpm to remove re-stacking grains and aggregates, to obtain graphene nanosheets with 1–3 layers. The graphene flake thickness is 0.80 nm. It possesses large potential applications in flexible and elastic electrical applications [85, 92]

Organic solar cells (OSCs) have surpassed 16% PCE by developing a substance that can store and release electrical charges. Flexible OSCs performance is still lower compared to stiff OSCs. In this context, plastic substrates are high-temperature annealing-sensitive, affecting solar panels' operation and outcome. Integrating polyimide (PI) into graphene creates a flexible, resilient, and thermally stable electrode. The graphene electrode modified with phosphorus iodide has a spotless exterior, 92% optical transmittance, and stable temperature. Direct incorporation of PI increased graphene electrode durability by preventing delamination under stress. An OSC with a PCE of 15.2% was realised using a PI-aided graphene electrode. The suggested electrode offers excellent efficiency and versatility for optoelectronic devices [96].

## Perovskite Solar Cell

CNTs and graphene are carbon-rich and mechanically resilient, making them ideal PSC electrode materials. Therefore, CNT and graphene sheets were evaluated as PSC electrode materials. Graphene has more excellent morphology and transparency than SWNTs; hence, it provides higher PCE in inverted PSCs. Thicker MoO<sub>3</sub> layers reduce solar cells' current density in a short circuit and fill factor. With increased MoO deposition thickness, the fermi level also increased, and photoelectron spectra were indicated. For AM 1.5G's artificial sunlight, in comparison with MoO-based PSCs, graphene-based PSCs demonstrated more excellent performance. HNO<sub>3</sub>-doped SWNT-based PSCs had a power conversion efficiency (PCE) of 15.3%, much more significant than MoO-coated SWNT films. SWNT sheets are rougher than graphene and ITO. AFM pictures confirm these results. SWNT sheets were significantly rougher than graphene films ( $R_a = 15.1$  nm). SWNT-based PSCs had more excellent repeatability when the transfer procedure was considered. Due to its entangled geometry, SWNT films were dry-transferrable and did not crumple. We tested the carbon electrodes' sheet resistance ( $R_{sheet}$ ) 100 times. SWNT films, a network of nanotubes, require more significant stretching to bend and distort [91].

Planar perovskite solar cells (PSCs) that are regulated by I-GQDs attain efficiency at 22.37% which is relatively high whilst maintaining stability over the long term. The graphene quantum dots functionalized with imidazole bromide regulate the ETL/formamidinium lead iodide interface (FAPbI<sub>3</sub>). As a result, GQDs have the potential to enhance the quality and stability of PSCs whilst simultaneously reducing the amount of interface trap states. Perovskite solar cells, often known as PSCs, are now in the lead in the competition to develop the next generation of photovoltaic technology. The currently available PSCs still have problems with the device's stability, which will significantly influence the commercialisation of these products [93].

Through coupling, optical transmittance was increased to 69% by using transparent graphene electrodes coated with organic polymers at 550 nm. Graphene has no polymer residue since just one transfer is necessary to create a monolayer. Compared to devices using ITO electrodes, gra-neutrino electrodes can withstand higher bending stress. The transfer method is substrate-agnostic and may be used on any flat surface. Physics research has demonstrated that graphene electrodes can bend superior to their ITO and PEN counterparts, making them ideal for use in flexible electronics. The crucial radius for ITO/Gr devices is least flexible at 2.0 mm and most flexible at 0.7 mm for Gr/Gr devices [97].

Organic semiconductors can be used to make low-temperature planar heterojunction perovskite solar cells. However, forming mesoporous TiO<sub>2</sub> at high temperatures is incompatible with flexible polymer substrates. Graphene is a potentially transparent and flexible electrode material. Gr-Mo/PEN photovoltaic characteristics were compared to PEDOT: PSS and graphene. Scientists have shown the potential flexibility using graphene-based perovskite solar cells. Following one thousand 2-mm-radius bending cycles, graphene electrodes preserved 49% of their initial PCEs. This is the first study to show steady functioning after tens of thousands of bending cycles [2].

In South Korea, scientists have developed perovskite solar cells that efficiently convert energy to usable form (PCE) of 18.9% for a stationary gadget and 18.3% for a mobile, flexible one. The voltage at the open circuit of 1.01 and 1.02 V for the novel perovskite solar cells based on the gamma-ray emitting transition metal dichalcogenide (GR TCE) with efficiencies of 12.8 and 13.8%, respectively, has been achieved (PCE). Perovskite solar cells doped with TFSA had improved performance from 300 to 850 nm. Researchers at Savitribai Phule Pune University said that they reached the high  $J_{sc}$  value by limiting light loss in GR TCE boosted with TFSA/PDMS-based FAPbI photovoltaic devices based on perovskite. Researchers at the University of Illinois at Urbana-Champaign suggest solar cells made on perovskite based on graphene TCE might power sophisticated gadgets and wearable electronic/photonic appliances [98].

Flexible C-PSCs were created by Jin and colleagues using a low-cost SnO<sub>2</sub> ETL that operates at room temperature and a transparent graphene-AgNWs/PET composite electrode. When graphene-AgNWs were sprayed over a polyethylene terephthalate sheet, they generated a thin and bendable electrode. Power conversion efficiency was maintained at 89% for the flexible C-PSCs, even after 1000 bending cycles at a 10 mm radius. Perovskite solar cells (C-PSCs) based on a carbon electrode and without a hole transport layer are a reasonable option because of their inexpensive cost, simplicity of manufacture, and long lifespan. Preparing these solar cells on flexible substrates at low temperatures is difficult, though. Polyethylene terephthalate (PET)/graphene-silver nanowires (graphene-AgNWs)/sn-oxide (SnO<sub>2</sub>)/chlorotrimethylp-biphenyl (carbon (C)/CH<sub>3</sub>NH<sub>3</sub>PbI<sub>3</sub>) electrodes are used to produce all flexible carbon-based C-PSCs effectively. When production circumstances are optimised, the efficiency of these flexible C-PSCs may reach 9.73%, the greatest of any such device. Compared to ITO/PET devices, the mechanical toughness of these bendable devices is far higher, and they offer exceptional long-term durability. The paper presents a simple method for producing high-efficiency and long-lasting perovskite solar cells at a cheap cost [89].

### Solar Cells with Schottky Junctions

Schottky connections form by connecting metal and doped semiconductors. Graphene-based solar cells are low-cost, high-performing, and stable compared to ITO-based ones. Graphene/n-type semi-crystal heterojunction is a Schottky solar cell. Due to the graphene-semiconductor work function discrepancy, a pre-installed potential occurs near the contact. Graphene-on-silicon, Feng et al. showed that doping Schottky junction solar cells with HNO and SOCl can enhance them. Au and graphene can be used to generate different device topologies. Zhang et al. also made as-fabricated Schottky junction solar cells. Thanks to developments like graphene/NW (NB) solar cells, graphene/silicon solar cells, and Schottky solar cells, high-efficiency and low-cost energy sources are within reach [95].

## Flexible Heterojunction Solar Cells

Aberystwyth University researchers have developed low-priced, high-performance, and adaptable heterojunction solar cells. Fabricating large-scale thin silicon (c-Si) solar cells is challenging. Low-thickness carriers and solar cells can benefit from thin Si substrates due to their short diffusion length. Because of their unique features, graphene transparent electrodes are popular. Their uses in LEDs, touch displays, and solar cells are currently being researched. The use of CVD allowed for produce graphene on Cu foil. The graphene layer was applied to C-Si. Swedish and British researchers created graphene/heterojunction solar cells made of crystalline silicon for photovoltaics. Ultrathin c-Si substrates were made by depositing graphene on SiO<sub>2</sub> of varying thicknesses. Ultrathick ultrathin c-Si substrates may be warped around a 6-mm glass rod to display flexibility and bending resilience—ultrathin graphene/c-Si solar cell. There was electron-blocking material sandwiched between the graphene and the Si of the P<sub>3</sub>HT 40 m thick silicon substrate. Graphene layers increase optical conductivity. As in prior work, P<sub>3</sub>HT was spin-coated between graphene and c-Si to prevent electrons. As an insulator, A 4-mm-diameter hole-punctured PDMS membrane was attached to an ultrathin c-Si. Photovoltaic electrodes employ graphene films. Light absorption and conductivity were compromised by using 40 m c-Si substrates. PCE of 3-layer graphene devices is 7.61%, double that of 1-layer devices [99].

## Polymer Solar Cell

With their mechanical adaptability, cheap cost of manufacture through solution processing, and light weight, polymer solar cells have shown promising growth. Superior to competing for solar cells, they are amenable to the widespread use of the production in a continuous roll form method in industrial settings. For this reason, polymer indium tin oxide (ITO) is a common material used in solar cells as their electrode that is translucent since it is both conductive and transparent. However, ITO's inherent limitations, such as a high manufacturing price utilising a method of deposition using a vacuum at high temperatures, issues with indium availability, fragility, and resistance that grows proportionally to surface area, limit its potential large-scale uses. Various alternatives have recently been developed to replace flexible polymer solar cells that use indium tin oxide (ITO) [100, 101].

Flexible electrodes made from functionalized graphene were disclosed by Tiwari et al. [9] for use in polymer photovoltaics. Graphene films fabricated using a variety of exfoliation, deposition, and manufacturing procedures find use in several solar cell applications. Graphene electrodes outperform ITO electrodes in terms of physical and thermal stability, leading to greater photoconversion efficiency and longer device lifetimes [9].

Bulk heterojunction (BHJ) solar cells based on conjugated polymers are generally recognised as a possible substitute for their inorganic analogues, as reported



in 2012 by a team at the “State Key Laboratory of Molecular Engineering of Polymers” led by Ming He, titled “graphene-based transparent flexible electrodes for polymer solar cells.” Conjugated block copolymers, such as rod-coil or rod-rod BCPs, show excellent adaptability in modifying the bandgap of semiconductor polymers [100, 101].

In the past three decades, organic solar cells (OSCs) have attracted a great deal of research and development investment from both the academic and commercial sectors, as reported in “recent developments in graphene/polymer nanocomposites for application in polymer solar cells,” written by a team of researchers from the Department of Analytical Chemistry led by Dez-Pascual (2018). These devices have significant benefits over their silicon-based counterparts, including reduced processing costs, greater portability, and less weight. Solar panels made from polymers and tiny molecules are two subcategories of OSCs. Spin-coating and printing are two solution-based processes for depositing the active layers. G/polymer nanocomposites may be helpful in many device components, including active and interfacial layers and transparent electrodes. The team suggests that further study is needed to determine how to regulate the structure and characteristics of G and how to enhance the device manufacturing process to create PSCs with better PCE [101].

## Others

Due to the intrinsic features of graphene, such as high mechanical strength, low density, high electrical conductivity, and specific solid surface area, three-dimensional graphene-based materials have been exciting. They have undergone research for various prospective uses, including supercapacitors and energy storage batteries. Especially for supercapacitors and batteries, graphene has recently attracted a lot of interest as an electrode material. Three-dimensional (3D) designs of graphene (such as foam, network, and gels) have been newly created to improve graphene electrodes’ performance significantly. These substances are low in density and have a large specific surface area, outstanding mechanical strength, excellent electrical conductivity, and the inherent features of grapheme [94].

The graphene electrode has more excellent physical and thermal stability than the ITO electrode, extending the device’s lifetime and photo conversion efficiency. Renewable energy sources, like wind turbines, solar energy, and geothermal heat energy, spontaneously replenish themselves over time. A device’s external quantum efficiency may be defined as the fraction of incoming photons converted into charges by photogeneration (EQE). Different exfoliation, deposition, and manufacturing techniques may be used to create graphene sheets, which can be applied in various ways to solar cells. In addition, graphene electrodes are more physically and thermally stable than ITO electrodes, increasing the lifetime of devices and their photo conversion efficiencies. When these solar cells’ environmental effects are considered, let us look at how these cells stack up against the competition for photovoltaics, like multi-Si, CdTe, and mono-Si. Copper indium gallium selenide (CIGS) exhibits reduced climate variability by 16–50% and total environmental consequences by 6–90%.

There are still several cutting-edge materials and technologies that might transform how we think about solar cells and pave the way for a promising future for photovoltaic technologies [9].

The bandgap of semiconductor polymers may be finely adjusted with the help of conjugated block copolymers (BCPs), which show a high degree of adaptability. A transparent ITO glass, photoactive layer, cathode buffer layer, and top metal electrode are the essential components of an ideal polymer BHJ solar cell. The PCE of inverted P3HT: PCBM-based devices are 2.5% when graphene is used as the top electrode. Using an innovative chemical method, graphite may be transformed into the highly conductive material known as graphene. Compared to a PEDOT: PSS-based device, the reduced GO (rGO) variant exhibits superior conductivity and resistance to oxygen and moisture. Doping graphene electrodes with AuCl improves their conductivity, transparency, and shape in an inverted P3HT: PCBM solar cell [102].

An anisotropic Si etching approach created a graphene-ultrathin Si sheet with exceptional flexibility. In addition, A PMMA film anti-reflection layer might be used to bring the reflectance down from 40 to 20%. Consequently, even after 60 bends, indefinitely, the solar cell's efficiency might stay at 93%. Few-layer graphene-Si (Gr-Si) solar cells were published in 2010 by Li et al. with efficiencies of up to 1.5%; this figure was subsequently increased to 8.6%. At 90 °C, a 50 wt% KOH solution was used to etch the Si-film from 100 polished Si wafers (n-type, 400 mm, 0.05–0.2  $\mu\text{m}$ ). A PMMA layer might be identified as a planar anti-reflection to lessen light reflection from the Si surface. For this bending evaluation, a brand-new PMMA-Gr-Si solar cell was built on a polyethylene terephthalate substrate with an active area of 0.096  $\text{cm}^2$ . PMMA-Gr-Si film solar cells could maintain 92% of their initial PCE [103].

## 2.7 Issues Need to Be Addressed

1. The graphene TCE's surface roughness and electrical conductance trade-offs and reductions in power conversion efficiency may be expected as the number of layers in a device increases (PCE) [85].
2. Genuinely, constructing these solar cells on bendable substrates at low temperatures is challenging [89].
3. The increased number of layers of graphene decreases its optical transparency as well as sheet resistance. Due to the correlation between layer count and transparency and sheet resistance, this is the case. Approximately, 97.7% of light may pass through a single sheet of graphene. Graphene stacks with three layers have an optical transparency of around 90.8%, and the transparency decreases by 2.3% for every additional layer. A single-layer graphene sheet may have a resistance of 2.1  $\text{ksq}^{-1}$  or 350  $\text{sq}^{-1}$  whilst still being 90% transparent. Due to its increased hole-accepting density, the quenching effect of multilayer graphene may be as much higher by 11% than in monolayer graphene.

## 2.8 Graphene in the Integrated Circuit

Graphene is a carbon substance; its chemical composition is equal to diamond or graphite. The difference is in the way atoms of this element which are structured (known as allotropy). Although graphene was initially discovered in the 1960s, its standardisation is hampered by a lack of specific terminology and categorization, which prevents a precise characterisation of many forms of graphene. Graphene's super-thin and honeycomb structure are very light, having a density of just  $300.77 \text{ mg/m}^2$ . Due to its innovative nanostructure and unique physical and chemical characteristics, it attracted much attention. Graphene is a highly elastic, hard substance with a hardness significantly higher than steel. It is also capable of self-cooling and self-healing. With a particular surface area of  $2630 \text{ m}^2/\text{g}$ , graphene has huge thermal cognovits (up to  $8000 \text{ W/mK}$ ). The carbon chain along the edges of graphene may be found in three distinct configurations: zigzag, armchair, as well as arbitrary. A nanoribbon with carbon chain armchair arrangements acts as a metal or semiconductor [104].

These days, integrated circuits are often made using CMOS technology, which stands for complementary metal-oxide semiconductors. Whilst manufacturing technology continues to progress, the pace at which transistors can be shrunk may eventually reach a plateau. Applying fully calibrated TCAD over a significant portion of the overall size of the gadget, regardless of the active channel area, an innovative and workable process technique to reduce the source/drain (S/D) epitaxially grown bulk fin-shaped field-effect transistors (FinFETs) at the 5-nm node were developed. Epitaxy, also known as S/D patterning (SDP), PFET drive current decrease was reduced, and channel regions enhanced short-channel effects. In addition, gate capacitances significantly lowered due to smaller active areas and decreased capacitances on the periphery, between the metal-gate stack and the bulk oxide at the bottom FinFETs, showing promise for future reductions [105].

Graphene is considered a capable replacement for electronics after Si [106]. However, the graphene manufacturing era has begun. Low-power devices based on graphene technology are still in the development stage, and there is a need to improve the production of large-area graphene films with superior electrical properties on dielectric surfaces. This is because graphene has unique properties that make it a promising material for electronic devices, such as its high electron mobility, high mechanical strength, and excellent thermal conductivity. However, the challenge lies in producing high-quality graphene films on a large scale, which requires the development of improved methods and techniques for synthesizing and transferring graphene onto dielectric substrates. Researchers are actively working on addressing these challenges to unlock the full potential of graphene in low-power electronics. Monolayer graphene was used to create a top-gated field-effect transistor, according to Lemme et al. in 2021. SOI MOSFETs with silicon and ultrathin bodies, the carrier mobility value was more significant than the universal mobility. The researchers also assumed that adjusting the device's bandgap was essential to enhancing its performance [107].

## Graphene in FETs

Sun et al. realised that the double gate graphene electric field-effect transistor (GFET) was manufactured using CVD growth graphene as a channelled conductor and spin-coated P (VDF-TRFE) organic dielectric solid film as the insulator of the upper gate. Introducing the double gate graphene electric transistor with a field-effect architecture, it has been reported that the charging properties of the graphene sheet may be effectively modulated with the insertion of organic strong electricity P (VDF-TRFE) as a top gate dielectric. Furthermore, using a gate dielectric made of available P (VDF-TRFE) helps regulate graphene charcoal transport characteristics with a polarised doping effect, eliminating the environmental impact on graphene and obtaining an alternative method to obtain GFET with improved performance provides. In addition, BGI, or bottom gate induction, has become clear that a static doping effect is a powerful tool for tightly regulating the top gate transmission properties of GFETs [108].

Vieira et al. [109] proposed a new plan for fabricating electrolyte-gated graphene field-effect transistors (EGFETs). There would be no gate electrode required from the outside due to the fact that the source, gate, and drain would form a single plane. Due to the simplicity of this planar construction, the innovative carrier mobility of up to  $1800 \text{ cm}^2/\text{Vs}$  in graphene EGFETs may be produced on wafer size. As proof of concept, they also created a chemical sensor and showed that it could discriminate between various saline liquid concentrations.

When using an electrolyte-gated FET (EGFET), an external, problematic gate electrode that is not in the plane is required. Li et al. [110] found a chemical method of producing bottom-width graphene nanoribbons (GNRs). Ten nanometers and individual bands varying in width along the length or using graphene connections defined by a lattice structure, a promising material for use in molecular electronics. GNR was in the resolution stage derivative and stably suspended in a solvent by polymer functionalization without covalent bonds. It had a refined edge, like a zigzag or a chair, and was relatively smooth. All of the sub-10 nm GNRs produced were semiconducting and produced graphene arrays during electro-transport tests, in comparison with single-walled carbon nanotubes. At room temperature, this effect transistor has an on/off ratio of roughly  $10^7$ .

Lee et al. [111] constructed his GFET having He is very nimble for someone with a cutoff frequency around 25 GHz with mechanical strength up to a 0.7 mm bend radius, measuring in at  $3900 \text{ cm}^2/\text{V s}$ . They also found that functional bilayer coatings on devices in the short term, thin films containing inorganic and organic components generated adequate hydrophobic surfaces. Or long-term exposure to deionized water, which provides water resistance as well as trustworthy electrical properties. It has also been reported to produce outcomes.

A bendable GFET with a 300 nm gate length was reported by Lan et al. made of PET substrate [112]. Covering the PET substrate with a polyimide sheet made it possible to obtain hole mobility of  $1738 \text{ cm}^2/\text{V s}$ . The Au-assisted graphene transfer approach made it easier to maintain output resistance close to 50. Changes in manufacturing helped achieve an external  $f_{\text{max}}$  of 28 GHz.

Montanaro et al. [113] manufactured optoelectronic mixers (OEM) operating at frequencies up to 67 GHz using GFETs. The gate terminal electrical signal and the modulated optical signal may be combined in the device inside the single-layer graphene channel. In the photodetection process, the sign of the related photocurrent was dictated by the value of the graphene fermi level.

Llinas et al. [114] created armchair-graphene nanoribbons of 0.95 nm in width and were used as the channel material in short-channel (20 nm) GFETs, together with a thin, high K-gate dielectric. The fabricated GFETs had outstanding switching behaviour at room temperature and had a high ION/IOFF ratio of  $10^5$ .

Fakih et al. [115] created a large-area graphene ion-sensitive FET (ISFET) for the selective simultaneous detection of multiple ions. The authors used the Nikolskii-Eisenman hypothesis to, whilst demonstrating the functionality in an aquatic setting, calculate, from the values of the appropriate currents, the concentration of a large number of ions with a LOD of 105 M.

## Graphene in Transistors

Martini et al. [116] represent novel and fascinating materials for use in nanoelectronics due to their characteristics, defined only because of their breadth and edge type, and can be controlled directly from synthesis with high precision. Here, we investigate the correlation between GNR structures and the electrical characteristics of the corresponding devices. They studied field-effect devices composed of chair-shaped GNR films with various structures as transistor channels (width and length) in contact as source-drain electrodes with neighbouring graphene layers. By examining a large number of transitions in each GNR type, it is found that the width-dependent behaviour and theoretically-predicted electronic bandgaps of the output current values hold. These findings light on how band structure and device features have contributed to the evolution of GNR-based electronics. Additionally, Jangid et al. presented a GNR-based transistor [117], made by etching Pt-coated nanoribbons onto mechanically exfoliated graphene at a  $2 \times 10^7$  ION/IOFF ratio. Using the measured properties, the hole-and-electron mobilities at 6 K were determined to be  $400 \text{ cm}^2/\text{V s}$  and  $1100 \text{ cm}^2/\text{V s}$ , respectively.

Graphene-based transistors for high-performance frequencies (in gigahertz) were used by Lin et al. [118], and the frequency response is analysed using conventional S-parameter measurements. The transistor based on graphene with a 150 nm gate length exhibited the highest possible frequency cutoff is 26 GHz. If graphene's remarkable mobility could be preserved throughout the manufacturing process, it would be a game-changer; the authors anticipated that gate-field-effect transistor (GFET) gates 50 nm in length could attain a cutoff frequency approaching a terahertz. The same group synthesised graphene transistors with higher operating frequencies [119] on 2-inch graphene wafers with high-frequency cutoff frequencies as high as 100 GHz. Graphene FETs have power gains up to 14 and 10 GHz using 550 nm and 240 nm gate lengths, respectively. Graphene synthesis and manufacturing technologies at the wafer size are used to make them. In a study by Wu et al., cutoff frequencies up to

155 GHz have been reported [120] on the characteristics of top-gated (40 nm gate length), inversely frequency-dependent graphene RF transistors. They also found that a large working window was possible since no noticeable performance improvement was hindered until the temperature reached 4.3 K. Organic semiconductors are the primary components of flexible electronics. Nonetheless, the charge carrier velocities of polymers and molecular films restrict their employment over a specific frequency MHz.

In contrast, graphene's significant potential for high-frequency electronics on stiff substrates has recently been established. Sire et al. [121] have conducted the first research on graphene transistors operating at gigahertz frequencies using a solution-based approach, showing that single-layer graphene based on a solution offers an ideal combination of properties required for achieving flexible electronics operating at high speed on plastic substrates. In these flexible graphene transistors' in terms of current and power increase, the upper limits are set at 2.2 GHz as well as 550 MHz, respectively.

In high-frequency applications, the high emitter barrier height is a common issue for graphene-based transistors. They have been put forward [122] owing to the low base delay brought on by the atomic thickness of graphene for high-frequency applications. The performance of transistors is nonetheless restricted to terahertz operation by the high emitter potential barrier heights associated with frequently employed tunnel emitters. However, transistor performance is limited to terahertz operation because of the large emitter possible barrier heights associated with regularly used tunnel emitters. Theoretically, graphene-based heterojunction transistors with a silicon base sandwiched between graphene layers have been suggested to address this issue. They show a vertical silicon-graphene-germanium transistor with a monocrystalline silicon and monolayer graphene Schottky emitter. A Schottky emitter with those characteristics has  $692 \text{ A cm}^{-2}$  of current and  $41 \text{ nF cm}^{-2}$  of capacitance. Therefore, using the prior tunnel emitter should allow the transistor's alpha cutoff frequency to rise from roughly 1 MHz to more than 1 GHz. This is a graphene transistor; a semiconductor device anticipated growing into promising technology at very high frequencies.

A method for creating high-speed nanowire-aligned graphene transistor gates was developed by Liao et al. [123]. Self-alignment technique, which involves automated and exact placement of the gate, source, and drain electrodes, allows for a decrease in the access resistance whilst maintaining improved carrier mobility due to the use of graphene in the nanowire gate's physical construction. Evidence also showed that the built transistor had a high natural transition (cutoff) frequency in the 100–300 GHz range.

The booming manufacturing of wafer-scale graphene circuits in 2011 by Lin et al. [124] was announced. This circuit's components, notably a graphene field-effect transistor (GFET) and an inductor, were successfully integrated into a single SiC wafer. Less than  $1 \text{ mm}^2$  was used for the whole integrated circuit (IC) as well as its connection pads. The wire acted as a 10 GHz-capable RF mixer with a wide frequency range.

Cheng et al. [123] have created a scalable procedure to produce transistors made of transfer-gate-stacked self-aligned graphene on glass. The graphene transistors have the most significant cutoff frequency to date thanks to a safe and reliable handoff method, including a self-adjusting design for the apparatus (427 GHz). This technique outlines a route to manufacturing on a large scale of high-speed self-aligned graphene transistor arrays on any substrate by first performing standard lithographic, deposition, and etching processes on a waste substrate and then integrating them with CVD-grown graphene across a broad region. However, the maximum oscillation frequency for a 220 nm channel length transistor was just 29 MHz.

Raising the highest oscillation frequency may be possible by enhancing graphene quality, lowering gate resistance, and boosting source-drain current saturation. Using an ultra-clean manufacturing technique, Feng et al. [125], graphene is protected from photo resistance, e-beam, and air by a layer of the pre-deposited gold film. GFETs have great DC and RF characteristics with a  $f_{max}$  of 105 GHz because of this extremely clean manufacturing and optimised device shape. Furthermore, this method of making graphene transistors is simple to use and compatible with a range of substrates.

A practical technique for producing high-performance graphene transistors needs to be defined, which is an essential first step towards applying graphene-based components in RF circuits. Yeh et al. [126] demonstrated how to make a graphene transistor on a PET substrate, paving the way for real progress in wearable electronics. Using a recently developed AlOx T-gate structure, we can significantly increase the device's transconductance whilst simultaneously decreasing the associated parasitic resistance. As a result, the highest oscillation frequency is 20 GHz, and the extrinsic cutoff frequency is 32 GHz, substantially higher than previously reported working frequencies.

According to Han et al. [127], a three-stage and high-performance graphene-integrated circuit was used to illustrate the fabrication method's complete preservation of the graphene transistor's quality. To accomplish down-conversion, the course acts as an RF receiver by amplifying, filtering, and mixing incoming signals. The integration of all circuit components into an area of 0.06 mm<sup>2</sup> and production in silicon wafers 200 mm in diameter show the extraordinary complexity of graphene circuits and the compatibility of the silicon complementary metal-oxide-semiconductor technology. According to proven circuit performance, graphene-integrated circuits may perform proper wireless communication operations, receiving, and retrieving digital text conveyed on 4.3 GHz carrier signals. In addition, future electronics must consider how electronic device scaling may impact IC technology's packing density and operating speed.

Graphene IC scaling was investigated by Bianchi et al. [128]. It could produce high-performance transistor-based integrated circuits (ICs) with various lead thicknesses, access lengths, and channel widths sub-micron graphene ROs oscillating at 4.3 GHz, the highest oscillation frequency ever recorded in a material, produced the minor gate delay of 31 ps per step.

Hanna et al. [129], an integrated power amplifier device operating at 2.5 GHz is shown using a graphene field-effect transistor thermally deposited on a SiC substrate



(FET). This is the first full-scale analysis of signals in graphene RF power amplifiers; the highest recorded power output and power addition efficiency are, respectively, with a 5.1 dBm output and 2.2% modulation. The comparison of Si and graphene CMOS amplifiers also revealed that the power-added efficiency was inferior to that of the silicon version.

Vaziri et al. [130] developed a vertical hot-electron transistor based on graphene and studied the wafer-scale production method using silicon to achieve direct-current (DC) functioning. The transistor's base was built of graphene, which caused it to go from ON to OFF and vice versa when an electric field was applied, with an ON/OFF current ratio of up to  $10^4$ .

A semiconductor-graphene-semiconductor transistor was made by Liu et al. [131] using the Si membrane transfer technique. According to the electrical characterisation, the common-base current gain might be 10% better than the standard gain.

Mol et al. [132] suggested a graphene-molecule-graphene transistor design in a theoretical investigation. Since the molecular junction remained always charged with a single electron, it was unaffected by the atomic arrangement of the graphene electrodes. The extraordinarily constant single-electron charge was responsible for the molecular junction's insensitivity to the graphene electrodes' nuclear structures.

Chemical vapour deposition uses vast regions of graphene crystals that are single-crystal (LSG) larger than half a millimetre. Ning et al. created a field-effect transistor made of graphene that is gated by ion gel (FET) [132] to investigate the based on the idea of electronic double layers, the material's electrical characteristics. A novel development technique for large single-crystal graphene was developed and enhanced by employing chemical vapour deposition's cyclical oxidation/hydrogen-annealing techniques to rebuild the copper foil surface (CVD). LSG in the channel layer on a polyethene terephthalate substrate and an ion gel sheet that was spun-coated functioned as the gate dielectric to make a flexible FET. The flexible device exhibits superior electrical characteristics and remarkable flexibility. As the object bent, the on/off current rose by 8.1%.

Currently, synthetic methods operating from the bottom up and the surface are manufactured using techniques optimised for graphene nanoribbons, which provide the atomic accuracy required for NPG production (GNRs) [133]. But until now, bottom-up synthesised NPG's promise in electronics has mostly been untapped. Here, FETs are shown using bottom-up synthesised chevron-type NPG (C-NPG), composed of arranged arrays of nanopores delineated by interconnected chevron GNRs. Field-effect transistors with a C-NPG gate symbol show on-off ratios greater than  $10^4$ , demonstrating extraordinary switching capability intrinsically linked to C-structural NPG's integrity. Furthermore, the components function as p-type transistors when air is present. Still, when tested in a vacuum, n-type transport is evident, related to the adsorption and desorption of gases and water vapour. Charge vehicles in C-NPG are theoretically examined using the electronic structure and transport simulations, and these calculations reveal that C-NPG has high conductance anisotropy effects. This study provides significant insights into the fabrication of high-performance graphene-based electrical devices with ballistic conductance and



conduction anisotropy, as well as sensors capable of picking up the slightest traces of chemicals or organisms. Obtaining a gate length of under 1 nm requires Wu et al. [134] to construct a vertical MoS<sub>2</sub> transistor with a gate electrode made from the ragged end of a graphene sheet. The device's on/off ratio can reach  $1.02 \times 10^5$ , and its subthreshold swing values can drop to 117 mV/dec.

## 2.9 Limitations of Graphene for Flexible Electronic Devices

Graphene's exceptional mechanical strength, low thermal conductivity, and rapid charge mobility set it apart from other materials. However, pure graphene has significant limitations that prevent it from being widely used as an electrode. Since graphene's Rsh is much higher than ITO's (10 V/sq), and its work function is much lower (4.4 eV), because of this, it cannot function as an electrode in either purely organic or purely organic–inorganic hybrid circuits. When the work function is low, there is a significant energy gap (or offset) between the anode and the covering layer, which decreases the hole boosts open circuit voltage in OSCs and causes current injection in OLEDs. When the applied bias is high, the maximum current through or into the device is also high. The device's efficiency is reduced compared to what it would be if it were made using ITO because of the alterations [135–138]. There are various doping methods, such as substitutional and charge transfer doping. [135, 136, 139–142] have been applied to pure graphene to alter its electrical properties, reducing its disadvantages for practical applications.

Substitutional doping has the potential to alter graphene's properties [138, 143]. Several electrical characteristics, such as the absence of a bandgap, high conductivity, and a high WF, are affected by altering the graphene lattice's electrical structure to accommodate the inclusion of hetero-atoms [138, 143, 144]. Graphene is often substituted with atoms of nitrogen and boron since they are about the same size as carbon atoms [143]. Create substitutionally-doped graphene from forms of hetero-atoms using CVD. These N-doped graphenes are synthesised by getting nitrogen and carbon from the gases NH<sub>3</sub> and CH<sub>4</sub>. Boronic acid and other B-containing precursors may also be utilised to produce B-doped graphene. [144] Because it disrupts the material's electronic structure, substitutional doping may change graphene's unique electrical characteristics, but at the expense of the material's conductivity [139].

Another technique for modifying the electrical characteristics of graphene is charge transfer doping [135, 136, 139, 140, 145]. Electronic charge transfer occurs spontaneously between graphene and an acceptor or donor due to the disparity in their ionisation potential or electron affinities [141, 142] When a semiconducting dopant contributes its electrons to graphene, its electron concentration increases because its highest occupied molecular orbital (HOMO) energy level is greater than graphene's fermi energy level [141, 142] Dopants, on the other hand, increase the concentration of holes in graphene by displacing electrons when their LUMO energy level is lower than graphene's fermi energy level [141, 146]. Additionally, Electrochemical charge transfer doping occurs when a surface-adsorbed dopant molecule participates in an

electrochemical redox interaction with graphene; the rate at which this happens is proportional to the reduction potential of the dopant molecule and the Gibbs free energy of the reaction. It is generally accepted that graphene may be converted to the n-type by depositing a dopant molecule that contains an electron-donating group. In contrast, doping using a dopant molecule that includes electron-withdrawing group results in a p-type doped material [147]. The doping effect is caused by the electrostatic potential between graphene and the dopant molecule, which is caused by the dipole moment of the charge transfer complex [148].

The electrical structure of graphene is not severely compromised by accidental charge transfer-based doping. Using the charge transfer method, graphene may be doped with various dopants, from inorganic acids to metal chlorides. Graphene is often doped with inorganic acids (such as HCl, HNO<sub>3</sub>, and H<sub>2</sub>SO<sub>4</sub>) to make it p-type because these acids may remove electrons from the material through charge transfer complex formation. This is due to the fact that graphene's electrical conductivity and WF have improved as their hole concentrations have grown [135, 139, 149].

Graphene doped with an inorganic small-molecule acid has a steady rise in Rsh at room temperature because these dopants are very unstable [135, 136].

Metal chlorides have likewise been used to sanitise graphene in the p-type charge transfer form. They demonstrated p-type doping effectiveness, resulting in a large WF of 5 eV and solid electrical conductivity of 30 V/sq [135, 140]. However, due to the reduction of metal cations, the graphene surface starts accumulating massive metal particles. Because these particles on graphene stick out so far, they could cause electrical leakage or short current in thin-film devices because of how far they stick out [135]. The potential reduction of T by metal chloride doping of graphene is a problem with optoelectronic devices [140].

Aqueous liquids do not entirely cover graphene because it repels water. To create flexible electronic devices processed in solutions, this problem has to be overcome. An interfacial buffer layer must entirely protect the graphene so that charges may be injected or extracted without creating local shorts at the electrode's exposed surface.

When graphene is exposed to oxygen-containing functional groups through treatment of the surface with O<sub>2</sub> plasma or UV-ozone, its hydrophobic surface may become hydrophilic. But since these procedures damage the hybridised carbon networks, graphene's electrical characteristics are drastically diminished [148, 150–152]. Therefore, techniques for surface modification do not affect graphene's electrical. Characteristics must be devised to ensure a thick layer of an intermediate film on a graphene electrode [153].

## ***2.10 Conclusion and Future Lookout***

Recent advancements in flexible solar cells, energy storage devices, and integrated circuits made from graphene have been explored. Graphene's potential electron mobility, a high T, and mechanical durability benefit flexible electronics. As a result,

graphene has undergone testing in various flexible electronic component applications. However, the problems with graphene must be overcome before being used effectively in flexible electronics. For example, the current through graphene-based devices is constrained by its relatively large  $R_{sh}$  for a given applied bias. In addition, its potential for causing voltage loss in SCs is also unsuitable for usage in WFs and LEDs.

As a result of the high energy barrier, it presents to charge injection (4.4 eV); pure graphene cannot be employed as a channel in field-effect transistors (FETs). In several productions to alter its electrical characteristics, scientists have created new techniques, including chemical and physical changes of graphene. Graphene film produced by chemical or mechanical exfoliation of graphite has limited applications. Still, the advent of large-scale graphene manufacturing via CVD has dramatically expanded the opportunities for graphene-based stretchable electronic devices. Graphene's band gap might be widened, providing a channel for field-effect transistors. The device's charge conduction has been improved using several doping procedures that create the necessary  $R_{sh}$  and WF. These methods have increased switching devices' on-off ratio and the lumen efficiency of LEDs and PCE of SCs. Multiple methods, including oxidation, hydrogenation, and GNRs, have been proposed for creating a small band gap in graphene. In addition, because of the interfacial layers, the high energy barrier to charge injection from the graphene electrode is lowered, significantly improving the gadget's electrical or illuminating capabilities. Because of its very impermeable structure to gas molecules and its tightly packed structure, graphene is a desirable and versatile encapsulant.

To advance the study of flexible electronics based on graphene, it is necessary to develop methods for synthesising graphene with large and single-crystal domains that are defect-free and easily transferred to other substrates without leaving any unwanted residue. Additionally, doping graphene's effects on increasing energy transfer and work output must be investigated further. Whilst doing so, graphene's possible that the interfacial layer is engineered to facilitate the injection of charge carriers from graphene to functional layers above, potentially allowing for the modification of pure graphene's electrical properties without sacrificing its unique qualities. Future flexible electronics will benefit from developing novel strategies for producing defect-free, high-quality graphene, and engineering methods for improving graphene's properties. Stretchable electronics need considerably more work on graphene's mechanical properties.

Next-generation flexible and wearable electronics might benefit from the use of graphene if methods could be devised to improve the pliability of electrodes and encapsulants made from graphene.

**Acknowledgements** These works were completed at the College of Engineering at Bharati Vidyapeeth (Deemed to be University), Pune, and the writers would like to express their gratitude to the university.

## References

1. Han, T., Kim, H., Kwon, S., Lee, T.: Graphene-based flexible electronic devices. *Mater. Sci. Eng. R.* **118**, 1–43 (2017)
2. Yoon, J., et al.: Superflexible, high-efficiency perovskite solar cells utilizing graphene electrodes: Towards future foldable power sources, *Energy Environ. Sci.*, **10**(1), 337–345 (2017)
3. Gupta, G., Zeng, M.: Applications of graphene-based materials in electronic devices (2017)
4. Olabi, A.G., Ali, M., Wilberforce, T., Taha, E.: Application of graphene in an energy storage device—A review. *Renew. Sustain. Energy Rev.* **135**, 110026 (2021)
5. Castro Neto, A.H., Guinea, F., Peres, N.M.R., Novoselov, K.S., Geim, A.K.: The electronic properties of grapheme. *Rev. Mod. Phys.* **81**(1), 109–162 (2009)
6. Jose Varghese, R., et al.: Introduction to nanomaterials: Synthesis and applications. Elsevier Inc. (2019)
7. Outline, C.: Optical properties of nanomaterials (2018)
8. Iqbal, T., Fatima, S., Bibi, T., Zafar, M.: Graphene and other two-dimensional materials in advance solar cells. *Opt. Quantum Electron.* **53**(5), 1–22 (2021)
9. Tiwari, S., Purabgola, A., Kandasubramanian, B.: Functionalised graphene as flexible electrodes for polymer photovoltaics. *J. Alloys Compd.* **825**, 153954 (2020)
10. Dong, Z., Kennedy, S.J., Wu, Y.: Electrospinning materials for energy-related applications and devices. *J. Power Sources* **196**(11), 4886–4904 (2011)
11. Saleh, T.A.: Nanomaterials: classification, properties, and environmental toxicities. *Environ. Technol. Innov.* **20**, 101067 (2020)
12. Ke, Q., Wang, J.: Graphene-based materials for supercapacitor electrodes—A review. *J. Mater.* **2**(1), 37–54 (2016)
13. Randviir, E.P., Brownson, D.A.C., Banks, C.E.: A decade of graphene research: production, applications and outlook. *Mater. Today* **17**(9), 426–432 (2014)
14. Bakandritsos, A., Jakubec, P., Pykal, M., Otyepka, M.: Covalently functionalized graphene as a supercapacitor electrode material. *FlatChem* **13**, 25–33 (2019)
15. Tsang, C.H.A., Huang, H., Xuan, J., Wang, H., Leung, D.Y.C.: Graphene materials in green energy applications: recent development and future perspective. *Renew. Sustain. Energy Rev.* **120**, 109656 (2020)
16. Mbayachi, V.B., Ndayiragije, E., Sammani, T., Taj, S., Mbuta, E.R., Ullah khan, A.: Graphene synthesis, characterization and its applications: a review. *Results Chem.* **3**, 100163 (2021)
17. Mishra, R.K., Choi, G.J., Sohn, Y., Lee, S.H., Gwag, J.S.: Nitrogen-doped reduced graphene oxide as excellent electrode materials for high-performance energy storage device applications. *Mater. Lett.* **245**, 192–195 (2019)
18. Dhinakaran, V., Stalin, B., Sai, M.S., Vairamuthu, J., Marichamy, S.: Recent developments of graphene composites for energy storage devices. *Mater. Today Proc.* **45**, 1779–1782 (2021)
19. Zheng, X., Hu, Q., Zhou, X., Nie, W., Li, C., Yuan, N.: Graphene-based fibers for the energy devices application: a comprehensive review. *Mater. Des.* **201**, 109476 (2021)
20. Liu, T., Zhang, L., Cheng, B., Hu, X., Yu, J.: Holey Graphene for electrochemical energy storage. *Cell Reports Phys. Sci.* **1**, 100215 (2020)
21. Lin, Y., et al.: Holey graphene nanomanufacturing: Structure, composition, and electrochemical properties. *Adv. Funct. Mater.* **25**, 2920–2927 (2015)
22. Dutta, D., et al.: Nanocatalyst-assisted fine tailoring of pore structure in holey-graphene for enhanced performance in energy storage. *ACS Appl. Mater. Interfaces* **11**, 36560–36570 (2019)
23. Wang, J., et al.: Scalable synthesis of holey graphite nanosheets for supercapacitors with high volumetric capacitance. *Nanoscale Horizons* **4**, 452–456 (2019)
24. Xu, Y., et al.: Holey graphene frameworks for highly efficient capacitive energy storage. *Nat. Commun.* **5**, (2014)
25. Bai, Y., et al.: Formation process of holey graphene and its assembled binder-free film electrode with high volumetric capacitance. *Electrochim. Acta* **187**, 543–551 (2016)

26. Liu, D., Li, Q., Zhao, H.: Electrolyte-assisted hydrothermal synthesis of holey graphene films for all-solid-state supercapacitors. *J. Mater. Chem. A* **6**(24) 11471–11478 (2018)
27. Han, X., et al.: Scalable holey graphene synthesis and dense electrode fabrication toward high-performance ultracapacitors. *ACS Nano* **8**(8), 8255–8265 (2014)
28. Walsh, E.D., et al.: Article for supercapacitors with ultrahigh areal loadings dry-processed, binder-free holey graphene electrodes for supercapacitors with ultrahigh areal loadings (2016)
29. Pei, J.: Three-dimensional nitrogen and sulfur co-doped holey-reduced graphene oxide frameworks anchored with MoO<sub>2</sub> nanodots for advanced rechargeable lithium-ion batteries. (2017)
30. Sammed, K.A., et al.: Reduced holey graphene oxide film and carbon nanotubes sandwich structure as a binder-free electrode material for supercapacitor. *Sci. Rep.* **10**(1), 1–10 (2020)
31. Lv, J., Liang, T.: Nanoporous graphene obtained by the hydrothermal process in H<sub>2</sub>O<sub>2</sub> and its application for supercapacitors. *Chem. Phys. Lett.* **659**, 61–65 (2016)
32. Manuscript, A.: *ChemComm* (2017)
33. Guo, C., Zhang, Y., Zeng, T., Huang, D., Wan, Q., Yang, N.: High-performance asymmetric supercapacitors using holey graphene electrodes and redox electrolytes. *Carbon N. Y.* **157**, 298–307 (2020)
34. Yang, C., Huang, P., Luo, X., Wang, C., Li, C.: Holey graphene nanosheets with surface functional groups as high-performance supercapacitors in ionic- liquid electrolyte. 1–9
35. Zang, P., Gao, S., Dang, L., Liu, Z., Lei, Z.: Green synthesis of holey graphene sheets and their assembly into aerogel with improved ion transport property. *Electrochim. Acta* **212**, 171–178 (2016)
36. Zhang, Y., et al.: Highly defective graphite for scalable synthesis of nitrogen-doped holey graphene with high volumetric capacitance. *J. Power Sources* **334**, 104–111 (2016)
37. Jiang, Z.J., Jiang, Z., Chen, W.: The role of holes in improving the performance of nitrogen-doped holey graphene as an active electrode material for supercapacitor and oxygen reduction reaction. *J. Power Sources* **251**, 55–65 (2014)
38. Xu, P., et al.: A high surface area N-doped holey graphene aerogel with low charge transfer resistance as high performance electrode of non-flammable thermostable supercapacitor. *Carbon N. Y.* **149**, 452–461 (2019)
39. Kan, Y., Ning, G., Ma, X.: Sulfur-decorated nanomesh graphene for high-performance supercapacitors. *Chinese Chem. Lett.* **28**, 2277–2280 (2017)
40. Online, V.A.: Sustainable energy & fuels hydrogel as a binder-free electrode material for 17–19 (2019)
41. Liu, J., Zhu, Y., Chen, X., Yi, W.: Nitrogen, sulfur and phosphorus tri-doped holey graphene oxide as a novel electrode material for application in supercapacitor. *J. Alloys Compd.* **815**, 152328 (2020)
42. Jia, S.: et al.: Microporous and mesoporous materials A 3-D covalently crosslinked N-doped porous carbon/holey graphene composite for quasi-solid-state supercapacitors. *Microporous Mesoporous Mater* 109796 (2019)
43. Wu, S., Hui, K.S., Hui, K.N., Yun, J.M., Kim, K.H.: School of Materials Science and Engineering, Pusan National University, San 30 Global Frontier R & D Center for Hybrid Interface Materials, Pusan National University, Corresponding author. *Chem. Eng. J.* (2017)
44. Chai, Y., Li, Z., Wang, J., Mo, Z., Yang, S.: *AC SC. J. Alloys Compd.* (2018)
45. Wang, L., Deng, D., Salley, S.O., Ng, K.Y.S.: Facile synthesis of 3-D composites of MnO<sub>2</sub> nanorods and holey graphene oxide for supercapacitors. *J. Mater. Sci.* **50**(19), 6313–6320
46. Lalwani, S., Sahu, V., Marichi, R.B., Singh, G., Sharma, R.K.: In situ immobilized, magnetite nanoplatelets over holey graphene nanoribbons for high performance solid state supercapacitor. *Electrochim. Acta* **224**, 517–526 (2017)
47. Song, Y., Wang, H., Liu, W., Wang, H., Yan, L.: Na<sub>2</sub>MoO<sub>4</sub> as both etcher for three-dimensional holey graphene hydrogel and pseudo-capacitive feedstock for asymmetric supercapacitors. *J. Alloys Compd.* **780**, 55–64 (2019)
48. Zhai, S., et al.: Nano-RuO<sub>2</sub>-decorated holey graphene composite fibers for micro-supercapacitors with ultrahigh energy density. *Small* **14**(29), 28–34 (2018)

49. Li, S., et al.: Hierarchical interpenetrating rHGO-decorated NiCo<sub>2</sub>O<sub>4</sub> nanowires architectures for high-performance supercapacitors. *Appl. Surf. Sci.* **473**(December 2018), 326–333 (2019)
50. Wang, C., et al.: Electrochimica acta A core-sheath holey graphene/graphite composite fiber intercalated with MoS<sub>2</sub> nanosheets for high-performance fiber supercapacitors. **305** (2019)
51. Tiruneh, S.N., Kang, K., Kwag, H., Lee, Y.: Synergistically active NiCo<sub>2</sub>S<sub>4</sub> nanoparticles coupled with holey defect graphene hydrogel for high-performance solid-state supercapacitors (2018) 1–9
52. Fan, Z., Zhu, J., Sun, X., Cheng, Z., Liu, Y., Wang, Y.: High density of free-standing holey graphene/PPy Films For Superior Volumetric Capacitance Of Supercapacitors. *ACS Appl. Mater. Interfaces* **9**(26), 21763–21772 (2017)
53. Liu, J., Du, P., Wang, Q., Liu, D., Liu, P.: Mild synthesis of holey N-doped reduced graphene oxide and its double-edged effects in polyaniline hybrids for supercapacitor application. *Electrochim. Acta* **305**, 175–186 (2019)
54. Du, P., Dong, Y., Kang, H., Wang, Q., Niu, J.: Electrochimica Acta Synthesis of holey graphene networks functionalized with *p*-phenylene diamine monomers for superior performance flexible solid-state supercapacitors. *Electrochim. Acta* **320**, 134610 (2019)
55. Wang, X., et al.: Organic molecule electrode with high capacitive performance originating from efficient collaboration between caffeic acid and graphene & graphene nanomesh hydrogel. *Electrochim. Acta* **326**, 134953 (2019)
56. Fan, Z., Wang, Y., Xie, Z., Wang, D., Yuan, Y., Kang, H.: Modified mxene/holey graphene films for advanced supercapacitor electrodes with superior energy storage, vol. 1800750 (2018)
57. Han, J., Li, H., Yang, Q.H.: Compact energy storage enabled by graphenes: challenges, strategies and progress. *Mater. Today* **51**, 552–565 (2021)
58. Lv, W.: Graphene-based materials for electrochemical energy storage devices: opportunities and challenges (2018)
59. Alsharaeh, E., Ahmed, F., Aldawsari, Y., Khasawneh, M.: Novel synthesis of holey reduced graphene oxide (HRGO) by microwave irradiation method for anode in lithium-ion batteries. *Nat. Publ. Gr.* 1–13 (2016)
60. Online, V.A.: Ion batteries with enhanced electrochemical performance † (2013)
61. Zhao, X., Hayner, C.M., Kung, M.C., Kung, H.H.: Flexible holey graphene paper electrodes with enhanced rate capability for energy storage applications. *ACS Nano* **5**(11), 8739–8749 (2011)
62. Liang, J., et al.: Vacuum-dried 3D holey graphene frameworks enabling high mass loading and fast charge transfer for advanced batteries. *Energy Technol.* **8**(3), 1–6 (2020)
63. Xu, J., Lin, Y., Connell, J.W., Dai, L.: Nitrogen-doped holey graphene as an anode for lithium-ion batteries with high volumetric energy density and long cycle life. *Small* **11**(46), 6179–6185 (2015)
64. Dong, X., et al.: SC (2017)
65. Wang, X., et al.: High-density monolith of N-doped holey graphene for ultrahigh volumetric capacity of li-ion batteries. *Adv. Energy Mater.* **6**(6) 1–7.
66. Online, V.A., Wang, L., Yang, S.: RSC Advances (2015)
67. Jiang, Z., Jiang, Z.: Fabrication of nitrogen-doped holey graphene hollow microspheres and their use as an active electrode material for lithium ion batteries fabrication of nitrogen-doped holey graphene hollow microspheres and their use as an active electrode material for lit (2014)
68. Zhu, X., Song, X., Ma, X., Ning, G.: Enhanced electrode performance of Fe<sub>2</sub>O<sub>3</sub> nanoparticle-decorated nanomesh graphene as anodes for lithium-ion batteries. *ACS Appl. Mater. Interfaces* **6**(10) 7189–7197 (2014)
69. Chen, Z., Chen, J., Bu, F., Agboola, P.O., Shakir, I., Xu, Y.: Double-hole-heterostructure frameworks enable fast, stable, and simultaneous ultrahigh gravimetric, areal, and volumetric lithium storage. *ACS Nano* **12**(12), 12879–12887 (2018)
70. Wu, D., et al.:  $\gamma$ -Fe<sub>2</sub>O<sub>3</sub> nanoparticles stabilized by holey reduced graphene oxide as a composite anode for lithium-ion batteries. *J. Colloid Interface Sci.* **552**, 633–638 (2019)
71. Chen, C., Chen, H.W., Wu, C.Y., Huang, J.C., Duh, J.G.: Heterostructural modulation of in situ growth of iron oxide/holey graphene framework nanocomposites as excellent electrodes for advanced lithium-ion batteries. *Appl. Surf. Sci.* **485**(March), 247–254 (2019)

72. Materials Chemistry A (2019)
73. Ma, Z., Cao, H., Zhou, X., Deng, W., Liu, Z.: Hierarchical porous MnO/graphene composite aerogel as high-performance anode material for lithium ion batteries. *RSC Adv.* **7**(26), 15857–15863 (2017)
74. Wang, B.: 3D nanoporous graphene films converted from liquid-crystalline holey graphene oxide for thin and high-performance supercapacitors (2018)
75. Wu, D., Zhao, W., Wu, H., Chen, Z., Li, H., Zhang, L.Y.: Holey graphene confined hollow nickel oxide nanocrystals for lithium ion storage. *Scr. Mater.* **178**, 187–192 (2020)
76. Online, V.A.: Electrochemical process : ultra-high capacity and rate, 14023–14030 (2013)
77. *Inorganic chemistry* (2019)
78. Stolyarova, S.G.: et al.: High-pressure high-temperature synthesis of MoS<sub>2</sub>/holey graphene hybrids and their performance in li-ion batteries. **1700262**, 1–6 (2017)
79. Xu, L., et al.: Holey graphenes as the conductive additives for LiFePO<sub>4</sub> batteries with an excellent rate performance. *Carbon N. Y.* **149**, 257–262 (2019)
80. Xiang, Y., Zhang, W., Chen, B., Jin, Z., Zhang, H.: Nano-Li<sub>4</sub>Ti<sub>5</sub>O<sub>12</sub> particles in-situ deposited on compact holey-graphene framework for high volumetric power capability of lithium ion battery anode. *J. Power Sources* **447**, 227372 (2020)
81. Lu, C., Chen, X.: Silver decorated graphene nanocomposites toward electrochemical energy storage. *Chem. Phys. Lett.* **771**, 138534 (2021)
82. Kumar, H., Sharma, R., Yadav, A., Kumari, R.: Recent advancement made in the field of reduced graphene oxide-based nanocomposites used in the energy storage devices: a review. *J. Energy Storage* **33**, 102032 (2021)
83. Tian, Y., Yu, Z., Cao, L., Zhang, X.L., Sun, C., Wang, D.W.: Graphene oxide: an emerging electromaterial for energy storage and conversion. *J. Energy Chem.* **55**, 323–344 (2021)
84. Fu, X., Xu, L., Li, J., Sun, X., Peng, H.: Flexible solar cells based on carbon nanomaterials. *Carbon N. Y.* **139**, 1063–1073 (2018)
85. Du, J., et al.: Extremely efficient flexible organic solar cells with a graphene transparent anode: Dependence on number of layers and doping of graphene. *Carbon N. Y.* **171**, 350–358 (2021)
86. Yusoff, R.b.M.: Graphene-based energy devices (2015)
87. Dhinakaran, V., Stalin, B. Sai, M.S., Vairamuthu, J., Marichamy, S.: Materials today: proceedings recent developments of graphene composites for energy storage devices. *Mater. Today Proc.* (2020)
88. Riverola, A., et al.: Fundamentals of solar cells. *Nanomater. Sol. Cell Appl.* **7**(May), 3–33 (2019)
89. Jin et al. J.J.: Efficient and stable flexible perovskite solar cells based on graphene-AgNWs substrate and carbon electrode without hole transport materials. *J. Power Sources* **482**, 228953 (2021)
90. Liu, Z., Li, J. Yan, F.: Package-free flexible organic solar cells with graphene top electrodes. *Adv. Mater.* **25**(31), 4296–4301 (2013)
91. Jeon, I., et al.: Carbon nanotubes versus graphene as flexible transparent electrodes in inverted perovskite solar cells. *J. Phys. Chem. Lett.* **8**(21), 5395–5401 (2017)
92. Ricciardulli, A.G., Yang, S., Feng, X., Blom, P.W.M.: Solution-processable high-quality graphene for organic solar cells. *ACS Appl. Mater. Interfaces* **9**(30), 25412–25417 (2017)
93. Gao, Z.W., et al.: Tailoring the interface in FAPbI<sub>3</sub> planar perovskite solar cells by imidazole-graphene-quantum-dots. *Adv. Funct. Mater.* **31**(27), 1–7 (2021)
94. Foster, C.W.: 3D printed graphene based energy storage devices (2017)
95. Ye, Y., Dai, L.: Graphene-based Schottky junction solar cells. *J. Mater. Chem.* **22**(46), 24224–24229 (2012)
96. Koo, D., et al.: Flexible organic solar cells over 15% efficiency with polyimide-integrated graphene electrodes. *Joule* **4**(5), 1021–1034 (2020)
97. Song, Y., Chang, S., Gradecak, S., Kong, J. (2016). Visibly-transparent organic solar cells on flexible substrates with all-graphene electrodes, *Adv. Energy Mater.* **6**(20), 1–8 (2016)
98. Heo, J.H., Shin, D.H., Song, D.H., Kim, D.H., Lee, S.J., Im, S.H.: Super-flexible bis(trifluoromethanesulfonyl)-amide doped graphene transparent conductive electrodes for photo-stable perovskite solar cells. *J. Mater. Chem. A* **6**(18), 8251–8258 (2018)

99. Ruan, K. et al.: Flexible graphene/silicon heterojunction solar cells. *J. Mater. Chem. A* **3**(27), 14370–14377 (2015)
100. Lu, S., Sun, Y., Ren, K., Liu, K., Wang, Z., Qu, S.: Recent development in ITO-free flexible polymer solar cells. *Polymers (Basel)* **10**(1) (2018)
101. Fahlman, B.D., Materials chemistry. *Mater. Chem.* **207890**, 1–485 (2007)
102. He, M., Jung, J., Qiu, F., Lin, Z.: Graphene-based transparent flexible electrodes for polymer solar cells. *J. Mater. Chem.* **22**(46), 24254–24264 (2012)
103. Jiao, T., et al.: Flexible solar cells based on graphene-ultrathin silicon Schottky junction. *RSC Adv.* **5**(89), 73202–73206 (2015)
104. Sengupta, J.: Graphene-induced performance enhancement of batteries, touch screens, transparent memory, and integrated circuits : a critical review on a decade of developments (2022)
105. Yoon, J.S., et al.: Source/drain patterning finfets as solution for physical area scaling toward 5-nm node. *IEEE Access* **7**, 172290–172295 (2019)
106. Lu, H.W., et al.: The promise of graphene-based transistors for democratizing multiomics studies. *Biosens. Bioelectron.* **195**, 113605 (2022)
107. Lemme, M.C., Member, S., Echtermeyer, T.J., Baus, M., Kurz, H.: **28**(4), 1–12 (2007)
108. Sun, Y.L., et al.: Tunable transport characteristics of double-gated graphene field-effect transistors using P(VDF-TrFE) ferroelectric gating. *Carbon N. Y.* **96**, 695–700 (2016)
109. Vieira, N.C.S., et al.: Graphene field-effect transistor array with integrated electrolytic gates scaled to 200 mm. *J. Phys. Condens. Matter* **28**(8), 85302 (2016)
110. Li, X., Wang, X., Zhang, L., Lee, S., Dai, H.: Chemically derived, ultrasoft graphene nanoribbon semiconductors. *Science (80-.)* **319**(5867), 1229–1232 (2008)
111. Lee, J., et al.: 25 GHz embedded-gate graphene transistors with high-K dielectrics on extremely flexible plastic sheets. *ACS Nano* **7**(9), 7744–7750 (2013)
112. Lan, Y., et al.: Flexible graphene field-effect transistors with extrinsic f<sub>max</sub> of 28 GHz. *IEEE Electron Device Lett.* **39**(12), 1944–1947 (2018)
113. Montanaro, et al.: Optoelectronic mixing with high-frequency graphene transistors. *Nat. Commun.* **12**(1) (2021)
114. Llinas, J.P., et al.: Short-channel field-effect transistors with 9-atom and 13-atom wide graphene nanoribbons. *Nat. Commun.* **8**(1), 8–13 (2017)
115. Ning, J., et al.: Flexible field-effect transistors with a high on/off current ratio based on large-area single-crystal graphene. *Carbon N. Y.* **163**, 417–424 (2020)
116. Martini, L., et al.: Structure-dependent electrical properties of graphene nanoribbon devices with graphene electrodes. *Carbon N. Y.* **146**, 36–43 (2019)
117. Jangid, P., Pathan, D., Kottantharayil, A.: Graphene nanoribbon transistors with high ION/IOFF ratio and mobility. *Carbon N. Y.* **132**, 65–70 (2018)
118. Lin, Y., Jenkins, K.A., Valdes-garcia, A., Small, J.P., Farmer, D.B., Avouris, P.: N1803316H.Pdf. *Nano Lett.* **9**(1), 422–426 (2009)
119. Lin, Y., et al.: 100-GHz transistors from. *NANO* **327**(5966), 100 (2010)
120. Wu, Y., et al.: High-frequency, scaled graphene transistors on diamond-like carbon. *Nature* **472**(7341), 74–78 (2011)
121. Sire, C., et al.: Flexible gigahertz transistors derived from solution-based single-layer graphene. *Nano Lett.* **12**(3), 1184–1188 (2012)
122. Liu, C., Ma, W., Chen, M., Ren, W., Sun, D.: A vertical silicon-graphene-germanium transistor. *Nat. Commun.* **10**(1), 1–7 (2019)
123. Liao, L., et al.: High-speed graphene transistors with a self-aligned nanowire gate. *Nature* **467**(7313), 305–308 (2010)
124. Lin, Y.M., et al.: Wafer-scale graphene integrated circuit. *Science (80-.)* **332**(6035), 1294–1297 (2011)
125. Feng, Z.H., et al.: An ultra clean self-aligned process for high maximum oscillation frequency graphene transistors. *Carbon N. Y.* **75**, 249–254 (2014)
126. Yeh, C.H., et al.: Gigahertz flexible graphene transistors for microwave integrated circuits. *ACS Nano* **8**(8), 7663–7670 (2014)



127. Han, S.J., Garcia, A.V., Oida, S., Jenkins, K.A., Haensch, W.: Graphene radio frequency receiver integrated circuit. *Nat. Commun.* **5**, 1–6 (2014)
128. Bianchi, M., et al.: Scaling of graphene integrated circuits. *Nanoscale* **7**(17), 8076–8083 (2015)
129. Hanna, T., Deltimple, N., Khenissa, M.S., Pallecchi, E., Happy, H., Frégonèse, S.: 2.5 GHz integrated graphene RF power amplifier on SiC substrate. *Solid. State. Electron.* **127**, 26–31 (2017)
130. Vaziri, S., et al. NI304305X.Pdf. no. c (2013)
131. Liu, C., et al.: A silicon-graphene-silicon transistor with an improved current gain. *J. Mater. Sci. Technol.* **104**, 127–130 (2022)
132. Fakhri, I., et al.: Selective ion sensing with high resolution large area graphene field effect transistor arrays. *Nat. Commun.* **11**(1) 1–12 (2020)
133. Mutlu, Z., et al.: Bottom-up synthesized nanoporous graphene transistors. *Adv. Funct. Mater.* **31**(47), 1–8 (2021)
134. Wu, F., et al.: Vertical MoS<sub>2</sub> transistors with sub-1-nm gate lengths. *Nature* **603**(7900) 259–264 (2022).
135. Han, T.H., et al.: Extremely efficient flexible organic light-emitting diodes with modified graphene anode. *Nat. Photonics* **6**(2), 105–110 (2012)
136. Han, T.H., et al.: Versatile p-type chemical doping to achieve ideal flexible graphene electrodes. *Angew. Chemie Int. Ed.* **55**(21), 6197–6201 (2016)
137. Han, T.H., Kwon, S.J., Seo, H.K., Lee, T.W.: Controlled surface oxidation of multi-layered graphene anode to increase hole injection efficiency in organic electronic devices. *2D Mater* **3**(1) (2016)
138. Denis, P.A.: Band gap opening of monolayer and bilayer graphene doped with aluminium, silicon, phosphorus, and sulfur. *Chem. Phys. Lett.* **492**(4–6), 251–257 (2010)
139. Bae, S., et al.: Roll-to-roll production of 30-inch graphene films for transparent electrodes. *Nat. Nanotechnol.* **5**(8), 574–578 (2010)
140. Güneş, F., et al.: Layer-by-layer doping of few-layer graphene film. *ACS Nano* **4**(8), 4595–4600 (2010)
141. Pinto, H., Markevich, A.: Electronic and electrochemical doping of graphene by surface adsorbates. *Beilstein J. Nanotechnol.* **5**(1), 1842–1848 (2014)
142. Mali, K.S., Greenwood, J., Adisojoso, J., Phillipson, R., De Feyter, S.: Nanostructuring graphene for controlled and reproducible functionalization. *Nanoscale* **7**(5), 1566–1585 (2015)
143. Wei, D., Liu, Y., Wang, Y., Zhang, H., Huang, L., Yu, G.: Synthesis of n-doped graphene by chemical vapor deposition and its electrical properties. *Nano Lett.* **9**(5), 1752–1758 (2009)
144. Urban, J.M., et al.: Nitrogen doping of chemical vapor deposition grown graphene on 4H–SiC(0001). *J. Appl. Phys.* **115**(23) (2014)
145. Dr. Xu, W., et al.: Controllable n-type doping on CVD-grown single—And double-layer graphene mixture. *Adv. Mater.* **27**(9), 1619–1623 (2015)
146. Shin, H., et al.: Control of electronic structure of graphene by various dopants and their effects on a nanogenerator. *J. Am. Chem. Soc.* pdf **16**, 15603–15609 (2010)
147. Liu, H., Liu, Y., Zhu, D.: Chemical doping of grapheme. *J. Mater. Chem.* **21**(10), 3335–3345 (2011)
148. Lee, W.H., et al.: Acsnano\_doping of CVD grown graphene b fluoropolymer for transparent.pdf. **2**, 1284–1290 (2012)
149. Kim, K.K., et al.: Enhancing the conductivity of transparent graphene films via doping. *Nanotechnology* **21**(28) (2010)
150. Jung, S.M., Jung, H.Y., Dresselhaus, M.S., Jung, Y.J., Kong, J.: A facile route for 3D aerogels from nanostructured 1D and 2D materials. *Sci. Rep.* **2**(i), 1–6 (2012)

151. Park, H., et al.: Graphene cathode-based ZnO nanowire hybrid solar cells. *Nano Lett.* **13**(1), 233–239 (2013)
152. Kim, H., et al.: On-fabrication solid-state N-doping of graphene by an electron-transporting metal oxide layer for efficient inverted organic solar cells. *Adv. Energy Mater.* **6**(12), 1–8 (2016)
153. Wang, Y., Chen, X., Zhong, Y., Zhu, F., Loh, K.P.: Large area, continuous, few-layered graphene as anodes in organic photovoltaic devices. *Appl. Phys. Lett.* **95**(6), 2012–2015 (2009)

# Catalytic Performance of Graphene-Based Nanocomposites



Prasenjit Mandal and Hari Shankar Biswas

**Abstract** For the past decade, two-dimensional graphene-based nanomaterials are at risk of global interest in scientists and incentives to detect various potential application in energy storage, sensor, electronic device, and catalysis due to their outstanding chemical and physical feature, which has quickly improved. Recently, researchers very much interested have also targeted on carbon-based materials such as graphene oxide or graphene-based nanocomposite, which lead to the progress of several applications in catalysis, e.g., coupling reaction, oxidation, reduction, and organic catalytic reaction. There is a significant interrelation between structural shape with the catalytic performance of the nanocomposite materials, which is a central focus to develop a high-performance catalyst in the research area, which is discussed. The challenges of the future developments of such associated materials are proposed and discussed. In this study, the effective approaches of the synthesized methods and their recent development of various catalytic applications of graphene or graphene oxide nanocomposites have been discussed.

**Keywords** Graphene · Graphene oxide · Nanocomposite · 2D-material · Catalysis

## 1 Introduction

For the advancement of elemental science knowledge, the importance of nanotechnology and nanoscience is a foremost driving force for nanomaterials to be accepted mostly. The superiority of our day-to-day life has excellently improved from time to time because of the discovery of suitable nanomaterials, and such novel nanomaterials are carbon-based nanomaterials. Such type of 2D material is graphene.

---

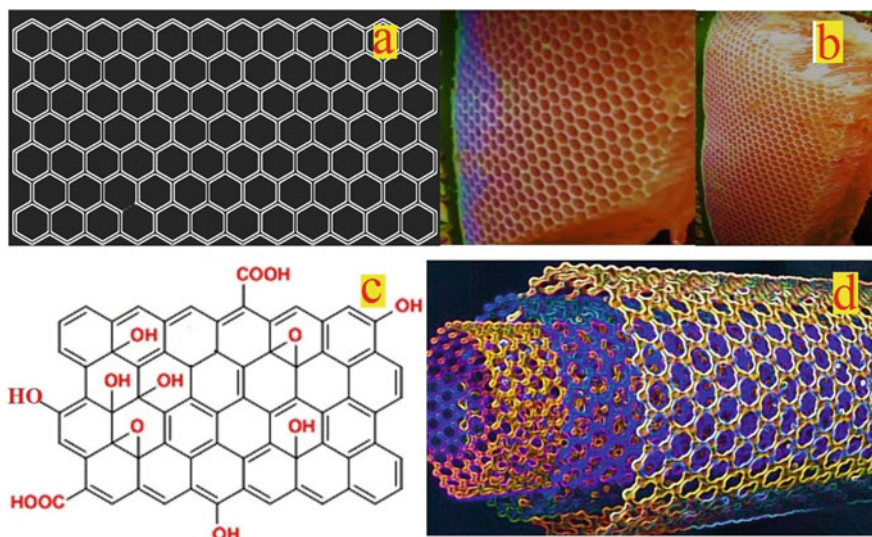
P. Mandal · H. S. Biswas (✉)

Department of Chemistry, Surendranath College, Kolkata, West Bengal 700009, India  
e-mail: [harishankarb7@gmail.com](mailto:harishankarb7@gmail.com)

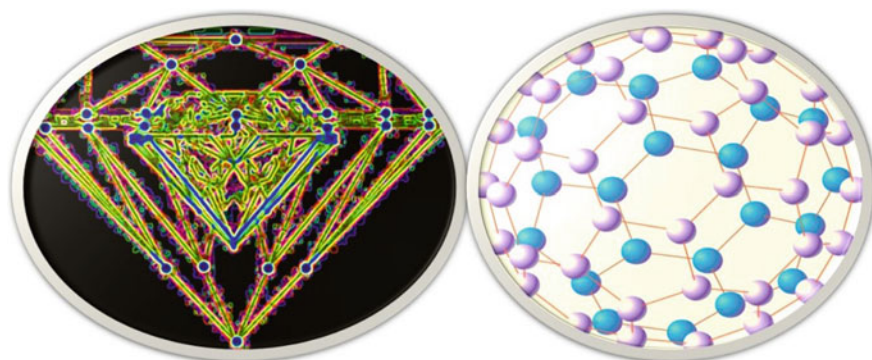
Department of Chemistry, Santipur College, Nadia, West Bengal 741404, India

Andre Geim and Konstantin Novoselov jointly won Nobel prize for their breakthrough experiment on the most attractive nanomaterial graphene in 2010. The wonder material graphene formation promises the future transformation, which is already the matter of scientific interest and legend around the globe. Geim and Novoselov extracted graphene material at first from pure graphite by micromechanical cleavage [1]. This chapter reviews the brief history and further work on graphene. It also deals with various synthetic methods of obtaining graphene-based or graphene oxide-based nanomaterials, the general properties of such materials, and their various application in different fields. Such types of applications are electronic industries, energy storage devices, catalysis, electrochemistry, and in biotechnology. The term “graphene” originated in 1987 when it was applied to  $sp^2$ -hybridized single-layer carbon, linked together in a hexagonal fashion lattice. Technically, it is 2D honeycomb structure lattice of the allotrope of carbon. (Scheme 1a, b). In 1962, it was first observed through the electron microscope. This 2D structure is the basic building block structure of graphite (three-dimensional), carbon nanotubes (quasi-one-dimensional), and buckyballs or fullerenes (Scheme 2) (quasi-zero-dimensional). Diamond (Scheme 2) is another allotrope of carbon, with an  $sp^3$  hybridized and tetrahedral structure. Although graphene has a two-dimensional structure and is not very stable in pure form [2], it has attracted much attention and has been subject to numerous investigations due to its unique physicochemical [3], electrochemical [4], and electronic graphene-based nanophotonic devices [5]. Graphene shows exceptionally good mobility of charge carriers ( $2 \times 10^5 \text{ cm}^2\text{V}^{-1} \text{ s}^{-1}$ ) [6] and high thermal conductivity ( $5000 \text{ Wm}^{-1} \text{ K}^{-1}$ ) [7]. This property was obtained by depositing the layers of graphene on solid support. The ruffled graphene became super hydrophobic. When used as a battery electrode, electrochemical current density increases in this material. Graphene is a candidate for future solar cells, wearable electronics, and other media, as a sensor for various types of materials, as an efficient catalyst, as a supercapacitor, and as a gas storage medium. The focus on industrial applications of graphene is likely to be of special interest, and there is outstanding demand for a good sample produced in laboratories. The features of each of the different allotropes of carbon are summarized in Table 1. For example, graphene and carbon nanotubes can be exceptionally good adsorbing materials [8] and have environmental applications [9] by removing heavy metals such as chromium, copper, cadmium, lead, and nickel from wastewater [10–12].

Graphene can be functionalized by various functional groups on the surface. Hydrophilic functional groups may be used to synthesize nanocomposites with other materials. Graphene is an excellent matrix for nanocomposite due to its excellent biocompatibility, high surface area, high electrical conductivity, exceptional chemical tolerance, etc. The research group of R. S. Ruoff at Northwestern University first reported graphene-based nanocomposites, in 2006. According to them, by modifying graphene sheets with inorganic nanomaterials, the electrical conductivity has been enhanced significantly for the nanocomposite. These properties helped to introduce a new type of graphene-based nanocomposite materials. Various synthetic methods like



**Scheme 1** **a** Schematic drawing of graphene, **b** original honeycomb structure by mobile click, **c** schematic drawing of graphene oxide, **d** schematic drawing of carbon nanotube



**Scheme 2** Schematic drawing of diamond and  $C_{60}$

ex-situ hybridization, in-situ formation, or crystallization on the surface of graphene (such as chemical reduction method, hydrothermal/solvothermal routes, electrochemical deposition, and sonochemical method) have been used for the synthesis of such composites. Through, the introduction of several types of functional materials, important properties of graphene material, and derivatives of its may be harnessed. To date, many such types of graphene-based nanocomposite have been prepared successfully with inorganic nanostructures such as silver, gold, tin, copper, cobalt, and some metal oxides like  $ZnO$ ,  $SnO_2$ ,  $TiO_2$ ,  $Fe_3O_4$ ,  $Fe_2O_3$ ,  $NiO$ ,  $MnO_2$  [13–19], polymers [20], organic crystals [21], metal-organic frameworks (MOFs) [22, 23],

**Table 1** Summary of features of the common allotropes of carbon

Properties	Fullerene (C <sub>60</sub> )	Diamond	Carbon nanotube	Graphite	Graphene
Color	Black solid	Colorless	Black	Steel black to gray	Black
Hybridization	sp <sup>2</sup> trigonal planar	sp <sup>3</sup> tetrahedral	sp <sup>2</sup> trigonal planar	sp <sup>2</sup> trigonal planar	sp <sup>2</sup> planar sheet
<i>Crystal formation</i>	Hexagonal, cubic	Octahedral	Carbon multi-layer tubular	Tubular	Hexagonal lattice
<i>C–C length (Å)</i>	1.53	1.54	1.42	1.39	1.42
<i>Density (gcm<sup>-3</sup>)</i>	1.7–1.9	3.52	2	1.99–2.3	> 1
<i>Crystal structure</i>	Face-centered cubic	Cubic	Cylindrical	Hexagonal	Honeycomb
<i>Electric Conductivity</i>	Semiconductor	Insulator	Conductor to semiconductor	Conductor	Conductor to semiconductor
<i>Melting point (K)</i>	> 553	3700	3970	3800	4900
<i>Bulk modulus (G Pa)</i>	9.1	1200	141.8	207	280
<i>Resistivity (ohm m)</i>	1 × 10 <sup>14</sup>	1 × 10 <sup>18</sup>	Constant	1.37 × 10 <sup>-5</sup>	1 × 10 <sup>-3</sup>

carbon nanotubes (CNTs) [24, 25], and biomaterials [26, 27]. These nanocomposites may be used in various fields, as energy storage [28, 29], solar cells [30–34], lithium-ion batteries, supercapacitors, pseudocapacitors, memory devices [35–37], Raman enhancement [38–40], sensing platforms [41–44], molecular imaging [45, 46], catalysis [47–56], and even drug delivery [57]. Recently, a few review articles have shorted the development graphene-based nanocomposite materials. Especially as advanced catalysts, these nanocomposites have shown outstanding performance. In this scenario, our main focus on the preparation of graphene oxide-based nanocomposite. We also deal with and focus on their catalytic applications in several types of chemical reactions to synthesize industrial, eco-friendly, biocompatible materials, pharmaceuticals, and other organic compounds. In this review, we have discussed effective approaches for the preparation of graphene or graphene oxide-based nanocomposite with their currently various types of catalytic applications. Until now, nonstop, quick research has progressed to expand simple and greener methods to the synthesis of graphene or graphene oxide-based nanocomposite materials and their organic catalytic reaction.

## 1.1 *Synthesis of Graphene*

Graphene has been synthesized in numerous ways and on several substrates. As the method of preparation of graphene is varied, the resulting purity, crystallinity, size, and transport properties of the product also may vary. Earlier, several techniques were known for producing graphitic thin films. The thin layers of graphite were prepared on a transition metal surface by precipitation method [58, 59] in the 1970s. In 1975, multi-layer graphite was prepared on a single-crystal platinum surface via the chemical decomposition method. But the name “graphene” was still not known in scientific circles and may be due to several factors [60]. Since the 1980s, there has been an explosive growth of surface characterization techniques, especially on the micro- and nanoscale. Nowadays, vastly, superior techniques are known for the preparation of nanostructured **graphene** [61]. Some of these techniques are chemical synthesis, electron beam lithography, electrochemical preparation, the catalytic transformation of fullerene, graphene oxide (GO) reduction, microwave-assisted hydrothermal (MAH), hydrothermal method, ultrasonic exfoliation method, and the soft-template method. In the present work, the chemical method has been the method of choice.

### **Exfoliation**

In 2004, graphene was first exfoliated mechanically from graphite. Graphene obtained by exfoliation shows the highest electron mobility and the lowest number of defects. It is a low-budget technique and was initially attributed as the cause of the unpredictable development of interest in graphene. Graphene flakes obtained by this method have proved to be invaluable for clarification of its basic structural characteristic. The preparation of graphene by the exfoliation method includes the use of adhesive tapes, graphite oxidation–reduction, shearing, wedge-based method, solvent-aided method, electrochemical synthesis, application of immiscible liquids and molten salts, etc.

### **Adhesive Tape**

Andre Geim and his co-workers first used the adhesive tape method to separate the graphene layer from graphite sheets [62]. Obtaining a monolayer (or ultra-pure) graphene sheet usually requires several exploitation steps, and each step produces fewer and fewer levels ultimately remaining one layer. Generally, the flakes are deposited onto a silicon plate or other surface after exfoliation. Crystallites can be visible to the naked eye if their size is greater than 1 mm [63].

## Reduction of Graphene Oxide

The generation of single-layer flakes of reduced graphene oxide (rGO) was first reported by P. Boehm in 1962 [64, 65]. Heating of graphite oxide rapidly and exploitation produced quick heating of graphite oxide and exfoliation produced powder of dispersed carbon with less percentage of graphene or rGO. The graphite oxide reduction single-layer sheets like reduction by hydrazine in an argon/hydrogen environment can produce graphene sheets. Afterward, this reduction procedure has been improved to produce rGO with an integral framework of carbon which allows the complete elimination of any functional group. The charge carrier mobility has been measured more than  $1000 \text{ cm}^2 (\text{393.70 in})^2/\text{Vs}$  [66]. The characterization of rGO was conducted by spectroscopic techniques [67, 68].

## Shearing

D graphene-containing defect-free and unoxidized liquids can be prepared from graphite powder using mixers which form local shear rates larger than  $10 \times 10^4$  in 2004 [69, 70]. This technique was deemed to apply to other two-dimensional materials, such as sheets of BN, MoS<sub>2</sub>, and other layered crystals [71, 72].

## Solvent-Aided Methods

In an appropriate aqueous medium, graphite powder was dispersed to create a graphene sheet by sonication. Centrifugation is used to separate graphene from graphite [73]. The concentration of prepared graphene was initially about 0.01 mg/ml N-methyl pyrrolidone (NMP) then afterward improved to 2.1 mg/ml [74]. Applying an appropriate ionic solution as a dispersing agent in an aqueous medium created a 5.33 mg/ml concentration [75]. The yield obtained in this method is still quite low compared to other methods, as there is nothing to prevent graphene sheets from restacking due to van der Waals's force of attraction. The highest concentration in each case is achieved when the van der Waals force of attraction matches with interaction forces between the solvent molecules and sheets of graphene. The restacking can be prevented by adding a surfactant to the solvent before sonication to get adsorbed to the graphene. This technique produces a higher concentration of graphene, but surfactant removal needs some extra care.

## Using Immiscible Liquids

To get macro-scale graphene sheets, two immiscible liquids like water-heptane are used at the interface for the sonication of graphite. The sheets of graphene are adsorbed at the high-energy interface of water and heptane, and the restacking is



prevented. The solvents may then be evaporated. The graphene films thus obtained are up to ~ 95% transparent and conducting [76].

### **From Molten Salts**

Graphene can be synthesized by reducing of graphite particles into molten salts along with different carbon nanostructures [77]. In the molten lithium chloride,  $H^+$  ion can be discharged on the cathodically polarized graphite that intercalated and peeled graphene films. Single-crystalline structure of graphene nanosheets may be formed with a lateral size of up to 100  $\mu\text{m}$ , with a high degree of crystallinity and high thermal stability [78].

### **Electrochemical Syntheses**

Exfoliated graphene can be made by electrochemical method, in which tuning the pulsed value, control thickness, flake area, number of defects, and other effects of features of the products. The exploitation starts by bathing the graphite in the solvent during intercalation. It is the transparent solutions, monitored with a photodiode and LED [79] which can make by such a process.

### **Hydrothermal Self-assembly**

Graphene sheet can be synthesized by using sugar like glucose, fructose, and some other sugar. The substrate-free hydrothermal self-assembly “bottom-up” process is harmless, eco-friendly, and easier than exploitation method. This technique is used to control the thickness from single-layer to multi-layer [61], which is known as the “Tang-Lau method.”

### **Deposition by Chemical Vapor Method**

The chemical vapor deposition (CVD) technique is an important method to prepare very high-quality, high-performance, solid materials, in which a wafer is exposed to gaseous compounds. The technique is frequently applied to create graphene thin film and other various nanomaterials in the semiconductor industries. It is a well-tested process to deposit of graphene as industrial scale to obtain thin films with a large surface area. The thin film is developed by decomposing the gaseous compounds on the solid surface. But several volatile by-products may also form, which must be removed.

## Epitaxy

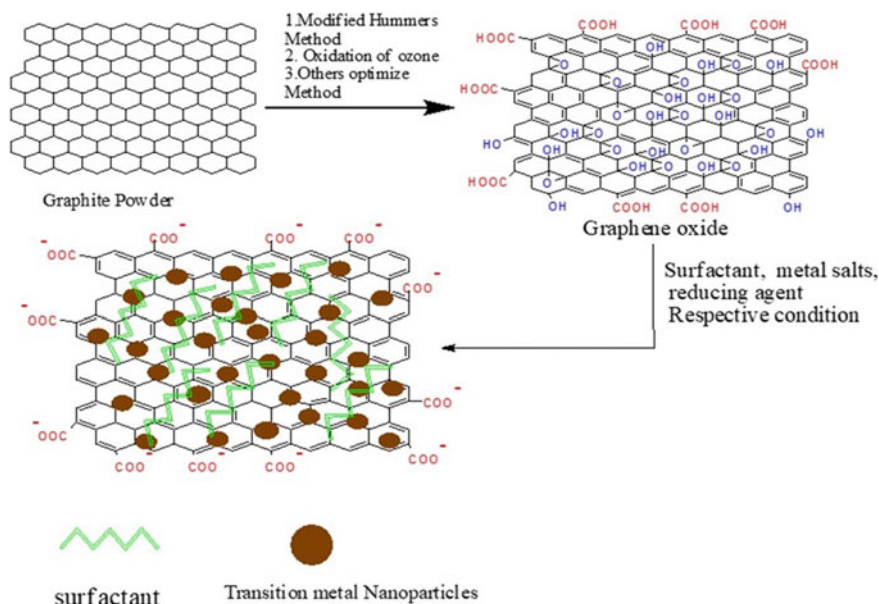
Epitaxy is the process in which a crystalline overlayer deposited on a crystalline substrate. In this method, the graphene layers are attached to the surfaces by the van der Waals force of interactions. This helps in retaining the 2D of isolated graphene of electronic band structure [80, 81]. A very good example of such epitaxial graphene on silicon carbide crystal [82]. At 1100 °C and at very low pressure (c.  $10^{-6}$  torr), silicon carbide reduces the graphite layer deposited on it to graphene [83–86]. Graphene can also be synthesized using several other epitaxial methods, e.g., using metal substrates [87–89], pyrolysis of sodium ethoxide [90], method of roll-to-roll [91], cold wall epitaxy [92], with wafer-scale CVD [93–96], by nanotube slicing [97, 98], by intercalation [99], by carbon dioxide reduction [100, 101], by spin coating and supersonic spray [102, 103], and using lasers [104].

## Microwave-Assisted Reduction

Direct synthesis of graphene, which was reported in 2012, using a one-step microwave-assisted method [105]. In this method, the graphene produced is associated with a low amount of oxygen and does not require any further treatment. This method does not need  $\text{KMnO}_4$  in the reaction mixture. Also, defect formation can be controlled by controlling the microwave time which can be considered as enhanced Hummer's method. In a modified version, the microwave heating process was used instead of traditional heating.

### *1.2 A Journey from Graphite Powder to Graphene Oxide*

The oxidized form of graphene is known as graphene oxide. It contains the variable ratio of carbon, oxygen, and hydrogen, made by the strong oxidation of graphite, which is low-cost and plentiful. So, the layered sheets of graphene oxide have been used to create strong paper-like materials, thin films, membranes, and various nanocomposite materials. It is considered to be a simple method of preparation and GO dispersible in deionized water and many other solvents. It is usually obtained in dispersed form, as a coating on substrates, and may be purchased in powder form as well. In 1898, Staudenmaier proposed an idea to oxidize graphite flakes using concentrated nitric acid, sulphuric acid, and  $\text{KMnO}_4$  to produce oxygen, carbon, and hydrogen-containing functionalized groups on graphite, known as graphite oxide. Such an oxidation process is practical but hazardous. Therefore, the method has been modified by Hummers and Offeman in 1958. The modified method improved the safety of the oxidizing process of graphite flakes and completed the oxidation in less than two hours. They used oxidizing reagents (water-acid mixture and  $\text{NaNO}_3$ ), resulting in a comparable level of oxidation. From then onwards, the synthesis of graphene oxide was made using Hummer's method with some extra modifications



**Scheme 3** Synthesis of several graphene or graphene oxide-based nanocomposite

to avoid long oxidation time and generation of toxic gases. In this way, a high degree of oxidation is ensured. Marcano et al. discover a method to synthesize graphene oxide in 2010. They increase the amount of potassium permanganate, and instead of  $\text{HNO}_3$ , they used  $\text{H}_3\text{PO}_4$  (9:1,  $\text{H}_2\text{SO}_4/\text{H}_3\text{PO}_4$ ). This method has been proven to create a large amount of hydrophilic graphene oxide. Also, no toxic gas is generated by this method. It also enhanced the oxidation efficiency of graphite flakes, making them more oxidized as compared to Hummer's method. Therefore, GO can be prepared by various methods like mechanical, thermal, chemical, etc. [106]. It is a very interesting material in material science, to be applied in areas such as capacitors [107], batteries [108], sensors [109], conducting materials [110, 111], biotechnology [112, 113], and as support of other nanoparticles and in catalytic applications. Synthesis of several graphene or graphene oxide-based nanocomposite is shown by Scheme 3.

### 1.3 Overview of Nanocomposite

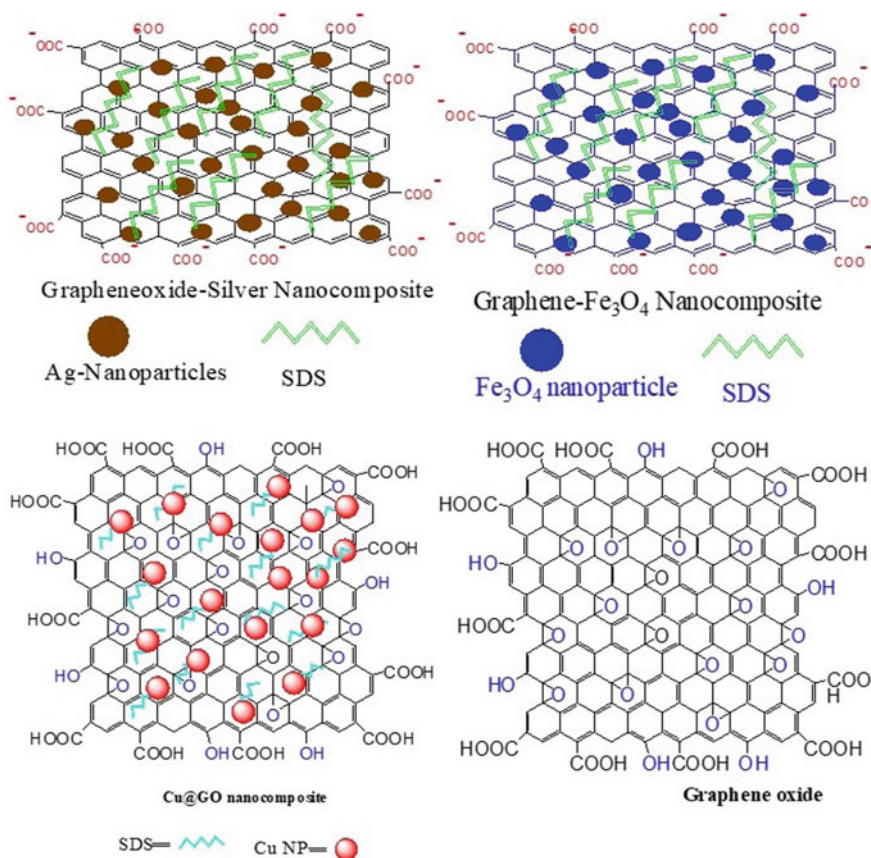
The word “nanotechnology” can be defined as the restrained manipulation, synthesis, characterization, and application of nanomaterial with at least one dimension less than 1000 nm. The dimensionality plays a vital role to assess the distinctness of matter. In the twenty-first century, nanotechnology is an exceptionally promising field of materials science. This technology offers physics, chemistry, materials science,

biology, and medicinal chemistry a full set of new materials with properties that can be tuned at will. The progress to increasingly facile methods for manufacturing of such materials may lead to a plethora of cheaper biomedical products, electronic devices, high-performance materials, and cosmetic articles. The commercialization of nanotechnology is prospective to massive increases in technological development, betterment of the quality of life, concomitant to social and environmental benefits around the world. There may certainly be changes as well in the fields of organic synthesis, inorganic materials, energy storage, semiconductors, and in biotechnology. In this sense, nanocomposite materials are defined as nanoscale materials that contain unique chemical and physical features with novel applications. Nanocomposite materials are nanosized particles incorporated into a standard matrix material. The nanometer unit evolved from the prefix nano from a Greek word meaning “dwarf” or very small. The nano-world lies intermediate between the quantum phenomena and atomic structure and the scale of bulk materials. The laws of atomic physics influenced some material features at the nanoscale level, and thus, behavior different from the conventional bulk materials is observed. There are two main classes of nanomaterials: engineered and environmental (metal sulfides and metal oxides frequently obtained as minerals). The engineered nanoparticles are defined as synthetically constructed nanoparticles. The work embodied in the present thesis deals with the investigation of several types of engineered nanoparticles. These nanomaterials, with important properties which are also discussed herein, may play a significant role in the society in future. Some examples of GO nanocomposite and graphene oxide sheets have been shown in Scheme 4.

### **Synthesis of graphene or graphene oxide-based nanocomposite**

## ***1.4 Graphene-Based Nanocomposite Catalyzed Reactions***

In recent years, large numbers of catalytic systems using graphene-based nanomaterials have been reported [114–116]. Many of these catalytic systems contain metals or metal nanoparticles or metal oxides. Such graphene-based nanomaterials are widely used for oxidation, reduction, and for different coupling reactions [13–57, 61, 66–122]. In the case of oxidation reactions, the use of graphene-based nanomaterials catalyzing the aerial oxidation of benzyl alcohol to benzaldehyde was reported by Bielawski et al. [123]. A similar application of graphene-based nanocomposite as catalysis in the oxidation of benzene to phenol in presence of hydrogen peroxide (30%) was reported by Ma et al. [124]. The application of graphene-based nanocatalyst in the oxidation of 5-hydroxymethylfurfural to 2,5-diformylfuran in presence of oxygen was reported by Hou et al. [125]. Cyclohexane to cyclohexanol, adipic acid, and cyclohexanone, in presence of oxygen as an oxidant and catalyzed by graphene-based nanomaterials, was reported by Peng et al. [125]. In the case of reduction or hydrogenation reactions, the conversion of nitrobenzene to aniline in presence of hydrazine hydrate as the reductant and catalyzed by graphene-based nanomaterials was reported by Ma et al. [126–128]. Oxygen reduction reaction was first carried out

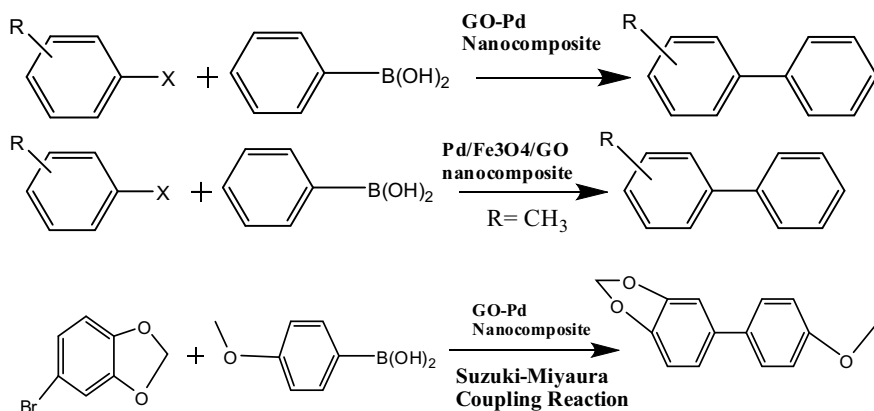


**Scheme 4** Examples of graphene oxide nanocomposite and graphene oxide sheet

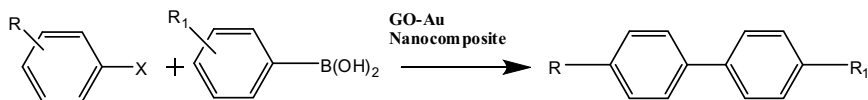
in presence of graphene-based nanomaterials as reported by Yang et al. [129]. The conversion of cinnamaldehyde to hydrocinnamaldehyde in presence of hydrogen and catalyzed by graphene-based nanomaterials was reported by Li et al. [130]. Reduction of 4-nitrophenol to 4-aminophenol in presence of  $\text{NaBH}_4$  as a reductant and catalyzed by graphene-based nanomaterials was reported by Ghosh et al. [131]. In the case of coupling reactions, the conversion of indoles to  $\alpha$ ,  $\beta$ -unsaturated ketones, and nitro-styrene catalyzed by graphene-based nanomaterials was reported by Rao et al. [132]. Transformation of primary amide to imine by oxidative coupling reaction in presence of graphene-based nanocatalyst was reported by Yang et al. [133]. The coupling reaction (alkylation) between alcohols and styrenes in presence of graphene-based nanomaterials was reported by Szostak et al. [134]. The alkylation reaction

between benzene and iodobenzene in presence of graphene-based nanomaterials was reported by Ma et al. and others [135].

### Example of (C–C) Coupling Reaction



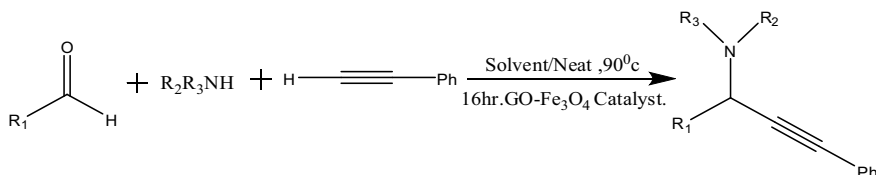
Cross Suzuki–Miyaura coupling reaction using Au-GO nanocomposite.



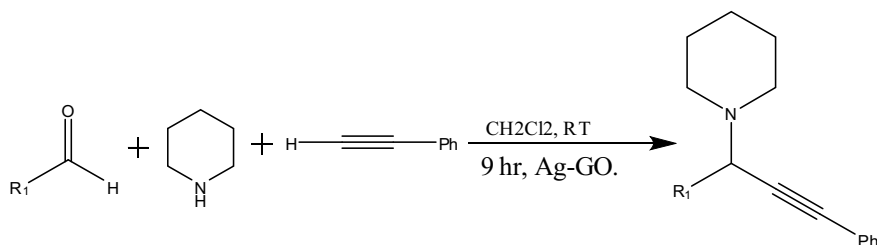
### A<sup>3</sup> Coupling Reaction

In the present scenario of organic synthesis, there is a lot of interest in coupling or multi-component reactions in one-pot synthesis. Such methods are termed “green,” and certainly reduce time and cost. Separation (and purification) of the product remains the only problem. Propargylamines are essential starting points for the synthesis of numerous nitrogen-containing biological active compounds, such as oxotremorine analogs, beta-lactams, isosteres, conformationally restricted peptides, and therapeutic drug molecules. These are also important structural elements of many natural products. Propargylamines are adaptable intermediates for the manufacture of various agrochemicals and proto-drug molecules. In 1998, Dax and co-workers first reported the solid phase synthesis of propargyl amines via the coupling of an aldehyde, an alkyne, and a secondary amine. This three-component coupling reaction, promoted by two equivalents of copper chloride, is termed the A<sup>3</sup> coupling reaction and is a supreme example of solid phase one-pot synthetic methodology [136]. Li and co-workers reported the A<sup>3</sup> coupling reaction using CuBr–RuCl<sub>3</sub> catalytic system

in water and under solvent-free conditions in 2002. They also reported that various copper salts like CuCl, CuCl<sub>2</sub>, CuBr, and CuI can be used as catalysts in this reaction [137]. In 2003, propargylamine was synthesized using the same reaction with salts of Au(I) and Au (III) as catalysts. The gold salts and gold-supported nanocatalysts are highly efficient catalysts for this reaction as the loading of gold is generally very low (<1 mol%) for the effective reaction [138]. Although the procedures reported by Li and co-workers provided eco-friendly and direct access to a range of propargyl amines [139, 140], all existing protocols have various substrate limitations and usually require a long time to complete. In t 2004, Tu and co-workers were the first to identify this problem and reported a rapid reaction method, and microwave-assisted copper-catalyzed A<sup>3</sup> coupling [141]. This methodology was restricted to the homogeneous catalyst to prepare propargyl amines under such reaction conditions. There are certain disadvantages related to the application of homogeneous catalysts, they are not cost-effective, and separation of them is not easy from their mixture. Moreover, even with the decrease in the reaction time and substrate scope developments, a significant challenge remains in the A<sup>3</sup>-coupling field, viz. that of recycling of the catalyst. After completion of the reaction, the loss of costly transition metal catalyst becomes a drawback. Park and Alper first reported a study on the recyclability of catalysts in A<sup>3</sup> coupling in 2005 [142]. The A<sup>3</sup> coupling reaction proceeds via direct dehydrative condensation [143] and requires several homogeneous and heterogeneous transition metal or supported metal nanocomposite catalysts like gold nanoparticles



[144], silver nanoparticles [145], Fe<sub>3</sub>O<sub>4</sub> nanoparticles, zinc, iridium [146], copper in solid phase systems, or some supported catalysts such as copper-doped alumina [147]. In continuation of attempts to enhance scope of A<sup>3</sup> coupling reaction to produce propargylamines, we reported graphene oxide-Fe<sub>3</sub>O<sub>4</sub> nanocomposites as outstanding catalysts for the same reaction [148]. The catalyst is easy to prepare, economical, robust, and recyclable.



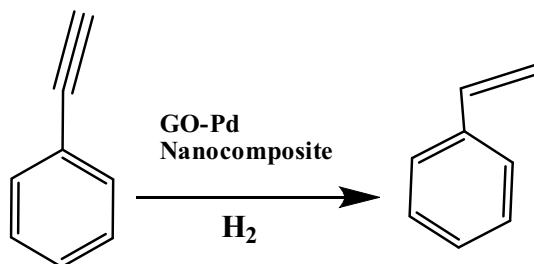
### Example of A<sup>3</sup> coupling reaction with Chemdraw structure

### Reduction of Nitroarenes

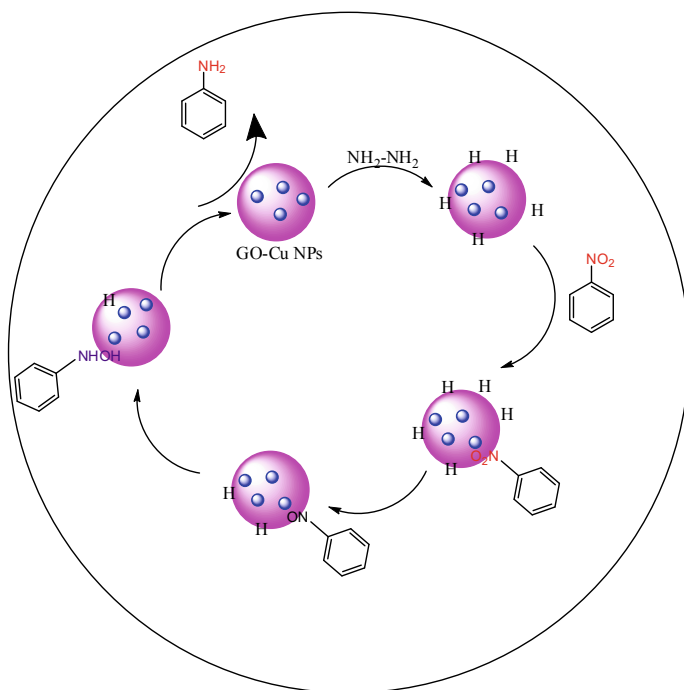
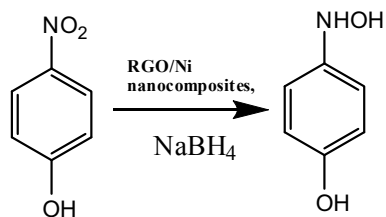
The reduction of nitro compounds can be altered by using various reagent and conditions. One of the first functional groups is the nitro to be reduced, by history. The hydrogenation reduction of many substituted nitrobenzene is a significant reaction of enormous interest, because aniline that is produced, and its derivatives are very important substances for the fabrication in the chemical industry of polymer agrochemical, pigments herbicides, dyes, and pharmaceuticals [149–153]. They are also important intermediates and key precursors to produce various organic compounds such as amines, hydroxylamine, and azo compounds. In the literature, several processes are reported for this reduction, including homogeneous and heterogeneous catalytic hydrogenation reduction [154, 155], electrolytic reduction [156], and reduction using metals. In recent times, catalytic hydrogenation was broadly reported for many substrates. A vital and adaptable methodology for the preparation of amines and its derivatives by reduction of functionalized nitro compounds uses many homogeneous and heterogeneous catalysts. Some examples of such stoichiometric reducing agents are NaBH<sub>4</sub>, H<sub>2</sub>O, hydrazine, propan-2-ol [157–162], and some metal-based catalysts such as Pd [163], Au [164], Ni [165], Fe [166], Pt [167], Co [168], Rh [169, 170], and Ru [171, 172]. For the reduction of nitrobenzene to amines, homogeneous catalysts are not beneficial anymore. The use of heterogeneous catalysts is more profitable because they are easy to separate from the reaction mixture and hence can be further used for the reaction. It would be an advantage if there is no significant loss of stability, selectivity, or catalytic activity.

Hydrogenation reduction of phenylacetylene to styrene synthesis using prepared GO-Pd nanocomposite catalyst is shown below.





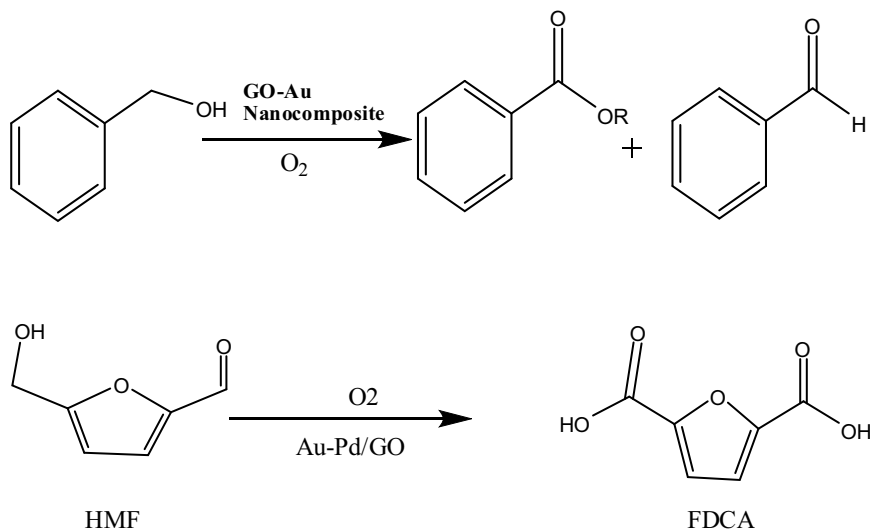
$\text{NaBH}_4$  is used for reduction of p-nitrophenol as a model system for quantitative evaluation of catalytic activity of as-prepared nanocomposites is shown in Scheme 5.



**Scheme 5** General scheme of reaction mechanism for the reduction of nitroarenes

### Oxidation Reaction

Au-GO nanocomposite catalyzed aerobic oxidative esterification reactions of such oxidation [173].



## 2 Conclusion Outlook and Remarks

Confidently, this chapter, we have assisted the reader to understand that the graphene is really a 2D honeycomb structure, has unique optical, electronic, nanophotonic, thermal, mechanical, and chemical properties. Since, to date, there has been no suitable practical technique for the production of graphene sheet in large scale, a new skill for synthesis of scalable graphene sheets needs to be developed. In our view, graphene nanocomposites and conventional catalysts may give some unexpected properties for further investigation. Similarly, design and tuned characterization techniques are welcome to explore. Again, it is difficult to get metal-free graphene-based catalyst, but it is the most attractive field for the future sustainable catalyst. Discovery of more reactions is expected to explore its applications on nanophotonic and electrochemical processes. Besides that, researchers are very much interested on graphene oxide-based nanocomposite materials, which lead to the progress of several applications in catalysis, e.g., coupling reaction, oxidation, reduction, and organic catalytic reaction. A very important topic is the significance of the relationship between catalytic performance materials and structural shape of nanocomposite that has become a hot topic of research to develop high-performance catalytic system, discussed in this review. The challenges of the future developments

of such associated materials are proposed and discussed. In this review, we have also discussed achievement of the effective approaches for preparation of graphene and graphene oxide-based nanocomposite materials with their application as catalyst in various field very recent. We think these efforts will help our scientific community with the tune fabrication and design of novel graphene nanocomposite material with excellent efficiency for future catalytic applications around the globe.

**Acknowledgements** One (H. S. Biswas) of the authors thanks to UGC minor research project, Reference No. F.PSW-140/15-16 for funding. The authors also thank, Mr. U.S. Sil of PPD, SINP, Dr. Indranil Kar, Principal, Surendranath College for their valuable suggestion and help.

**Conflicts of Interest** There are no conflicts of interest.

## References

1. Chen, C., Yang, Q.H., Yang, Y., Lev, W., Wen, Y., Hou, P.-X., Wang, M., Cheng, H.-M.: Self-assembled free-standing graphite oxide membrane. *Adv. Mat.* **21**, 3007–3011 (2009)
2. Novoselov, K.S., Geim, A.K., Morozov, S.V., Jiang, D., Zhang, Y., Dubonos, S.V., Grigorieva, I.V., Firsov, A.A.: Electric field effect in atomically thin carbon films. *Science* **306**, 659–666 (2004)
3. Meyer, J.C., Geim, A.K., Katsnelson, M.I., Novoselov, K.S., Booth, T.J., Roth, S.: The structure of suspended graphene sheets. *Nature* **446**, 60–63 (2007)
4. Huang, H.P., Zhu, J.J.: Preparation of novel carbon-based nanomaterial of graphene and its applications electrochemistry. *Chin. J. Anal. Chem.* **39**, 963–971 (2011)
5. Pandya, A., Sorathiya, V., Lavadiya, S.: Graphene-based nanophotonic devices. *Recent Advances in Nanophotonics–Fundamentals and Applications* (2020). <https://doi.org/10.5772/intechopen.93853>
6. Bolotin, K.I., Sikes, K.J., Jiang, Z., Klima, M., Fudenberg, G., Hone, J., Kim, P., Stormer, H.L.: Ultrahigh electron mobility in suspended graphene. *Solid State Commun.* **146**, 351–355 (2008)
7. Balandin, A.A., Ghosh, S., Bao, W.Z., Calizo, I., Teweldebrhan, D., Miao, F., Lau, C.N.: Superior thermal conductivity of single-layer graphene. *Nano Lett.* **8**, 902–907 (2008)
8. Liu, Q., Shi, J., Zeng, L., Wang, T., Cai, Y., Jiang, G.: Evaluation of graphene as an advantageous adsorbent for solid-phase extraction with chlorophenols as model analytes. *Chromatogr. A.J.: Epub* **1218**, 197–204 (2011)
9. Tariq, W., Ali, F., Arslan, C., Nasir, A., Hamza Gillani, S., Rehman, A.: Synthesis and applications of graphene and graphene-based nanocomposites: conventional to artificial intelligence approaches. *Front. Environ. Chem.* (2022). <https://doi.org/10.3389/fenvc.2022.890408>
10. Kuo, C.Y., Lin, H.Y.: Adsorption of aqueous cadmium (II) onto modified multi-walled carbon nanotubes following microwave/chemical treatment. *Desalination* **249**, 792–796 (2009)
11. Pillay, K., Cukrowska, E.M., Coville, N.J.: Multi-walled carbon nanotubes as adsorbents for the removal of parts per billion levels of hexavalent chromium from aqueous solution. *J. Hazard. Mater.* **166**, 1067–1075 (2009)
12. Kandah, M.I., Meunier, J.L.: Removal of nickel ions from water by multi-walled carbon nanotubes. *J. Hazard. Mater.* **146**, 283–288 (2007)
13. Wu, S., Yin, Z., He, Q., Huang, X., Zhou, X., Zhang, H.: Electrochemical deposition of semiconductor oxides on reduced graphene oxide-based flexible, transparent, and conductive electrodes. *J. Phys. Chem. C* **114**, 11816–11821 (2010)

14. Yin, Z., Wu, S., Zhou, X., Huang, X., Zhang, Q., Boey, F., Zhang, H.: Electrochemical deposition of ZnO nanorods on transparent reduced graphene oxide electrodes for hybrid solar cells. *Small* **6**, 307–312 (2010)
15. Mandal, P., Molla, R.A., Chattopadhyay, A.P., Poddar, S., Biswas, H.S.: GO-APTES-Cu (II) Schiff base complex as efficient heterogeneous catalyst for aerobic decarboxylation reaction of phenylacetic acids. *Inorg. Chem. Commun.* **144**, 109825 (2022)
16. Muszynski, R., Seger, B., Kamat, P.V.: Decorating graphene sheets with gold nanoparticles. *J. Phys. Chem. C* **112**, 5263–5266 (2008)
17. Shi, W., Zhu, J., Sim, D.H., Tay, Y.Y., Lu, Z.Y., Zhang, X.J., Zhang, H., Hng, H.H., Yan, Q.: Achieving high specific charge capacitances in Fe<sub>3</sub>O<sub>4</sub>/reduced graphene oxide nanocomposites. *J. Mater. Chem.* **21**, 3422–3427 (2011)
18. Zhu, J., Zhu, T., Zhou, X., Zhang, Y., Lou, X.W., Chen, X., Chen, H., Zhang, H., Hng, H.H., Ma, J., Yan, Q.: Facile synthesis of metal oxide/reduced graphene oxide hybrids with high lithium storage capacity and stable cyclability. *Nanoscale* **3**, 1084–1089 (2011)
19. Huang, X., Li, S., Huang, Y., Wu, S., Zhou, X., Li, S., Gan, C.L., Boey, F., Mirkin, C.A., Zhang, H.: Synthesis of hexagonal close-packed gold nanostructures. *Nat. Commun.* **2**, 292–297 (2011)
20. Han, T.H., Lee, W.J., Lee, D.H., Kim, J.E., Choi, E.Y., Kim, S.O.: Peptide/graphene hybrid assembly into core/shell nanowires. *Adv. Mater.* **22**, 2060–2064 (2010)
21. Jahan, M., Bao, Q., Yang, J.-X., Loh, K.P.: Structure-directing role of graphene in the synthesis of metal–organic framework nanowire. *J. Am. Chem. Soc.* **132**, 14487–14495 (2010)
22. Petit, C., Bandoz, T.J.: Enhanced adsorption of ammonia on metal-organic framework/graphite oxide composites: analysis of surface interactions. *Adv. Funct. Mater.* **20**, 111–118 (2010)
23. Petit, C., Burrell, J., Bandoz, T.J.: The synthesis and characterization of copper-based metal–organic framework/graphite oxide composites. *Carbon* **49**, 563–572 (2011)
24. Dong, X., Li, B., Wei, A., Cao, X., Chan-Park, M.B., Zhang, H., Li, L.-J., Huang, W., Chen, P.: One-step growth of graphene-carbon nanotube hybrid materials by chemical vapor deposition. *Carbon* **49**, 2944–2949 (2011)
25. Fan, Z., Yan, J., Zhi, L., Zhang, Q., Wei, T., Feng, J., Zhang, M., Qian, W., Wei, F.: A three-dimensional carbon nanotube/graphene sandwich and its application as electrode in supercapacitors. *Adv. Mater.* **22**, 3723–3728 (2010)
26. Lu, C.H., Yang, H.H., Zhu, C.L., Chen, X., Chen, G.N.: A graphene platform for sensing biomolecules. *Angew. Chem. Int. Ed.* **121**, 4879–4881 (2009)
27. Wang, Y., Li, Z., Hu, D., Lin, C.-T., Li, J., Lin, Y.: Aptamer/graphene oxide nanocomplex for in situ molecular probing in living cells. *J. Am. Chem. Soc.* **132**, 9274–9276 (2010)
28. Zhang, L.L., Zhou, R., Zhao, X.S.: Graphene-based materials as supercapacitor electrodes. *J. Mater. Chem.* **20**, 5983–5989 (2010)
29. Vivekchand, S., Rout, C., Subrahmanyam, K., Govindaraj, A., Rao, C.: Graphene-based electrochemical supercapacitors. *J. Chem. Sci.* **120**, 9–14 (2008)
30. Wang, X., Zhi, L., Mullen, K.: Transparent, conductive graphene electrodes for dye-sensitized solar cells. *Nano Lett.* **8**, 323–329 (2007)
31. Guo, C.X., Yang, H.B., Sheng, Z.M., Lu, Z.S., Song, Q.L., Li, C.M.: Layered graphene/quantum dots for photovoltaic devices. *Angew. Chem. Int. Ed.* **49**, 3014–3021 (2010)
32. Chang, H., Lv, X., Zhang, H., Li, J.: Quantum Dots Sensitized Graphene: In situ growth and application in photoelectrochemical cells. *Electrochem. Commun.* **12**, 483–488 (2010)
33. Wang, P., Jiang, T., Zhu, C., Zhai, Y., Wang, D., Dong, S.: One-step, solvothermal synthesis of graphene-CdS and graphene-ZnS quantum dot nanocomposites and their interesting photovoltaic properties. *Nano Res.* **3**, 794–799 (2010)
34. Liu, Z., He, D., Wang, Y., Wu, H., Wang, J.: Solution-processable functionalized graphene in donor/acceptor-type organic photovoltaic cells. *Sol. Energy Mater. Sol. Cells* **94**, 1196–1202 (2010)
35. Mandal, P., Bala, S., Poddar, S., Sarkar, S., Biswas, H.S.: Fabrication of graphene-Fe<sub>3</sub>O<sub>4</sub>-polypyrrole based ternary material as an electrode for pseudocapacitor application. *Mater. Today: Proceed.* **65(2)**, 1001–1010 (2022)

36. Navarro, C.G., Weitz, R.T., Bittner, A.M., Scolari, M., Mews, A., Burghard, M., Kern, K.: Electronic transport properties of individual chemically reduced graphene oxide sheets. *Nano Lett.* **7**, 3499–3503 (2007)
37. Zhang, L., Liang, J., Huang, Y., Ma, Y., Wang, Y., Chen, Y.: Size-controlled synthesis of graphene oxide sheets on a large scale using chemical exfoliation. *Carbon Carbon* **47**, 3365–3368 (2009)
38. Xie, L., Ling, X., Fang, Y., Zhang, J., Liu, Z.: Graphene as a substrate to suppress fluorescence in resonance raman spectroscopy. *J. Am. Chem. Soc.* **131**, 9890–9891 (2009)
39. Ling, X., Xie, L., Fang, Y., Xu, H., Zhang, H., Kong, J., Dresselhaus, M.S., Zhang, J., Liu, Z.: Can graphene be used as a substrate for raman enhancement? *Nano Lett.* **10**, 553–561 (2009)
40. Ling, X., Zhang, J.: First-layer effect in graphene-enhanced raman scattering. *Small* **6**, 2020–2025 (2010)
41. Chang, H., Tang, L., Wang, Y., Jiang, J., Li, J.: Graphene fluorescence resonance energy transfer aptasensor for the thrombin detection. *Anal. Chem.* **82**, 2341–2346 (2010)
42. Park, S., Mohanty, N., Suk, J.W., Nagaraja, A., An, J., Piner, R.D., Cai, W., Dreyer, D.R., Berry, V., Ruoff, R.S.: Biocompatible, robust free-standing paper composed of a TWEEN/graphene composite. *Adv. Mater.* **22**, 1736–1740 (2010)
43. Wang, Z., Zhang, J., Chen, P., Zhou, X., Yang, Y., Wu, S., Niu, L., Han, Y., Wang, L., Boey, F., Zhang, Q., Liedberg, B., Zhang, H.: Label-free, electrochemical detection of methicillin-resistant staphylococcus aureus DNA with reduced graphene oxide-modified electrodes. *Biosens. Bioelectron.* **26**, 3881–3887 (2011)
44. Schedin, F., Geim, A.K., Morozov, S.V., Hill, E.W., Blake, P., Katsnelson, M.I., Novoselov, K.S.: Detection of individual gas molecules adsorbed on graphene. *Nat. Mater.* **6**, 652–657 (2007)
45. Cai, W., Chen, X.: Nanoplatforms for targeted molecular imaging in living subjects. *Small* **3**, 1840–1854 (2007)
46. Peng, C., Hu, W., Zhou, Y., Fan, C., Huang, Q.: Intracellular imaging with a graphene-based fluorescent probe. *Small* **6**, 1686–1692 (2010)
47. Scheuermann, G.M., Rumi, L., Steurer, P., Bannwarth, W., Mu, R., Haupt, L.: Palladium nanoparticles on graphite oxide and its functionalized graphene derivatives as highly active catalysts for the Suzuki–Miyaura coupling reaction. *J. Am. Chem. Soc.* **131**, 8262–8270 (2009)
48. Singh, R.N., Awasthi, R.: Graphene support for enhanced electrocatalytic activity of Pd for alcohol oxidation. *Catal. Sci. Technol.* **1**, 778–783 (2011)
49. Zhang, N., Qiu, H., Liu, Y., Wang, W., Li, Y., Wang, X., Gao, J.: Fabrication of gold nanoparticle/graphene oxide nanocomposites and their excellent catalytic performance. *J. Mater. Chem.* **21**, 11080–11083 (2011)
50. He, H., Gao, C.: Graphene nanosheets decorated with Pd, Pt, Au, and Ag nanoparticles: Synthesis, characterization, and catalysis applications. *Sci. China: Chem.* **54**, 397–404 (2011)
51. Li, Y., Fan, X., Qi, J., Ji, J., Wang, S., Zhang, G., Zhang, F.: Gold nanoparticles–graphene hybrids as active catalysts for Suzuki reaction. *Mater. Res. Bull.* **45**, 1413–1418 (2010)
52. Mastalir, A., Kiraly, Z., Patzko, A., Dekany, I., Argentiere, P.L.: Synthesis and catalytic application of Pd nanoparticles in graphite oxide. *Carbon* **46**, 1631–1637 (2008)
53. Dreyer, D.R., Bielawski, C.W.: Carbocatalysis: Heterogeneous carbons finding utility in synthetic chemistry. *Chem. Sci.* **2**, 1233–1240 (2011)
54. Long, Y., Zhang, C., Wang, X., Gao, J., Wang, W., Liu, Y.: Oxidation of SO<sub>2</sub> to SO<sub>3</sub> catalyzed by graphene oxide foams. *J. Mater. Chem.* **21**, 13934–13941 (2011)
55. J. Pyun.: Graphene oxide as catalyst: application of carbon materials beyond nanotechnology. *Angew. Chem. Int. Ed.* **50**, 46–54 (2011)
56. Jia, H.P., Dreyer, D.R., Bielawski, C.W.: C–H oxidation using graphite oxide. *Tetrahedron* **67**, 4431–4434 (2011)
57. Akhavan, O., Ghaderi, E., Esfandiari, A.: Wrapping bacteria by graphene nanosheets for isolation from environment, reactivation by sonication, and inactivation by near-infrared irradiation. *J. Phys. Chem. B* **115**, 6279–6288 (2011)

58. Eizenberg, M., Blakely, J.M.: Carbon monolayer phase condensation on Ni(111). *Surf. Sci.* **82**, 228–236 (1979)
59. Eizenberg, M., Blakely, J.M.: Carbon interaction with nickel surfaces: Monolayer formation and structural stability. *J. Chem. Phys.* **71**, 3467–3479 (1979)
60. Lang, B.: A LEED study of the deposition of carbon on platinum crystal surfaces. *Surf. Sci.* **53**, 317–329 (1975)
61. Novoselov, K.S., Geim, A.K., Morozov, S.V., Jiang, D., Zhang, Y., Dubonos, S.V., Grigorieva, I.V., Firsov, A.A.: Electric field effect in atomically thin carbon films. *Science* **306**, 666–669 (2004)
62. Geim, A.K., MacDonald, A.H.: Graphene: exploring carbon flatland. *Phys. Today* **60**, 35–41 (2007)
63. Boehm's 1961 Isolation of Graphene. *Graphene Times*. 7 December 2009; Archived from the original on October 8, 2010
64. Many Pioneers in Graphene Discovery. *Letters to the Editor. Aps.org*. Vol.9, January 2010
65. Eigler, S., Enzelberger-Heim, M., Grimm, S., Hofmann, P., Kroener, W., Geworski, A., Dotzer, C., Röckert, M., Xiao, J., Papp, C., Lytken, O., Steinrück, H.P., Müller, P., Hirsch, A.: Wet chemical synthesis of graphene. *Adv. Mater.* **25**, 3583–3587 (2013)
66. Yamada, Y., Yasuda, H., Murota, K., Nakamura, M., Sodesawa, T., Sato, S., Analysis of heat-treated graphite oxide by X-ray photoelectron spectroscopy; *J. M. Sci.* **48**, 8171–8190 (2013)
67. Ji, L., Xin, H.L., Kuykendall, T.R., Wu, S.L., Zheng, H., Rao, M., Cairns, E.J., Battaglia, V., Zhang, Y.: SnS<sub>2</sub> nanoparticle loaded graphene nanocomposites for superior energy storage. *Phys. Chem. Chem. Phys.* **14**, 6981–6994 (2012)
68. Mohandoss, M., Gupta, S.S., Nelleri, A., Pradeep, T., Maliyekkal, S.M.: Solar mediated reduction of graphene oxide. *RSC Adv.* **7**, 957–963 (2017)
69. Pato, K.R. et al: Scalable production of large quantities of defect-free few-layer graphene by shear exfoliation in liquids. *Nat. Mater.* **13**, 624–630 (2014)
70. Hernandez, Y., Nicolosi, V., Lotya, M., Blighe, F.M., Sun, Z., De, S., McGovern, I.T., Holland, B., Byrne, M., Gun'Ko, Y.K., Boland, J.J., Niraj, P., Duesberg, G., Krishnamurthy, S., Goodhue, R., Hutchison, J., Scardaci, V., Ferrari, A.C., Colema, J.N.: High-yield production of graphene by liquid-phase exfoliation of graphite. *Nat. Nanotechnol.* **3**, 563–568 (2008)
71. Alzari, V., Nuvoli, D., Scognamillo, S., Piccinini, M., Gioffredi, E., Malucelli, G., Marceddu, S., Sechi, M., Sanna, V., Mariani, A.: Graphene-containing thermoresponsive nanocomposite hydrogels of poly(N-isopropylacrylamide) prepared by frontal polymerization. *J. M. Chem.* **21**, 8727–8733 (2011)
72. Nuvoli, D., Valentini, L., Alzari, V., Scognamillo, S., Bon, S.B., Piccinini, M., Illescas, J., Mariani, A.: High concentration few-layer graphene sheets obtained by liquid phase exfoliation of graphite in ionic liquid. *J. M. Chem.* **21**, 3428–3431 (2011)
73. Woltornist, S.J., Oyer, A.J., Carrillo, J.M.Y., Dobrynin, A.V., Adamson, D.H.: Conductive thin films of pristine graphene by solvent interface trapping. *ACS Nano* **7**, 7062–7066 (2013)
74. Kamali, A.R., Fray, D.J.: Molten salt corrosion of graphite as a possible way to make carbon nanostructures. *Carbon* **56**, 121–131 (2012)
75. Kamali, A.R., Fray, D.J.: Large-scale preparation of graphene by high temperature insertion of hydrogen into graphite. *Nanoscale* **7**, 11310–11320 (2015)
76. Mario, H., Yu, C.W., Tuân, N.D., Ping, H.Y.: Controlling the properties of graphene produced by electrochemical exfoliation. *Nanotechnology* **26**, 335607–335621 (2015)
77. Tang, L., Li, X., Ji, R., Teng, K.S., Tai, G., Ye, J., Wei, C., Lau, S.P.: Bottom-up synthesis of large-scale graphene oxide nanosheets. *J. M. Chem.* **22**, 5676–5683 (2012)
78. Gall, N.R., Rut'Kov, E.V., Tontegode, A.Y.: Two dimensional graphite films on metals and their intercalation. *Int. J. Mod. Phys.* **11**, 1865–1911 (1997)
79. Gall, N.R., Rut'Kov, E.V., Tontegode, A.Y.: Influence of surface carbon on the formation of silicon-refractory metal interfaces. *Thin Solid Films* **226**, 229–233 (1995)
80. Jobst, J., Waldmann, D., Speck, F., Hirner, R., Duncan, D.K., Thomas, S.W., Weber, B.H.: Quantum oscillations and quantum Hall effect in epitaxial graphene. *Phys. Rev. B.* **81**, 195434–195447 (2009)

81. Shen, T., Gu, J.J., Xu, M., Wu, Y.Q., Bolen, M.L., Capano, M.A., Engel, L.W., Ye, P.D.: Observation of quantum-Hall effect in gated epitaxial graphene grown on SiC (0001). *App. Phys. Letters*. **95**, 172105–172113 (2009)
82. Wu, X., Hu, Y., Ruan, M., Madiomanana, N.K., Hankinson, J., Sprinkle, M., Berger, C., de, H., Walt, A.: Half integer quantum Hall effect in high mobility single layer epitaxial graphene. *App. Phys. Lett.* **95**(22), 223108–223123 (2009)
83. Alexander-Webber, J.A., Baker, A.M.R., Janssen, T.J.B.M., Tzalenchuk, A., Lara-Avila, S., Kubatkin, S., Yakimova, R., Piot, B.A., Maude, D.K., Nicholas, R.J.: Phase space for the breakdown of the quantum Hall effect in epitaxial graphene. *Phys. Rev. Lett.* **111**, 96601–96613 (2013)
84. Pletikosić, I., Kralj, M., Pervan, P., Brako, R., Coraux, J., n'Diaye, A., Busse, C., Michely, T.: Dirac cones and minigaps for graphene on Ir(111). *Phys. Rev. Lett.* **102**, 056808 (2009)
85. Mattevi, C., Kim, H., Chhowalla, M.: A review of chemical vapour deposition of graphene on copper. *J. Mat. Chem.* **21**, 3324–3334 (2011)
86. Ghoneim, M.T., Smith, C.E., Hussain, M.M.: Simplistic graphene transfer process and its impact on contact resistance. *App. Phys. Lett.* **102**, 103104–103109 (2013)
87. Choucair, M., Thordarson, P., Stride, J.A.: Gram-scale production of graphene based on solvothermal synthesis and sonication. *Nat. Nanotechnol.* **4**, 30–33 (2008)
88. Chhowalla, M., Teo, K.B.K., Ducati, C., Rupesinghe, N.L., Amaratunga, G.A.J., Ferrari, A.C., Roy, D., Robertson, J., Milne, W.I.: Growth process conditions of vertically aligned carbon nanotubes using plasma enhanced chemical vapor deposition. *J. Appl. Phys.* **90**, 5308–5317 (2001)
89. Bae, S., Kim, H., Lee, Y., Xu, X., Park, J.S., Zheng, Y., Balakrishnan, J., Lei, T., Kim, H.-R.: Roll-to-roll production of 30-inch graphene films for transparent electrodes. *Nat. Nanotech.* **5**, 574–578 (2010)
90. Bointon, T.H., Barnes, M.D., Russo, S., Craciun, M.F.: High quality monolayer graphene synthesized by resistive heating cold wall chemical vapor deposition. *Adv. Mat.* **27**, 4200–4206 (2015)
91. Tao, L., Lee, J., Chou, H., Holt, M., Ruoff, R.S., Akinwande, D.: Synthesis of high quality monolayer graphene at reduced temperature on hydrogen-enriched evaporated copper (111) films. *ACS Nano* **6**, 2319–2325 (2012)
92. Rahimi, S., Tao, L., Chowdhury, Sk.F., Park, S., Jouvray, A., Buttress, S., Rupesinghe, N., Teo, K., Akinwande, D.: Toward 300 mm wafer-scalable high-performance polycrystalline chemical vapor deposited graphene transistors. *ACS Nano* **8**, 10471–10479 (2014)
93. Tao, L., Lee, J., Holt, M., Chou, H., McDonnell, S.J., Ferrer, D.A., Babenco, Matías, G., Wallace, R.M., Banerjee, S.K.: Uniform wafer-scale chemical vapor deposition of graphene on evaporated Cu (111) film with quality comparable to exfoliated monolayer. *J. Phys. Chem C*. **116**, 24068–24074 (2012)
94. Kosynkin, D.V., Higginbotham, A.L., Sinitskii, A., Lomeda, J.R., Dimiev, A., Price, B.K., Tour, J.M.: Longitudinal unzipping of carbon nanotubes to form graphene nanoribbons. *Nature* **458**, 872–876 (2009)
95. Liying, J., Zhang, L., Wang, X., Diankov, G., Dai, H.: Narrow graphene nanoribbons from carbon nanotubes. *Nature* **458**, 877–880 (2009)
96. Chakrabarti, A., Lu, J., Skrabutenas, J.C., Xu, T., Xiao, Z., Maguire, J.A., Hosmane, N.S.: Conversion of carbon dioxide to few-layer graphene. *J. Mat. Chem.* **21**, 9491–9497 (2011)
97. Kim, D.Y., Ray, S.S., Park, J.J., Lee, J.G., Cha, Y.H., Bae, S.H., Ahn, J.H., Jung, Y.C., Kim, S.M., Yarin, A.L., Yoon, S.S.: Self-healing reduced graphene oxide films by supersonic kinetic spraying. *Adv. Fun. Mat.* **24**, 4986–4995 (2014)
98. Vimalanathan, K., Gascooke, J.R., Martinez, I.S., Marks, N.A., Kumari, H., Garvey, C.J., Atwood, J.L., Lawrance, W.D., Raston, C.L.: Fluid dynamic lateral slicing of high tensile strength carbon nanotubes. *Sci. Rep.* **6**, 22865–22872 (2016)
99. Tang, Y.P., Paul, D.R., Chung, T.S.: Free-standing graphene oxide thin films assembled by a pressurized ultrafiltration method for dehydration of ethanol. *J. Membr. Sci.* **458**, 199–208 (2014)

100. Kovtyukhova, N.I., Wang, Y., Berkdemir, A., Silva, R.C., Terrones, M., Crespi, V.H., Mallouke T.E.: Non-oxidative intercalation and exfoliation of graphite by Brønsted acids. *Nat. Chem.* **6**, 957–963 (2014)
101. Maher, F., Kady, E., Strong, V., Dubin, S., Kaner, R.B.: Laser scribing of high-performance and flexible graphene-based electrochemical capacitors. *Sci.* **335**, 1326–1330 (2012)
102. Viana, M.M., Lima, M.C.F.S., Forsythe, J.C., Gangoli, V.S., Cho, M., Cheng, Y., Silva G.G., Wong, M.S., Caliman, V.: Facile graphene oxide preparation by microwave-assisted acid method. *J. Braz. Chem. Soc.* **26**, 30535–901 (2015)
103. Li, G., Shi, L., Zeng, G., Zhang, Y., Sun, Y.: Efficient dehydration of the organic solvents through graphene oxide (GO)/ceramic composite membranes. *Rsc. Adv.* **4**, 52012–52015 (2014)
104. Nair, R.R., Wu, H.A., Jayaram, P.N., Grigorieva, I.V., Geim, A.K.: Unimpeded permeation of water through helium-leak-tight graphene-based membranes. *Science* **335**, 442–444 (2012)
105. Liu, H.Y., Wang, H.T., Zhang, X.W.: Facile fabrication of freestanding ultrathin reduced graphene oxide membranes for water purification. *Adv. Mater.* **27**, 249–254 (2015)
106. Biswas, H.S., Bala, S., Kundu, A.K., Saha, I., Poddar, S., Sarkar, S., Mandal, P.: Tuned synthesis and designed characterization of graphene oxide thin film. *Inorg. Chem. Commun.* **139**, 109356 (2022)
107. Liu, C., Yu, Z., Neff, D., Zhamu, A., Jang, B.Z.: Graphene-based supercapacitor with an ultrahigh energy density. *Nano Lett.* **10**, 4863–4869 (2010)
108. Dreyer, D.R., Park, S., Bielawski, C.W., Ruoff, R.S.: The chemistry of graphene oxide. *Chem. Soc. Rev.* **39**, 228 (2010)
109. Lin, Y.H., Shao, Y.Y., Wang, J., Wu, H., Liu, J., I.A.: Graphene based electrochemical sensors and biosensors: a review. *Electroanalysis* **22**, 1027–1038 (2010)
110. Zhou, M., Wang, Y.L., Zhai, Y.M., Zhai, J.F., Ren, W., Wang, F.A., Dong, S.J.: Controlled synthesis of large-area and patterned electrochemically reduced graphene oxide films. *Chem. Eur. J.* **15**, 6116–6121 (2009)
111. Hu, W., Peng, C., Luo, W., Lv, M., Li, X., Li, D., Huang, Q., Fan, C.: Graphene-based antibacterial paper. *ACS Nano* **4**, 4317–4322 (2010)
112. Zhang, L., Li, Y., Li, D.W., Karpuzov, D., Long, Y.T.: Electrocatalytic oxidation of NADH on graphene oxide and reduced graphene oxide modified screen-printed electrode. *Int. J. Electrochem. Sci.* **6**, 819–829 (2011)
113. Wan, L., Song, Y., Zhu, H., Wang, Y., Wang, L.: Electron transfer of co-immobilized cytochrome c and horseradish peroxidase in chitosan-graphene oxide modified electrode. *Int. J. Electrochem. Sci.* **6**, 4700–4706 (2011)
114. Fecheté, I., Wang, Y., Védrine, J.C.: The past, present and future of heterogeneous catalysis. *Catal. Today.* **189**, 22–27 (2012)
115. Li, Y., Shen, W.J.: Morphology-dependent nanocatalysts: rod-shaped oxides. *Chem. Soc. Rev.* **43**, 1543–1574 (2014)
116. (a) Zaera, F.: Nanostructured materials for applications in heterogeneous catalysis. *Chem. Soc. Rev.* **42**, 2746–2762 (2013); (b) Mandal, P., Chattopadhyay, A.N., Chattopadhyay, A.P.: Highly efficient and recyclable silver-graphene oxide nano-composite catalyst in the acylation of amines under solvent-free condition. *MOJ Biorg. Org. Chem.* **2**(4) 201–211 (2018)
117. Qi, X., Pu, K.Y., Li, H., Zhou, X., Wu, S., Fan, Q.-L., Liu, B., Boey, F., Huang, W., Zhang, H.: Amphiphilic graphene composites. *Angew. Chem. Int. Ed.* **49**, 9426–9429 (2010)
118. Mishra, A.K., Ramaprabhu, S.: Functionalized graphene-based nanocomposites for supercapacitor application. *J. Phys. Chem. C* **115**, 14006–14011 (2011)
119. Su, C.L., Loh, K.P.: Carbocatalysts: graphene oxide and its derivatives. *Accounts. Chem. Res.* **46**, 2275–2285 (2013)
120. Navalon, S., Dhakshinamoorthy, A., Alvaro, M., Garcia, H.: Carbocatalysis by graphene-based materials. *Chem. Rev.* **114**, 6179–6212 (2014)
121. Sengupta, A., Su, C.L., Bao, C.L., Nai, C.T., Loh, K.P.: Graphene oxide and its functionalized derivatives as carbocatalysts in the multicomponent strecker reaction of ketones. *Chemcatchem* **6**, 2507–2511 (2014)



122. Su, D.S., Perathoner, S., Centi, G.: Nanocarbons for the development of advanced catalysts. *Chem. Rev.* **113**, 5782–5816 (2013)
123. Dreyer, D.R., Jia, H.P., Bielawski, C.W.: Graphene oxide: a convenient carbocatalyst for facilitating oxidation and hydration reactions. *Angew. Chem. Int., Edit.* **49**, 6813–6816 (2010)
124. Yang, J.H., Sun, G., Gao, Y.J., Zhao, H.B., Tang, P., Tan, J., Lu, A.H., Ma, D.: Direct catalytic oxidation of benzene to phenol over metal-free graphene-based catalyst. *Energy. Environ. Sci.* **6**, 793–798 (2013)
125. Lv, G.Q., Wang, H.L., Yang, Y.X., Deng, T.S., Chen, C.M., Zhu, Y.L., Hou, X.L.: Graphene oxide: a convenient metal-free carbocatalyst for facilitating aerobic oxidation of 5-Hydroxymethylfurfural into 2, 5-Diformylfuran. *Acs Catal.* **5**, 5636–5646 (2015)
126. Cao, Y.H., Luo, X.Y., Yu, H., Peng, F., Wang, H.J., Ning, G.Q.: sp<sup>2</sup>- and sp<sup>3</sup>-hybridized carbon materials as catalysts for aerobic oxidation of cyclohexane. *Catal. Sci. Technol.* **3**, 2654–2660 (2013)
127. Hirashima, T., Manabe, O.: Catalytic reduction of aromatic nitro compounds with hydrazine in the presence of iron(iii) chloride and active carbon. *Chem. Lett.* **3**, 259–260 (1975)
128. Larsen, J.W., Freund, M., Kim, K.Y., Sidovar, M., Stuart, J.L.: Mechanism of the carbon catalyzed reduction of nitrobenzene by hydrazine. *Carbon* **38**, 655–661 (2000)
129. Han, B.H., Shin, D.H., Cho, S.Y.: Graphite catalyzed reduction of aromatic and aliphatic nitro compounds with hydrazine hydrate. *Tetrahedron. Lett.* **26**, 6233–6234 (1985)
130. Byon, R.B., Jin, S., Yang, S.H.: Graphene-based non-noble-metal catalysts for oxygen reduction reaction in acid. *Chem. Mater* **23**, 3421–3428 (2011)
131. Xie, R., Fan, G., Ma, Q., Yang, L., Li, F.: Facile synthesis and enhanced catalytic performance of graphene-supported Ni nanocatalyst from a layered double hydroxide-based composite precursor. *J. Mater. Chem. A* **2**, 7880–7889 (2014)
132. Moitra, D., Ghosh, B.K., Chandel, M., Ghosh, N.N.: Synthesis of a BiFeO<sub>3</sub> nanowire-reduced graphene oxide based magnetically separable nanocatalyst and its versatile catalytic activity towards multiple organic reactions. *RSc adv.* **6**, 97941–97952 (2016)
133. Kumar, A.V., Rao, K.R.: Recyclable graphite oxide catalyzed friedel–crafts addition of indoles to  $\alpha,\beta$ -unsaturated ketones. *Tetrahedron. Lett.* **52**, 5188–5191 (2011)
134. Wu, S., Wen, G., Schloglb, R., Su, D.S.: Carbon nanotubes oxidized by a green method as efficient metal-free catalysts for nitroarene reduction. *Phys. Chem. Chem. Phys.* **17**, 1567–1572 (2015)
135. Hu, F., Patel, M., Luo, F.X., Flach, C., Mendelsohn, R., Garfunkel, E., He, H.X., Szostak, M.: Graphene-catalyzed direct friedel–crafts alkylation reactions: mechanism, selectivity, and synthetic utility. *J. Am. Chem. Soc.* **137**, 14473–14480 (2015)
136. For example, see. (a) Gao, Y., Tang, P., Zhou, H., Zhang, W., Yang, H., Yan, N., Hu, G., Mei, D., Wang, J., Ma, D.: Graphene oxide promoted C–H arylation of benzene with aryl halides. *Angew. Chem. Int. Ed.* **55**, 3124–3128 (2016) (b) Santra, S., Hota, P.K., Bhattacharyya, R., Bera, Ghosh, P., Mandal, S.K.: *ACS Catal.* **3**, 2776–2789 (2013). (c) Hu, J., Wang, Y., Han, M., Zhou, Y., Jiang, X., Sun, P.: *Catal. Sci. Technol.* **2**, 2332–2340 (2012). (d) Gil, M.S., Luigi, R., Peter, S., Willli, B., Rolf, M.L.: *J. Am. Chem. Soc.* **131**, 8262–8270 (2009). (e) Mondal, P., Salam, N., Mondal, A., Ghosh, K., Khatun, T., Islam, Sk.M.: *J. C.I. Sci.* **459**, 97–106 (2015)
137. Dyatkin, A.B., Rivero, R.A.: The solid phase synthesis of complex propargylamines using the combination of sonogashira and mannich reactions. *Tetra. Lett.* **39**, 3647–3650 (1998)
138. Li, C.J., Wei, C.: Highly efficient Grignard-type imine additions via C–H activation in water and under solvent-free conditions. *Chem. Commun.* **0**, 268–269 (2002)
139. We, C., Li, C.J.: A highly efficient three-component coupling of aldehyde, alkyne, and amines via C–H activation catalyzed by gold in water. *J. Am. Chem. Soc.* **125**, 9584–9585 (2003)
140. Wei, C., Li, Z., Li, C.J.: The first silver-catalyzed three-component coupling of aldehyde, alkyne, and amine. *Org. Lett.* **5**, 4473–4475 (2003)
141. Shi, L., Tu, Y.Q., Wang, M., Zhang, F.M., Fan, C.A.: Microwave-promoted three-component coupling of aldehyde, alkyne, and amine via C–H activation catalyzed by copper in water. *Org. Lett.* **6**, 1001–1003 (2004)

142. For examples, see: (a) Polshettiwar, V., Baruwati, B., Varma, R.S.: Magnetic nanoparticle-supported glutathione: a conceptually sustainable organocatalyst. *Chem. Commun.* 1837–1839 (2009); (b) Luo, S., Zheng, X., Xu, H., Mi, X., Zhang, L., Cheng, J.-P.: *Adv. Synth. Catal.* **349**, 2431–2434 (2007); (c) Polshettiwar, V., Baruwati, B., Varma, R.S.: *Green Chem.* **11**, 127–131 (2009); (d) Kotani, M., Koike, T., Yamaguchi, K., Mizuno, N.: *Green Chem.* **8**, 735–741 (2006); (e) Zhang, D.H., Li, G.D., Lia, J.X., Chen, J.S.: *Chem. Commun.* **5**, 3414–3416 (2008); (f) Kawamura, M., Sato, K.: *Chem. Commun.*, **7**, 4718–4719 (2006); (g) Kawamura, M., Sato, K.: *Chem. Commun.* **8**, 3404–3405 (2007); (h) Hu, A., Yee, G.T., Lin, W.: *J. Am. Chem. Soc.* **127**, 12486–12487 (2005); (i) Chouhan, G., Wang, D., Alper, H.: *Chem. Commun.* **8**, 4809–4811 (2007); (j) Abu-Reziq, R., Wang, D., Post, M., Alper, H.: *Adv. Synth. Catal.* **349**, 2145–2150 (2007); (k) Polshettiwar, V., Varma, R.S.: *Chem. Eur. J.* **15**, 1582–1586 (2009); (l) Ge, J., Zhang, Q., Zhang, T., Yin, Y.: *Angew. Chem. Int. Ed.* **47**, 8924–8928 (2008)
143. Peshkov, V.A., Pereshivko, O.P., Van der Eycken, E.V.: A walk around the A<sup>3</sup>-coupling. *Chem. Soc. Rev.* **41**, 3790–3807 (2012)
144. Seidel, D.: The redox-A<sup>3</sup> reaction. *Org. Chem. Front.* **1**, 426–429 (2014)
145. Kidwai, M., Bansal, V., Kumar, A., Mozumdar, S.: The first Au-nanoparticles catalyzed green synthesis of propargylamines via a three-component coupling reaction of aldehyde, alkyne and amine. *Green Chem.* **9**, 742–745 (2007)
146. Teimouri, A., Chermahini, A.N., Nariman, M.: Simple and efficient one-pot three-component synthesis of propargylamines using bismuth(iii) chloride. *Bull. Korean Chem. Soc.* **33**, 1556–1560 (2012)
147. Satoshi, S., Takashi, K., Ishii, Y.: A three-component coupling reaction of aldehydes, amines, and alkynes. *Angew. Chem. Int. Ed.* **40**, 2534–2536 (2001)
148. (a) Youngman, M.A., Dax, S.L.: Solid-phase mannich condensation of amines, aldehydes, and alkynes: investigation of diverse aldehyde inputs. *J. Comb. Chem.* **3**, 469–472 (2001); (b) Dax, S.L., Youngman, M.A., Kocis, P., North, M.: *Solid-Phase Org. Synth.* **1**, 45–53 (2001); (c) Dyatkin, A.B., Rivero, R.A.: *Tetrahedron Lett.* **39**, 3647–3650 (1998); (d) McNally, J.J., Youngman, M.A., Dax, S.L.: *Tetrahedron Lett.* **39**, 967–970 (1998); (e) Youngman, M.A., Dax, S.L.: *Tetrahedron Lett.* **38**, 6347–6350 (1997)
149. (a) Liu, Y.H., Zhang, Z.H., Li, T.S.: Efficient conversion of epoxides into β-Hydroperoxy alcohols catalyzed by antimony trichloride/SiO<sub>2</sub>. *Synthesis*, 3314–3318 (2008); (b) Zhang, Z.H., Tao, X.Y.: *Aust. J. Chem.*, **61**, 77–79 (2008); (c) Liu, Y.-H., Liu, Q.-S., Zhang, Z.H.: *J. Mol. Catal. A: Chem.* **296**, 42–46 (2008); (d) Liu, Y.-H., Liu, Q.-S., Zhang, Z.H.: *Tetrahedron Lett.* **50**, 916–921 (2009); (e) Zhang, P., Zhang, Z.H.: *Monatsh. Chem.* **140**, 199–203 (2009); (f) Mandal, P., Chattopadhyay, A.P.: *Dalton Trans.* (2015), **44**, 11444–11456. (g) Salam, N., Sinha, A., Roy, A.S., Mondal, P., Jana, N.R., Islam, S.M.: *RSC Adv.* **4**, 10001–10012 (2014)
150. Downing, R.S., Kunkeler, P.J., van Bekkum, H.: Catalytic syntheses of aromatic amines. *Catal. Today* **37**, 121–136 (1997)
151. Ram, S., Ehrenkaufe, R.E.: A general procedure for mild and rapid reduction of aliphatic and aromatic nitro compounds using ammonium formate as a catalytic hydrogen transfer agent. *Tetrahedron Lett.* **25**, 3415–3418 (1984)
152. Yuste, F., Saldana, M., Walls, F.: Selective reduction of aromatic nitro compounds containing o- and n-benzyl groups with hydrazine and raney nickel. *Tetrahedron Lett.* **23**, 147–148 (1982)
153. Gowda, D.C., Gowda, S.: Formic acid with 10% palladium on carbon: a reagent for selective reduction of aromatic nitro compounds. *Indian J. Chem.* **398**, 709–711 (2000)
154. Onopchenko, A., Sabourin, E.T., Selwitz, C.M.: Selective catalytic hydrogenation of aromatic nitro groups in the presence of acetylenes. Synthesis of (3-aminophenyl)acetylene via hydrogenation of (3-nitrophenyl)acetylene over cobalt polysulfide and ruthenium sulfide catalysts. *J. Org. Chem.* **44**, 3671–3676 (1979)
155. Welton, T.: Room-temperature ionic liquids. Solvents for synthesis and catalysis. *Chem. Rev.* **99**, 2071–2083 (1999)
156. Wasserscheid, P., Keim, W.: Ionic liquids-new “solutions” for transition metal catalysis. *Angew. Chem. Int. Ed. Engl.* **39**, 3772–3789 (2000)

157. Popp, F.D., Schultz, H.P.: Electrolytic reduction of organic compounds. *Chem. Rev.* **62**, 19–27 (1962)
158. Bae, J.W., Cho, Y.J., Lee, S.H., Yoon, C.O.M., Yoon, C.M.: A one-pot synthesis of N-alkylaminobenzenes from nitroaromatics: reduction followed by reductive amination using B10H14. *Chem. Commun.* **8**, 1857–1858 (2000)
159. Rahaim, R.J., Maleczka, R.E.: Pd-catalyzed silicon hydride reductions of aromatic and aliphatic nitro groups. *Org. Lett.* **7**, 5087–5090 (2005)
160. Redemann, C.T., Redemann, C.E.: 5-amino-2,3-dihydro-1,4-phthalazinedione. *Org. Synth. Collective* **3**, 69–73 (1955)
161. (a) Imai, H., Nishiguchi, T., Fukuzumi, K.: Homogeneous catalytic reduction of aromatic nitrocompounds by hydrogen transfer. *Chem. Lett.* 655–656 (1976); (b) Berthold, H., Schotten, T., Honig, H.: Transfer hydrogenation in ionic liquids under microwave irradiation. *Synthesis*, **8**, 1607–1610 (2002)
162. Watanabe, Y., Ohta, T., Tsuji, Y., Hiyoshi, T., Tsuji, Y.: Bull. Ruthenium catalyzed reduction of nitroarenes and azaaromatic compounds using formic acid. *Chem. Soc. Jpn.* **57**, 2440–2444 (1984)
163. Taleb, A.B., Jenner, G.: Synthesis of aminoarenes in homogeneously catalyzed nitroarene—methyl formate reactions. *J. Mol. Catal.* **91**, 149–153 (1994)
164. Corma, A., Serna, P., Concepcion, P., Calvino, J.J.: Transforming nonselective into chemoselective metal catalysts for the hydrogenation of substituted nitroaromatics. *J. Am. Chem. Soc.* **130**, 8748–8753 (2008)
165. Maity, P., Basu, S., Bhaduri, S., Lahiri, G.K.: Superior performance of a nanostructured platinum catalyst in water: hydrogenations of alkenes, aldehydes and nitroaromatics. *Adv. Synth. Catal.* **349**, 1955–1962 (2007)
166. Takasaki, M., Motoyama, Y., Higashi, K., Yoon, S.H., Mochida, I., Nagashima, H.: Chemoselective hydrogenation of nitroarenes with carbon nanofiber-supported platinum and palladium nanoparticles. *Org. Lett.* **10**, 1601–1604 (2008)
167. Corma, A., Serna, P.: Chemoselective hydrogenation of nitro compounds with supported gold catalysts; *Science* **313**, 332–334 (2006)
168. He, L., Wang, L.C., Sun, H., Ni, J., Cao, Y., He, H.Y., Fan, K.N.: Efficient and selective room-temperature gold-catalyzed reduction of nitro compounds with CO and H<sub>2</sub>O as the hydrogen source. *Angew. Chem. Int. Ed.* **48**, 9538–9541 (2009)
169. Yamane, Y., Liu, X., Hamasaki, A., Ishida, T., Haruta, M., Yokoyama, T., Tokunaga, M.: One-pot synthesis of indoles and aniline derivatives from nitroarenes under hydrogenation condition with supported gold nanoparticles. *Org. Lett.* **11**, 5162–5165 (2009)
170. Jagadeesh, R.V., Surkus, A.E., Junge, H., Pohl, M.M., Radnik, J., Rabeah, J., Huan, H., Schunemann, V., Bruckner, A., Beller, M.: Nanoscale Fe<sub>2</sub>O<sub>3</sub>-based catalysts for selective hydrogenation of nitroarenes to anilines. *Science* **342**, 1073–1076 (2013)
171. Wienhofer, G., Kruger, M.B., Ziebart, C., Westerhaus, F.A., Baumann, W., Jackstell, R., Junge, K., Beller, M.: Hydrogenation of nitroarenes using defined iron–phosphine catalysts. *Chem. Commun.* **49**, 9089–9091 (2013)
172. Westerhaus, F.A., Jagadeesh, R.V., Wienhofer, G., Pohl, M.M., Radnik, J., Surkus, A.E., Rabeah, J., Junge, K., Junge, H., Nielsen, M., Bruckner, A., Beller, M.: Heterogenized cobalt oxide catalysts for nitroarene reduction by pyrolysis of molecularly defined complexes. *Nat. Chem.* **5**, 537–543 (2013)
173. Shi, Q., Lu, R., Lu, L., Fu, X., Zhao, D.: Efficient reduction of nitroarenes over nickel-iron mixed oxide catalyst prepared from a nickel-iron hydroxalcite precursor. *Adv. Synth. Catal.* **349**, 1877–1881 (2007)

# Graphene-Based Nanophotonic Biosensors



Alma Mejri, Ahmed Hichem Hamzaoui, Hamza Elfil,  
and Abdelmoneim Mars

**Abstract** Currently, biosensors have gained significant market acceptance in several crucial fields, such as disease diagnosis, medicine, pharmaceuticals, environmental surveillance, water and food quality control, and forensics. To meet market demands, it is vital to provide stable and effective biosensing platforms. Besides, the main challenges involved in the progress of biosensors are the efficient capture of biorecognition signals and their transformation into measurable signals, the improvement of the performance of transducers, and the miniaturization of biosensing devices using nanotechnologies. In this perspective, graphene has received tremendous due to its exceptional properties such as zero bandgap at its Dirac point, high electronic and thermal conductivity, and broadband saturable optical absorption. This chapter summarized the recent advances in using graphene as photonic nanomaterials in the development of various types of biosensors. Several applications of optical sensing are examined in detail to demonstrate the effect of graphene integration on improved detection performance. The future perspective and challenges in developing graphene-based nanophotonic biosensors are also discussed to give the reader a clear vision of the implementation of these two-dimensional nanomaterials in biosensors architectures.

**Keywords** Biosensors · Nanophotonic · Point-of-care · Food safety · Environmental monitoring

---

A. Mejri (✉) · H. Elfil · A. Mars

Desalination and Natural Water Valorization Laboratory (LaDVEN), Water Researches and Technologies Center (CERTE), BP 273, 8020 Borj-Cedria, Tunisia  
e-mail: [almaa.mejri@gmail.com](mailto:almaa.mejri@gmail.com)

A. H. Hamzaoui

Valorization Laboratory of Useful Materials (LVMU), National Center of Material Science Research (CNRSM), BP 273, 8020 Borj-Cedria, Tunisia

# 1 Introduction

Several studies have demonstrated that biosensors, which are analytical tools that generate an interpretable signal proportional to the concentration of target analytes, have contributed to improving the effectiveness of numerous vital areas including food quality control, surveillance system, security, medicine, and health care [1]. The latter is one of the leading markets in the biosensor sector, supporting about 70% of medical decisions [2]. Although conventional biosensing methods remain crucial in the decisive decision, the manufacture and validation of highly accurate, portable, inexpensive, and easy-to-handle biosensors are highly demanded because they lead to highly accurate and decentralized diagnoses without having to return to the central analytical laboratory [3]. Besides, biosensors can be categorized using various criteria including the kind of the bioreceptor and the transducer which are the responsible components for the biorecognition process and its conversion into a measurable analytical signal, respectively (Fig. 1).

Depending on the nature of the transducers, biosensors can be thermal, electrochemical, mechanical, or optical devices [4]. The chapter discusses the recent development in the fields of nanophotonic biosensors, a subset of optical biosensors. These devices have been created to address the limitation of conventional bioanalytical sensing techniques by improving the light-matter interactions through light control in subwavelength volumes. Indeed, nanophotonic biosensors have succeeded in achieving high performances in terms of sensitivity, efficiency, usability, and miniaturization [5]. In this regard, an important number of nanophotonic biosensors has been described in the literature including resonant dielectric, plasmonic, and surface-enhanced spectroscopies biosensors. At the same time, particular focus was

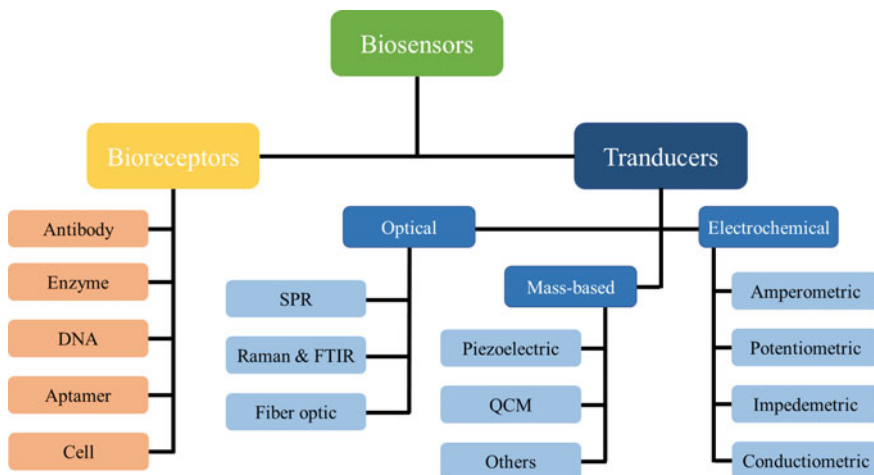


**Fig. 1** Classification of biosensors by type of transducers and bioreceptors

paid to the integration of nanomaterials in the architecture of nanophotonic biosensors, in particular to graphene derivatives due to their distinctive properties, especially high surface-to-volume ratio, and outstanding bio-compatibility with a variety of macromolecules, including deoxyribonucleic acid (DNA), antibodies, enzymes, cells, and proteins [6]. It has demonstrated that the unique chemical, electric, and optical features of graphene-based nanomaterials drastically enhanced the accuracy, sensitiveness, and detection limits (LODs) reaching femtomolar scales [7]. It is worth noting that, according to Google Scholar, the number of recently reported studies of the application of nanophotonic platforms based on graphene and its nanocomposites for the sensing of various biomolecules in several sectors such as medicine, food quality control, and environmental surveillance has considerably increased these last decades.

## 2 Key Parameters for Photonic Sensing

### 2.1 Nanophotonic Response

As is known, light has a dual nature defined as wave–particle duality. This means that light has the properties of both a continuous electromagnetic wave and a particle, called also a photon [8]. Besides, photonics refers to light manipulation for different applications such as biomedicine, nanotechnology, physics, and electronics. Indeed, the term “photonic” was intended to describe the study of light phenomena where the photon nature of light is important [9]. Therefore, nanophotonic is defined as light control at nanometer scales producing excellent features in the sensing of several bio-analytes and pathogenic agents with high performances with respect to conventional sensing methods [10]. Moreover, the confinement of light can be performed by three techniques: (i) the creation of light-matter connections by confining light to nanometric dimensions below the wavelength of light, (ii) the confinement of matter to the nanometric domain, limiting light-matter interactions only at nanoscopic scales, and (iii) the confinement of the photon, generated by a photochemical process or light-induced phase transition and its application to manufacturing nanometric photonic structures [11]. Among the nanomaterials used for the design of photonic biosensors, graphene nanocomposites have been extensively applied because they offer enhanced light response owing to their capacity to confine light to small sizes, their exceptional optical responses, which can be monitored by subjecting them to electrical potential, their strong and stable structures, and their ability to act as highly transparent thin conductors and light absorbers, depending on the manner they are prepared [12]. Concerning the detection approach, it is carried out by monitoring the variation of the photonic response mainly proportional to the changes in the concentration of the target bio-analytes.

## 2.2 *Modification of Graphene Surface*

### **Graphene Surface Modification**

Graphene, the honeycomb-shaped monolayer carbon, is a very attractive nanomaterial in many potential applications because of its unique properties such as stiffness, stability, and thickness. Nonetheless, the chemical inertness, the hydrophobicity, as well as its zero-band gap, weaken the competitiveness of graphene in various fields including the biosensing application [13]. Thus, graphene functionalization with several species, including organic and inorganic molecules, is in high demand for different applications. Several studies investigated the dispersion of graphene in common solvents and its application as a precursor for the preparation of several hybrid nanocomposite materials [14]. The latter offer new properties demonstrated by the combination of graphene properties and functional groups used in the modification such as conductivity, stability, and optics. As the covalent modification of the graphene surface, it includes two main pathways: the establishment of new bonds by sharing electrons between (i) free radicals (such as Sandmeyer reaction) or electron-withdrawing (EWD) groups and alkene bonds of graphene or (ii) organic functional groups (amino, hydroxyl, acid carboxylic, epoxide, etc.) and the oxygenated groups of graphene oxide [15]. Besides, the non-covalent route has been widely used for the modification of the pristine graphene surface because it enables the attachment of functional groups without affecting the electrical network; therefore, its interactions with atoms and molecules have been extensively studied [16].

### **Decoration with Nanomaterials**

Because graphene sheet has an important surface area and high mechanical stability, it has been widely used as a two-dimensional substrate for many forms of nanomaterials including nanoparticles, quantum dots, nanorods, nanoflower, etc. Interestingly, the hybridization between graphene and other materials allows the gathering of the properties of graphene and the involved nanomaterials. From this perspective, research has been focused on decorating graphene nanosheets with semiconductor quantum dots, metallic nanoparticles, and metal oxide nanoparticles [17]. Metallic nanoparticles are usually deposited on the graphene surface by reducing their relative salt dissolved in the solvent that contains dispersed graphene or its derivatives (GO and rGO) [18]. Besides, alkaline hydrolysis of the metal salt or the in-situ hydrothermal technique is frequently used to prepare metal oxide-modified graphene nanocomposite, whereas the spin casting technique is commonly used to deposit semiconductor quantum dots on the 2D graphene surface [19].

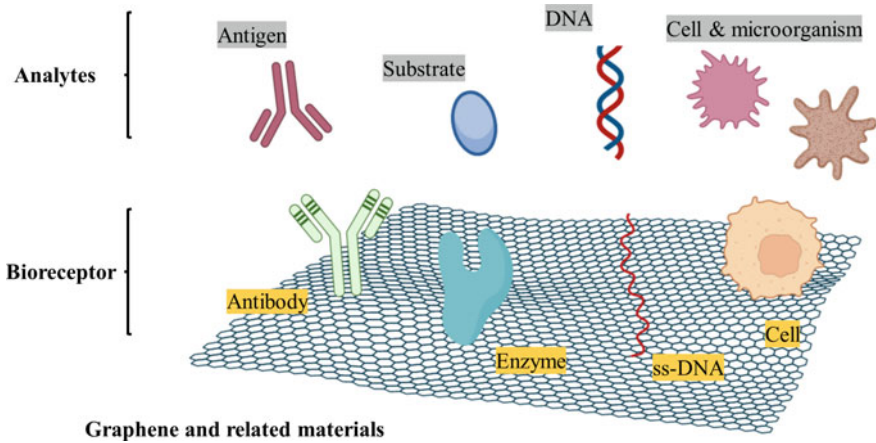


**Fig. 2** Graphene-based biosensors are biofunctionalized with various biomolecules for the detection of bio-analytes

### Biofunctionalization of the Graphene Surface

There is considerable interest in graphene-based nanomaterials in biological studies due to their capacity to quench electron donors and to prevent enzymatic cleavage of biomolecules, thus, their excessive use in the development of nucleic acids, peptides, proteins, and cells-based biosensors [20] (Fig. 2). For this reason, the interface graphene-biomolecules have been broadly studied to understand the immobilization mechanisms on the carbon honeycomb surface. Two biofunctionalization approaches have been commonly used until now to immobilize biomolecules on the graphene derivative surface [21]. The first involves a covalent interaction between the oxygenated groups graphene derivatives (rGO, GO, GQDs) surface and the functional groups of the biomolecule or the cross-linking agents, commonly peptide linkage, while the second refers to a non-covalent interaction.

## 3 Graphene-Based Nanophotonic Biosensors

Recently, many groups of researchers have focused on developing accurate and highly sensitive biosensors that produce results in a short analysis time. Besides, remarkable advances have been realized during the last global sanitary crisis (coronavirus disease 2019) in the field of optical biosensors, mainly nanophotonic devices [22]. Biosensing nanotechnologies, developed during the pandemic, have been eventually transferred to many other applications including point-of-care testing, pharmaceuticals, environmental monitoring, and food quality control [23]. The nanophotonic sensing platforms can easily be miniaturized, offering the possibility of chip integration. Indeed, it is possible to integrate several features, namely microfluidics, to



make a lab-on-a-chip device. Furthermore, optical studies on graphene materials demonstrated that graphene absorption capacity of light depends on its constant fine structure  $\alpha$  and that absorption has reached a universal value of 2.3% [24]. Although graphene shows strong optical absorption, the weak interaction between the graphene atomic thickness and the incident light remains a major drawback in the construction of nanophotonic biosensors based on graphene [25]. Accordingly, different methods were used to improve the coupling of light and graphene, citing the coverage of plasmonic nanostructures on graphene, the use of graphene with periodic patterns, or double-layer graphene [26].

### ***3.1 Nanophotonic Biosensors for Near-Patient Testing***

Nowadays, infection by mortal disorders such as human immunodeficiency viruses, coronavirus, tuberculosis, and malaria has increased significantly causing more than 10 million deaths worldwide [27]. Therefore, the development of effective and timely diagnostic tools is of great interest. Before getting into the details, it is worth defining the point-of-care test (POC). Indeed, POC is presented as a diagnostic tool that performs in vitro analyses, and the result can be obtained in a brief amount of time without special staff or sophisticated equipment [28]. The World Health Organization (WHO) has created standards for POC devices that are labialized (ASSURED) and described as Affordably, Sensitive, Specific, User-friendly, Rapid and Robust, Equipment-Free, and Delivered [29]. It is important to notice that most optical sensing platforms use the evanescent field to monitor the sensing process (Fig. 3) [30].

Interestingly, the biorecognition of the target analytes by the immobilized bioreceptors, onto the surface of the waveguide, affects the guiding properties of the waveguide due to the variation of the concentration of the analytes or the biomolecular conformation. Precisely, offsets in the effective mode index are observed and can be assessed by various optical properties of the waveguide, mainly the phase, amplitude, and resonant momentum. With a deterioration length of several hundred nanometers, the evanescent field gradually decreases across a perpendicular pivot to the detection surface [31]. This configuration prevents most non-specific interactions and renders biosensors evanescent among the detection systems the most promising techniques for the sensing of targets in complex biological samples. In this perspective, W. S. Jiang et al. have demonstrated the applicability of reduced graphene oxide (rGO)-based label-free nanophotonic biosensing platform for the quantification of rabbit immunoglobulin G (IgG) [32]. The surface plasmon resonance (SPR) responses of reduced graphene oxide nanosheets with a thickness of 8.1 nm to the presence of various rabbit IgG antigen concentrations have been investigated using graphene's tunable absorption effect. The findings demonstrated an increased control of rabbit IgG with a limit of detection of 62.5 ng/ml. In a similar study, N. F. Chiu and collaborators reported the exploitation of carboxyl graphene oxide composites to develop an SPR biosensing platform [33]. The platform was applied as an immunoaffinity sensor to detect the protein model, the bovine serum

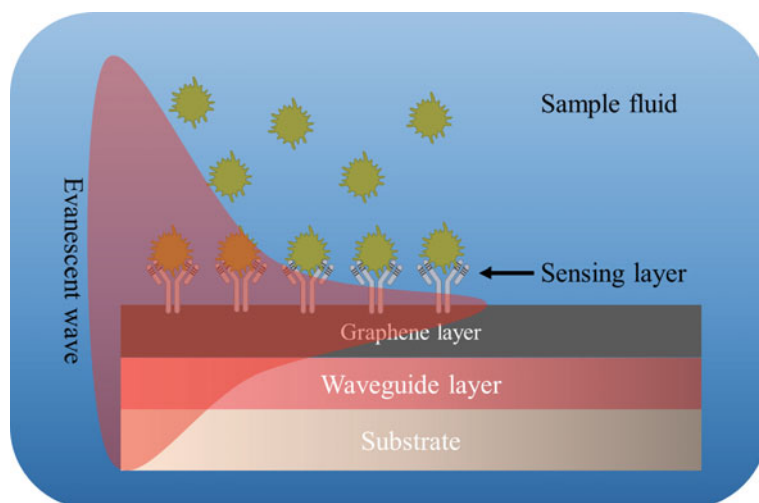


**Fig. 3** Functionality of evanescent wave-based nanophotonic biosensors. The parameters of the optical mode contained on a graphene substrate are influenced by the crossing between the evanescent field and the environmental elements

albumin. The authors demonstrated that functionalizing graphene enables the modification of its visible range, which can then be used to improve plasmonic pairing process control by up to 5.15 times over unfunctionalized graphene oxide. The results demonstrated that the developed nanophotonic biosensor is efficient for the immediate monitoring of blood within bodies and diagnoses based on the detection of cancer tumor markers. Recently, A. Vasilescu and coworkers have investigated the ability of graphene oxide-decorated gold chips to quantify the amount of lysozyme regulated in leukemia, kidneys, and digestive diseases [34]. To this end, the authors suggested the biofunctionalization of the rGO/Au interface with whole cells of *Micrococcus lysodeikticus*, a typical enzyme substrate for lysozyme. The data revealed that exposure of the nanophotonic platform to a serum containing lysozyme exhibited cell detachment and damage to the bacterial cell–SPR interface, provoking a drastic reduction in the surface plasmon resonance response providing the determination of lysozyme amounts in concentrated real serum. More interestingly, the functionalization of the gold layer with graphene–MoS<sub>2</sub> nanohybrid (Gr–MoS<sub>2</sub>) has been described by M. Rahman et al. as having an influence on the sensing capabilities of ss-DNA as a biomolecule model [35]. The findings revealed that nanohybrid modification increased the responsiveness of the nanophotonic platform while decreasing detection accuracy. To resolve this issue, the authors suggest including a layer of silicon between gold and Gr–MoS<sub>2</sub> layers. It was proven that silicone inclusion proved successful in maintaining high sensitivity. Despite that SPR is the common nanophotonic technique applied in studying biochemical interaction in medical diagnosis, it is still limited to small molecules or low amounts of the targets [36]. As an effective solution, research has demonstrated the effect of graphene and its related

materials on improving the surface plasmons resonance signals. During the coronavirus pandemic, the SPR technique demonstrated its effectiveness in rapidly determining the SARS-CoV-2 virus. The real-time reverse transcriptase polymerase chain reaction (RT-PCR) method was commonly utilized as a standard. [37]. Nevertheless, the RT-PCR process is very long and complicated; thus, analysis can take at least a day to get results. Therefore, scientists have adopted the development of SPR-based graphene nanomaterials to identify cases of SARS-CoV-2. Recently, T. B. Abdul-Akib et al. have described the fabrication of an SPR biosensing platform based on graphene for the early-stage determination of coronavirus [38]. The authors proposed to coat the BK7 (prism)—gold layer with both platinum-di-selenide (PtSe<sub>2</sub>) and graphene layers. The researchers discovered that incorporating graphene into the platform structure increases the sensitivity of the proposed nanophotonic biosensor, allowing it to determine the coronavirus in a variety of biological forms. By the same token, Moznuzzaman et al. have reported the design of a six-layer SPR biosensor (prism/TiO<sub>2</sub>/silver/MoSe<sub>2</sub>/Gr/CR3022 antibodies) for the SARS-CoV-2 detection process [39]. To this end, a silver layer was interposed between the two layers, a MoSe<sub>2</sub>-graphene composite and TiO<sub>2</sub> thin sheet. The authors have justified the utility of each used material by the examination of all the refractive index values at 633 nm wavelength. In addition, silver was used due to its plasmonic property. Moreover, the nanoscale biosensor showed significant sensor capabilities, including high sensitivity, large quality factor, and high sensor accuracy. As the last design, black phosphorus-graphene nanocomposite was used to develop a sensitively improved guided-wave SPR biosensing platform [40]. The choice of the hybrid nanomaterial was based on its effect on enhancing the sensitivity of the nanophotonic platform through its electrical conductivity in the lower plane. The results showed that the graphene-based nanocomposite has excellent properties, including strong antioxidant properties and a high affinity for a large number of biomolecules. Further, the proposed graphene-based biosensor has excellent sensing performance, with indices of refraction ranging from 1.33 to 1.78 RIU, responsiveness of 148.2°/RIU, and detection target index of refraction of 1.33 RIU. Graphene optical fiber biosensors, on the other hand, have attracted great attention because of their accuracy and sensitivity of detection. As a model, dual-peak long-period grating decorated with graphene oxide was applied recently to construct a label-free biosensing platform for the real-time determination of antibodies. L. Chen's research team has reported an efficient approach for the depositing of graphene oxide on a fiber surface by the combination of chemical bonding and physical adsorption [41]. The method offers excellent advantages such as a robust bonding between graphene oxide and fiber surface, as well as a steady graphene oxide with high stability and reliability. In 2014, S. Sridevi and colleagues described the application of graphene oxide modified with mannose-modified dendrimers based on poly(propyl ether imine) in the development of engraved fiber nanophotonic biosensing [42]. The authors demonstrated that the designed platform showed an excellent specificity to Concanavalin-A protein even in the presence of an excess amount of several interfering proteins such as bovine serum albumin. Furthermore, B. C. Yao and collaborators have reported the fabrication of a D-type Bragg fiber splitting platform based on graphene for the determination of

red blood cells level [43]. For this end, a D-shaped micro-structured polymer fiber Bragg grating was coated with decorated with a graphene-silica nanocomposite, and the nanophotonic platform exhibited high sensitivity, fast response, and high selectivity to human erythrocyte (red blood cell). The authors suggested that the designed biosensor shows great promise for in vivo cell and in-situ sensing applications. Photonic crystal fibers, with their distinct structure and adaptable design, have been demonstrated to be a great prism. Indeed, their single-mode transmission, tunable dispersion, and effective birefringence are the main advantages [44]. Interestingly, the integration of graphene in the photonic crystal fiber structure increased drastically the sensing performances unlike their counterparts, biosensing platforms based on conventional photonic crystal fiber. Accordingly, graphene SPR crystal fiber biosensors were widely investigated. For instance, a bi-refractive SPR crystal fiber platform based on a graphene-silver layer was developed by [45]. Graphene has been used in this study to improve the detection platform sensitivity because it prevents the degradation of the silver layer. The findings demonstrated that biosensor displays fascinating performances including a resolution of  $4 \times 10^{-5}$  RIU<sup>-1</sup> and a sensibility in the range of 860 RIU<sup>-1</sup>. Likewise, Yang et al. have proposed an SPR biosensing platform based on plasmonic crystal fiber [46]. In this configuration, the authors reported that the nanophotonic platform exhibited a wavelength sensitivity and a resolution of 2520 nmRIU<sup>-1</sup> and  $3.97 \times 10^{-5}$  RIU, respectively. Furthermore, surface-enhanced Raman scattering (SERS) is commonly employed to sense selectively biomolecules, especially biomarkers [47]. This technique is based on exploiting the effect of biomolecules (adsorbed onto rough metal surfaces such as gold or silver) in the scattering of inelastic light. The adsorption

### ***3.2 Nanophotonic Biosensors for Food Quality Control***

Currently, the increasing demand for food production, storage, and long-term preservation has created an urgent need for a technique to easily track the purity and quality of food from manufacture to consumption for the lifetime of the product [52, 53]. Indeed, contaminants, citing toxins, antibiotics, pesticides, and microbial contamination, can provoke several foodborne diseases in humans and animals, namely norovirus infection, salmonellosis, shigellosis, toxoplasmosis, and vibrio infection [54–56]. As a result, the scientific community is addressing this serious problem by developing and establishing rapid, portable, inexpensive, sensitive, and accurate methods of food quality control [57]. For this purpose, several research groups have focused on the fabrication of nanophotonic biosensing platforms based on graphene and its associated nanomaterials, e.g., graphene, graphene oxide, and graphene quantum dot, using several recognition biomolecules including aptamers, ribonucleic acid, enzymes, etc. [58–60]. Consequently, the number of scientific paper number published on the development of nanophotonic biosensors including SPR, optical fiber, and SERS biosensors for food safety has grown significantly over this

decade [61]. Recently, R. Kant has developed an SPR-optical fiber biosensing platform based on tantalum(V) oxide nanoparticles incorporated in rGO matrices for the determination of fenitrothion pesticide levels in food samples [62]. For this end, a thin layer of silica optical fiber decorated with a thin layer of silver was modified with the developed rGO nanocomposite. The report reveals that the designed nanophotonic platform exhibited a linear sensitive photonic response ranging from 0.25 to 4  $\mu\text{M}$  with a low detection limit of 38 nM. On the other hand, the sensing of herbicide and the determination of napropamide have been widely studied. Interestingly, a polypyrrole chitosan graphene oxide nanocomposite layer-decorated gold layer was used as SPR substrate to quantify napropamide in various real matrices with a wide concentration area ranging from 0.01 to 100 ppm and a low detection limit of 0.1 ppm [63]. Furthermore, Y. Song and collaborators have described the application of a functional silver-gold shell-core-modified rGO-based SERS biosensing platform for the determination of thiram pesticides [64]. According to the results, the rGO-Au@AgNRs nanohybrid enabled the detection of thiram at a low level of about  $10^{-7}$  M. In a similar approach, H. Zheng and collaborators have reported the development of SERS-based platform for the quantification of L-Theanine levels in tea samples [65]. The authors proposed that prepared graphene nanocomposite can be applied as an efficient sensor for SERS quantification of L-Theanine with a promised detection limit of  $10^{-7}$  M. More interestingly, C. Zhou group has described the application of silver nanoparticles-modified rGO for the development of an SPR fiber optic biosensor for E. coli O157:H7 detection in juice samples [66]. The results demonstrated that modification of the surface of a gold layer-coated optical fiber with the reduced graphene oxide nanocomposite enhances considerably the SPR response, and the graphene prevents the oxidation of silver nanoparticles. The reported nanophotonic method possesses high performances in terms of sensitivity, selectivity, reproducibility, and stability with satisfactory recoveries of 88–110% for sensing in fruit and vegetable juices. On the other hand, mycotoxins, which are formed by several fungi, including *Aspergillus*, *Penicillium*, and *Fusarium*, pose an increasing risk to both human and animal health [67, 68]. Through contaminated food, they can easily access human cells and blood and provoke serious damage including inflammation, immunosuppression, cancer, and hepatic necrosis [69]. Aflatoxins, one of the most important mycotoxins, are of great importance because of their harmful effects ranging from acute poisoning to long-term effects such as immunodeficiency and cancer [70]. In this framework, P. Chen et al. have described the design of a graphene oxide-based SERS sensing platform for the detection of aflatoxin B1 [71]. The graphene oxide and AFB1 aptamer were used, respectively, as a signal amplifier and signal probe. As a biosensor design, the indium tin oxide glass was coated sequentially with GO and AuNPs and was used as a SERS substrate. The AFB1 aptamer was immobilized onto the modified substrate through  $\pi$ - $\pi$  interaction. The results demonstrated that a proportional Raman signal to the increase in AFB1 concentration ranging from 0.1  $\text{pg mL}^{-1}$  to 100  $\text{ng mL}^{-1}$  was observed with a limit detection of 0.1  $\text{pg mL}^{-1}$ . The authors suggested that the developed nanophotonic system can be considered a sensitive analytical method for the control of food quality. More interestingly, Fumonisin B1, aflatoxin B1, and zearalenone were simultaneously determined by S.

Zheng and colleagues using a robust nanophotonic approach based on a multiplexed SERS-based immunochromatographic test [72]. For this reason, a polyethyleneimine layer was used to coat a three-dimensional gold nanofilm based on graphene oxide. The polyethyleneimine layer can be used as a built-in nanogap and host molecules and produce robust hotspots between the internal graphene oxide-modified gold thin film and the externally constructed gold nanoparticles satellites, as shown by the authors. Further, the nanophotonic biosensor allowed the simultaneous quantification of fumonisin B1, aflatoxin B1, and zearalenone, with low limits of detection of the order of 0.529, 0.745, and 5.90  $\text{pg mL}^{-1}$ , respectively. Additionally, the nanophotonic biosensor enabled the simultaneous quantification of the target bio-analytes with low detection limits of around 0.529  $\text{pg mL}^{-1}$ . For real food samples, testing with high accuracy takes just 20 min.

### ***3.3 Nanophotonic Biosensors for Environmental Monitoring***

Environmental pollution, which is mainly caused by uncontrollable anthropogenic, agricultural, and industrial activities, is a major concern worldwide [73–75]. However, environmental monitoring is progressing slowly despite significant interest and investment. Therefore, the construction of rapid and effective tools for on-site and rapid monitoring of water, soil, and air pollution is crucial to managing environmental degradation [76–79]. On the other hand, nanophotonic biosensors were considered promising control assays due to their miniaturization capability and on-site accuracy; thus, their application in environmental surveillance is of great interest [80]. Within this framework, graphene-based nanophotonic biosensors including SPR and SERS platforms are the most common analytical tools for environmental monitoring [81]. Nowadays, the significant increase in industrial and mining activities is causing serious diseases to humans and the environment which heavy metals and related forms (pure elements, ions, or complexes) are one of the generators [82, 83]. Recently, N. H. Kamaruddine et al. have applied an accurate chitosan-modified GO nanocomposite SPR sensor for the determination of lead (II) level in water [84]. The authors demonstrated that the modification of the metallic layers (gold-silver-gold layers) enhances the sensitivity of the nanophotonic platform where findings showed that the improved scattering domain at the detection barrier layer increased the shifting of the SPR orientation by up to  $3.5^\circ$  within the concentration ranging from 0.1 to 1 ppm. Further, the results revealed that investigated sensing platform exhibited excellent analytic performance for the sensing of Pb (II) in wastewater samples. In the same context, Q. He and collaborators have reported the determination of Pb (II) using a regenerable DNAzyme bio-conjugated graphene SERS biosensor [85]. For this purpose, the hybrid metal (gold-silver) nanostructure was biofunctionalized with Cy3-labeled thiolated DNAzyme probe and its complementary substrate strand. The authors reported that the sensing process was monitored by the measurement of the Cy3 probe Raman signal intensity. The Raman studies showed that the nanophotonic platform possesses a broad linear response ranging

from 10 pM to 100 nM with a detection limit of 4.31 pM. Further, the authors suggested that reusable SERS biosensors exhibited an efficient heavy ion detection method for environmental monitoring. As a final example of heavy metal sensing, heterojunctions of AuNPs and rGO were applied for the biosensing of a trace of mercury (II) through the coordination between thymine and  $\text{Hg}^{2+}$  [86]. The SERS substrate was constructed via seed-assisted growth of AuNPs/rGO nanocomposite on  $\text{SiO}_2/\text{Si}$  substrates. The findings demonstrated extremely low detection limits of the order of 0.1 nM, suggesting that the integration of graphene is appropriate as a method of improving the Raman signal. On the other hand, antibiotics are one of the main pollutants of water and the environment which are recently produced in large quantities provoking their diffusion in environmental ecosystems; thus, the determination of their levels in water is highly demanded [87–89]. In this context, Y. Wang and collaborators have recently described the application of a graphene-based SERS biosensing platform for the sensing of ultra-trace of ampicillin and nitrofurantoin antibiotics [90]. To this end, the designed platform was constructed using AuNPs-modified GO nanocomposite. The studies revealed that the linear response is ranging from 500 ng mL<sup>-1</sup> to 5 ng mL<sup>-1</sup> with a limit of detection for nitrofurantoin and ampicillin of 5 and 0.01 ng mL<sup>-1</sup>, respectively. More interestingly, a novel accurate SERS biosensing platform for a polar antibiotic was developed by Y. T. Li's group [91]. In this work, silver-graphene nanocomposite was used to coat the screen-printed electrode. The  $\pi$ - $\pi$  interactions provided by graphene have been used to increase the concentration of antibiotics immobilized on the SERS substrate which subsequently increases the sensitivity of the designed biosensing platform. The findings indicated that the proposed nanophotonic platform is useful for fast and accurate quantification of target antibiotics without performing a pre-separation process. However, it should be noted that detection techniques based on Raman spectroscopy suffer from reproducibility and reliability [92, 93]. As a solution, integrating graphene nanomaterials into the biosensor structure can be an effective way to improve this weakness [94–96]. L. Zhang et al. have recently proposed the embedding of graphene oxide into a sandwich of gold-silver nanocomposites [97]. The designed platform was applied as a SERS substrate to quantify rhodamine-6G and the pesticide thiram in grape juice sold commercially. The results showed that Raman signals were significantly increased owing to the existence of plenty of hotspots on gold-silver nanocomposites surface and the excellent properties of graphene oxide sheets. The findings demonstrated that target analytes were quantified with an enhancement factor of  $7 \times 10^7$  and a limit of detection of 0.1  $\mu\text{M}$  suggesting that the designed graphene oxide-based nanophotonic sensing platform can be applied to future real-world use for field-based sensing of pesticide residues in a variety of real matrices.

## 4 Conclusion

The present chapter emphasized the integration of graphene and its related nanomaterials into nanophotonic sensing platforms including SPR, optical fiber, and

SERS platforms. The reported works demonstrated that the modification of photonic substrates with graphene nanomaterials enhances drastically the optical signals, thereby the sensitivities and the analytical performances of nanophotonic biosensors were improved and can sense various analytes in trace levels. Research teams are starting to pay attention to nanophotonic platforms based on graphene, and its related materials gave that the number of scientific publications describing the application of graphene-based nanophotonic biosensors in many fields, namely health care, food safety, and environmental monitoring has begun to increase significantly. Furthermore, the effect of graphene on the functionality of various photonic systems was described, and analytical performances, in particular, linear ranges, limits of detection, and applicability in various real matrices were also highlighted to demonstrate the graphene role in the determination of trace levels of viruses, biomarkers, mycotoxins, pesticides, heavy metals, and many others hazardous species, therefore the improvement of people's health. Nevertheless, the miniaturization and commercialization of compact graphene-based nanophotonic biosensors for clinical diagnosis and environmental monitoring must still be done, as it requires the validation of an accurate, reliable, reproducible system, and cost-effective biosensors with high specificity in real matrices where the interfering effect of various molecules and biomolecules, presented in biological and physiological fluids, disturbs the photonic signal.

## References

1. Singh, S., Kumar, V., Dhanjal, D.S., Datta, S., Prasad, R., Singh, J.: Biological biosensors for monitoring and diagnosis. *Microb. Biotechnol. Basic Res. Appl.* 317–335 (2020)
2. Ngo, A., Gandhi, P., Miller, W.G.: Frequency that laboratory tests influence medical decisions. *J. Appl. Lab. Med.* 1(4), 410–414 (2017)
3. Srinivasan, B., Tung, S.: Development and applications of portable biosensors. *J. Lab. Autom.* 1–25 (2015)
4. Polat, E.O., Cetin, M.M., Tabak, A.F., Güven, E.B., Uysal, B.O., Arsan, T., Kabbani, A., Hamed, H., Gül, S.B.: Transducer technologies for biosensors and their wearable applications. *Biosensors* 12(6), 385 (2022)
5. Chocarro-Ruiz, B., Fernandez-Gavela, A., Herranz, S., Lechuga, L.M.: Nanophotonic label-free biosensors for environmental monitoring. *Curr. Opin. Biotechnol.* 45, 175–183 (2017)
6. Krishnan, S.K., Singh, E., Singh, P., Meyyappan, M., Nalwa, H.S.: A review on graphene-based nanocomposites for electrochemical and fluorescent biosensors. *RSC Adv.* 9, 8778–8881 (2019)
7. Justino, C.I.L., Gomes, A.R., Freitas, A.C., Duarte, A.C., Rocha-Santos, T.A.P.: Graphene based sensors and biosensors. *Trends Anal. Chem.* 91, 53–66 (2017)
8. Rab, A.S., Polino, E., Man, Z.X., An, N.B., Xia, Y.J., Spagnolo, N., Franco, R.L., Sciarino, F.: Entanglement of photons in their dual waveparticle nature. *Nat. Commun.* 8, 915 (2017)
9. Amiri, I.S., Azzuhri, S.R.B., Jalil, M.A., Hairi, H.M., Ali, J., Bunruangses, M., Yupapin, P.: introduction to photonics: principles and the most recent applications of microstructures. *RSC Adv.* 9, 778–8881 (2019)
10. Mohammadi, E., Tsakmakidis, K.L., Askarpour, A.N., Dehkhoda, P., Tavakoli, A., Altug, H.: Nanophotonic platforms for enhanced chiral sensing. *ACS Photonics* 5(7), 2669–2675 (2018)
11. Iqbal, M.A., Ashraf, N., Shahid, W., Awais, M., Durrani, A.K., Shahzad, K., Ikram, M.: Nanophotonics: fundamentals, challenges, future prospects and applied applications. In:



- Nonlinear Optics—Nonlinear Nanophotonics and Novel Materials for Nonlinear Optics. IntechOpen (2021)
12. Pandya, A., Sorathiya, V., Lavadiya, S.: Graphene-based nanophotonic devices. Recent Advances in Nanophotonics—Fundamentals and Applications. IntechOpen (2021)
  13. Magne, T., Vieira, M., Alencar, L.M.R.: Graphene and its derivatives: understanding the main chemical and medicinal chemistry roles for biomedical applications. *J. Nanostruct. Chem.* **12**, 693–727 (2022)
  14. Perumal, S., Atchudan, R., Cheong, W.: Recent studies on dispersion of graphene-polymer composites. *Polymers* **13**, 2375 (2021)
  15. Criado, A., Melchionna, M., Marchesan, S., Prato, M.: The Covalent functionalization of graphene on substrates. *Angew. Chem. Int. Ed.* **54**, 10734–10750 (2015)
  16. Georgakilas, V., Otyepka, M., Bourlinos, A.B., Chandra, V., Kim, N., Kemp, C.K., Hobza, P., Zboril, R., Kim, K.S.: Functionalization of graphene: covalent and non-covalent approaches, derivatives and applications. *Chem. Rev.* **112**, 6156–6214 (2012)
  17. Parnianchi, F., Nazari, M., Maleki, J., Mohebi, M.: Combination of graphene and graphene oxide with metal and metal oxide nanoparticles in fabrication of electrochemical enzymatic biosensors. *Int. Nano Lett.* **8**, 229–239 (2018)
  18. Low, S., Shon, Y.-S.: Molecular interactions between pre-formed metal nanoparticles and graphene families. *Adv. Nano Res.* **6**(4), 357–375 (2018)
  19. Khan, M., Tahir, M.N., Adil, S.F., Khan, H.U., Siddiqui, M.R.H., Warthan, A.A.A., Tremel, W.: Graphene based metal and metal oxide nanocomposites: synthesis, properties and their applications. *J. Mater. Chem. A* **3**, 18753–18808 (2015)
  20. Mustapha O, Mekhzoum MER, Bouhfid R, Qaiss AK (2019) Surface functionalization of graphene-based nanocomposites by chemical reaction. In: Functionalized graphene nanocomposites and their derivatives, pp 21–45
  21. Shahriari, S., Sastry, M., Panjkar, S., Singh Raman, R.K.: Graphene and graphene oxide as a support for biomolecules in the development of biosensors. *Nanotechnol. Sci. Appl.* **14** (2021)
  22. Gisela, R.V., Maria, S., Laura, M.L.: Nanophotonic biosensors for point-of-care COVID-19 diagnostics and coronavirus surveillance. *J. Phys. Photonics* **3**, 011002 (2021)
  23. Kulkarni, M.B., Ayachit, N.H., Aminabhavi, T.M.: Biosensors and microfluidic biosensors: from fabrication to application. *Biosensors* **12**(7), 543 (2020). [2079-6374]
  24. Tiwari, S.K., Sahoo, S., Wang, N., Huczko, A.: Graphene research and their outputs: status and prospect. *J. Sci. J. Sci. Adv. Mater. Dev.* **5**, 10–29 (2020)
  25. Zhang, S., Li, Z., Xing, F.: Review of polarization optical devices based on graphene materials. *Int. J. Mol. Sci.* **21**(5), 1608 (2020) [1422-0067]
  26. Frank, H.L.K., Darrick, E.C., Javier García de Abajo, F.: Graphene plasmonics: a platform for strong light–matter interactions. *Nano Lett.* **11**(8), 3370–3377 (2011)
  27. Ong, C.W.M., Migliori, G.B., Raviglione, M., et al.: Epidemic and pandemic viral infections: impact on tuberculosis and the lung. *Eur. Respir. J.* **56**, 2001727 (2020)
  28. Vashist, S.K.: Point-of-care diagnostics: recent advances and trends. *Biosensors* **7**(4), 62 (2017)
  29. Land, K.J., Boeras, D.I., Chen, X.S., et al.: Reassured diagnostics to inform disease control strategies, strengthen health systems and improve patient outcomes. *Nat. Microbiol.* **4**, 46–54 (2019)
  30. Juan-Colás, J., Johnson, S., Krauss, T.F. Dual-mode electro-optical techniques for biosensing applications: a review. *Sensors* **17**, 2047 (2017)
  31. Jeffrey, S.G., Peter, H., Kenneth, S.B.: Evanescent wave microscopy encyclopedia of microfluidics and nano fluidics (2008). 978-0-387-32468-5
  32. Wen-S, J., Wei, X., Shuang, X., Shao-Nan, C., Xiao-Guang, G., Zhi-Bo, L., Jian-Guo, T.: Reduced graphene oxide-based optical sensor for detecting specific protein. *Sens. Actuators B Chem.* **249**(142–148), 0925–4005 (2017)
  33. Chiu, N.-F., Fan, S.-Y., Yang, C.-D., Huang, T.-Y. Carboxyl-functionalized graphene oxide composites as SPR biosensors with enhanced sensitivity for immunoaffinity detection. *Biosens. Bioelectron.* **89**(1), 370–376 (2017). [0956-5663]

34. Lina, V., Szilveszter, G., Mihaela, G., Sorin, D., Valentina, D., Serban, P., Qian, W., Musen, L., Rabah, B., Sabine, S.: Surface plasmon resonance based sensing of lysozyme in serum on *Micrococcus lysodeikticus*-modified graphene oxide surfaces. *Biosens. Bioelectron.* **89**(Part 1):525–531 (2017). [0956–5663]
35. Rahman, M.S., Shamim, A.M., Rabiul, H., Hossain, M.B., Haque, M.I.: Design and numerical analysis of highly sensitive Au–MoS<sub>2</sub>-graphene based hybrid surface plasmon resonance biosensor. *Opt. Commun.* **96**, 36–43. (0030-4018)
36. Jonde, J., Rosa, J., Lima, J.C., Baptista, P.V.: Nanophotonics for molecular diagnostics and therapy applications. *Int. J. Photoenergy* **11** (2012). <https://doi.org/10.1155/2012/619530>
37. Alireza, T., Abdollah, A.: Real-time RT-PCR in COVID-19 detection: issues affecting the results. *Expert Rev. Mol. Diagn.* **20**(5), 453–454 (2020)
38. Akib, T.B.A., Mou, S.F., Rahman, M.M., Rana, M.M., Islam, M.R., Mehedi, I.M., Mahmud, M.A.P., Kouzani, A.Z.: Design and numerical analysis of a graphene-coated SPR biosensor for rapid detection of the novel coronavirus. *Sensors* **21**, 3491 (2021)
39. Moznuzzaman, M., Imran, K., Islam, R.M.: Nano-layered surface plasmon resonance-based highly sensitive biosensor for virus detection: a theoretical approach to detect SARS-CoV-2. *AIP Adv.* **11**, 065023 (2021)
40. Mingyang, S., Xueyu, C., Linwei, T., Bo, Y., Haijian, Z., Junmin, L., Ying, Li., Shuqing, C., Dianyan, F.: Black phosphorus (BP)-graphene guided-wave surface plasmon resonance (GWSPR) biosensor. *Nanophotonics* **9**(14), 4265–4272 (2020)
41. Chen, L., Qi, C., Baojian, X., Weidong, Z., Lin, Z., Jianlong, Z., Xianfeng, C.: Graphene oxide functionalized long period grating for ultrasensitive label-free immunosensing. *Biosens. Bioelectron.* **94**(200–206), 0956–5663 (2017)
42. Sridevi, S., Vasu, K.S., Sampath, S., Asokan, S., Sood, A.K.: Optical detection of glucose and glycated haemoglobin using etched fiber Bragg gratings coated with functionalized reduced graphene oxide. *J. Biophotonics* **9**(7), 760–769 (2016)
43. Yao, B., Wu, Y., Webb, D., Zhou, J., Rao, Y., Pospori, A., Yu, C., Gong, Y., Chen, Y.: Graphene-based D-shaped polymer FBG for highly sensitive erythrocyte detection. In: *Proceedings of Frontiers in Optics* (2015). <https://doi.org/10.1364/FIO.2015.FTh2E.3>
44. Gui, F., Jiang, P., Yang, H., Qin, Y., Caiyang, W.: Design for a high birefringence photonic crystal fiber with multimode and low loss. *Appl. Opt.* **57**, 6–13 (2018)
45. Jitendra, N.D., Rajan, J.: Graphene-based birefringent photonic crystal fiber sensor using surface plasmon resonance. *IEEE Photonics Technol. Lett.* **26**, 1041–1135 (2014)
46. Yang, X., Lu, Y., Liu, B., et al.: Analysis of Graphene-based photonic crystal fiber sensor using birefringence and surface plasmon resonance. *Plasmonics* **12**, 489–496 (2017)
47. Nguyen, A.H., Peters, E.A., Schultz, Z.D.: Bioanalytical applications of surface-enhanced Raman spectroscopy: de novo molecular identification. *Rev. Anal. Chem.* **364** (2017). <https://doi.org/10.1515/revac-2016-0037>
48. Shan, C., Xiaohong, L., Yuxiao, J., Wei, Z., Zhigang, Z.: Surface enhanced Raman scattering revealed by interfacial charge-transfer transitions. *Innov.* **1**, 100051 (2020)
49. Lin, Y., Shu, J.Z., Yuan, F.L., Cheng, Z.H.: Silver nanoparticles deposited on graphene oxide for ultrasensitive surface-enhanced Raman scattering immunoassay of cancer biomarker. *J. Name. Nanoscale* **25** (2018)
50. Xiuli, F., Yunqing, W., Yongming, L., Huitao, L., Longwen, F., Jiahui, W., Jingwen, L., Peihai, W., Lingxin, C.: A graphene oxide/gold nanoparticle-based amplification method for SERS immunoassay of cardiac troponin. *Analyst* **144**, 1582–1589 (2019)
51. Zhou, C., Yu, Z., Yu, W., et al.: Split aptamer-based detection of adenosine triphosphate using surface enhanced Raman spectroscopy and two kinds of gold nanoparticles. *Microchim Acta* **186**, 251 (2019)
52. Jon, A., Mohammad-Ali, S., Krishna, K., Vinayaka, A.C., Anders, W., Dang, D.B., Yi, S. Molecularly imprinted polymers for sample preparation and biosensing in food analysis: progress and perspectives. *Biosens. Bioelectron.* **91**, 606–615 (2017) [0956-5663]
53. Neethirajan, S., Jayas, D.S.: Nanotechnology for the food and bioprocessing industries. *Food Bioprocess Technol.* **4**, 39–47 (2011)

54. Thomas, B.: Foodborne pathogens review. *AIMS Microbiol.* **3**, 529–563 (2017)
55. Simothy, L., Mahomoodally, F., Neetoo, H.: A study on the potential of ants to act as vectors of foodborne pathogens. *AIMS Microbiol.* **4**(2), 319–333 (2018)
56. Bintsis, T.: Microbial pollution and food safety. *AIMS Microbiol.* **4**(3), 377–396 (2018)
57. Visciano, P., Schirone, M.: Rapid methods for assessing food safety and quality. *Foods* **9**(4), 533 (2020). <https://doi.org/10.3390/foods9040533>
58. Altug, H., Oh, S.H., Maier, S.A., et al.: Advances and applications of nanophotonic biosensors. *Nat Nanotechnol* **17**, 5–16 (2022)
59. Kobun, R.: Nanotechnology-based optical biosensors for food applications. In: *Adv Food Anal Tools* 147–165 (2021). [Academic Press] [9780128205914]
60. Hashim, N., Abdullah, S., Yusoh, K. Graphene nanomaterials in the food industries: quality control in promising food safety to consumers. *Graphene 2D Mater.* **7**, 1–29 (2022)
61. Chiu, N.F.: The current status and future promise of SPR. *Biosensors* **12**(11), 933 (2022)
62. Kant, R.: Surface plasmon resonance-based fiber-optic nanosensor for the pesticide fenitrothion utilizing Ta<sub>2</sub>O<sub>5</sub> nanostructures sequestered onto a reduced graphene oxide matrix. *Microchim. Acta* **187**, 8 (2020)
63. Reza, A., Suraya, S.A., Soleimani, H., Shafie, S., Noor, A.S.M., Mohammadi, A.: Application of surface plasmon resonance sensor with polypyrrole chitosan graphene oxide layer to detect the napropamide. *IOP Conf. Ser. J. Phys. Conf. Ser.* **1123**, 012016 (2018)
64. Song, Y., Zhang, Y., Huang, Y., Fan, Y., Lai, K.: Rapid determination of Thiram residues in fruit juice by surface-enhanced Raman scattering coupled with a Gold@Silver nanoparticle-graphene oxide composite. *Anal. Lett.* **53**(7), 1003–1018 (2020)
65. Zheng, H., Ni, D., Yu, Z., Liang, P.: Preparation of SERS-active substrates based on graphene oxide/silver nanocomposites for rapid detection of l-Theanine. *Food Chem.* **217**(511–516), 0308–8146 (2017)
66. Zhou, C., Zou, H., Li, M., Sun, C., Ren, D., Li, Y. Fiber optic surface plasmon resonance sensor for detection of *E. coli* O157:H7 based on antimicrobial peptides and AgNPs-rGO. *Biosens. Bioelectron.* **117**, 347–353 (2018). [0956-5663]
67. Reza, E.K., Pashazadeh, P., Maryam, H., de la Guardia, M., Mokhtarzadeh, A.: Recent advances in nanomaterial-mediated Bio and immune sensors for detection of aflatoxin in food products. *TrAC Trends Anal. Chem.* **87**, 112–128 (2017). [0165-9936]
68. Cheat, S., Pinton, P., Cossalter, A.M., Cognie, J., Vilariño, M., Callu, P., Raymond-Letron, I., Oswald, I.P., Kolf-Clauw, M.: The mycotoxins deoxynivalenol and nivalenol show in vivo synergism on jejunal enterocytes apoptosis. *Food Chem. Toxicol.* **87**, 45–54 (2016). [0278-6915]
69. Awuchi, C.G., Ondari, E.N., Nwozo, S., Odongo, G.A., Eseoghene, I.J., Twinomuhwezi, H., Ogbonna, C.U., Upadhyay, A.K., Adeleye, A.O., Okpala, C.O.R. Mycotoxins' toxicological mechanisms involving humans, livestock and their associated health concerns: a review. *Toxins* **14**, 167 (2022)
70. Mahato, D.K., Lee, K.E., Kamle, M., Devi, S., Dewangan, K.N., Kumar, P., Kang, S.G.: Aflatoxins in food and feed: an overview on prevalence, detection and control strategies. *Front. Microbiol.* **10**, 2266 (2019)
71. Chen, P., Li, C., Ma, X., Wang, Z., Zhang, Y.: A surface-enhanced Raman scattering aptasensor for ratiometric detection of aflatoxin B1 based on graphene oxide-Au@Ag core-shell nanoparticles complex. *Food Control* **134**, 108748 (2022). ISSN 0956-7135
72. Zheng, S., Wang, C., Li, J., Wang, W., Yu, Q., Wang, C., Wang, S.: Graphene oxide-based three-dimensional Au nanofilm with high-density and controllable hotspots: a powerful film-type SERS tag for immunochromatographic analysis of multiple mycotoxins in complex samples. *J. Chem. Eng.* **448**(137760), 1385–8947 (2022)
73. Naseem, A., Ishak, M.I.S., Bhawani, S.A., Umar, K.: Various natural and anthropogenic factors responsible for water quality degradation: a review. *Water* **13**(19), 2660 (2021)
74. Hoang, H.G., Chiang, C.F., Lin, C., Wu, C.-Y., Lee, C.-W., Cheruiyot, N.K., Tran, H.-T., Bui, X.-T.: Human health risk simulation and assessment of heavy metal contamination in a river affected by industrial activities. *Environ. Pollut.* **285**, 0269–7491 (2021). <https://doi.org/10.1016/j.envpol.2021.117414>

75. Proshad, R., Islam, Md.S., Kormoker, T., Sayeed, A., Khadka, S., Idris, A.M.: Potential toxic metals (PTMs) contamination in agricultural soils and foodstuffs with associated source identification and model uncertainty. *Sci. Total Environ.* **789**, 147962 (2021)
76. Du, H., Xie, Y., Wang, J.: Nanomaterial-sensors for herbicides detection using electrochemical techniques and prospect applications. *Trends Analyt. Chem.* **135**(116178), 0165–9936 (2021)
77. Grzegorz, L.: Reliable environmental trace heavy metal analysis with potentiometric ion sensors—reality or a distant dream. *Environ. Pollut.* **289**(117882), 0269–7491 (2021)
78. Long, C., Jiang, Z., Shangguan, J., Qing, T., Zhang, P., Feng, B.: Applications of carbon dots in environmental pollution control: a review. *Chem. Eng. J.* **406**(126848), 1385–8947 (2021)
79. Hassan, M.M., Xu, Y., Zareef, M., Li, H., Rong, Y., Chen, Q.: Recent advances of nanomaterial-based optical sensor for the detection of benzimidazole fungicides in food: a review. *Crit. Rev. Food Sci. Nutr.* (2021). <https://doi.org/10.1080/10408398.2021.1980765>
80. Wang, J., Maier, S.A., Tittel, A.: Trends in nanophotonic-enabled optofluidic biosensors. *Adv. Optical Mater.* **10**, 2102366 (2022)
81. Shandilya, R., Bhargava, A., Ratre, P., Kumari, R., Tiwari, R., Chauhan, P., Mishra, K.P.: Graphene quantum-dot-based nanophotonic approach for targeted detection of long noncoding RNAs in circulation. *ACS Omega* **7**, 26601–26609 (2022)
82. Long, Z., Huang, Y., Zhang, W., et al.: Effect of different industrial activities on soil heavy metal pollution, ecological risk, and health risk. *Environ. Monit. Assess.* **193**, 20 (2021)
83. Cai, L.M., Wang, Q.S., Luo, J., Chen, L.G., Zhu, R.L., Wang, S., Tang, C.H.: Heavy metal contamination and health risk assessment for children near a large Cu-smelter in central China. *Sci. Total Environ.* **650**(1), 725–733 (2019). [0048-9697]
84. Kamaruddin, N.H., Bakar, A.A.A., Yaacob, M.H., Mahdi, M.A., Zan, M.S.D., Shaari, S.: Enhancement of chitosan-graphene oxide SPR sensor with a multi-metallic layer of Au–Ag–Au nanostructure for lead (II) ion detection. *Appl. Surf. Sci.* **361**, 177–184 (2016) [0169-4332]
85. He, Q., Han, Y., Huang, Y., Gao, J., Gao, Y., Han, L., Zhang, Y.: Reusable dual-enhancement SERS sensor based on graphene and hybrid nanostructures for ultrasensitive lead (II) detection. *Sens. Actuators B Chem.* **341**, 130031 (2021). [0925-4005]
86. Ding, X., Kong, L., Wang, J., Fang, F., Li, D., Liu, J.: Highly sensitive SERS detection of Hg<sup>2+</sup> ions in aqueous media using gold nanoparticles/graphene heterojunctions. *ACS Appl. Mater. Interfaces* **5**(15), 7072–7078 (2013)
87. Karthik, V., Selvakumar, P., Senthil Kumar, P., Sathesekumar, P., Vijaysunder, M.G., Hariharan, S, Antony, K.: Recent advances in electrochemical sensor developments for detecting emerging pollutant in water environment. *Chemosphere* **304**, 0045–6535 (2022). <https://doi.org/10.1016/j.chemosphere.2022.135331>
88. Dong, X., Liu, D., Meng, X., et al.: Research progress on photoelectrochemical sensors for contamination analysis in agricultural fields. *Anal. Sci.* **38**, 459–481 (2022)
89. Zhao, Y.L., Chen, Q., Lv, J., et al.: Specific sensing of antibiotics with metal-organic frameworks based dual sensor system. *Nano. Res.* **15**, 6430–6437 (2022)
90. Wang, Y., Chen, H., Jiang, L.: A highly reproducible SERS sensor based on an Au nanoparticles/graphene oxide hybrid nanocomposite for label-free quantitative detection of antibiotics. *Analyst* **146**, 5740–5746 (2021). <https://doi.org/10.1039/D1AN01185E>
91. Li, Y.T., Qu, L.L., Li, D.W., Song, X., Fathi, F., Long, Y. Rapid and sensitive in-situ detection of polar antibiotics in water using a disposable Ag–graphene sensor based on electrophoretic preconcentration and surface-enhanced Raman spectroscopy. *Biosens. Bioelectron.* **43**, 94–100 (2013). <https://doi.org/10.1016/j.bios.2012.12.005>
92. Guo, S., Beleites, C., Neugebauer, U., et al.: Comparability of Raman spectroscopic configurations: a large-scale cross-laboratory study. *Anal Chem* **92**, 15745–15756 (2020)
93. Orlando, A., Franceschini, F., Muscas, C., Pidkova, S., Bartoli, M., Rovere, M., Tagliaferro, A.: A comprehensive review on Raman spectroscopy applications. *Chemosensors* **9**, 262 (2021)
94. Lu, L., Hou, S., Zhao, X., Liu, C., Li, Z., Li, C., Xu, S., Wang, G., Yu, J., Zhang, C., Man, B.: Role of graphene in constructing multilayer plasmonic SERS substrate with graphene/AgNPs as chemical mechanism—electromagnetic mechanism unit. *Nanomaterials* **10**(12), 2020–2371 (2020). <https://doi.org/10.3390/nano10122371>

95. Lai, H., Xu, F., Zhang, Y., Wang, L.: Recent progress on graphene-based substrates for surface-enhanced Raman scattering applications. *J. Mater. Chem. B* **6**, 4008–4028 (2018). <https://doi.org/10.1039/C8TB00902C>
96. Cao, Y., Cheng, Y., Sun, M.: Graphene-based SERS for sensor and catalysis. *Appl Spectrosc Rev* (2021)
97. Zhang, L., Jiang, C., Zhang, Z.: Graphene oxide embedded sandwich nanostructures for enhanced Raman readout and their applications in pesticide monitoring. *Nanoscale* **5**, 3773–3779 (2013)

# An Investigation on Unique Graphene-Based THz Antenna



Rachit Jain, P. K. Singhal, and Vandana Vikas Thakare

**Abstract** Terahertz band in the electromagnetic spectrum has not been able to establish itself as an advantageous band for communication operations, even though there are not reliable, affordable sources and detectors that can operate at terahertz frequencies. The electromagnetic spectrum's terahertz band lies somewhere between the optical and microwave spectrums. Numerous potentially significant uses, particularly in the areas of short-distance communication, security, and defense, have been envisioned. Therefore, it is imperative that Terahertz sources and detectors be properly analyzed and designed. Graphene has recently gained popularity and has become a material of interest for several uses. It is a two-dimensional hexagonal structure of connected carbon particles, which is utilized for various generations of signals, signal propagation, signal detection, and modulation. These functions are made possible by graphene's broad band, high speed, small dimensions, and especially reduced losses as compared to traditional materials like silicon. Among all of graphene's great qualities, its capacity to support the surface plasmon polariton (SPP) wave, which travels at terahertz frequency range, is the most significant one. As a result, it is excellent for use in terahertz (THz) band technology. The chapter will focus on the recent development of flexible, compact, and effective terahertz (THz) antennas using graphene, their applications, and challenges.

**Keywords** Graphene · THz · Antenna · 6G Communication

---

R. Jain (✉) · P. K. Singhal · V. V. Thakare  
Department of Electronics Engineering, Madhav Institute of Technology and Science, Gwalior,  
Madhya Pradesh, India  
e-mail: [rachit2709@gmail.com](mailto:rachit2709@gmail.com)

P. K. Singhal  
e-mail: [pks\\_65@mitsgwalior.in](mailto:pks_65@mitsgwalior.in)

V. V. Thakare  
e-mail: [vandana@mitsgwalior.in](mailto:vandana@mitsgwalior.in)

## 1 Introduction

Graphene has received much interest from its very discovery in 2004. Due to this exceptional material's superior electromechanical conductivities for future high-speed electronic devices having electrical and electro-magnetic properties, many gadgets are constructed from it. A high density 2-dimensional cluster of carbon is termed graphene. It has incredible mechanical strength, extraordinarily high electrical and thermal conductivities and gas impermeability. Modulators, wearable technologies, semiconductors, and molecular equipment's work in high frequency, and THz gadgets might all make use of graphene [1, 2]. Exploring microstrip antennas at terahertz frequency is motivated by the growing need for smart antenna at faster communication rate of speed. The terahertz band, according to the International Telecommunication Union (ITU), spans 300 GHz to 10 THz. The microstrip patch antenna is an attractive technology for the terahertz frequency range because it can be miniaturized. Versatile and narrow antennas based on graphene are needed since the thin metallic layer that employs graphene often cracks or breaks in response to physical variations. The domain for THz networking is becoming increasingly interested in graphene-based plasmonic antennas. [3, 4]. The capacity for graphene to support the surface plasmon polariton (SPP) wave, which has frequency band in THz, stands out among the numerous remarkable qualities of graphene. Moreover, the transmission done through graphene is dynamically controlled by using bias voltage through external gate and, consequently, the applied electric field. As a result, radiation characteristics, frequency, and polarization of tunable antenna may be created by dynamically adjusting the SPP wave propagation properties in graphene. Patch antenna frequency and radiation patterns were already covered in the research as per electromechanical and optical principles. Changing the current distribution on an antenna's radiating is basically invented for the above-mentioned reconfigurations. In comparison, graphene-based antenna reflects material's tunable property of conductivity and various reconfigurable properties can be generated with very minor modifications. The present project illustrates the structure and radiating properties of array of reconfigurable patch based on graphene on a polyimide substrate in the THz range [5, 6].

We provide a brief overview and context for the recent advancements in THz graphene-based antenna research and make an effort to pinpoint current research trends, as well as short-, mid-, and long-term obstacles and opportunities. The simulation technique is quite complex to show the fundamentals of antenna resonance because of the sophisticated technique and modeling of graphene-based antenna. Transmitter dimensions, graphene characteristics, and substrate characteristics have the biggest impact on performance. A variety of parameters should be taken into consideration in order to improvise the antenna for the desired performance. To fully comprehend such antennas, the graphene-based antenna resonant circuit model was explored to aid in the early structure of the antenna and comprehension of antenna resonance feature. Our analysis of the most cutting-edge resonant antenna, leaky wave antennas, and reflect arrays is followed by a look at their feeding network and

the most fascinating THz system and graphene antenna applications that have been proposed.

In addition to theoretical research, empirical establishments of graphene’s material characteristics have been accelerated by its discovery. One of graphene’s appealing qualities like a semi-metal substance is its distinctive conductivity, which may be managed by external power. Opportunities for the development of graphene-based devices that can influence electromagnetic (EM) waves at the THz range are offered by both a deeper knowledge of the characteristics of graphene and improved manufacturing techniques that produce high-quality graphene [4, 6].

### 1.1 Graphene Fabrication Techniques

Industrialists have now been developing appropriate manufacturing techniques for good-quality, less defective, robust, and less costly approaches since graphene was found. The manufacturing of graphene is a difficult challenge since the usage of this material for various purposes mainly relies on large-scale manufacturing techniques [7]. Various fabrication techniques generally used for production of graphene are shown in Fig. 1.

**Fig. 1** Graphene fabrication techniques

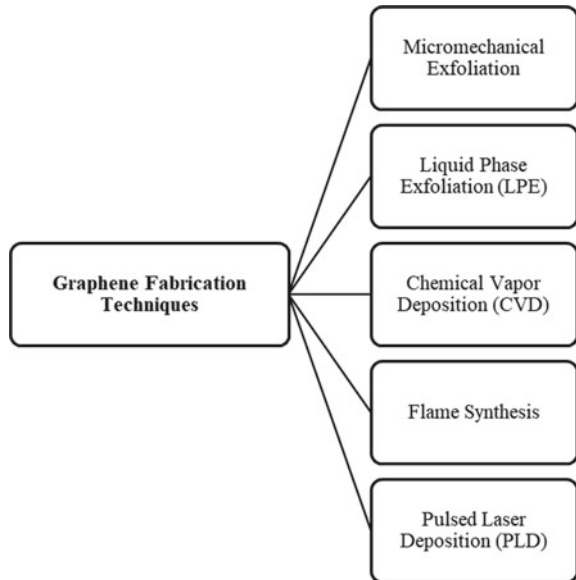
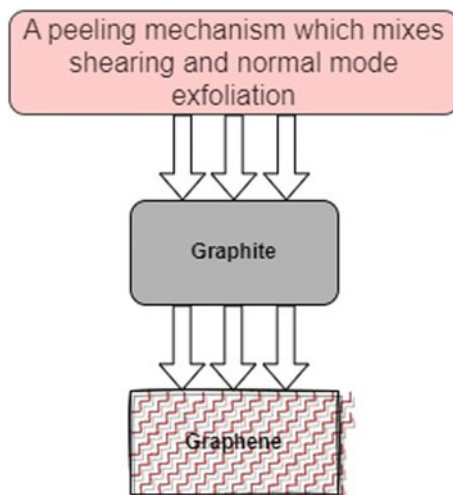




**Fig. 2** Micromechanical exfoliation technique



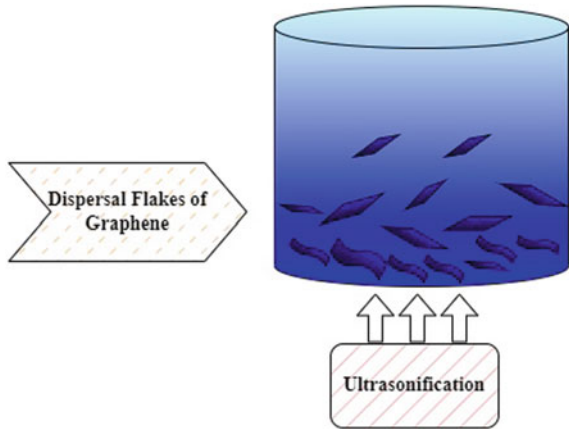
### Micromechanical Exfoliation

Micromechanical exfoliation is a procedure for fabricating graphene-based substances which includes removing sequentially arranged pyrolytic graphite using sticky tape. This is a graphene-synthesized procedure in which graphene is extracted from graphite crystals. Peeling represents the process of extracting graphene from graphite. After peeling, multi-layer graphenes appear mostly on tape. Graphene gets repeatedly peeled into sheets over a few layers. Although it is a straightforward and simple production process, graphene cannot be grown on a large scale using this technology. Documentation on the steps involved in producing graphene is available in article [8]. Process is shown in Fig. 2.

### Liquid Phase Exfoliation (LPE)

LPE is a technique represented in Fig. 3 that generates graphene substances via ultrasonically exfoliating graphite while utilizing solvents including acetic acid, sulfuric acid, and hydrogen peroxide. Since graphite includes many layers of graphene that are held together, the LPE process employs sonication to exfoliate the substance and separate graphene from the graphite. Such a technique was applied to originate graphene nano-ribbons, but producing graphene on a large scale is extremely difficult. Documentation on LPE to make graphene is available in the papers [9, 10].

**Fig. 3** Liquid phase exfoliation technique



### Chemical Vapor Deposition (CVD)

CVD is a vital deposition technique for metallic elements. Nickel and copper are utilized in this technique to synthesize graphene on a massive scale. During the CVD process, a layer of metallic catalysts coats the substrates. Chemical etching is performed on substance that has been applied to substrate. Following chemical etching, a carbon-containing mixture is introduced into the reaction chamber. The CVD process experimental setup is depicted in Fig. 4. The graphene produced by this technique is of superb quality. In the article [11], more details are available.

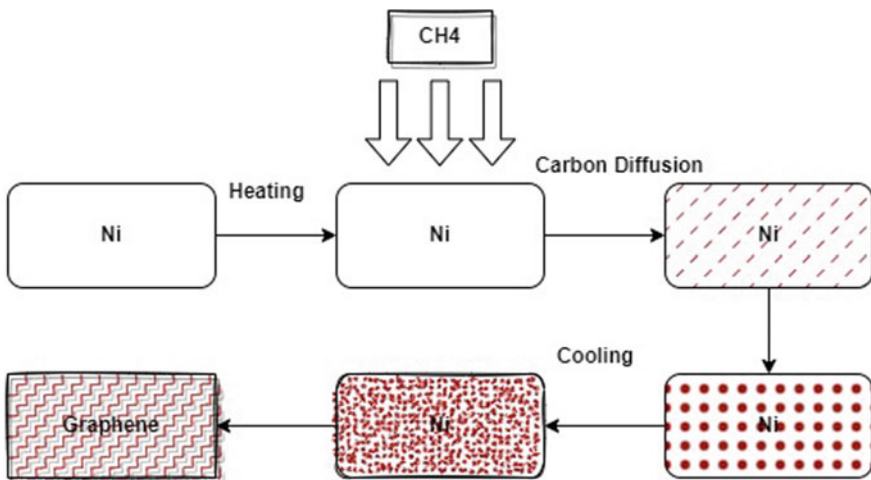


**Fig. 4** Chemical vapor deposition process

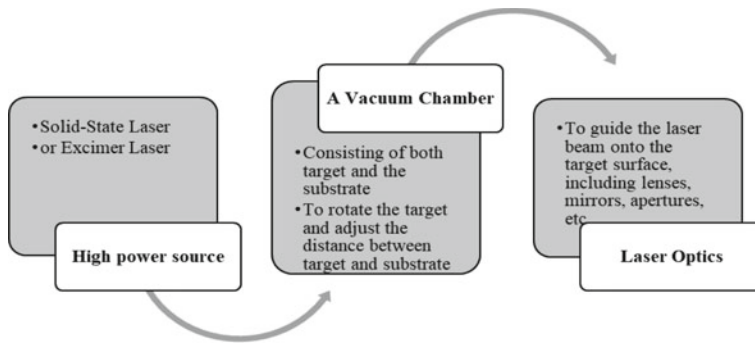


**Fig. 5** Pulsed laser deposition (PLD) framework

## Flame Synthesis

A widely used approach for creating nanoparticles in massive amounts is flame synthesis. This approach was not as popular for the fabrication of graphene-like chemical vapor deposition. Due to its benefits, including expandability and affordability, several researchers have accumulated on using flame synthesis to produce graphene substances. Some authors suggest that flame synthesis may be used to inexpensively synthesize graphene [12].

## Pulsed Laser Deposition (PLD)

This is a prominent growth strategy that is utilized to produce practically all sorts of materials. Laser power is used throughout the PLD procedure, and a high vacuum is maintained inside the capsule. Figure 5 shows the PLD framework.

Material is placed at a 45° angle by stoichiometry transfer between target and substrate material in this process. Substrates are added to its surfaces parallel to the target at a range of 2–10 mm during procedure.

The primary benefit of the PLD technique is the small temperature growth rate that is accomplished, resulting in the production of flawless graphene [13].

### 1.2 About Graphene Conductivity

Graphene conductivity is directly influenced by a variety of factors, including chemical doping, frequency of operation, Fermi energy (chemical potential), mobility of electrons, temperature of environment, and relaxation time. Such variables are not independent, although they could be connected [14, 15].

At THz frequencies, the graphene conductivity may be calculated using only the intraband component of the Kubo formula [16] represented in Eq. 1, where  $\omega$

= angular frequency,  $\mu_c$  = chemical potential of graphene,  $\tau$  = graphene electron relaxation time,  $T$  = Temperature,  $k_B$  = Boltzmann's constant,  $\hbar$  = Planck's constant, and  $e$  = charge of electron.

At millimeter and microwave frequencies, graphene is frequency dependent from an electromagnetic aspect. The conductivity of this material responds to THz and infrared frequencies due to its inherent kinetic inductance, which is connected to the interference pattern of the conductivity and serves as a negative real permeability in a base material. The development of antenna has recently been inspired by the fact that graphene encourages surface plasmon polaritons (SPP) propagation at high frequencies, somewhat like metals do so in optics.

The dispersion relation and characteristic impedance of transverse magnetic (TM) plasmons in an available sheet of graphene of conductivity  $\sigma$  could be calculated using Eqs. 2 and 3, where  $k_0$  = free-space wavenumber,  $\eta$  impedance,  $\epsilon_0$  = permittivity of vacuum, and  $\epsilon_{\text{eff}}$  = effective permittivity [16, 17].

$$\sigma = -j \frac{e^2 k_B T}{\pi \hbar^2 (\omega - j\tau^{-1})} \ln \left\{ 2 \left[ 1 + \cosh \left( \frac{\mu_C}{k_B T} \right) \right] \right\} \quad (1)$$

$$k_{\text{SPP}} = k_0 \sqrt{1 - \left( \frac{2}{\eta \sigma} \right)^2} \quad (2)$$

$$Z_C = \frac{k_{\text{SPP}}}{\omega \epsilon_0 \epsilon_{\text{eff}}} \quad (3)$$

## 2 Recent Work on Graphene Antenna

Numerous surface antenna with graphene-holographic artificial impedance in the THz range was suggested in this work [18]. The presented surface THz antenna graphene-holographic impedance could be structured through uniformly sizing and spacing patch cells by taking advantage of its conductive adaptive property. The anticipated impedance pattern can then be easily accomplished by changing the DC values for every patch.

According to [18], by altering the DC values, scanning of the beam and polarization conversion might also be accomplished without the use of conventional techniques. The general construction of the proposed antennas is made up of  $51 \times 51$  graphene patches of equal size. A DC gate-pad which is 100 nm thick polysilicon was positioned beneath each patch to allow for local control of graphene conductivity. Moreover, due to its exceptional mechanical properties and atomic thickness, it is ideally suited for conformal antenna design.

In this article [19], author proposes that due to the unique qualities of graphene material, graphene-patch antennas had already recently been extensively for use in wireless communication, especially in THz applications. On FR4 substrate material,

a rectangular patch antenna based on graphene is fabricated. To improve overall antenna's performance and to protect the patch antenna from various hazards, and provide a multiband resonance frequency, the radiating patch antenna is covered with a single- or double-faced superstrate metamaterial. A dual-band frequency at 3.5 and 4.33 THz had been obtained using a single-face triangle SRR (Split Ring Resonator), with a bandwidth of 400 and 460 GHz, and the dual-band structure's return loss reached  $-26.7$  and  $-46.2$  dB, respectively. The triangle SRR designed on the reverse side of the dual-face metamaterial unit cell generates a 3rd resonant frequency, leading to the generation of three distinct frequency bands, each with bandwidth of 230, 520, and 610 GHz, corresponding to 2.32, 3.35, and 4.38 THz. This not only improves that antenna's performance but also introduces a new resonance frequency that might be employed for another 6G services.

Author of this paper [20] discusses enhanced data transfer rates and less transmit power needed for dependable wireless networks at high frequency ranges (THz). With this article, a solution to the issue of reconfiguration of radiation characteristics with a patch antenna has been suggested. This solution satisfies the need for multifunctional systems with greater performance in restricted spaces at higher frequencies.

Design and analysis of monolayer reconfigurable graphene-based array antenna at THz band for three reconfiguration frequencies and radiation patterns are presented in this study. The presented design produces 60% efficiency, 12.69 dB of directivity, and 10.17 dB of gain at 0.71 THz. With chemical potential varying from 0.4 to 0.8 eV, reconfiguration of frequency is accomplished between 0.64 and 0.74 THz. Resonating frequency changed to a higher frequency when chemical potential increased. Linear, right-hand circular, and left-hand circular polarization can be reconfigured. Beam variation between  $82^\circ$  and  $115^\circ$  is utilized to reconfigure the radiation pattern.

In this article [21], a rectangular graphene loop antenna with a good radiation efficiency for terahertz (THz) band is presented and analyzed. This antenna outperforms the earlier-designed antenna in terms of fractional bandwidth and radiation efficiency as compared to similar graphene dipole antennas. Based on a single layer of graphene, this antenna is resistant to slight deviations in graphene characteristics. It was demonstrated that an array of equivalent dipole formulation may accurately forecast the antenna's simulated performance. The proposed antenna has some resilience to the fundamental graphene properties, which makes it a promising choice for wideband communications in THz spectrum.

The author of this manuscript [22] describes a circular microstrip patch antenna for use in the terahertz band at almost 7 THz, with graphene working as main patch element on substrate of Teflon having  $\epsilon_r = 2.1$ . Superstrate layer is utilized to improve the radiation characteristics of the presented antenna and to provide high gain and directivity. The author tested various dielectric materials, such as Teflon ( $\epsilon_r = 2.1$ ), Arlon AD 250 ( $\epsilon_r = 2.5$ ), Roger RO3003 ( $\epsilon_r = 3$ ), Roger RO4003C ( $\epsilon_r = 3.25$ ), polyimide ( $\epsilon_r = 3.5$ ), and glass ( $\epsilon_r = 0.82$ ), utilized as the overlaying superstrate layer, and evaluated their effects on the performance of the proposed antenna at the terahertz band. At the resonance frequency of 6.994 THz, the proposed antenna gives antenna gain of 7.286 dB, efficiency of 97.2%, directivity of 7.4 dB, and bandwidth

of 386 GHz. The author came to the conclusion that using materials with greater dielectric constants as even the superstrate layer greatly enhances antenna gain. However, it decreases the proposed antenna's efficiency and bandwidth.

The concept of graphene-based microstrip patch antenna as well as its cluster is represented in this work [23]. The graphene-based single patch receiving wire with a  $1 \times 2$  cluster of patch antenna is also considered in this research. In order to take a resonant frequency of 27.92 GHz into consideration, this article provides a 5G spectrum beyond 6 GHz band that is located around 24.5 and 29.5 GHz. Through the use of HFSS software, these researchers analyzed the gain, radiation pattern, and return loss of a single fixed radio wire and its array.

The results showed that the presented graphene-patch antenna with two component cluster has multiband with high gain of 2.43 and 6.5 dB. Additionally, the results show that a single patch graphene receiving wire has less cross polarization than a metallic (copper) patch reception antenna. In comparison with metallic receiving antenna, the structured antenna's data transmission capacity has increased.

Numerous graphene-based multiple-beam reconfigurable THz antenna configurations were examined. Few techniques of modulation in THz antennas which are graphene based are proposed in this paper [24].

By varying the chemical potentials of the graphene in the antenna, the key characteristics of the proposed antenna, including direction of beam, resonant frequency, front-to-back ratio, and peak gain could be varied. Through selecting the appropriate chemical potentials for said proposed two-beam reconfigurable THz antenna, outstanding unidirectional symmetrical radiation patterns are obtained, with a front-to-back ratio of 10 dB.

In this article [25], a graphene nanoplate-based grounded coplanar waveguide (GCPW) attenuator was presented. In this article, a brand-new, graphene nanoplate-based grounded coplanar waveguide (GCPW) attenuator was presented. A 50-GCPW transmission line and 3 pairs of graphene nanoplate pads spaced evenly apart across the signal line as well as the top metal ground comprise the attenuator. By raising the voltage levels, attenuation level of the graphene pad may be controlled from high to low resistance. To obtain appropriate impedance matching in various operating bands, it is possible to modify the spacing among 2 pairs of graphene pads in particular. The theory of impedance matching is examined.

Two attenuator specimens are structured, fabricated, as well as evaluated (8–18 and 18–28 GHz). Modeling and simulation are used to validate the other two samples (3.5–8 and 28–38 GHz). As the voltage level change between 0 and 6 V, the attenuators' attenuation amplitude could be tuned from 2.5 to 14 dB with return loss less than  $-10$  dB and the operating frequency bands ranges between 3.5 and 38 GHz.

This author proposed [26] graphene-based, flexibly reconfigurable antenna that operates in the range of microwaves and has a voltage-controlled far-field radiation pattern. The presented antenna comprises 2 radiating patches along with a planer feed that is primarily made up of a power divider with a hybrid graphene-metal phase shifter and graphene-based attenuator. A bias voltage applied to graphene causes the

phase shifter's output phase to vary. When the voltage level varies between 0.7 and 5 V, the antenna can operate in two separate states with differing beam orientations.

The phase shift behavior of the graphene-metal phase shifter is examined using analogous circuit model. This article explains how a new form of reconfigurable antenna may be created using a graphene-metal combination throughout the microwave frequency band. By using a simplified pasting approach rather than soldering, this type of graphene-based tuning construction may be simply stacked through another circuitry, enabling graphene to build composite structures with materials that not able to tolerate soldering heat. That is feasible to continuously scan the beam within a specific range by adding multiple radiating elements toward the antenna. Future flexible radio frequency systems could make use of this feature.

A graphene-based adjustable resistor-based reconfigurable Vivaldi antenna for millimeter wave (MMW) is presented in this article [27]. First, similar proportional slot on the ground patch is used to create a reformed Vivaldi antenna, which gives higher front-to-back ratio (FBR). Moreover, to perform dynamic gain modification, a pattern-reconfigurable antenna composed of two end-to-end redesigned Vivaldi antennas with 2 symmetrical loaded graphene nanoplate pads on the feed line is provided. The resistance of such graphene pad could be gradually decreased from 200 to 20  $\Omega$  by providing voltage level between 0 and 4 V. Patch and ground slots enable the dc interruption of two graphene pads for separate resistance tuning. Vivaldi antenna's radiation pattern could be changed from two opposing beams to one beam by adjusting the resistance of two graphene pads. According to the research observations, the presented antenna for millimeter waves can change the direction of its radiation beams to 90° or 270°, and this capability can be expanded to a variety of pattern-reconfigurable antennas.

The structure and radiation properties for graphene-based patch antenna on SiO<sub>2</sub> (Glass Substrate) in the THz band are investigated and explained in detail in this paper [28]. Electric current's capability passing across screen eliminates the area constraint issue associated with this same antenna upon that phone's screen, suppressing the electrical interference from the antenna.

To comprehend the antenna's resonance behavior, an analogous circuit of antenna having R, L, and C linked through series is described and utilized to simulate the graphene-patch antenna which is proposed. With excellent frequency reconfiguration, a low return loss, and an omnidirectional radiation characteristics, this antenna attained a sidelobe level of 212.7 dB.

The basic constraints on this design are brought due to the characteristics of graphene, including its relaxation duration, the limit of acceptable voltages, and also the appropriateness for substrates in the terahertz spectrum. With reference to the design examined in this article, it appears to be noted that when the outcomes of the graphene-based patch antennas are compared to that of the copper-patch antenna, suggesting that even this graphene-based antenna may be incorporated in future every reconfigurable graphene THz transmitters, receivers, and various sensors instead of compromising electrical performance.

In this work [29], author introduces a square spiral antenna made of graphene that can be tuned for frequency and radiation pattern for the THz spectrum. The achieved maximum impedance bandwidth of the proposed antenna is almost 26.39%.

The designed antenna has a frequency range of 0.1–2 THz. Changing chemical potentials can also alter radiation patterns within a specific frequency band. The suggested antenna is a suitable choice to develop wireless communication for nano-systems, electrically frequency-tunable photoconductive terahertz sources, as well as for beam scanning systems in the terahertz band due to the reconfigurability of frequency and radiation pattern.

The author proposes a graphene loop antenna with a reconfigurable operating frequency band [30]. A photomixer-excited ring graphene element makes up this antenna. The device can function at various terahertz frequencies by altering the chemical potential of graphene. The working band of this device can be changed from 2.2 to 2.3 THz (with bandwidth of 4.4%) and 2.6–3.3 THz (with bandwidth of 21%) for voltage levels of 0.5 and 1 eV, respectively, based on modifying the graphene antenna's chemical potential.

This research presents [31] a novel method for constructing graphene-based microstrip antennas. The microstrip antenna is specifically cut through the flexible graphene-based conductors using a commonly available micro-cutter, and then this piece is adhered to a ground FR4 substrate to construct an innovative fabricated antenna.

The copper of such a conventional conformal antenna, though, can be a problem. Due to the weight and the possibility of copper failure from repeated bending deformations, this is the case. A bendable graphene-based conducting substance is being investigated as a potential replacement for the traditional use of copper in a conformal antenna in an attempt to resolve some of these problems. ADS was used to simulate the antenna design, and a prototype was built and tested and shown relative complex designs can be produced with simple and inexpensive commonly available micro-cutter.

It was investigated how a carbon nanotube could be used as a nano-dipole antenna, in this paper along with EM communications with nano-devices [32]. Authors are able to identify the energy band structure for several CNT forms and calculate its corresponding transmission line attributes using tight-binding model. Analysis has been done on how the essential resonance frequency, antenna input impedance, and system energy rely on the nanotube width. The wave propagation velocity in CNTs is shown to be governed by quantum effects down to a few nanometers in diameter, where it is nearly a hundred times slower than that of the light speed. The impact of quantum effects is lessened as nanotube diameter increases, and wave propagation tends to approach the light speed. A CNT-based antenna's input impedance also reduces as system energy and nanotube width increase. Short patch antenna built on the GNR has demonstrated similar results. The cumulative results highlight that graphene-based nano-antenna would be able to radiate EM waves in THz band for the size that nano-devices are intended to be, in any of the dimensions less than 1 mm.



### 3 Technical Requirements Toward Communication (in 6G)

The 5th (5G) mobile networks were unable to meet performance requirements; thus, the 6th (6G) technology of cellular operators will create new standards to do so. Owing to a variety of causes, including their demanding needs for faster networks with lower latency and higher intelligence, there are various goals for 6G, such as offering worldwide coverage, and the AI applications will set 6G apart from earlier generations because of these goals. The THz frequency band has a vital role in 6G communication. Between 0.1 and 10 THz, the THz spectrum is located between the microwaves and infrared spectrums. The microwave frequency band has recently become more prevalent in various uses, such as high data rate transmission in Internet of Things applications [33, 34]. Many antennas, including Yagi–Uda antenna, the Monopole antenna, and the log-periodic antenna, have been designed for the THz spectrum. Microstrip patch antenna, on the other hand, has a lot of benefits over the other types of antennas. Figure 6 illustrates several 6G essential requirements.

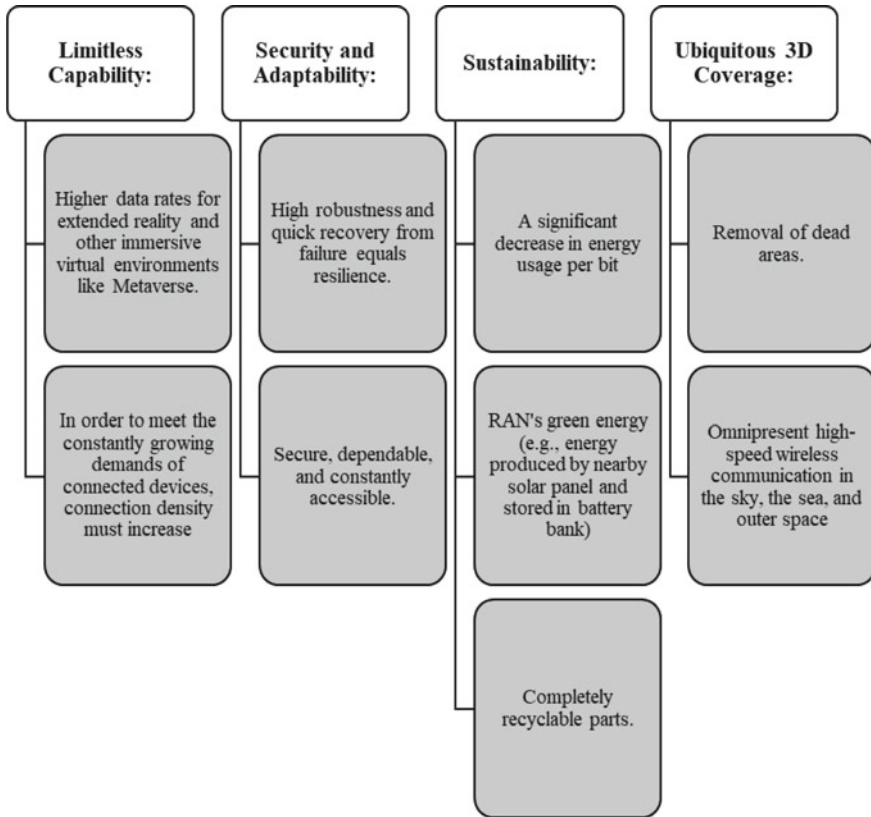
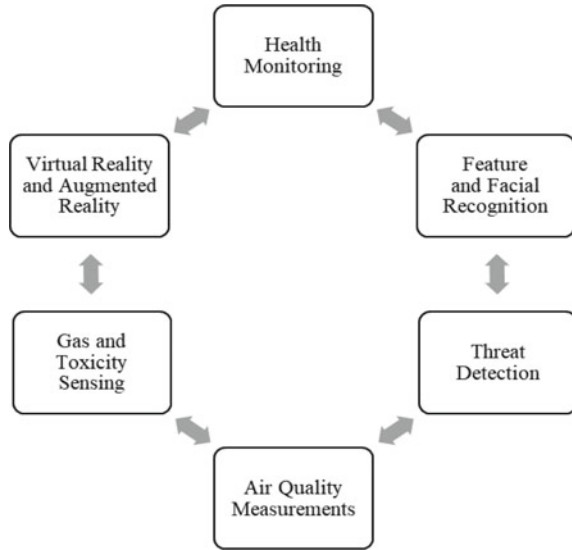


Fig. 6 6G essential requirements

Fig. 7 Significance of 6G



Great significance of 6G on national security and public health and safety is represented in Fig. 7.

### 3.1 How Graphene Antenna Is Important for 6G Communication

The 6G wireless communication system uses the terahertz frequency range to support user demand for increased data rates and extremely high data speed connectivity for numerous future applications. An essential function of the terahertz frequency range in 6G communication omnipresent high-speed wireless connectivity in the sky, the sea, and outer space. THz band has recently been popular in a variety of applications, such as high data transmission in Internet of Things applications. Figure 8 represents graphene antenna for 6G communication importance.

### 3.2 Advantages

Advantages are well elaborated in Fig. 9, and the frequencies are not bounded for THz antenna which is made up of graphene, nor do they require high voltage levels.

Highly desirable for applications having compact size, candidate for a nano-sized antenna, after reading the research reports on graphene-based THz antennas,

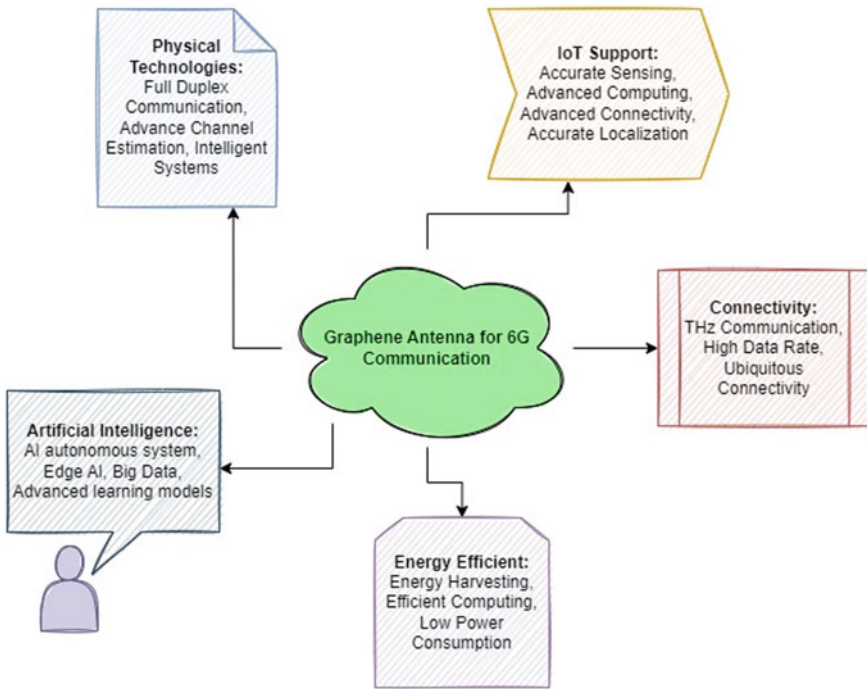


**Fig. 8** Graphene antenna for 6G communication

demonstrates that the antennas exhibit good values for good gain and antennas and radiative efficiency at THz frequency.

Based on the reference [35, 36], graphene based THz antenna for area constricted applications have remarkable compactness and adjustability attributes in THz bands, but those features occur with the expense of decreased radiation characteristics until the property of the graphene monolayers has been enhanced soon.

### 3.3 Challenges

THz band has various limitations, such as a short communication range, i.e., not useful for long-distance communication. Very high surface resistance results in more energy consumption. Less efficiency was compared to traditional antennas. The main difficulty with employing graphene as a nano element is modeling the material mathematically such that it has superior THz frequency characteristics. Any mechanical variation can cause graphene to crack or break. Fig. 10 depicts potential graphene-based challenges.

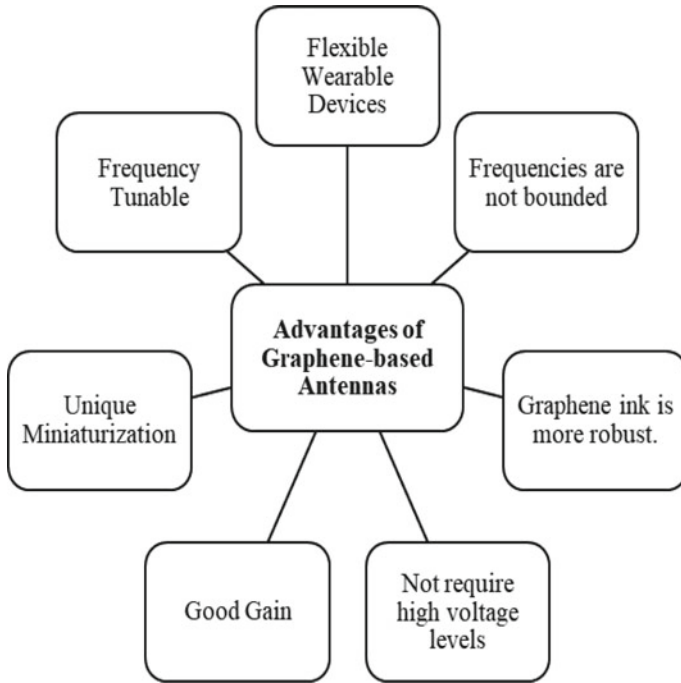
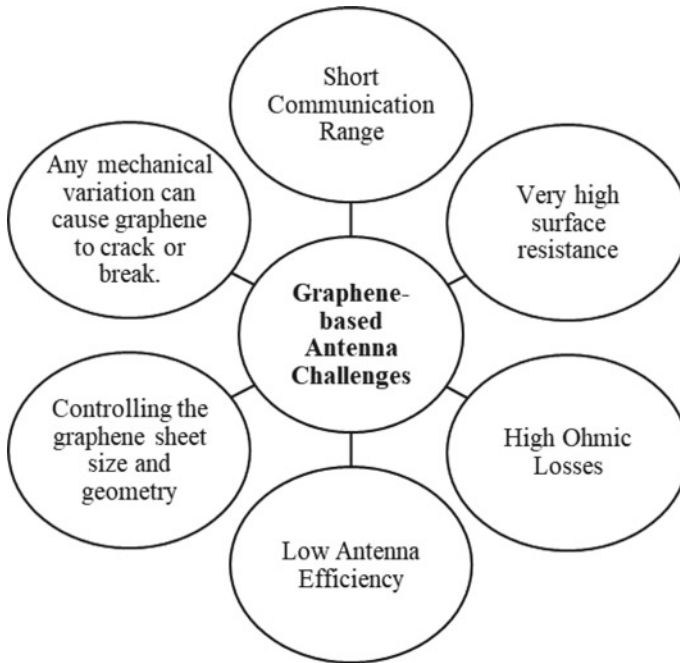


Fig. 9 Advantages of graphene-based antennas

## 4 Conclusion

Graphene has gained interest recently as a material for wide range of applications. It has numerous roles for signal emission, transmission, modulation, and detection. It is 2D (two-dimensional) hexagonal network of interconnected carbon sheets. Due to graphene’s broadband, small size, high speed, and especially little loss when compared with conventional materials like silicon, various applications are made possible. For the terahertz (THz) evolution for modern communications, antenna must have micro size range and have excellent far-field gain. This technology satisfies the need for a multipurpose system that performs better at greater frequency and occupies less space. Both thermally and electrically, graphene is very conductive. It examines the impact of graphene’s chemical potential on the antenna’s return loss and resonant frequency. The best way to change the radiation characteristics would be to change the graphene surface impedance. The recent advantage of graphene to create flexible, small, and efficient THz antennas, as well as their uses and difficulties, were the main topics of this chapter.



**Fig. 10** Graphene-based antenna challenges

## References

1. Anand, S., Kumar, D.S., Wu, R.J., Chavali, M.: Graphene nanoribbon based terahertz antenna on polyimide substrate. *Optik* **125**(19), 5546–5549 (2014)
2. Geim, A.K., Novoselov, K.S.: The rise of graphene. *Nat. Mater.* **6**(3), 183–191 (2007)
3. Llatser, I., Kremers, C., Cabellos-Aparicio, A., Jornet, J.M., Alarcón, E., Chigrin, D.N.: Graphene-based nano-patch antenna for terahertz radiation. *Photonics Nanostruct. Fundam. Appl.* **10**(4), 353–358 (2012)
4. Perruisseau-Carrier, J.: Graphene for antenna applications: opportunities and challenges from microwaves to THz. In: 2012 Loughborough Antennas & Propagation Conference (LAPC), pp. 1–4. IEEE (2012, November)
5. Jornet, J.M., Akyildiz, I.F.: Graphene-based plasmonic nano-antenna for terahertz band communication in nanonetworks. *IEEE J. Sel. Areas Commun.* **31**(12), 685–694 (2013)
6. Leng, T., Huang, X., Zhang, X., Hu, Z.: Reconfigurable dipole antenna design using graphene based switch. In: 2015 IEEE International Symposium on Antennas and Propagation & USNC/URSI National Radio Science Meeting, pp. 2295–2296. IEEE (2015, July)
7. Rudrapati, R.: Graphene: Fabrication methods, properties, and applications in modern industries. *Graphene Prod. Appl.* 9–22 (2020)
8. Sinclair, R.C., Suter, J.L., Coveney, P.V.: Micromechanical exfoliation of graphene on the atomistic scale. *Phys. Chem. Chem. Phys.* **21**(10), 5716–5722 (2019)
9. Cui, X., Zhang, C., Hao, R., Hou, Y.: Liquid-phase exfoliation, functionalization and applications of graphene. *Nanoscale* **3**(5), 2118–2126 (2011)
10. Monajjemi, M.: Liquid-phase exfoliation (LPE) of graphite towards graphene: an ab initio study. *J. Mol. Liq.* **230**, 461–472 (2017)

11. Kidambi, P.R., Ducati, C., Dlubak, B., Gardiner, D., Weatherup, R.S., Martin, M.B., Seneor, P., Coles, H., Hofmann, S.: The parameter space of graphene chemical vapor deposition on polycrystalline Cu. *J. Phys. Chem. C* **116**(42), 22492–22501 (2012)
12. Memon, N.K., Stephen, D.T., Al-Sharab, J.F., Yamaguchi, H., Goncalves, A.M.B., Kear, B.H., Chhowalla, M.: Flame synthesis of graphene films in open environments. *Carbon* **49**(15), 5064–5070 (2011)
13. Tite, T., Donnet, C., Loir, A.S., Reynaud, S., Michalon, J.Y., Vocanson, F., Garrelie, F.: Graphene-based textured surface by pulsed laser deposition as a robust platform for surface enhanced Raman scattering applications. *Appl. Phys. Lett.* **104**(4), 041912 (2014)
14. Neto, A.C., Guinea, F., Peres, N.M., Novoselov, K.S., Geim, A.K.: The electronic properties of graphene. *Rev. Mod. Phys.* **81**(1), 109 (2009)
15. Falkovsky, L.A., Varlamov, A.A.: Space-time dispersion of graphene conductivity. *Eur. Phys. J. B* **56**(4), 281–284 (2007)
16. Hanson, G.W.: Dyadic Green's functions and guided surface waves for a surface conductivity model of graphene. *J. Appl. Phys.* **103**(6), 064302 (2008)
17. Correias-Serrano, D., Gomez-Diaz, J.S., Perruisseau-Carrier, J., Alvarez-Melcon, A.: Graphene-based plasmonic tunable low-pass filters in the terahertz band. *IEEE Trans. Nanotechnol.* **13**(6), 1145–1153 (2014)
18. Ren, P., Jiang, L., Li, P.: Graphene based tunable terahertz holographic antennas. *IEEE Open J. Antennas Propagation* **3**, 324–332 (2022)
19. Khaleel, S.A., Hamad, E.K., Saleh, M.B.: High-performance tri-band graphene plasmonic microstrip patch antenna using superstrate double-face metamaterial for THz communications. *J. Electr. Eng.* **73**(4), 226–236 (2022)
20. Chandra, S., Dwivedi, S. (2021, April). Design and simulation of graphene based antenna for radiation pattern. In: 2021 6th International Conference for Convergence in Technology (I2CT), pp. 1–4. IEEE
21. Dmitriev, V., Rodrigues, N.R., de Oliveira, R.M., Paiva, R.R.: Graphene rectangular loop antenna for terahertz communications. *IEEE Trans. Antennas Propagation* **69**(6), 3063–3073 (2020)
22. Khan, M., Kaium, A., Ullah, M., Kabir, R., Alim, M.A.: High-performance graphene patch antenna with superstrate cover for terahertz band application. *Plasmonics* **15**(6), 1719–1727 (2020)
23. Singh, A.K., Kaur, P.: Design of graphene based antenna for 5G MIMO system. In: 2019 International Conference on Computing, Power and Communication Technologies (GUCON), pp. 503–507. IEEE (2019, September)
24. Luo, Y., Zeng, Q., Yan, X., Wu, Y., Lu, Q., Zheng, C., Hu, N., Xie, W., Zhang, X.: Graphene-based multi-beam reconfigurable THz antennas. *IEEE Access* **7**, 30802–30808 (2019)
25. Wu, B., Zhang, Y., Zu, H., Fan, C., Lu, W.: Tunable grounded coplanar waveguide attenuator based on graphene nanoplates. *IEEE Microwave Wirel. Components Lett.* **29**(5), 330–332 (2019)
26. Wang, J., Lu, W.B., Liu, Z.G., Zhang, A.Q., Chen, H.: Graphene-based microwave antennas with reconfigurable pattern. *IEEE Trans. Antennas Propagation* **68**(4), 2504–2510 (2019)
27. Fan, C., Wu, B., Hu, Y., Zhao, Y., Su, T.: Millimeter-wave pattern reconfigurable Vivaldi antenna using tunable resistor based on graphene. *IEEE Trans. Antennas Propagation* **68**(6), 4939–4943 (2019)
28. Goyal, R., Vishwakarma, D.K.: Design of a graphene-based patch antenna on glass substrate for high-speed terahertz communications. *Microwave Optical Technol. Lett.* **60**(7), 1594–1600 (2018)
29. Zhang, X., Ruan, C., Dai, J.: Reconfigurable antenna based on graphene at terahertz frequency. In: 2018 Progress in Electromagnetics Research Symposium (PIERS-Toyama), pp. 2311–2313. IEEE (2018)
30. Rodrigues, N.R.N.M., Dmitriev, V., de Oliveira, R.M.S.: Graphene loop antenna for THz band. In: 2018 SBFoton International Optics and Photonics Conference (SBFoton IOPC), pp. 1–5. IEEE (2018)

31. Sajal, S.Z., Braaten, B.D., Marinov, V.R.: A microstrip patch antenna manufactured with flexible graphene-based conducting material. In: 2015 IEEE International Symposium on Antennas and Propagation & USNC/URSI National Radio Science Meeting, pp. 2415–2416. IEEE (2015)
32. Jornet, J.M., Akyildiz, I.F.: Graphene-based nano-antennas for electromagnetic nanocommunications in the terahertz band. In: Proceedings of the Fourth European Conference on Antennas and Propagation, pp. 1–5. IEEE (2010)
33. Kranz, G., Christensen, G.: What is 6G? Overview of 6G networks & technology. In: SearchNetworking (2017). <https://www.techtarget.com/searchnetworking/definition/6G>
34. Jain, R., Aole, K., Mittal, S., Ranjan, P.: An analysis on wireless communication in 6G THz network and their challenges. In: Terahertz Devices, Circuits and Systems, pp. 167–181. Springer, Singapore (2022)
35. Abadal, S., Hosseininejad, S. E., Cabellos-Aparicio, A., & Alarcón, E.: Graphene-based terahertz antennas for area-constrained applications. In: 2017 40th International Conference on Telecommunications and Signal Processing (TSP), pp. 817–820. IEEE (2017)
36. Tripathi, S.K., Kumar, A.: Performance comparison of graphene terahertz antenna and copper terahertz antenna. In: Advances in Computational Intelligence and Communication Technology, pp. 489–497. Springer, Singapore (2021)

# Two-Dimensional Carbon Nanomaterial-Based Biosensors: Micromachines for Advancing the Medical Diagnosis



Shalini Bhatt, Vinay Deep Punetha, Rakshit Pathak, and Mayank Punetha

**Abstract** The current era has seen a sharp increase in maladies in the form of diseases and infections that have negatively affected the health, standard of life, healthcare expenditure as well as mortality of the individual. Diagnosis of such diseases requires identifying the biomarker molecules that are specific for the infection or diseased condition. The rapid evolution of biosensors in the field of disease diagnosis has provided the medical fraternity with an advanced level of diagnostics having high sensitivity, specificity and reproducibility. Biomarkers that are present in very less amounts require a highly sensitive biosensor that can even detect its pico-molar quantities in the sample. Graphene owing to its exceptionally diverse functionalities has gained worldwide recognition for use as a biosensor. This chapter explores the current advancement of graphene-based biosensors in medical diagnostics and treatment by the detection of different biomarkers in the biological sample. Impetus has been given on various methods for the development of graphene-based biosensors. In addition, future challenges and prospects have been discussed that may provide research in the field of graphene biosensors in a more channelled way for exceedingly specific, sensitive and throughput detection of the emerging fatal diseases.

**Keywords** Biomarker · Biosensor · Diagnostics · Graphene · Field effect transistors · Surface plasmon resonance

---

S. Bhatt (✉) · V. D. Punetha · R. Pathak · M. Punetha  
Centre of Excellence for Research, PP Savani University, Surat, Gujarat 394125, India  
e-mail: [shalini.bhatt@pps.ac.in](mailto:shalini.bhatt@pps.ac.in)

V. D. Punetha  
e-mail: [vinaydeep.punetha@pps.ac.in](mailto:vinaydeep.punetha@pps.ac.in)

R. Pathak  
e-mail: [rakshit.pathak@pps.ac.in](mailto:rakshit.pathak@pps.ac.in)

M. Punetha  
e-mail: [mayank.punetha@pps.ac.in](mailto:mayank.punetha@pps.ac.in)



## 1 Introduction

Disease diagnosis requires development of highly specific and sensitive detection method and biomarkers [1]. The use of early-stage diagnosis tools is essential for achieving better treatment outcomes while reliably battling deadly illnesses and infections. There are numerous conventional and novel methods available for detecting these fatal diseases. Conventional methods encompass enzyme-linked immunosorbent assay (ELISA), DNA sequencing, electrochemical methods, fluorescent microarray and lateral flow immunoassay [2–6]. However, to obtain accurate and sensitive detection, these approaches need expensive reagents, intricate sample preparation procedures and laborious quantification methodologies [7, 8]. These conventional methods lag in the real-time diagnosis of the diseases. On the other hand, novel methods employ the use of sensors, which are cheap, easy to use and highly sensitive in detecting the target biomolecule. These sensors may be employed in the real-time monitoring of diseases and therefore find their vast clinical applications in disease theranostics [9, 10]. Biosensors (BS) are self-contained diagnostic device which combines a biological component, termed as biosensing element, with a physicochemical one, termed as bio-transducer element to yield a quantitative signal generated upon the interaction of biosensing element with the target termed as analyte (Fig. 1) [11–13]. The two categories of often utilized biosensing components are catalytic and affinity type. The catalytic type of BS comprises the cell, tissues, enzymes, microbes, etc., while affinity-type sensors include antibodies, receptors and nucleic acids [14, 15].

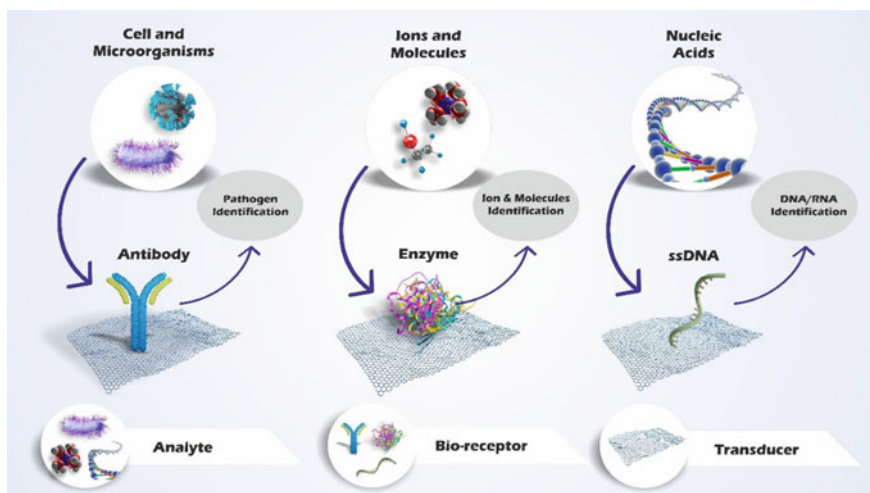


**Fig. 1** Graphene as a biosensor for the detection of various analytes

In contemporary times, various health hazards due to disrupted lifestyles possess a serious threat to mankind making biosensing and diagnosis as a crucial part of health management. Furthermore, with the development of the first oxygen biosensor by Led and Clark in 1952, BS have enabled highly specific, sensitive and rapid detection of biomarkers to fulfil the objectives of diagnostics and testing procedures [16–18]. A biomarker is defined as a biological molecule that is found in cells, tissues, blood or other body fluids and is truly a representative of a normal or abnormal as well as diseased condition of the body. Moreover, these BS have demonstrated excellent potential for use in a wide range of fields including biotechnology, pharmaceuticals, food, environment and agriculture [19–21]. Biomarker screening allows for an early and accurate detection of the infectious agent. They have emerged as a major tool for healthcare science for the accurate identification as well as eradication of various chronic diseases including Alzheimer’s disease (AD), allergy, asthma, cancer, diabetes, dementia, epilepsy, renal calculi, etc. Furthermore, they can successfully be used as an economical and highly efficacious tool which makes use of biological components namely, antibodies, cells, enzymes, tissues, microorganisms, nucleic acids (DNA and RNA), synthetic ligands for quick, unambiguous and highly sensitive detection of the analytes (Fig. 2). Bio-transducer elements detect the stimulus generated by the interaction of the biosensing component with its specific analyte and transform it into a detectable signal. Commonly used transducers include Optical, Electrochemical, Piezoelectric and Thermal/Calorimetric Sensors as explained in Table 1.

The amalgamation of BS with nanotechnology has provided immense potential in medical diagnosis delivering high throughput, real-time, label-free analysis with

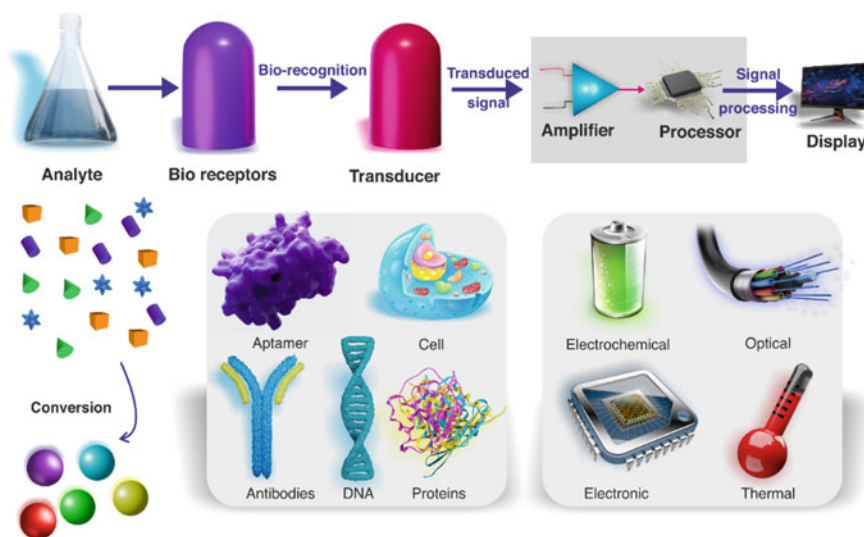


**Fig. 2** Schematic illustration of biosensor design and working

**Table 1** Commonly used transducer element in a biosensor

Transducer type		Examples	Analytes
Electrochemical	Amperometric	Clark O <sub>2</sub> electrode and mediated electrode system	Immunological analytes, cell, tissue, organelle, enzymes and gases
	Potentiometric	Redox and ion-selective electrodes, FETs, light addressable potentiometric sensors	
	Conductometric	Au/Pt electrodes for detecting the conductivity changed due to the ion formation	
Optical		Integrate optical sensors, photodiode, wave-guide system	Enzymes, various immunological analytes
Piezoelectric/ acoustic		Piezoelectric crystals, surface acoustic devices	Volatile gases, antibodies
Calorimetric		Thermistor	Antibiotics, enzyme, gases, organelle, pollutants, antibiotics

lower detection limits requiring lesser sample volume. In this regard, various nanomaterials in conjunction with biological molecules have been investigated for being a successful BS [22, 23]. The rising demand of carbon nanomaterials (CNM) for the development of BS is principally owing to the intrinsic properties including dimensional and thermal stability, chemical resistance, electrical conductivity, reduced water permeability, surface appearance, optical clarity and flame retardance, which all assist for their applicability in the biosensing platform. These inherent properties of various 0D, 1D, 2D and 3D CNM such as graphene, CNT (Carbon nanotubes), CQD (Carbon quantum dots), GQD (Graphene quantum dots), CNOs (Carbon nano-onions), CNHs (carbon nanohorns) and CB (carbon black) are being employed in the contemporary time for the evolution of advanced technology in the sensing applications [24]. Particularly, 2D-CNM, graphene (G), presents the most promising carbon-based nanomaterial for use as a BS and has drawn much attention of the researchers as a potential candidate in the diagnostic field owing to its exceptionally remarkable properties of adsorption performance, electrochemical conductivity, mechanical strength and pliability. Moreover, it can withstand the strong ionic solutions prevalent in bodily fluids [25–27]. Its planar surface along with its high surface-volume ratio allows specific and sensitive detection [26]. The present chapter is an effort to provide its readers with holistic knowledge about the graphene-based BS. Basic principles of biosensing using BS have been elaborated and illustrated with the diagram along with a thorough description of the history and properties of the BSs. A brief discussion on the general properties of the graphene imparting the characteristic feature of BS is provided. Comprehensive information about the classification of graphene-based BSs with a main focus on their biosensing ability and signal generation is provided.

Further, the chapter briefly analyses the contemporary research and development concerning graphene-based studies along with its role in medical diagnostics for the early detection and treatment of various diseases. It thus generates a thoughtful insight into the development along with the role of various graphene-based BS. This chapter will resourcefully highlight the current state of knowledge on graphene-based BS highly specific, sensitive and early detection of emerging fatal diseases.

## 2 Biosensor: History, Principle and Properties

BS is defined as device that detects chemical or biological interactions by producing signals corresponding to the analyte concentration in the reaction [28]. They are actively employed in applications including monitoring of disease, drug development, detection of contaminating agents, disease-causing microbes and biomarkers that serve as disease indicators in body fluids (blood, saliva, sweat, urine). This scientific analytical instrument consists of three major components, namely sensing bio-receptors, transducers and detector connected with the digital output. Upon interaction between the bio-receptors with the specific analyte, the transducer converts this reaction into a measurable signal which is further detected by the detector.

### 2.1 Principle

Biosensor is an analytical device which is composed of a biological molecule/element, to name a few, enzymes, proteins, antibodies and nucleic acids, with an electrical component to generate a signal output that can be measured or quantified. BS consists of various components as explained below [28] (Fig. 1).

**Analyte:** Analyte is the substance that is to be detected from the sample and forms the major point of interest. For example, p53 and Tau protein are an “analyte” for the BS that is designed to identify cancer [29, 30] and AD [31].

**Bio-receptor:** A bio-receptor is a molecule that uniquely recognizes the analyte of interest. It includes elements like antibodies, aptamers, cells, enzymes and nucleic acids (DNA/RNA). Signal generation in the form of pH change, light, charge/mass change, heat, etc., in response to the contact of the bio-receptor with the analyte is termed as bio-recognition. Bio-catalysis and bio-affinity are the two major types of bio-recognitions involved in biosensing [32].

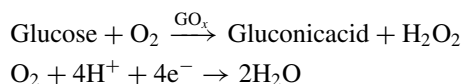
**Transducer:** Transducer converts energy from one form to another by a process termed as signalization. This element transforms bio-recognition process into a quantifiable signal, which is either electrical or optical and is generally proportional to the number of analyte bio-receptor interactions.

**Electronics:** This section of a BS is responsible for processing the specific transduced signal and getting it ready for exhibiting the output. It is made up of intricate circuits that carry out signal conditioning tasks like signal amplification and conversion from analogue to digital form. The BS's display device then quantifies the signals that have been processed.

**Display:** The display comprises a user interpretation system that provides readable figures or curves for the user. This component consists of a hardware and software combination that produces user-friendly BS data output. Based on the need of the end user, output signal on the display may be a picture, numerical, tabular or visual.

## 2.2 *Brief History*

Historical prospective of BS has been arranged into 3 generation based on attachment of the bio-receptor element to the transducer. In the 1st generation, analytes and the products of bio-receptor reactions diffuse through the transducer surface and generate an electrical response, which is measured by the BS. These types of sensors were termed as mediator-less amperometric BS. The first BS was invented in 1906 when M. Cremer suggested that the “electric potential which develops between fluid components which are on opposing sides of a glass membrane is proportional to the acid concentration in the liquid” [33]. Though, concept of hydrogen ion concentration (pH) and electrodes for pH measurements were introduced in 1909 by Soren Peder Lauritz Sorensen and 1922 by W.S. Hughes, respectively [34]. In the middle of 1902–1922, Griffin and Nelson illustrated immobilization of the invertase enzyme on charcoal and aluminium hydroxide [35, 36]. Leland C. Clark Jr. created the first “real” BS in 1956 to detect oxygen. He is regarded as the “Father of BSs,” and the oxygen electrode he invented is designated after his name as “Clark electrode”. Leland Clark created the amperometric enzyme electrode to detect glucose later in 1962, after which, Guilbault and Montalvo Jr. discovered the first potentiometric BS for detecting urea in 1969 [37, 38]. This BS enables monitoring of blood sugar in diabetic patients. In their work, glucose oxidase ( $GO_x$ ) acting as a bio-receptor, remained entrapped in a “Clark Electrode” via a semi-permeable dialysis membrane. Following reactions represent the catalytic reactions occurring in the electrode:



They demonstrated that the oxygen concentration was proportional to the concentration of glucose. Finally, in 1975, Yellow Spring Instruments (YSI) manufactured the first commercialized BS.

In the 2nd generation, specialized components such as enzymes and co-reactants are inserted into the biological element layer of the BS with the main aim of increasing

their analysis efficiency. These types of BS are termed as Mediator Amperometric BS. In 1976, Clemens and co-workers integrated an electrochemical glucose BS in a “bedside artificial pancreas” [39, 40]. Later, a glucose analyser which was based on a catheter was introduced by VIA Medica, followed by the introduction of lactate analyser, LA 640 by transporting electrons from LDH to an electrode [41].

In the 3rd generation, the incorporation of the bio-receptor molecule into the basal sensing component led to revolutionary progress by integrating enzymes and mediators on the single electrode rather than easily diffusible mediators in the electrolytic solution. Thereafter, since the advent of the i-STAT sensors remarkable advancements have been made in the BS domain. The field of BS research has evolved into a multidisciplinary one that combines the fundamentals of applied medicine, electronics and micro/nanotechnology, and with those of the basic sciences (physics, chemistry and biology) [42, 43]. Figure 3 illustrates the historical summary of BS.

### 2.3 Properties of a Biosensor

Every BS possesses a certain set of dynamic and static properties. Optimization as well as fine-tuning of these features is necessary for the ideal performance of the BS. The following section discusses some of these characteristics of a BS:

**Selectivity:** This property of a BS enables it to selectively detect the analyte molecule from the sample where different kinds of molecules or substances are present. For example, BS having antibody (Ab) as a bio-receptor immobilized on a transducer surface when exposed to the sample specifically reacts with the antigen molecule present in it. Selectivity is the main attribute that determines the working of a BS. False-positive results are obtained when a signal or response is generated by the interaction of the bio-receptor with the molecule that is similar to the analyte molecule. These false-positive results are often obtained with the BS that have poor selectivity. This property of a BS is very important in medical applications where biological samples such as blood/urine contain different kinds of similar molecules resembling the target analyte and thus compete for binding with the bio-receptor [61, 62].

**Reproducibility:** This characteristic enables the generation of identical results when experimental procedure is performed in replicates. The higher reproducibility of a BS represents the higher precision and accuracy of the electronics and transducer. Reproducible results obtained during repeated experiments for a particular sample relate to the extremely reliable and efficient response of the BS [28].

**Stability:** Stability forms the major attribute for BS which is used during continuous monitoring. It determined the capability of a BS to resist change in its performance over time concerning the disturbances/interruption caused by external factors. These factors include temperature, pH, humidity, ionic concentration, etc., variation and disturbances which lead to errors in the generated output signals, thereby influencing the accuracy and precision of the BS [28, 61].

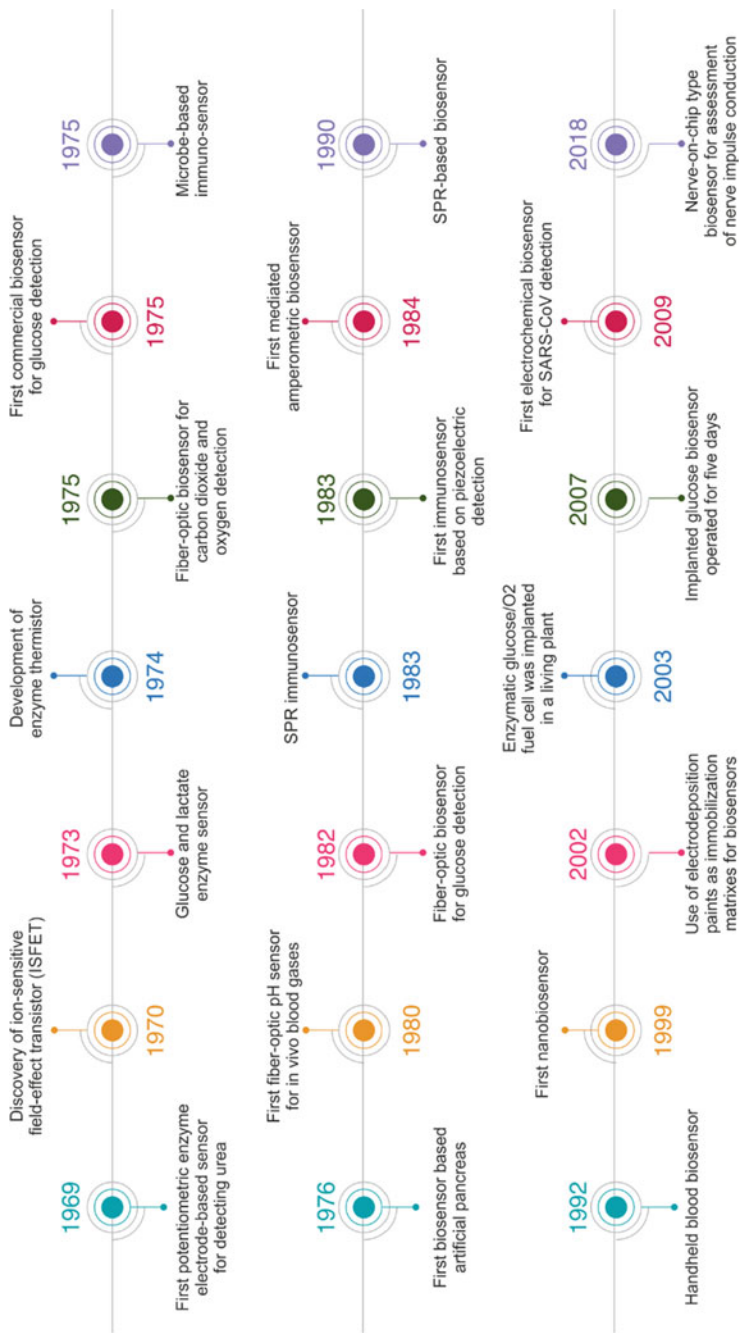


**Fig. 3** Historical summary of the biosensor development [38, 39, 44–60]



**Sensitivity:** This attribute defines the ability of a BS to detect the traces of analyte, i.e. minimal concentration in the sample, in the range of ng/mL or fg/mL. Highly sensitive BS is capable of generating signals in response to slight variations in the target analyte concentration. This characteristic is usually important during the processing of medical and environmental samples [63, 64].

**Detection limit:** Detect limit is expressed as the least concentration of the target analyte that is able to stimulate a detectable signal or response. An ideal BS is ought to have a minimum detection limit, particularly in medical diagnostic applications where the target analyte may be present in very trace concentrations in the sample [65, 66].

**Response time:** Response time is the time needed by a BS to produce a measurable response/ signal upon the interaction of a bio-receptor molecule with that of the analyte molecule of interest [66, 67].

**Range or linearity:** Linearity of a BS governs the accuracy of the produced signals in response to the measurements with varying concentrations. This characteristic provides an understanding about resolution capability of the BS, which is defined as the least minimum change in the concentration of target analyte which is essential to produce an observable signal [28].

### 3 Graphene and Its Derivatives

2D-CNM graphene possesses a special honeycomb lattice-like structure in which carbon atoms are joined by  $sp^2$  hybridization including  $s$ ,  $p_x$  and  $p_y$  with a  $120^\circ$  angle. This creates a strong C–C bond with an interatomic length of about 1.42 (Fig. 4) [68]. With a Young modulus of around 1 TPa, which corresponds to a breaking strength of about 42 N/m, and an intrinsic tensile strength of roughly 130 GPa, it is also one of the strongest materials discovered to date. Besides, the absorption rate of the graphene sheet is 2.3% which is practically constant. It can be synthesized by top-down and bottom-up approaches [69, 70]. Former use procedures such as arc discharge, liquid phase and mechanical exfoliation to break down the precursor graphite together with interlayer segregation to create graphene sheets. Contrarily, the bottom-up process uses a carbon source gas and techniques namely chemical vapour deposition (CVD) method or epitaxial growth to produce graphene.

Graphene derivatives include graphene oxide (GO) and reduced graphene oxide (rGO) (Fig. 4). GO is derived by graphitic oxidation and possesses several oxygen-carrying functional groups like C–O–C, –COON, –OH and C=O, exhibiting robust reactivity, superior dispersibility as well as suitable binding sites for future functionalization [71, 72]. Removing these oxygen-containing functional groups from GO by heat or chemical process generates rGO which too exhibits properties such as higher electron mobility, larger specific surface area, higher chemical as well as thermal stability.



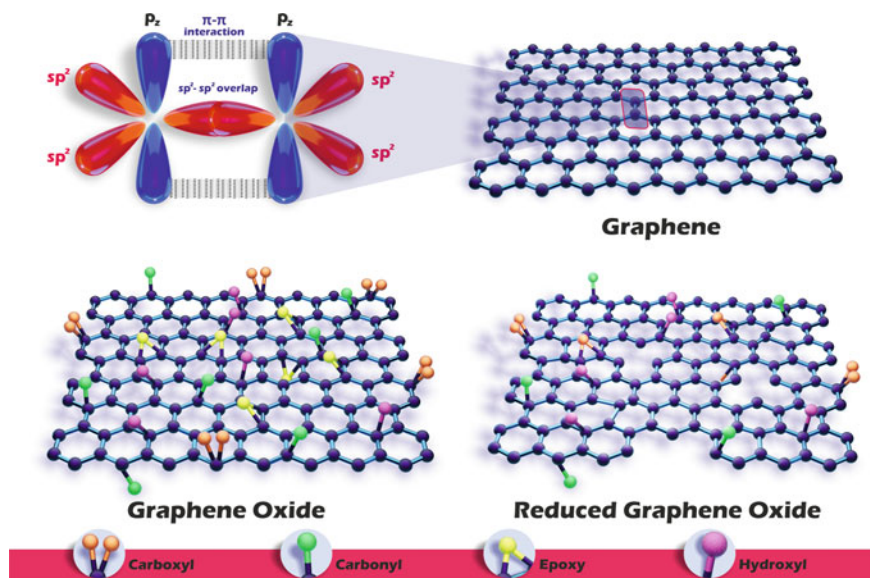


Fig. 4 Graphene and its derivatives highlighting  $sp^2$  hybridization in C-atom

### 3.1 Properties Supplementing Biosensing Platform

With the emergence of G in 2004, it gained widespread research interest among scientific community to be used as a BS, owing to its wide range of properties as mentioned above such as biocompatibility, high stability and sustained signal amplification even in harsh environmental conditions and low production cost. Graphene-based BS have demonstrated to be effective in detecting various biological as well as chemical species including antibodies, bacteria, viruses, DNA, peptides, lipids, proteins and metal ions, resulting in increasing research interest among scientists for the revolutionary objective of multiplexed medical diagnostic BS to deliver early and accurate detection of emerging fatal diseases [73]. The following section discusses the major properties of the G supplementing its biosensing capability.

**a. Large specific surface area:** G has a large specific surface area hypothetically of about  $2630 \text{ m}^2/\text{g}$  for a single layer of G. This property leads to extremely high packing capacity for drugs and biomolecules. In biosensing applications, this property leads to the high density of the attached analyte molecule of interest [74].

**b. High electrical conductivity:** High electronic conductivity of graphene is mainly owed to the zero-overlap semi-metal using electron and holes for charge carriers. Every carbon atom contains six electrons, out of this, four valance electrons, with one  $s$  and three  $p$  orbitals are accessible for chemical bonding. In-plane strong covalent bonds are formed by one  $s$  and two  $p$  orbitals. Conductivity is predominantly determined by the  $p$  orbital which is out of plane [75–77]. Gs hexagonal structure

has an alternative double-bond conformation that enables optimal conjugation in  $sp^2$  hybridization. Thus, its remaining  $p_z$  orbital has just one electron, but its  $p_x$  and  $p_y$  orbitals each contain one electron [78]. The carbo-carbon bonds are strengthened by free electrons ( $\pi$  electrons) of this  $p_z$  orbital of adjacent carbon atoms forming pi ( $\pi$ ) bond. On the other hand, electrons from other orbitals ( $p_x$  and  $p_y$ ) for sigma ( $\sigma$ ) bond with the neighbouring C-atoms. The electronic characteristics are controlled by the bonding and antibonding of these  $p$  orbitals at low energies [79]. Studies using reciprocal lattices show that the Fermi energy in the corner of the Brillouin zone, where  $\pi$  and  $\pi^*$  bands touch in the 2D crystal of  $sp^2$ -hybridized carbon, is a zero-band gap semiconductor [78]. The bands exhibit linear dispersion very close to point called as Dirac point (Fig. 5). This arrangement gives rise to fascinating electron transport properties [75, 77].

**c. Mechanical strength:** Graphene has high mechanical strength and pliability having maximum elastic modulus and tensile strength. Due to atomic plane C=C bonding, it is harder than diamond, on the other hand, Van der Waals forces in interlayers are responsible for its softness, providing it a greater potential for use in wearable BS [80]. The presence of functional groups on the G surface offers the additional advantage of higher dispersion in polar and aqueous solvents resulting in enhanced mechanical properties [81, 82].

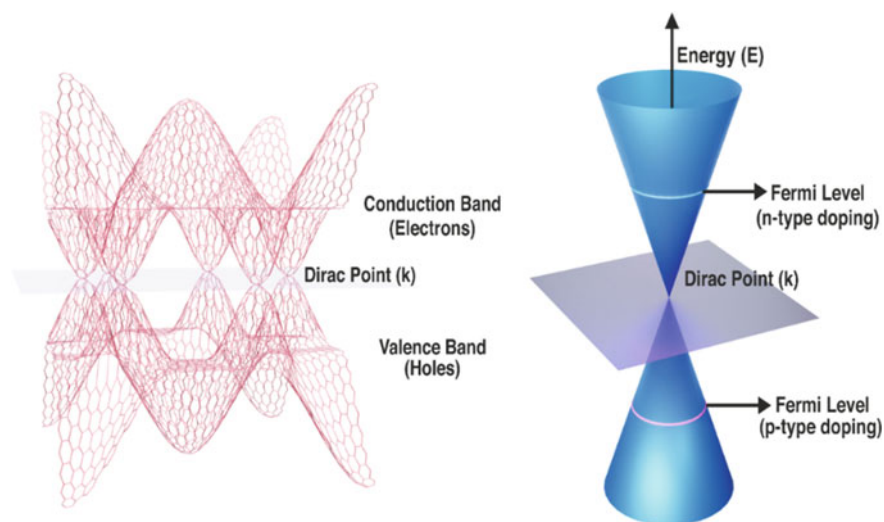


**Fig. 5** 3D Band Structure of graphene and position of Fermi level in n and p type doping

## 4 Classification of Graphene-Based Biosensors

As explained in previous sections, BS consist of a bio-receptor element, that binds specifically with its target molecule and transducer element, converting this binding reaction into a measurable/quantitative signal [83, 84]. Graphene-based nanomaterial are widely employed in BS as transducer elements transforming the incident of binding of bio-receptor with its target analyte into the signals that can be detected thermally, optically or electrochemically [85–87]. These molecules such as DNA, RNA, antibodies, aptamers, proteins and enzymes must be attached to the transducer element, for the biosensing reaction to proceed. The most frequently used method for attaching single-stranded (ss) DNA and antibodies to graphene and its derivatives (GO, rGO) is EDC/NHS (EDC: 1-Ethyl-3-(3-dimethylaminopropyl) carbodiimide; NHS: N-hydroxy succinimide) chemistry [88]. ssDNA binds to graphene's surface by noncovalent interaction like electrostatic, H-bonding and  $\pi$ - $\pi$  stacking. On the contrary, enzymes are usually immobilized by physical adsorption, i.e. physisorption. Proteins are attached chemically by their amine groups to carboxylic groups of GO [89]. Because of its huge surface area, faster electron transfer, higher electrical conductivity and ability to immobilize diverse compounds, graphene has been used in the creation of numerous BS with various transduction modalities [90]. In electrochemical sensors, the  $\pi$ -conjugated structure of graphene expedites the transfer of electrons between the transducer and bio-receptor [88]. Graphene-based nanomaterials can also function as a quencher in the transducer for fluorescent BS. Studies have illustrated that G, GO and rGO have exceedingly high efficiency of fluorescent quenching [91, 92]. Graphene and its derivatives are used in 6 BS systems, namely Electrochemical, Optical (Fluorescent), Surface Plasmon Resonance (SPR), Surface-enhanced Raman Scattering (SERS) and Field Effect Transistor (FET). Sections below discussed these BS along with their applications in medical sector (Fig. 6).

### 4.1 Graphene-Based Optical Biosensing Platform

Graphene has remarkable optical properties as compared to other nanomaterials [93, 94]. Properties like large specific surface area, greater chemical stability, high biocompatibility and easy absorbance of biomolecule through  $\pi$ - $\pi$  stacking, all of which favour the biosensing platform. Its derivatives namely GO and rGO have been extensively used in optical biosensing [95, 96]. The optical biosensing system utilizes the changes in the intrinsic optical properties such as absorbance, fluorescence, light absorption, reflectance, scattering, chemiluminescence, photoluminescence and fluorescence resonance energy transfer (FRET), upon binding of the sensor element with its analyte. Many optical sensors have been created thus far based on the fundamental principles of colourimetric, fluorescence and plasmonic sensing [97]. Colourimetric-based sensors offer easy-to-use, economical and absorbance response upon binding of analyte which could be detected with the naked eye but have sensitivity issues

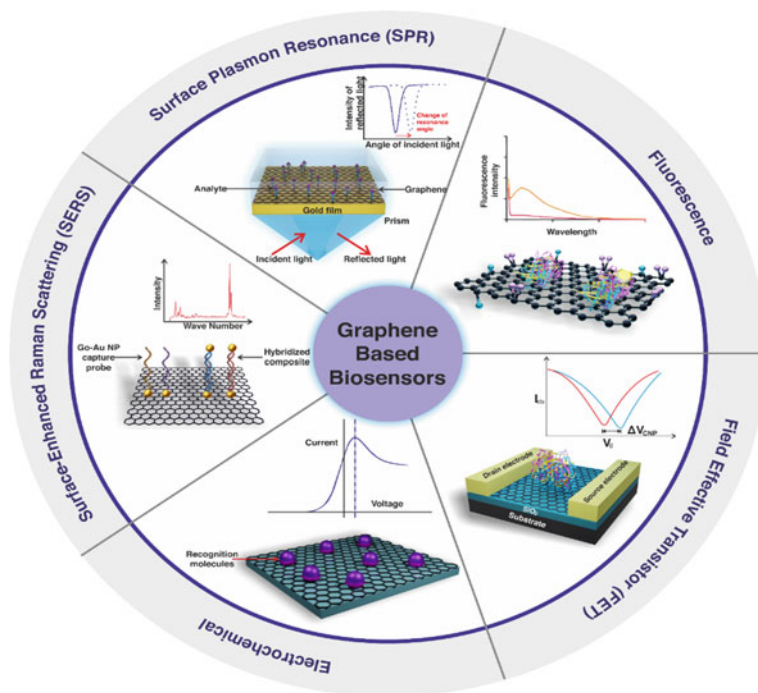


**Fig. 6** Schematic representation of various graphene-based biosensors

when the analyte concentration is very less and limited multiplexing capabilities. Plasmonic-based sensors utilizing SPR localize SPR (LSPR), SERS and propagating surface plasmon polaritons (SPP) and offer higher sensitivity as well as multiplexing capabilities.

### Fluorescence-Based Optical Biosensors

Fluorescence-based BS employ specific fluorescent probes that are attached to the transducer element and generate a quantifiable fluorescent signal upon binding of its specific analyte. Changes in these fluorescent signals might occur due to fluorescent quenching, fluorescent enhancement or FRET. These fluorescence-based BS have been widely employed in medical diagnostics for the detection of cancer biomarkers, cancerous cell tissues *in vitro* as well as *in vivo*, and tumorous cell identification at early stages [98]. The tuneable band gap exhibited by pristine graphene has enabled its wide use in optical BS due to the photo-excited photoluminescence. Defect-derived photoluminescence and the conjugated  $\pi$ -domain are responsible for the production of photoluminescence by graphene derivatives [96, 99, 100].

Fluorescence in GO and rGO owed to the  $O_2$ -containing groups that allow for  $sp^2$  as well as  $sp^3$  hybridization, thus giving them band gap as well as fluorescence [101,

[102]. As pH of the environment changes, GO displays a broad fluorescence peak at a wavelength of around 680 nm; when pH increases one peak (680 nm) slowly declines to melt and another peak (500 nm) starts appearing under alkaline conditions. These differences in the fluorescence properties are due to the proton transfer in the excited state by pH variation [103]. However, in fluorescence-based biosensing, GO serve as a fluorescent chromophore whose property may be modified by altering the size of the sheets and chemical composition, sheet size and chemical composition. Likewise, employing carrier transport and resonance energy transfer, GO is also utilized as a fluorescent quencher. The tuneable fluorescence and quenching capability of GO direct its use in biosensing which further depends upon the oxidation time, shape, size as well as fraction of the  $sp^2$ -hybridized clusters. Due to the heterogeneous structure, GO can fluoresce by photo-excitation within a diverse range of wavelengths ranging from near infra-red (NIR) region to ultraviolet (UV) range [104, 105]. In NIR biosensing, GO is used in bio-imaging via two-photon excitation spectroscopy due to the red-edge effect [106].

The potential of the above-discussed optical techniques incorporated with graphene has paved several paths for the fabrication of graphene-based optical BS that are small, economical and multifunctional readable devices. Two-photon imaging utilizing GO as a fluorescent marker has been extensively used in the imaging of cancer cell, pathogenic microbial cells and food safety sectors [106–108]. The tuneable wavelength of the two-photon fluorescence of GO sheet by changing its excitation energy leads to the multi-coloured bio-imaging of the bacterial cell [106, 109]. By varying NIR excitation energy from 760 to 1120 nm, two-photon luminescence has been used in multi-coloured bio-imaging of methicillin-resistant *Staphylococcus aureus* (MRSA) [106]. GO-based fluorescent DNA aptasensors are being devised to target liver cancer cells and provide *in vitro* as well as *in vivo* bio-imaging assisting medical diagnosis and chemotherapy [108]. Graphene is used in FRET-based BS to determine molecular distances and interactions between proteins or different realms of a particular protein [110, 111]. Tuneable graphene-based plasmonic BS has been designed for label-free detection and identification of protein monolayers utilizing their electro-optical properties. Here, the protein is probed selectively at varying frequencies using the dynamically tuned plasmon resonance of graphene to determine its composite refractive index. Additionally, the extraordinarily high overlap between the biomolecules and the spatial light confinement in graphene allows for higher sensitivity in the observation of their vibrational state and refractive index. It provided selectivity with the enhanced sensitivity of graphene for use in biosensing [112].

### Surface Plasmon Resonance (SPR)-Based Optical Biosensors

SPR-BS have evidenced to be one of the most efficient methods for real-time monitoring of various biomarkers including proteins, lipids, cells, nucleic acids, etc. [113–115]. The surface of these sensors has a major role in the gross efficacy of the sensors. It offers a potent label-free method for examining noncovalent molecular interactions

and has been extensively employed in the study of protein–DNA, DNA–DNA/RNA and protein–protein interactions [116]. SPR-BS are extensively used in the detection of biomarkers due to the very high sensitivity of surface plasmon to changes in the reflective index (RI) of the dielectric medium. Interaction of the analyte molecule with the attached receptor on the metal surface leads to the changes in the RI of the sensing medium which further alters the propagation constant of associated surface plasmons. This disturbs the resonance situation of surface plasmons with specific surface plasmon waves (SPW). A sharp dip is formed in the SPR curve as a result of the energy of the light photon transferred to the surface plasmons at resonance angle and decrease in the reflectance of light [117, 118].

Graphene-based nanomaterials (GBN) are being extensively utilized in SPR-BS owing to their large surface:volume ratio which increases the number of biomolecules interacting on its surface by  $\pi$ - $\pi$  stacking. This further increases the sensitivity of the BS due to efficient light absorption by the increased number of interactions [119]. GBNs are capable of effective transmission and excitation of surface plasmon, and their use in SPR-BS markedly enhances the sensitivity to the change in RI due to their remarkable optical absorption and plasmonic features [120, 121]. Certain features such as signal-to-noise ratio and quality factor of these BS get reduced, adversely affecting the functioning of the BS. Further multiple graphene layers often tend to lower the resolution of BS by the rise in the FWHM (full width at half maximum) in the SPR curve by widening the reflectance dip and reducing the depth of the dip [122]. Further during SPR-BS fabrication, these drawbacks are eliminated along with the amplification of their advantages. Graphene and graphene-MoS<sub>2</sub> (molybdenum disulphide)-based SPR-BS were evaluated for their sensitivity in biomolecular recognition, and it was observed that later has 175% more sensitivity than graphene SPR-BS [123]. In dual sensing BS by coupling SPR-LSPR-BS, the sensing panel was coated with GO/Au modified with goat anti-human anti-IgG to detect human Ig G in the sample coated with Au nanoparticles. Here, GO coating in the sensing channel enhances the loading of biomolecules thereby strengthening the response signal [10]. Alternatively, prism-coupled SPR-based BS exhibits excellent sensitivity for sensing blood glucose gas [124]. Kretschmann prism configuration with SPR graphene-based BS is used to sense the urea in urine samples. This configuration is composed of 6-components namely a glass of soda lime, adhesion layer of chromium (Cr), thin film of Au, the monolayer of molybdenum disulphide (MoS<sub>2</sub>), layer of graphene and sensing medium [125]. GO/silver-coated polymer cladding silica (PCS) fibre was used in SPR-BS. Surface of GO was attached with Staphylococcal protein A and goat anti-human IgG to detect human IgG in infected blood samples [126].



## 4.2 *Graphene-Based Field Effect Transistors (FET) Biosensor*

Semiconductor Field Effect Transistors (FET) have been utilized in BS owing to their wide range of properties including the capability for mass production, ultra-sensitivity detection and low-cost manufacturing as well as easy use in the portable devices [127–129]. FET-BS have been a great option for the label-free transducers. These FET-based transducers include 3 electrodes, namely source, drain and gate. As a biological detection component, the area between the drain and the source interacts with the target analyte/biomolecules to detect their existence, concentration and electrical activity. The BS then transforms the biological data right away into a discernible signal [130]. The signal thus obtained can be demonstrated, amplified, stored and examined, or it can be transferred to the data centre for extra processing [131]. In FET-BS, a change in the sample solution's concentration results in a difference in the charge near the sensor's interface which causes a lowering of the effectual gate voltage. This change in the gate voltage leads to changes in the current flow of the drain [42].

Graphene has outstanding carrier mobilities and a very less effective mass due to linear dispersion of the charge carriers [132]. These charge transfer properties of the graphene facilitate an exceptional channel material that has the potential for replacing silicon and other semiconductors in these FETs. Moreover, these do not necessitate impurity doping like other semiconductors for the conduction of electricity. They exhibit the phenomenon of self-doping, which with the help of an external electric field can regulate the carrier type and its concentration [133–135]. Graphene-based FET has been used for bacterial and viral diseases as well as for cancer detection [136–138]. They provide ultra-sensitive and less noise due to higher biocompatibility, ease of functionalization and bio-catalyst in oxygen reduction reaction [134, 136, 139]. Zhou and co-workers developed a label-free immunological sensor that relied on the Ab-modified graphene FET. They immobilized Ab's targeting the carcinoembryonic antigen (anti-CEA) on the graphene surface and the resulting anti-CEA modified graphene FET effectively observed the reaction between the CEA protein and the anti-CEA Ab with relatively high sensitivity and specificity [140]. Wu et al. carried out the theoretical demonstration of graphene-based FET for bacterial detection and observed that graphene-bacterial distance, bacterial concentration and probe size are the parameters that determine the sensitivity of the BS [141].

These BS have been effectively utilized for the label-free detection of exosomes by conjugating graphene FET with anti-CD63 antibodies. These antibodies are produced against the exosomal membrane protein namely CD63 and worked as a biomarker for the early-stage diagnosis of cancer and other diseases [142]. Seo et al. produced graphene-based FET-BS for detecting coronavirus disease 2019 (COVID-19), by coating graphene sheets with the anti-SARS-CoV-2 spike protein antibody. The SARS-CoV-2 spike protein from the infected samples can be detected from the suggested device and provide an ultra-sensitive immunological method for COVID-19 detection without sample pre-treatment and labelling [136]. Lin and co-workers

utilized these graphene FET for detecting food contamination by bacteria *Escherichia coli*. They employed a volatile molecule indole released by a bacterium to detect the bacterial contamination of the food samples. Exposure of the FET with the indole leads to  $\pi$ - $\pi$  stacking interaction between them and hence change in the electrical signal [9].

### 4.3 Graphene-Based Electrochemical Biosensors

Electrochemical BS require 3 electrodes, namely reference electrode, counter electrode (or auxiliary electrode) and a working electrode (or sensing /redox electrode). The counter electrode connects the electrolytic solution; thus, current can be transferred to the working electrode; on the other hand, the working electrode acts as a transduction component in the biochemical process. These electrodes must be conductive and chemically stable. The electrochemical reaction between the analyte and bio-receptor occurs on the surface of the transducer, thus producing observable electrochemical signals in terms of current, voltage, capacitance and impedance [22]. Improvement in electrodes and intermediates further leads to an increase in the sensitivity, specificity as well as stability of the electrochemical sensors [143]. A vast range of molecular detection elements can be employed by electrochemical BS for the identification of biomarkers. In recent years, high sensitivity for biomarkers has been made possible by the use of nanomaterials and electrochemically active compounds in bioassays involving electrochemical techniques. Some of the elements contributing to the high compatibility of electrochemical BS based on nanomaterials include the coupling of various bio-receptors with nanomaterials [144]. These nanomaterials increase signal transmission by generating synergistic effects between conductivity, catalytic activity and biocompatibility.

Based on the transduction principle, these sensors are categorized as Potentiometric, Amperometric, Conductometric, Impedimetric and Voltammetric BSs detecting changes in the charge, current, conductivity, impedance and applied potential, respectively [66]. Graphene's use in these BS provides faster electron transport, higher thermal conductivity, good mechanical flexibility as well as biocompatibility properties, which enhance the BS's functioning [145]. Modification of the electrodes with graphene nanomaterials causes the uniform distribution of electrochemical species and their higher surface-to-volume ratio results in the appropriate substrate for the identification of adsorbed analytes. The electron transfer rate in these BS is directly dependent on the distance between the electrode surface and the bioreceptor's electrochemically active centre, and graphene-based modifications can significantly shorten this distance to facilitate electron transfer. This process occurs at the edges of graphene sheets or basal plane defects via direct electron transmission by nano-wiring between electrode surfaces and active electrochemical sites [146, 147]. Tezerjani et al. developed a hybrid structure for detecting DNA using a nanocomposite of polyaniline (PANI) and GO nanosheets for the detection of prostate cancer. The binding of the complementary DNA sequences with the



mon-complementary DNA sequence generates an electrochemical response which is measured via electrochemical impedance spectroscopy (EIS) method [148]. Electrochemical BS with tightly packed gold nanoparticles on the rGO multi-walled carbon nanotubes (MWCNT) platform was devised to detect the presence of prostate-specific antigen (PSA) in the serum of patients with prostate cancer. This very antigen serves as a biomarker for detecting prostate cancer in patients, and the developed electrochemical bioassay provide ultra-sensitive detection of the PSA in cancer patients [149]. In another approach to detecting prostate cancer, a sandwich-type electrode made up of rGO/gold nanoparticles, anti-total PSA monoclonal Ab and anti-free PSA Ab were constructed together. The generated BS possessed higher sensitivity for detecting total as well as free PSA in the serum samples from the patients [150]. Electrochemical BS built on a glassy carbon electrode (GCE) was constructed to detect miRNA-21, which serves as a biomarker for the early-stage identification of prostate cancer [151]. Saeed and co-workers developed DNA BS using ErbB2 (erythroblastic oncogene B Receptor Tyrosine Kinase 2) gene and cluster differentiation 24 c gene (CD24c) modified gold nanoparticles and GO which are further loaded onto the GCE for early detection of breast cancer. ErbB2 gene is amplified and overexpressed in human breast cancers and acts as a biomarker for cancer detection. The electrochemical signals are enhanced by the gold nanoparticles and GO which aid in the highly specific and sensitive detection of breast cancer biomarker ErbB2 [152]. An electrochemical immunosensor for the recognition of carcinoembryonic antigen (CEA) was developed. The electrochemical conduction of the antibody-modified electrode upon binding with the antigen present in the sample was analysed by voltammetry and impedance analysis. The developed immunosensor exhibits higher sensitivity and outstanding selectivity to CEA and hence can be used in analysis of clinical samples [153].

#### ***4.4 Graphene-Based Surface-Enhanced Raman Scattering (SERS) Biosensors***

The loss and gain of energy due to molecular vibration process represent the information about the molecular structure enabling real-time in situ identification of molecules [154]. SERS is a sub-class of widely used sensing practice, Raman Scattering, in which in-elastic light scattering by the molecules is significantly enhanced by adsorption of molecules on metal surfaces like silver or gold nanoparticles [155]. The use of plasmonic nanostructures enhances the sensitivity of molecular detection to a million-fold. SERS enhancement is achieved by electromagnetic and chemical processes [156]. Graphene owing to its large surface:volume ratio, great optical transparency, excellent charge mobility, strong chemical interaction with a vast range of biomolecules and biocompatibility has proved to be a potent substrate for SERS [157].

Graphene-based SERS-BS are used for quantitative detection of various biomolecules present in trace amounts [126, 158]. Hybrid substrates formed by combining graphene and metal nanoparticles, serve as a highly efficient substrate for SERS sensors, finding its huge potential in the biomedical field, medical diagnosis, disease monitoring and food inspection [159]. Different processes including coating, combined assembly of graphene and nanoparticles, and accumulation of metals on top of pre-deposited graphene layer have been shown to improve the efficiency of SERS-BS. Pico-molar quantities of the analyte have been successfully detected by using a hybrid system consisting of graphene with metal nanoparticles as a substrate for SERS [95]. rGO sandwiched in between gold and silver nanoparticles is used as a substrate for SERS for ultra-sensitive detection of tumour cells [160].

## 5 Advances in Graphene-Based Biosensors in Medical Diagnostics

Graphene is extensively used in the synthesis of the biological sensors with ultra-high sensitivity, specificity as well as low detection limit. The following sections present an overview of various application of graphene in biosensing platform for detecting various biomarkers for disease diagnosis.

### 5.1 Graphene-Based Biosensors for DNA

A major issue in clinical diagnosis is the requirement for quick and accurate DNA analysis. Detection of the single nucleotide polymorphisms (SNPs) and the sequence-specific identification of ssDNA have gained global attention in the past years by the scientists. SNPs are a frequent type of genetic variation that occurs every 100–300 bp and is linked to several serious illnesses and disorders, including Parkinson's disease (PD), AD, diabetes and several types of cancer. Therefore, the development of cost-effective DNA analysis methods with the motive of fast, accurate, easy and cheap detection system for the diagnosis of these diseases could bring a breakthrough in modern diagnostics. Graphene and its derivatives have been utilized for developing DNA-based BSs by adsorbing DNA onto graphene-based nanomaterials. Pristine graphene being hydrophobic in nature gets rarely dispersed in water, hence limiting the adsorption of DNA onto its surface. GO has oxygen-containing functional groups (esters, epoxides, carboxyl, hydroxyl) and is hence extensively used for DNA detection. These groups may provide a pH-dependent net negative charge and thus colloidal stability in organic solvents and water which is perilous for DNA detection [161, 162]. Functional groups carrying oxygen present in GO can be partly removed by physical or chemical treatment to generate rGO to restore its electrical conductivity. This rGO further proves to be an effective material for DNA BSs [163,

[164]. Various graphene-based DNA biosensors providing information about target analyte, biosensing platform, biosensor type as well as detection limit are outlined in Table 2.

Adsorption of biological molecule forms a crucial step in the construction of a DNA BS because this can affect the sensor's response and operational stability. DNA detection using graphene-based BSs is classified into two approaches [165]. First, force between charge-biomolecule at  $\pi$ - $\pi$  domains and electrostatic forces all

**Table 2** Graphene-based biosensors for detecting nucleic acid/gene

Analyte/Target	Sensing platform	Biosensor type	Detection limit	Refs.
ssDNA	Capture DNA sequence (CP), AuNPs and Thi-functionalized rGO	Electrochemical	$4.28 \times 10^{-19}$ M $1.58 \times 10^{-13}$ M	[170]
DNA/RNA	Deformed monolayer graphene channel	FET	600 zM, 20 aM	[171]
dsDNA	rGO rods decorated with AuNPs and use PNA	Electrochemical	0.86 pM	[172]
RNA	Single-strand DNA probe immobilized on G surface using PBASE as a linker	FET	0.1 fM	[139]
cDNA	Fluorescein-labelled DNA probe and graphene species	FRET	-	[173]
DNA hybridization	AGNR interconnected between gold electrodes	FET	-	[174]
Nucleic Acids	Zirconia reduced GO–thionine (ZrO <sub>2</sub> -rGO–Thi)	Electrochemical	24 fM	[143]
HIV-1 gene	AuNPs–GO	FRET	15 fM	[175]
DNA hybridization	Single-layer CVD-grown graphene	Liquid-gated multichannel FET	15 fM	[176]
HPV-16 DNA	NH <sub>2</sub> -IL-rGO immobilized on a MWCNT and loaded with aminated DNA probes	Electrochemical	1.3 nM	[177]

*Abbreviations* AGNR: Armchair graphene nanoribbon; Thi: Thionine; AuNPs: Gold nanoparticles; PNA: Peptide Nucleic Acid; FET: Field Effect Transistor; PBASE: 1-pyrenebutanoic acid succinimidyl ester; FRET: Fluorescence resonance energy transfer; HPV: Human Papillomavirus; HIV: Human Immunodeficiency Virus; MWCNT: Multiwalled Carbon Nano Tube; IL: Interleukin; GO: Graphene oxide; rGO: Reduced GO; CVD: Chemical vapour deposition; DNA: Deoxyribonucleic acid

lead to difference in electrical properties of pristine graphene. The second involves the immobilization of receptor molecules on the surface of GO and rGO by their defects and functionalization. The DNA molecule when get attached to the surface of graphene-based materials leads to the changes in electronic, optical as well as electrochemical properties of the materials, which forms the basis for BS detection. DNA sensing using electrochemical BSs provides rapid, cost-effective as well as simple detection methods for various diseases [166]. The specific hybridization between the probe DNA and the target DNA is the basis of electrochemical DNA BSs. To hybridize with the target complementary DNAs, the probe DNA is physically or covalently attached to the electrode surface. An electrochemical workstation might then monitor the change in electrochemical signals caused by hybridization [88]. Electrochemical DNA BS is based on the change in the voltage, impedance or current that is caused by the hybridization of DNA or oxidation of bases adenine, guanine, cytosine and thymine in DNA. They can be labelled free and labelled based on inherent electrochemical properties of nucleic acids and the use of radioactive species with nucleic acids, respectively. Label-free DNA BSs can be made using a scalable and highly reproducible (>90% yield) fabrication approach based on GFETs that have been functionalized with ssDNA-probe. Upon hybridization with its complementary DNA analyte, a swing in the Dirac point voltage of the GFET sensor occurs. These DNA BSs provide a broad analysis range and LOD of 1fM for 60-mer oligonucleotide DNA [167]. An electrochemical BS fabricated from graphene draped with graphitic nanosphere. DNA probe is covalently attached to the graphene nanosphere, and the constructed BS showed high sensitivity and selectivity for the target DNA [168].

DNA detection using fluorescent BSs employs signal transducer element such as graphene derivatives (in this context) as well as molecular recognition element as the main component. Molecular recognition elements can be synthetic oligonucleotide or DNA aptamers (ssDNA/RNA), which are complementary to the target DNA sequence. Interaction between these aptamer sequences and graphene derivatives is assisted by strong  $\pi$ - $\pi$  interaction and hydrophobic interactions between the graphene derivatives and the ring-shaped structure in nucleotides. When there is no analyte present in the sample, fluorescent dye-labelled aptameric DNA sequence in bound to the graphene derivatives and quenched. On the contrary, when analytes are recognized by the complementary labelled aptameric DNA sequence, it is detached from the graphene derivatives. As a result, the graphene derivative weakly interacts with the aptamer-target complex, allowing the dye-labelled ssDNA to regain its fluorescence. Photoluminescence quenching capability of GO has been employed in the detection of *Escherichia coli* (*E. coli*). [169].

## 5.2 Graphene-Based Biosensors for Enzymes

Enzymatic BSs involve enzymes as sensing element, which specifically binds with the target analyte termed as substrate (in this context), and a transduction system

which converts the binding/recognition event into a quantifiable signal. Graphene-based BS for enzymes finds its utility in detecting various diseases by identifying the enzymes which is representative of a disease's condition. These BSs consist of the enzyme which is immobilized on the membrane and electrode transducer system, that combines enzyme and electrode system [178]. Various physiological/biological processes occurring inside the body involve enzymes and elevated levels of certain enzymes are associated with severe medical conditions. Therefore, their detection finds its application in biosensors [179]. Enzymes such as bilirubin oxidase, laccase and horseradish peroxidase have been immobilized onto the graphene BSs using covalent bonding, EDC/NHS chemistry, physical entrapment and adsorption method [180]. These BS have been used to detect a variety of compounds, including caffeic acid, phenols (2,6-dimethoxyphenol), glucose, hydrogen peroxide, 17-estradiol and bilirubin. Table 3 outlines various graphene-based BS for detecting enzymes along with information about target analyte, biosensing platform and biosensor type as well as the limit of detection.

**Table 3** Graphene-based biosensors for detecting enzymes/biomolecules

Analyte/Target	Sensing platform	Biosensor type	Detection limit	Refs.
Protease	Graphene with a panel of fluorescently tagged peptides	Fluorescence	–	[185]
17 $\beta$ -estradiol	GCE supported with GO–rhodium nanoparticles	Electrochemical	0.54 pM	[186]
GSH	GSH-Px immobilized on GCE decorated with GO and nafion	Electrochemical	1.5 nM	[187]
CT	Laccase enzyme immobilized on graphene-CMF composite modified SPCE	Amperometric	0.085 $\mu$ M	[188]
DA	Platinum–silver graphene (Pt–Ag/Gr) nanocomposite immobilized on GCE	Electrochemical	0.012 M	[189]
DA	GO-CMF/PdSPs composite sensor	Electrochemical	23 nM	[190]
DA and AA	GO/P (ANI-co-THI) immobilized on GCE	Electrochemical	DA: 2 M AA:242 M	[191]
DA and AA	PVP graphene-modified GCE	Electrochemical	DA:0.002 M AA: 0.8 M	[192]
CT	Poly (Adenine)-modified graphene paste electrode	Voltametric	CC: 0.24 M	[193]
CT and HQ	Graphene oxide-LaMnO <sub>3</sub> nanocomposite	Electrochemical	HQ: 0.06 M CT: 0.05 M	[194]

*Abbreviations:* GSH-Px: Glutathione Peroxidase, GCE: Glassy Carbon Electrode; GO: Graphene oxide; SPCE screen printed carbon electrode; GO-CMF: Graphene Oxide-Cellulose Microfiber; PdSPs: spindle-like palladium nanostructures; P(ANI-co-THI): poly(aniline-co-thionine); DA: Dopamine; AA: Ascorbic acid; PVP: Poly vinyl pyrrolidone; CT: Catechol; HQ: Hydroquinone

Graphene-based enzyme BS are extensively used in the detection of serum glucose levels by immobilizing glucose oxidase ( $\text{GO}_x$ ) enzyme on graphene's surface. Graphene FET as devised by Huang and co-workers allows the detection of glucose [181]. Recently, laser-induced graphene-based enzymatic BS have been devised, providing highly sensitive, low-cost and rapid detection of glucose. Laser-induced graphene electrodes were immobilized with  $\text{GO}_x$ /chitosan composite for specific detection of glucose. This employs amperometric glucose sensing in which  $\text{GO}_x$  catalyses the oxidation of glucose present in samples [182]. Graphene-based FET-BS have been devised for the determination of lactic acid in human fluids. Elevated levels of lactate in human body serve as a prognosis marker used for various disorders such as failure of left ventricles and septic shock [183, 184]. Lactic acid was detected by lactate dehydrogenase enzyme (LDH) to catalyse the lactate present in the samples. LDH enzyme was immobilized over the graphene layer of FET-BS to sense the lactate present in biological samples [179].

### 5.3 Graphene-Based Biosensors for Proteins/Antibodies

Protein biomarkers are used for the identification and efficient prediction of various diseases. These biomarkers are proteinaceous existing in blood, body fluids or tissues and can be of great value in the diagnosis, prognosis as well as monitoring of diseases [195]. Graphene-based BSs are employed in detecting antibodies present in the serum samples of the person infected with the particular microbe. These antibodies are produced as a part of the human immune response against the specific epitope of the antigen. The antigen is a foreign substance or toxin which can induce a specific immune response inside the body. The structure, characteristics and reactivity of the antibodies play a major role in this specific high-affinity recognition of antibodies with their antigen for a specific antibody-antigen response, making them highly efficient candidates for sensing applications.

Antibodies can be attached on the surface of graphene and its derivatives by different ways involving EDC/NHS chemistry, PASE (1-pyrenebutanoic acid succinimidyl ester) and electrostatic reactions. Functionalization of GO with a PASE linker is the most popular and adaptable method for generating biochemical conjugates. EDC is a water-soluble cross-linking agent by amide bond between carboxy and amine group present in the molecules [196]. Detection of target molecules may be achieved through various methods. An electrochemical method as discussed in above sections measures any change in the electrical or chemical concentration at the electrolyte–electrode interface due to the conformational changes induced by the bio-recognition of the antibody with the target antigen [10]. These immunosensors are widely used methods being highly sensitive, requiring less sample volume, simple procedure and yielding rapid results [197]. However, these immunosensors have certain limitations including irreversible antigen–antibody reaction and binding affinity [198].

Antibody BSs based on graphene-based nanomaterials provide a wide range of adaptability in terms of pathogen detection. Various antibody BSs based on graphene along with information about target analyte, biosensing platform, biosensor type as well as detection limit are outlined in Table 4. Electrical graphene-based BS functionalized with *E. coli* strain O157:H7-specific antibodies for sensitive detection of foodborne pathogenic bacteria. *E. coli* strain O157:H7 [199]. Field-effective BS was devised for detecting Zika virus infection thereby providing an ideal candidate for use in medical diagnostics against the infection. It utilizes Zika viral monoclonal antibodies and provides real-time as well as quantitative detection of native Zika viral antigen [200]. These are also utilized to detect fibrinogen in the serum or whole blood and serve as biomarker in trauma-induced coagulopathy [201]. Furthermore, vertical graphene-based BSs functionalized with anti-EpCAM (epithelial cellular adhesion molecule) antibody is used for differentiating one breast cancer and two colon cancers by utilizing the dielectric signatures of three different types of tumour cell lines namely MCF-7, HT-29 and SW403 [202]. EpCAM used in this study is a widely used biomarker in cancer diagnostics.

Prions are infectious protein molecules capable of causing severe neurological disorders in humans as well as animals [203]. The abnormal 3D structure of the protein lead to protein collapse, severe infections and protein misfolding diseases. Amyloids are the prions formed by the aggregation of abnormal proteins and are the major cause of AD and PD [203, 204]. GO-based fluorescent BSs have been used for quantitative detection and measurement of amyloid-beta ( $\beta$ )-oligomer [205]. Recently, GO-silver nanoparticle conjugated aptamer for detecting amyloid- $\beta$ -oligomer employing ELISA immunoassay has been developed for the diagnosis of AD [206]. Moreover, ultra-sensitive electrochemical BS for detecting AD have been devised using Au nanoparticle-modified vertical graphene/carbon cloth as substrate electrode and poly(thymine)—template copper nanoparticles as the signal probe [207].

#### **5.4 Graphene-Based Biosensors for Microbial Cells**

Infectious diseases caused by bacteria and viruses pose a serious threat to society. Graphene-based BSs are widely employed for specific and sensitive detection of various disease-causing pathogenic microbes [217]. Early detection of these pathogenic microbes is crucial for clinical point-of-care testing (POCT) [218, 219]. Moreover, various antibacterial treatments require evaluation of the bacterial population before and after antibacterial therapy. A FRET-based immune sensor for detecting *Campylobacter jejuni* whole cells in food samples was designed with the use of GO and graphene quantum dots [220]. The bacterium is known to cause campylobacteriosis, a type of bacterial gastroenteritis. BS is constructed in a way that the polyclonal antibodies are conjugated with the graphene quantum dots and interact with the membrane protein of the bacterium. Electrochemical aptasensor utilizing reduced GO-titanium dioxide composite for detecting the whole cell of *Salmonella*

**Table 4** Graphene-based biosensors for detecting Antibodies/Antigen

Analyte/Target	Sensing platform	Biosensor type	Detection limit	Refs.
CEA antigen	CNTs/COOH/rGO/Ag@BSA/PEDOT/anti-CEA	Electrochemical	$1 \times 10^{-4}$ ng/mL	[208]
CEA antigen	Graphene-zirconia nanocomposite functionalized with PYSE followed by the immobilization of CEA antibody	Electrochemical	4.25 pg/ml	[9]
SARS-CoV-2 nucleocapsid (N-) antigens	Buffer-based zinc oxide/rGO nanocomposite coated on carbon screen-printed electrode	Electrochemical	21 fg/mL	[209]
SARS-CoV-2 protein antigen	GO/G van der Waals hetero-structure having immobilized SARS-CoV-2 capture antibody	FET	8 fg/mL	[210]
$\alpha$ -synuclein antigen	Bio-conjugation of biotinylated antibody with AuNPs-modified graphene	Electrochemical	4 ng/mL	[211]
Epithelial cellular adhesion molecule antigen	Vertically aligned graphene nanosheets on surface of interdigitated electrodes functionalized with anti-EpCAM antibodies	Electrochemical, impedimetric	-	[212]
CEA antigen	AuNPs-TiO <sub>2</sub> -graphene nanocomposite prepared for sandwich immunosensor	Amperometric	3.33 pg/mL	[213]
Early secreted antigenic target 6-kDa protein (ESAT-6)	ESAT-6 MAbs on the N-doped GO (N-GO) functionalized electrode	Electrochemical impedimetric	7.0 pg/mL	[214]

(continued)



**Table 4** (continued)

Analyte/Target	Sensing platform	Biosensor type	Detection limit	Refs.
CEA antigen	Au NR and HRP in the channels of amine-functionalized SBA-15 followed by subordinate antibody (Ab2) conjugation [Au NR@SBA-15/Ab2-HRP]	Electrochemical	5.25 fg/mL	[215]
CEA antigen	Anti-CEA attached with core shell of Fe <sub>3</sub> O <sub>4</sub> @Au NPs immobilized on a carbon electrode modified with MnO <sub>2</sub> decorating on graphene nanoplatelets	Electrochemical	0.10 pg/mL	[216]

*Abbreviations:* Carcinoembryonic antigen: CEA; anti-CEA: CEA antibody; CNTs-COOH: Carboxylated single-walled carbon nanotubes; Ag@BSA: Bovine Serum Albumin-Ag; PEDOT: poly (3,4 ethylenedioxythiophene); PYSE: 1-pyrenebutyric-acid-N-hydroxysuccinimide-ester; SARS-CoV-2: Severe Acquired Respiratory Syndrome-Corona Virus-2; FET: Field Effect Transistor; AuNPs: Gold Nanoparticle; EpCAM: Epithelial cellular adhesion molecule; AuNPs-TiO<sub>2</sub>: Gold nanoparticles-titanium dioxide; MAbs: Monoclonal antibodies; NR: Nanorods; HRP: Horseradish peroxidase; MnO<sub>2</sub>: Manganese dioxide

*enterica* capable of causing foodborne diseases [221]. Recently, *Mycobacterium tuberculosis*, a tuberculosis-causing bacterium, has been detected using label-free graphene-based refractive index BS [222]. Another label-free pristine graphene-based sensor for detecting the bacterial colonization and biofilm formation on the surface of biomedical devices has been developed. This sensor could successfully detect *Pseudomonas aeruginosa* and *Staphylococcus epidermidis* colonization on the devices, thus preventing further transmission of nosocomial infections [223].

BSs for detecting viral pathogens have been an area of research among the scientific community. Various BSs detecting viral pathogens, namely Influenza, Hepatitis C virus, Human Immunodeficiency Virus, Severe acute respiratory syndrome coronavirus 2 (SARS-CoV-2) virus, Zika, Rota viruses, Dengue fever virus, have been developed [224]. FET-BS detecting SARS-CoV-2 virus from the saliva samples have been developed using DNA aptamer conjugated to the graphene FET-BS platform. These FET-BS have high precision in detecting coronavirus and provide an easy, rapid and accurate point-of-care (POC) platform for detecting as well as controlling the spread of the pathogen [225]. Furthermore, electrochemical BS for detecting coronavirus cDNA using graphene polylactic electrode modified with gold particles have been developed [226].

Fungal pathogens affect humans by causing severe skin infections and contaminating food samples [227, 228]. Electrochemical BS for detecting fish fungal pathogen, *Aphanomyces invadans*, have been developed. The BS was developed by immobilization of anti-mycelium antibodies on nanocomposite of graphene-silver nanoparticles. Further, Graphene and its derivatives as well as nanocomposites can be potentially used for fungal detection used for fungal pathogen detection [229]. Table 5 outlines various graphene-based BS for detecting microbial cells along with information about target analyte, biosensing platform, biosensor type as well as detection limit.

## 5.5 Graphene-Based Biosensors in Inflammatory Diseases

Chronic inflammatory diseases (CIDs) namely cancer, diabetes mellitus, neurodegenerative diseases and ischaemic heart diseases are a cause of mortality worldwide. Specific biomarker detection for these CIDs can markedly lower the death rate induced by these diseases. Graphene-based BSs are widely employed for biosensing of biomarkers specific for these inflammatory diseases. Various biomarkers used in disease diagnosis include pro-inflammatory cytokines and interleukins (IL): IL-1 $\beta$ , IL-6, IL-8, IL-15, IL-17, IL-18 for rheumatoid arthritis, oral cancer, AD and osteoarthritis [238–241]; anti-inflammatory cytokines: IL-4, IL-10, IL-13 for Asthma, inflammatory pain, ulcerative colitis, systemic sclerosis [242–245]; serum cardiac troponin I (cTn-I) for Cardiac troponin T, coronary artery disease [246, 247]; B-type natriuretic peptide (BNP) for coronary artery disease [248, 249]; high-mobility group box 1 (HMGB1) for COVID-19, oral inflammation, etc [250, 251].

**Table 5** Graphene-based biosensors for detecting microbial cells

Analyte/Target	Biosensor design	Biosensor type	Detection limit	Refs.
<i>E. coli</i>	Anti- <i>E.coli</i> linked on the surface of graphene aerogel	Electrochemical impedimetric	–	[230]
DNAzymes specific for <i>Vibrio alginolyticus</i>	DNAzyme-based fluorescent sensor	Fluorescent	31 CFU/mL	[231]
<i>E. coli</i>	Electro-statically functionalized GO with oxygen-containing functional groups	Electrochemical	100 CFU/mL	[232]
<i>S. enterica</i>	Label-free Aptamer on rGO-TiO <sub>2</sub> nanocomposite	Electrochemical	10 CFU/mL	[221]
Glycoprotein of Ebola virus	Anti-EBOV glycoprotein antibody immobilized on the surface of FET modified with rGO	FET	2.4 pg/mL	[233]
Zika viral antigen of Zika virus	Monoclonal antibodies linked on the surface of graphene	FET	0.45 nM	[200]
Hepatitis C virus DNA	mrGO-CuNCs nanocomposite	Electrochemical	405 pM	[234]
Influenza virus surface protein HA	H <sub>1</sub> N <sub>1</sub> and H <sub>5</sub> N <sub>2</sub> peptide bound to Nio-rGO/MXene nanocomposite coated on GCE surface	Electrochemical	H1N1: 3.63 nM H5N2: 2.39 nM	[235]
Chikungunya virus	Si and graphene layer coated on glass prism base coated with Ag	SPR		[236]
<i>M. tuberculosis</i>	PNA probe-modified NH <sub>2</sub> -rGO/TEMPO-NCC films immobilized on SPE	Electrochemical		[237]

*Abbreviations:* *E. coli*: *Escherichia coli*; CFU: Colony forming unit; rGO: reduced graphene oxide; TiO<sub>2</sub>: Titanium dioxide; FET: Field Effect Transistor; EBOV: Ebola virus; mrGO: magnetic reduced graphene oxide; CuNCs: Copper nanocomposites; GCE: Glassy carbon electrode; HA/H: Hemagglutinin; N: Neuraminidase; SPR: Surface plasmon resonance; Ag: Silver; SPE: Screen printed carbon electrode; TEMPO-NCC: 2,2,6,6-tetramethylpiperidin-1-yl) oxyl nanocrystalline cellulose; PNA: Peptide nuclide acid; *S. enterica*: *Salmonella enterica*; *M. tuberculosis*: *Mycobacterium tuberculosis*

Table 6 depicts various graphene BS used in biomarker detection along with information about target analyte, biosensing platform, biosensor type as well as the detection limit.

Graphene-based BSs have been used for detecting various biomarkers. Interleukin-6 (IL-6) is a pro-inflammatory and anti-inflammatory cytokine serving as a biomarker for sepsis and various pathological inflammation [252]. This immune sensor is based on gold nanoparticles functionalized with sulphur-doped GQDs and

**Table 6** Graphene-based biosensors for detecting inflammatory biomarkers

Analyte/Target	Biosensor design	Biosensor type	Detection limit	Refs.
GFAP	Hybrid graphene nano-sheet intermixed with the conductive PEDOT:PSS polymers embedded within the base carbon matrix	Electrochemical	281.7 fg/mL	[255]
Beta-amyloid (A $\beta$ <sub>1-40</sub> )	Graphene/rGO dual-layer screen-printed electrode immobilized with H31L21 antibody	Electrochemical	2.398 pM	[256]
IL-6	Pyrene-tagged DNA Aptamer (PTDA) Probes immobilized on graphene	FET	100 pM	[257]
IL-6	Aptamer immobilized on the surface of graphene	FET	139 fM	[258]
IL-6	Crumpled graphene	FET	–	[259]
Cytokines namely IL-6, TNF- $\alpha$ and IFN- $\gamma$	Graphene sheets deposited on a copper substrate	Electrochemical impedimetric	175 kDa total cytokine mass	[254]
Cytokines namely VEGF, IFN- $\gamma$ and TNF- $\alpha$	Three biotinylated molecular beacon aptamers tagged by redox probes namely AQ for VEGF, MB for IFN- $\gamma$ and Fc for TNF- $\alpha$	Electrochemical	5 pg/mL	[260]
Oral cancer biomarker IL-8	ZnO-(rGO)nanocomposite	Electrochemical	51 pg/mL	[261]
cTn-I biomarker	LSG-ZnFe <sub>2</sub> O <sub>4</sub> NPs electrodes-aptasensor	Electrochemical	0.001 ng/mL	[262]
cTn-I biomarker	Aptamer immobilized on Ag NPs/MoS <sub>2</sub> /rGO nanocomposite	Electrochemical	0.27 pg/mL	[263]

*Abbreviations:* GFAP: Glial fibrillary acidic protein; PEDOT-PSS : poly(3,4-ethylenedioxythiophene) polystyrene sulfonate; A $\beta$ <sub>1-40</sub>: beta-amyloid (A $\beta$ <sub>1-40</sub>) peptide of 40 amino acids; PTDA: Pyrene-Tagged DNA Aptamer; VEGF: Vascular endothelial growth factor; TNF: Tumor necrosis factor; IFN: Interferon; IL: Interleukin; FET: Field Effect Transistor; AQ: Anthraquinone; AQ; Methyl blue: MB; Ferrocene: Fc; ZnO: Zinc oxide; rGO: reduced graphene oxide; ZnFe<sub>2</sub>O<sub>4</sub>: Zinc ferrite; NPs: nanoparticles; LSG: Laser scribed graphene; cTn-I: cardiac Troponin-I; MoS<sub>2</sub>: Molybdenum disulfide

hollow zinc sulphide and cadmium sulphide nanocage both of which were immobilized with anti-IL-6 antibodies and provide highly selective and sensitive detection of IL-6 in serum sample. Graphene-based electrochemical BS is utilized in quantification of multiple cytokines for monitoring of pathological and physiological conditions in the body [253]. Electrochemical impedance spectroscopy (EIS) BSs based on graphene, gold and carbon electrodes are utilized for detection of cytokine

storms in the blood due to hyperactivity of the multiplication of the pathogens, such as in case of COVID-19 virus infections [254].

## 6 Challenges

With the ongoing research and development in the field of BSs, biosensing is developing into a commercial reality. For a better understanding of BS's market trend and feasibility, the "Biomedical Sensor Market Forecast" is being released by industry ARC<sup>TM</sup>, offering industry market analytics, research and consulting (ARC) [264]. It states that these BSs tailored themselves to each patient's genetic makeup and are configured to emit alert signals when abnormalities or unexpected bodily readings are obtained in real time. According to the ten-year Graphene Market and 2D Material Assessment for 2021–2031, the graphene market forecast for 18 key application areas demonstrates that graphene materials are progressing along their rising trend and have moved out of the laboratory into the market [265]. Commercialization has been expanding gradually, and the market is expected to grow significantly over the next decades. However, before being commercially available as well as worthy product, the graphene-based BS will undoubtedly encounter certain challenges including quality control, durability and scalability; and needs to be properly addressed. Thorough attention must be given to the inherent properties of graphene, their functionalization as well as the fabrication procedure and diagnostic need for designing the BS. The activity of some graphene-based sensors in biological samples frequently fell short of the desired detection results, even though a large number of these sensors had been published and reported in previous articles. This was primarily due to some non-specificity of several biochemical molecules during the graphene and targets interfacial reactions. Even though some sample pre-processing for biological samples is required before the final testing, which is often time-consuming complex procedure [266]. Moreover, the performance of BS in actual biological samples is frequently not published, even though these sensors as described in the literature display strong storage stability and repeatability.

## 7 Conclusion

The chapter explores the recent progress in graphene-based BSs. It provides comprehensive knowledge about the design strategies of these BSs along with their potential uses in detecting microbial infection, inflammatory biomarkers, DNA, enzymes and antibodies, all of which are related to the diseased or abnormal state of the body. With graphene-based BS, a wide variety of detection techniques may be employed and sensor size and read out may be adjusted as needed depending on the intended use. However, there is still a vital need to move above the research by constructing new concepts for obtaining higher sensitivity as well as specificity, such that the present

BS could be modified and brought into biological applications. In vivo application of these BSs still needs a practical focus such that it can be used in the biomedical field. Major limiting features including non-specific interaction of graphene-based surfaces along with the large-scale reproducibility of the graphene BS fabrications needs to be highlighted as they form a key factor preventing their commercialization. Furthermore, to prevent any unintended secondary health impacts, toxicity and biocompatibility problems still need to be properly addressed. The bio-stability of the sensors has been evaluated in vivo and in vitro, and the results are favourable and promising for future technology transfer. Despite the worldwide research on graphene-based BSs, there are still several impediments to overcome, such that research in the lab can fruitfully serve the biomedical sector easing diseased free as well as healthy lives. To advance this subject and suggest graphene-based BS as a point-of-care option, there is an urgent need for coordinated teamwork between scientists of diverse fields including chemistry, physics, material, science as well as medical professionals.

## References

1. Mousavi, S.M., et al.: Recent advances in plasma-engineered polymers for biomarker-based viral detection and highly multiplexed analysis. *Biosensors* **12**(5), 286 (2022). <https://doi.org/10.3390/BIOS12050286>
2. Zhu, H., Fohlerová, Z., Pekárek, J., Basova, E., Neužil, P.: Recent advances in lab-on-a-chip technologies for viral diagnosis. *Biosens. Bioelectron.* **153**, 112041 (2020). <https://doi.org/10.1016/J.BIOS.2020.112041>
3. Peng, P., et al.: Emerging ELISA derived technologies for in vitro diagnostics. *TrAC, Trends Anal. Chem.* **152**, 116605 (2022). <https://doi.org/10.1016/J.TRAC.2022.116605>
4. Miller, S., Chiu, C.: The role of metagenomics and next-generation sequencing in infectious disease diagnosis. *Clin. Chem.* **68**(1), 115–124 (2021). <https://doi.org/10.1093/CLINCHEM/HVAB173>
5. Lopes, L.C., Santos, A., Bueno, P.R.: An outlook on electrochemical approaches for molecular diagnostics assays and discussions on the limitations of miniaturized technologies for point-of-care devices. *Sens. Actuators Rep.* **4**, 100087 (2022). <https://doi.org/10.1016/J.SNR.2022.100087>
6. de Travensolo, R.F., Ferreira, V.G., Federici, M.T., de Lemos, E.G.M., Carrilho, E.: Microarrays application in life sciences: the beginning of the revolution. In: *Tools and Trends in Bioanalytical Chemistry*, pp. 483–496 (2022). [https://doi.org/10.1007/978-3-030-82381-8\\_25](https://doi.org/10.1007/978-3-030-82381-8_25)
7. Schulze, H., Rubtsova, M., Bachmann, T.T.: DNA microarrays for pathogen detection. In: *Modern Techniques for Pathogen Detection*, pp. 113–220 (2015). <https://doi.org/10.1002/9783527687978.CH4>
8. Lindsley, M.D., et al.: Evaluation of a newly developed lateral flow immunoassay for the diagnosis of cryptococcosis. *Clin. Infect. Dis.* **53**(4), 321–325 (2011). <https://doi.org/10.1093/CID/CIR379>
9. Lin, Z., Wu, G., Zhao, L., Lai, K.W.C.: Detection of bacterial metabolic volatile indole using a graphene-based field-effect transistor biosensor. *Nanomaterials* **11**, 1155 (2021). <https://doi.org/10.3390/NANO11051155>
10. Wang, C.F., Sun, X.Y., Su, M., Wang, Y.P., Lv, Y.K.: Electrochemical biosensors based on antibody, nucleic acid and enzyme functionalized graphene for the detection of disease-related biomolecules. *Analyst* **145**(5), 1550–1562 (2020). <https://doi.org/10.1039/C9AN02047K>

11. Patel, S., Nanda, R., Sahoo, S., Mohapatra, E.: Biosensors in health care: The milestones achieved in their development towards lab-on-chip-analysis. *Biochem. Res. Int.* **2016** (2016). <https://doi.org/10.1155/2016/3130469>.
12. Xu, T., et al.: Electrochemical hydrogen sulfide biosensors. *Analyst* **141**(4), 1185–1195 (2016). <https://doi.org/10.1039/C5AN02208H>
13. Huang, R., He, N., Li, Z.: Recent progresses in DNA nanostructure-based biosensors for detection of tumor markers. *Biosens. Bioelectron.* **109**, 27–34 (2018). <https://doi.org/10.1016/J.BIOS.2018.02.053>
14. Hasan, M.M., et al.: Analgesic and anti-inflammatory activities of leaf extract of *mallotus repandus* (Willd.) Muell. *Arg. Biomed. Res. Int.* **2014** (2014). <https://doi.org/10.1155/2014/539807>
15. Asal, M., Özen, Ö., Şahinler, M., Polatoğlu, I.: Recent developments in enzyme, DNA and immuno-based biosensors. *Sensors* **18**(6), 1924 (2018). <https://doi.org/10.3390/S18061924>
16. Dincer, C., et al.: Disposable sensors in diagnostics, food, and environmental monitoring. *Adv. Mater.* **31**(30), 1806739 (2019). <https://doi.org/10.1002/ADMA.201806739>
17. Pirsaeheb, M., Mohammadi, S., Salimi, A.: Current advances of carbon dots based biosensors for tumor marker detection, cancer cells analysis and bioimaging. *TrAC, Trends Anal. Chem.* **115**, 83–99 (2019). <https://doi.org/10.1016/J.TRAC.2019.04.003>
18. Qian, L., et al.: Biosensors for early diagnosis of pancreatic cancer: a review. *Transl. Res.* **213**, 67–89 (2019). <https://doi.org/10.1016/J.TRSLS.2019.08.002>
19. Griesche, C., Baumner, A.J.: Biosensors to support sustainable agriculture and food safety. *TrAC, Trends Anal. Chem.* **128**, 115906 (2020). <https://doi.org/10.1016/J.TRAC.2020.115906>
20. Qian, L., Durairaj, S., Prins, S., Chen, A.: Nanomaterial-based electrochemical sensors and biosensors for the detection of pharmaceutical compounds. *Biosens Bioelectron* **175**, 112836 (2021). <https://doi.org/10.1016/J.BIOS.2020.112836>
21. Chadha, U., et al.: Recent progress and growth in biosensors technology: a critical review. *J. Ind. Eng. Chem.* **109**, 21–51 (2022). <https://doi.org/10.1016/J.JIEC.2022.02.010>
22. Malhotra, B.D., Ali, Md. A.: Nanomaterials in biosensors: fundamentals and applications. *Nanomater. Biosens.* **1** (2018). <https://doi.org/10.1016/B978-0-323-44923-6.00001-7>
23. Malik, P., Gupta, R., Malik, V., Ameta, R.K.: Emerging nanomaterials for improved biosensing. *Measurement: Sens.* **16**, 100050 (2021). <https://doi.org/10.1016/J.MEASEN.2021.100050>
24. *Handbook of Graphene*, vol. 8, pp. 1–800 (2019). <https://doi.org/10.1002/9781119468455>
25. Geim, A.K., Novoselov, K.S.: The rise of grapheme. *Nat. Mater.* **6**(3), 183–191 (2007). <https://doi.org/10.1038/nmat1849>
26. Ferrari, A.C., et al.: Science and technology roadmap for graphene, related two-dimensional crystals, and hybrid systems. *Nanoscale* **7**(11), 4598–4810 (2015). <https://doi.org/10.1039/C4NR01600A>
27. Xu, Y., Cao, H., Xue, Y., Li, B., Cai, W.: Liquid-phase exfoliation of graphene: an overview on exfoliation media, techniques, and challenges. *Nanomaterials* **8**(11) (2018). <https://doi.org/10.3390/NANO8110942>
28. Bhalla, N., Jolly, P., Formisano, N., Estrela, P.: Introduction to biosensors. *Essays Biochem.* **60**(1), 1–8 (2016). <https://doi.org/10.1042/EBC20150001>
29. Deepa, Pundir, S., Pundir, C.S.: Detection of tumor suppressor protein p53 with special emphasis on biosensors: a review. *Anal. Biochem.* **588**, 113473 (2020). <https://doi.org/10.1016/J.AB.2019.113473>
30. Hou, L., Huang, Y., Hou, W., Yan, Y., Liu, J., Xia, N.: Modification-free amperometric biosensor for the detection of wild-type p53 protein based on the in situ formation of silver nanoparticle networks for signal amplification. *Int. J. Biol. Macromol.* **158**, 580–586 (2020). <https://doi.org/10.1016/J.IJBIOMAC.2020.04.271>
31. Ameri, M., et al.: Biosensors for detection of Tau protein as an Alzheimer’s disease marker. *Int. J. Biol. Macromol.* **162**, 1100–1108 (2020). <https://doi.org/10.1016/J.IJBIOMAC.2020.06.239>

32. Soleymani, L., Li, F.: Mechanistic Challenges and Advantages of Biosensor Miniaturization into the Nanoscale. *ACS Sens.* **2**(4), 458–467 (2017). [https://doi.org/10.1021/ACSSENSORS.7B00069/ASSET/IMAGES/MEDIUM/SE-2017-00069T\\_0004.GIF](https://doi.org/10.1021/ACSSENSORS.7B00069/ASSET/IMAGES/MEDIUM/SE-2017-00069T_0004.GIF)
33. Über die Ursache der elektromotorischen Eigenschaften der Gewebe, zugleich ein Beitrag zur Lehre von polyphasischen Elektrolytke by Cremer, Max [1865–1935]; orig. wrappers (1906) | Expatriate Bookshop of Denmark. <https://www.abebooks.com/Ursache-elektromotorischen-Eigenschaften-Gewebe-zugleich-Beitrag/15914123739/bd>. Accessed 03 Nov 2022
34. Hughes, W.S.: The potential difference between glass and electrolytes in contact with the glass. *J. Am. Chem. Soc.* **44**(12), 2860–2867 (1922). [https://doi.org/10.1021/JA01433A021/ASSET/JA01433A021.FP.PNG\\_V03](https://doi.org/10.1021/JA01433A021/ASSET/JA01433A021.FP.PNG_V03)
35. Griffin, E.G., Nelson, J.M.: The influence of certain substances on the activity of invertase. *J. Am. Chem. Soc.* **38**(3), 722–730 (1916). [https://doi.org/10.1021/JA02260A027/ASSET/JA02260A027.FP.PNG\\_V03](https://doi.org/10.1021/JA02260A027/ASSET/JA02260A027.FP.PNG_V03)
36. Nelson, J.M., Griffin, E.G.: Adsorption of invertase. *J. Am. Chem. Soc.* **38**(5), 1109–1115 (1916). [https://doi.org/10.1021/JA02262A018/ASSET/JA02262A018.FP.PNG\\_V03](https://doi.org/10.1021/JA02262A018/ASSET/JA02262A018.FP.PNG_V03)
37. Clark, L.C., Lyons, C.: Electrode systems for continuous monitoring in cardiovascular surgery. *Ann. N. Y. Acad. Sci.* **102**(1), 29–45 (1962). <https://doi.org/10.1111/J.1749-6632.1962.TB13623.X>
38. Guilbault, G.G., Montalvo, J.G.: A urea-specific enzyme electrode. *J. Am. Chem. Soc.* **91**(8), 2164–2165 (1969). [https://doi.org/10.1021/JA01036A083/ASSET/JA01036A083.FP.PNG\\_V03](https://doi.org/10.1021/JA01036A083/ASSET/JA01036A083.FP.PNG_V03)
39. Clemens, A.H., Chang, P.H., Myers, R.W.: Development of an automatic system of insulin infusion controlled by blood sugar, its system for the determination of glucose and control algorithms. *J. Annu. Diabetol. Hotel Dieu*, 269–78 (1976)
40. Clemens, A.H., Chang, P.H., Myers, R.W.: The development of biostator, a glucose controlled insulin infusion system (GCIIS). *Horm. Metab. Res.* **7**, 23–33 (1977). Available <https://pubmed.ncbi.nlm.nih.gov/873440/>. Accessed 03 Nov 2022
41. Geysant, A., Dormois, D., Barthelemy, J.C., Lacour, J.R.: Lactate determination with the lactate analyser LA 640: a critical study. **45**(2), 145–149 (2009). <https://doi.org/10.3109/00365518509160987>
42. Wadhwa, T., Kakkar, D., Wadhwa, ., Raj, B.: Recent advances and progress in development of the field effect transistor biosensor: a review. *J. Electron. Mater.* **48**(12), 7635–7646 (2019). <https://doi.org/10.1007/S11664-019-07705-6>
43. Metkar, S.K., Girigoswami, K.: Diagnostic biosensors in medicine—A review. *Biocatal. Agric. Biotechnol.* **17**, 271–283 (2019). <https://doi.org/10.1016/J.BCAB.2018.11.029>
44. Bergveld, P.: Short communications: development of an ion-sensitive solid-state device for neurophysiological measurements. *IEEE Trans Biomed Eng BME*-**17**(1), 70–71 (1970). <https://doi.org/10.1109/TBME.1970.4502688>.
45. Guilbault, G.G., Lubrano, G.J.: An enzyme electrode for the amperometric determination of glucose. *Anal. Chim. Acta.* **64**(3), 439–455 (1973). [https://doi.org/10.1016/S0003-2670\(01\)82476-4](https://doi.org/10.1016/S0003-2670(01)82476-4)
46. Mosbach, K., Danielsson, B.: An enzyme thermistor. *Biochimica et Biophysica Acta (BBA) Enzymol.* **364**(1), 140–145 (1974). [https://doi.org/10.1016/0005-2744\(74\)90141-7](https://doi.org/10.1016/0005-2744(74)90141-7)
47. Lübbers, D.W., Opitz, N.: Die pCO<sub>2</sub>-pO<sub>2</sub>-Optode: Eine neue pCO<sub>2</sub>- bzw. pO<sub>2</sub>-Meßsonde zur Messung des pCO<sub>2</sub> oder pO<sub>2</sub> von Gasen und Flüssigkeiten. *Zeitschrift für Naturforschung Sect. C J. Biosci.* **30**(7–8), 532–533 (1975). [https://doi.org/10.1515/ZNC-1975-7-819/MAC\\_HINEREADEABLECITATION/RIS](https://doi.org/10.1515/ZNC-1975-7-819/MAC_HINEREADEABLECITATION/RIS)
48. Newman, J.D., Turner, A.P.F.: Home blood glucose biosensors: a commercial perspective. *Biosens. Bioelectron.* **20**(12), 2435–2453 (2005). <https://doi.org/10.1016/J.BIOS.2004.11.012>
49. D’Orazio, P.: Biosensors in clinical chemistry. *Clin. Chim. Acta* **334**(1–2), 41–69 (2003). [https://doi.org/10.1016/S0009-8981\(03\)00241-9](https://doi.org/10.1016/S0009-8981(03)00241-9)
50. Suzuki, S., Takahashi, F., Satoh, I., Sonobe, N.: Ethanol and lactic acid sensors using electrodes coated with dehydrogenase—Collagen membranes. *Bull. Chem. Soc. Jpn.* **48**(11), 3246–3249 (1975). <https://doi.org/10.1246/bscj.48.3246>



51. Peterson, J.I., Goldstein, S.R., Fitzgerald, R.V., Buckhold, D.K.: Fiber optic pH probe for physiological use. *Anal. Chem.* **52**(6), 864–869 (1980). <https://doi.org/10.1021/AC50056A022>
52. Schultz J.S.: Oxygen sensor of plasma constituents. U.S. Patent No. 4,344,438A, 17 Aug 1982
53. Cass, A.E.G., et al.: Ferrocene-mediated enzyme electrode for amperometric determination of glucose. *Anal. Chem.* **56**(4), 667–671 (1984). [https://doi.org/10.1021/AC00268A018/ASSET/AC00268A018.FP.PNG\\_V03](https://doi.org/10.1021/AC00268A018/ASSET/AC00268A018.FP.PNG_V03)
54. Vestergaard, M.C., Tamiya, E.: Nanobiosensors and nanobioanalyses: a review. In: *Nanobiosensors and Nanobioanalyses*, pp. 3–20 (2015). [https://doi.org/10.1007/978-4-431-55190-4\\_1/COVER](https://doi.org/10.1007/978-4-431-55190-4_1/COVER)
55. Poncharal, P., Wang, Z.L., Ugarte, D., de Heer, W.A.: Electrostatic deflections and electromechanical resonances of carbon nanotubes. *Science* (1979) **283**(5407), 1513–1516 (1999). <https://doi.org/10.1126/SCIENCE.283.5407.1513>
56. Kurzawa, C., Hengstenberg, A., Schuhmann, W.: Immobilization method for the preparation of biosensors based on pH shift-induced deposition of biomolecule-containing polymer films. *Anal. Chem.* **74**(2), 355–361 (2002). <https://doi.org/10.1021/ac010830a>
57. Mano, N., Mao, F., Heller, A.: Characteristics of a miniature compartment-less glucose–O<sub>2</sub> biofuel cell and its operation in a living plant. *J. Am. Chem. Soc.* **125**(21), 6588–6594 (2003). <https://doi.org/10.1021/ja0346328>
58. Weinstein, R.L., Schwartz, S.L., Brazg, R.L., Bugler, J.R., Peyser, T.A., McGarraugh, G.V.: Accuracy of the 5-day freestyle navigator continuous glucose monitoring system. *Diabetes Care* **30**(5), 1125–1130 (2007). <https://doi.org/10.2337/dc06-1602>
59. Ishikawa, F.N., et al.: Label-free, electrical detection of the SARS virus n-protein with nanowire biosensors utilizing antibody mimics as capture probes. *ACS Nano* **3**(5), 1219–1224 (2009). <https://doi.org/10.1021/NN900086C>
60. Gribi, S., du Bois de Dunilac, S., Ghezzi, D., Lacour, S.P.: A microfabricated nerve-on-a-chip platform for rapid assessment of neural conduction in explanted peripheral nerve fibers. *Nature Commun* **9**(1), 1–10 (2018). <https://doi.org/10.1038/s41467-018-06895-7>
61. Wilkins, E., Atanasov, P.: Glucose monitoring: state of the art and future possibilities. *Med. Eng. Phys.* **18**(4), 273–288 (1996). [https://doi.org/10.1016/1350-4533\(95\)00046-1](https://doi.org/10.1016/1350-4533(95)00046-1)
62. Polatoğlu, I., Aydın, L., Nevruz, B.Ç., Özer, S.: A novel approach for the optimal design of a biosensor. **53**(9), 1428–1445 (2020). <https://doi.org/10.1080/00032719.2019.1709075>
63. Ajami, S., Teimouri, F.: Features and application of wearable biosensors in medical care. *J. Res. Med. Sci.* **20**(12), 1208 (2015). <https://doi.org/10.4103/1735-1995.172991>
64. Jain, S., et al.: Internet of medical things (IoMT)-integrated biosensors for point-of-care testing of infectious diseases. *Biosens. Bioelectron.* **179**, 113074 (2021). <https://doi.org/10.1016/J.BIOS.2021.113074>
65. Saylan, Y., Erdem, Ö., Ünal, S., Denizli, A.: An alternative medical diagnosis method: biosensors for virus detection. *Biosensors* **9**(2), 65 (2019). <https://doi.org/10.3390/BIOS9020065>
66. Naresh, V., Lee, N.: A review on biosensors and recent development of nanostructured materials-enabled biosensors. *Sensors* **21**(4), 1109 (2021). <https://doi.org/10.3390/S21041109>
67. Ali, J.: Biosensors: their fundamentals, designs, types and most recent impactful applications: a review. *Biosens.: Their Fundam. Des. Types Most Recent Impactful Appl.: Rev. J. Biosens. Bioelectron.* **8**(1), 235 (2017). <https://doi.org/10.4172/2155-6210.1000235>
68. Yang, G., Li, L., Lee, W.B., Ng, M.C.: Structure of graphene and its disorders: a review. *Sci Technol Adv Mater* **19**(1), 613 (2018). <https://doi.org/10.1080/14686996.2018.1494493>
69. Zhang, Z., Fraser, A., Ye, S., Merle, G., Barralet, J.: Top-down bottom-up graphene synthesis. *Nano Futures* **3**(4), 042003 (2019). <https://doi.org/10.1088/2399-1984/AB4EFF>
70. Gutiérrez-Cruz, A., Ruiz-Hernández, A.R., Vega-Clemente, J.F., Luna-Gazcón, D.G., Campos-Delgado, J.: A review of top-down and bottom-up synthesis methods for the production of graphene, graphene oxide and reduced graphene oxide. *J. Mater. Sci.* **57**(31), 14543–14578 (2022). <https://doi.org/10.1007/S10853-022-07514-Z>

71. Aliyev, E., Filiz, V., Khan, M.M., Lee, Y.J., Abetz, C., Abetz, V.: Structural characterization of graphene oxide: surface functional groups and fractionated oxidative debris. *Nanomaterials* **9**(8), 1180 (2019). <https://doi.org/10.3390/NANO9081180>.
72. Georgakilas, V., et al.: Noncovalent functionalization of graphene and graphene oxide for energy materials, biosensing, catalytic, and biomedical applications. *Chem. Rev.* **116**(9), 5464–5519 (2016). <https://doi.org/10.1021/ACS.CHEMREV.5B00620>
73. Haleem, A., Javaid, M., Singh, R.P., Suman, R., Rab, S.: Biosensors applications in medical field: a brief review. *Sen. Int.* **2**, 100100 (2021). <https://doi.org/10.1016/J.SINTL.2021.100100>
74. Zhang, S., Wang, H., Liu, J., Bao, C.: Measuring the specific surface area of monolayer graphene oxide in water. *Mater. Lett.* **261**, 127098 (2020). <https://doi.org/10.1016/J.MATLET.2019.127098>
75. Deshpande, A., Leroy, B.J.: Scanning probe microscopy of graphene. *Physica E Low Dimens. Syst. Nanostruct.* **44**(4), 743–759 (2012). <https://doi.org/10.1016/J.PHYSE.2011.11.024>
76. Mbayachi, V.B., Ndayiragije, E., Sammani, T., Taj, S., Mbuta, E.R., Ullah khan, A.: Graphene synthesis, characterization and its applications: a review. *Results Chem.* **3**, 100163 (2021). <https://doi.org/10.1016/J.RECHEM.2021.100163>
77. Sang, M., Shin, J., Kim, K., Yu, K.J.: Electronic and thermal properties of graphene and recent advances in graphene based electronics applications. *Nanomaterials* **9**(3) (2019). <https://doi.org/10.3390/NANO9030374>.
78. Atta, N.F., Galal, A., El-Ads, E.H., Atta, N.F., Galal, A., El-Ads, E.H.: Graphene—A platform for sensor and biosensor applications. *Biosens. Micro Nanoscale Appl.* (2015). <https://doi.org/10.5772/60676>
79. Malik, R., Tomer, V.K., Chaudhary, V.: Hybridized graphene for chemical sensing. In: *Functionalized Graphene Nanocomposites and Their Derivatives: Synthesis, Processing and Applications*, pp. 323–338 (2019). <https://doi.org/10.1016/B978-0-12-814548-7.00016-7>
80. Qi, X., et al.: Mulberry paper-based graphene strain sensor for wearable electronics with high mechanical strength. *Sens. Actuators Phys.* **301**, 111697 (2020). <https://doi.org/10.1016/J.SNA.2019.111697>
81. Xin, G., et al.: Highly thermally conductive and mechanically strong graphene fibers. *Science* (1979) **349**(6252), 1083–1087 (2015). <https://doi.org/10.1126/SCIENCE.AAA6502>
82. Yu, X., Cheng, H., Zhang, M., Zhao, Y., Qu, L., Shi, G.: Graphene-based smart materials. *NatRM* **2**(9), 17046 (2017). <https://doi.org/10.1038/NATREVMATS.2017.46>
83. Baig, N., Kawde, A.N., Elgamouz, A.: A cost-effective disposable graphene-based sensor for sensitive and selective detection of uric acid in human urine. *Biosens. Bioelectron.* **X** **11**, 100205 (2022). <https://doi.org/10.1016/J.BIOSX.2022.100205>
84. Hossain, B., Kumar Paul, A., Arefin Islam, M., Faruk Hossain, M., Mahabubur Rahman, M.: Design and analysis of highly sensitive prism based surface plasmon resonance optical salinity sensor. *Results Opt.* **7**, 100217 (2022). <https://doi.org/10.1016/J.RIO.2022.100217>
85. Ahmad, R., Wolfbeis, O.S., Hahn, Y.B., Alshareef, H.N., Torsi, L., Salama, K.N.: Deposition of nanomaterials: a crucial step in biosensor fabrication. *Mater. Today Commun.* **17**, 289–321 (2018). <https://doi.org/10.1016/j.mtcomm.2018.09.024>
86. Cho, I.H., Kim, D.H., Park, S.: Electrochemical biosensors: perspective on functional nanomaterials for on-site analysis. *Biomater. Res.* **24**(1), 1–12 (2020). <https://doi.org/10.1186/S40824-019-0181-Y>
87. Pratts, I., Hui, E., Gubeljak, P., Kaminski Schierle, G.S., Lombardo, A., Occhipinti, L.G.: Graphene for biosensing applications in point-of-care testing. *Trends Biotechnol.* **39**(10), 1065–1077 (2021). <https://doi.org/10.1016/J.TIBTECH.2021.01.005>
88. Peña-Bahamonde, J., Nguyen, H.N., Fanourakis, S.K., Rodrigues, D.F.: Recent advances in graphene-based biosensor technology with applications in life sciences. *J. Nanobiotechnol.* **16**(1), 1–17 (2018). <https://doi.org/10.1186/S12951-018-0400-Z>
89. Li, D., Zhang, W., Yu, X., Wang, Z., Su, Z., Wei, G.: When biomolecules meet graphene: from molecular level interactions to material design and applications. *Nanoscale* **8**(47), 19491–19509 (2016). <https://doi.org/10.1039/C6NR07249F>

90. Yildiz, G., Bolton-Warberg, M., Awaja, F.: Graphene and graphene oxide for bio-sensing: General properties and the effects of graphene ripples. *Acta Biomater.* **131**, 62–79 (2021). <https://doi.org/10.1016/J.ACTBIO.2021.06.047>
91. Wu, X., Xing, Y., Zeng, K., Huber, K., Zhao, J.X.: Study of fluorescence quenching ability of graphene oxide with a layer of rigid and tunable silica spacer. *Langmuir* **34**(2), 603–611 (2018). <https://doi.org/10.1021/ACS.LANGMUIR.7B03465>
92. Batır, G.G., Arik, M., Caldıran, Z., Turut, A., Aydoğan, S.: Synthesis and characterization of reduced graphene oxide/rhodamine 101 (rGO-Rh101) nanocomposites and their heterojunction performance in rGO-Rh101/p-Si device configuration. *J. Electron. Mater.* **47**(1), 329–336 (2017). <https://doi.org/10.1007/S11664-017-5758-4>
93. Obratsova, E.D., Rybin, M.G., Obratsov, P.A.: Optical properties of graphene. In: *Graphene: Properties, Preparation, Characterization and Applications*, 2nd edn., pp. 133–142 (2021). <https://doi.org/10.1016/B978-0-08-102848-3.00006-2>
94. Gangwar, P., Singh, S., Khare, N.: Study of optical properties of graphene oxide and its derivatives using spectroscopic ellipsometry. *Appl. Phys. A* **124**(9), 1–8 (2018). <https://doi.org/10.1007/S00339-018-1999-1>
95. Zhao, Y., Li, X.G., Zhou, X., Zhang, Y.N.: Review on the graphene based optical fiber chemical and biological sensors. *Sens. Actuators B Chem.* **231**, 324–340 (2016). <https://doi.org/10.1016/J.SNB.2016.03.026>
96. Gao, X.G., Cheng, L.X., Jiang, W.S., Li, X.K., Xing, F.: Graphene and its derivatives-based optical sensors. *Front. Chem.* **9**, 5 (2021). <https://doi.org/10.3389/FCHEM.2021.615164>
97. Yoo, S.M., Lee, S.Y.: Optical biosensors for the detection of pathogenic microorganisms. *Trends Biotechnol.* **34**(1), 7–25 (2016). <https://doi.org/10.1016/J.TIBTECH.2015.09.012>
98. Zhang, H., Zhang, H., Aldabahi, A., Zuo, X., Fan, C., Mi, X.: Fluorescent biosensors enabled by graphene and graphene oxide. *Biosens. Bioelectron.* **89**(Pt 1), 96–106 (2017). <https://doi.org/10.1016/J.BIOS.2016.07.030>
99. Morales-Narváez, E., Merkoçi, A.: Graphene oxide as an optical biosensing platform: a progress report. *Adv. Mater.* **31**(6), 1805043 (2019). <https://doi.org/10.1002/ADMA.201805043>
100. Ji, G., Tian, J., Xing, F., Feng, Y.: Optical biosensor based on graphene and its derivatives for detecting biomolecules. *Int. J. Mole. Sci.* **23**(18), 10838 (2022). <https://doi.org/10.3390/IJM231810838>
101. Huang, H., Li, Z., She, J., Wang, W.: Oxygen density dependent band gap of reduced graphene oxide. *J. Appl. Phys.* **111**(5), 054317 (2012). <https://doi.org/10.1063/1.3694665>
102. Mathkar, A., et al.: Controlled, stepwise reduction and band gap manipulation of graphene oxide. *J. Phys. Chem. Lett.* **3**(8), 986–991 (2012). <https://doi.org/10.1021/JZ300096T>
103. Cushing, S.K., Li, M., Huang, F., Wu, N.: Origin of strong excitation wavelength dependent fluorescence of graphene oxide. *ACS Nano* **8**(1), 1002–1013 (2014). [https://doi.org/10.1021/NN405843D/SUPPL\\_FILE/NN405843D](https://doi.org/10.1021/NN405843D/SUPPL_FILE/NN405843D)
104. Romero-Aburto, R., et al.: Fluorinated graphene oxide; a new multimodal material for biological applications. *Adv. Mater.* **25**(39), 5632–5637 (2013). <https://doi.org/10.1002/ADMA.201301804>
105. He, X.P., Tian, H.: Photoluminescence architectures for disease diagnosis: from graphene to thin-layer transition metal dichalcogenides and oxides. *Small* **12**(2), 144–160 (2016). <https://doi.org/10.1002/SMLL.201502516>
106. Pramanik, A., Fan, Z., Chavva, S.R., Sinha, S.S., Ray, P.C.: Highly efficient and excitation tunable two-photon luminescence platform for targeted multi-color MDRB imaging using graphene oxide. *Sci. Rep.* **4**(1), 1–6 (2014). <https://doi.org/10.1038/srep06090>
107. Zhao, H., et al.: Graphene-based nanomaterials for drug and/or gene delivery, bioimaging, and tissue engineering. *Drug Discov. Today* **22**(9), 1302–1317 (2017). <https://doi.org/10.1016/J.DRUDIS.2017.04.002>
108. Ma, K., Xie, W., Liu, W., Wang, L., Wang, D., Tang, B.Z.: Graphene oxide based fluorescent dna aptasensor for liver cancer diagnosis and therapy. *Adv. Funct. Mater.* **31**(36), 2102645 (2021). <https://doi.org/10.1002/ADFM.202102645>

109. Galande, C., et al.: Quasi-molecular fluorescence from graphene oxide. *Sci. Rep.* **1**(1), 1–5 (2011). <https://doi.org/10.1038/srep00085>
110. Martins, T.D., et al.: New insights on optical biosensors: techniques, construction and application. *State Art Biosens. Gen. Aspects* (2013). <https://doi.org/10.5772/52330>
111. Lei, Z.L., Guo, B.: 2D material-based optical biosensor: status and prospect. *Adv. Sci.* **9**(4), 2102924 (2022). <https://doi.org/10.1002/ADVS.202102924>
112. Rodrigo, D., et al.: Mid-infrared plasmonic biosensing with grapheme. *Science* (1979) **349**(6244), 165–168 (2015). <https://doi.org/10.1126/SCIENCE.AAB2051>
113. Nie, W., et al.: Low-fouling surface plasmon resonance sensor for highly sensitive detection of microRNA in a complex matrix based on the DNA tetrahedron. *Anal. Chem.* **90**(21), 12584–12591 (2018). <https://doi.org/10.1021/ACS.ANALCHEM.8B02686>
114. Daems, D., Pfeifer, W., Rutten, I., Saccà, B., Spasic, D., Lammertyn, J.: Three-dimensional DNA origami as programmable anchoring points for bioreceptors in fiber optic surface plasmon resonance biosensing. *ACS Appl. Mater. Interfaces* **10**(28), 23539–23547 (2018). <https://doi.org/10.1021/ACSAMI.8B04757>
115. Bian, S., et al.: Development and validation of an optical biosensor for rapid monitoring of adalimumab in serum of patients with Crohn's disease. *Drug Test Anal.* **10**(3), 592–596 (2018). <https://doi.org/10.1002/DTA.2250>
116. Bakhtiar, R.: Surface plasmon resonance spectroscopy: A versatile technique in a biochemist's toolbox. *J. Chem. Educ.* **90**(2), 203–209 (2013). <https://doi.org/10.1021/ED200549G>
117. Nesterenko, D.V., Sekkat, Z.: Resolution estimation of the Au, Ag, Cu, and Al single- and double-layer surface plasmon sensors in the ultraviolet, visible, and infrared regions. *Plasmonics* **8**(4), 1585–1595 (2013). <https://doi.org/10.1007/S11468-013-9575-1>
118. Maurya, J.B., Prajapati, Y.K.: A comparative study of different metal and prism in the surface plasmon resonance biosensor having MoS<sub>2</sub>-graphene. *Opt. Quantum Electron.* **48**(5), 1–12 (2016). <https://doi.org/10.1007/S11082-016-0562-6>
119. Maharana, P.K., Jha, R., Palei, S.: Sensitivity enhancement by air mediated graphene multi-layer based surface plasmon resonance biosensor for near infrared. *Sens. Actuators B Chem.* **190**, 494–501 (2014). <https://doi.org/10.1016/J.SNB.2013.08.089>
120. Cen, C., et al.: Numerical investigation of a tunable metamaterial perfect absorber consisting of two-intersecting graphene nanoring arrays. *Phys. Lett. A* **383**(24), 3030–3035 (2019). <https://doi.org/10.1016/J.PHYSLETA.2019.06.028>
121. Yi, Z., et al.: Band plasmonic perfect absorber based on graphene metamaterials for refractive index sensing application. *Micromachines* **10**(7), 443 (2019). <https://doi.org/10.3390/MI10070443>
122. Wu, B., Mathews, N., Sum, T.C.: Surface plasmon resonance. *SpringerBriefs Appl. Sci. Technol.* **9789811020193**, 25–31 (2017). [https://doi.org/10.1007/978-981-10-2021-6\\_2](https://doi.org/10.1007/978-981-10-2021-6_2)
123. Habib, M.M., et al.: Study of graphene-MoS<sub>2</sub> based SPR biosensor with graphene based SPR biosensor: comparative approach. *Int. J. Nat. Sci. Res.* **7**(1), 1–9 (2019). <https://doi.org/10.18488/JOURNAL.63.2019.71.19>
124. Panda, A., Pukhrabam, P.D., Keiser, G.: Performance analysis of graphene-based surface plasmon resonance biosensor for blood glucose and gas detection. *Appl. Phys. A* **126**(3), 1–12 (2020). <https://doi.org/10.1007/S00339-020-3328-8>
125. Jamil, N.A., Menon, P.S., Said, F.A., Tarumaraja, K.A., Mei, G.S., Majlis, B.Y.: Graphene-based surface plasmon resonance urea biosensor using Kretschmann configuration. In: *Proceedings of the 2017 IEEE Regional Symposium on Micro and Nanoelectronics, RSM 2017*, pp. 112–115 (2017). <https://doi.org/10.1109/RSM.2017.8069122>
126. Wang, Q., Wang, B.T.: Surface plasmon resonance biosensor based on graphene oxide/silver coated polymer cladding silica fiber. *Sens. Actuators B Chem.* **275**, 332–338 (2018). <https://doi.org/10.1016/J.SNB.2018.08.065>
127. Pathak, S., Estrela, P.: Field-effect transistors: Current advances and challenges in bringing them to point-of-care. In: *Nanobiosensors and Nanobioanalyses*, pp. 353–371 (2015). [https://doi.org/10.1007/978-4-431-55190-4\\_17](https://doi.org/10.1007/978-4-431-55190-4_17)

128. Mehrotra, P.: Biosensors and their applications—A review. *J. Oral. Biol. Craniofac. Res.* **6**(2), 153–159 (2016). <https://doi.org/10.1016/J.JOBCR.2015.12.002>
129. Syu, Y.-C., Hsu, W.-E., Lin, C.-T.: Review—Field-effect transistor biosensing: devices and clinical applications. *ECS J. Solid State Sci. Technol.* **7**(7), Q3196–Q3207 (2018). <https://doi.org/10.1149/2.0291807JSS>
130. Sze, S.M. (Professor of electrical engineering) Li, Y., Ng, K.K.: *Physics of Semiconductor Devices*, p. 944 (2021). [https://books.google.com/books/about/Physics\\_of\\_Semiconductor\\_Devices.html?id=svYkEAAAQBAJ](https://books.google.com/books/about/Physics_of_Semiconductor_Devices.html?id=svYkEAAAQBAJ). Accessed 04 Nov 2022
131. Kaisti, M.: Detection principles of biological and chemical FET sensors. *Biosens. Bioelectron.* **98**, 437–448 (2017). <https://doi.org/10.1016/J.BIOS.2017.07.010>
132. Sharma, S., Prakash, V., Mehta, S.K.: Graphene/silver nanocomposites-potential electron mediators for proliferation in electrochemical sensing and SERS activity. *TrAC Trends Anal. Chem.* **86**, 155–171 (2017). <https://doi.org/10.1016/J.TRAC.2016.10.004>
133. Fahim-Al-Fattah, M., Rahman, M.T., Islam, M.S., Bhuiyan, A.G.: A study on theoretical performance of graphene FET using analytical approach with reference to high cutoff frequency. **15**(3) (2016). <https://doi.org/10.1142/S0219581X16400019>
134. Hu, S., Jia, Y.: Function of tetra (4-aminophenyl) porphyrin in altering the electronic performances of reduced graphene oxide-based field effect transistor. *Molecules* **24**(21), 3960 (2019). <https://doi.org/10.3390/MOLECULES24213960>
135. Aspermair, P., et al.: Reduced graphene oxide-based field effect transistors for the detection of E7 protein of human papillomavirus in saliva. *Anal. Bioanal. Chem.* **413**(3), 779–787 (2020). <https://doi.org/10.1007/S00216-020-02879-Z/FIGURES/5>
136. Seo, G., et al.: Rapid detection of COVID-19 causative virus (SARS-CoV-2) in human nasopharyngeal swab specimens using field-effect transistor-based biosensor. *ACS Nano* **14**(4), 5135–5142 (2020). <https://doi.org/10.1021/ACS.NANO.0C02823>
137. Novodchuk, I., Bajcsy, M., Yavuz, M.: Graphene-based field effect transistor biosensors for breast cancer detection: a review on biosensing strategies. *Carbon N. Y.* **172**, 431–453 (2021). <https://doi.org/10.1016/J.CARBON.2020.10.048>
138. Sengupta, J., Hussain, C.M.: Graphene-based field-effect transistor biosensors for the rapid detection and analysis of viruses: a perspective in view of COVID-19. *Carbon Trends* **2**, 100011 (2021). <https://doi.org/10.1016/J.CARTRE.2020.100011>
139. Tian M., et al., RNA detection based on graphene field-effect transistor biosensor. *Adv. Condens. Matter Phys.* **2018** (2018). <https://doi.org/10.1155/2018/8146765>
140. Zhou, L., et al.: Label-free graphene biosensor targeting cancer molecules based on non-covalent modification. *Biosens. Bioelectron.* **87**, 701–707 (2017). <https://doi.org/10.1016/J.BIOS.2016.09.025>
141. Wu, G., Meyyappan, M., Lai, K.W.C.: Simulation of graphene field-effect transistor biosensors for bacterial detection. *Sensors* **18**(6), 1715 (2018). <https://doi.org/10.3390/S18061715>
142. Kwong Hong Tsang D., et al.: Chemically functionalised graphene FET biosensor for the label-free sensing of exosomes. *Scientific Reports* **9**(1), 1–10 (2019). <https://doi.org/10.1038/s41598-019-50412-9>
143. Chen, L.C., et al.: Improving the reproducibility, accuracy, and stability of an electrochemical biosensor platform for point-of-care use. *Biosens. Bioelectron.* **155**, 112111 (2020). <https://doi.org/10.1016/J.BIOS.2020.112111>
144. Quinchia, J., Echeverri, D., Cruz-Pacheco, A.F., Maldonado, M.E., Orozco, J.A.: Electrochemical biosensors for determination of colorectal tumor biomarkers. *Micromachines* **11**(4), 411 (2020). <https://doi.org/10.3390/MII1040411>
145. Jin, B., et al.: Multi-nanomaterial electrochemical biosensor based on label-free graphene for detecting cancer biomarkers. *Biosens. Bioelectron.* **55**, 464–469 (2014). <https://doi.org/10.1016/J.BIOS.2013.12.025>
146. Anik, U., et al.: Electrochemical medical biosensors for POC applications. In: *Medical Biosensors for Point of Care (POC) Applications*, pp. 275–292 (2017). <https://doi.org/10.1016/B978-0-08-100072-4.00012-5>

147. Dinani, H.S., Pourmadadi, M., Rashedi, H., Yazdian, F.: Fabrication of nanomaterial-based biosensor for measurement of a microRNA involved in cancer. In: 27th National and 5th International Iranian Conference of Biomedical Engineering, ICBME 2020, pp. 47–54, Nov 2020. <https://doi.org/10.1109/ICBME51989.2020.9319450>
148. Tezerjani, M.D., et al.: An impedimetric biosensor based on a composite of graphene nanosheets and polyaniline as a suitable platform for prostate cancer sensing. *Anal. Methods* **8**(41), 7507–7515 (2016). <https://doi.org/10.1039/C6AY01524G>
149. Heydari-Bafrooei, E., Shamszadeh, N.S.: Electrochemical bioassay development for ultra-sensitive aptasensing of prostate specific antigen. *Biosens. Bioelectron.* **91**, 284–292 (2017). <https://doi.org/10.1016/J.BIOS.2016.12.048>
150. Akbari jonous, Z., Shayeh, J.S., Yazdian, F., Yadegari, Hashemi, M., Omid, M.: An electrochemical biosensor for prostate cancer biomarker detection using graphene oxide–gold nanostructures. *Eng. Life Sci.* **19**(3), 206–216 (2019). <https://doi.org/10.1002/ELSC.201800093>
151. Asadi, H., Ramasamy, R.P.: Graphene-based electrochemical biosensor for impedimetric detection of miRNAs as potential cancer biomarkers. *J. Electrochem. Soc.* **167**(16), 167523 (2020). <https://doi.org/10.1149/1945-7111/ABD284>
152. Saeed, A.A., Sánchez, J.L.A., O’Sullivan, C.K., Abbas, M.N.: DNA biosensors based on gold nanoparticles-modified graphene oxide for the detection of breast cancer biomarkers for early diagnosis. *Bioelectrochemistry* **118**, 91–99 (2017). <https://doi.org/10.1016/J.BIOELECHEM.2017.07.002>
153. Jozghorbani, M., Fathi, M., Kazemi, S.H., Alinejadian, N.: Determination of carcinoembryonic antigen as a tumor marker using a novel graphene-based label-free electrochemical immunosensor. *Anal. Biochem.* **613**, 114017 (2021). <https://doi.org/10.1016/J.AB.2020.114017>
154. Li, P., Long, F., Chen, W., Chen, J., Chu, P.K., Wang, H.: Fundamentals and applications of surface-enhanced Raman spectroscopy–based biosensors. *Curr. Opin. Biomed. Eng.* **13**, 51–59 (2020). <https://doi.org/10.1016/J.COBME.2019.08.008>
155. Langer, J., et al.: Present and future of surface-enhanced Raman scattering. *ACS Nano* **14**(1), 28–117 (2020). <https://doi.org/10.1021/ACS.NANO.9B04224>
156. Ding, S.Y., You, E.M., Tian, Z.Q., Moskovits, M.: Electromagnetic theories of surface-enhanced Raman spectroscopy. *Chem. Soc. Rev.* **46**(13), 4042–4076 (2017). <https://doi.org/10.1039/C7CS00238F>
157. Zhang C., Lin K., Huang Y., Zhang J.: Graphene-Ag hybrids on laser-textured SI surface for SERS detection. *Sensors* **17**(7), 1462 (2017). <https://doi.org/10.3390/S17071462>
158. Ling, X., et al.: Lighting up the raman signal of molecules in the vicinity of graphene related materials. *Acc. Chem. Res.* **48**(7), 1862–1870 (2015). <https://doi.org/10.1021/AR500466U>
159. Cao Y., Cheng Y., Sun, M.: Graphene-based SERS for sensor and catalysis (2021). <https://doi.org/10.1080/05704928.2021.1910286>
160. Yi, N., Zhang, C., Song, Q., Xiao, S.: A hybrid system with highly enhanced graphene SERS for rapid and tag-free tumor cells detection. *Sci. Rep.* **6**(1), 1–8 (2016). <https://doi.org/10.1038/srep25134>
161. Lerf, A., He, H., Forster, M., Klinowski, J.: Structure of graphite oxide revisited. *J. Phys. Chem. B* **102**(23), 4477–4482 (1998). <https://doi.org/10.1021/JP9731821>
162. Park, S., et al.: Colloidal suspensions of highly reduced graphene oxide in a wide variety of organic solvents. *Nano. Lett.* **9**(4), 1593–1597 (2009). <https://doi.org/10.1021/NL803798Y>
163. Lord, H., Kelley, S.O.: Nanomaterials for ultrasensitive electrochemical nucleic acids biosensing. *J. Mater. Chem.* **19**(20), 3127–3134 (2009). <https://doi.org/10.1039/B814569E>
164. Kagan, V.E., et al.: Carbon nanotubes degraded by neutrophil myeloperoxidase induce less pulmonary inflammation. *Nat. Nanotechnol.* **5**(5), 354–359 (2010). <https://doi.org/10.1038/nnano.2010.44>
165. Suvarnaphaet, P., Pechprasarn, S.: Graphene-based materials for biosensors: a review. *Sensors* **17**(10), 2161 (2017). <https://doi.org/10.3390/S17102161>.



166. Trotter, M., Borst, N., Thewes, R., von Stetten, F.: Review: electrochemical DNA sensing—Principles, commercial systems, and applications. *Biosens. Bioelectron.* **154**, 112069 (2020). <https://doi.org/10.1016/J.BIOS.2020.112069>
167. Ping, J., Vishnubhotla, R., Vrudhula, A., Johnson, A.T.C.: Scalable Production of high-sensitivity, label-free DNA biosensors based on back-gated graphene field effect transistors. *ACS Nano* **10**(9), 8700–8704 (2016). <https://doi.org/10.1021/ACS.NANO.6B04110>
168. Raja Jamaluddin, R.Z.A., Tan, L.L., Chong, K.F., Heng, L.Y.: An electrochemical DNA biosensor fabricated from graphene decorated with graphitic nanospheres. *Nanotechnology* **31**(48) (2020). <https://doi.org/10.1088/1361-6528/ABAB2E>
169. Morales-Narváez, E., Hassan, A.-R., Merkoçi, A.: Graphene oxide as a pathogen-revealing agent: sensing with a digital-like response. *Angew. Chem.* **125**(51), 14024–14028 (2013). <https://doi.org/10.1002/ANGE.201307740>
170. Ye, Y., et al.: A label-free electrochemical DNA biosensor based on thionine functionalized reduced graphene oxide. *Carbon N. Y.* **129**, 730–737 (2018). <https://doi.org/10.1016/J.CARBON.2017.12.060>
171. Hwang M.T., et al. Ultrasensitive detection of nucleic acids using deformed graphene channel field effect biosensors. *Nat. Commun.* **11**(1), 1–11 (2020). <https://doi.org/10.1038/s41467-020-15330-9>
172. Safarzadeh, M., Pan, G.: Detection of a double-stranded MGMT gene using electrochemically reduced graphene oxide (ErGO) electrodes decorated with AuNPs and peptide nucleic acids (PNA). *Biosensors* **12**(2), 98 (2022). <https://doi.org/10.3390/BIOS12020098>
173. Becheru, D.F., Vlăsceanu, G.M., Banciu, A., Vasile, E., Ioniță, M., Burns, J.S.: Optical graphene-based biosensor for nucleic acid detection; influence of graphene functionalization and ionic strength. *Int. J. Mol. Sci.* **19**(10), 3230 (2018). <https://doi.org/10.3390/IJMS19103230>
174. Bagherzadeh-Nobari, S., Kalantarinejad, R.: Real-time label-free detection of DNA hybridization using a functionalized graphene field effect transistor: a theoretical study. *J. Nanopart. Res.* **23**(8) (2021). <https://doi.org/10.1007/S11051-021-05295-1>
175. Qaddare, S.H., Salimi, A.: Amplified fluorescent sensing of DNA using luminescent carbon dots and AuNPs/GO as a sensing platform: A novel coupling of FRET and DNA hybridization for homogeneous HIV-1 gene detection at femtomolar level. *Biosens. Bioelectron.* **89**(Pt 2), 773–780 (2017). <https://doi.org/10.1016/J.BIOS.2016.10.033>
176. Kong, X., et al.: Graphene-based liquid gated field-effect transistor for label-free detection of DNA hybridization. In: 18th IEEE International Multi-Conference on Systems, Signals and Devices, SSD 2021, Mar. 2021, pp. 387–391. <https://doi.org/10.1109/SSD52085.2021.9429414>
177. Farzin, L., Sadjadi, S., Shamsipur, M., Sheibani, S.: Electrochemical genosensor based on carbon nanotube/amine-ionic liquid functionalized reduced graphene oxide nanoplatfrom for detection of human papillomavirus (HPV16)-related head and neck cancer. *J. Pharm. Biomed. Anal.* **179**, 112989 (2020). <https://doi.org/10.1016/J.JPBA.2019.112989>
178. Liu, C., et al.: Enzyme biosensors for point-of-care testing. In: *MEMS Sensors—Design and Application* (2018). <https://doi.org/10.5772/INTECHOPEN.73249>
179. Schuck, A., et al.: A graphene-based enzymatic biosensor using a common-gate field-effect transistor for L-lactic acid detection in blood plasma samples. *Sensors* **21**(5), 1852 (2021). <https://doi.org/10.3390/S21051852>
180. Alhazmi, H.A., et al.: Graphene-based biosensors for disease theranostics: development, applications, and recent advancements. *Nanotechnol. Rev.* **11**(1), 96–116 (2021). <https://doi.org/10.1515/NTREV-2022-0009>
181. Huang, Y., Dong, X., Shi, Y., Li, C.M., Li, L.J., Chen, P.: Nanoelectronic biosensors based on CVD grown graphene. *Nanoscale* **2**(8), 1485–1488 (2010). <https://doi.org/10.1039/C0NR00142B>
182. Settu, K., Chiu, P.T., Huang, Y.M.: Laser-induced graphene-based enzymatic biosensor for glucose detection. *Polymers* **13**(16), 2795 (2021). <https://doi.org/10.3390/POLYM13162795>

183. Rathee, K., Dhull, V., Dhull, R., Singh, S.: Biosensors based on electrochemical lactate detection: a comprehensive review. *Biochem. Biophys. Rep.* **5**, 35–54 (2016). <https://doi.org/10.1016/J.BBREP.2015.11.010>
184. Yu, G., et al.: Utility of the early lactate area score as a prognostic marker for septic shock patients in the emergency department. *Acute Crit. Care* **34**(2), 126–132 (2019). <https://doi.org/10.4266/ACC.2018.00283>
185. Dempsey, P.W., et al.: Detection of early-stage lung cancer with an in vitro panel of activity-based biosensors to measure inflammatory protease enzymes. **40**(16), e20551–e20551 (2022). <https://doi.org/10.1200/JCO.2022.40.16>
186. Povedano, E., et al.: Decoration of reduced graphene oxide with rhodium nanoparticles for the design of a sensitive electrochemical enzyme biosensor for 17 $\beta$ -estradiol. *Biosens Bioelectron* **89**, 343–351 (2017). <https://doi.org/10.1016/J.BIOS.2016.07.018>
187. Cheraghi, S., et al.: Novel enzymatic graphene oxide based biosensor for the detection of glutathione in biological body fluids. *Chemosphere* **287**, 132187 (2022). <https://doi.org/10.1016/J.CHEMOSPHERE.2021.132187>
188. Palanisamy, S., et al.: A novel Laccase biosensor based on laccase immobilized graphene-cellulose microfiber composite modified screen-printed carbon electrode for sensitive determination of catechol. *Sci. Rep.* **7** (2017). <https://doi.org/10.1038/SREP41214>
189. Anuar, N.S., Basirun, W.J., Shalauddin, M., Akhter, S.: A dopamine electrochemical sensor based on a platinum–silver graphene nanocomposite modified electrode. *RSC Adv.* **10**(29), 17336–17344 (2020). <https://doi.org/10.1039/C9RA11056A>
190. Palanisamy, S., et al.: Facile synthesis of cellulose microfibers supported palladium nanospindles on graphene oxide for selective detection of dopamine in pharmaceutical and biological samples. *Mater. Sci. Eng. C* **98**, 256–265 (2019). <https://doi.org/10.1016/J.MSEC.2018.12.112>
191. Nan Song, N., et al.: A novel electrochemical biosensor for the determination of dopamine and ascorbic acid based on graphene oxide /poly(aniline-co-thionine) nanocomposite. *J. Electroanal. Chem.* **873**, 114352 (2020). <https://doi.org/10.1016/J.JELECHEM.2020.114352>
192. Wu, Y., et al.: Simultaneous and sensitive determination of ascorbic acid, dopamine and uric acid via an electrochemical sensor based on PVP-graphene composite. *J. Nanobiotechnol.* **18**(1), 1–13 (2020). <https://doi.org/10.1186/S12951-020-00672-9>
193. Manjunatha, J.G.: Poly (adenine) modified graphene-based voltammetric sensor for the electrochemical determination of catechol, hydroquinone and resorcinol. *Open Chem. Eng. J.* **14**(1), 52–62 (2020). <https://doi.org/10.2174/1874123102014010052>
194. Akbari, S., Foroughi, M.M., Nadiki, H.H., Jahani, S.: Synthesis and characterization of LaMnO<sub>3</sub> nanocrystals and graphene oxide: fabrication of graphene oxide–LaMnO<sub>3</sub> sensor for simultaneous electrochemical determination of hydroquinone and catechol. *J. Electrochem. Sci. Eng.* **9**(4), 255–267 (2019). <https://doi.org/10.5599/JESE.634>
195. Szunerits, S., Boukherroub, R.: Graphene-based biosensors. *Interface Focus* **8**(3) (2018). <https://doi.org/10.1098/RFSFS.2016.0132>
196. Cho, I.H., et al.: Current technologies of electrochemical immunosensors: perspective on signal amplification. *Sensors* **18**(1), 207 (2018). <https://doi.org/10.3390/S18010207>
197. Wan, Y., Su, Y., Zhu, X., Liu, G., Fan, C.: Development of electrochemical immunosensors towards point of care diagnostics. *Biosens. Bioelectron.* **47**, 1–11 (2013). <https://doi.org/10.1016/J.BIOS.2013.02.045>
198. Singh, P., Pandey, S.K., Singh, J., Srivastava, S., Sachan, S., Singh, S.K.: Biomedical perspective of electrochemical nanobiosensor. *Nanomicro. Lett.* **8**(3), 193–203 (2016). <https://doi.org/10.1007/S40820-015-0077-X>
199. Pandey, A., Gurbuz, Y., Ozguz, V., Niazi, J.H., Qureshi, A.: Graphene-interfaced electrical biosensor for label-free and sensitive detection of foodborne pathogenic *E. coli* O157:H7. *Biosens. Bioelectron.* **91**, 225–231 (2017). <https://doi.org/10.1016/J.BIOS.2016.12.041>
200. Afsahi, S., et al.: Novel graphene-based biosensor for early detection of Zika virus infection. *Biosens. Bioelectron.* **100**, 85–88 (2018). <https://doi.org/10.1016/J.BIOS.2017.08.051>



201. Saleem, W., Salinas, C., Watkins, B., Garvey, G., Sharma, A.C., Ghosh, R.: Antibody functionalized graphene biosensor for label-free electrochemical immunosensing of fibrinogen, an indicator of trauma induced coagulopathy. *Biosens. Bioelectron.* **86**, 522–529 (2016). <https://doi.org/10.1016/J.BIOS.2016.07.009>
202. Tincu, B., et al.: Vertical graphene-based biosensor for tumor cell dielectric signature evaluation. *Micromachines (Basel)* **13**(10), 1671 (2022). <https://doi.org/10.3390/MI13101671>
203. Woerman, A.L., et al.: Kinetics of  $\alpha$ -synuclein prions preceding neuropathological inclusions in multiple system atrophy. *PLoS Pathog.* **16**(2), e1008222 (2020). <https://doi.org/10.1371/JOURNAL.PPAT.1008222>
204. Salahuddin, P., Fatima, M.T., Uversky, V.N., Khan, R.H., Islam, Z., Furkan, M.: The role of amyloids in Alzheimer's and Parkinson's diseases. *Int. J. Biol. Macromol.* **190**, 44–55 (2021). <https://doi.org/10.1016/J.IJBIOMAC.2021.08.197>
205. Liu, L., Xia, N., Zhang, J., Mao, W., Wu, Y., Ge, X.: A graphene oxide-based fluorescent platform for selective detection of amyloid- $\beta$  oligomers. *Anal. Methods* **7**(20), 8727–8732 (2015). <https://doi.org/10.1039/C5AY02018B>
206. Zhao, J., et al.: Graphene oxide-gold nanoparticle-aptamer complexed probe for detecting amyloid beta oligomer by ELISA-based immunoassay. *J. Immunol. Methods.* **489**, 112942 (2021). <https://doi.org/10.1016/J.JIM.2020.112942>
207. Zhou, Y., et al.: Ultrasensitive assay of amyloid-beta oligomers using Au-vertical graphene/carbon cloth electrode based on poly(thymine)-templated copper nanoparticles as probes. *Sens. Actuators B Chem.* **331**, 129429 (2021). <https://doi.org/10.1016/J.SNB.2020.129429>
208. Zhang, X., Yu, Y., Shen, J., Qi, W., Wang, H.: Design of organic/inorganic nanocomposites for ultrasensitive electrochemical detection of a cancer biomarker protein. *Talanta* **212**, 120794 (2020). <https://doi.org/10.1016/J.TALANTA.2020.120794>
209. Haghayegh, F., Salahandish, R., Hassani, M., Sanati-Nezhad, A.: Highly stable buffer-based zinc oxide/reduced graphene oxide nanosurface chemistry for rapid immunosensing of SARS-CoV-2 antigens. *ACS Appl. Mater. Interfaces* **14**(8), 10844–10855 (2022). <https://doi.org/10.1021/ACSAMI.1C24475>
210. Gao, J., et al.: Graphene oxide-graphene Van der Waals heterostructure transistor biosensor for SARS-CoV-2 protein detection. *Talanta* **240**, 123197 (2022). <https://doi.org/10.1016/J.TALANTA.2021.123197>
211. Aminabad, E.D., Mobed, A., Hasanzadeh, M., Hosseinpour Feizi, M.A., Safaralizadeh, R., Seidi, F.: Sensitive immunosensing of  $\alpha$ -synuclein protein in human plasma samples using gold nanoparticles conjugated with graphene: an innovative immuno-platform towards early stage identification of Parkinson's disease using point of care (POC) analysis. *RSC Adv.* **12**(7), 4346–4357 (2022). <https://doi.org/10.1039/D1RA06437A>
212. Duong Ngo, H., et al.: Vertical graphene-based biosensor for tumor cell dielectric signature evaluation. *Micromachines* **13**(10), 1671 (2022). <https://doi.org/10.3390/MI13101671>
213. Chen, Y., et al.: Effective immobilization of Au nanoparticles on TiO<sub>2</sub> loaded graphene for a novel sandwich-type immunosensor. *Biosens. Bioelectron.* **102**, 301–306 (2018). <https://doi.org/10.1016/J.BIOS.2017.11.009>
214. Xia, Y., et al.: Picogram level electrochemical impedimetric immunosensor for monitoring Mycobacterium tuberculosis based on specific and sensitive ESAT-6 monoclonal antibody. *Talanta* **124052** (2022). <https://doi.org/10.1016/J.TALANTA.2022.124052>
215. Krishnan, S., He, X., Zhao, F., Zhang, Y., Liu, S., Xing, R.: Dual labeled mesoporous silica nanospheres based electrochemical immunosensor for ultrasensitive detection of carcinoembryonic antigen. *Anal. Chim. Acta* **1133**, 119–127 (2020). <https://doi.org/10.1016/J.ACA.2020.07.080>
216. Butmee, P., Tumcharern, G., Thouand, G., Kalcher, K., Samphao, A.: An ultrasensitive immunosensor based on manganese dioxide-graphene nanoplatelets and core shell Fe<sub>3</sub>O<sub>4</sub>@Au nanoparticles for label-free detection of carcinoembryonic antigen. *Bioelectrochemistry* **132**, 107452 (2020). <https://doi.org/10.1016/J.BIOELECHEM.2019.107452>

217. Samota, S., Rani, R., Chakraverty, S., Kaushik, A.: Biosensors for simplistic detection of pathogenic bacteria: a review with special focus on field-effect transistors. *Mater. Sci. Semicond. Process* **141**, 106404 (2022). <https://doi.org/10.1016/J.MSSP.2021.106404>
218. Kozel, T.R., Burnham-Marusch, A.R.: Point-of-care testing for infectious diseases: past, present, and future. *J. Clin. Microbiol.* **55**(8), 2313–2320 (2017). <https://doi.org/10.1128/JCM.00476-17>
219. Hansen, S., el Wahed, A.A.: Point-of-care or point-of-need diagnostic tests: time to change outbreak investigation and pathogen detection. *Trop. Med. Infect. Dis.* **5**(5), 151 (2020). <https://doi.org/10.3390/TROPICALMED5040151>
220. Dehghani, Z., Mohammadnejad, J., Hosseini, M., Bakhshi, B., Rezayan, A.H.: Whole cell FRET immunosensor based on graphene oxide and graphene dot for *Campylobacter jejuni* detection. *Food Chem.* **309**, (2020). <https://doi.org/10.1016/J.FOODCHEM.2019.125690>
221. Muniandy, S., et al.: A reduced graphene oxide-titanium dioxide nanocomposite based electrochemical aptasensor for rapid and sensitive detection of *Salmonella enterica*. *Bioelectrochemistry* **127**, 136–144 (2019). <https://doi.org/10.1016/J.BIOELECTROCHEM.2019.02.005>
222. Parmar, J., Patel, S.K., Katkar, V., Natesan, A.: Graphene-Based Refractive Index sensor using machine learning for detection of mycobacterium tuberculosis bacteria. *IEEE Trans. Nanobiosci.* (2022). <https://doi.org/10.1109/TNB.2022.3155264>
223. Pandit, S., et al.: Graphene-based sensor for detection of bacterial pathogens. *Sensors* **21**(23), 8085 (2021). <https://doi.org/10.3390/S21238085>
224. Vermisoglou, E., et al.: Human virus detection with graphene-based materials. *Biosens. Bioelectron.* **166**, 112436 (2020). <https://doi.org/10.1016/J.BIOS.2020.112436>
225. Ban, D.K., et al.: Rapid self-test of unprocessed viruses of SARS-CoV-2 and its variants in saliva by portable wireless graphene biosensor. *Proc. Natl. Acad. Sci. U. S. A.* **119**(28), e2206521119 (2022). <https://doi.org/10.1073/PNAS.2206521119>
226. Silva, L.R.G., et al.: Electrochemical biosensor for SARS-CoV-2 cDNA detection using AuPs-modified 3D-printed graphene electrodes. *Biosensors* **12**(8), 622 (2022). <https://doi.org/10.3390/BIOS12080622>
227. Kainz, K., Bauer, M.A., Madeo, F., Carmona-Gutierrez, D.: Fungal infections in humans: the silent crisis. *Microbial. Cell* **7**(6), 143 (2020). <https://doi.org/10.15698/MIC2020.06.718>
228. Pitt, J.I., Hocking, A.D.: Spoilage of stored, processed and preserved foods. In: *Fungi and Food Spoilage*, pp. 537–568 (2022). [https://doi.org/10.1007/978-3-030-85640-3\\_12](https://doi.org/10.1007/978-3-030-85640-3_12)
229. Pourmadadi, M., Yazdian, F., Hojjati, S., Khosravi-Darani, K.: Detection of microorganisms using graphene-based nanobiosensors. *Food Technol. Biotechnol.* **59**(4), 496–506 (2021). <https://doi.org/10.17113/FTB.59.04.21.7223>
230. Shi, C., et al.: Capture and detection of *Escherichia coli* with graphene aerogels. *J. Mater. Chem. B* **10**(40), 8211–8217 (2022). <https://doi.org/10.1039/D2TB01749K>
231. Tian, X., et al.: Fast and sensitive graphene oxide-DNAzyme-based biosensor for *Vibrio alginolyticus* detection. *J. Fish. Dis.* **45**(5), 687–697 (2022). <https://doi.org/10.1111/JFD.13594>
232. Nair, S., Kumar, V., Kumar, R., Jain, V.K., Nagpal, S.: Electrostatic graphene oxide-based biosensor for rapid direct detection of *E. coli*. *Int. J. Mater. Res.* **113**(6), 560–568 (2022). <https://doi.org/10.1515/IJMR-2021-8288>
233. Jin, X., et al.: A field effect transistor modified with reduced graphene oxide for immunodetection of Ebola virus. *Mikrochim Acta* **186**(4) (2019). <https://doi.org/10.1007/S00604-019-3256-5>
234. Li, J., et al.: Sensitive electrochemical detection of hepatitis C virus subtype based on nucleotides assisted magnetic reduced graphene oxide-copper nano-composite. *Electrochem. Commun.* **110**, 106601 (2020). <https://doi.org/10.1016/J.ELECOM.2019.106601>
235. Manohara Reddy, Y.V., et al.: Fine-tuning of MXene-nickel oxide-reduced graphene oxide nanocomposite bioelectrode: Sensor for the detection of influenza virus and viral protein. *Biosens. Bioelectron.* **214**, 114511 (2022). <https://doi.org/10.1016/J.BIOS.2022.114511>
236. Yupapin, P., Trabelsi, Y., Vigneswaran, D., Taya, S.A., Daher, M.G., Colak, I.: Ultra-high-sensitive sensor based on surface plasmon resonance structure having si and graphene layers

- for the detection of chikungunya virus. *Plasmonics* **17**(3), 1315–1321 (2022). <https://doi.org/10.1007/S11468-022-01631-W>
237. Zaid, M.H.M., et al.: Reduced graphene oxide/TEMPO-nanocellulose nanohybrid-based electrochemical biosensor for the determination of mycobacterium tuberculosis. *J. Sens.* **2020** (2020). <https://doi.org/10.1155/2020/4051474>
238. Bishnoi, R.J., Palmer, R.F., Royall, D.R.: Serum interleukin (IL)-15 as a biomarker of Alzheimer's disease. *PLoS ONE* **10**(2), e0117282 (2015). <https://doi.org/10.1371/JOURNAL.PONE.0117282>
239. Pimentel, G.D., dela Vega, M.C.M., Laviano, A.: High neutrophil to lymphocyte ratio as a prognostic marker in COVID-19 patients. *Clin. Nutr. ESPEN* **40**, 101–102 (2020). <https://doi.org/10.1016/J.CLNESP.2020.08.004>
240. Cheng, R., Wu, Z., Li, M., Shao, M., Hu, T.: Interleukin-1 $\beta$  is a potential therapeutic target for periodontitis: a narrative review. *Int. J. Oral. Sci.* **12**(1) (2020). <https://doi.org/10.1038/S41368-019-0068-8>
241. Forouzandeh, M., Besen, J., Keane, R.W., de Rivero Vaccari, J.P.: The inflammasome signaling proteins ASC and IL-18 as biomarkers of psoriasis. *Front. Pharmacol.* **11**, 1238 (2020). <https://doi.org/10.3389/FPHAR.2020.01238>
242. Fuschioti, P., Larregina, A.T., Ho, J., Feghali-Bostwick, C., Medsger, T.A.: Interleukin-13-producing CD8+ T cells mediate dermal fibrosis in patients with systemic sclerosis. *Arthritis Rheum* **65**(1), 236–246 (2013). <https://doi.org/10.1002/ART.37706>
243. Motomura, Y., et al.: Basophil-derived interleukin-4 controls the function of natural helper cells, a member of ILC2s, in lung inflammation. *Immunity* **40**(5), 758–771 (2014). <https://doi.org/10.1016/J.IMMUNI.2014.04.013>
244. Eijkelkamp, N., et al.: IL4-10 fusion protein is a novel drug to treat persistent inflammatory pain. *J. Neurosci.* **36**(28), 7353–7363 (2016). <https://doi.org/10.1523/JNEUROSCI.0092-16.2016>
245. Hoving, J.C.: Targeting IL-13 as a host-directed therapy against ulcerative colitis. *Front Cell Infect. Microbiol.* **8**, 395 (2018). <https://doi.org/10.3389/FCIMB.2018.00395>
246. Ostermann, M., et al.: Cardiac troponin release is associated with biomarkers of inflammation and ventricular dilatation during critical illness. *Shock* **47**(6), 702 (2017). <https://doi.org/10.1097/SHK.0000000000000811>
247. Welsh, P., et al.: Cardiac Troponin T and Troponin I in the general population. *Circulation* **139**(24), 2754–2764 (2019). <https://doi.org/10.1161/CIRCULATIONAHA.118.038529>
248. Okumura, T., Hiraiwa, H., Takefuji, M., Murohara, T.: Benefits and precautions in using B-type natriuretic peptide—N-terminal-pro-B-type natriuretic peptide conversion formula. *Circ. J. CJ-22-0343* (2022). <https://doi.org/10.1253/CIRCJ.CJ-22-0343>
249. Liu, H.L., Tseng, Y.T., Lai, M.C., Chau, L.K.: Ultrasensitive and rapid detection of N-terminal pro-B-type natriuretic peptide (NT-proBNP) using fiber optic nanogold-linked immunosorbent assay. *Biosensors* **12**(9), 746 (2022). <https://doi.org/10.3390/BIOS12090746>
250. Chen, R., et al.: HMGB1 as a potential biomarker and therapeutic target for severe COVID-19. *Heliyon* **6**(12), e05672 (2020). <https://doi.org/10.1016/J.HELİYON.2020.E05672>
251. Yamashiro, K., et al.: High mobility group box 1 expression in oral inflammation and regeneration. *Front. Immunol.* **11**, 1461 (2020). <https://doi.org/10.3389/FIMMU.2020.01461>
252. Atar, N., Yola, M.L.: A novel QCM immunosensor development based on gold nanoparticles functionalized sulfur-doped graphene quantum dot and h-ZnS-CdS NC for Interleukin-6 detection. *Anal. Chim. Acta* **1148** (2021). <https://doi.org/10.1016/J.ACA.2021.338202>
253. Wei, H., Ni, S., Cao, C., Yang, G., Liu, G.: Graphene oxide signal reporter based multifunctional immunosensing platform for amperometric profiling of multiple cytokines in serum. *ACS Sens.* **3**(8), 1553–1561 (2018). <https://doi.org/10.1021/ACSENSORS.8B00365>
254. Khayamian, M.A., et al.: A label-free graphene-based impedimetric biosensor for real-time tracing of the cytokine storm in blood serum; suitable for screening COVID-19 patients. *RSC Adv.* **11**(55), 34503–34515 (2021). <https://doi.org/10.1039/D1RA04298J>
255. Salahandish, R., Haghayegh, F., Khetani, S., Hassani, M., Nezhad, A.S.: Immuno-affinity potent strip with pre-embedded intermixed PEDOT:PSS conductive polymers and graphene

- nanosheets for bio-ready electrochemical biosensing of central nervous system injury biomarkers. *ACS Appl. Mater. Interfaces* **14**(25), 28651–28662 (2022). <https://doi.org/10.1021/ACSAMI.2C07322>
256. Sethi, J., van Bulck, M., Suhail, A., Safarzadeh, M., Perez-Castillo, A., Pan, G.: A label-free biosensor based on graphene and reduced graphene oxide dual-layer for electrochemical determination of beta-amyloid biomarkers. *Microchim. Acta* **187**(5), 1–10 (2020). <https://doi.org/10.1007/S00604-020-04267-X>
  257. Khan, N.I., Song, E.: Detection of an IL-6 biomarker using a GFET platform developed with a facile organic solvent-free Aptamer immobilization approach. *Sensors* **21**(4), 1335 (2021). <https://doi.org/10.3390/S21041335>
  258. Hao, Z., Pan, Y., Huang, C., Wang, Z., Zhao, X.: Sensitive detection of lung cancer biomarkers using an aptameric graphene-based nanosensor with enhanced stability. *Biomed. Microdev.* **21**(3), 1–9 (2019). <https://doi.org/10.1007/S10544-019-0409-6>
  259. Hwang, M.T., et al.: Ultrasensitive detection of dopamine, IL-6 and SARS-CoV-2 proteins on crumpled graphene FET biosensor. *Adv. Mater. Technol.* **6**(11), 2100712 (2021). <https://doi.org/10.1002/ADMT.202100712>
  260. Shen, Z., Ni, S., Yang, W., Sun, W., Yang, G., Liu, G.: Redox probes tagged electrochemical aptasensing device for simultaneous detection of multiple cytokines in real time. *Sens. Actuators B Chem.* **336**, 129747 (2021). <https://doi.org/10.1016/J.SNB.2021.129747>
  261. Verma, S., Singh, S.P.: Non-invasive oral cancer detection from saliva using zinc oxide-reduced graphene oxide nanocomposite based bioelectrode. *MRS Commun.* **9**(4), 1227–1234 (2019). <https://doi.org/10.1557/MRC.2019.138>
  262. Rauf, S., Mani, V., Lahcen, A.A., Yuvaraja, S., Beduk, T., Salama, K.N.: Binary transition metal oxide modified laser-scribed graphene electrochemical aptasensor for the accurate and sensitive screening of acute myocardial infarction. *Electrochim. Acta* **386**, 138489 (2021). <https://doi.org/10.1016/J.ELECTACTA.2021.138489>
  263. Li, J., et al.: A novel graphene-based nanomaterial modified electrochemical sensor for the detection of cardiac Troponin I. *Front. Chem.* **9**, 339 (2021). <https://doi.org/10.3389/FCHEM.2021.680593>
  264. Medical device market: market size, industry outlook, market forecast, demand analysis, market share, market report 2021–2026. <https://www.industryarc.com/Research/Medical-Device-Market-Research-514107>. Accessed 05 Nov 2022
  265. Collins, R.: Graphene market & 2D materials assessment 2021–2031 copyright. Use and disclaimer (2021). Available <https://www.idtechex.com/en/research-report/graphene-market-and-2d-materials-assessment-2021-2031/789>. Accessed 05 Nov 2022
  266. Huang, Y., et al.: Lateral flow biosensors based on the use of micro- and nanomaterials: a review on recent developments. *Mikrochim Acta* **187**(1) (2019). <https://doi.org/10.1007/S00604-019-3822-X>

# Micro-sized Graphene-Based UWB Annular Ring Patch Antenna for Short-Range High-Speed Terahertz Wireless Systems



Asma Khabba, Jamal Amadid, Zakaria El Ouadi, Layla Wakrim, Saida Ibnyaich, Ahmed Jamal Abdullah Al-Gburi, and Abdelouhab Zeroual

**Abstract** Owing to the fascinating features of graphene material, graphene-based patch antennas have quickly attracted attentions in communication technologies for high-speed data transfer in terahertz band. Herein, we present in this chapter a careful study of a new ultra-wide band (UWB) graphene-based plasmonic terahertz (THz) antenna operating in the range of 7.4–8.4 THz, with a huge bandwidth of 1000 GHz. The resonant part of the antenna consists of a modified circular ring patch, designed on 2.4  $\mu\text{m}$ -thick silicon laminate with a high permittivity of 11.9. The resonating frequencies and the antenna operation band can be controllable by adjusting the graphene layers' chemical potential, where the desired UWB behavior is attained with a chemical potential of 2 eV. The suggested antenna possesses a super compact geometry of  $24 \times 24 \mu\text{m}$  along with attractive radiation behavior in terms of gain (up to 5.5 dB) radiation efficiency (>97%). In addition, a high impedance matching is achieved which contributes in very low reflection coefficient of  $-53.5$  dB. According to the outcomes realized, it can be inferred that the proffered THz antenna would be an excellent solution for various applications in terahertz regime, including the explosive detection, material characterization, homeland defense, security scanning, biomedical imaging, sensing, video rate imaging system and the upcoming short-range high-speed wireless indoor communications.

**Keywords** Graphene · Terahertz · UWB · Antenna · Plasmonic · Indoor communication · High speed

---

A. Khabba (✉) · J. Amadid · Z. E. Ouadi · S. Ibnyaich · A. Zeroual  
Instrumentation, Signals and Physical Systems (I2SP) Team, Faculty of Sciences Semlalia, Cadi Ayyad University, Marrakesh, Morocco  
e-mail: [asma.khabba@edu.uca.ac.ma](mailto:asma.khabba@edu.uca.ac.ma)

L. Wakrim  
Laboratory of Innovation in Management and Engineering for Business (LIMIE), Higher Institute of Engineering and Business (ISGA), Marrakesh, Morocco

A. J. A. Al-Gburi  
Department of Electronic and Computer Engineering (FKEKK), Center of Telecommunication Research and Innovation (CeTRI), Universiti Teknikal Malaysia Melaka (UTeM), Durian Tunggal, Malacca, Malaysia

## 1 Introduction

During the past few years, the revolutionary advancement in wireless communications technologies generated a real need to an inexhaustible frequency bandwidth to fulfill the requirements of channel capacity, colossal data traffic rate, and uninterrupted connectivity [1–6]. These needs have attracted the researchers' interests toward a new massive frequency band spectrum, namely terahertz (THz) band. The latter is an electromagnetic (EM) spectrum lying between millimeter wave and infrared regions and occupying the spectral band from 0.1 to 10 THz. The region of THz band has appeared as a key solution to achieve high speed, secure, highly reliable wireless communications and unprecedented advanced technologies [7, 8]. The THz band technologies are gaining a rapid development to support several high potential applications such as ultra-fast communication [9], medical diagnostic [10], explosive detection [11], chemical, viruses' detection [12], remote sensing [13], imaging system [14], material characterization [15] and spectroscopic detection [16]. Indeed, the terahertz spectrum are able to hold up all these data-hungry applications due to many benefits like the enormous available frequency band, improved anti-interference performance, low diffraction and high spectral resolution compared to millimeter wave (mm-Wave) spectrum. However, the severe atmospheric path attenuation constitutes a significant hurdles for the commercialization of THz wireless systems. Accordingly, developing a compact antenna with high efficient performance is of first concern to indemnify the wasted energy referred to the considerable path loss in THz regime [17]. The antenna is the key unit enabling the transmission of EM waves in THz wireless communication where its characteristics, including the compactness, the bandwidth, efficiency and gain, etc., affect directly the THz system performance. This will inherently raise several defiances to the experts of antenna community and usher in a new era in the realm of planar antenna technology. In the other side, graphene material arouses a considerable scientific attentiveness due to its exceptional mechanical and electrical traits. It is explored as miracle substance enabling the good exploitation of terahertz portion [18]. Accordingly, many existing works are focused on graphene to design different antennas structures for THz applications, for instance, in Ref. [19], a THz antenna with graphene material is proposed for multiband application at 1.73/2.6/4.01/4.72 THz. In Ref. [20], a photoconductive dipole antenna is designed using graphene layer and put in comparison with a photoconductive dipole antenna made with gold metal, where a high emitted spectrum is reached while using graphene. In Ref. [21], a graphene patch antenna with superstrate is suggested to operate at 7 THz with total bandwidth of 386 GHz. Another graphene-based antenna with narrow bandwidth of 25 GHz is reported in [22]. In Ref. [23], a conventional patch antenna is presented with a total bandwidth of 280 GHz at 0.72 THz. In Ref. [24], a rectangular path antenna is created at 0.67 THz with only 40 GHz of bandwidth. Similarly in Ref. [25], a modified patch antenna is modeled using graphene as radiating material to work at 0.62 THz. The photonic band gaps were implanted in the substrate, while a restricted bandwidth of 34.9 GHz is reached.

Taking into account the wide bandwidth requirement for high data rate transmission, the main objective of this research work is the development of a new THz antenna supporting the ultra-wide band operation while preserving a suitable radiation performance and extremely small dimensions. This purpose is successfully accomplished by developing a teeny circular ring antenna powered by a 50  $\Omega$  microstrip feed line and backed by a full ground plane. The conducting parts of the proposed antenna are made of graphene material, while silicon substrate is chosen to build the design.

The remaining of the paper is organized as follows: The next section is allowed to introduce the graphene material and modeling. Section 3 presents the proffered antenna geometry. The antenna evolution procedures is studied in Sect. 4. A careful parametric study is done in Sect. 5. Section 6 brings the main achieved results. A comparative study is taken place in Sect. 7. Finally, Sect. 8 summarizes the performed study.

## 2 Modeling of Graphene Material

Graphene is a staggering carbon-based material with spectacular optical, electrical and mechanical properties. It is considered the magic key to entering the terahertz world through its wide door. In addition, one of the most advantage of graphene is the capability to support the transmission of surface plasmon polaritons (SPPs) waves on its surface which can be employed for miniaturization process even for antennas or other applications [26]. Indeed, the graphene surface plasmon polaritons are highly tunable and marked by low consumption, ultra-fast carrier mobility and strong localization [27]. The SPPs propagation as well as the graphene resonance are heavily depending on its complex electrical conductivity, where the latter is mainly depends on the key parameters, namely relaxation time ( $\tau$ ) and chemical potential ( $\mu_c$ ), i.e., (Fermi energy). Hence, the chemical potential can be altered through chemical doping or by applying electrostatic gate bias [28]. For an infinitesimally thin graphene surface with random-phase approximation (RPA), the surface electric conductivity ( $\sigma_s$ ) can be represented mathematically with the assistance of Kubo Formula which is denoted by Eq. (1) [21, 29], where, Fermi Dirac distribution is denoted by  $fd(\varepsilon) = \left( e^{\frac{\varepsilon - \mu_c}{k_B T}} + 1 \right)$ , and the collision frequency is represented by  $\Gamma = 1/2\tau$ .

Furthermore, the graphene total conductivity ( $\sigma_g$ ) [30] can be obtained by summing the two conductivity parts, the first part is the intra-band conductivity ( $\sigma_{\text{intra}}$ ), while the second is the inter-band conductivity ( $\sigma_{\text{inter}}$ ). The intra-band conductivity controls the graphene characteristics in infrared region, where the approximated Eq. (2) is given by Dured model, where  $q$  is the electron charge, Boltzmann constant is denoted by  $k_B$ ,  $T$  is the effective carrier temperature in Kelvin, reduced Plank constant is given by  $\hbar = h/2\pi$  and  $\omega$  is the angular frequency of the incident wave. Damping constant is expressed as  $\Gamma_c = q \hbar v_F^2 / \mu \mu_c$ , where,



$\mu = 10^4 \text{m}^2 \cdot \text{V}^{-1} \cdot \text{s}^{-1}$  is the electron mobility and  $v_F^2 = 10^6 \text{m} \cdot \text{s}^{-1}$  is the Fermi velocity. The other conductivity part, i.e., the inter-band conductivity, is dominating at higher frequency spectrum and it is expressed by Eq. (3).

$$\sigma_s = j \frac{q^2(\omega - j2\Gamma)}{\pi h^2} \left[ \frac{1}{(\omega - j2\Gamma)^2} \int_0^\infty \varepsilon \left( \frac{\partial f d(\varepsilon) - \partial f d(-\varepsilon)}{\partial \varepsilon} \right) \partial \varepsilon - \int_0^\infty \frac{f d(-\varepsilon) - f d(\varepsilon)}{(\omega - j2\Gamma)^2 - 4\left(\frac{\varepsilon}{h}\right)^2} \partial \varepsilon \right] \quad (1)$$

$$\sigma_{\text{intra}} = j \frac{q^2 k_B T}{\pi h(h\omega + j2\Gamma_c)} \left[ \frac{\mu_c}{k_B T} + 2 \ln \left( e^{\frac{\mu_c}{k_B T}} + 1 \right) \right] \quad (2)$$

$$\sigma_{\text{inter}} = j \frac{q^2}{4\pi h} \ln \left[ \frac{2|\mu_c| - (h\omega + j\Gamma_c)}{2|\mu_c| + (h\omega + j\Gamma_c)} \right] \quad (3)$$

The graphene material can be roughly modeled using the FIT-based (Finite Integration Technique) electromagnetic software, namely CST microwave studio for optical applications and terahertz spectrum. Accordingly, Fig. 1a and b expose the real and imaginary parts of the of the simulated graphene conductivity for various values of chemical potential ( $\mu_c$ ) and relaxation time ( $\tau$ ), respectively.

As illustrated, it can be clearly observed that the conductivity behavior changes significantly when augmenting the chemical potential ( $\mu_c$ ) and relaxation time ( $\tau$ ), which leads to produce a strong resonance at higher frequency range. Indeed, with the increase of chemical potential ( $\mu_c$ ), the absorption cross section raises and the resonance shifts toward high frequencies, where the same goes for relaxation time ( $\tau$ ). Hence, to tune the antenna resonance at high terahertz frequency, the graphene characteristics are chosen in the following manner; chemical potential ( $\mu_c$ ) is fixed at 2 eV, for the relaxation time ( $\tau$ ) is specified at  $10^{-12}$  s and the temperature T is chosen at 300 K.

### 3 Geometry of the Proposed THz Antenna

The configuration of the proposed antenna structure is exposed in Fig. 2. The antenna geometry is wisely built of  $2.4 \mu\text{m}$ -thick silicon substrate with permittivity  $\varepsilon_r$  of 11.9, tangent loss of 0.00025 and full area ( $W_s \times L_s$ ) of  $24 \times 24 \mu\text{m}^2$ . The proposed layout consists of a radiating annular ring with outer radius  $r_1$  and inner radius  $r_2$  of  $6.5$  and  $5 \mu\text{m}$ , respectively, powered by a  $50 \Omega$  microstrip feed line of length  $L_f = 5.6 \mu\text{m}$  and width  $W_f = 1.5 \mu\text{m}$ . A rectangular strip of width  $W_1 = 1.7 \mu\text{m}$  and length  $L_1 = 1.42 \mu\text{m}$  is placed at the outer edge of the annular ring, in the opposite direction to the feeding line for bandwidth enhancement goal. A full ground plane is used to back the structure, where the antenna conductive parts are made using  $0.4 \mu\text{m}$ -thick graphene layer.



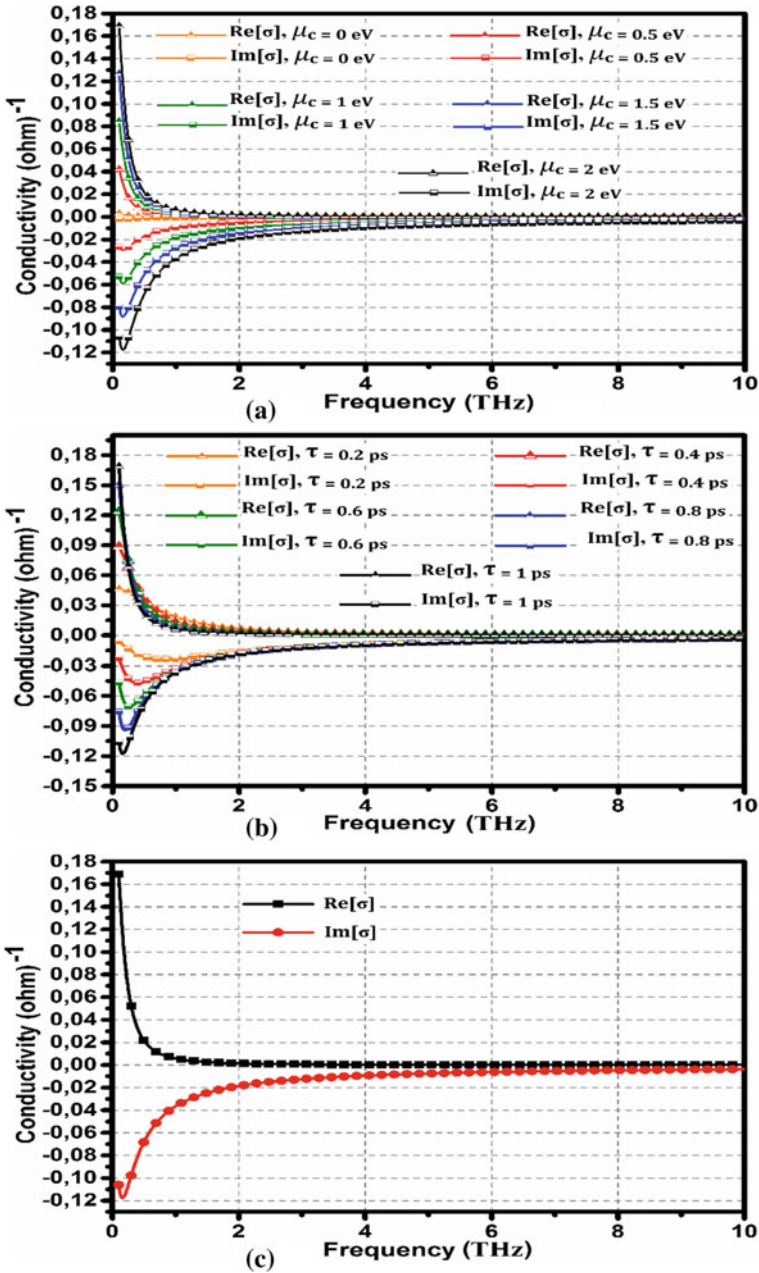
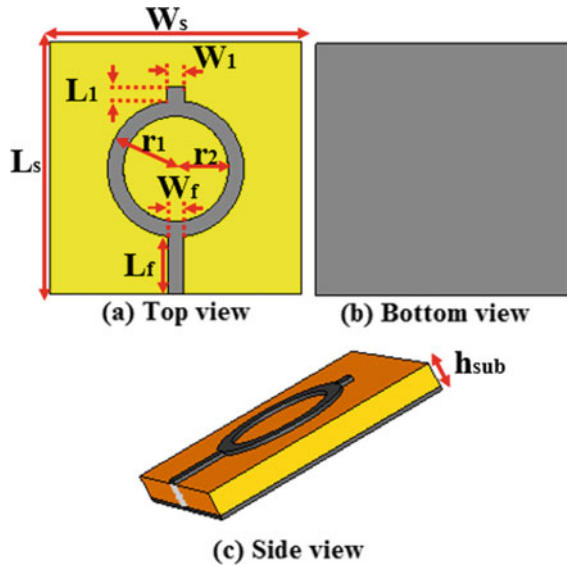


**Fig. 1** Conductivity variation with respect to **a** Chemical potential ( $\mu_c$ ), **b** relaxation time, **c** conductivity of proposed graphene with  $\mu_c = 2$  eV,  $\tau = 10^{-12}$  s and  $T = 300$  K

**Fig. 2** Layout of the graphene-based suggested antenna



A careful design construction and intense parameter optimization are made using the above mentioned software to reach the most-refined version of the suggested antenna providing the desirable operation. To find out the antenna design methodology, the next section investigates the antenna evolution procedure.

#### 4 Evolutionary Stages of the Suggested Antenna

In order to comprehend the operation principle of the proposed antenna design, Fig. 3 displays the essential evolution steps through which the final antenna geometry with the desired operation is reached. As clarified, the proposed antenna is the ameliorated version of the basic Circular Microstrip Patch Antenna (CMPA) developed over three essential steps, where the frequency response for all design steps is collected in Fig. 4. As demonstrated in Fig. 3a, the first step is accomplished by designing a conventional CMPA with complete ground plane, where the patch radius  $r_1$  is preliminary approximated using Eqs. (4–5). Then the overall dimensions refinement is done with the assistance of CST software to bring the antenna resonance in the band of interest. As perceived in Fig. 4, the conventional CMPA (Antenna-1) was firstly modeled to resonate around 8 THz frequency, however, the total bandwidth is only 177 GHz, while the impedance matching needs a considerable improvement. Hence, to extend the operating bandwidth and the impedance matching, geometrical modifications are required. Accordingly, in the second step exposed in Fig. 4, the basic CMPA is converted to an annular ring microstrip patch antenna (Antenna-2) by creating a circular slot with a radius  $r_2$  inside the resonant patch. As expected,

the reflection coefficient in Fig. 4 shows a great bandwidth enhancement from 177 to 720 GHz after adding the circular slot where a strong resonance is created at 8.11 THz. This is obtained through a fine refinement of the slot radius  $r_2$  which is fixed at  $5 \mu\text{m}$ , where the latter is approximately seventh wavelength ( $\frac{\lambda}{7}$ ) at 8.11 THz.

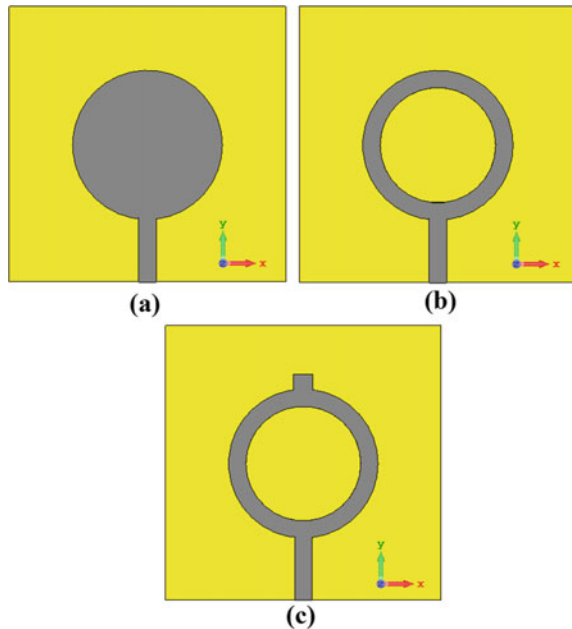
$$r_1 = \frac{F}{\left\{ 1 + \frac{2h_{\text{sub}}}{\pi \epsilon_r F} \left[ \ln\left(\frac{\pi F}{2h_{\text{sub}}}\right) + 1.7726 \right] \right\}^{1/2}} \tag{4}$$

$$F = \frac{8.791 \times 10^9}{f_r \sqrt{\epsilon_r}} \tag{5}$$

Hence, to well comprehend the circular slot effect, Fig. 5 shows the electric field distribution of the SPP before and after adding the slot. As configured, the etched slot has led to a strong confinement of the electric field propagation in the substrate inside the annular ring which enables the antenna to form its first resonance around 8.11 THz. Finally, as visualized in Fig. 3c, to get the coveted operation, a rectangular strip is inserted on the top edge of the annular ring which consequently contributes to reach the final design of the suggested antenna.

As can be seen in Fig. 4, the resonant strip engenders a new resonating frequency at 7.5 THz which bestowed further bandwidth-extension toward lower frequencies. The strip dimensions are properly tuned to extract the optimal antenna behavior

**Fig. 3** Stepwise design evolution, **a** Antenna-1 (Conventional antenna), **b** Antenna-2 (Ring antenna), **c** Proposed antenna



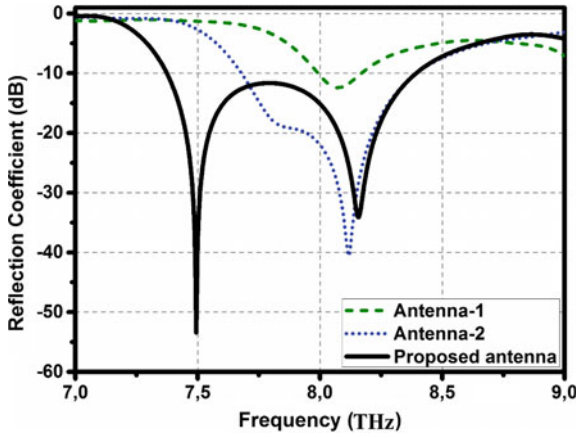


Fig. 4 Reflection coefficient of the evolutionary designs

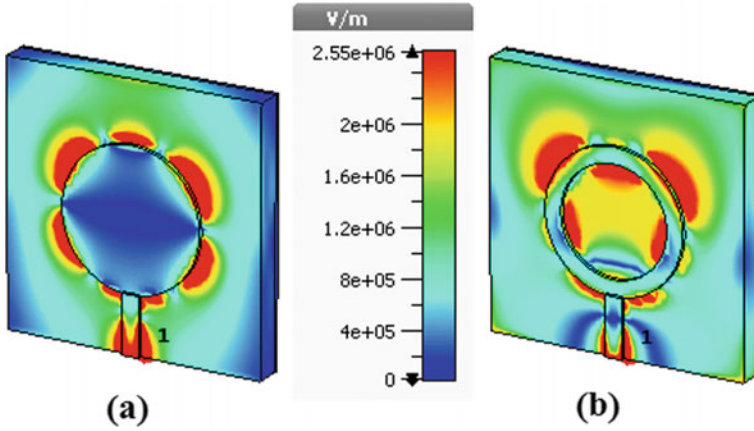


Fig. 5 SPP electric field distribution, a Antenna-1 at 8.07 THz, b Antenna-2 at 8.11 THz

where its effect can be easily glimpsed by observing the electric field pervasion in Fig. 6.

As described, a strong electric field intensity is surrounding the rectangular strip at 7.5 THz which indicates its main rule to generate the mentioned resonating frequency, whereas at 8.15 THz, the electric field propagation remains intense in the annular ring slot. So, to deeply analyze the effect of the antenna parameters on its operation behavior, an accurate parametric study is done in the next section.

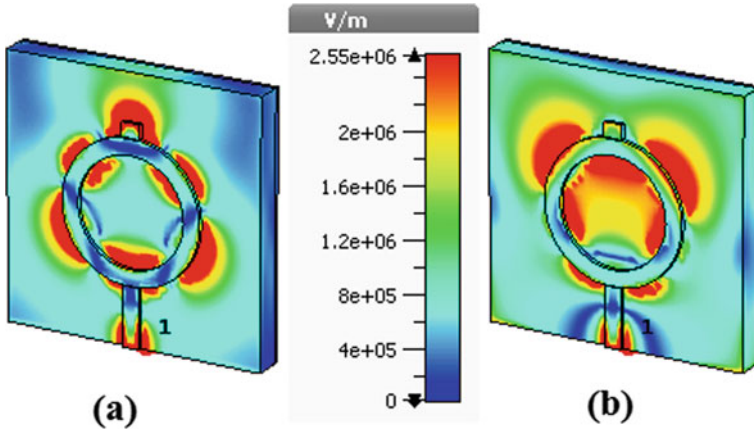


Fig. 6 SPP electric field distribution of the proposed antenna, a 7.5 THz, b 8.15 THz

### 5 Parametrical Analysis

Parametric analysis is an inevitable phase in antenna design to discover the optimal dimensions allowing the best antenna performance. Hence, this parametric analysis is performed with the intention to reveal the effect of the some basic parameters related to the annular ring and the rectangular strip on the antenna performance including the operating bandwidth, the impedance matching and the resonant frequencies. The influence of the inner radius  $r_2$ , the strip width  $W_1$  and length  $L_1$  is configured in Fig. 7. During the parametrical study, when altering a parameter, the other ones remain constant. As manifested in Fig. 7a, the reflection coefficient shows a hyper sensitivity and changes drastically when the inner radius  $r_2$  is increased from 3 to 6  $\mu\text{m}$ . Indeed, with  $r_2 = 3 \mu\text{m}$ , the antenna acts as multiband antenna with two resonant frequencies at 8.12 and 8.65 THz. The multiband operation converts to monoband operation around 8.21 THz when  $r_2$  is 4  $\mu\text{m}$ . The required operation is glimpsed when the inner radius  $r_2$  is 5  $\mu\text{m}$ , where the antenna bears an ultra-wide band of 1000 GHz and two resonant frequencies at 7.5 THz and 8.15 THz. However, when the inner radius  $r_2$  is augmented to 6  $\mu\text{m}$ , the impedance matching is distorted over the whole frequency range and inherently the operational bandwidth get lost. The effect of varying the rectangular strip width  $W_1$  is displayed in Fig. 7b. As shown, the slight variation of the parameter  $W_1$  from 1.3 to 1.9  $\mu\text{m}$  with a step of 0.1  $\mu\text{m}$  has a clear impact on the impedance matching of both resonating frequencies as well as the adjustment of the lower resonating frequency.

Indeed, it can be remarked that the latter is decreased from 7.59 to 7.5 THz when the width  $W_1$  increases from 1.3 to 1.7  $\mu\text{m}$  while it rising back to 7.53 THz when  $W_1$  is 1.9  $\mu\text{m}$ . The most suitable result is attained at  $W_1 = 1.7 \mu\text{m}$ . The outcome of swapping the strip length  $L_1$  is plotted if Fig. 7c.

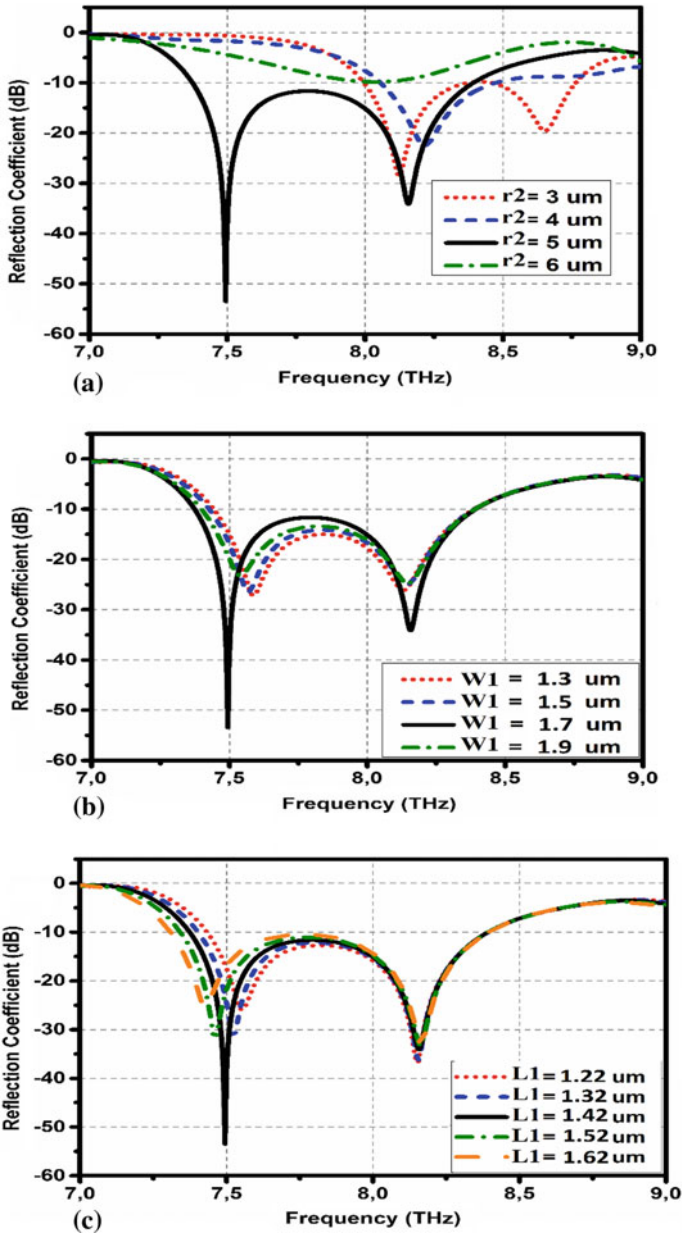


Fig. 7 Parametric analysis of the some key parameters, **a** inner radius  $r_2$ , **b** strip width  $W_1$ , **c** strip length  $L_1$

As exposed, the effect of altering the parameter  $L_1$  from 1.22 to 1.62  $\mu\text{m}$  has principally a direct influence on the lower resonance frequency and the impedance matching, while the higher resonance frequency value still unchanged. By increasing  $L_1$ , the first resonance shifts down from 7.55 to 7.42 THz, while the sought-after frequency response is acquired with  $L_1 = 1.42 \mu\text{m}$ . Consequently, the performed parametrical analysis assures the main role of the parameters, namely the inner radius  $r_2$ , the strip length  $L_1$  and width  $W_1$  to neatly control the reflection coefficient and adjust the resonant frequencies and operating bandwidth. In addition, they can properly amend the impedance matching to offer the best performance operation. After wisely analyzing the antenna parameters and describing their effect on the frequency response, the next section is dedicated to present the results and antenna performance.

## 6 Performance Results and Discussions

This section is allowed to present and describe the traits of the suggested antenna including the impedance and radiation characteristics.

### 6.1 Reflection Coefficient

As illustrated in Fig. 8, the suggested antenna bears an ultra-wide bandwidth of 1000 GHz from 7.4 to 8.4 THz with high impedance matching where the reflection coefficient at the first and second resonant frequencies reaches to  $-54 \text{ dB}$  and  $-34 \text{ dB}$ . The attained bandwidth could be used for various high-speed wireless applications in terahertz spectrum.

**Fig. 8** Reflection coefficient of the proposed antenna

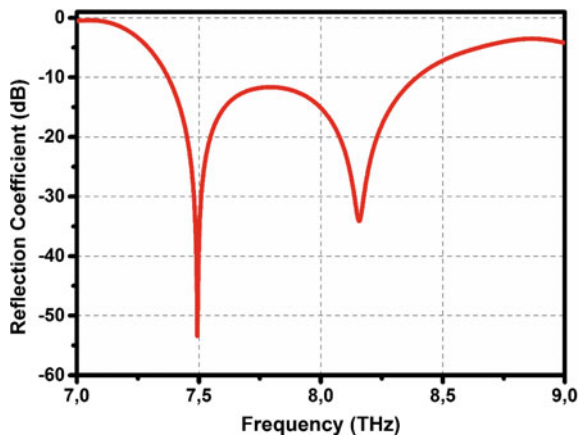
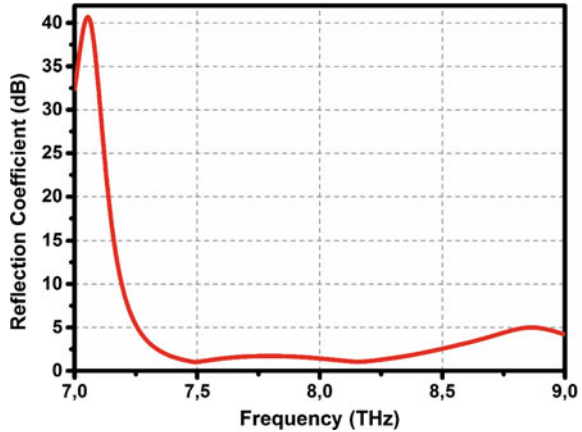


**Fig. 9** VSWR of the suggested antenna



## 6.2 Voltage Standing Wave Ratio

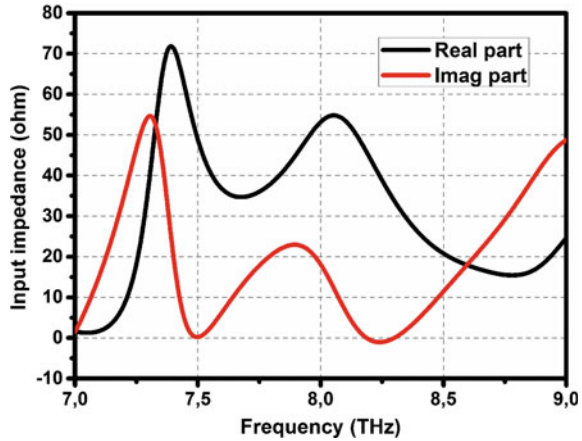
As the reflection coefficient, the Voltage Standing Wave Ratio (VSWR) can be used to visualize the impedance bandwidth of the proposed antenna. Indeed, the operational bandwidth can be determined when the VSWR is below 2. Accordingly, same as the reflection coefficient, the plotted VSWR in Fig. 9 shows a large operating bandwidth from 7.4 to 8.4 THz at VSWR < 2 which in turn indicates a good agreement and validates the operating band.

## 6.3 Input Impedance

The antenna input impedance ( $Z_{in}$ ) is the voltage to current ratio at the input of the antenna. It is a complex number where the input resistance is the real part  $\text{Re}[Z_{in}]$ , while the imaginary part  $\text{Im}[Z_{in}]$  is the input reactance. To fulfill a high impedance matching at a given frequency which inherently means a highly radiated power, the input impedance should be close to  $50 \Omega$ . This signifies that the real part must be close to  $50 \Omega$ , while the imaginary part should be near to zero. In the ideal case, the imaginary part of the input impedance is null and the real part is exactly  $50 \Omega$  which indicates that the antenna receives and radiates the total incident power. The input impedance of the proposed antenna is configured in Fig. 10, as can be seen the antenna realizes a high impedance matching at both resonance frequencies, where the real and imaginary parts ( $\text{Re}[Z_{in}]$ ,  $\text{Im}[Z_{in}]$ ) at the lower and higher resonance frequencies are  $(50.02, 0.2) \Omega$  and  $(49.23, 1.8) \Omega$ , respectively.



**Fig. 10** Antenna input impedance



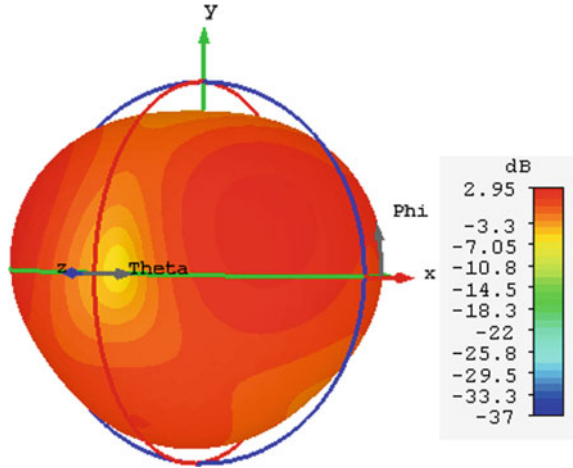
### 6.4 Radiation Patterns

The radiation pattern describes the variations of the radiated power in function of the direction away from the antenna. Hence, the three-dimensional radiation patterns 7.5, 7.8, 8 and 8.15 THz are plotted in Figs. 11, 12 and 13 and 14, respectively. In addition, the polar (2D) representation of the radiation pattern at the mentioned frequencies is illustrated in Figs. 15, 16, 17 and 18, respectively. As displayed, the 3D configuration assures a good and stable radiation behavior of the suggested antenna at all selected frequencies where the maximum gain achieved is 2.95, 3.57, 3.82 and 4.6 dB at 7.5 THz, 7.8 THz, 8 THz and 8.15 THz, respectively. Furthermore, the 2D radiation patterns at the above mentioned frequencies in the two cutting planes, i.e., H-plane ( $\phi = 0^\circ$ ) and E-plane ( $\phi = 90^\circ$ ) show for most frequencies a quasi-omnidirectional pattern in H-plane and bidirectional pattern in E-plane which demonstrates a uniform radiation. In the other side, the gain and radiation efficiency along the operating bandwidth are traced in Fig. 19. As displayed, the proposed design is marked by a good gain characteristic varying between 2.6 and 5 dB over the working band. In addition, an excellent radiation efficiency trait is remarked along the whole bandwidth where the minimum value is more than 97.5% and the maximum reached is up to 99.72%. After describing the achievements of the suggested antenna, a brief comparison with some existing work is reported in the next section to well evaluate the antenna performance.

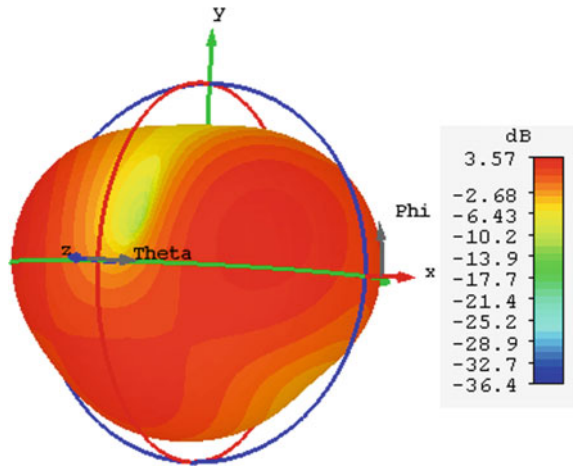
## 7 Comparison with Other Reported Work

Table 1 presents a comparative study of the proffered antenna performance with some other previous works. Certainly, many research are reported in the literature to propose different antenna design structure for the upcoming terahertz applications.

**Fig. 11** 3D radiation pattern at 7.5 THz



**Fig. 12** 3D radiation pattern at 7.8 THz



Indeed, as summed in the Table, the researchers was focusing on both lower and higher frequencies of terahertz spectrum to develop different antennas structures. However, all the assembled designs were marked by a narrow bandwidth, while some of them are limited by their low radiation efficiency. Hence, compared to the other previous works, the suggested antenna offers the widest bandwidth of about 1000 GHz with the highest radiation efficiency of 99.72%. Moreover, it provides a good comparable gain while preserving the most compact structure. As a result, all the mentioned traits allows the proposed antenna to be a suitable option for the wireless devices of terahertz applications.

**Fig. 13** 3D radiation pattern at 8 THz

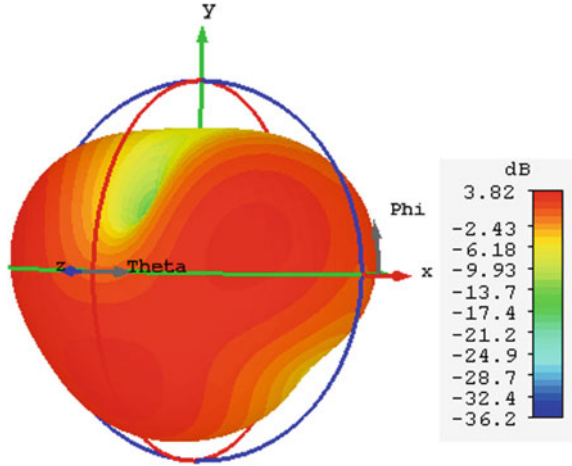
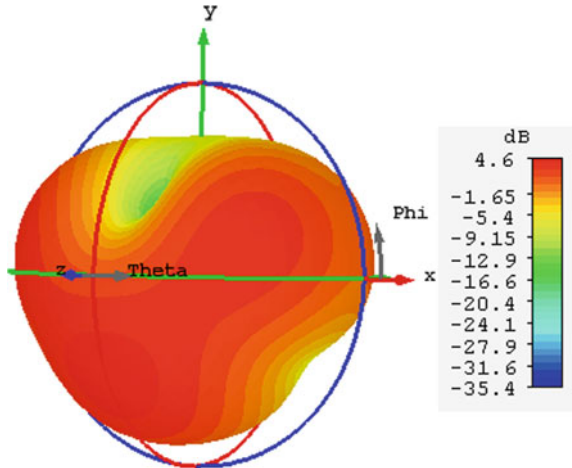


**Fig. 14** 3D radiation pattern at 8.15 THz



## 8 Conclusion

In this manuscript, an ultra-simple, ultra-wide band and super-tiny graphene-based annular ring antenna was developed and optimized for terahertz applications. The antenna was neatly designed using CST software to operate along a very wide terahertz spectrum range from 7.4 to 8.4 THz with high radiation efficiency reaches to 99.72% and maximum gain of 5 dB. The achieved results qualifies the proffered antenna to be a strong contender for terahertz wireless applications.

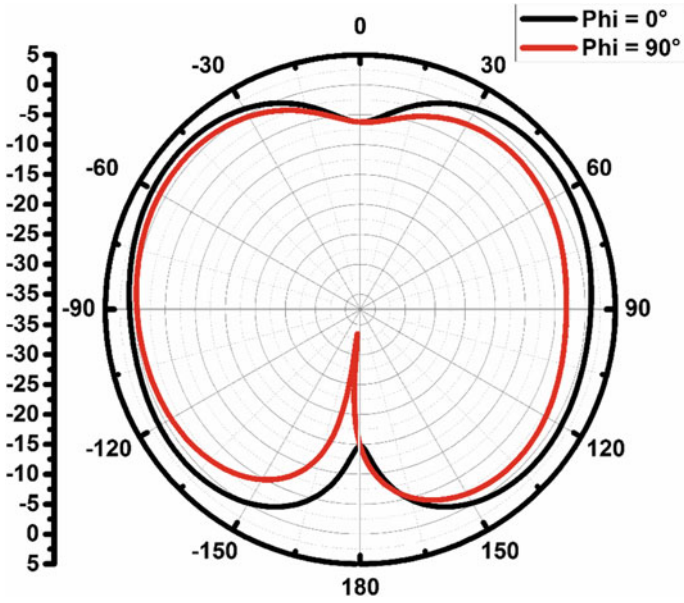


Fig. 15 Two dimension radiation pattern at 7.5 THz

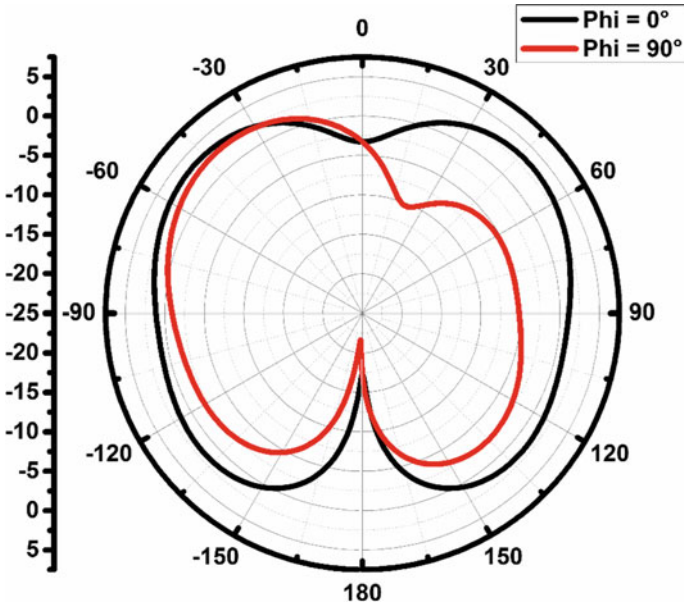


Fig. 16 Two dimension radiation pattern at 7 THz

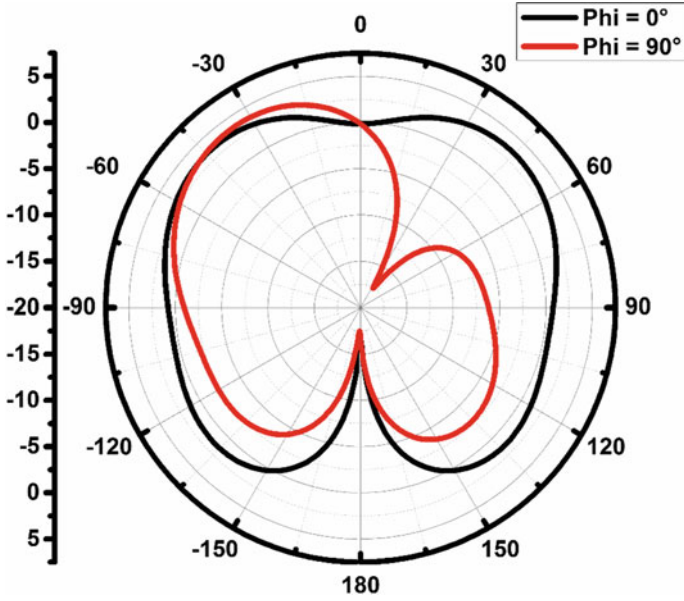


Fig. 17 Two dimension radiation pattern at 8 THz

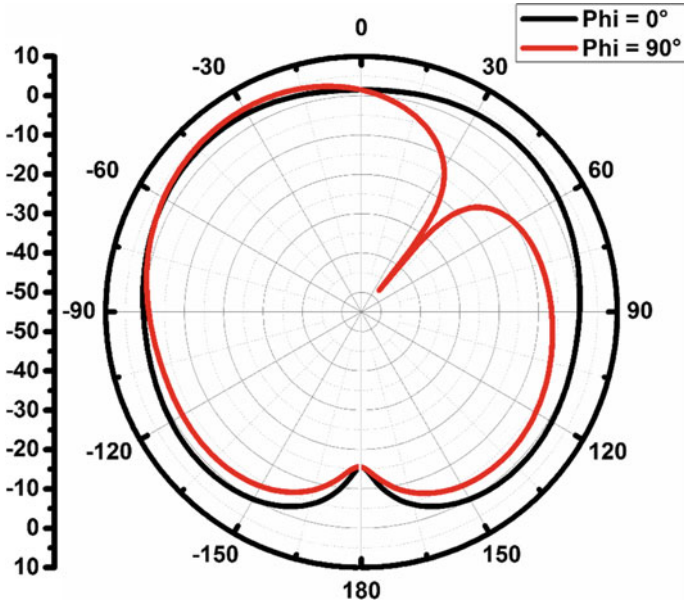


Fig. 18 Two dimension radiation pattern at 8.15 THz

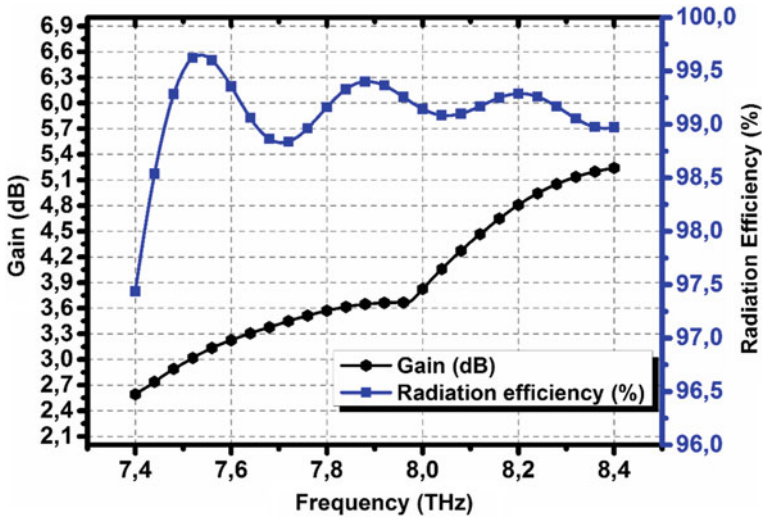


Fig. 19 Radiation efficiency and gain versus frequency

**Table 1** Comparison with other published works

References	Size ( $\mu\text{m}$ )	Substrate	Resonant frequency (THz)	Frequency range (THz)	Bandwidth (GHz)	Gain (dB)	Radiation efficiency (%)
[21]	$24 \times 24 \times 4.8$	Teflon ( $\epsilon_r = 2.1$ )	7	–	386	7.3	97.2
[23]	$120 \times 120 \times 45$	Arlon AD 1000 ( $\epsilon_r = 2.1$ )	0.72	0.57–0.84	270	–	–
[24]	$208 \times 422 \times 20$	Polyimide ( $\epsilon_r = 3.5$ )	0.67	0.65–0.69	40.16	5.22	–
[31]	$208 \times 433 \times 20$	Polyimide ( $\epsilon_r = 3.5$ )	0.75	0.725–0.775	50	5.09	86.58
[32]	$24 \times 24 \times 1.6$	Teflon ( $\epsilon_r = 2.1$ )	7.32	–	371	6.3	69.81
[33]	$28 \times 66.67 \times 2.5$	Polyimide ( $\epsilon_r = 3.5$ )	6.2	5.66–6.43	770	3.3	38.15
This work	$24 \times 24 \times 0.4$	Silicon ( $\epsilon_r = 11.9$ )	7.5 8.15	7.4–8.4	1000	5	99.72

## References

1. Xu, F., Lin, Y., Huang, J., Wu, D., Shi, H., Song, J., Li, Y.: Big data driven mobile traffic understanding and forecasting: a time series approach. *IEEE Trans. Serv. Comput.* **9**(5), 796–805 (2016)
2. Khabba, A., Wakrim, L., El Ouadi, Z., Amadid, J., Ibnyaich, S., Zeroual, A.: High gain double u-shaped slots microstrip patch antenna array for 28ghz 5g applications. In: 2022 International Conference on Decision Aid Sciences and Applications (DASA), pp. 1589–1592. IEEE (2022)
3. Khabba, A., Amadid, J., Ibnyaich, S., Zeroual, A.: Pretty-small four-port dual-wideband 28/38 ghz mimo antenna with robust isolation and high diversity performance for millimeter-wave 5g wireless systems. *Analog Integr. Circ. Sig. Process* **112**(1), 83–102 (2022)
4. Krishna, C.M., Das, S., Nella, A., Lakrit, S., Madhav, B.T.P.: A micro-sized rhombus-shaped thz antenna for high-speed short-range wireless communication applications. *Plasmonics* **16**(6), 2167–2177 (2021)
5. Khabba, A., Mohapatra, S., Wakrim, L., Ez-zaki, F., Ibnyaich, S., Zeroual, A.: Multiband antenna design with high gain and robust spherical coverage using a new 3d phased array structure for 5g mobile phone mm-wave applications. *Analog Integr. Circ. Sig. Process* **110**(2), 331–348 (2022)
6. Khabba, A., Amadid, J., Mohapatra, S., El Ouadi, Z., Ahmad, S., Ibnyaich, S., Zeroual, A.: Uwb dual-port self-decoupled o-shaped monopole mimo antenna with small-size easily extendable design and high diversity performance for millimeter-wave 5g applications. *Appl. Phys. A* **128**(8), 1–23 (2022)
7. Yang, P., Xiao, Y., Xiao, M., Li, S.: 6g wireless communications: Vision and potential techniques. *IEEE Netw.* **33**(4), 70–75 (2019)
8. Shafie, A., Yang, G.N., Han, C., Jornet, J.M., Juntti, M., Kurner, T.: Terahertz communications for 6g and beyond wireless networks: challenges, key advancements, and opportunities. *IEEE Netw.* (2022)
9. Huq, K.M.S, Rodriguez, J., Otung, I.E.: 3d network modeling for thzenabled ultra-fast dense networks: A 6g perspective. *IEEE Commun. Stand. Mag.* **5**(2), 84–90 (2021)
10. Yin, X.-X., Baghai-Wadji, A., Zhang, Y.: A biomedical perspective in terahertz nano-communications—a review. *IEEE Sens J* (2022)
11. Singh, M., Singh, S.: Design and performance investigation of miniaturized multi-wideband patch antenna for multiple terahertz applications. *Photonics Nanostruct. Fundam. Appl.* **44**, 100900 (2021)
12. Amin, M., Siddiqui, O., Abutarboush, H., Farhat, M., Ramzan, R.: thz graphene metasurface for polarization selective virus sensing. *Carbon* **176**, 580–591 (2021)
13. Dong, P., Liu, L., Li, S., Hu, S., Bu, L.: Application of m5 model tree in passive remote sensing of thin ice cloud microphysical properties in terahertz region. *Remote Sens* **13**(13), 2569 (2021)
14. Li, H., Li, C., Wu, S., Zheng, S., Fang, G.: Adaptive 3d imaging for moving targets based on a simo inisar imaging system in 0.2 Thz band. *Remote Sens.* **13**(4), 782 (2021)
15. Abdullah-Al-Shafi, M., Akter, N., Sen, S., Hossain, M.S.: Design and performance analysis of background material of zeonex based high core power fraction and extremely low effective material loss of photonic crystal fiber in the terahertz (thz) wave pulse for many types of communication areas. *Optik* **243**, 167519 (2021)
16. Hasan, M.M., Pandey, T., Habib, M.A.: Highly sensitive hollow-core fiber for spectroscopic sensing applications. *Sens. Bio-Sens. Res.* **34**, 100456 (2021)
17. Khaleel, S.A., KI Hamad, E., Parchin, N.O., Saleh, M.B.: Mtm-inspired graphene-based thz mimo antenna configurations using characteristic mode analysis for 6g/iot applications. *Electronics* **11**(14), 2152 (2022)
18. Tassin, P., Koschny, T., Soukoulis, C.M.: Graphene for terahertz applications. *Science* **341**(6146), 620–621 (2013)
19. Nissiyah, G.J., Madhan, M.G.: Graphene based microstrip antenna for triple and quad band operation at terahertz frequencies. *Optik* **231**, 166360 (2021)



20. Nissiyah, G.J., Madhan, M.G.: Graphene-based photoconductive antenna structures for directional terahertz emission. *Plasmonics* **14**(4), 891–900 (2019)
21. Khan, M., Kaium, A., Ullah, M., Kabir, R., Alim, M.A., et al.: High-performance graphene patch antenna with superstrate cover for terahertz band application. *Plasmonics* **15**(6), 1719–1727 (2020)
22. Nissiyah, G.J., Madhan, M.G.: A narrow spectrum terahertz emitter based on graphene photoconductive antenna. *Plasmonics* **14**(6), 2003–2011 (2019)
23. Shamim, S., Uddin, M.S., Hasan, M., Samad, M., et al.: Design and implementation of miniaturized wideband microstrip patch antenna for high-speed terahertz applications. *J. Comput. Electron.* **20**(1), 604–610 (2021)
24. Dhillon, A.S., Mittal, D., Sidhu, E.: Thz rectangular microstrip patch antenna employing polyimide substrate for video rate imaging and homeland defence applications. *Optik* **144**, 634–641 (2017)
25. Kushwaha, R.K., Karuppanan, P., Malviya, L.D.: Design and analysis of novel microstrip patch antenna on photonic crystal in thz. *Physica B Condens. Matter* **545**, 07–112 (2018)
26. Tang, W.X., Zhang, H.C., Ma, H.F., Jiang, W.X., Cui, T.J.: Concept, theory, design, and applications of spoof surface plasmon polaritons at microwave frequencies. *Adv. Opt. Mater.* **7**(1), 1800421 (2019)
27. Wang, Y., Liu, H., Wang, S., Cai, M., Ma, L.: Optical transport properties of graphene surface plasmon polaritons in mid-infrared band. *Curr. Comput.-Aided Drug Des.* **9**(7), 354 (2019)
28. Dash, S., Patnaik, A.: Impact of silicon-based substrates on graphene thz antenna. *Phys. E.* **126**, 114479 (2021)
29. Aloui, R., Zairi, H., Mira, F., Llamas-Garro, I., Mhatli, S.: Terahertz antenna based on graphene material for breast tumor detection. *Sens. Bio-Sens. Res.* 100511 (2022)
30. Cao, M., Xiong, D.-B., Yang, L., Li, S., Xie, Y., Guo, Q., Li, Z., Adams, H., Gu, J., Fan, T., et al.: Ultrahigh electrical conductivity of graphene embedded in metals. *Adv. Funct. Mater.* **29**(17), 1806792 (2019)
31. Anand, S., Kumar, D.S., Wu, R.J., Chavali, M.: Graphene nanoribbon based terahertz antenna on polyimide substrate. *Optik* **125**(19), 5546–5549 (2014)
32. Khan, M.A.K., Shaem, T.A., Alim, M.A.: Graphene patch antennas with different substrate shapes and materials. *Optik* **202**, 163700 (2020)
33. Thampy, A.S., Darak, M.S., Dhamodharan, S.K.: Analysis of graphene based optically transparent patch antenna for terahertz communications. *Phys. E Lowdimensional Syst. Nanostruct.* **66**, 67–73 (2015)

# Surrogate Optimization-Assisted Dual-Band THz Inverted-F Coplanar Graphene Antenna



K. C. Rajarajeshwari, T. Sathiyapriya, and E. L. Dhivya Priya

**Abstract** In this chapter, we employed graphene to design a dual-band terahertz patch antenna. The computational results demonstrate that the proposed inverted-F coplanar graphene antenna (IFCGA) structure could provide outstanding dual wide-band performance and frequency reconfiguration by incorporating some parameter optimization on graphene conductor. The conductivity and Fermi level of graphene will change as that the attributes of host material could be modified through varying external voltage level and also by changing the doping level of graphene. Due to its excellent electrical conductivity and optoelectronic characteristics in the THz frequency regime, graphene coplanar antenna possesses better functionality in terms of more stable UWB performance, increased miniaturization, and simple adjustment. At higher frequency, there exists an aberrant condition of cross-polarization in conventional microstrip transmitter and receiver antennas. To cover a long-distance connection, a graphene-based antenna structure is employed to provide higher efficiency and low cross-polarization in comparison with conventional transmitter and receiver antennas. Initially, the antenna was constructed using pure graphene versus doped graphene, and then the optimizations were carried out to enhance the antenna performance at the desired frequency. Initially, the optimization parameters were fixed as multiple objectives like small size, front-to-back ratio, S11 (dB), and graphene purity. The reflection coefficient, gain, directivity, and efficiency increased when a reflective mesh was used below the antenna structure. The maximum results were achieved at 0.8 and 2.2 THz which can be used for various THz communications.

**Keywords** Surrogate optimization · THz range · IFCGA

---

K. C. Rajarajeshwari (✉) · T. Sathiyapriya  
Department of ECE, Dr Mahalingam College of Engineering and Technology, Pollachi,  
Tamil Nadu, India  
e-mail: [rajarajeshwari@drmcet.ac.in](mailto:rajarajeshwari@drmcet.ac.in)

E. L. D. Priya  
Department of ECE, Erode Sengunthar Engineering College, Erode, India

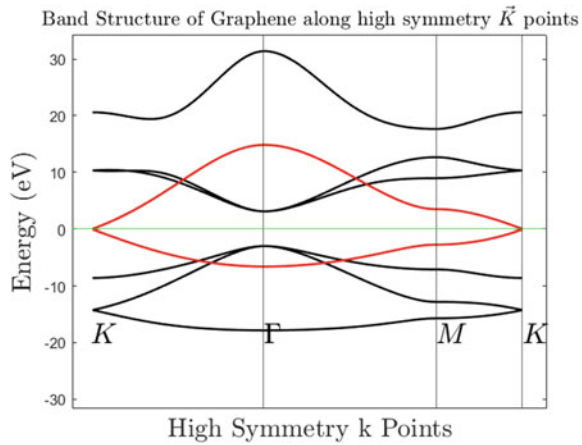
## 1 Introduction

Graphene is indeed the finest material that man has discovered around one atom thick, the lightest substance known, and the hardest compound found with a tensile strength 300 times that of steel. Keeping this in consideration, it may sound surprising to learn that carbon is the second most prevalent material inside the human system and the fourth highest common material in the world (by mass), behind all elements. As carbon is the elemental basis for all existing life on this planet, graphene has the potential to be an environmentally friendly, viable solution for an almost infinite number of uses. One of the main goals of contemporary technology is to supplant metals with lightweight, more affordable, and much less energy-intensive materials.

For engineering applications like aviation and the automobile industries, where the use of nitrogen materials (such as bio composites and elevated polymeric materials) is being pushed in the direction of substituting up to 50% of the metal components of the vehicle, this metal remediation primary objective is currently well defined. Humongous production of graphene thin films is currently required in order to supersede seamless conductors in applications like flexible screens, transparent TV, and solar cells. However, sheet resistance  $\ll 1 \Omega$  is necessary for potential implementation demanding the passage of large currents, such NFC antennae or microelectronics. Such structures do not demand substantial annealing, are made entirely of nanoparticles that include graphene without even any extra binders or metallic additives, and can sustain tens of millions of deformation cycles without losing function [4]. In this work a graphene-based antenna with a high ionic conductivity ( $4.20 \times 10^5$  S/m) that is equivalent to single crystal graphene but considerably better malleable and consumable structure is used. With these favorable characteristics as a foundation, we show the substance's technological maturity by creating, characterizing, and modeling antennas based on it. Such antennas outrank all other carbon-based conductor and can be used to satisfactorily completely replace electrically conductive commercial antennas in short range. We achieved high success through rigorous device optimization. Initially, we conducted a thorough comparison and selection of various materials, whether generated in the laboratory or commercially available at a low cost and in large quantities [3] (Fig. 1).

The electromechanical behavior of the concentration intra- and inter and the near electromagnetic field distribution is analyzed in terms of center frequency position, magnitude, and amplitude width. Furthermore, the structural elements' impact is assessed. Comprehensive simulation results are used to generate the radio frequency analysis. Simulation studies suggest that the nanoparticles may be utilized to effectively create subsequent graphene-based antenna elements functioning in the terahertz range [5]. It is impossible to just shrink conventional metallic transmitter and receiver antennas to nanoscale dimensions since doing so would necessitate ultrahigh resonant frequency. Therefore, it would take a significant amount of energy to run them. Additionally, the typical graphene antenna electrons really are not increasingly

**Fig. 1** Band structure analysis for grapheme [12]



dynamic at nanoscales, preventing the formation of the required electromagnetic radiation. Furthermore, given the special properties of graphene, these restrictions will not be a problem [1].

A collection of conductive material may fit inside a graphene flakes. As a result, it would therefore be feasible to implement an antenna from this substance. As a result, graphene is commonly used in microstrip antennas rather than copper since it can withstand continuous bending deformation. Researchers found that the graphene-based sheets possess higher conductivity than that of the copper or aluminum of both the rectangular frequency selective radiators, which is ideal for radio communication. Hence using carbon materials sheets for metamaterial array antennas to create radiofrequency antennas provides unique performances, compact design, and great adaptability. The approach of a nanoparticles inverted coplanar microstrip antenna for dual-band applications that rely on  $TM_{11}$  modes is discussed in this paper [2].

This paper deals with lot of subsections such as.

1. Design of feed/U-shaped slot for input feeding purpose.
2. Design of patch antenna with graphene as metal.
3. Addition of reflector plate structure to improve the radiation gain.
4. Replacement of reflector plate with reflector meshes to further enhancement of results.
5. Optimization using surrogate method for fixing the mesh and output results.

## 2 Design of U-Slot for Feeding Inverted-F Element

In this work, initially U-slot antenna was designed for feeding the proposed antenna as given in Fig. 2. The reflection coefficient must be reduced utilizing the short-pin approach to increase antenna gain. The input and short-pin locations are changed at each point of distance 0.45 mm from the previous one and the observations were noted

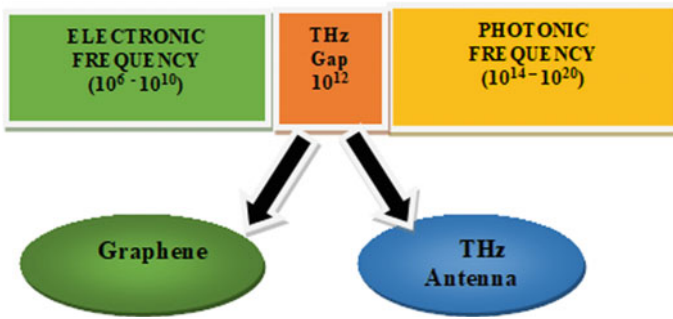


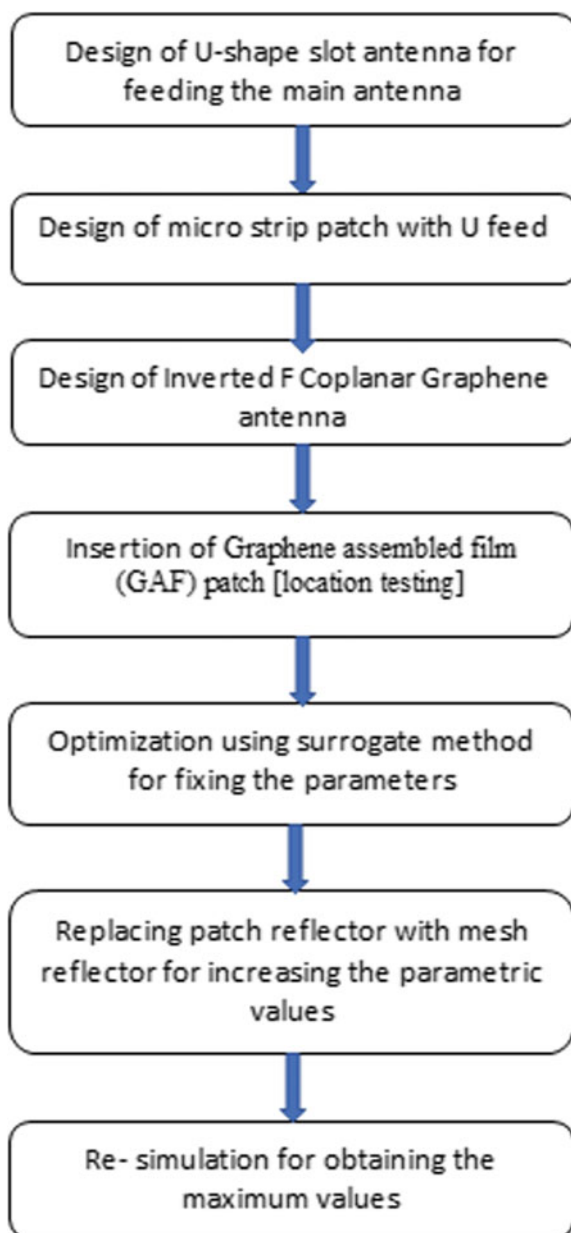
**Fig. 2** Role of graphene material in THz antenna

[10]. The U-slot antenna gave reflection coefficient of  $-18$  dB at 2.2 THz with a gain of 3 dB which will not be sufficient for long-distance applications. THz and sub-THz telecommunications involve the utilization of a frequency that covers the spectrum between (0.1–10) THz and (0.1–0.3) THz [11]. THz networks will be crucial in situations when very higher network speeds over small distances are demanded. Inside a 5 m range, the terahertz spectrum can be utilized for greater information transfer. This reception region is made up of mobile network tiny cells [8]. THz information can be communicated both indoors and outdoors, with both fixed and mobile users. Terabit wireless local area networks (T-WLAN) may connect wide range of data to fiber optical cables to portable smartphones and tablets with ease. In terahertz telecommunication, mobile and fixed channels have the same performance [6]. This reflection coefficient can be further improved by adding this slot as feed network for the proposed antenna. The detailed process involved in the design of the proposed antenna is given in Fig. 3.

The layout proposes an integrated model and then modifies it by using simulations in three phases. Firstly, the required bonding factor is determined. Secondly, CMA is employed to construct separable patches and slots with about similar frequency ranges. These two designs are then joined to form a complete U-slot patched antenna structure, and the comprehensive impedance is determined. If required, the shape can be adjusted using a few basic rules to provide a better resistance region. However, any array can be created entirely using simulation and quantitative optimization, and next designs are important for each fast-making great design also knowing the constraints and opportunities of system efficiency.

Regrettably first-principle explanation that involved the use of statistical procedure based on such is unusual in the research for broad range, linearly polarized U-slot antenna. This research applies characteristic mode analysis (CMA) [7] as well as coupled mode theory (CMT) to characterize the U-slot antenna in a novel manner and evolves a modeling approach relying mostly promised to give precepts, spanning previous analysis that provided evidence that now the dual bands of the

**Fig. 3** Process involved in design of inverted-F coplanar graphene antenna



U-slot antenna are pertaining to CMT, as shown in Fig. 4. The study advances knowledge and development of U-slot patch antenna by establishing that now the traditional U-slot patch antenna is regulated through CMT, as well as correctly defining both transceivers of the U-slot patch while creating an effective analogous device that specifically illustrates interaction between two resonators. Furthermore, a data transmission process for calculating resonance and a methodological approach based on the operating concept are presented. U-slot patch could well be created rapidly and effectively using the approach given.

The reflection coefficient was simulated for frequency between 0.1 and 3 THz, and the values are given below in Table 1. The best values are tabulated for reference, and the dual-band frequencies are 0.9 and 2.2 THz which deserve the maximum reflection coefficient. The dielectric volume distribution is shown in Fig. 4, and the dimensions of the U-slot are made as  $0.006 \times 0.04$  mm. In these, various feeds like edge, offset, center, and so on were employed, and among them, center feed best

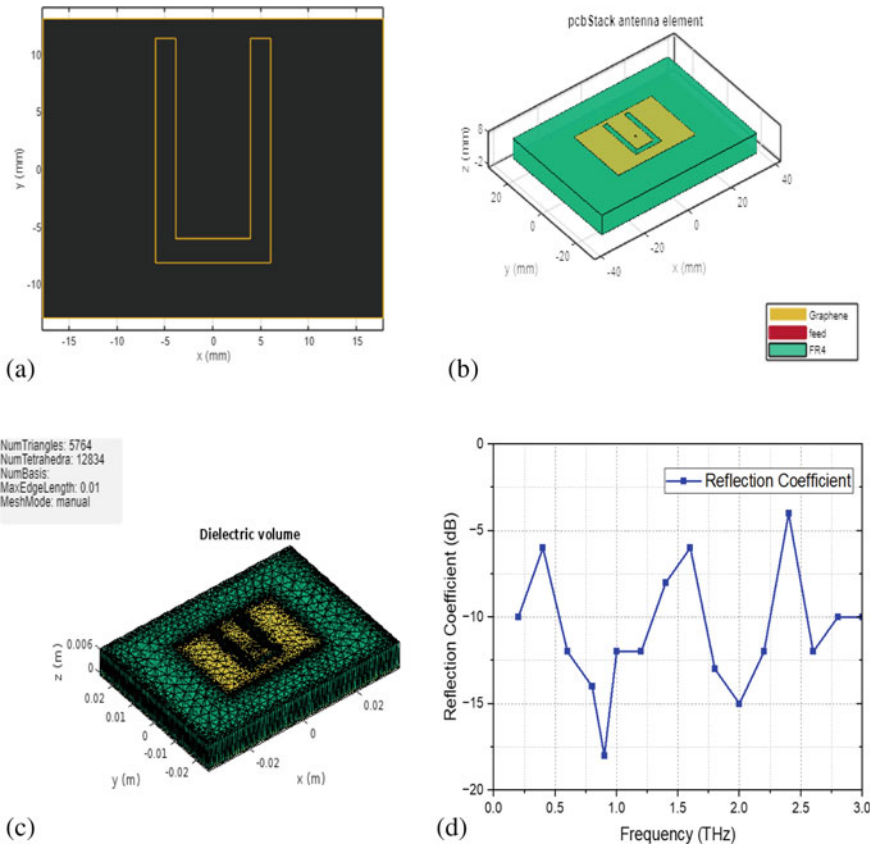


**Fig. 4** a Design of U-slot antenna, b design of U-shaped antenna with graphene and FR-4 substrate, c dielectric volume distribution for the proposed antenna, d reflection coefficient for U-slot antenna

**Table 1** Frequency versus reflection coefficient for U-slot

S. No.	Frequency (THz)	Reflection coefficient (dB)
1.	0.9	-18
2.	1.1	-12
3.	1.4	-15
4.	2.2	-18
5.	2.6	-13

suitied which will also be used to match with the inverted-F coplanar antenna feed [11].

### 3 Design of Inverted-F Coplanar Antenna

In the telecom sector, the planar inverted-F antenna (PIFA) is becoming more popular. This resonator is shaped like an inverted-F, therefore, named as PIFA. The planar inverted-F antenna is well-liked furthermore to its reduced size and omni-directional radiation pattern which can be used for dual- and multi-band applications. This feeding configuration enables the input to be flexibility coupled to slots available in the limited ground to introduce new frequency. To model and simulate approach, two *U*-slot designs followed by *F*-shaped antenna are developed and optimized. The perfect match between the predicted and experimental findings verifies the proposed dual-band antenna design. Initially, *U*-shaped antenna is designed, then a straight slotted line is inserted to form inverted-F shape, and then the feed is given. Graphene-assembled film (GAF) is used as reflector substrate to enhance the radiation properties and to avoid the spill over rays of antenna.

In the first stage without any reflector surface, the maximum reflection coefficient obtained is -18 dB and - 19 dB at 0.9 THz and 2.2 THz, respectively. Since the reflection coefficient is not sufficient for THz applications in order to enhance this, we have to find an alternate method. One such method is inserting the reflector sheet or mesh to improvise the reflection coefficient and gain of the antenna which is employed in this work. In order to enhance this, we can insert slot, change the feed system, add reflector surface, and so on [9]. Utilizing the layout of a rectangular or square radiating patch on the surface below, a specular reflection layer is generated with dual-layer rectangular microstrip patch antenna design [11]. Figure 5 depicts the shape and configuration of a graphene-assembled film (GAF). Gain improvement will be enhanced by altering multiple parameters like inner spacing dimension, external spacer equivalent diameter, linear slot diameter, and air gap/reflector distance. In this proposed system, a reflector of graphene-assembled film (GAF) sheet is inserted below the proposed antenna which gives maximum reflection coefficient of -23 dB and -25 dB at 0.9 THz and 2.2 THz, respectively [10], and further to increase the reflection coefficient to -39 and -41 dB at 0.9 THz and 2.2 THz, respectively. The reflection coefficient at various frequencies is listed in Table 2. The location of feed



point was fixed based on surrogate optimization technique. A surrogate optimization technique is frequently utilized to substitute the antenna modeling software in improving the effectiveness of antenna optimization design. Broad learning system (BLS) offers an alternate way for cognitive structure, which overcomes the time-consuming traditional simulation process, even though the accuracy not meets with traditional simulation methods.

The bottom sheet of commonly used antennae with such a graphene ground sheet reflects the EM waves, suppressing the spill over and losses of the field radiation pattern and improving reflection coefficient. But even so, the coplanar structure's central graphene antenna and GAF sheet are in the same plane. The antenna

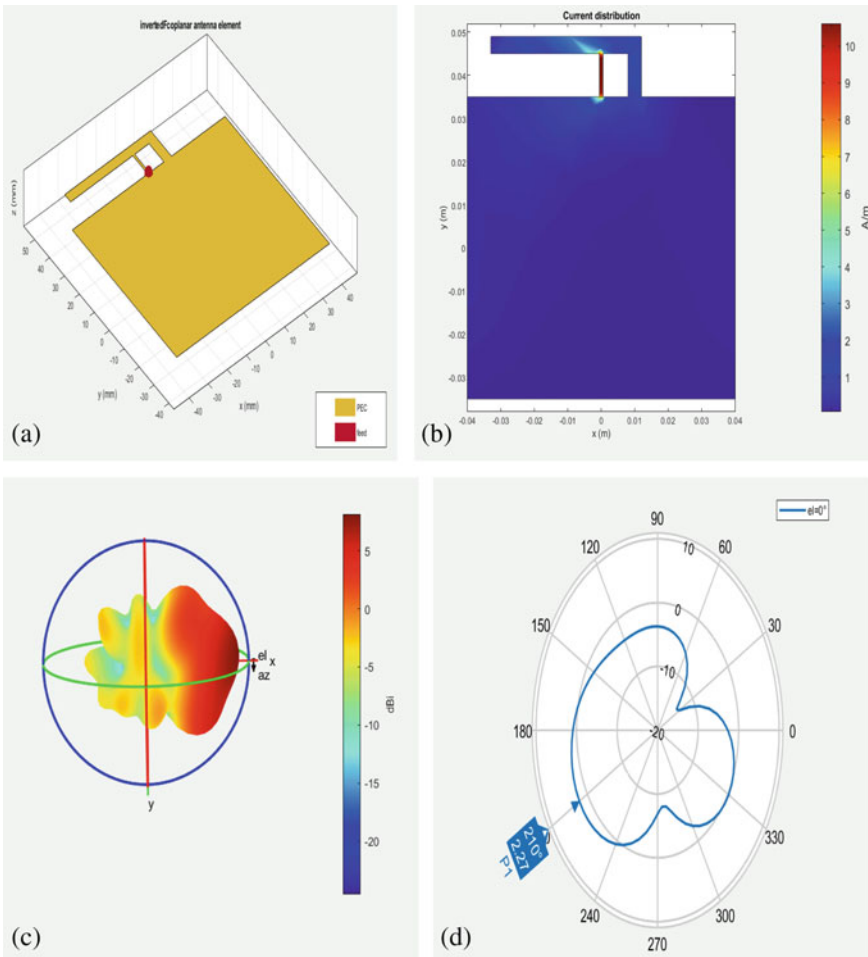


**Fig. 5** a Design of proposed system. b Current distribution pattern. c Directional pattern of the antenna. d Directional angle for the proposed antenna

**Table 2** Reflection coefficient of the proposed antenna

S. No.	Frequency (THz)	Reflection coefficient (dB)		
		Planar inverted-F antenna without any reflector	Planar inverted-F antenna with GAF reflector sheet	Planar inverted-F antenna with GAF reflector mesh
1.	0.2	-10	-11	-12
2.	0.4	-6	-16	-6
3.	0.6	-12	-18	-12
4.	0.8	-14	-16	-14
5.	0.9	-18	-23	-39
6.	1	-12	-13	-12
7.	1.2	-13	-14	-10
8.	1.4	-5	-18	-6
9.	0.6	-9	-9	-10
10.	0.8	-11	-11	-11
11.	2	-12	-14	-13
12.	2.2	-19	-25	-41
13.	2.4	-12	-17	-11
14.	2.6	-13	-15	-21
15.	2.8	-8	-13	-13
16.	3	-6	-9	-10

provides same radiation field pattern for both the top and the bottom parts. Perhaps as consequence, irrespective of whether the antenna is flexure bended, the resonance frequency moves consistently, and the susceptibility experimental findings of the radiating patch with all these different states show a comparable pattern.

The graphene film antenna’s flexibility may be considered as just a sensing material. When compressed, the device bends toward the graphene patch, and when tensioned, it bends toward the substrate. The physical elasticity of a graphene antenna detector is measured by conforming for varying diameters. Implantable electrical equipment are the fundamental building blocks of a human body LAN. Because of its near proximity toward the patient’s psyche, antenna adaptability and seclusion must be improved in order to retain excellent data signal quality. A stretchy wearable antenna device is made of graphene-assembled film (GAF).

The conformal mix of strong new components and elastic elastomer increases the antenna’s elasticity and thermal durability and, furthermore, the proposed coplanar inverted-F antenna. Hence, it can be very well used for IoT-coupled wearable antenna device which will assist in patient- and doctor-friendly environment.

### 4 Gain and Reflection Coefficient Enhancement Methods Using Reflector Mesh

Graphene array antenna can produce incredibly thin, maneuverable antenna waves; however, it is physically hard to form reflectors which produce electromagnetic waves having equivalent ranges with existing technology. Regardless of whether the physical dimension of reflectors and antenna arrays seems to be the same, smart antenna arrays allow the operator various degrees of freedom (DOF), spanning between internal rays to resultant beam patterns, but they are complicated to implement. On the other hand, reflector sheet or mesh does the job simpler on low cost without altering any angle.

The current distribution pattern and other parameters are shown in Figs. 6 and 7. In Fig. 6, the reflector used is solid surface, and the gain obtained is 7 dB, whereas in Fig. 7, the reflector used is mesh surface, and the gain obtained is 9 dB at 0.9 THz which is shown in Table 3.

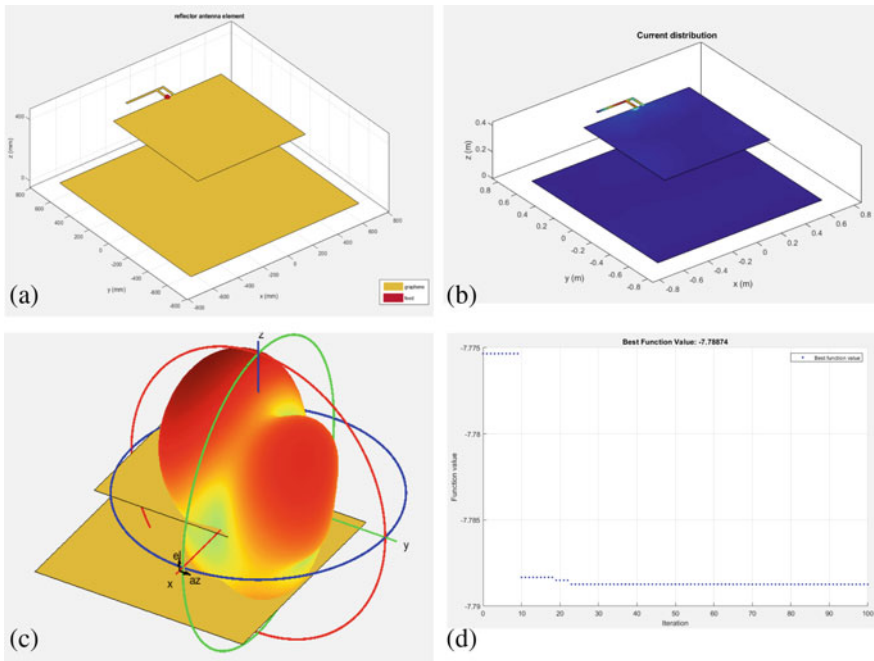


**Fig. 6** a Inverted-F coplanar antenna with reflector sheet, b current distribution of inverted-F coplanar antenna with reflector sheet, c directivity of inverted-F coplanar antenna with reflector sheet, d location of plane reflector based on surrogate optimization technique

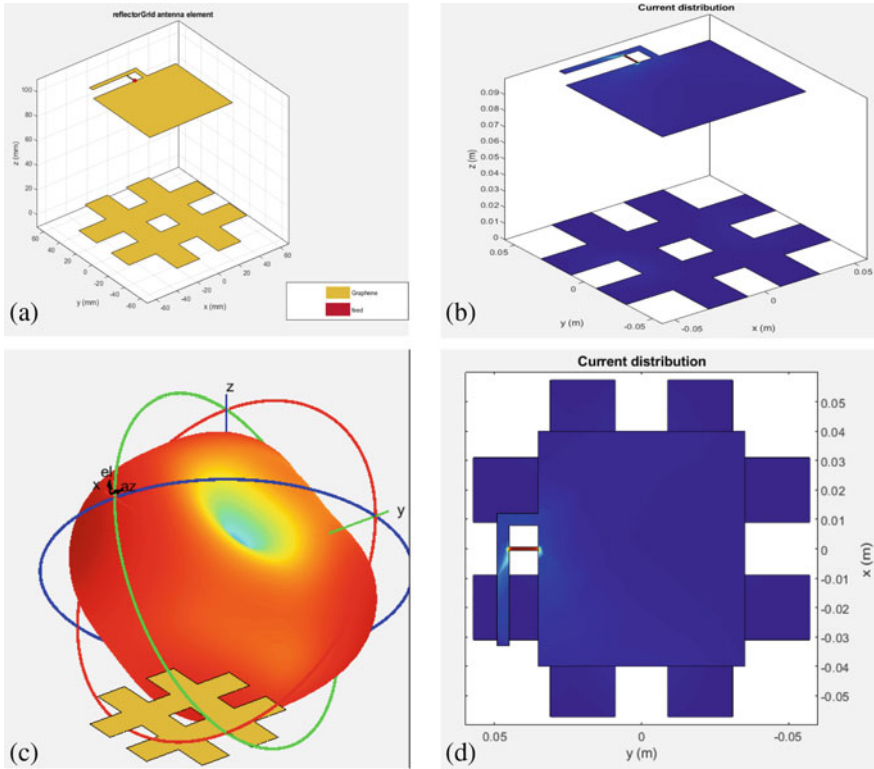


**Fig. 7** **a** Inverted-F coplanar antenna with mesh reflector sheet, **b** current distribution of inverted-F coplanar antenna with mesh reflector sheet, **c** directivity of inverted-F coplanar antenna with mesh reflector sheet, **d** top view

**Table 3** Gain of the proposed antenna

S. No.	Frequency (THz)	Gain (dB)		
		Planar inverted-F antenna without any reflector	Planar inverted-F antenna with GAF reflector sheet	Planar inverted-F antenna with GAF reflector mesh
1.	0.9	6	7	9
2.	2.2	5.6	6.8	8.6

### 5 Parametric Studies

The parametric studies section mainly involves the comparison of the different parametric value changes with respect to the reflection coefficient. In this section, we discuss on various results and their comparisons. In Fig. 8, the reflection coefficients for inverted planar graphene antenna without reflector, with planar reflector,

and mesh reflector are discussed. Out of all, mesh reflector gives the maximum gain and reflection coefficient. Similarly, Fig. 9 shows various gains for different antenna structures.

For further improvement, we replaced the normal reflector with mesh type and the dielectric constant of graphene. The mesh graphene provides improved results which are shown in Fig. 7. The reflection coefficient initially without reflector was just  $-18$  dB at  $0.9$  THz which is further enhanced to  $-23$  dB by using planar reflector and further enhanced to  $-39$  dB by using mesh reflector which is given in Table 4. Similarly, reflection coefficient initially without reflector was just  $-19$  dB at  $2.2$  THz which is further enhanced to  $-25$  dB by using planar reflector and further enhanced to  $-41$  dB by using mesh reflector and with dielectric constant of  $3.5$  which is given in Table 4.

**Fig. 8** Comparison of reflection coefficient for the proposed antenna without reflector, with planar, and grid reflector

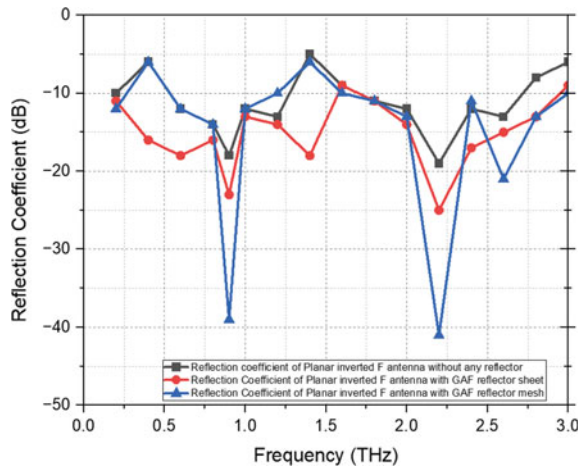


**Fig. 9** Comparison of gain for the proposed antenna without reflector, with planar, and grid reflector

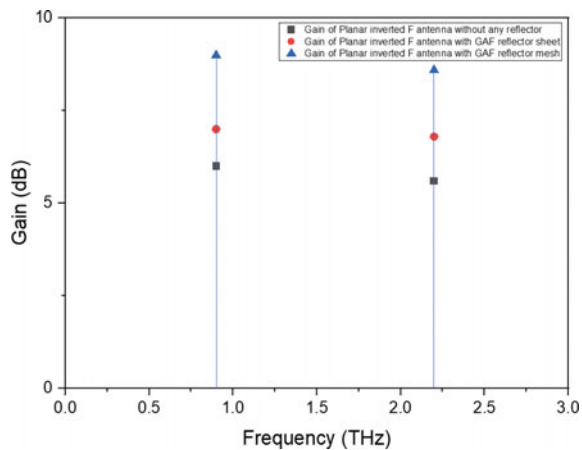


**Table 4** Reflection coefficient of the proposed antenna

S. No.	Frequency (THz)	Dielectric constant ( $\epsilon_r$ )	Reflection coefficient (dB)		
			Planar inverted-F antenna without any reflector	Planar inverted-F antenna with GAF reflector sheet	Planar inverted-F antenna with GAF reflector mesh
1.	0.9	3.5	-18	-23	-39
		4.5	-11	-15	-23
		6.5	-10	-13	-15
		9.5	-8	-11	-12

## 6 Conclusion

In this work, we designed a dual-band terahertz patch antenna. The simulation results show that the proposed inverted-F coplanar graphene antenna (IFCGA) structure provided an outstanding dual wide-band performance and frequency reconfiguration by incorporating some parameter optimization on graphene conductor. Initially, *U*-shaped slot was constructed for feeding and then inverted-F coplanar antenna. For further improvement, we replaced the normal reflector with mesh type and the dielectric constant of graphene. The mesh graphene provides improved parameters. The reflection coefficient initially without reflector was just -18 dB at 0.9 THz which is further enhanced to -23 dB by using planar reflector and further enhanced to -39 dB by using mesh reflector. Similarly, reflection coefficient initially without reflector was just -19 dB at 2.2 THz which is further enhanced to -25 dB by using planar reflector and further enhanced to -41 dB by using mesh reflector and with dielectric constant of 3.5 (Table 5).

**Table 5** Reflection coefficient of the proposed antenna

S. no	Frequency (THz)	Dielectric constant ( $\epsilon_r$ )	Reflection coefficient (dB)		
			Planar inverted-F antenna without any reflector	Planar inverted-F antenna with GAF reflector sheet	Planar inverted-F antenna with GAF reflector mesh
1.	2.2	3.5	-19	-25	-41
		4.5	-10	-13	-12
		6.5	-9	-11	-13
		9.5	-6	-8	-16

## References

1. Kazemi, A.H., Mokhtari, A.: Graphene-based patch antenna tunable in the three atmospheric windows. *Inter. J. Light Electron Opt.* **142**, 475–482 (2017)
2. Sirisha, M., Arun, M.: Dual-band reconfigurable graphene-based patch antenna in terahertz band for wireless network-on-chip applications. *IET Micr. A. Prop.* **11**, 2104–2108 (2017)
3. Tang, W., Politano, A., Guo, C., Guo, W., Liu, C., Wang, L., Chen, X., Lu, W.: Ultrasensitive room-temperature terahertz direct detection based on a bismuth selenide topological insulator. *Adv. Funct. Mater.* 1–9 (2018)
4. Shafi, M., Molisch, A.F., Smith, P.J., Haustein, T., Zhu, P., De Silva, P., Tufvesson, F., Benjebbour, A., Wunder, G.: 5G: a tutorial overview of standards, trials, challenges, deployment, and practice. *IEEE J. Sel. Areas Commun.* **35**, 1201–1221 (2017)
5. Wang, C.-X., Haider, F., Gao, X., You, X.-H., Yang, Y., Yuan, D., Aggoune, H., Haas, H., Fletcher, S., Hepsaydir, E.: Cellular architecture and key technologies for 5G wireless communication networks. *IEEE Commun. Mag.* **52**, 122–130 (2014)
6. Liao, L., Duan, X.: Graphene for radio frequency electronics. *Mater. Today* **15**, 328–338 (2012)
7. Kim, E., Ko, S.-T., Lee, Y.J., Oh, J.: Millimeter-wave tiny lens antenna employing U-shaped filter arrays for 5G. *IEEE Antennas Wirel. Propag. Lett.* **17**, 845–848 (2018)
8. Kazemi, A.H., Mokhtari, A.: Graphene-based patch antenna tunable in the three atmospheric windows. *Optik* **142**, 475–482 (2017)
9. Rajarajeshwari, K.C., Poornima, T., Gokul Anand, K.R., Kumari, S.V.: SIMO array characterized THz antenna resonating at multiband ultra high frequency range for 6G wireless applications. In: Das, S., Nella, A., Patel, S.K. (eds) *Terahertz Devices, Circuits and Systems*. Springer, Singapore (2022). [https://doi.org/10.1007/978-981-19-4105-4\\_7](https://doi.org/10.1007/978-981-19-4105-4_7)
10. Fan, H., Du, G., Lankanath, D., Yang, Q., Liu, F., Dong, Y., Chen, F., Uddin, N., Hou, X.: Tuning localized surface resonances in graphene based Au nanosphere dimer antenna. In: *Proceedings of SPIE 11052, 3rd International Conference on Photonics and Optical Engineering*, p. 110521E (2019). <https://doi.org/10.1117/12.2522151>
11. Song, R., Chen, X., Jiang, S., Hu, Z., He, D.: Graphene assembled film based millimeter wave antenna array for 5G mobile communications. In: *2021 IEEE MTT-S International Wireless Symposium (IWS)*, 2021, pp. 1–3. <https://doi.org/10.1109/IWS52775.2021.9499635>
12. Ali, M.A.: Tight Binding Electronic Structure of Graphene. <https://www.mathworks.com/matlabcentral/fileexchange/104035-tight-binding-electronic-structure-of-graphene> (2022). MATLAB Central File Exchange. Retrieved 16 Nov 2022

# Recent Advances in Graphene Oxide-Ferrite Hybrid Framework as Radar Absorbing Material



Ajay Singh, Sunil Sambyal, and Vishal Singh

**Abstract** The excessive usage of electronic devices results in tremendous increase in electronic pollutions such as electromagnetic interference (EMI) and electronic noise. In order to safeguard the electronic equipments from excessive electromagnetic waves, microwave absorbing/electromagnetic interference shielding materials has been continuously explored. These EMI shielding materials can be layered on military aircrafts, missiles, tanks, etc., so that they cannot be detected by the RADAR. Blocking of electromagnetic (EM) waves can be achieved by using shielding material such as conductive or magnetic. Owing to their superior electric, mechanical, thermal properties and large aspect ratio, graphene has gained much importance as microwave absorbing material. Electromagnetic shielding efficiency of graphene is 135 dB. On the other hand, the ferrites such as hexaferrite/spinel have attracted researchers as radar absorbing materials because these materials possess good magnetic as well as dielectric properties. However, neither ferrites nor carbon-containing materials (graphene, reduced graphene oxide, carbon black or carbon nanotubes) independently meet the EMI shielding properties such as large absorption peak, thin absorption layer and wide frequency range. To achieve high EM absorption properties, a material based on graphene oxide-ferrite nanocomposite has been synthesized and extensively investigated. As complex permittivity, permeability of material decides the EM absorption properties. The electric loss in composite is achieved by substituting losing fillers such as graphene/reduced graphene oxide to a matrix, and magnetic loss is provided by hexaferrite or spinel ferrite by means of big hysteresis attenuation in a matrix. This chapter reviews the research conducted in the field of

---

A. Singh (✉)

Department of Physics, GGM Science College, (Constituent College of Cluster University of Jammu), Canal Road, Jammu, UT of J&K 180002, India  
e-mail: [ajay.dadwal1234@gmail.com](mailto:ajay.dadwal1234@gmail.com)

S. Sambyal

School of Sciences, School of Applied Sciences, Shri Venkateshwara University, Gajraula, U.P. 244236, India

V. Singh

Department of Nano Sciences and Materials, Central University of Jammu, Bagla, Rahya Suchani, Jammu, UT of J&K 181143, India



microwave absorbing materials. The focus will be on the uniqueness and universality of graphene oxide-ferrite nanocomposites versus other unconventional materials in terms of materials chemistry and physics, electronic, magnetic characteristics, synthesis strategies and selected applications in an electromagnetic interference shielding.

**Keywords** Ferrites · Dielectric properties · Magnetic properties · EMI shielding

## Abbreviations

CFs	Carbon fibres
CNTs	Carbon nanotubes
dB	Decibels
EG	Expanded graphite
EM	Electromagnetic
EMI	Electromagnetic interference
ESD	Electrostatic discharge
FCI	Flaky carbonyl Iron
GO	Graphene oxide
ICPs	Intrinsic conducting polymers
$M_s$	Saturated magnetization
MUT	Material under test
MW	Microwave
MWCNTs	Multi-walled carbon nanotubes
NRW	Nicolson–Ross–Weir
PANI	Polyaniline
PMCs	Polymer matrix composites
PP	Polypropylene
PPy	Polypyrrole
RF	Radio frequency
RGO	Reduced graphene oxide
$RL_{\min}$	Minimal reflection
RL	Reflection loss
SCL	Short-circuit line
$SE_A$	Shielding effectiveness absorption
$SE_M$	Shielding effectiveness multiple reflection
$SE_R$	Shielding effectiveness reflection
SE	Shielding effectiveness
$SE_T$	Shielding effectiveness transmitted
SNA	Scalar network analyser
SWCNTs	Single-walled carbon nanotubes
VNA	Vector network analyser

## 1 Introduction

Electromagnetic pollution is escalating in our day-to-day life with steady extension of electronic technique such as advanced navigation and excessive usage of electronic devices such as computers, radio and mobile phones. The electromagnetic (EM) wave irradiation like microwave (MW) and radiofrequency (RF) has adverse effect on the functioning of electronic equipment and at the same time is also harmful to human health [1] in various forms such as psychological disorders, affect the immune system and also causing a problem in hereditary [2]. These EM waves produced from various components of electronic devices affect the functioning of other electronic devices and is called as electromagnetic interference (EMI). Source of EMI can be from other portable and compact electronic devices or from natural incidences such as solar flare and thunder [3, 4]. Due to EMI pollution, radar surveillance system is highly affected as it works in microwave frequency. Electromagnetic shielding of electronics without producing harmful effect on nearby devices and human health is the solution to eliminate EMI pollution [5, 6]. The history of EMI shielding is reported way back in 1830s when Faraday cage was discovered which is an encircled conducting house with zero electric field [7]. Another method to achieve EMI shielding is by developing lightweight and cost-effective materials which protect the environment and human health from EM waves.

Graphene/reduced graphene oxide (RGO) is most extensively explored for EMI shielding at high frequencies [8] owing to its excellent electrical properties [9], thermal stability, structural flexibility and high dielectric loss. However, graphene/RGO independently is not suitable for absorbing EM waves because for attenuation of EM waves in the material, both dielectric and magnetic losses are required. Therefore, a composite material consisting of hard/soft ferrite in combination with RGO/graphene is explored, and these composites complement the superior properties of graphene as well as ferrites.

This chapter reviews the research conducted in the field of microwave absorbing materials. The focus will be on the uniqueness and universality of graphene oxide-ferrite nanocomposites versus other unconventional materials in terms of materials chemistry and physics, electronic, magnetic characteristics, synthesis strategies and selected applications in an electromagnetic interference shielding.

## 2 Mechanism of EMI Shielding Process

EM waves undergo various mechanisms such as reflection, absorption, multiple reflection and transmission when interacting with the surface of any system. Out of these four, the main process involved to stop harmful EM waves is reflection and absorption.

For the attenuation of EM wave by reflection, the absorbing material should possess mobile charge carriers, i.e., fair conductivity ' $\sigma$ ' ( $S/m$ ) and permeability ' $\mu$ '. Example of such materials are Au, Ag, Cu and Al.

For absorption (or adsorption) mechanism, the electric and/or magnetic dipoles should be present in the absorbing material. For example, BaTiO<sub>3</sub> or dielectric material provide electric dipoles, and ferrous oxide (Fe<sub>2</sub>O<sub>3</sub>) provides magnetic dipoles. The electric ( $E$ ) and magnetic ( $H$ ) component of EM wave is decimated by the dipoles present in absorbing substance and converts it into thermal energy.

Another shielding mechanism is the multiple reflection. For multiple reflection, the absorbing materials should have large surface/interface area. For example, a composite material having one or more fillers (porous) is used as shielding material involving multiple reflection. Multiple reflections come into play when reflecting surfaces are at larger distance than the skin depth ( $\delta$ ).

When EM waves penetrate without attenuation through the shielding material, transmission is said to be high, for example, glass, polyester, and polypropylene (PP).

EMI shielding effectiveness (SE) of the material is due to attenuation because of reflection ( $SE_R$ ), absorption ( $SE_A$ ) and multiple reflections ( $SE_M$ ) and is measured in decibels (dB). EMI SE can be expressed in terms of electric ( $E$ ), magnetic ( $H$ ) or power ( $P$ ) intensities as the ratio of  $E$  (or  $H$  or  $P$ ) before and after attenuation is expressed as:

$$SE = 20 \log_{10} \frac{E_T}{E_I}; SE = 20 \log_{10} \frac{H_T}{H_I}; SE = 20 \log_{10} \frac{P_T}{P_I} \quad (1)$$

where subscripts ' $T$ '—transmitted EM wave and ' $I$ '—incident EM waves, respectively.

As the Schelkunoff's theory predicted that the EMI SE ( $SE_T$ ) is given by:

$$SE_T = SE_R + SE_A + SE_M \quad (2)$$

Reflection loss ( $SE_R$ ) at the surface of shielding material occurs due to mismatch between incident EM wave and impedance of shielding material and is given by:

$$SE_R = -10 \log_{10} \left( \frac{\sigma_T}{16f\epsilon\mu_r} \right) \quad (3)$$

where ' $\epsilon$ '—electric permittivity, ' $\mu_r$ '—relative magnetic permeability, and ' $f$ '—frequency and ' $\sigma_T$ '—total conductivity (in  $S/cm$ ).

From expression (3),  $SE_R$  depends on the ratio of  $\left( \frac{\sigma_T}{\mu_r} \right)$  and decreases with increasing ' $f$ ' for fixed  $\sigma_T$  and  $\mu_r$ .

When EM wave passes through the medium, its amplitude reduces exponentially. Absorption loss ( $SE_A$ ) of the absorbing material depends upon physical characteristics of the material and mainly occur due to the ohmic loss which results in the

heating of the material and is given by:

$$SE_A = 3.34t\sqrt{(f\mu_r\sigma_T)} \quad (4)$$

On rearranging the above equation, the expression for EMI  $SE_A$  is given as:

$$SE_A = -20\left(\frac{t}{\delta}\right)\log_{10} e = -8.68\left(\frac{t}{\delta}\right) = -8.68t\frac{\sqrt{(f\mu_r\sigma_T)}}{2} \quad (5)$$

where 't' is the material thickness. From Eq. (4),  $SE_A$  is the function of  $\mu_r$ ,  $\sigma_T$  and  $f$ . An absorbing material should have high ' $\sigma_T$ ', sufficient 't' and high ' $\mu$ ' to attain required ' $\delta$ ' at lower frequency 'f' [10, 11].

Attenuation due to multiple reflection ( $SE_M$ ) occurs in thin shielding material and is mathematically expressed as:

$$SE_M = 20\log_{10}\left(1 - e^{-\frac{2t}{\delta}}\right) = 20\log_{10}\left(1 - 10^{-\frac{SE_A}{10}}\right) \quad (6)$$

From Eq. (6), it is clear that  $SE_M$  and  $SE_A$  is closely related to each other. For thick shielding material,  $SE_A$  is high; thus,  $SE_M$  can be neglected. In other words, when  $SE_A \geq 10$  dB,  $SE_M \approx 0$  [12]. For thin metals, at high EM band frequencies ( $\geq$  GHz),  $SE_M$  plays a vital role.

The value of EMI SE of shielding material describes its application. For example, for a shielding material,  $SE < 10$  dB shows no shielding. For commercial and industrial applications, value of  $SE \geq 20$  dB as it attenuates 99% of striking EM waves [13, 14].

### 3 Techniques for the Preparation of Effective Absorbing Materials.

A better EMI shielding material should have improved complex permeability ( $\mu$ ), larger impedance matching value and strong interface polarization which results in the conversion of incident EM thermal energy into thermal energy. This combination of properties is offered by Fe-related materials. The various strategies for producing EMI shielding materials is discussed below:

#### 3.1 Hierarchical or Substituted Ferrites (Divalent/Trivalent Ion)

The two main processes that decide the absorption of EM wave are dielectric and magnetic losses. To achieve this, various morphologies of hierarchical Fe-based

structures such as flakes of  $\alpha$ -Fe<sub>2</sub>O<sub>3</sub> and Fe [15, 16], octahedral Fe<sub>3</sub>O<sub>4</sub> [17], Fe nanowires, urchin-like structures of Fe<sub>3</sub>O<sub>4</sub>,  $\alpha$ -Fe<sub>2</sub>O<sub>3</sub> [18], nanocapsules such as  $\alpha$ -Fe/ZnO,  $\alpha$ -Fe/SnO and Fe/Fe<sub>3</sub>B/Y<sub>2</sub>O<sub>3</sub> [19], dendritic structures of Fe, Fe<sub>3</sub>O<sub>4</sub> and  $\alpha$ -Fe<sub>2</sub>O<sub>3</sub> [20] and loose nano-Fe<sub>3</sub>O<sub>4</sub> [21] are explored. Shang et al. [17] investigated octahedral Fe<sub>3</sub>O<sub>4</sub> nanoparticles and showed that anisotropic structure of octahedral results in excellent magnetic properties. Zhang et al. [22] investigated flake carbonyl iron particles and observed reflection loss  $\sim$  12.2 dB at 4.4 GHz at 1 mm thickness. Substitution of divalent and trivalent impurities in ferrites showed great effect on EMI properties. For example, Al substituted Ba<sub>1.5</sub>Sr<sub>0.5</sub>CoZnAl<sub>x</sub>Fe<sub>12-x</sub>O<sub>22</sub>; (for  $x = 0-1$ ) hexaferrites, showed effective microwave absorption due to natural and domain wall resonance [23], NdCo substituted Sr<sub>1-x</sub>Nd<sub>x</sub>Fe<sub>12-x</sub>Co<sub>x</sub>O<sub>19</sub>; ( $x = 0-0.4$ ) showed enhanced electron hopping between Nd<sup>3+</sup> and Co<sup>2+</sup> ions, which results in complex permittivity of these ferrites and magnetic loss [24]. Li et al. [25] investigated Fe<sub>3</sub>O<sub>4</sub>/NiFe<sub>2</sub>O<sub>4</sub>/Ni heterostructures and showed that controlling Ni content and NiFe<sub>2</sub>O<sub>4</sub> interface layers results in improved impedance matching and dielectric losses and hence a broader absorption band.

### 3.2 Fe Alloying with Other Metals

An effective EMI shielding material should have high saturation magnetization ( $M_S$ ); therefore, Fe-based alloys are investigated because in comparison to pure metals, alloying increases saturation magnetization, interfacial polarization and permittivity, etc. For example, a lot of research activities are noticed in Fe alloying within dielectric materials such as carbon, ZnO, conducting and non-conducting polymers [26–30]. Feng et al. [31] investigated FeNi@C nanocomposites and observed that the interaction of dielectric and magnetic losses in this nanocomposite results in excellent microwave absorption performance. Choi et al. [32] investigated FeCo/EPDM composite and observed enhanced reflection loss by impedance mismatching.

### 3.3 Core@Shell Structures

A high-performance material can be synthesized by using core–shell strategy of Fe containing materials. Du et al. [33] investigated Fe<sub>3</sub>O<sub>4</sub>@C Core@Shell structure and observed that carbon coating increased complex dielectric permittivity owing to multiple relaxation processes. Guo et al. [34] investigated iron oxide@nSiO<sub>2</sub>@mSiO<sub>2</sub> core–shell structure and observed that the composites showed enhanced EMI SE in comparison to pure Fe<sub>2</sub>O<sub>3</sub>. Yu et al. [35] synthesized yolk–shell Fe<sub>3</sub>O<sub>4</sub>@ZrO<sub>2</sub> core@shell structure and observed that at 500 °C, the composite exhibits 90% reflection loss (RL). Liu et al. [36] investigated double-shelled Fe<sub>3</sub>O<sub>4</sub>@SnO<sub>2</sub> microspheres and observed synergistic effect between Fe<sub>3</sub>O<sub>4</sub> cores and SnO<sub>2</sub> shells and improved microwave absorption properties.

Chen et al. [37] synthesized  $\text{Fe}_3\text{O}_4$ @carbon nanorods structure and showed that the composite exhibit outstanding EM wave absorption properties because of porous structure and enhanced dielectric and magnetic loss. Zhu et al. [38] investigated  $\text{Fe}_3\text{O}_4$  polyelectrolyte (PE)@PANI/paraffin composite and observed that this composite exhibit an  $\text{RL}_{\min}$  of  $-6.5$  dB at  $14.3$  GHz. Thus, Fe-based core-shell composites show enhanced microwave absorption. The core@shell structure can be binary, ternary and quaternary.

The binary core@shell structures containing two different elements can be synthesized in following configuration: magnetic core@magnetic shell, magnetic core@dielectric shell and dielectric core@magnetic shell. The magnetic core@magnetic shell exhibits superior SE but result in reduction of dielectric loss and hence favour impedance mismatching. Example of magnetic core@magnetic shell is  $\text{Fe}_3\text{O}_4/\text{Co}$ . The magnetic core@dielectric shell has protective encapsulation which prevent agglomeration and oxidation of Fe metal nanoparticle as well as acts as link between dielectric and magnetic losses. Examples of magnetic core@dielectric shell materials are  $\text{Fe}_3\text{O}_4$ @ZnO core-shell [39], ZnO-coated iron nanocapsules [40], SnO-coated-Fe(Sn) nanocapsules [19], Fe@ $\text{Al}_2\text{O}_3$  [41],  $\text{Fe}_3\text{O}_4$ @ $\text{SnO}_2$  double shells [36], Fe@ $\text{SiO}_2$  nanoflakes [42], spinel  $\text{Fe}_3\text{O}_4$ @ $\text{TiO}_2$  [43], Fe nanoparticles with amorphous  $\text{Al}_2\text{O}_3/\text{FeO}_x$  composites shells [44] and yolk-shell  $\text{Fe}_3\text{O}_4$ @ $\text{ZrO}_2$  [35]. These composites show enhanced EMI SE. The dielectric core@magnetic shell structures show improved dielectric properties and interfacial polarization because of increased O-vacancy concentration. Example of dielectric core@magnetic shell is  $\text{CeO}_2$ @ $\text{Fe}_3\text{O}_4$  core-shell.

The ternary core@shell structures containing three different elements can be obtained by the dispersion of the core@shell structure into graphene, PPy or PVDF, etc. Examples of ternary core@shell structure are (CIP)@ $\text{SiO}_2$ @ $\text{Mn}_{0.6}\text{Zn}_{0.4}\text{Fe}_2\text{O}_4$  ferrite [45],  $\text{Fe}_3\text{O}_4$ @ZnO decorated graphene (GN-p $\text{Fe}_3\text{O}_4$ @ZnO) [46].  $\text{RL}_{\min}$  obtained of GN-p $\text{Fe}_3\text{O}_4$ @ZnO is  $-40$  dB at  $11.4$  GHz frequency.

The quaternary composites containing four different elements and can be obtained by the distribution of core@shell@shell heteronanostructures on substrates like graphite, graphene, CNTs, PANI, etc. In quaternary core@shell structures, the presence of multiple interfaces increases dielectric loss and hence promote multiple reflection because of complicated morphologies. Example of quaternary core@shell structures is  $\text{Fe}_3\text{O}_4$ @ $\text{SiO}_2$ @polyaniline wrapped with a graphene substrate [47] in which triple interface and junctions enhance the interfacial polarization and presence of active sites/void space between  $\text{Fe}_3\text{O}_4$  and PANI increases the reflection of EM waves.

## 4 Measurement Techniques for EMI Shielding

To measure the EMI SE of material experimentally, network analysers (NA) is used which can be classified into two types: scalar network analysers (SNA) and vector network analysers (VNA). To record the amplitude of electric signal only SNA is

employed, however, to record both amplitude as well as phase of different signal, VNA is employed. Thus, VNA can measure complex permittivity ( $\epsilon^*$ ), complex permeability ( $\mu^*$ ) and is widely used instrument.

In VNA, S—parameters viz.  $S_{12}$  (or  $S_{21}$ ) and  $S_{11}$  (or  $S_{22}$ ) are used to indicate incident and transmitted waves which are related to the coefficient of shielding mechanisms and is given as  $R = |S_{11}|^2 = |S_{22}|^2$  and  $T = |S_{12}|^2 = |S_{21}|^2$ ; where  $S_{11}$  or  $S_{22}$  and  $S_{21}$  or  $S_{12}$  are referred as forward reflection coefficient ( $S_{11}$ ), the reverse reflection coefficient ( $S_{22}$ ), the forward transmission coefficient ( $S_{12}$ ) and the backward transmission coefficient ( $S_{21}$ ). If the material under test (MUT) is uniform, then  $S_{11} = S_{22}$  and  $S_{12} = S_{21}$ . These S—parameters are related to the coefficients of shielding mechanism and are given as [49, 50]:

$$SE_T = 10 \log_{10} \left( \frac{1}{T} \right) = 10 \log_{10} \left( \frac{1}{S_{21}^2} \right) \quad (7)$$

$$SE_R = 10 \log_{10} \left( \frac{1}{1-R} \right) = 10 \log_{10} \left( \frac{1}{1-S_{11}^2} \right) \quad (8)$$

$$SE_A = 10 \log_{10} \left( \frac{1-R}{T} \right) = 10 \log_{10} \left( \frac{1-S_{11}^2}{S_{21}^2} \right) \quad (9)$$

and

$$R + T + A = 1 \quad (10)$$

The various conversion approaches have been used for calculating parameters such as  $\epsilon$ ,  $\mu$ , RL and Z: transmission line theory, short circuit line (SCL), Nicolson–Ross–Weir (NRW) technique and delta-function method. Among all techniques, transmission line and NRW techniques are widely used [48]. Parameters such as  $Z(\Omega)$  and RL(dB) are given by following equations:

$$Z = Z_0 \left[ \frac{1 + S_{11}}{1 - S_{11}} \right] \quad (11)$$

and

$$RL = 20 \log[S_{11}] \quad (12)$$

For measuring EMI SE, the three most commonly used configurations are described below:

(i) Rectangular Waveguide Method

For different frequency ranges, different size of rectangular waveguide is used. It has been observed that the dimensions of waveguide decreases as frequency increases. The benefit of this approach is that sample preparation is easy and very

simple, whereas its disadvantage is many waveguides are needed when measuring frequencies are in narrow range [49].

(ii) Coaxial Airline Method

In this approach, material under investigation needs to be synthesized in rectangular toroid shape and is placed at an accurate distance between internal and external conductors. The advantage of this procedure is that same sample is used in any frequency ranges; however, the disadvantage of this procedure is that much attention needs to be paid to prepare thin ring-shaped sample to avoid air gaps [49, 50].

(iii) Free Space Method

It is a contact-free procedure in which MUT is placed between two antennas. In this method, broad range of frequencies of EM radiations are incident on material under investigation. However, this approach requires thicker material in comparison to aforementioned methods.

## 5 EMI Absorbing Materials: A Brief Description

### 5.1 Iron (Fe) Ingredient

Iron is one of the most promising transition metals used in microwave absorption application. Fe-based nanostructures prepared by using DC arc plasma, ball milling and sputtering methods [51] have many advantages (high magnetic moment, high aspect ratio) as compared to bulk materials [52]. With changing air conditions, structural changes occur in Fe (orthorhombic, spinel) which results in changing electric, magnetic and optical properties. It has been observed that by pelleting Fe NPs in a paraffin matrix, the reflection loss  $RL_{\min} = 11$  dB at 13.6 GHz for Fe/paraffin = 4/1. In a dendrite-like microstructures of Fe, reflection loss  $RL_{\min} = 25.0$  dB at 2.5 GHz is observed. This is because of large surface area and defects [53, 54]. However, Fe exists in different size, shape and dimensions which results in enhancing reflection loss but have small value of conductivity. To solve this issue, ferric oxide, iron oxide, ferrous oxide (FeO), magnetite and iron hydroxide (FeOOH) have been preferred as EM shielding material because of their semiconductor behaviour (highly resistive) [55].

### Ferrites

Ferrite contain iron oxide along with other metal oxides and are useful in microwave devices because of their large saturation magnetization ( $M_S$ ) and high resistivity ( $0.1-10^{-5}$   $\Omega$ -m). Based on crystal structure, ferrites are of various types.

Spinel ferrite having formula  $PFe_2O_4$ , where  $P$  is divalent metal ions. Because of their moderate conductivity (semiconductor property) and large magnetic loss,



they are used as microwave absorbing materials, however, their natural magnetic resonance frequency is very low.

Garnet ferrites having formula  $\text{Pe}_3\text{Fe}_5\text{O}_{12}$ , where Pe is trivalent ion. Due to the presence of some extra sites (a dodecahedral  $c$  axis), their physical properties can be tuned by doping of cations at these sites [56]. Garnet ferrites having good chemical stability and magnetic properties (ferromagnetic) and can be used for EMI suppression.

Ortho-ferrites having formula  $\text{PeFeO}_3$ . Ortho-ferrites show good multi-ferroelectricity and tunable magnetic properties (weak/canted antiferromagnetism) [57].

Hexagonal ferrites having magnetoplumbite structure and possess high intrinsic magneto crystalline anisotropy which enables them to be useful in entire GHz range [58]. There are six types of hexagonal ferrites:  $M$ -type ( $\text{PFe}_{12}\text{O}_{19}$ , where  $P = \text{Ba, Sr, Mg, Pb}$  etc.),  $Y$ -type ( $\text{P}_2\text{Q}_2\text{Fe}_{12}\text{O}_{22}$  where  $P = \text{Ba, Sr, Mg, Pb}$ , and  $Q = \text{Cu, Co, Zn}$  etc.),  $W$ -type ( $\text{P}_2\text{Q}_2\text{Fe}_{16}\text{O}_{27}$ ),  $X$ -type ( $\text{P}_2\text{Q}_2\text{Fe}_{28}\text{O}_{46}$ ),  $Z$ -type ( $\text{P}_3\text{Q}_2\text{Fe}_{14}\text{O}_{41}$ ), and  $U$ -type ( $\text{P}_4\text{Q}_2\text{Fe}_{36}\text{O}_{60}$ ). In  $Y$ -type ferrite, substitution species such as divalent, trivalent and tetravalent improves their magnetic characteristics and hence enhanced microwave absorption [59].  $X$ -type ferrite is basically a combination of  $M$ - and  $W$ -type hexagonal ferrites and shows high Curie temperature and large ' $M_s$ ', and hence can be employed as excellent EM shielding materials.  $Z$ -type ferrites are used in antennas, inductors and absorbers [60].

### Ferric Oxide ( $\text{Fe}_2\text{O}_3$ )

Ferric oxides consist of four polymorphs:  $\alpha$ - $\text{Fe}_2\text{O}_3$ ,  $\beta$ - $\text{Fe}_2\text{O}_3$ ,  $\gamma$ - $\text{Fe}_2\text{O}_3$  and  $\epsilon$ - $\text{Fe}_2\text{O}_3$ .  $\alpha$ - $\text{Fe}_2\text{O}_3$  is known as hematite (rhombohedral-hexagonal structure),  $\gamma$ - $\text{Fe}_2\text{O}_3$  is known as maghemite (cubic spinel structure),  $\beta$ - $\text{Fe}_2\text{O}_3$  has cubic bixbyite structure, and  $\epsilon$ - $\text{Fe}_2\text{O}_3$  has orthorhombic structure. The  $\alpha$ - $\text{Fe}_2\text{O}_3$  is antiferromagnetic in nature and exist in different morphologies, whereas  $\gamma$ - $\text{Fe}_2\text{O}_3$  is ferromagnetic in nature [20]. These two are widely investigated and show excellent EMI shielding application.

### Magnetite ( $\text{Fe}_3\text{O}_4$ )

Magnetite ( $\text{Fe}_3\text{O}_4$ ) exists in various morphologies and is widely used in EMI applications [61]. In  $\text{Fe}_3\text{O}_4$ , the electron hopping occurs between  $\text{Fe}^{2+}$  and  $\text{Fe}^{3+}$  [62, 63]; as a result, it shows outstanding magnetic/dielectric properties and is a favourable candidate for EMI shielding mechanism.

### **Wüstite (FeO)**

FeO (Iron (II) oxide) is rarely investigated because of higher temperature ( $> 560\text{ }^{\circ}\text{C}$ ) and pressure requirement of its stability. Zhu et al. [64] investigated Fe@FeO NPs dispersed in polyurethane (PU) matrix and observed that Fe@FeO/PU shows eddy current effect and RL  $> 20\text{ dB}$ . SiO<sub>2</sub>-coated Fe@FeO/PU composites show even better performance in EMI application.

### **Iron Oxy-Hydroxide (FeOOH)**

FeOOH has poor electrical and magnetic properties. They find their application in electrode materials and lithium batteries. They exist in four forms such as goethite ( $\alpha$ -FeOOH), akaganeite ( $\beta$ -FeOOH), lepidocrocite ( $\gamma$ -FeOOH) and feroxyhyte ( $\delta$ -FeOOH). They are not good candidates for EMI applications.

### **Carbonyl Iron (CI)**

Carbonyl iron (CI) has superior  $M_s$ , high Curie temperature and magnetic loss which makes them as an excellent magnetic absorbing material. With changing shape, size and morphology, its magnetic properties can be varied. For example, in CI nanoflakes, the planar anisotropy improves its Snoek's limit which results in increasing its permeability and resonance frequency [65].

Although Fe materials have several advantages for EMI shielding applications, it suffers from drawback like skin depth problem and Snoek's limit. Another drawback of Fe oxides is that of poor permittivity in comparison to the permeability. A good EMI shielding material should have good permittivity and permeability. Therefore, carbon-based materials, Fe-based composites and conducting polymers gained researchers attention.

## ***5.2 Metals/Metal Oxides for EMI Shielding***

The combination of metal oxides such as BaTiO<sub>3</sub>, SnO<sub>2</sub>, ZnO, SiO<sub>2</sub>, TiO<sub>2</sub> with Fe ingredients increases dielectric and magnetic loss which are the requirement for microwave absorption applications. The major drawback of Fe/metal oxides composites are agglomeration during preparation, poor dispersion, and galvanic corrosion. The most commonly used metals for shielding materials are: alloy of Fe, Cu, Cr, Ni, Ag, Al, Ni, conductive carbon/graphite particles or fibres. They too suffer from various limitations such as high density, brittleness, low impact resistance and corrosion. Magnesium (Mg) is preferred for EMI shielding application in which reflection loss dominates due to its active response over entire frequency range [66].

### 5.3 Carbonaceous Materials

Carbonaceous materials have high permittivity that lies between ingredients of Fe- and carbon-based materials which makes them useful for microwave absorbing applications. Apart from high permittivity, carbonaceous material possesses high chemical, thermal and mechanical stability, low density and excellent conductivity. Carbonaceous/Fe composites are excellent for EM reflection /or absorption materials due to its lightweight. The carbonaceous materials investigated for EMI shielding applications are discussed in latter subsection.

#### Graphite/Expanded Graphite

Graphite due to its lightweight, good mechanical/thermal stability and high aspect ratio is used in the fields of electronics, energy and optical devices. Due to poor dispersion of graphite in solvents, composites are prepared from functionalized graphite by acid treatment such as HCl and H<sub>2</sub>SO<sub>4</sub>. Expanded graphite (EG) synthesized by thermal treatment show poor magnetic properties. However, integrating graphite or expanded graphite with Fe ingredients improves their magnetic properties and can be used for enhanced EMI performance.

#### Graphene

Graphene has superior electric properties, thermal stability, mechanical strength and dielectric loss as compared to metal oxides such as ZnO, TiO<sub>2</sub> or SnO<sub>2</sub> [67]. Graphene synthesized by physical and chemical process possesses high carrier mobility and lack surface functionalities and are not useful for EM absorption. However, the derivatives of graphene such as graphene oxide (GO) and reduced graphene oxide (RGO) are mostly used in EMI applications.

Graphene oxide (GO) is hydrophilic and is synthesized from graphite by strong oxidizing agent. GO is easily dispersed in polymer matrix and in any organic or inorganic solvent which is the most appealing property of GO. Samadi et al. [68] investigated Fe<sub>3</sub>O<sub>4</sub>-GO/PVDF composite and observed that GO affect the reflection loss and bandwidth in the composite because GO acts as electrical insulator; however, Fe improves the conductivity of composite to certain extent.

In reduced graphene oxide (RGO), hydrazine hydrate, NaBH<sub>4</sub> or NaOH, etc. is used to remove oxygen functional group. The remanent functional groups and defects present in RGO enhance electronic dipole relaxation which results in improved EM absorption. Apart from this, RGO shows higher dielectric and magnetic loss in the process of microwave absorption. He et al. [69] investigated RGO/flaky carbonyl iron (FCI) composites and observed better absorption properties (−65.4 dB at 5.2 GHz at 3.87 mm thickness). Further, RGO and Fe-, Fe<sub>3</sub>O<sub>4</sub>- and Fe<sub>2</sub>O<sub>4</sub>-based composites are investigated for EMI shielding applications.

## 5.4 Carbon Nanotubes (CNTs)

CNTs is a one-dimensional (1-D) nanostructure having fascinating electrical, mechanical (> GPa) and thermal properties and can be semiconductor or metallic in nature depending upon their structure and diameter. CNTs are used as nanofillers in enhancing properties of composites. Che et al. investigated CNTs/CoFe<sub>2</sub>O<sub>4</sub>, and Qi et al. investigated Fe/CNTs. Both these composites show enhanced dielectric and magnetic losses. CNTs can be single-walled carbon nanotubes (SWCNTs) and multi-walled carbon nanotubes (MWCNTs).

### Single-Walled Carbon Nanotubes (SWCNTs)

SWCNTs having  $sp^2$  hybridized carbon atom and have good electric properties because of their smaller diameter (diameter ~ 1.4 nm) and large aspect ratio. SWCNTs possess high conductivity and poor magnetic properties which make them as excellent microwave absorbing materials. To improve its magnetic and electric properties, Fe is incorporated in SWCNTs such as Fe<sub>3</sub>O<sub>4</sub>/SWCNT composites [70].

### Multi-walled Carbon Nanotubes (MWCNTs)

MWCNTs is 1-D material consists of multiple layers of graphite separated from each layer by a distance of 0.34 nm and wrapped to form tube shape [71]. The structural disorder such as Stone–Wales defects, and atomic defects present in MWCNTs result in high aspect ratio and low percolation threshold which makes MWCNTs more favourable than SWCNTs in EMI shielding applications.

### Carbon Fibres (CFs)

Carbon fibres (CFs) are like other carbon materials have lower magnetism but have high conductivity which result in impedance mismatching in EMI shielding application. To overcome this problem, CFs is used in composite with Fe ingredients such as Fe, Fe<sub>3</sub>O<sub>4</sub>, Fe<sub>2</sub>O<sub>3</sub> or alloy for EMI applications. CFs is used as filler; however, high weight % ratio of CFs as fillers is required for impedance matching in polymers, but it reduces the mechanical strength of polymers.

## 5.5 Composite Materials for EMI Shielding

The combination of two or more immiscible materials having distinct characteristics than that of individual materials form composites. In composite, the host material or

matrix can be ceramic, polymer, glass or metal, and the filler can be fibres, flakes and platelets. Polymer matrix-containing conducting fillers (polymer matrix composites or PMCs) are used for microwave absorbing applications because of low density and fair conductivity. Intrinsic conducting polymers (ICPs) such as polyaniline (PANI), polyacetylene, polypyrrole (PPy), polyacetylene, etc. are used in shielding mechanism of reflection and absorption. Nanomaterial-based conducting polymer composites have gained attention of scientific community because of desired EMI shielding applications [72–74]. The basic requirement of composites is the minimum value of  $\sigma > 10^{-2}$  S/m and for electrostatic discharge (ESD) application in the range of  $10^{-3}$  to  $10^{-7}$  S/m [75].

### 5.6 Polymer-Based Nanocomposite for EMI Shielding

The filler's properties such as conductivity, physical geometry, aspect ratio, dielectric constant and magnetic properties [76] decide the EMI shielding applications of composites. Percolation threshold limit decides the concentration of critical conducting filler for forming electrical conduction network in insulating polymer matrix which influence conductivity and shielding effectiveness of the composites [74]. Nanofiller in conducting polymer nanocomposites improves electrical properties because of excellent interface formation and interaction [77]. Examples of conductive fillers incorporated into the polymer matrix to produce lightweight and excellent shielding efficient polymer nanocomposites [78] are metal nanoparticles, RGO, CNTs and CFs.

## 6 Graphene Oxide-Ferrite Hybrid as the EMI Shielding Material

The prominent structural properties of carbon nanomaterials and their physiochemical reaction with other materials open many new applications such as mechanical sensors and wave absorption. To reduce the thickness and loading percentage to obtain wide absorption bandwidth, adding of different type of carbon to magnetic ferrites has been investigated. Ahmad et al. [79] investigated Ni–Zn ferrite/carbon nanotube composite synthesized by physical mixing and observed absorption threshold  $-10$  dB at two frequencies 3.7 GHz and 0.9 GHz at 1.0 mm thickness. Liu et al. [80] investigated  $\text{Fe}_3\text{O}_4/\text{C}$  composite and observed  $\epsilon_r = 5.1 - i3.2$ ;  $\mu_r = 1.01 + i0.019$  and  $\text{RL} = -23.6$  dB for thickness of 2 mm at 17.5 GHz frequency. For the thickness of 2.5 mm at the frequency of 15.5 GHz for a 1:1 loading percentage by weight in  $\text{Fe}_3\text{O}_4/\text{C}$  composite,  $\epsilon_r = 4.5 - i2.5$ ;  $\mu_r = 1.04 + i0.019$  and  $\text{RL} = -39.3$  dB is observed. Wang et al. [81] investigated 17.84 wt% C, and 23.41 wt% C  $\text{Fe}_3\text{O}_4@C$  composite synthesized by in-situ polymerization and observed  $\epsilon_r = 9.4$

i2.9;  $\mu_r = 1.1 - i0.2$  and  $RL = -35.8$  dB for 17.84 wt % C at the frequency of 4.7 GHz for the thickness of 5 mm, and  $\epsilon_r = 9.4 - i2.9$ ;  $\mu_r = 1.1 - i0.2$  and  $RL = -40.2$  dB for 23.41 wt% C at the thickness of 1.5 mm at the 15.8 GHz frequency. Feng et al. [82] investigated CF@CoFe<sub>2</sub>O<sub>4</sub> and CF@CoFe<sub>2</sub>O<sub>4</sub>@MnO<sub>2</sub> composites synthesized by sol-gel and hydrothermal technique. CF@CoFe<sub>2</sub>O<sub>4</sub>@MnO<sub>2</sub> composite shows  $RL_{min} = -34$  dB at thickness of 1.5 mm and superior EM matching than CF@CoFe<sub>2</sub>O<sub>4</sub> composite.

Addition of graphene to ferrite has been attempted by large number of researchers. Huang et al. [83] investigated magnetically garnished graphene (GR)@CuS and observed  $RL = -54.5$  dB for the thickness of 2.5 mm at the frequency of 11.4 GHz, and the absorption bandwidth under  $-10$  dB was 4.5 GHz. Zhang et al. [84] investigated CoFe<sub>2</sub>O<sub>4</sub>:SnS<sub>2</sub>/RGO composite and observed  $RL = -54.4$  dB at 16.5 GHz frequency for 1.6 mm thickness and absorption bandwidth under  $-10$  dB was 12 GHz. Huang et al. [85] investigated RGO/CoFe<sub>2</sub>O<sub>4</sub> composite synthesized by hydrothermal technique and observed  $RL = -37.2$  dB at 11.6 Hz frequency for the thickness of 2.5 mm. Thus, owing to large surface area, graphene is suitable for loading ferrite nanoparticles [86–88].

## 7 Parameters/Factors Affecting EMI Performance

### 7.1 Permittivity and Permeability

Impedance matching is related to permittivity and permeability of composites and is an important characteristic for ideal EMI shielding material which is mathematically expressed as:

$$\alpha = \pi f c \sqrt{2 \left( \mu'' \epsilon'' - \mu' \epsilon' + \sqrt{(\mu''^2 + \mu'^2)(\epsilon'^2 + \epsilon''^2)} \right)} \quad (13)$$

where  $\epsilon'/\mu'$  represents electric/magnetic energy storage capacity,  $\epsilon''/\mu''$  represents dielectric/magnetic losses and  $\alpha$  is the attenuation constant of shielding material/slab.

Dielectric loss ( $\epsilon''$ ) is because of conductivity and polarization loss in the shielding material. According to the free electron theory, dielectric loss is given by:

$$\epsilon'' = \frac{\sigma}{2\pi \epsilon_0 f} \quad (14)$$

From above equation, it is clear that high electric conductivity increases dielectric loss ( $\epsilon'' \propto \sigma$ ). Also, ionic and electronic polarization dominates at higher frequency ( $> 10^3$  GHz). Dipole polarization is due to bound charges or defects and comes into the picture because of synthesis technique, material used and annealing temperature,

etc. However, interfacial polarization is because of trapped space charges at the interfaces and mostly occur in multi-interface composites.

Magnetic loss occurs due to ferromagnetic resonance and eddy current loss in the microwave frequency region. The resonance frequency  $f_r$  is related to an anisotropy field  $H_0$  by the relation:

$$f_r = \frac{\gamma H_0}{2\pi} \quad (15)$$

and  $H_0 = \frac{2K}{\mu_0 M_s}$ ;  $K$  is the anisotropy constant.

An excellent magnetic shielding material should retain magnetic permeability at GHz frequency range; however, at cut off frequency  $f_r$ , permeability decreases according to the relation given by Snoek's limit:

$$f_r(\mu - 1)\alpha M_s \quad (16)$$

Thus, a good magnetic shielding materials should have high  $M_s$  at high  $f_r$ . Due to semiconducting nature, bulk ferrites have lower  $M_s$  value and hence lower  $f_r$  (low GHz range). Therefore, nanosized ferrites are focussed because as the dimension of material is lowered eddy current loss is decreased.

## 7.2 Snoek's Limit

Snoek's limit determines the limitation on the value of permeability in case of ferrites. The complex permeability of magnetic materials is due to the domain wall and the spin rotation motion, and their contribution in the material is of the resonance type and the relaxation type [89]. Thus, permeability can be expressed mathematically as:

$$\mu(\omega) = 1 + \chi_{sr}(\omega) + \chi_{dw}(\omega) \quad (17)$$

where  $\chi_{sr}(\omega) = \frac{K_{sr}}{1+j(\omega/\omega_{sr})}$  and  $\chi_{dw}(\omega) = \frac{K_{dw}\omega_{dw}^2}{\omega_{dw}^2 - \omega^2 + j\beta\omega}$

Here,  $\omega$ ,  $\omega_{sr}$ , and  $\omega_{dw}$  are *rf* magnetic field resonance frequency, spin resonance frequency and domain wall motion resonance frequency. The terms  $K_{sr}$ , and  $K_{dw}$  are susceptibilities due to static spin and domain wall motion while  $\beta$  is the damping factor. It was noticed that at higher frequencies ( $> 10^2$  MHz),  $\mu(\omega)$  is a function of  $\chi_{sr}(\omega)$  and  $\chi_{dw}(\omega)$  part can be ignored. The expression for  $\chi_{sr}(\omega)$  and  $\omega_{sr}$  in terms of saturation magnetization ( $M_s$ ), crystalline anisotropy ( $K$ ) and gyromagnetic ratio ( $\gamma$ ) is given by:

$$\chi_{sr} = \frac{2\pi M_s^2}{K} \quad \text{and} \quad \omega_{sr} = C'\gamma \frac{2K}{M_s} \quad (18)$$

The product of these two equation gives:

$$\chi_{sr} \omega_{sr} = 2C' \pi \gamma M_s \quad (19)$$

Therefore, at  $\omega_{sr} = \omega_r = 2\pi f_r$  (resonance frequency)

$$f_r(\mu - 1)\alpha M_s \quad (20)$$

The above expression is known as Snoek's limit, and it determines the limitation on the value of permeability in case of ferrites.

### 7.3 Temperature and Time

In case of ferrites, it has been observed that heat treatment and reaction time reverse the reflection loss and enhance attenuation [90]. This is because of defects/structural changes which create extra energy level near the fermi level. Reaction time and annealing temperature decide the reflection loss in FeCo/ZnO composites [91].

### 7.4 Size, Shape and Morphology

The size of the magnetic particle decides the value of its permeability and hence eddy current loss. It has been found that below critical small size of the magnetic particle, the eddy current losses decrease because of decrease in induced eddy voltage ( $E_{eddy} \propto \text{area}$ ). In addition to this, due to small size of nanostructures, magnetic anisotropy energy dominates because of breaking of some exchange bonds which modifies the spin relaxation time or frequency. Due to small size, spin fluctuation is very fast in superparamagnetic state and hence relaxation is observed at higher frequencies [92, 93]. In multi-interface materials, bound charges accumulate at the interfaces result in Maxwell–Wagner effect and unsaturated bonds result in dipolar polarization. Thus, multi-interface materials such as Fe and Fe-alloy show good EM attenuation because of conductivity loss and interfacial/dipolar polarization. Bayat et al. [94] studied the effect of particle size and thickness on EMI performance of Fe<sub>3</sub>O<sub>4</sub>/carbon nanofibre composite and observed that as particle size varies from 10–20 to 20–30 nm, SE<sub>T</sub> varies from 47 to 68 dB and as sample thickness varies from 0.1 to 0.7 mm, SE<sub>T</sub> varies from 24 to 68 dB. This is due to increasing conductivity which increases the SE<sub>A</sub> and hence SE<sub>T</sub>.



## 7.5 Mass Ratio

The threshold percolation value of conductivity and the electrical properties of the material are related and are given as:

$$\sigma = \sigma_0(V - V_c)^C \quad (21)$$

where  $\sigma$ —electrical conductivity of the material;  $\sigma_0$ —natural conductivity;  $V$ —volume fraction of filler;  $V_c$ —volume fraction at the percolation threshold;  $C$ —critical exponent.

The value  $V_c$  depends upon various factors such as shape, aspect ratio, conductivity, concentration and compatibility of filler [95]. For example, in nano-Fe<sub>2</sub>O<sub>3</sub>-coated CNTs, reflection loss is related to CNT—to-Fe<sup>3+</sup> mass ratio [96].

## 7.6 Thickness

The minimal reflection ‘RL<sub>min</sub>’ of microwave power is related to the thickness ( $t$ ) of shielding material. RL<sub>min</sub> occurs when thickness ( $t$ ) of absorber is equal to the odd number multiple of propagating wavelength and is given by:

$$t_m = n \frac{\lambda_m}{4}$$

$$\text{And } \lambda_m = \frac{\lambda_0}{\sqrt{\mu\epsilon}} \quad (22)$$

where  $n = (1, 2, 3, 5, 7 \dots)$ ;  $n = 1$  determines first dip at low frequency and for  $t = 7$  mm, the dip occurred at  $1.0 \frac{\lambda_m}{4}$ ,  $3.0 \frac{\lambda_m}{4}$  and so on.

Reflection peaks shift towards the lower frequencies if sample thickness is increased. For example, in Fe<sub>3</sub>O<sub>4</sub>@C, carbon shell thickness in the range 20–70 nm shows superior dielectric behaviour [33].

## 8 Summary and Future Perspective

In summary, we have systematically reviewed the recent advances in graphene oxide-ferrite hybrid framework and their application as radar absorbing material. In order to deal with the complex electromagnetic environment, the radar absorbing materials need to be further improved. The important research areas in this directions are: (i) optimizing microstructure, morphology, thickness, density and frequency bandwidth of the composite; (ii) to extend the application of EMI shielding materials in the harsh battle field, a high-temperature and corrosion resistance materials need to be

investigated; (iii) simple environmental friendly preparation techniques need to be used for the synthesis of microwave absorbing materials without sacrificing their performances; and (iv) to explore two-dimensional materials and their composites that can be used in flexible devices.

## References

1. Raagulan, K., Kim, B.M., Chai, K.Y.: Recent advancement of electromagnetic interference (EMI) shielding of two dimensional (2D) MXene and graphene aerogel composites. *Nanomaterials* **10**, 702 (2020)
2. Li, Y., Chen, S., Zhao, K., Gui, Y., Fang, S., Xu, Y., Ma, Z.: Effects of electromagnetic radiation on health and immune function of operators. *Chin. J. Indus. Hyg. Occup. Dis.* **31**(8), 602–605 (2013)
3. Sharma, A.K., Bhardwaj, P., Singh, K.K., Dhawan, S.K.: Improved microwave shielding properties of polyaniline grown over three-dimensional hybrid carbon assemblage substrate. *Appl. Nanosci.* **5**, 635–644 (2014)
4. Narendra, J., Harnadek, M.: xGnP for electromagnetic interference shielding application. *XG Sci.* **5**, 1–11 (2012)
5. Li, N., Zheng, M., Lu, H., Hu, Z., Shen, C., Chang, X., Ji, G., Cao, J., Shi, Y.: High-rate lithium–sulphur batteries promoted by reduced graphene oxide coating. *Chem. Commun.* **48**, 4106 (2012)
6. Pawar, S.P., Biswas, S., Kar, G.P., Bose, S.: High frequency millimetre wave absorbers derived from polymeric nanocomposites. *Polymer* **84**, 398–419 (2016)
7. Chung, D.D.L.: Electromagnetic interference shielding effectiveness of carbon materials. *Carbon* **39**, 279–285 (2001)
8. Sun, X., He, J., Li, G., Tang, J., Wang, T., Guo, Y., Xue, H.: Laminated magnetic graphene with enhanced electromagnetic wave absorption properties. *J. Mater. Chem. C.* **1**, 765–777 (2013)
9. Singh, K., Ohlan, A., Pham, V.H., Balasubramanian, R., Varshney, S., Jang, J., Hur, S.H., Choi, W.M., Kumar, M., Dhawan, S.K., Kong, B.-S., Chung, J.S.: Nanostructured graphene/Fe<sub>3</sub>O<sub>4</sub> incorporated polyaniline as a high performance shield against electromagnetic pollution. *Nanoscale.* **5**, 2411 (2013)
10. Joshi, A., Datar, S.: Carbon nanostructure composite for electromagnetic interference shielding. *Pramana* **84**, 1099–1116 (2015)
11. Choudary, V., Dhawan, S.K., Saini, P.: Polymer based nanocomposites for electromagnetic interference (EMI) shielding. In: Jaroszewski, M., Ziaja, J. (eds.) *EMI Shielding Theory and Development of New Materials*, pp. 67–100. India, Research Signpost (2012)
12. Saini, P., Aror, M.: Microwave absorption and EMI shielding behavior of nanocomposites based on intrinsically conducting polymers, graphene and carbon nanotubes. *New Polym. Spec. Appl.* 71–112 (2012)
13. Al-Ghamdi, A.A., Al-Hartomy, O.A., El-Tantawy, F., Yakuphanoglu, F.: Novel polyvinyl alcohol/silver hybrid nanocomposites for high performance electromagnetic wave shielding effectiveness. *Microsyst. Technol.* **21**, 859–868 (2014)
14. Deshmukh, K., Sankaran, S., Ahamed, B., Sadasivuni, K.K., Pasha, K.S.K., Ponnamma, D., Rama Sreekanth, P.S., Chidambaram, K.: Dielectric spectroscopy. In: *Spectroscopic Methods for Nanomaterials Characterization*, pp. 237–299 (2017)
15. Yang, Z., Li, M., Zhang, Y., Lyu, X., Hu, D.: Hierarchical formation mechanism of anisotropic magnetite microflakes and their superior microwave attenuation properties. *J. Alloy. Compd.* **781**, 321–329 (2019)
16. Fu, L.-S., Jiang, J.-T., Xu, C.-Y., Zhen, L.: Synthesis of hexagonal Fe microflakes with excellent microwave absorption performance. *Cryst. Eng. Comm.* **14**, 6827–6832 (2012)

17. Shang, C., Ji, G., Liu, W., Zhang, X., Lv, H., Du, Y.: One-pot in situ molten salt synthesis of octahedral Fe<sub>3</sub>O<sub>4</sub> for efficient microwave absorption application. *RSC Adv.* **5**, 80450–80456 (2015)
18. Tong, G., Wu, W., Guan, J., Qian, H., Yuan, J., Li, W.: Synthesis and characterization of nano-sized urchin-like  $\alpha$ -Fe<sub>2</sub>O<sub>3</sub> and Fe<sub>3</sub>O<sub>4</sub>: microwave electromagnetic and absorbing properties. *J. Alloy. Compd.* **509**, 4320–4326 (2011)
19. Wang, Z.H., He, X., Wang, X., Han, Z., Geng, D.Y., Zhu, Y.L., Zhang, Z.D.: Magnetic and microwave-absorption properties of SnO-coated  $\alpha$ -Fe(Sn) nanocapsules. *J. Phys. D Appl. Phys.* **43**, 495404 (2010)
20. Sun, G., Dong, B., Cao, M., Wei, B., Hu, C.: Hierarchical dendrite-like magnetic materials of Fe<sub>3</sub>O<sub>4</sub>,  $\gamma$ -Fe<sub>2</sub>O<sub>3</sub>, and Fe with high performance of microwave absorption. *Chem. Mater.* **23**, 1587–1593 (2011)
21. Jia, K., Zhao, R., Zhong, J., Liu, X.: Preparation and microwave absorption properties of loose nanoscale Fe<sub>3</sub>O<sub>4</sub> spheres. *J. Magn. Magn. Mater.* **322**, 2167–2171 (2010)
22. Baoshan, Z., Feng, Y., Xiong, J., Yang, Y., Lu, H.: Microwave-absorbing properties of deaggregated flake-shaped carbonyl-iron particle composites at 2–18 GHz. *IEEE Trans. Magn.* **42**, 1778–1781 (2006)
23. Song, W.-L., Guan, X.-T., Fan, L.-Z., Cao, W.-Q., Zhao, Q.-L., Wang, C.-Y., Cao, M.-S.: Tuning broadband microwave absorption via highly conductive Fe<sub>3</sub>O<sub>4</sub>/graphene heterostructures nanofillers. *Mater. Res. Bull.* **72**, 316–323 (2015)
24. Zhang, Z., Liu, X., Wang, X., Wu, Y., Li, R.: Effect of Nd–Co substitution on magnetic and microwave absorption properties of SrFe<sub>12</sub>O<sub>19</sub> hexaferrites. *J. Alloy. Compd.* **525**, 114–119 (2012)
25. Li, Y., Wu, T., Jin, K., Qian, Y., Qian, N., Jiang, K., Wu, W., Tong, G.: Controllable synthesis and enhanced microwave absorbing properties of Fe<sub>3</sub>O<sub>4</sub>/NiFe<sub>2</sub>O<sub>4</sub>/Ni heterostructures porous rods. *Appl. Surf. Sci.* **387**, 190–201 (2016)
26. He, F., Li, J., Chen, L., Chen, L., Huang, Y.: Fabrication and characterization of novel Fe–Ni alloy coated carbon fibers for high-performance shielding materials. *Surf. Rev. Lett.* **22**, 1550028 (2015)
27. Liu, X.G., Ou, Z.Q., Geng, D.Y., Han, Z., Jiang, J.J., Liu, W., Zhang, Z.D.: Influence of a graphite shell on the thermal and electromagnetic characteristics of FeNi nanoparticles. *Carbon* **48**, 891–897 (2010)
28. Han, Z., Li, D., Wang, H., Liu, X.G., Li, J., Geng, D.Y., Zhang, Z.D.: Erratum: Broad-band electromagnetic-wave absorption by FeCo/C nanocapsules. *Appl. Phys. Lett.* **95**, 209901 (2009)
29. Ding, X., Huang, Y., Wang, J.: Synthesis of feni3 nanocrystals encapsulated in carbon nanospheres/reduced graphene oxide as a light weight electromagnetic wave absorbent. *RSC Adv.* **5**, 64878–64885 (2015)
30. Bhingardive, V., Suwas, S., Bose, S.: New physical insights into the electromagnetic shielding efficiency in PVDF nanocomposites containing multiwall carbon nanotubes and magnetic nanoparticles. *RSC Adv.* **5**, 79463–79472 (2015)
31. Feng, C., Liu, X., Sun, Y.P., Jin, C.: Enhanced microwave absorption of flower-like FeNi@C nanocomposites by dual dielectric relaxation and multiple magnetic resonance. *RSC Adv.* **4**, 22710–22715 (2014)
32. Choi, J. R., Jung, B. M., Choi, U. H., Cho, S. C., Park, K. H., Kim, W.-Jung, Lee, S.-K., Lee, S. B.: Characterization of FeCo magnetic metal hollow fiber/EPDM composites for electromagnetic interference shielding. *Compos. Res.* **28**, 333–339 (2015)
33. Du, Y., Liu, W., Qiang, R., Wang, Y., Han, X., Ma, J., Xu, P.: Shell thickness-dependent microwave absorption of core–shell Fe<sub>3</sub>O<sub>4</sub>@C composites. *ACS Appl. Mater. Interf.* **6**, 12997–13006 (2014)
34. Guo, X., Deng, Y., Gu, D., Che, R., Zhao, D.: Synthesis and microwave absorption of uniform hematite nanoparticles and their core-shell mesoporous silica nanocomposites. *J. Mater. Chem.* **19**, 6706–6712 (2009)
35. Yu, M., Liang, C., Liu, M., Liu, X., Yuan, K., Cao, H., Che, R.: Yolk–shell Fe<sub>3</sub>O<sub>4</sub>@ZrO<sub>2</sub> prepared by a tunable polymer surfactant assisted sol–gel method for high temperature stable microwave absorption. *J. Mater. Chem. C.* **2**, 7275–7283 (2014)

36. Liu, J., Cheng, J., Che, R., Xu, J., Liu, M., Liu, Z.: Double-shelled yolk-shell microspheres with Fe<sub>3</sub>O<sub>4</sub> cores and SnO<sub>2</sub> double shells as high-performance microwave absorbers. *J. Phys. Chem. C* **117**, 489–495 (2012)
37. Chen, Y.-J., Xiao, G., Wang, T.-S., Ouyang, Q.-Y., Qi, L.-H., Ma, Y., Gao, P., Zhu, C.-L., Cao, M.-S., Jin, H.-B.: Porous Fe<sub>3</sub>O<sub>4</sub>/carbon core/shell nanorods: synthesis and electromagnetic properties. *J. Phys. Chem. C* **115**, 13603–13608 (2011)
38. Zhu, Y.-F., Ni, Q.-Q., Fu, Y.-Q., Natsuki, T.: Synthesis and microwave absorption properties of electromagnetic functionalized Fe<sub>3</sub>O<sub>4</sub>-polyaniline hollow sphere nanocomposites produced by electrostatic self-assembly. *J. Nanopart. Res.* **15**, 1988 (2013)
39. Sun, X., Ma, G., Lv, X., Sui, M., Li, H., Wu, F., Wang, J.: Controllable fabrication of Fe<sub>3</sub>O<sub>4</sub>/ZnO core-shell nanocomposites and their electromagnetic wave absorption performance in the 2–18 GHz frequency range. *Materials* **11**, 780 (2018)
40. Liu, X.G., Geng, D.Y., Meng, H., Shang, P.J., Zhang, Z.D.: Microwave-absorption properties of ZnO-coated iron nanocapsules. *Appl. Phys. Lett.* **92**, 173117 (2008)
41. Zhang, Z., Shi, Z., Fan, R., Gao, M.: Guo,.: Microwave absorption properties of Fe@Al<sub>2</sub>O<sub>3</sub> nano embedment prepared by mechano-synthesis. *Mater. Chem. Phys.* **130**, 615–618 (2011)
42. Yan, L., Wang, J., Han, X., Ren, Y., Liu, Q., Li, F.: Enhanced microwave absorption of Fe nanoflakes after coating with SiO<sub>2</sub> nanoshell. *Nanotechnology* **21**, 095708 (2010)
43. Liu, J., Che, R., Chen, H., Zhang, F., Xia, F., Wu, Q., Wang, M.: Microwave absorption enhancement of multifunctional composite microspheres with spinel Fe<sub>3</sub>O<sub>4</sub> cores and anatase TiO<sub>2</sub> shells. *Small* **8**, 1214–1221 (2012)
44. Liu, X., Sun, Y., Feng, C., Jin, C., Li, W.: Synthesis, magnetic and electromagnetic properties of Al<sub>2</sub>O<sub>3</sub>/Fe oxides composite-coated polyhedral Fe core-shell nanoparticles. *Appl. Surf. Sci.* **280**, 132–137 (2013)
45. Chen, Q., Li, L., Wang, Z., Ge, Y., Zhou, C., Yi, J.: Synthesis and enhanced microwave absorption performance of CIP@ SiO<sub>2</sub>@Mn<sub>0.6</sub>Zn<sub>0.4</sub>Fe<sub>2</sub>O<sub>4</sub> ferrite composites. *J. Alloys Compd.* **779**, 720–727 (2019)
46. Sun, D., Zou, Q., Wang, Y., Wang, Y., Jiang, W., Li, F.: Controllable synthesis of porous Fe<sub>3</sub>O<sub>4</sub>@ZnO sphere decorated graphene for extraordinary electromagnetic wave absorption. *Nanoscale* **6**, 6557–6562 (2014)
47. Wang, L., Zhu, J., Yang, H., Wang, F., Qin, Y., Zhao, T., Zhang, P.: Fabrication of hierarchical graphene@Fe<sub>3</sub>O<sub>4</sub>@SiO<sub>2</sub>@polyaniline quaternary composite and its improved electrochemical performance. *J. Alloy. Compd.* **634**, 232–238 (2015)
48. Ahmad, A.F., Abbas, Z., Obaiys, S.J., Ibrahim, N., Hashim, M., Khaleel, H.: Theoretical and numerical approaches for determining the reflection and transmission coefficients of OPEFB-PCL composites at X-band frequencies. *PLOS ONE*. **10** (2015)
49. Micheli, D., Pastore, R., Vricella, A., Delfini, A., Marchetti, M., Santoni, F.: Electromagnetic characterization of materials by vector network analyzer experimental setup. In: *Spectroscopic Methods for Nanomaterials Characterization*, pp. 195–236 (2017)
50. González, M., Mokry, G., de Nicolás, M., Baselga, J., Pozuelo, J.: Carbon nanotube composites as electromagnetic shielding materials in GHz Range. In: *Carbon Nanotubes—Current Progress of their Polymer Composites*, p. 292 (2016)
51. Ping, H., Lu, K., Jun, Y., Fan, Y., Kuaishe, W., Jinjing, D., Zhanlin, Y., Weicheng, C., Dongxin, L.: Synthesis of Fe nanoparticles via one-step reduction method. *Rare Metal Mater. Eng.* **45**, 3112–3114 (2016)
52. Huber, D.L.: Synthesis, properties, and applications of iron nanoparticles. *Small* **1**, 482–501 (2005)
53. Chu, X.T., Ta, B.N., Ngo, L.T., Do, M.H., Nguyen, P.X., Nam, D.N.: Microwave absorption properties of iron nanoparticles prepared by ball-milling. *J. Electron. Mater.* **45**, 2311–2315 (2015)
54. Zeng, G., Zhang, H., Chen, Y., et al.: Electromagnetic compatibility (APEMC). *Asia-Pac. Symp.* **2012**, 533–536 (2012)
55. Bae, H., Ahmad, T., Rhee, I., Chang, Y., Jin, S.-U., Hong, S.: Carbon-coated iron oxide nanoparticles as contrast agents in magnetic resonance imaging. *Nanoscale Res. Lett.* **7**, 44 (2012)

56. Akhtar, M.N., Saleem, M., Khan, M.A.: Al doped spinel and garnet nanostructured ferrites for microwave frequency c and X- band applications. *J. Phys. Chem. Solids* **123**, 260–265 (2018)
57. Kumar, A., Shen, J., Zhao, H., Zhengjian, Q., Li, Q.: Crystallographic and magnetic properties of nanocrystalline perovskite structure  $\text{SmFeO}_3$  orthoferrites. *J. Cryst. Growth* **490**, 1–5 (2018)
58. Kumar, S., Dubey, D.P., Shannigrahi, S., Chatterjee, R.: Complex permittivity, permeability, magnetic and microwave absorbing properties of  $\text{Ni}^{2+}$  substituted mechanically milled U-type hexaferrites. *J. Alloy. Compd.* **774**, 52–60 (2019)
59. Song, Y., Zheng, J., Sun, M., Zhao, S.: The electromagnetic and microwave absorbing properties of polycrystalline Y-type  $\text{Ba}_{1.5}\text{Sr}_{0.5}\text{CoZnFe}_{12-x}\text{Al}_x\text{O}_{22}$  hexaferrites over the microwave range. *J. Mater. Sci. Mater. Electron.* **27**, 4131–4138 (2016)
60. Guo, D., Kong, W., Feng, J., Li, X., Fan, X.: Microwave absorption properties of  $\text{Sr}_x\text{Ba}_{3-x}\text{Co}_2\text{Fe}_{24}\text{O}_{41}$  hexaferrites in the range of 0.1–18 GHz. *J. Alloys Compds.* **751**, 80–85 (2018)
61. Zhou, W., Hu, X., Bai, X., Zhou, S., Sun, C., Yan, J., Chen, P.: Synthesis and electromagnetic, microwave absorbing properties of core-shell  $\text{Fe}_3\text{O}_4$ -poly(3,4-ethylenedioxythiophene) microspheres. *ACS Appl. Mater. Interfaces.* **3**, 3839–3845 (2011)
62. Ghandoor, H.E., Zidan, H., Khalil, M.M., Ismail, M.: *Int. J. Electrochem. Sci.* **7**, 5734–5745 (2012)
63. Singh, A.K., Srivastava, O.N., Singh, K.: Shape and size-dependent magnetic properties of  $\text{Fe}_3\text{O}_4$  nanoparticles synthesized using piperidine. *Nanoscale Res. Lett.* **12**, 298 (2017)
64. Zhu, J., Wei, S., Haldolaarachchige, N., Young, D.P., Guo, Z.: Electromagnetic field shielding polyurethane nanocomposites reinforced with core-shell Fe-silica nanoparticles. *J. Phys. Chem. C.* **115**, 15304–15310 (2011)
65. Weng, X., Li, B., Zhang, Y., Lv, X., Gu, G.: Synthesis of flake shaped carbonyl iron/reduced graphene oxide/polyvinyl pyrrolidone ternary nanocomposites and their microwave absorbing properties. *J. Alloy. Compd.* **695**, 508–519 (2017)
66. Geetha, S., Satheesh Kumar, K.K., Rao, C.R., Vijayan, M., Trivedi, D.C.: EMI shielding: methods and materials-a review. *J. Appl. Polym. Sci.* **112**, 2073–2086 (2009)
67. LV, H., Ji, G., Liang, X.H., Zhang, H., Du, Y.: A novel rod-like  $\text{MnO}_2$ @Fe loading on graphene giving excellent electromagnetic absorption properties. *J. Mater. Chem. C.* **3**, 5056–5064 (2015)
68. Samadi, A., Hosseini, S.M., Mohseni, M.: Investigation of the electromagnetic microwaves absorption and piezoelectric properties of electrospun  $\text{Fe}_3\text{O}_4$ -rgo/PVDF hybrid nanocomposites. *Org. Electron.* **59**, 149–155 (2018)
69. He, L., Zhao, Y., Xing, L., Liu, P., Wang, Z., Zhang, Y., Wang, Y., Du, Y.: Preparation of reduced graphene oxide coated flaky carbonyl iron composites and their excellent microwave absorption properties. *RSC Adv.* **8**, 2971–2977 (2018)
70. Kuchi, R., Nguyen, H.M., Dongquoc, V., Van, P.C., Surabhi, S., Yoon, S.-G., Kim, D., Jeong, J.-R.: In-situ Co-arc discharge synthesis of  $\text{Fe}_3\text{O}_4$ /SWCNT composites for highly effective microwave absorption. *physica status solidi (a)*. **215**, 1700989 (2018)
71. Mantena, K.V: Electrical and mechanical properties of MWCNT filled conductive adhesives on lead free surface finished PCB's, Master's Thesis, University of Kentucky (2009)
72. Fu, X., Chung, D.D.L.: Submicron-diameter-carbon-filament cement-matrix composites. *Carbon* **36**, 459–462 (1998)
73. Luo, X., Chung, D.D.L.: Electromagnetic interference shielding using continuous carbon-fiber carbon-matrix and polymer-matrix composites. *Compos. B Eng.* **30**, 227–231 (1999)
74. Al-Saleh, M.H., Gelves, G.A., Sundararaj, U.: Copper Nanowire/polystyrene nanocomposites: lower percolation threshold and higher EMI shielding. *Compos. A Appl. Sci. Manuf.* **42**, 92–97 (2011)
75. Sudha, J.D., Sivakala, S., Patel, K., Radhakrishnan Nair, P.: Development of electromagnetic shielding materials from the conductive blends of polystyrene polyaniline-clay nanocomposite. *Compos. A Appl. Sci. Manuf.* **41**, 1647–1652 (2010)
76. Joshi, A., Bajaj, A., Singh, R., Alegaonkar, P.S., Balasubramanian, K., Datar, S.: Graphene nanoribbon-PVA composite as EMI shielding material in the X band. *Nanotechnology* **24**, 455705 (2013)

77. Shen, L., Wang, F.Q., Yang, H., Meng, Q.R.: The combined effects of carbon black and carbon fiber on the electrical properties of composites based on polyethylene or polyethylene/polypropylene blend. *Polym. Testing* **30**, 442–448 (2011)
78. Kuang, T., Chang, L., Chen, F., Sheng, Y., Fu, D., Peng, X.: Facile preparation of lightweight high-strength biodegradable polymer/multi-walled carbon nanotubes nanocomposite foams for electromagnetic interference shielding. *Carbon* **105**, 305–313 (2016)
79. Yu, L.J., Sahrim, A.H., Kong, I., Mouad, A.T.: Microwave absorbing properties of nickel-zinc ferrite/multiwalled nanotube thermoplastic natural rubber composites. *Adv. Mater. Res.* **501**, 24–28 (2012)
80. Liu, X., Guo, H., Xie, Q., Luo, Q., Wang, L.-S., Peng, D.-L.: Enhanced microwave absorption properties in GHz range of Fe<sub>3</sub>O<sub>4</sub>/C composite materials. *J. Alloy. Compd.* **649**, 537–543 (2015)
81. Liu, X., Ma, Y., Zhang, Q., Zheng, Z., Wang, L.-S., Peng, D.-L.: Facile synthesis of Fe<sub>3</sub>O<sub>4</sub>/C composites for broadband microwave absorption properties. *Appl. Surf. Sci.* **445**, 82–88 (2018)
82. Feng, A., Hou, T., Jia, Z., Wu, G.: Synthesis of a hierarchical carbon fiber@cobalt ferrite@Manganese dioxide composite and its application as a microwave absorber. *RSC Adv.* **10**, 10510–10518 (2020)
83. Liu, P., Huang, Y., Yan, J., Yang, Y., Zhao, Y.: Construction of CUS nanoflakes vertically aligned on magnetically decorated graphene and their enhanced microwave absorption properties. *ACS Appl. Mater. Interfaces.* **8**, 5536–5546 (2016)
84. Zhang, N., Huang, Y., Zong, M., Ding, X., Li, S., Wang, M.: Coupling CoFe<sub>2</sub>O<sub>4</sub> and SnS<sub>2</sub> nanoparticles with reduced graphene oxide as a high-performance electromagnetic wave absorber. *Ceram. Int.* **42**, 15701–15708 (2016)
85. Zong, M., Huang, Y., Wu, H., Zhao, Y., Wang, Q., Sun, X.: One-pot hydrothermal synthesis of RGO/CoFe<sub>2</sub>O<sub>4</sub> composite and its excellent microwave absorption properties. *Mater. Lett.* **114**, 52–55 (2014)
86. Bhattacharyya, R., Prakash, O., Roy, S., Singh, A.P., Bhattacharya, T.K., Maiti, P., Bhattacharyya, S., Das, S.: Graphene oxide-ferrite hybrid framework as enhanced broadband absorption in gigahertz frequencies. *Sci. Rep.* **9** (2019)
87. Li, J., Zhou, D., Liu, W.-F., Su, J.-Z., Fu, M.-S.: Novel and facile reduced graphene oxide anchored Ni-Co-Zn-Nd-ferrites composites for microwave absorption. *Scripta Mater.* **171**, 42–46 (2019)
88. Acharya, S., Alegaonkar, P., Datar, S.: Effect of formation of heterostructures of SrAl<sub>4</sub>Fe<sub>8</sub>O<sub>19</sub>/RGO/PVDF on the microwave absorption properties of the composite. *Chem. Eng. J.* **374**, 144–154 (2019)
89. Acher, O., Dubourg, S.: Generalization of Snoek's law to ferromagnetic films and composites. *Phys. Rev. B* **77**, 104440 (2008)
90. Liu, Y., Wei, S., Xu, B., Wang, Y., Tian, H., Tong, H.: Effect of heat treatment on microwave absorption properties of Ni-Zn-Mg-La ferrite nanoparticles. *J. Magn. Magn. Mater.* **349**, 57–62 (2014)
91. LV, H., Ji, G., Wang, M., Shang, C., Zhang, H., Du, Y.: FeCo/ZnO composites with enhancing microwave absorbing properties: effect of hydrothermal temperature and Time. *RSC Adv.* **4**, 57529–57533 (2014)
92. Dosoudil, R., Usakova, M., Franek, J., Slama, J., Gruskova, A.: Particle size and concentration effect on permeability and em-wave absorption properties of hybrid ferrite polymer composites. *IEEE Trans. Magn.* **46**, 436–439 (2010)
93. Habib, A.H., Xu, S., Walker, E., Ondeck, M., Swaminathan, R., McHenry, M.E.: The role of eddy currents and nanoparticle size on AC magnetic field-induced reflow in solder/magnetic nanocomposites. *J. Appl. Phys.* **111** (2012)
94. Bayat, M., Yang, H., Ko, F.K., Michelson, D., Mei, A.: Electromagnetic interference shielding effectiveness of hybrid multifunctional Fe<sub>3</sub>O<sub>4</sub>/carbon nanofiber composite. *Polymer* **55**, 936–943 (2014)

95. Saini, P., Aror, M.: Microwave absorption and EMI shielding behavior of nanocomposites based on intrinsically conducting polymers, graphene and carbon nanotubes. *New Polym. Spec. Appl.* (2012)
96. Li, Y., Yu, M., Yang, P., Fu, J.: Enhanced microwave absorption property of Fe nanoparticles encapsulated within reduced graphene oxide with different thicknesses. *Ind. Eng. Chem. Res.* **56**, 8872–8879 (2017)

# Graphene-Based THz Antenna: Rudiments, Fabrication, and Forthcoming Opportunity



Sunil Lavadiya, Vishal Sorathiya, Kumutha Duraisamy,  
Delshi Howsalya Devi, and Sudipta Das

**Abstract** High-tech electromagnetic antennas that can receive and transmit at micro- and millimeter wave frequencies are crucial in the modern era of information. Multimedia broadcasting, wireless and satellite communications, radars, environmental sensing, and even medical equipment use them. Raising the working frequency of existing antennas using the terahertz (THz) band is a simple method for satisfying such requirements. Graphene, a form of carbon with just two dimensions, has recently attracted intensive and varied study. Graphene has swiftly become a leading substrate for THz transceivers and optoelectronic devices due to its plasmonic response occurring in the THz and IR frequency ranges. This chapter provides a high-level summary of the development of THz graphene-based antennas, its backdrop, current research trends, and anticipated challenges and possibilities in the intermediate and far future. Finally, we examine the exciting potential of graphene antennas after analyzing the current state of the art in many THz antennas and building a THz MIMO antenna.

**Keywords** MIMO antenna · Terahertz spectrum · Graphene · ECC · DG · CCL

---

S. Lavadiya (✉)

Department of Information and Communication Technology, Marwadi University, Rajkot,  
Gujarat 360002, India

e-mail: [sunil.lavadiya@marwadieducation.edu.in](mailto:sunil.lavadiya@marwadieducation.edu.in)

V. Sorathiya

Faculty of Engineering and Technology, Parul Institute of Engineering and Technology, Parul  
University, Waghodia Road, Vadodara, Gujarat 391 760, India

K. Duraisamy

Department of Biomedical Engineering, Karpaga Vinayaga College of Engineering and  
Technology, Chengalpattu, Tamilnadu, India

D. H. Devi

Department of AI & DS, Karpaga Vinayaga College of Engineering and Technology,  
Chengalpattu, Tamil Nadu, India

S. Das

Department of Electronics and Communication Engineering, IMPS College of Engineering and  
Technology, Malda, West Bengal, India



## 1 Introduction

In today's information age, highly developed electromagnetic antennas capable of working at micro- and millimeter-wave frequencies are an absolute need [1]. As a result, they are used to a large extent in a diverse array of applications, some examples of which include medical systems, broadcasting, radars, satellite communications, and weather sensing systems. Due of the vast number of potential applications, there has been an explosion of research and technical development in this sector over the last several decades. Growing at an exponential rate, the information society is placing ever-greater and sometimes incompatible demands on our technology. These requirements include, but are not limited to, the following: increased bandwidth for data transmission; many functions in a single, compact device; completely integrated and compact sensing systems; efficient use of spectrum and energy resources; and so on [2].

Increasing the operating frequency of existing antennas to take advantage of the terahertz (THz) band is a simple method that may be implemented to meet such requirements [3], that is, electromagnetic (EM) waves that have frequencies that range from 0.1 to 10 terahertz [4]. This band offers excellent chances for the development of new applications like imaging systems, screening, and spectroscopy [5]. This frequency band is referred to as the "THz gap" since it fills a technological void between the fields of electronics and photonics that have reached a high level of development [6].

Graphene, a two-dimensional carbon material, has lately spurred pervasive and diversified research efforts owing to its remarkable mechanical, electromagnetic, electrical, and thermal capabilities. This is connected to the fact that graphene has just been around for the last few years [7]. Graphene allows for the propagation of surface plasmon polaritons (SPPs). Graphene is a two-dimensional material. Because of the plasmonic response in the IR and THz frequency bands. Even though composite materials may hold up SPPs at THz [8]. Due to plasmonic response of graphene opened up exciting and unanticipated possibilities for the manipulation of waves and their emission in this frequency range. Utilizing graphene's one-of-a-kind features, researchers have proposed tiny and leaky-wave [9], reconfigurable resonant [10], and reflect array antennas [11] that offer unsurpassed radiation efficiency and functionality at THz frequencies. These graphene antennas leverage the reconfigurable nature of graphene's conductivity to their full potential, allowing them to resonate at frequencies far lower than those of their metallic counterparts. In addition, graphene plasmonic may be used to implement all of the essential building blocks required for front-end transceiver systems. These building blocks include modulators, switches, phase shifters, low-pass filters, and band-pass filters. When graphene is influenced by magnetostatic fields, non-reciprocal propagation and gigantic Faraday rotation have also been achieved; however, the large magnets that are needed for this technique are antagonistic to the downsizing of graphene plasmonics that is desired [12].

Their electromagnetic responses have only been predicted through the use of numerical simulations. Nevertheless, we would like to bring to your attention that

recent investigations have conclusively proven the propagation of restricted and controllable SPPs in graphene [13]. This is the underlying physical process that every antenna and component that has been detailed here relies upon. In earlier operations, graphene of inferior quality was produced. This graphene was unsuitable for any electrodynamic use other than acting as a tunable resistor. As a result, the practical viability of most research was severely hindered. Despite this, considerable headway has been made in this area over the last several years due to the concerted efforts of dozens of organizations located all over the globe to advance manufacturing methods. For instance, it has been reported that graphene structures that have a layer of hexagonal boron nitride sandwiched between them have mobility increases that are many orders of magnitude greater [14], which are far superior to the quality standards required by any antennas or devices that are included in this evaluation. The responsiveness of several interesting THz detectors and modulators has already been experimentally proven. This is despite the fact that the manufacturing and testing procedures required are very difficult. When compared to prior art, these detectors and modulators perform better and more closely match numerical predictions [15, 16]. Currently, THz reconfigurable antenna plays a vital role in targeting multiple wireless applications [17, 18]. Better application covering will be attained by choosing liquid-based reconfigurable antennae [19–21].

## 2 Graphene Conductivity

The conductivity of graphene is directly determined by its one-of-a-kind band structure and a set of special characteristics [22]. We emphasize that these criteria are not independent of one another but may be connected to one another in some way. Just the Kubo formula's intraband element is needed to represent graphene's conductivity at THz frequencies. This modeling may be done by using a semiclassical, local model and considering that there is no magnetic bias present [23].

$$\sigma = -j \frac{e^2 k_B T}{\pi \hbar^2 (\omega - j\tau^{-1})} \ln \left\{ 2 \left[ 1 + \cos h \left( \frac{\mu_c}{k_B T} \right) \right] \right\} \quad (1)$$

$$k_{SPP} = k_0 \sqrt{1 - \left( \frac{2}{\eta\sigma} \right)^2} \quad (2)$$

$$Z_C = \frac{k_{SPP}}{\omega \epsilon_0 \epsilon_{eff}} \quad (3)$$

where  $k_B$  is Boltzmann's constant,  $\tau$  is the electron relaxation time in graphene,  $e$  is the electron charge,  $T$  is temperature,  $\hbar$  is the reduced Planck's constant,  $\omega$  is the angular frequency, and the  $\mu_c$  is graphene's chemical potential. The mentioned equation is valid for the condition of  $\hbar \omega < 2|\mu_c|$ . These are for the different values

of  $\mu_c$ . Interband contributions of graphene conductivity become essential at higher frequencies [24, 25].

Graphene exhibits frequency-dependent behavior from an electromagnetic point of view and demonstrates the characteristics of a surface resistor. However, its conductivity develops a distinct response at terahertz and infrared frequencies. Due to the inherent kinetic inductance of the material serves the function of negative absolute permittivity in a bulk material, this has resulted in the recent invention of steered antennas and devices [26].

Where  $\eta$  is impedance,  $k_0$  is the free-space wavenumber,  $\epsilon_0$  is vacuum permittivity, and effective permittivity is  $\epsilon_{eff}$ . This straightforward model assumes laterally infinite sheets. Graphene's complicated conductivity may be manipulated, without question, one of the fascinating aspects of this material's features [27].

The bias will either inject holes/electrons into the sheet, which will change the chemical potential of the graphene. Recent investigations have shown that this tunability may be pretty considerable and quick, reaching hundreds of gigahertz. Graphene's band structure. The conductivity of graphene transforms into a gyrotropic tensor at this point, which results in fascinating non-reciprocal reactions like Faraday rotation or isolators. In addition, optical pumping has been utilized to change the characteristics of graphene, which has made THz lasing and the functioning of graphene as a reconfigurable gain medium possible [28–30].

### 3 Graphene-Based Antenna Structure

#### 3.1 Resonant Antenna

Because resonant antennas are so common in our everyday lives, it was only logical for researchers to focus their first theoretical attention on these particular types of graphene antennas. For the difficult-to-reach THz frequency band, subwavelength graphene patches are an attractive antenna option due to their resonant properties. These pioneering experiments were carried out by Jornet and colleagues [31].

Having these resonant frequencies at hand allows one to readily extract the structure's absorption and scattering cross sections by retrieving the effective polarizability of the subwavelength patch. Quick on the heels of this research, Tamagnone and coworkers presented the first "real" graphene antenna, one that connects sheet-propagating (SPPs) and far-field radiation [32]. The most significant improvement is a connection for effectively stimulating SPPs across graphene (or detecting them in reception using resonant detection) [33].

The electrical size of the antenna provides a simple explanation for this phenomenon. The antenna's electrical length, measured in terms of free-space wavelength, grows when the chemical potential  $\mu$  is increased, causing a corresponding upshift in the resonant frequency. All graphene antennas have this characteristic since doing so allows for incredibly compact devices to be created by using graphene's

high inductance for small  $c$ , albeit at the expense of radiation efficiency. However, there is a hidden cost to utilizing big  $cc$ : Graphene SPP characteristics become less responsive to bias voltages, reducing their electrical reconfigurability. Designing and analyzing graphene-based dipoles using full-wave simulations allowed the researchers to determine the resonant frequency and input impedance [34].

Another technique to take use of graphene's tunability in building THz antennas is to employ it as a perturbation in other structures that may have superior radiation efficiency, commonly utilizing metals. This research aims to use graphene not as the (main) radiating element but as a resonant frequency that can be electronically tuned. Similar to how previous planar dipoles could be tuned by changing the conductivity of graphene, this new antenna design allows for fine-tuning of the input impedance of the entire structure, allowing for fine-grained control over the antenna's overall efficiency while barely affecting the antenna's radiation efficiency. The graphene resonant antennas we have examined here can all be integrated into larger array structures. The device comprises multiple graphene nanopatch antennas with individually adjustable resonance frequencies. This arrangement makes it possible to have a tiny footprint and integrated subwavelength components for MIMO responses at THz while still accomplishing efficiency and tuning [35].

### 3.2 *Leaky-Wave Antennas*

The unique beam-scanning feature makes leaky-wave antennas (LWAs) makes popular in last several decades. Their foundation is the concept of electromagnetic waves traveling through a waveguide and leaking energy into free space faster than the speed of light due to the waveguide's dielectric properties. Most LWAs are optimized for operation at micro- and millimeter-wave frequencies. Still, the physics behind them is essential to understanding seemingly fantastical phenomena like "extraordinary transmission," "electromagnetically induced transparency," and "Cherenkov radiation." Graphene's unique properties make it ideal for directing leaky waves at THz and infrared frequencies, enabling the creation of reconfigurable structures and, more crucially, the realization of hitherto unattainable magnet-less non-reciprocal responses [36].

Sinusoidal modulation of reactance surfaces is the foundation of a popular and influential class of leaky-wave antennas. This idea, first introduced by Professor Oliner in the 1950s, has lately garnered much attention in the microwave domain. The reactance of device has to be inductive, and the value it takes on defines the constancy of the wave's propagation and its confinement. The radiation rate and angle are both controlled by the modulation amplitude and period. This allows us to write an expression for the effectively modulated surface reactance as per Eq. (4).

$$X'_S = X_S[1 + M\sin(2\pi y/p)] \quad (4)$$

$$k_y = \beta_{SPP} + \Delta\beta_{SPP} - j(\alpha_{SPP} + \alpha_{rad}) \quad (5)$$

$$\theta_0 = \text{asin}(\beta_{-1}/k_0) \approx \text{asin}\left(\frac{\beta_{SPP}}{k_0} - \frac{\lambda_0}{p}\right) \quad (6)$$

Graphene's inductive response makes it an ideal substrate for realizing this idea at THz frequencies. Esquiús-Morote and colleagues suggested the first graphene-based LWA in 2014. The structure comprises a graphene sheet and several polysilicon DC gating pads on a back-metallized substrate. Individual voltages may be applied to each place independently to execute arbitrary modulations of the reactance profiles throughout the sheet and enable the propagation of leaky waves. Modifying the modulation's characteristics allows for real-time adjustment of the emitted beam's pointing angle  $\theta_0$  and leakage rate  $\alpha_{rad}$  [37]. The equation for the fundamental harmonic wavenumber  $k_y$  in a sheet of modified graphene equation, where  $\beta_{SPP}$  is the SPP propagation constant,  $\Delta\beta_{SPP}$  is a minor fluctuation in the wavenumber owing to the modulation,  $\alpha_{SPP}$  is the dissipative attenuation constant, and  $\alpha_{rad}$  is the leaky radiation attenuation constant. The radiating beam on the pointing angle is represented by Eq. (6). Graphene plasmons are relatively lossy, so achieving highly directive beams is difficult, while maintaining high-radiation efficiency is difficult. However, the modulation amplitude  $M$  can favor one of these two goals over the other: A large  $M$  will result in a smaller effective aperture, reducing directivity, while a small  $M$  will increase efficiency [38].

Many writers have also suggested an alternative THz implementation of LWAs based on graphene. In order to excite leaky spatial harmonics, the antenna with gate pads regularly modifies the strip's width. The authors do this by capitalizing on the extreme sensitivity of the plasmon propagation constant. This structure's width-dependent plasmon dispersion may be mapped to practical changes in graphene's conductivity  $\sigma = 1/Z_s$ , allowing for detailed modeling of the structure's modulation of the reactance in design and computation. SPP analytical scaling over the strips width presented was used to carry out such analyses quickly, allowing for rapid realization of methods and studies of such antennas. This version is easier to build than the previous one since no gating pads are required underneath the graphene sheet. However, by providing a single DC bias voltage, the direction of the emitted beam may be precisely controlled at a particular frequency. However, unlike the prior setup, the modulation amplitude  $M$  and operating frequency are now fixed at manufacture based on the width modulation [39].

Composite RH transmission lines and antennas are only two examples of ideas that may be borrowed from the microwave domain and used in implementing LWAs. Other looked explored the possibility of employing graphene plasmonic to achieve similar methods at THz frequencies. Initial findings have been encouraging, but the complexity of the necessary structures and the need for high-quality graphene samples may postpone their practical use for some time.

To fully use graphene's interdisciplinary nature, it has been suggested that elastic vibrations based on flexural (mechanical) waves be used to produce leaky waves.

A wave propagating on graphene may be adequately described as a wave grating over the period  $p$ . The frequency of the flexural waves may be dynamically adjusted using a biharmonic source, allowing for fine-grained control over the emitted beam. The primary benefit of this antenna is that, since mechanical waves are so versatile, they can provide almost any modulation reactance profile. Furthermore, since its characteristics are analogue, the reactance profile does not need to be fixed or discretized by gate electrodes. That's why it's flexible enough to execute any radiation pattern and provide beam-scanning capabilities. However, since the structure relies on vibrating free-standing graphene, it may be challenging to produce and has certain non-planar qualities. In addition, it may be difficult to find the right balance between small plasmonic devices and mechanical parts, particularly in real-world applications [40].

Using graphene as a perturbation element, similar to what was proposed for resonant antennas, is another way to create graphene-based LWAs. The goal is to increase performance or lessen the need for high-quality graphene, both of which may be achieved by using the benefits of various technologies. Graphene is ubiquitously employed in these systems because of its capacity to provide near real-time electronic reconfiguration. Here, we look into LWAs with high-impedance surfaces that use graphene to improve beamforming and provide tuning flexibility.

Non-reciprocal responses without ferromagnetic materials have recently emerged as a potential concept in electromagnetics and the antenna community. Conventionally, this capability has required the use of large, costly magnets, which significantly restricts device downsizing and integration with other technologies. The THz graphene plasmonic applications benefit considerably from this since the silicon-incompatible magnets. Modulating a structure's attributes (permittivity) in space and time has been suggested as a new paradigm to break time-reversal symmetry. Applications of this method span the electromagnetic spectrum, acoustics, and even mechanics, resulting in breakthroughs like exciting high-performance circulators that are also compatible with modern integrated circuits. Essential devices like isolators, circulators, and non-reciprocal antennas may be made smaller and cheaper by shifting to a magnet-less non-reciprocal paradigm [41].

Exciting work by Correas-Serrano has turned such ideas into THz graphene plasmonic by fully leveraging the material's great reconfigurability using the field effect. More precisely, these approach enables the creation of terahertz antennas with a wide range of customizable transmission and reception characteristics. What's more intriguing is that the device's sent and received SPPs fluctuate at different frequencies when time is reversed. When these two events occur together, it may lead to LWAs responding in ways they never have before. We point out that similar methods have recently been used to create non-reciprocal LWAs at microwave frequencies [37, 42].

### 3.3 Reflect array Antennas

Many global and satellite communication systems have seen remarkable capacity gains because of the use of reflect arrays, a well-established issue in the RF, microwave, and antenna research communities. An enlightening feed antenna and a grid of reflecting unit cells combine to create these structures, with each cell introducing a unique phase shift to the reflected wave [43].

In this way, highly directional far-field beams may be synthesized in practically any direction by manipulating the phase fronts of the reflected beam. It's important to remember that the phenomena behind the "generalized Snell laws" that have sparked so much interest in the optics world in recent years are also at the heart of transmit and reflect arrays. Semiconductor diodes, microelectromechanical systems (MEMS) lumped components, and liquid crystals are only some of the technologies suggested for dynamically controlling the phase of the unit cell at micro- and mm waves. However, mainly owing to size and loss, they are inappropriate for use in the THz band. Graphene's high inductance and electric solid field effect, which allow for downsizing and the necessary tunability to synthesize any reflection phase, make it a desirable contender to fill this hole [44]. Reflect arrays made from graphene were initially developed by Carrasco et al. An article unit cell is shown as a square patch of Graphene deposited on a  $\text{SiO}_2$  base. Patches of traditional reflect arrays often constructed of gold or noble metals will resonate. If their size is about equal to half a wave's wavelength in the effective medium, this typically results in massive structures.

## 4 Proposed THz MIMO Antenna

Over the last several years, there has been a meteoric rise in the need for more data rates that boast substantial efficiencies and operate over a broad frequency range. This desire has been brought on by the significant development of wireless communication systems. As a result, research into the terahertz communication band the one presently underutilized for wireless communication services. Meanwhile, by 2021, it's expected that global smartphone traffic would reach over 50 PB/mo. As a result, many academics have begun researching different parts of the terahertz (THz) spectrum, which is located in the middle of the typical microwave and infrared spectral ranges. This spectrum has applications in sensing, imaging, screening, and time-domain spectroscopy [45, 46].

The THz frequency spectrum applies to a vast number of fields and offers a variety of benefits. It does, however, suffer from a shortage of suitable small sources, which is one of the reasons why the employment of this technology is constrained to a more limited scope [47]. Several methodologies have been thoroughly investigated to find a solution to this issue to create acceptable sources that may be used in the THz frequency band [48]. Successful application of the terahertz frequency domain

has been achieved by the Quantum Cascade Laser, or QCL, in this setting. The generation of THz radiation may also be accomplished by using techniques such as optical photo mixing and electro-optical rectification. Using these strategies, it is possible to create output power in the mW range. Along with various kinds of sources for antenna components, end devices need to have high efficiency.

In the terahertz band, there is also a substantial attenuation path loss, another problem preventing its broad deployment. To combat the issue of attenuation, a variety of researchers have developed a variety of high-gain antenna structures. However, due to their three-dimensional, intricate, and massive geometric forms of majority antennas, the majority of these antennas can readily be merged with tiny electronics. Because of this, planar MPA structures have attracted substantial research in the THz frequency range due to the ease with which they may be combined with tiny electronics. However, antenna configurations with a more considerable bandwidth are necessary to offer a greater number of wireless communication services at a higher data rate. The term “Super Wideband” (SWB) antenna refers to an antenna that has an availability that is more than ten times that of a decade ratio (10:1). Several S-Wave band antenna constructions have been given for operation in the THz frequency zone, and these structures are shown in the images. Each of these architectures has a patch with either an elliptical ring fractal or a hexagonal fractal applied to it in order to maximize bandwidth [49].

Two port-loaded THz MIMO antennas are presented to analyze different antenna performances. The proposed work is represented in Fig. 1. Upper view is illustrated in Fig. 1a, and the lower outlook is presented in Fig. 1b. The patch and ground regions are the perfect conductors. The size of the represented structure is  $35\ \mu\text{m}$  by  $50\ \mu\text{m}$ . There are two patches in the system that is considered and analyzed. First, the hexagonal-shaped patch regions are considered. Then, the patch elements are cropped by considering the C-shaped structure. It will help for minimizing the reflectance coefficients. Finally, the rectangular-shaped ground region is considered. Graphene is used for the material of patch elements, and polyimide material is used as a substrate material. The different dimensions of the proposed design are shown in Fig. 1.

The performance of isolation is observed in terms of transmittance and reflectance response in Fig. 2. The analysis is carried out over the 1–20 THz spectrum. There is good isolation observed over this entire range. The broad bandwidth is kept in the field of 3.95–9.65 THz (Bandwidth 5.7 THz).

The envelope correlation coefficient gives us information about the independence between the emission patterns of two antennas. In this scenario, the correlation between the two antennas would be 0 since one antenna would be horizontally polarized while the second antenna would be vertically polarized. The ECC response of the presented structure is shown in Fig. 3. The ECC response of the presented design is near the zero value.

The channel capacity loss of the design is observed in Fig. 4. CCL response of the design structure provides a lower amount of channel capacity loss for the broad spectrum range.



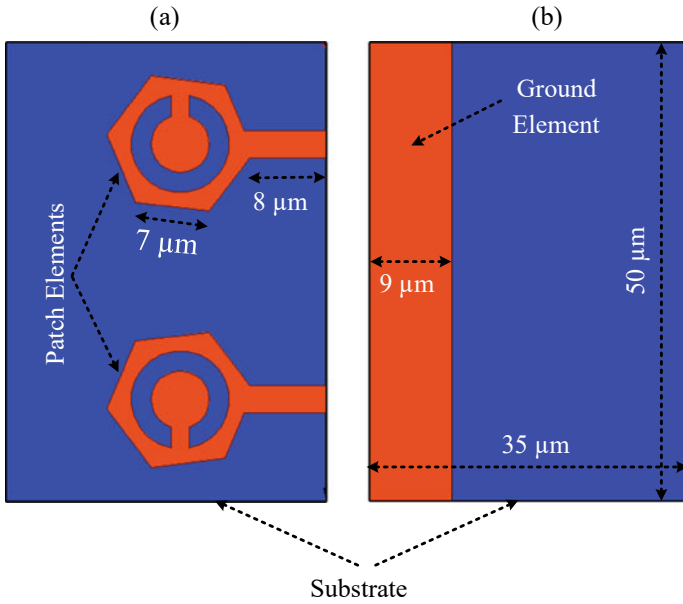


**Fig. 1** Proposed hexagonal patch-based THz MIMO antenna. **a** Top sight of the structure. **b** Bottom sight of the structure

**Fig. 2** Transmittance and reflectance response of the presented design

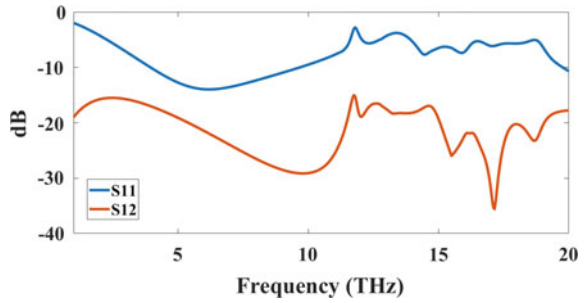


**Fig. 3** ECC response of proposed THz MIMO antenna

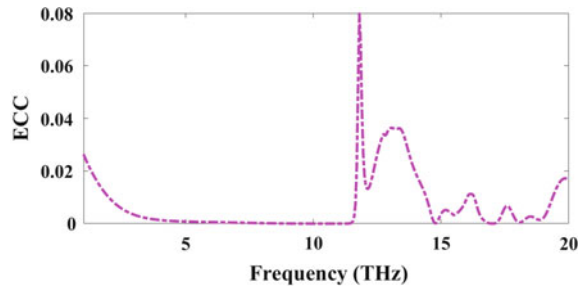


**Fig. 4** CCL response of proposed THz MIMO antenna

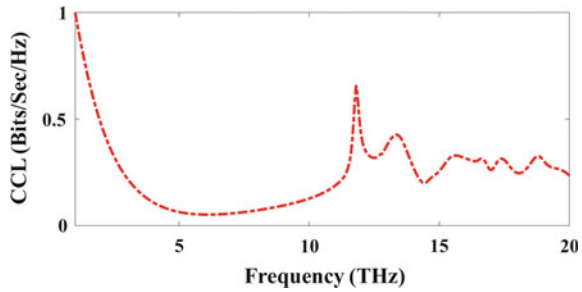
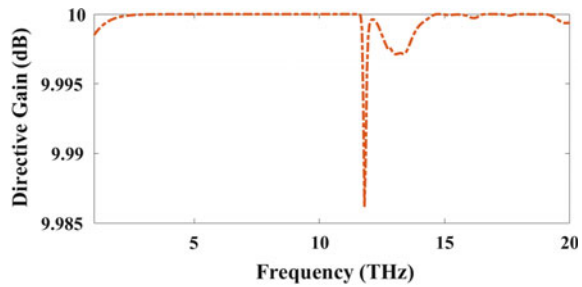


**Fig. 5** DG response of proposed THz MIMO antenna



The expected value of the proposed antenna structure’s directive gain is near 10 dB [50]. Figure 5 represents the DG of the presented antenna structure. The DG response of the system is almost near the 10 dB throughout the spectrum’s 1 THz to 20 THz range.

The healthy gain of the proposed design is 17.1 dB in Fig. 6. The gain response is analyzed for the resonating frequency. Overall, all performance indices are considered to observe the antenna structure’s performance. The necessary conditions like isolation, ECC, DG, CCL, and gain meet the standard requirements.

## 5 Fabrication Technology of Graphene-Based Nanomesh

Graphene, a single-layer sp<sup>2</sup>-hybridized carbon sheet with unusual optoelectronic features, including zero band gap, high carrier mobility, and frequency-independent absorption has garnered much interest in recent years. Nanoelectronics, photodetectors, and biosensors are just a few areas that might benefit from these characteristics. However, its use in electrical and photonic devices is constrained by graphene’s negligible energy gap. Consequently, energy gap reduction and increasing the ratio of  $I_{on}/I_{off}$  is greatly desired. It is generally accepted that several techniques can tune the band gap of graphene [51], strain, and the reforming of the graphene-based nanostructure [52]. Simplifying the material’s nanostructure to reduce its intrinsic

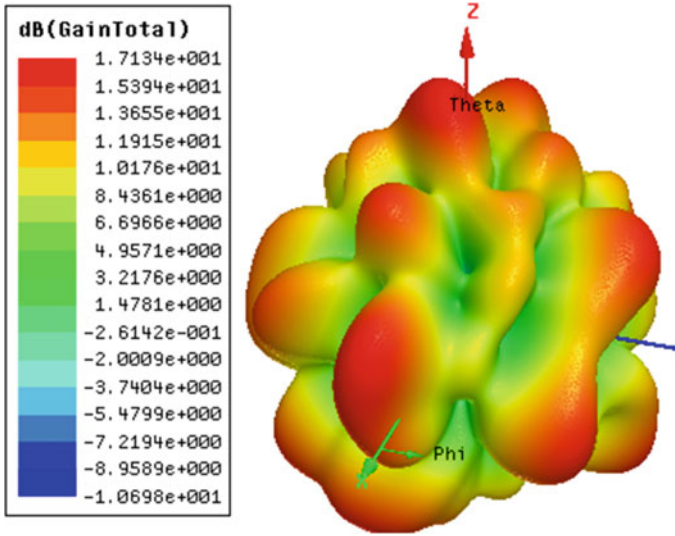


**Fig. 6** Total gain of proposed THz MIMO antenna structure

electronic characteristics is presently the most practical option [53] when graphene is reduced in size to nanostructures like a nanoribbon (GNR), nanoring, or nanomesh.

However, the difficulty in fabricating long, thin GNRs will limit the usefulness of nanoelectronics devices. In contrast to individual GNR devices, FETs based on graphene nanomesh (GNM) can handle currents roughly 100 times larger than personal GNR devices. Using mesoporous silicon (meso-SiO<sub>2</sub>) as a mold, Yang et al. developed highly sensitive biosensors that can specifically detect human epidermal growth. This proves that modifying graphene into GNMs is a potent method for increasing the band gap. To manufacture a large-surface GNM for this purpose. Unfortunately, the GNM's energy gap couldn't be closed since its neck width was too great (260 nm). Using anodic aluminum oxide membranes as pattern masks and O<sub>2</sub> plasma etching, Zang et al. many articles showed a unique template-assisted approach for preparing GNM. To reshape the graphene layer, most GNMs are prefabricated using a nanoparticles as a mask. In order to accomplish the manufacturing of large-scale uniform arrays, however, the nanomask synthesis is complicated.

Electron beam lithography was used to construct large-scale successfully, circular graphene nanomeshes (c-GNMs) and rectangular graphene nanomeshes (r-GNMs) array with varying widths. GNMs were also used to create terahertz detectors based on graphene's photoconductive properties. We conducted electrical experiments at room temperature to learn more about how the GNM neck width impacts detector performance. A more prominent current was seen in c-GNM-based devices, despite a lower  $I_{on}/I_{off}$  current ratio. The photoconductive impact of this unique structure was then assessed by measuring the THz photo currents of r-GNM structure for varying sizes. Finally, bifocal imaging system is used for THz imaging application based on r-GNM devices.

Chemical vapor deposition was used to create a single layer of graphene on a copper substrate across a large area. Polymethyl methacrylate (PMMA) was used to aid in the wet-transfer process before the pattern was transferred to strongly doped p-type Si substrates covered in SiO<sub>2</sub> layer. Electron beam evaporation was used to deposit the Au source and drain electrodes on the graphene, and then the standard metal lift-off technique was used to remove the electrodes. The average distance between electrodes was 14 μm. Second, we used electron beam lithography (EBL) to produce r-GNM and c-GNM, two distinct nanomesh graphene varieties. After the graphene sample was transferred to the substrate, positive e-beam resist for etching mask. Mask aids in specifying the needed shape and dimensions. The exposed graphene was then removed from the air using oxygen plasma [37]. After etching the PMMA away using a mixture of three parts isopropanol to one part methyl isobutyl ketone, the Si<sub>3</sub>N<sub>4</sub> gate dielectrics. After that, the Si<sub>3</sub>N<sub>4</sub> was coated with a gate electrode material vaporized by electron beam evaporation. Both r-GNM and c-GNM were analyzed for their appearance and structure using scanning electron microscopy after they were synthesized. At room temperature, a semiconductor parameter analyzer assessed the detector's electrical properties, while the optical features of the devices were investigated using improvised optical measuring equipment [54].

## 6 Forthcoming Research Scope of THz Antenna

THz antennas have several desirable characteristics: high gain, high radiation, cheap cost, resistance to alkalis and acids, and a wide working bandwidth. In response, the following factors should be prioritized in future THz antennas research.

### 6.1 *Structure Miniaturization*

The limited bandwidth of THz antennas is due to the tiny wavelength of this frequency range. The need for mobile antennas that can be worn increases as the number of intelligent devices proliferates. Efforts to shrink things down have great potential as an area for future study. Right now, it makes more sense to integrate various antennas into a smaller package. The lens's radius may be as small as practical. It is essential to proceed with care so that antenna performance is not degraded. The microstrip antenna offers the most minor return loss, gain, and directivity compared to other antenna types. Wearable antennas are portable antennas that are smaller, lighter, and easier to replicate [55].

## 6.2 *Healthy Gain of Structure*

THz antennas play a crucial role in the overall communication output of a wireless communication device due to their central role in the system. Normal measures of energy conversion and radiation output include gain and efficiency. Bandwidth indicates the possible frequency bandwidth of the antenna. Most significant challenge to THz connection is the attenuation that occurs in the atmosphere. Increasing the gain is a workable strategy since failure on a free-space path is inevitable. Due to the larger operating antenna and little impact on environmental loss, the antennas must be broad-band, high gain, and efficient for optimal use. With THz wave's broad output spectrum, researchers are primarily interested in building highly efficient. However, the low resistivity of silicon substrates makes this impossible. The vast majority of this power is dissipated as heat. Because of this, on-chip antennas built on silicon tend to have subpar radiation behavior.

Even in hostile environments, where the transmission signal is most likely to be degraded, high-gain THz antennas may still perform. THz antennas that are suitable for high-gain horn and lens antenna. Most challenging aspect of developing a THz antenna is constructing an array of individual parts. Miniature THz antennas are available. As a result, setting up the array requires caution and accuracy. The gain enhancement of THz antenna is attained technologically and materially since present manufacturing technologies cannot match the design criteria [56].

## 6.3 *Better Way of Integration*

Due to the increased customer demand several research has looked at THz antenna integration. If several antennas can be integrated on the same chip, then antenna integration will be significantly enhanced. Maintaining electromagnetic compatibility is a significant obstacle for THz packaging techniques (EMC). A small yet dense array of antennas is used to achieve a high gain. The elements of the array mutually interfere with one another. Including a filter, the arrangement makes the building bigger. Miniaturization of THz antennas requires a trade-off with efforts to reduce electromagnetic interference. Since the chip is larger than the wavelength, sophisticated packaging and processing methods must be created. It is well known that CMOS technology is responsible for the recent success of completely embedded applications. Due to this property, CMOS technology may be used in THz-wave circuit design. Integrated circuit's implementation regions have been expanded in THz devices thanks to CMOS and SiGe advancements, which have also affected THz-wave circuit design. Integration and packaging technologies need new architectural and modeling approaches to deal with the complicated activities of electromagnetic waves in embedded structures.

## 7 Concluding Remarks

The rudimentary notions and operational principles behind terahertz operating antennas are incorporated. THz-operated antennas need more careful planning than their lower frequency. Electron mobility, chemical doping, Fermi energy, operating frequency, relaxation time, and ambient temperature are only a few additional factors that contribute to the conductivity model of graphene. Several types of antenna architectures based on graphene are taken into account. These include leaky-wave antennas, resonating antennas, and reflect array antennas. In this article, we investigate the performance behavior of THz MIMO antennas and get insight into their architectures. The research considers the difficulties and the approach for the fabrication technology of graphene-based nanomesh, and it also comprehends the future research scope of the THz antenna.

## References

1. Balanis, C.A.: In: *Antenna Theory: Analysis and Design* (2016)
2. Parchin, N.O., Basherlou, H.J., Al-Yasir, Y.I.A., Abdulkhaleq, A.M., Abd-Alhameed, R.A.: Reconfigurable antennas: Switching techniques—a survey. *Electronics (Switzerland)* **9**(2) (2020). <https://doi.org/10.3390/electronics9020336>
3. “Recent Research Trends of Terahertz Measurement Standards. *IEEE J. Magazine, IEEE Xplore* (2022). <https://ieeexplore.ieee.org/abstract/document/7335435>. Accessed 27 Oct 2022
4. Nagatsuma, T.: *Antenna Technologies for Terahertz Communications* (2019)
5. Woolard, D.L., Brown, E.R., Pepper, M., Kemp, M.: Terahertz frequency sensing and imaging: a time of reckoning future applications? *Proc. IEEE* **93**(10), 1722–1743 (2005). <https://doi.org/10.1109/JPROC.2005.853539>
6. Nagatsuma, T., Ducourneau, G., Renaud, C.C.: Advances in terahertz communications accelerated by photonics. *Nat. Photon.* **10**(6), 371–379 (2016). <https://doi.org/10.1038/nphoton.2016.65>
7. Geim, A.K., Novoselov, K.S.: The rise of graphene. *Nat. Mater.* **6**(3), 183–191 (2007). <https://doi.org/10.1038/nmat1849>
8. Pendry, J.B., Martín-Moreno, L., Garcia-Vidal, F.J.: Mimicking surface plasmons with structured surfaces. *Science* (80-) **305**(5685), 847–848 (2004). <https://doi.org/10.1126/SCIENCE.1098999>
9. Gómez-Díaz, J.S., Esquiús-Morote, M., Perruisseau-Carrier, J.: Plane wave excitation-detection of non-resonant plasmons along finite-width graphene strips. *Opt. Expr.* **21**(21), 24856 (2013). <https://doi.org/10.1364/OE.21.024856>
10. Jornet, J.M., Akyildiz, I.F.: Graphene-based nano-antennas for electromagnetic nanocommunications in the terahertz band (2010). Accessed 06 Jul 2021. [Online]. Available <https://ieeexplore.ieee.org/abstract/document/5505569/>
11. Carrasco, E., Perruisseau-Carrier, J.: Reflectarray antenna at terahertz using graphene. *IEEE Antennas Wirel. Propag. Lett.* **12**, 253–256 (2013). <https://doi.org/10.1109/LAWP.2013.2247557>
12. Perruisseau-Carrier, J., Tamagnone, M., Gomez-Diaz, J.S., Carrasco, E.: In: *European Microwave Week 2013, EuMW 2013—Conference Proceedings; EuMC 2013:43rd European Microwave Conference*, pp. 369–372. (2013) Accessed 27 Oct 2022. [Online]. Available: <https://ieeexplore.ieee.org/abstract/document/6686668>

13. Woessner, A., et al.: Highly confined low-loss plasmons in graphene–boron nitride heterostructures. *Nat. Mater.* **14**(4), 421–425 (2015). <https://doi.org/10.1038/nmat4169>
14. Zomer, P.J., Dash, S.P., Tombros, N., van Wees, B.J.: A transfer technique for high mobility graphene devices on commercially available hexagonal boron nitride. *Appl. Phys. Lett.* **99**(23), 232104 (2011). <https://doi.org/10.1063/1.3665405>
15. Patel, S.K., Sorathiya, V., Sbeah, Z., Lavadiya, S., Nguyen, T.K., Dhasarathan, V.: Graphene-based tunable infrared multi band absorber. *Opt. Commun.* **474**, 126109 (2020). <https://doi.org/10.1016/j.optcom.2020.126109>
16. Sounas, D.L., Caloz, C.: Electromagnetic nonreciprocity and gyrotropy of grapheme. *Appl. Phys. Lett.* **98**(2), 021911 (2011). <https://doi.org/10.1063/1.3543633>
17. Lavadiya, S.P., Patel, S.K., Rayisyan, M.: High gain and frequency reconfigurable copper and liquid metamaterial tooth based microstrip patch antenna. *AEU—Int. J. Electron. Commun.* **137**, 153799 (2021). <https://doi.org/10.1016/j.aeue.2021.153799>
18. Patel, S.K., Lavadiya, S.P., Parmar, J., Ahmed, K., Taya, S.A., Das, S.: Low-cost, multi-band, high gain and reconfigurable microstrip radiating structure using PIN diode for 5G/WiMAX/WLAN applications. *Phys. B Condens. Matter.* **639**, 413972 (2022). <https://doi.org/10.1016/j.physb.2022.413972>
19. Nguyen, T.K., Patel, S.K., Lavadiya, S., Parmar, J., Bui, C.D.: Design and fabrication of multiband reconfigurable copper and liquid multiple complementary split-ring resonator based patch antenna. *Waves in Random and Complex Media* 1–24 (2022). <https://doi.org/10.1080/17455030.2021.2024623>
20. Sumathi, K., Lavadiya, S., Yin, P.Z., Parmar, J., Patel, S.K.: High gain multiband and frequency reconfigurable metamaterial superstrate microstrip patch antenna for C/X/Ku-band wireless network applications. *Wirel. Networks* **27**(3), 2131–2146 (2021). <https://doi.org/10.1007/s11276-021-02567-5>
21. Patel, S.K., Lavadiya, S.P., Parmar, J., Das, S., Ahmed, K., Taya, S.A.: Low-cost, compact, and reconfigurable antennas using complementary split-ring resonator metasurface for next-generation communication systems. *Int. J. Microw. Wirel. Technol.* 1–11 (2022). <https://doi.org/10.1017/S175907872200099X>
22. Fei, Z., et al.: Electronic and plasmonic phenomena at graphene grain boundaries. *Nat. Nanotechnol.* **8**(11), 821–825 (2013). <https://doi.org/10.1038/nnano.2013.197>
23. Pandya, A., Sorathiya, V., Lavadiya, S.: Graphene-based nanophotonic devices. In: *Recent Advances in Nanophotonics—Fundamentals and Applications*, IntechOpen (2020)
24. Patel, S.K., Sorathiya, V., Lavadiya, S., Nguyen, T.K., Dhasarathan, V.: Polarization insensitive graphene-based tunable frequency selective surface for far-infrared frequency spectrum. *Phys. E Low-Dimensional Syst. Nanostruct.* **120**, 114049 (2020). <https://doi.org/10.1016/j.physe.2020.114049>
25. Bonaccorso, F., Sun, Z., Hasan, T., Ferrari, A.C.: Graphene photonics and optoelectronics (2010). <https://doi.org/10.1038/nphoton.2010.186>
26. Correas-Serrano, D., Gomez-Diaz, J.S., Perruisseau-Carrier, J., Alvarez-Melcon, A.: Graphene-based plasmonic tunable low-pass filters in the terahertz band. *IEEE Trans. Nanotechnol.* **13**(6), 1145–1153 (2014). <https://doi.org/10.1109/TNANO.2014.2344973>
27. Novoselov, K.S. et al.: Electric field in atomically thin carbon films. *Science* (80-) **306**(5696), 666–669 (2004). <https://doi.org/10.1126/science.1102896>
28. Patel, S.K., Sorathiya, V., Lavadiya, S., Luo, Y., Nguyen, T.K., Dhasarathan, V.: Numerical analysis of polarization-insensitive squared spiral-shaped graphene metasurface with negative refractive index. *Appl. Phys. B Lasers Opt.* **126**(5), 80 (2020). <https://doi.org/10.1007/s00340-020-07435-2>
29. Phare, C.T., Daniel Lee, Y.-H., Cardenas, J., Lipson, M.: Graphene electro-optic modulator with 30 GHz bandwidth. *Nat. Photon.* **9**(8), 511–514 (2015). <https://doi.org/10.1038/nphoton.2015.122>
30. Lukose, V., Shankar, R., Baskaran, G.: Novel electric field effects on landau levels in grapheme. *Phys. Rev. Lett.* **98**(11), 116802 (2007). <https://doi.org/10.1103/PhysRevLett.98.116802>

31. Martí, I.L. et al.: Scattering of terahertz radiation on a graphene-based nano-antenna, pp. 144–146. (2011). <https://doi.org/10.1063/1.3644239>
32. Tamagnone, M., Gómez-Díaz, J.S., Mosig, J.R., Perruisseau-Carrier, J.: Analysis and design of terahertz antennas based on plasmonic resonant graphene sheets. *J. Appl. Phys.* **112**(11), 74106 (2012). <https://doi.org/10.1063/1.4768840>
33. Tamagnone, M., Gómez-Díaz, J.S., Mosig, J.R., Perruisseau-Carrier, J.: Reconfigurable terahertz plasmonic antenna concept using a graphene stack. *Appl. Phys. Lett.* **101**(21), 214102 (2012). <https://doi.org/10.1063/1.4767338>
34. de Arquer, F.P.G., Volski, V., Verellen, N., Vandenbosch, G.A.E., Moshchalkov, V.V.: Engineering the input impedance of optical nano dipole antennas: materials, geometry and excitation effect. *IEEE Trans. Antennas Propag.* **59**(9), 3144–3153 (2011). <https://doi.org/10.1109/TAP.2011.2161544>
35. Dragoman, M., Muller, A.A., Dragoman, D., Cocchetti, F., Plana, R.: Terahertz antenna based on graphene. *J. Appl. Phys.* **107**(10), 104313 (2010). <https://doi.org/10.1063/1.3427536>
36. Hu, Y., et al.: Extraordinary optical transmission in metallic nanostructures with a plasmonic nanohole array of two connected slot antennas. *Plasmonics* **10**(2), 483–488 (2015). <https://doi.org/10.1007/s11468-014-9831-z>
37. Hadad, Y., Soric, J.C., Alu, A.: Breaking temporal symmetries for emission and absorption. *Proc. Natl. Acad. Sci.* **113**(13), 3471–3475 (2016). <https://doi.org/10.1073/pnas.1517363113>
38. Rudramuni, K., Majumder, B., Rajanna, P.K.T., Kandasamy, K., Zhang, Q.: Dual-band asymmetric leaky-wave antennas for circular polarization and simultaneous dual beam scanning. *IEEE Trans. Antennas Propag.* **69**(4), 1843–1852 (2021). <https://doi.org/10.1109/TAP.2020.3026898>
39. Chu, D.A., Hon, P.W.C., Itoh, T., Williams, B.S.: Feasibility of graphene CRLH metamaterial waveguides and leaky wave antennas. *J. Appl. Phys.* **120**(1), 013103 (2016). <https://doi.org/10.1063/1.4955138>
40. Gomez-Diaz, J.S., Alvarez-Melcon, A., Bertuch, T.: A modal-based iterative circuit model for the analysis of CRLH leaky-wave antennas comprising periodically loaded PPW. *IEEE Trans. Antennas Propag.* **59**(4), 1101–1112 (2011). <https://doi.org/10.1109/TAP.2011.2109357>
41. Estep, N.A., Sounas, D.L., Alu, A.: Magnetless microwave circulators based on spatiotemporally modulated rings of coupled resonators. *IEEE Trans. Microw. Theory Tech.* 1–17 (2016). <https://doi.org/10.1109/TMTT.2015.2511737>
42. Patel, S.K., Sorathiya, V., Lavadiya, S., Thomas, L., Nguyen, T.K., Dhasarathan, V.: Multi-layered graphene silica-based tunable absorber for infrared wavelength based on circuit theory approach. *Plasmonics* **15**(6), 1767–1779 (2020). <https://doi.org/10.1007/s11468-020-01191-x>
43. Baracco, J.-M., Ratajczak, P., Brachet, P., Toso, G.: Dual frequency Ka-band reflectarray for ground terminal application. In *The 8th European Conference on Antennas and Propagation (EuCAP 2014)*, April 2014, pp. 1437–1440. (2014). <https://doi.org/10.1109/EuCAP.2014.6902050>
44. Legay, H., Pinte, B., Charrier, M., Ziaei, A., Girard, E., Gillard, R.: A steerable reflectarray antenna with mems controls. In: *IEEE International Symposium on Phased Array Systems and Technology*, pp. 494–499. (2003). <https://doi.org/10.1109/PAST.2003.1257031>
45. Mumtaz, S., Jornet, J.M., Aulin, J., Gerstaecker, W.H., Dong, X., Ai, B.: Terahertz communication for vehicular networks. *IEEE Trans. Veh. Technol.* **66**(7), 5617–5625 (2017). <https://doi.org/10.1109/TVT.2017.2712878>
46. Krozer, V. et al.: Terahertz imaging systems with aperture synthesis techniques. *IEEE Trans. Microw. Theory Tech.* **58**(7) PART 2, 2027–2039 (2010). <https://doi.org/10.1109/TMTT.2010.2050246>
47. Sharma, A., Singh, G.: Rectangular microstrip patch antenna design at THz frequency for short distance wireless communication systems. *J. Infrared, Millimeter, Terahertz Waves* **30**(1), 1–7 (2009). <https://doi.org/10.1007/s10762-008-9416-z>
48. Mukherjee, P., Gupta, B.: Terahertz (THz) frequency sources and antennas—a brief review. *Int. J. Infrared Millimeter Waves* **29**(12), 1091–1102 (2008). <https://doi.org/10.1007/s10762-008-9423-0>



49. Das, S., Mitra, D., Bhadra Chaudhuri, S.R.: Fractal loaded planar super wide band four element MIMO antenna for THz applications. *Nano Commun. Netw.* **30**, 100374 (2021). <https://doi.org/10.1016/j.nancom.2021.100374>
50. Dave, K., et al.: Graphene-based double-loaded complementary split ring resonator (CSRR) slotted MIMO patch antenna for spectroscopy and imaging THz applications. *Appl. Phys. A* **128**(8), 656 (2022). <https://doi.org/10.1007/s00339-022-05820-6>
51. Yu, W.J., Liao, L., Chae, S.H., Lee, Y.H., Duan, X.: Toward tunable band gap and tunable dirac point in bilayer graphene with molecular doping. *Nano Lett.* **11**(11), 4759–4763 (2011). <https://doi.org/10.1021/nl2025739>
52. Sun, J., Iwasaki, T., Muruganathan, M., Mizuta, H.: Lateral plasma etching enhanced on/off ratio in graphene nanoribbon field-effect transistor. *Appl. Phys. Lett.* **106**(3), 033509 (2015). <https://doi.org/10.1063/1.4906609>
53. Marmolejo-Tejada, J.M., Velasco-Medina, J.: Review on graphene nanoribbon devices for logic applications. *Microelectron. J.* **48**, 18–38 (2016). <https://doi.org/10.1016/j.mejo.2015.11.006>
54. Yuan, W. et al.: The fabrication of large-area, uniform graphene nanomeshes for high-speed, room-temperature direct terahertz detection. *Nanoscale Res. Lett.* **13**(1), 190 (2018). <https://doi.org/10.1186/s11671-018-2602-6>
55. Kalra, P.P., Sidhu, E.: Rectangular TeraHertz microstrip patch antenna design for riboflavin detection applications. In: *Proceedings 2017 International Conference Big Data Analysis Computing Intelligence ICBDAI 2017*, pp. 303–306. (2017). <https://doi.org/10.1109/ICBDACI.2017.8070853>
56. Rabbani, M.S., Ghafouri-Shiraz, H.: Liquid crystalline polymer substrate-based THz microstrip antenna arrays for medical applications. *IEEE Antennas Wirel. Propag. Lett.* **16**, 1533–1536 (2017). <https://doi.org/10.1109/LAWP.2017.2647825>

# Design of Monopole Ground Graphene Disc-Inserted THz Antenna for Future Wireless Systems



K. Vasu Babu, Gorre Naga Jyothi Sree, Kumutha Duraisamy,  
M. Jeyabharathi, and Sudipta Das

**Abstract** This paper demonstrates the basic circular patch and monopole ground plane with graphene patch underneath the substrate. The designed radiator performance has been evaluated in terms of chemical potentials, S-parameters, E-field, H-field and VSWR. In this design, using the substrate of polyimide with lower dielectric constant 3.5 and the thickness is 40.0  $\mu\text{m}$  has been considered in antenna design. In this design, the ground plane, patch and feed line are designed with copper having resistivity and conductivity are.  $1.68 \times 10^{-8} \Omega\text{-m}$  and  $5.8 \times 10^7 \text{ S/m}$ , respectively. The designed structure has been fed with microstrip feeding line of impedance 49.68  $\Omega$ . The current design structure has an impedance of real part is nearly zero, and imaginary part is with negative value which is resonating at 1.6 THz. The current designed structure is used in the applications like homeland defence and image of video rate systems. The simulation and designing of current THz system using CST MW Studio 2018 are based on the technique of FDTD.

**Keywords** Antenna · Tunable · Graphene · Terahertz · Strip radiator · E-field · H-field

---

K. Vasu Babu (✉)

BVRIT Hyderabad College of Engineering for Women, Bachupally, Hyderabad, India  
e-mail: [vasubabuece@gmail.com](mailto:vasubabuece@gmail.com)

G. N. J. Sree

Department of ECE, Vasireddy Venkatadri Institute of Technology, Guntur, A.P, India

K. Duraisamy

Department of Biomedical Engineering, Karpaga Vinayaga College of Engineering and Technology, Chengalpattu, Tamilnadu, India

M. Jeyabharathi

Department of Electronics and Communication Engineering, K.S.R. Institute for Engineering and Technology, Tiruchengode, Namakal, Tamilnadu 637215, India

S. Das

Department of Electronics and Communication Engineering, IMPS College of Engineering and Technology, Malda, West Bengal, India

## 1 Introduction

A significant transformation in the modern technology of wireless communications has been seen over past decades. Due to the growing of faster data rates mostly in the current communication wireless technology, the data connection enhancement in mobile communication technology due to research achievements resulting in the era of advanced research applications with new possibilities carrying out the research of variety of institutions. The various factors influence the system like restricted communication distance and propagation route loss including substantial amount. The frequency related to the communications of terahertz offers obstacles and exciting promise. The performance of THz system is directly impact on features of THz systems must not lose their sight of the system. The THz system must not be the forgotten it should be something. For the huge demand and better sensitivity and compact size of radiators, transmitting and sensing are two reasons for THz waves. Mobile communications, broadcasting and satellites, multimedia, identification of weapons and explosives (weapon identification system and development of explosive), medical systems and environmental sensing include development of radars are the some of the applications in the era of THz communication system. For the growing need of higher amount of data rates in wireless technology of communication related to current trend for the last several decades of communication. In [1] designed on glass material used as substrate for THz high-speed communications, a micro-scaled wideband MIMO-printed radiator for THz system [2], using the polyimide substrate-designed THz antenna for video rate systems for imaging and defence homeland area applications [3], using photonic crystal substrate designed THz patch antenna and analysed [4], using ohm & L-shape symbols designed MIMO radiating system [5], a ring-shaped THz wideband MIMO radiator with tetradecagonal system [6], a micro-sized optimization of MIMO system for THz range based on their characteristic analysis related to graphene material [7], for UWB applications designed THz microstrip patch antenna [8], for THz system range 0.33 THz-10.0 THz designed super wideband system with high-isolation [9], using DGS designed a MIMO UWB system reduce mutual coupling [10], a fractal shape structure like hexagonal designed for THz for super-wideband system [11], for the interference inherent designed a MIMO radiator system using DGS [12], in THz region graphene patch designed [13], compact U-shaped design designed [14] and metamaterial with graphene reflector explained [15].

## 2 Antenna Geometry

The final antenna structure of current design is shown in Fig. 1. The geometry consists of simple circular ring with microstrip feed line attached with diameter 'S' and strip line width ' $W_f$ ' and considered the height related to the substrate  $L_f = 1.6 \mu\text{m}$  and monopole ground with inserted graphene disc on back side design to improve

**Fig. 1** Proposed antenna geometry

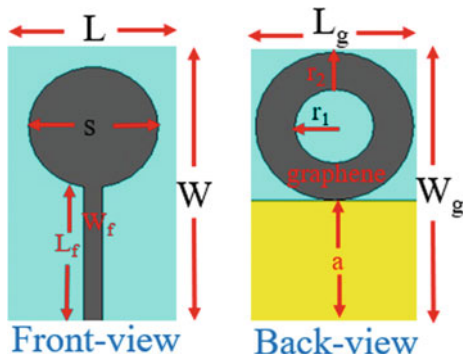


**Table 1** Description of symbols in  $\mu\text{m}$

Symbol	L	W	S	$L_f$	$W_f$	a	$r_1$	$r_2$	$L_g$	$W_g$
Value	50	30	18	1.6	2.5	14	12	6	50	30

bandwidth related to system. The permittivity of the designed substrate  $\epsilon_s = 3.5$  and thickness of  $40 \mu\text{m}$  having the structure dimensions indicates with  $L \times W$  is required for implementation of current THz system. By using the lithography of electronic beam patterned the ground plane radiator shape. The various expressions required to analyse the graphene material with chemical potentials are [15]. Table 1 shows design parameters related current designed structure.

$$\sigma_{\text{intra band}}(\omega, \mu_c, \Gamma, T) = -j \frac{e^2 K_B T}{\pi h^2 (\omega - j2\Gamma)} \times \left( \frac{\mu_c}{K_B T} + 2 \ln \left( e^{\frac{-\mu_c}{K_B T}} + 1 \right) \right) \quad (1)$$

Here, ‘e’ indicates the charge of electron, ‘h’ indicates Planck’s constant value and ‘ $k_v$ ’ indicates Boltzmann’s constant value.

$$\sigma_{\text{interband of graphene}}(\omega, \mu_c, \Gamma, T) \approx \frac{-je^2}{4.0 \pi h} \ln \left( \frac{2.0|\mu_c| - (\omega - j\Gamma)h}{2.0|\mu_c| + (\omega - j\Gamma)h} \right) \quad (2)$$

Here, conditions are considered as  $h\omega = 2|\mu_c|$ ,  $K_B T \approx |\mu_c|$  and  $K_B T \approx h\omega$ .

$$n_s = \frac{2}{\pi h^2 v_f^2} \int_0^\infty E (f_d(E) - f_d(E + 2\mu_c)) dE \quad (3)$$

Here, distribution of Fermi–Dirac function  $f_d(E)$  represents their required energy,  $f_d(E) = \left( e^{\frac{E - \mu_c}{k_B T}} + 1 \right)^{-1}$  and  $v_f$  represents the Fermi velocity which approximately ( $10^8 \text{ cm/s}$ ). The distribution function of electric field expression taken as [14].

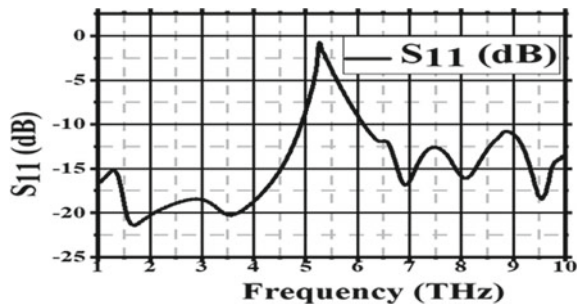
$$\frac{2\varepsilon_s E_0}{e} = \frac{2}{\pi h^2 v_f^2} \int_0^\infty E(f_d(E) - f_d(E + 2\mu_c)) dE \tag{4}$$

### 3 Results Analysis

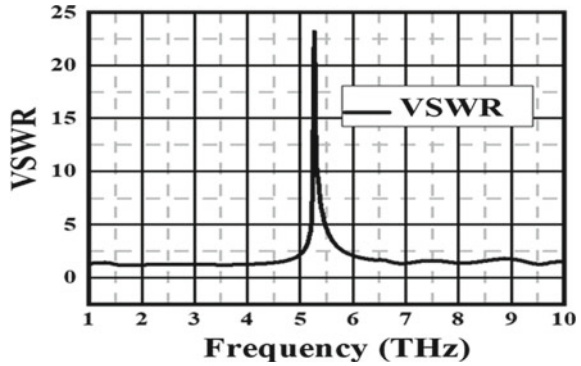
In the field of wireless technology, the spectrum of THz spectrum plays a satisfied major role in transmission related secured high-speed and ultra-wideband systems. In this paper designed, a high-performance THz antenna using CST MW Studio 2018. The designed antenna scrutinized by VSWR, E-field, H-field, radiation pattern including H-field, E-field and return loss ( $S_{11}$ ). Figure 2 shows the S-parameters of current design structure is obtained  $\leq -10.0$  dB at required system. Figure 3 displays the representation related VSWR of present designed which is  $\leq 2$  at the resonant band of the designed region which makes the proposed system is better of current THz design applications well suited. Figure 4 displays impedance representation in form of real part as well as imaginary part leads the real parts of the impedance is nearly zero, and imaginary part of the design is negative impedance acts like a capacitor and inductor.

Figure 5 shows the designed THz system by varying various chemical potentials varying from  $\mu_c = 0$  V to  $\mu_c = 1.0$  V with an increment of 0.2 V of reflection coefficient ( $S_{11}$ ) which is  $\leq -10.0$  dB at resonant required system. Figure 6 shows distribution-related E-field of present design which related fields of current are maximum along the horizontal directions of current designed structure. Figure 7 shows the distribution of H-field of the current design which the fields of current are maximum along the vertical directions of current designed structure. Figure 8 displays the distribution-related surface currents which lead at the edges of the design, and ground plane represents the maximum current flows through the monopole ground completely which improves the bandwidth of the system due to monopole ground structure. Figure 9 displays radiation pattern of E-field along with H-field which consists both principal plane radiations for both cross-pole and co-pole

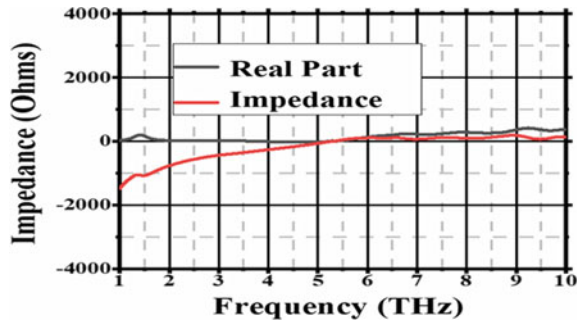
Fig. 2 S-parameters of design



**Fig. 3** VSWR related to design

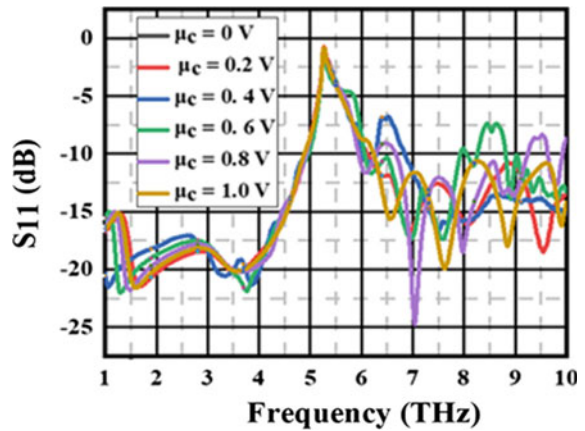


**Fig. 4** Impedance related to design



patterns. The plane of E-field produces omnidirectional radiation patterns, and for the H-plane, omnidirectional with maximum radiation at the azimuthal angle is observed. A difference of  $-30$  dB is identified among the radiation strengths of cross-pole and co-pole radiations.

**Fig. 5** Chemical potentials of the design



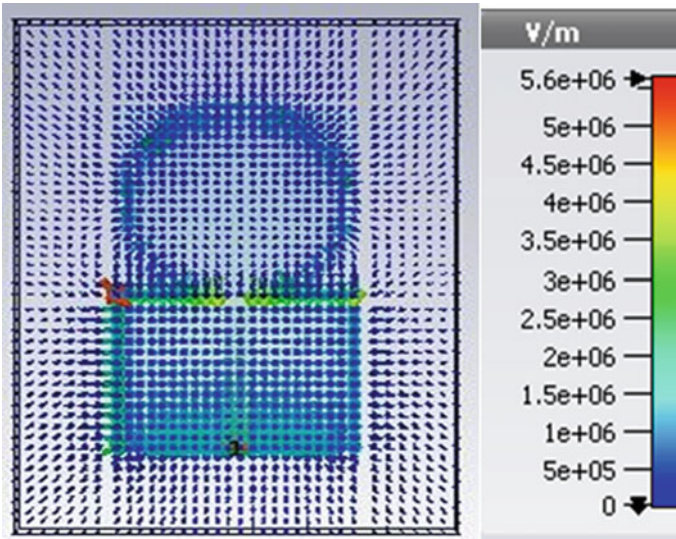


Fig. 6 E-field related to design

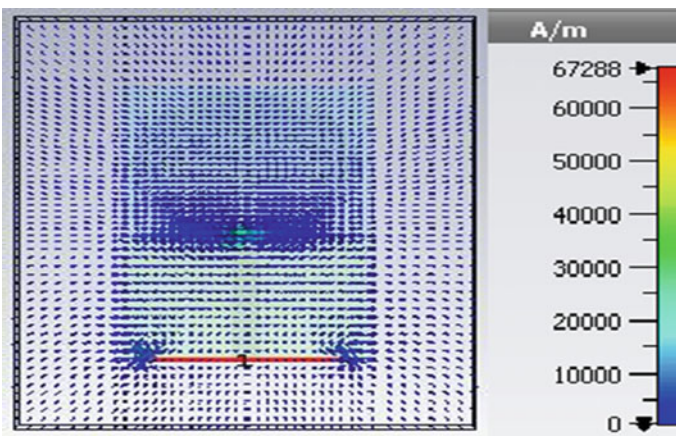


Fig. 7 H-field of elated to design

### 4 Conclusions

A graphene-based circular patch radiator has been designed in this paper at frequency of 1.6 THz. The performance of the current design radiator has reported the VSWR, S-parameters, impedance and chemical potentials by implementing on the substrate of polyimide substrate. The design has shown the acceptable parameters of the radiator. For the current, designed structure has been identified that  $VSWR \leq 2$  within the



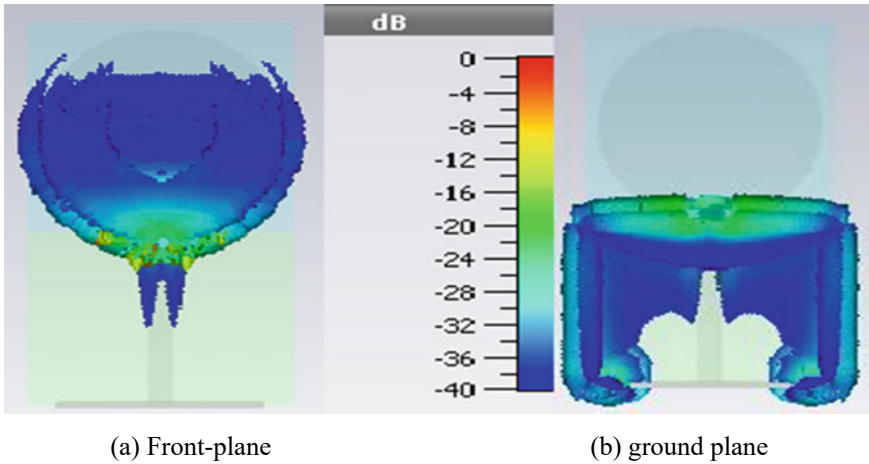


Fig. 8 Distribution of surface currents of the design

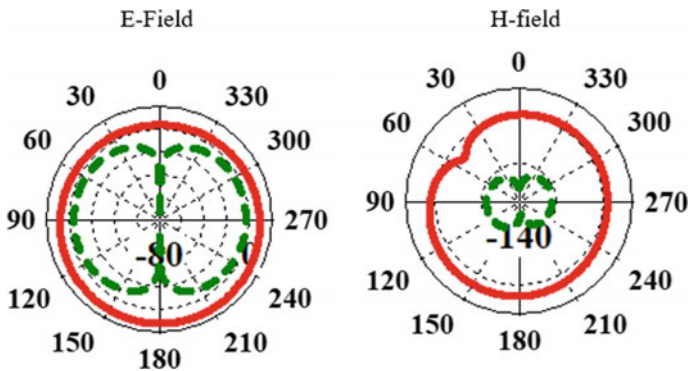


Fig. 9 Radiation pattern of current design

resonant band of frequencies with E-field, H-field and surface current distributions has been identified. The design antenna would be used for the applications of security-related technology system, spectroscopy-type materials and medical imaging, etc.

## References

1. Rahul, G., Kumar Vishwakarma, D.: Design of a graphene-based patch antenna on glass substrate for high-speed terahertz communications. *Microwave Opt. Technol. Lett.* **60.7**, 1594–1600 (2018)
2. Vasu Babu, K. et al.: A micro-scaled graphene-based tree-shaped wideband printed MIMO antenna for terahertz applications. *J. Comput. Electron.* 1–15 (2022)



3. Dhillon, A.S., Mittal, D., Sidhu, E.: THz rectangular microstrip patch antenna employing polyimide substrate for video rate imaging and homeland defence applications. *Optik* **144**, 634–641 (2017)
4. Kushwaha, R.K., Karuppanan, P., Malviya, L.D.: Design and analysis of novel microstrip patch antenna on photonic crystal in THz. *Phys. B: Condensed Matter* **545**, 107–112 (2018)
5. Vasu, B.K., Anuradha, B.: Design of inverted L-shape and ohm symbol inserted MIMO antenna to reduce the mutual coupling. *AEU-Int. J. Electron. Commun.* **105**, 42–53 (2019)
6. Sarthak, S.: Tetradecagonal ring shaped terahertz superwideband MIMO antenna. *Optik* **208**, 164066 (2020)
7. Kommanaboyina Vasu, B. et al.: Design and optimization of micro-sized wideband fractal MIMO antenna based on characteristic analysis of graphene for terahertz applications. *Opt. Quantum Electron.* **54.5**, 1–20 (2022)
8. Singhal, S.: Ultrawideband elliptical microstrip antenna for terahertz applications. *Microw. Opt. Technol. Lett.* **61**(10), 2366–2373 (2019)
9. Gaurav, S., Awasthi, Y.K., Jain, P.: High isolation and high gain super-wideband (0.33–10 THz) MIMO antenna for THz applications. *Optik* **223**, 165335 (2020)
10. Vasu, B.K., Anuradha, B.: Design of UWB MIMO antenna to reduce the mutual coupling using defected ground structure. *Wireless Personal Commun.* **118.4**, 3469–3484 (2021)
11. Sarthak, S.: Hexagonal fractal antenna for super wideband terahertz applications. *Optik* **206**, 163615 (2020)
12. Vasu, B.K., Anuradha, B.: Design of MIMO antenna to interference inherent for ultra-wide band systems using defected ground structure. *Microwave and Opt. Technol. Lett.* **61.12**, 2698–2708 (2019)
13. Bala, R., Marwaha, A.: Characterization of graphene for performance enhancement of patch antenna in THz region. *Optik* **127**(4), 2089–2093 (2016)
14. Vasu, B.K. et al.: Compact dual-band design and analysis of half-circular U-shape MIMO radiator for wireless applications. *Microsyst. Technol.* 1–14 (2022)
15. Deng, G et al.: Tunable terahertz metamaterial with a graphene reflector. *Mater. Res. Expr.* **3.11**, 115801 (2016)

# Graphene-Based D-Shaped Gold-Coated Photonic Crystal Fiber for Transformer Oil Moisture Sensing



M. S. Mani Rajan and N. Ayyanar

**Abstract** Graphene is a sheet of carbon atoms organized in a honeycomb lattice. It has great electrical, mechanical, thermal, and electrical properties due to its high electron mobility. Graphene absorbs light at any frequency, including THz, due to its broad spectrum of optical absorption properties, making it appropriate for various photonic applications. In terms of sensing technology, an optical fiber sensor with graphene coating will improve sensing performance and also have large research influence due to its low cost and scalability. Because of graphene's high specific surface area, it is more appropriate for biomolecule absorption, allowing for label-free, real-time detection of biological molecules such as protein and DNA. This chapter discusses the most recent advances in photonic crystal fiber for THz applications. In particular, a D-shaped graphene-covered PCF sensor for detecting the quality of transformer oil when it is contaminated is thoroughly examined.

**Keywords** Photonic crystal fibers · Graphene coating · D-shaped PCF · Photonic sensor · Transformer oil

## 1 Introduction

In 2010, the Nobel Prize has been awarded to physicist Geim and Novoselov for their significant contribution to findings the graphene's properties. Graphene can be considered as a peculiar material for many applications since its unexpected electronic band structure [1]. Since 2004, graphene has attracted great interest after the successful isolation from graphite [2], and pioneering works on experimental investigation have been carried out due to its unique quantum electromagnetic properties

---

M. S. Mani Rajan (✉)  
Department of Physics, Anna University, University College of Engineering,  
Ramanathapuram 623513, India  
e-mail: [senthilmanirajanofc@gmail.com](mailto:senthilmanirajanofc@gmail.com)

N. Ayyanar  
Department of Electronics and Communication Engineering, Thiagarajar College of Engineering,  
Madurai, Tamil Nadu, India

[3, 4]. Also, graphene unlocked the world of photonics for some new developments. Graphene exhibits more chemical reactivation nature which is hundred times better than thicker sheets. Graphene exhibits excellent optical absorption property with broadband which means that graphene can be regarded as perfect absorber of light at any frequency, especially in THz regime. In the frequency spectrum of THz and mid-infrared, graphene material employed in different dimensions because of excellent tunable electrical conductivity and optical properties like optically transparent [5], tunable electromagnetic [6], and high electron mobility [7]. The controllable property of the graphene can be attained by changing Fermi level through tuning the applied bias voltage. The graphene is an excellent conductor which is having zero band gap, large surface area and  $\pi$ -conjugation structure. Hence, it is suitable photonic material for SPR-based biosensing applications. Since it has zero band gap, its absorption coefficient has covered the 2.3% ranges in the electromagnetic spectrum between ultraviolet and far-infrared (FIR) wavelengths. In order to enhance the sensing performances, we should enhance the optical interaction with graphene material in an efficient manner. The combination of graphene with plasmonic materials like noble metals could be employed to improve the sensing characteristics of biosensors.

In terahertz regime, graphene effectively supports to plasmonic wave propagation in the subwavelength scale where it can be tunable for various applications. The conductivity layer model with complex conductivity  $\sigma_s(\omega, \mu_c, \tau, T)$  parameters is used to calculate graphene's electrical characteristics. Thus, the conductivity of graphene is equal to addition of conductivity belongs to intra- and inter-band [8], which are defined as follows:

$$\sigma_s = \sigma_{\text{inter}} + \sigma_{\text{intra}} \quad (1)$$

$$\sigma_{\text{intra}} = \frac{-je^2k_B T}{\pi \hbar^2(\omega - j2\Gamma)} \left( \frac{\mu_c}{k_B T} + 2 \ln \left( e^{-\frac{\mu_c}{k_B T}} + 1 \right) \right) \quad (2)$$

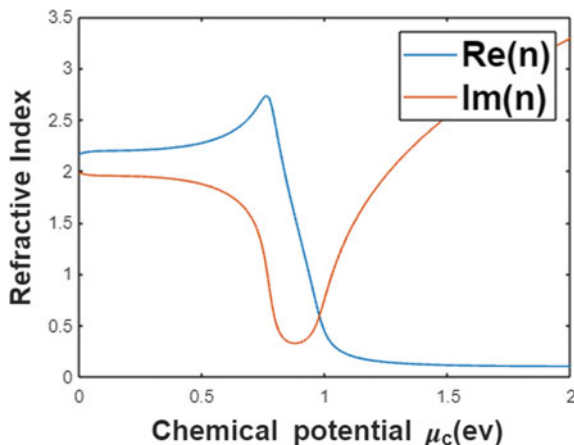
$$\sigma_{\text{inter}} = \frac{-je^2}{4\pi \hbar} \ln \left( \frac{2|\mu_c| - (\omega - j2\Gamma)\hbar}{2|\mu_c| + (\omega - j2\Gamma)\hbar} \right) \quad (3)$$

With  $\tau = \frac{\mu_m \mu}{ev_f^2}$ .

Here,  $\omega$  is angular frequency,  $\Gamma$  is the rate of scattering,  $\hbar$  and  $k_B$  are respectively denote the Planck's constant and Boltzmann's constant. Here, the values of  $\mu_c$  range from 0.2 eV to 1 eV, the value of  $\tau^{-1}$  is the electron relaxation time, which is  $10^{-13}$  s ( $\tau^{-1} = \Gamma$ ), and the temperature  $T$  is 300 K. The proposed structure is also dissected by the incident wave's varied polarization.

The chemical potential ( $\mu_c$ ) has major impact on conductivity of graphene surface. Chemical potential  $\mu_c$  is a parameter which could be control the properties of graphene. By using the value of surface conductivity ( $\sigma_G$ ), permittivity of graphene can be determined [9].

**Fig. 1** Refractive index ( $n$ ) variation with respect to chemical potential for graphene



$$\varepsilon_G = 1 - i \frac{\sigma_G}{\omega \varepsilon_0 d_G} \quad (4)$$

In Eq. (4),  $\varepsilon_0$  denotes the permittivity of vacuum and  $d_G$  represents the graphene layer's thickness which is 10 nm. Where is the angular frequency with a value of  $2\pi c/\lambda$  and  $i$  denotes the permittivity's imaginary quantity. The graphene refractive index varies with chemical potential, as illustrated in Fig. 1 at 800 nm.

where  $\omega = 2\pi c/\lambda$  is angular frequency and  $i$  implies the imaginary quantity of the permittivity. Variation of refractive index of graphene with respect to chemical potential is shown in Fig. 1 at the wavelength 800 nm.

Recently, creating graphene artificially has been receiving considerable attention due to controlling and managing in the field of photonics. Graphene possesses tremendous properties of electrical conductivity, luminescence, flexibility, etc. due to which graphene-based biosensor can be used in early cancer and tumor recognition [10]. Graphene perturbations added in waveguide structure increase the sensitivity by the shifted peak in terms of absorption and reflection [11]. The leakage in the optical leaky-wave antenna increases due to the addition of graphene by changing its chemical potential [12]. The excitation of localized surface plasmon resonance (LSPR) has been excited is observed when gold nanoparticles combined with graphene, and it increases the sensitivity and detection of ascorbic acid which is helpful in the immunity and is used in online monitoring, detection of microdroplets, etc. to fight against bacteria, viruses, etc., and they are fabricated from more doped photosensitive fiber to unit mode fiber [13]. Graphene-based plasmonic sensors and nanoring resonators are linked with biomolecules that are used for the detection of hybridization of DNA-related issues through the finite element method (FEM) and have been progressive in the field of photonics and helpful in developing nanosensors [14]. Graphene-based metasurface infrared sensor using C-shaped material tungsten material increases sensitivity, and it is obtained through shift absorption peak by adding biomolecules [15].

Graphene and plasmonic material-based biosensor can be used to improve the sensitivity and detection accuracy through 3D-finite difference time domain method (3D FDTD) [16]. Graphene-based long-period fiber grating is used in detection of glucose from a linear response of graph that helps in better detection [17]. The detection of the concentration of urea is needed for dialysis of kidney patients to calculate the value of PH, urease is used as a biomaterial with graphene detects composition of carbon and ammonia [18]. Nanomaterial-based optical sensors used in working with detection of all types of bacteria such as salmonella typhi, *Escherichia coli*, that bear the loss in social and economic progress compared to other materials that are used for detection of bacteria being so insensitive [19].

Graphene-based Bloch surface wave sensor with truncate layer 1-D photonic crystal (DPC) in which layer's thickness is optimized and adding up the graphene layer increases sensitivity which is not observed in surface plasmon resonance [20]. Graphene can be used to detect the bioanalyte like proteins, nucleic acids, DNA, etc. DNA strands from shorter to longer detection of polymer used technologies in treating the harmful diseases and can be recycled [21]. Single-mode fiber-based sensors are sensible for detection and protection from most harmful gases by depositing graphene through various techniques such as ultraviolet spectroscopy and atomic force microscope (AFM) and make a broad change in the optical band which is used in mines [22]. Plasmonic properties used with graphene in polarization-independent sensor observing them absorption in a limit wavelength range are applicable in environmental applications [23, 24].

## 2 Photonic Crystal Fibers

A special type of optical fibers which are having microstructure with the wavelength scale along their length is known as photonic crystal fibers [25]. Based on their guiding mechanisms, photonic crystal fibers classified as two types namely index-guiding PCF [26] and photonic bandgap fibers (PBF) [27]. Light is limited to a solid core in index directing PCFs using the modified total internal reflection (m-TIR) principle, whereas cladding regions with low effective index are created using an array of air holes. These fibers having various features like endlessly single-mode operation which can support only the fundamental mode for wide range of wavelength, high nonlinearity due to extremely smaller core radius, tunable dispersion property, excellent birefringent characteristics, etc. In the case of photonic bandgap fiber, however, light is trapped in the low index medium. In this kind of PCF, air-core is located at the center and silica-based photonic crystal cladding is comprised in the background with the triangular array of air holes. When compare with silica material, air-core has a lower refractive index value where TIR guidance is not possible [28]. Recently, the investigations on coated photonic crystal fiber (PCF) with suitable material for photonic sensing applications are exponentially increasing. Especially, for biosensing applications, numerous PCF-based biosensors have been developed and investigated [29]. Besides, PCF received huge attention because of freedom to

designing the structure with tailoring property. Through some pioneering techniques, numerous PCF structures are proposed to attain the desirable properties for various sensing applications to sense different analytes.

In order to investigate the PCF structures, various techniques of numerical analysis have been employed to investigate the Maxwell equations. The optical parameters like large mode area, anomalous or normal dispersion, two or more zero-dispersion wavelengths, high numerical aperture, high birefringence, effective area, and high nonlinearity parameters are essential parameters to evaluate the behavior of PCF. It must be noted that these parameters can be calculated using the effective index value. The effective refractive index is mostly determined by the geometrical structure of the PCF. By means of finite element analysis with the aid of COMSOL multi-physics which is a powerful module in the numerical modeling, the performance of the proposed PCF sensor is investigated. The electromagnetic wave propagation through an optical fiber can be represented by Maxwell's equations with macroscopic consideration in the absence of electric charges:

$$\nabla \times E(r, t) = -\frac{\partial B(r, t)}{\partial t} \tag{5}$$

$$\nabla \times H(r, t) = -J(r, t) + \frac{\partial D(r, t)}{\partial t} \tag{6}$$

$$\nabla \cdot D(r, t) = \rho(r, t) \tag{7}$$

$$\nabla \cdot B(r, t) = 0 \tag{8}$$

The Fourier components for electric field associated with wave equation can be described as given below:

$$\nabla \times (\nabla \times E(r, \omega)) - k_o^2 [\hat{\epsilon}_r(r, \omega)E(r, \omega)] = 0 \tag{9}$$

Similarly, for the magnetic field:

$$\nabla \times [\hat{\epsilon}_r(r, \omega)]^{-1} \nabla \times H(r, \omega) - k_o^2 H(r, \omega) = 0 \tag{10}$$

In the expressions (9) and (10),  $k$  is the wave number which is equal  $\omega c^{-1}$  and where  $c = \sqrt{\epsilon_0 \mu_0}$  is the speed of light. The term  $\hat{\epsilon}_r(r, \omega) = \epsilon_r(r, \omega) - j\sigma(r, \omega)/\omega\epsilon_0$  represents the relative dielectric parameter which is material-dependent and  $\sigma(r, \omega)$  represents the Ohmic conductivity of the material.

The modal properties of a solid-core PCF are mainly influenced by two parameters, namely diameter of the air hole and pitch. Moreover, distribution of air holes, tunable air hole size, and pitch value offers additional possibilities in the designing of photonic crystal fiber with desirable properties. This designing flexibility leads to

tailoring the excellent optical properties for various applications. For the determination of number of guided modes supported by any kind of optical fiber medium, the  $V$ -parameter or cutoff frequency is an important parameter which plays a vital role. As an example, for conventional optical fiber, optical fibers supported to multi-mode if  $V \gg 1$  and fibers can support to propagate within the core. The  $V$ -parameter condition for conventional optical fiber with single-mode operation is  $V < 2.405$ . The expression for  $V$ -parameter of conventional optical fiber given below.

$$V_{\text{SMF}} = \frac{2\pi a}{\lambda} \sqrt{n_{\text{co}}^2 - n_{\text{cl}}^2} \quad (11)$$

In the context of PCF,  $V$ -parameter calculated by

$$V_{\text{PCF}} = \frac{2\pi \wedge}{\lambda} \sqrt{n_{\text{FM}}^2(\lambda) - n_{\text{FSM}}^2(\lambda)} \quad (12)$$

From Eq. (11),  $a$  is radius of the core,  $n_{\text{co}}$  and  $n_{\text{cl}}$  means core and cladding refractive index, respectively. From Eq. (12),  $n_{\text{FM}}$  is wavelength dependent fundamental mode (FM) and  $n_{\text{FSM}}$  is the cladding mode index of periodic cladding structure.

The mode area with function of wavelength is inversely proportional to nonlinearity. The nonlinearity parameter ( $\gamma$ ) can be expressed below,

$$\gamma(\lambda) = \frac{2\pi}{\lambda} \frac{n_2}{A_{\text{eff}}(\lambda)} \quad (13)$$

Air-filling fraction is an essential parameter to illustrate the HC-PCF. When air-filling fraction (*aff*) is large, guided modes must have  $\beta/k_0 < 1$  for light freely propagates through the air medium. The air-filling fraction described as,

$$\text{aff} = \frac{\pi}{\sqrt[2]{3}} \frac{d_h^2}{\wedge^2} \quad (14)$$

According to the detection of biosamples in the sensing region, we have evaluated intensity variation in PCF biosensors. In dual-core PCF biosensor, light energy transferred from one core to another one core due to coupled-mode theory. Hence, output power can be calculated by,

$$P_{\text{out}}(\lambda) = \sin^2\left(\frac{\Delta n_{eo}^i \pi L}{\lambda}\right) = \sin^2\left(\frac{|n_{\text{even}}^i - n_{\text{odd}}^i| \pi L}{\lambda}\right) \quad (15)$$

where  $\Delta n_{eo}^i$ ,  $i = x$ - and  $y$ -polarization, index difference between super modes (even and odd mode),  $L$  is the fiber length, and it can evaluate the transferred optical energy from first core to second core at the fixed length. Further, it can be supported to calculate the transmission power by the following formula,

$$T_r = 10 \log_{10} \left( \frac{P_{\text{out}}}{P_{\text{in}}} \right) \quad (16)$$

In dual-core PCF, fiber length ( $L$ ) can be considered greater than the coupling length. Minimum length of coupling which light energy transferred from one core to another one core in an easy way and calculated by

$$L_c = \frac{\lambda}{2|n_{\text{even}}^i - n_{\text{odd}}^i|} \quad (17)$$

The PCF sensor's sensitivity can be determined shift of peak resonance wavelength by the variation of RI analyte in the sensing region. It is called a wavelength interrogation method. The expression for the sensitivity by wavelength interrogation method follows,

$$S \left( \frac{\text{nm}}{\text{RIU}} \right) = \frac{\Delta \lambda_{\text{peak}}}{\Delta n_s} \quad (18)$$

where  $\lambda_{\text{peak}}$  is resonance wavelength and  $n_s$  is RI value for the biosample.

### 3 Terahertz Regime

The terahertz (THz) range cover the frequency lies between 0.1 and 20 THz. In this frequency range, many materials are transparent but optically opaque in the visible and infrared spectra. The corresponding range in the wavelengths and energy levels is 3 mm to 30 mm and 0.4 to 41 meV, respectively. Specifically, ionization and chemical damage are not influenced by THz radiations, hence do not alter the analyte nature. The terahertz regime covers two different regions, namely higher-frequency side of photonic regime and lower-frequency side of electronic regime. This notable property of THz implies that utilize both optical and electronic in the various applications like source, detection, sensing, imaging, manipulation of electromagnetic waves. Since materials are opaque in THz regime, these waves are open new window for imaging technologies in the optical domain which offers numerous applications in nondestructive imaging and testing of hidden weapons or explosives, fault detection in packaged electronic circuits, etc. However, the research on transmission medium for terahertz wave and terahertz-based optical devices is still being explored.

The microwave and infrared frequency spectrum are covered by terahertz and most of materials like glass, plastics, etc. having a strong absorption in the microwave and optical bands. It limits the realization and application on the development of opto-electronic technology in terahertz band [30]. In the THz band, graphene supported for surface plasmons in the range between far infrared to the THz range [31]. When compare with noble metals, field localization is stronger and optical loss is low for graphene. In the terahertz regime, Eq. (1) can be simplified as



$$\sigma_g = \frac{ie^2\mu_c}{\pi(\omega + i2\Gamma)\hbar^2} \left( \frac{\mu_c}{k_B T} + 2 \ln \left( e^{-\frac{\mu_c}{k_B T}} + 1 \right) \right) \quad (19)$$

Very low attenuation, i.e.,  $\alpha < 0.5$  dB/km, exhibited by silica glass due to higher transparency nature. Furthermore, due to its thermo-optic properties, silica glass can be utilized to fabricate optical components based on optical fibers with intricate designs. However, in the THz domain, silica glass not suitable material for fabrication of THz devices. At 2 THz frequency, the refractive index of silica is 1.965. The vibrational frequencies of various biomolecules fall within the span of THz frequency coincides which enabling the detection of biomolecule vibrations. Terahertz spectroscopy, in particular, has emerged as an important tool for the label-free and nondestructive investigation of chemical and biological constituents. As a result, several academics are seeking to exploit this band for novel uses in the bio-medical field.

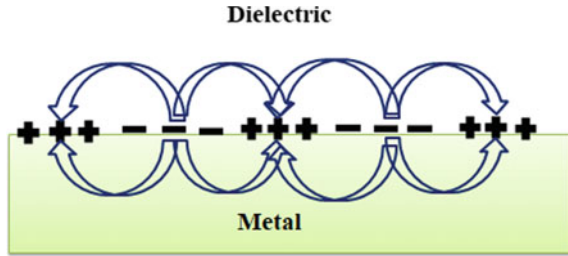
#### 4 Surface Plasmon Resonance (SPR)

The surface plasmons (SPs) are excited by collective oscillation of free electrons which are confined and induced by electromagnetic field on the metal surface [32]. A surface plasmon wave (SPWs) propagates in the transverse magnetic (TM) direction on the surface of metal. In plasmonics, we prefer the specific TM-polarized light for the excitation of SPs because TE-polarization of field component is the perpendicular to the incident plane which can't generate charge at the planar interface. When TM-polarized light is travel along the interface which affected to the incident light that time generate SP. In sensing, based on refractive index analyte, resonance position will be varied. The interaction between the photons and electric dipoles at the metal surface or in semiconductor leads to excitation of polaritons. Surface plasmons coupling with polaritons called surface plasmons polaritons (SPPs) [33]. The propagation of SPPs will be taken place at the interface between two different regions where metal and dielectric are present as shown in Fig. 2. With the resonance condition, at the boundary of metal and dielectric, plasmonic waves will be excited which is known as surface plasmon resonance (SPR). The improvement of coating technology with the combination of photonics and plasmonic is significantly contribute for the development of photonic sensor which has recently receiving huge attention among photonic community due to their potential applications. The PCF structures based on SPR coating with plasmonic materials provided extreme sensitivity [34].

At the resonance, the following condition must be satisfied.

$$\frac{2\pi}{\lambda} n_1 \sin\theta = \frac{2\pi}{\lambda} \sqrt{\frac{\epsilon_r n_2^2}{\epsilon_r + n_2^2}} \quad (20)$$

**Fig. 2** Plasmonic generation at the boundary in between metal and dielectric



The plasmonic wave profile is maximum at the metal–dielectric interface and exponentially decaying. In the expression (20), the left-hand and right-hand sides are respectively denoting the evanescent wave’s wave vector and surface plasmon wave’s wave vector. According to Eq. (20), resonance peak is very sensitive to the corresponding change in refractive index of analyte, incident angle, and wavelength of incident light. By employing SPR technique, numerous SPR-based PCF sensors have been reported [35–38]. In the SPR sensing mechanism, Kretschmann configuration is widely employed in which *p*-polarized light is a strike on a prism where the surface is coated with metals. These materials are called as plasmonic materials that can be used to excite the surface plasmon polaritons (SPP). SPR sensor has been proposed to detect the gas and biological analyte sensing [39]. The structural configuration of Kretschmann (prism)-based SPR sensor is bulky due to the requirement of many opto-mechanical-based components which are not suitable for many sensing applications [40]. In the SPR-based photonic sensors, gold (Au) and silver (Ag) metals are extensively employed as a plasmonic material to excite the plasmons [41]. In specific, gold gives an excellent support to the aqueous environments due to chemically stable. But its resonance peak is broad which is significantly affecting the detection [42]. On the other hand, when compared with other plasmonic materials, silver material is suitable plasmonic material which exhibits the minimum loss and narrowed resonance peak. However, silver material is chemically inert which causes oxidation process easily.

In the photonic sensors, SPR technology essential to enhance the sensitivity of sensors due to its various advantages such as label-free detection, high accuracy and extremely high sensitivity. Especially, SPR-based sensors used in the sensing of environmental parameters [43], detection of chemical agents [44], biological analytes sensing [45] and other SPR-based photonic devices [46]. At earlier days, plasmonic sensors were designed with the employment of prism [47], such as the Kretschmann–Raether prism [48] that can be used to detect up to  $10^{-6}$  RIU. When prism-based configuration is employed for SPR sensors, it has many disadvantages such as costly integration, limitation of mechanical reliability and mass production in ability. Notably, when compared with the coating of traditional metal and graphene, plasmonic waves are effectively supports to control the modulation of light through properly adjusting the graphene’s Fermi level. In this work, we obtained the dielectric constant of gold which is used as a plasmonic material and the value of dielectric constant is calculated from the Drude model [49].

$$\varepsilon = \varepsilon_{\infty} - \frac{\omega_p^2}{\omega(\omega + j\omega_c)} \quad (21)$$

In the expression (1),  $\varepsilon_{\infty}$  has the value of 9.75 which is the dielectric constant of gold at very high frequency and  $\omega_p$  has the value of  $1.36 \times 10^{16}$  rad/s which is the plasma frequency of gold.  $\omega_c$  is the electron's scattering frequency with the value of  $1.45 \times 10^{14}$  rad/s. The resonance angle in the SPR experiment is gradually increases with increasing RI sample. The maximum shift in the resonance angle illustrates the enhancing of sensitivity of biosensing device. This resonance peak shift is the sensing mechanism behind the working of SPR-based photonic sensors. PCF biosensors working based on surface plasmon have received huge attention among researchers in the area of photonic sensor technology. Many researchers have been investigated the SPR-based biosensing with the use of combination of metal or plasmonic materials, dielectric material, and semiconducting layers. With the aid of hybrid structure of photonic sensors, the sensitivity can be enhanced over the conventional optical sensors. In the development of photonic sensors, hybrid structures have supports to better field enhancement and sensitivity for wide range of refractive index of analytes as compared to the conventionally known photonic sensors by exhibiting full width half maximum (FWHM) as much as narrow. A graphene-based optical sensor has an excellent bridge between the infrared and THz regime. Also, they can be fabricated through employing electron beam lithography (EBL) which can be cost-effective method due to the simplicity.

## 5 Moisture in Transformer Oil

In the electrical transmission system, performance of transformer is determined by transmitting power of transformer. In order to maintain the performance of transformer, monitoring and the maintenance for the transformer is highly essential. Dielectric strength is another important parameter in transformer system and this parameter having higher values new transformer oil is higher than that of contaminated oil. Nowadays, society demands more electrical energy and it is increasing exponentially.

Since 1920s, the study on performance of transformer by calculating the moisture presence in the transformer oil has received huge attention. The working performance of transformer is degraded by several factors related to transformer oil like moisture contamination [50], irrelevant particles or foreign atoms present, and also variation of pressure [51]. Hence, the maintenance of the transformer is very essential, and level of moisture in the transformer should be monitored carefully. The periodic oil test must be performed to maintain the performance of transformer through monitoring the quality of insulating oil in the transformer and frequent checking is needed which depending upon the performance of the transformers[52]. At normal temperatures, new insulating oil has a water level of less than 10 ppm.

### 5.1 SPR-Based D-Shaped PCF with Graphene and Gold

Graphene material has been used for optical sensing application due to some remarkable properties like broad detection range, very thin atomic thickness (0.345 nm), nanosized particles, and carbon conductivity. From the reflection analysis, output spectrum can be analyzed by an optical spectrum analyzer (OSA). Many novel optical sensors based on graphene devoted so far [53, 54]. The effect of graphene layer on optical sensor based on photonic crystal fibers has been investigated in [55]. In this study, refractive index (RI)-based photonic sensor is proposed with D-shaped PCF by assisting the coating of some specific noble material. Particularly, gold (Au) is coated and coupled-mode theory (CMT) is followed with wide range of refractive index, i.e., 1.30 to 1.36, which corresponds to the wavelength range from 1.2 to 2.0  $\mu\text{m}$ . The background material of the sensor is fused silica ( $\text{SiO}_2$ ), and it is refractive index calculated by [56],

$$n^2 = 1 + \sum_{i=1}^3 \frac{A_i \lambda^2}{\lambda^2 - \lambda_i^2} \quad (22)$$

In Eq. (22),  $n$  represents RI of  $\text{SiO}_2$ .  $A_i$  and  $\lambda_i$  constants are used by fitting dispersion curve [56]. The RI of graphene evaluated by [57]:

$$n_g = 3 + \frac{i\lambda 5.446 \mu\text{m}^{-1}}{3} \quad (23)$$

As for the concerns with refractive index sensors, one can detect the various concentrations analytes through investigate the loss peak resonance. Simultaneously, the impacts of the geometrical structure of the developed PCF can be used to maximize resonance peak shifting. Tunability of the suggested sensor construction can be achieved by graphene's conductivity and chemical potential. Numerous researchers have published in the literature on the role of graphene in the photonic crystal structure. However, published works are tells about 1D photonic crystal which require simple computation. But the detection limit and sensing resolution are not much effective than PCFs.

Gold is one of the important plasmonic materials for getting better sensing performance in plasmonic sensor. Many plasmonic sensors employ the gold as plasmonic material because of several advantageous properties. Few among them are chemically inert, more stable, and simple structure. With help of Drude–Lorentz model, the permittivity of gold can be calculated by [58].

$$\varepsilon_{\text{Au}} = \varepsilon_{\infty} - \frac{\omega_D^2}{\omega(\omega + i\gamma_D)} - \frac{\Delta\varepsilon\Omega_L^2}{(\omega^2 - \Omega_L^2) + i\Gamma_L\omega} \quad (24)$$

In the expression (24),  $\varepsilon_{\infty}$  denotes the permittivity at high frequency and its value is 5.9673.  $\omega_p$  and  $\gamma_D$  are respectively signifies the plasma frequency and

damping frequency; their values are respectively 13,280.14 THz and 100.02 THz. The weighting factor for gold as a plasmonic material is  $\Delta\varepsilon = 1.09$ . In contrast, the oscillator strength and spectral breadth are denoted as  $\Omega_L$  and  $\Gamma_L$ , with values of 4084.51 THz and 658.85 THz, respectively. The graphene is deposited on the surface of the gold layer for obtaining better coupling condition of SPP and core modes. Furthermore, graphene layer proposed to manage the sensor's resonance peak. As a result of their exceptional electro-optical capabilities, better photonic sensors based on graphene materials are envisaged.

Figure 1 shows a cross section of the D-shaped PCF sensor. The sensing performances analyzed by the finite element method (FEM). In order to obtain the excellent sensitivity, the structural parameters (pitch value, hole size, the thickness of the gold layer, the graphene layer chemical potential (GCP), and the angle of incidence) are optimized. Here, we used the following design parameters as follows. In the designing of PCF structure is  $2\ \mu\text{m}$ , and the designed diameters of the air holes  $d$ ,  $d_1$ ,  $d_2$ , and  $d_3$  are 0.8, 0.6, 0.4, and  $1.2\ \mu\text{m}$ , respectively.

According to Fig. 3, combination of two materials like Au and graphene provides more stability in the designing of sensors for the advancement in photonic sensing technology. The electromagnetic wave propagation in a photonic crystal fiber depending on the angular frequency of incident wave and refractive index of the materials. By employing COMSOL Multiphysics for the proposed D-shaped PCF structure, the distribution of electric field intensity obtained through “mode Analyses” as portrays in Fig. 4. In the structure of PCF, a perfectly match layer (PML) is added around the outer boundary. This layer is used in the structure to avoid the effects due to the refraction and external effects. Many researchers proposed various D-shaped photonic crystal fiber for different kind of photonic sensing applications [59–64].

Especially for PCF with D-shape, penetration of electromagnetic field into the cladding region is significantly high when wavelength is gradually increased. At a particular wavelength, resonance condition is satisfied and plasmonic waves are

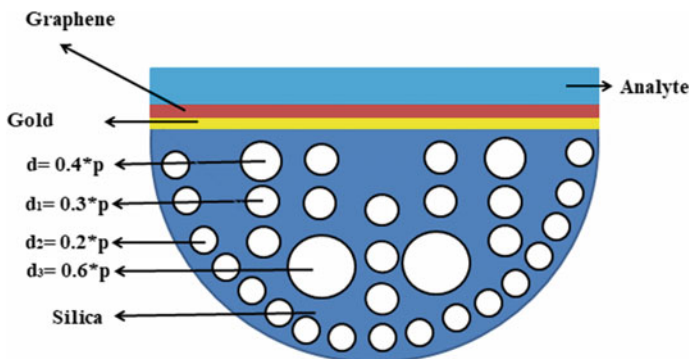
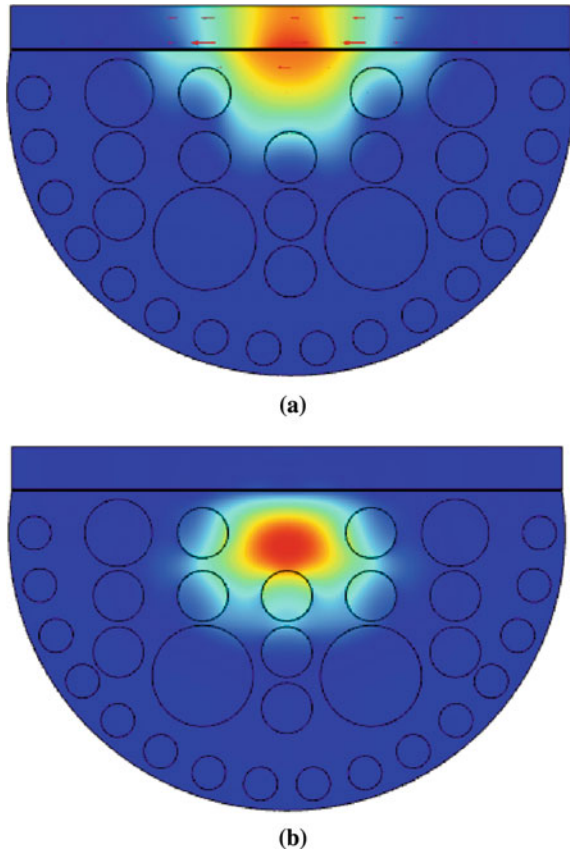


Fig. 3 Schematic cross-sectional view of D-shaped PCF

**Fig. 4** **a** Coupling mode confinement and **b** core mode confinement



generated. The free electrons are mainly affected by the evanescent field and electromagnetic field are significantly influenced by the resonant electrons. The variation of the real part of effective index for fiber core mode and SPP mode supports excited the plasmonic wave around the resonance wavelength which is the mechanism of physics this phenomenon.

The confinement loss (CL) is essential parameter to analyze the proposed PCF sensor. In the designed PCF model, guiding properties are depending upon the structural parameters like dimension of air holes, the number of air holes, and operating wavelength. The expression for confinement loss is given follows

$$\alpha \left( \frac{\text{dB}}{\text{m}} \right) = 8.686 \times \frac{2\pi}{\lambda} \times \text{Im}(n_{\text{eff}}) \times 10^6 \text{dB/m} \tag{25}$$

In the expression (25), respectively  $\lambda$  represents the wavelength of input optical light and  $\text{Im}(n_{\text{eff}})$  denotes complex part of the effective mode index of core-guided mode. The sensing mechanism can be implemented by linking the core mode and

the analyte to be sensed. Because the analyte layer is placed on top of the graphene layer, the TE mode coupling between the core and plasmonic material is considered (gold). There will be energy transfer between the core mode and the SPP mode at the point of connection. The absorption value is maximal at a specific wavelength, and the absorption peak that corresponds to this wavelength is known as the resonance wavelength. The resonance peak on the absorption spectra will vary depending on the refractive index of the analytes.

## 5.2 Results and Discussions

The detecting mechanism of the surface plasmon-based PCF sensor is the interaction of the evanescent field with the surface electron of the plasmonic metal. When an evanescent field strikes a metallic surface, it generates a surface plasmonic wave (SPW), which travels at the interface between the metal and the dielectric medium. A strong loss peak is evident at the resonance when the fundamental mode frequency and surface plasmon polariton (SPP) mode frequency are exactly matched. Changes in the refractive index of the liquid analyte will have an effect on the loss spectrum. As a result, analyte concentration will be determined using either the shift of the resonance peak or loss variations. The geometrical or structural features of the proposed sensor have a major impact on the performance of the proposed SPR-based PCF sensor. As a result, these parameters must be properly tuned in order for the metal surface and the evanescent field to interact effectively. Furthermore, the PCF sensor's strong link between SPP mode and core-guided mode considerably improves sensitivity.

By closely observing the Fig. 5, one can infer that transformer oil has shown high confinement loss for concentration of water with 21 ppm at  $0.75 \mu\text{m}$ . In the designed D-shaped PCF sensor, structural parameters are having a great impact on the performance of sensor. The influence of structural parameters on the proposed sensor is studied for various analyte with different concentration like 15, 16, 18, and 21 ppm. In Fig. 3, gold coating is act as plasmonic layer for the best performance. In this proposed structure, thickness of layer is 10 nm for both graphene and gold.

The sensing response behavior of proposed structure due to the result of interaction between the light and optical medium leads the wavelength resonance shift. Practically, optical spectrum analyzer (OSA) is used to measure this wavelength resonance shift. By carefully observing the transmission characteristics of the input optical signal through the optical medium, we can detect the unknown analyte is accurately. Thus, low resonance shift is observed for low concentration of water in the transformer oil is shown in Fig. 6.

By fixing the chemical potential as 1.2 eV, we observed the maximum confinement loss for various concentrations of contaminated oil in the transformer as illustrated in Fig. 7. Moreover, we obtained confinement loss as maximum value 2500 dB/m for 21 ppm.

**Fig. 5** Confinement loss versus wavelength

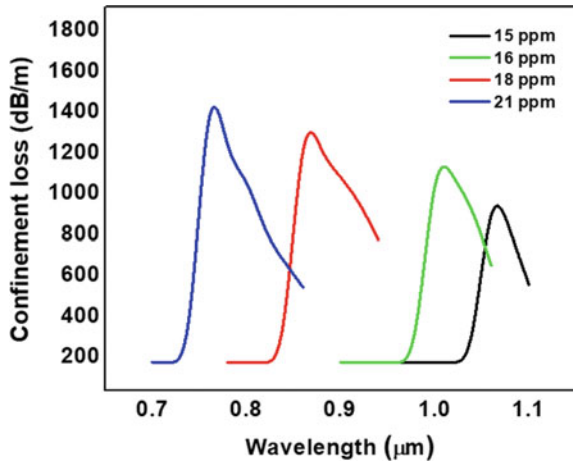
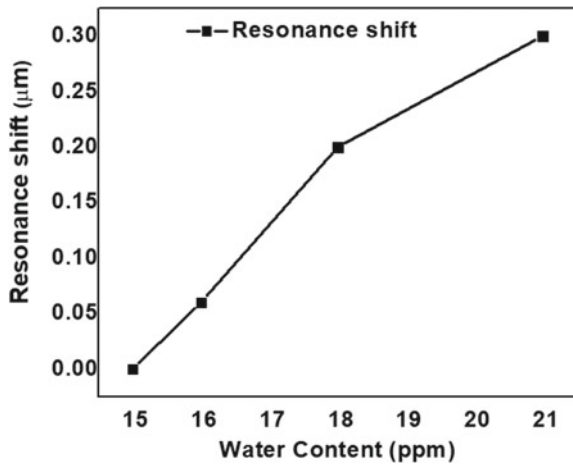


**Fig. 6** Resonance shift with water content in the transformer oil



By using the expression (18), for the proposed D-shaped PCF sensor, sensitivity is calculated for different chemical potential values 0.8 eV, 1 eV, 1.2 eV of graphene are 43.33 nm/ppm, 50 nm/ppm, and 46.66 nm/ppm, respectively. Thus, we observed higher sensitivity of D-shaped PCF sensor for chemical potential 1 eV.

## 6 Conclusions

In this chapter, novel D-shaped PCF sensors based on SPR have been proposed to detect the water content in the transformer oil. In order to excite the surface plasmon, gold is employed as plasmonic material. Moreover, designed D-shaped



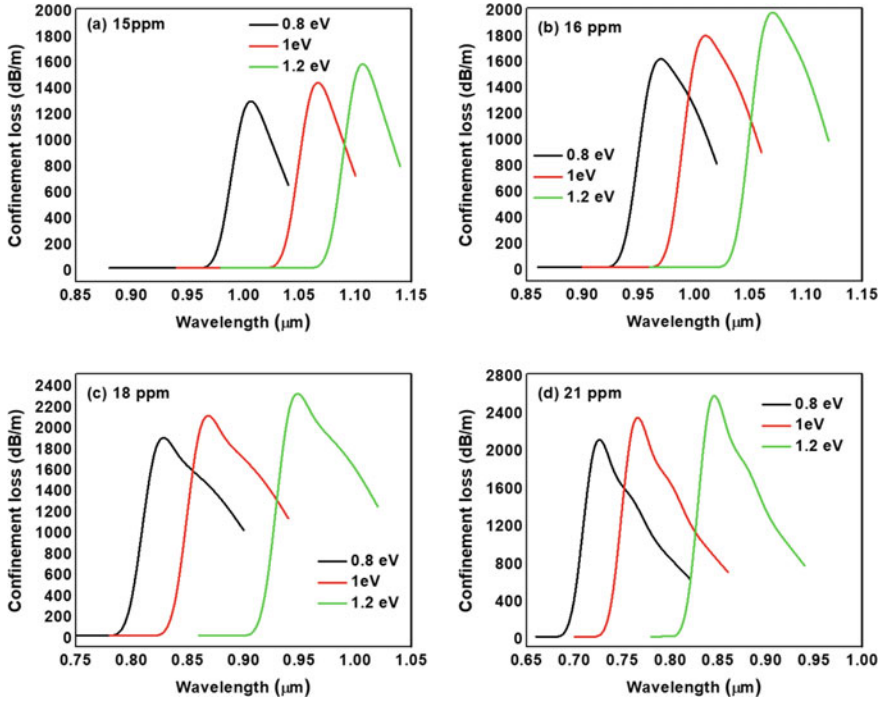


**Fig. 7** a Variation of confinement loss with wavelength for different chemical potential with 15 ppm. b 16 ppm, c 18 ppm, and d 21 ppm

PCF is coated with graphene and gold layers. The constructed photonic sensor has been investigated through varying water content in the transformer oil and attained maximum sensitivity of 50 nm/ppm for chemical potential 1 eV. The confinement loss for proposed structure is investigated in detailed with different concentration of water content such as 15, 16, 18 and 21 ppm in the transformer oil.

## References

1. Neto, A.C., Guinea, F., Peres, N.M.R., Novoselov, K.S., Geim, A.K.: The electronic properties of grapheme. *Rev. Mod. Phys.* **81**, 109 (2009)
2. Novoselov, K.S., Geim, A.K., Morozov, S.V., Jiang, D., Zhang, Y., Dubonos, S.V., Grigorieva, I.V., Firsov, A.A.: Electric field effect in atomically thin carbon films. *Science* **306**, 666–669 (2004)
3. Novoselov, K.S., Geim, A.K., Morozov, S.V., Jiang, D., Katsnelson, M.I., Grigorieva, I.V., Dubonos, S.V., Firsov, A.A.: Two-dimensional gas of massless Dirac fermions in grapheme. *Nature* **438**, 197–200 (2005)
4. Zhang, Y.B., Tan, Y.W., Stormer, H.L., Kim, P.: Experimental observation of the quantum hall effect and Berry's phase in grapheme. *Nature* **438**, 201–204 (2005)

5. Mak, K.F., Ju, L., Wang, F., Heinz, T.F.: Optical spectroscopy of graphene: from the far infrared to the ultraviolet. *Solid State Commun.* **152**, 1341–1349 (2012)
6. Tang, J.Y., Xiao, Z.Y., Xu, K.K.: Cross polarization conversion based on a new chiral spiral slot structure in THz region. *Opt. Quantum Electron.* **48**, 111 (2016)
7. Wu, J.B., Lin, M.L., Cong, X.: Raman spectroscopy of graphene-based materials and its applications in related devices. *Chem. Soc. Rev.* **47**, 1822–1873 (2018)
8. Sorathiya, V., Lavadiya, S., AlGhamdi, A.: Hilbert resonator-based multiband tunable graphene metasurface polarizer for lower THz frequency. *J. Comput. Electron.* **21**, 280–288 (2022)
9. Fu, G., Wang, Y., Wang, B., Yang, K., Wang, X., Fu, X., Jin, W., Bi, W.: A compact electro-absorption modulator based on graphene photonic crystal fiber. *Chin. Phys. B* **29**, 034209 (2020)
10. Balaji, A., Zhang, J.: Electrochemical and optical biosensors for early-stage cancer diagnosis by using graphene and graphene oxide. *Cancer Nanotechnol.* **8**, 10 (2017)
11. Patel, S.K., Parmar, J., Kosta, Y.P., Ladumor, M., Zakaria, R., Nguyen, T.K.: Design of graphene metasurface based sensitive infrared biosensor. *Sens. Actuators A Phys.* **301**, 111767 (2020)
12. Patel, S.K., Parmar, J., Ladumor, M., Ahmed, K., Nguyen, T.K., Dhasarathan, V.: Numerical simulation of a highly directional optical leaky wave antenna using diamond-shaped graphene perturbations. *Appl. Opt.* **59**, 2225 (2020)
13. Kumar, S., Singh, R., Yang, Q., Cheng, S., Zhang, B., Kaushik, B.K.: Highly sensitive, selective and portable sensor probe using germanium-doped photosensitive optical fiber for ascorbic acid detection. *IEEE Sens. J.* **21**, 62–70 (2021)
14. Khodadadi, M., Moshiri, S.M.M., Nozhat, N.: Theoretical analysis of a simultaneous graphene-based circular plasmonic refractive index and thickness bio-sensor. *IEEE Sens. J.* **20**, 9114–9123 (2020)
15. Patel, S.K., Parmar, J., Kosta, Y.P., Charola, S., Zakaria, R., Nguyen, T.K.: Graphene-based highly sensitive refractive index biosensors using C-shaped metasurface. *IEEE Sens. J.* **20**, 6359–6366 (2020)
16. Farmani, H., Farmani, A., Biglari, Z.: A label-free graphene-based nanosensor using surface plasmon resonance for biomaterials detection. *Phys. E. Low-Dimension. Syst. Nanostruct.* **116**, 113730 (2020)
17. Xu, B., Huang, J., Ding, L., Cai, J.: Graphene oxide-functionalized long period fiber grating for ultrafast label-free glucose biosensor. *Mater Sci. Eng. C* **107**, 110329 (2020)
18. Bonini, A., Vivaldi, F.M., Herrera, E., Melai, B., Kirchhain, A., Sajama, N.V.P.: A graphenic biosensor for real-time monitoring of urea during dialysis. *IEEE Sens. J.* **20**, 4571–4578 (2020)
19. Du, H., Li, Z., Wang, Y., Yang, Q., Wu, W.: Nanomaterial-based optical biosensors for the detection of foodborne bacteria. *Food Rev. Int.* 655–684 (2020)
20. Lin, Z., Jia, Y., Ma, Q., Wu, L., Ruan, B., Zhu, J.: High sensitivity intensity-interrogated bloch surface wave biosensor with graphene. *IEEE Sens. J.* **18**, 106–110 (2018)
21. Singh, M., Raghuvanshi, S.K., Prakash, O.: Ultra-sensitive fiber optic gas sensor using graphene oxide coated long period gratings. *IEEE Photonics Technol. Lett.* **31**, 1473–1476 (2019)
22. Vishnubhotla, R., Sriram, A., Dickens, O.O., Mandyam, S.V., Ping, J., Adu-Beng, E.: Attomolar detection of ssDNA without amplification and capture of long target sequences with graphene biosensors. *IEEE Sens. J.* **20**, 5720–5724 (2020)
23. Zainud-Deen, S.H., Malhat, H.A., El-Refaa, E.A.: Polarization-independent reconfigurable graphene gas sensor using crescent plasmonic antenna. *Plasmonics* **15**, 1115–1122 (2020)
24. Alrammouz, R., Podlecki, J., Vena, A., Garcia, R., Abboud, P., Habchi, R.: Highly porous and flexible capacitive humidity sensor based on self-assembled graphene oxide sheets on a paper substrate. *Sens. Actuators B Chem.* **298**, 126892 (2019)
25. Knight, J.C., Birks, T.A., Russell, P., St, J., Atkin, D.M.: All-silica single mode optical fiber with photonic crystal cladding. *Opt. Lett.* **21**(19), 1547–1549 (1996)
26. Birks, T.A., Knight, J.C., Russell, P.S.: Endlessly single-mode photonic crystal fiber. *Opt. Lett.* **22**, 961–963 (1997)

27. Cregan, R.F., Mangan, B.J., Knight, J.C., Birks, T.A., Russell, P.S., Roberts, P.J., Allan, D.C.: Single-mode photonic band gap guidance of light in air. *Science* **285**, 1537–1539 (1999)
28. Bjarklev, A., Broeng, J., Bjarklev, A.S.: *Photonic Crystal Fibres*. Springer Science & Business Media (2012).
29. Prakash, R., Chandra, P.: *Nanobiomaterial Engineering: Concepts and Their Applications in Biomedicine and Diagnostics*. Springer (2020)
30. Zhang, L., Ren, G.J., Yao, J.Q., Zhang, Y.M.: Design of the novel steering-wheel micro-structured optical fibers sensor based on evanescent wave of terahertz wave band. *Optik* **125**, 5936–5939 (2014)
31. Jafari, D., Danaie, M., Orouji.: Ultra-fast two-bit all-optical analog to digital convertor based on surface plasmons and Kerr-type nonlinear cavity. *Plasmonics* **16**, 2101–2108 (2021)
32. Homola, J.: Surface plasmon resonance sensors for detection of chemical and biological species. *Chem. Rev.* **108**, 462–493 (2008)
33. Fu, H.Y., Zhang, S.W., Chen, H., Weng, J.: Graphene enhances the sensitivity of fiber-optic surface plasmon resonance biosensor. *IEEE Sens. J.* **15**, 5478–5482 (2015)
34. Luan, N., Yao, J.: A hollow-core photonic crystal fiber-based SPR sensor with large detection range. *IEEE Photon J.* **9**, 1–7 (2017)
35. Otupiri, R., Akowuah, E.K., Haxha, S.: Multi-channel SPR biosensor based on PCF for multi-analyte sensing applications. *Opt. Exp.* **23**, 15716–15727 (2015)
36. Rifat, A., Mahdiraji, G.A., Shee, Y., Shawon, M.J., Adikan, F.M.: A novel photonic crystal fiber biosensor using surface plasmon resonance. *Proc. Eng.* **140**, 1–7 (2016)
37. Hasan, M.R., Akter, S., Rifat, A.A., Rana, S., Ahmed, K., Ahmed, R., Subbaraman, H., Abbott, D.: Spiral photonic crystal fiber-based dual-polarized surface plasmon resonance biosensor. *IEEE Sens. J.* **18**, 133–140 (2018)
38. Momota, M.R., Hasan, M.R.: Hollow-core silver coated photonic crystal fiber plasmonic sensor. *Opt. Mater.* **76**, 287–294 (2018)
39. Liedberg, B., Nylander, C., Lunström, I.: Surface plasmon resonance for gas detection and biosensing. *Sens. Actuators* **4**, 299–304 (1983)
40. Homola, J., Yee, S.S., Gauglitz, G.: Surface plasmon resonance sensors: review. *Sens. Actuators B Chem.* **54**, 3–15 (1999)
41. Naik, G.V., Shalae, V.M., Boltasseva, A.: Alternative plasmonic materials: beyond gold and silver. *Adv. Mater.* **25**, 3264–3294 (2013)
42. Dash, J., Jha, R.: Graphene based birefringent photonic crystal fiber sensor using surface plasmon resonance. *IEEE Photon. Technol. Lett.* **26**, 1092–1095 (2014)
43. Li, N., Zhang, D., Zhang, Q., Lu, Y., Jiang, J., Liu, G.L., Liu, Q.: Combing localized surface plasmon resonance with anodic stripping voltammetry for heavy metal ion detection. *Sens. Actuators B Chem.* **231**, 349–356 (2016)
44. Zhao, Y., Lei, M., Liu, S.X., Zhao, Q.: Smart hydrogel-based optical fiber SPR sensor for pH measurements. *Sens. Actuators B Chem.* **261**, 226–232 (2018)
45. Dash, J.N., Jha, R.: On the performance of graphene-based D-shaped photonic crystal fibre biosensor using surface plasmon resonance. *Plasmonics* **10**, 1123–1131 (2015)
46. Singh, P.: SPR biosensors: historical perspectives and current challenges. *Sens. Actuators B Chem.* **229**, 110–130 (2016)
47. Otto, A.: Excitation of nonradiative surface plasma waves in silver by the method of frustrated total reflection. *Z. Phys.* **216**, 398–410 (1968)
48. Kretschmann, E., Reather, H.: Radiative decay of non-radiative surface plasmons excited by light. *Z. Naturforsch.* **23**, 2135–2136 (1968)
49. Chu, S., Nakkeeran, K., Abobaker, A.M., Aphale, S.S., Babu, P.R., Senthilnathan, K.: Design and analysis of surface-plasmon-resonance-based photonic quasi-crystal fiber biosensor for high-refractive-index liquid analytes. *IEEE J. Sel. Top Quantum Electron.* **25**, 1–9 (2019)
50. Sparling, B., Aubin, J.: Assessing water content in insulating paper of power transformers. *Electr. Energy T&D Mag.* **11**, 30–34 (2007)
51. Luo, Y.T., Wang, H.B., Ma, G.M.: Research on high sensitive D-shaped FBG hydrogen sensors in power transformer oil. *Sensors* **16**, 1641 (2016)

52. Karthikeyan, S., Mezher, H., Ibrahim, F.: Graphene oxide-based optical waveguide for moisture sensing in transformer oil. *Photonics Nanostruct. Fundam. Appl.* **36**, 100727 (2019)
53. Gao, X., Cheng, L.X., Jiang, W.S., Li, X.K., Xing, F.: Graphene and its derivatives-based optical sensors. *Front. Chem.* **9**, 615164 (2021)
54. Shivananju, B.N., Yu, W., Liu, Y., Zhang, Y., Lin, B., Li, S., Bao, Q.: The roadmap of graphene-based optical biochemical sensors. *Adv. Func. Mater.* **27**, 1603918 (2017)
55. Haque, E., Md Anwar, H., Feroz, A., Yoshinori, N.: Surface plasmon resonance sensor based on modified D-shaped photonic crystal fiber for wider range of refractive index detection. *IEEE Sens. J.* **18**, 8287–8293 (2018)
56. Malitson, I.H.: Interspecimen comparison of the refractive index of fused silica. *J. Opt. Soc. Amer.* **55**, 1205–1209 (1965)
57. Dash, J.N., Jha, R.: Graphene-based birefringent photonic crystal fiber sensor using surface plasmon resonance. *IEEE Photonics Technol. Lett.* **26**, 1092–1095 (2014)
58. Kiroriwal, M., Singal, P.: Design and analysis of highly sensitive solid core gold-coated hexagonal photonic crystal fiber sensor based on surface plasmon resonance. *J. Nanophotonics* **15**, 026008 (2021)
59. Tian, P., Lu, L., Chen, C., Lv, D., Liu.: All-solid D-shaped photonic fiber sensor based on surface plasmon resonance. *Opt. Commun.* **285**, 1550–1554 (2012)
60. An, G., Li, S., Qin, W., Zhang, W., Fan, Z., Yajie, F.: High-sensitivity refractive index sensor based on d-shaped photonic crystal fiber with rectangular lattice and nanoscale gold film. *Plasmonics* **9**, 1355–1360 (2014)
61. Gupta, A., Singh, H., Singh, A., Singh, R.K., Tiwari, A.: D-shaped photonic crystal fiber-based surface plasmon resonance biosensors with spatially distributed bimetallic layers. *Plasmonics* **15**, 1–2 (2020)
62. Liang, H.Q., Liu, B., Hu, J.F.: An ultra-highly sensitive surface plasmon resonance sensor based on D-shaped optical fiber with a silver-graphene layer. *Optik* **149**, 149–154 (2017)
63. Luan, N., Wang, R., Lv, W., Yao, J.: Surface plasmon resonance sensor based on D-shaped micro-structured optical fiber with hollow core. *Opt. Express* **23**, 8576–8682 (2015)
64. Patnaik, A., Senthilnathan, K., Jha, R.: Graphene-based conducting metal oxide coated D-shaped optical fiber SPR sensor. *IEEE Photonics Technol. Lett.* **27**, 2437–2440 (2015)

# Recent Advances in Graphene-Based Adsorbents for Fluoride Removal from Groundwater



Swati Dubey, Avanish Kumar, and Abhishek Gupta

**Abstract** Nowadays, there is a major problem regarding drinking water scarcity due to the water contaminants present in the groundwater. Various fluoride removal techniques including coagulation, membrane filtration, electrocoagulation, and adsorption are applied. Amongst the different defluoridation techniques, adsorption technique is widely adopted due to easy operation, inexpensiveness, and high efficiency. Various adsorbents have been investigated for fluoride adsorption from groundwater, and activated alumina is extensively applied. However, there are some major drawbacks in using activated alumina including high cost and difficulty in regeneration. Graphene-based adsorbents have emerged as an efficient adsorbent for the defluoridation technique. The present study critically reviews the current advancements in the development of adsorbents for the defluoridation process and also suggests the upcoming solutions for the same.

**Keywords** Fluoride · Defluoridation · Adsorption · Graphene

---

S. Dubey · A. Kumar (✉)

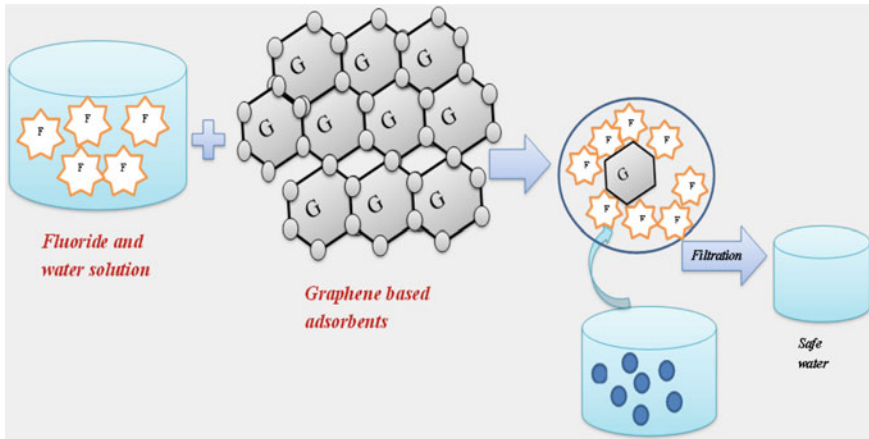
Department of Chemical Engineering, Marwadi University, Rajkot, Gujarat 360003, India  
e-mail: [avanish.kumar@marwadieducation.edu.in](mailto:avanish.kumar@marwadieducation.edu.in)

S. Dubey

e-mail: [swati.dubey@marwadieducation.edu.in](mailto:swati.dubey@marwadieducation.edu.in)

A. Gupta

Department of Chemical Engineering, Marwadi University, Rajkot, Gujarat 360003, India  
e-mail: [abhishek.gupta@marwadieducation.edu.in](mailto:abhishek.gupta@marwadieducation.edu.in)



## 1 Introduction

The water contamination because of the presence of fluoride above than the permissible limit has become a worldwide problem. The acceptable value for  $F^-$  ion in potable water prescribed by World Health Organisation is less than 1.5 mg/L. The nations those are affected with the problem are India, Bangladesh, China, Pakistan, Africa, Brazil, and Tanzania. The concentration of fluoride higher than the prescribed limit leads to serious health problems in human body including skeletal fluorosis, dental fluorosis, respiratory problems, muscular damage, etc. Several districts in India have been affected with the problem of fluoride contamination of drinking water [20, 18, 46, 60]. Some major health issues also include neurological disorders and endocrine issues, and therefore, there is an urgent requirement to adopt certain techniques that could remove fluoride from drinking water [4, 18, 37]. Figure 1 depicts the serious health issues due to the presence of fluoride in drinking water. Hence, several researches have been conducted for the defluoridation of drinking water to solve this major issue including coagulation, electrocoagulation, adsorption, membrane filtration, and ion exchange process. Figure 2 depicts the various defluoridation techniques with their advantages and disadvantages. Coagulation process is a simple and effective process, but the major drawback is the generation of large amount of sludge and high amount of Al left in defluoridated water. Electrocoagulation required significant quantity of electricity and generation of significant amount of sludge. Membrane filtration process is highly expensive, and there is problem of membrane fouling [19, 49]. Amongst all the defluoridation techniques, adsorption has shown a significant efficiency in removing fluoride from drinking water. Adsorption technique is able to remove fluoride even at lower concentrations, hence making the technique highly capable. The process of adsorption involves the exchange of fluoride ion by ion exchange or by chemical reaction taking place. Activated alumina

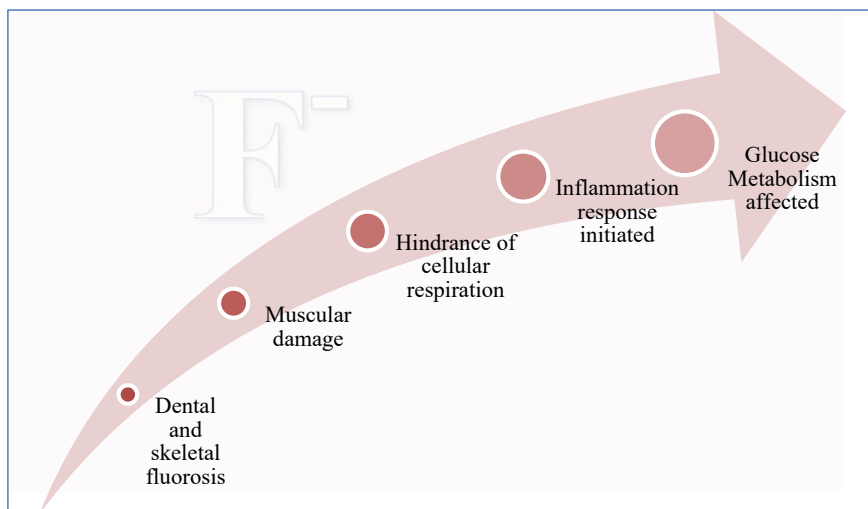


**Fig. 1** Harmful health effects of fluoride on human body

is the most used adsorbent for defluoridation, but this adsorbent also has some major limitations of adsorbent bed regeneration and residual Al in treated water [1, 21, 32, 69]. Several investigators have performed experiments for the modification of activated alumina for achieving the better efficiency for removing fluoride. Residual Al present in treated water causes neurological disorders and Alzheimer's disease. In the subsequent sections, various adsorbents used for fluoride removal have been discussed along with their limitations. Several adsorbents include calcium-based adsorbents, Al-based adsorbents, natural adsorbents, carbon-based adsorbents, and graphene-based adsorbents [69, 70].

Calcium has very low affinity towards fluoride ion; therefore, very few studies have been conducted for the application of calcium-based adsorbents for fluoride removal. To increase the efficiency, calcium has been modified with aluminium compound, and consequently, this leads to other limitations [52]. Natural adsorbents include clay, and soil built adsorbents are also applied for the fluoride removal and found to have no such detrimental effects but their extremely low efficiency makes them unsuitable for defluoridation. Carbon-based adsorbents include mainly activated carbon, carbon nanotubes, and graphene-based adsorbents. The major limitation of activated carbon includes large amount of cost in making the adsorbent and complications in regenerating it [17, 38]. The emerging substitutes for activated char are carbon nanotubes and graphene-based materials for efficient adsorption of fluoride [2, 21, 72]. Several researchers have contributed in applying carbon nanotubes for the fluoride removal, and these adsorbents are very promising in fluoride removal because of their large surface area, having oxygen-including functional groups, and they can be scaled up for treating larger quantity of water. On the contrary, graphene-based adsorbents have shown better efficiency towards fluoride removal as compared to carbon nanotubes.

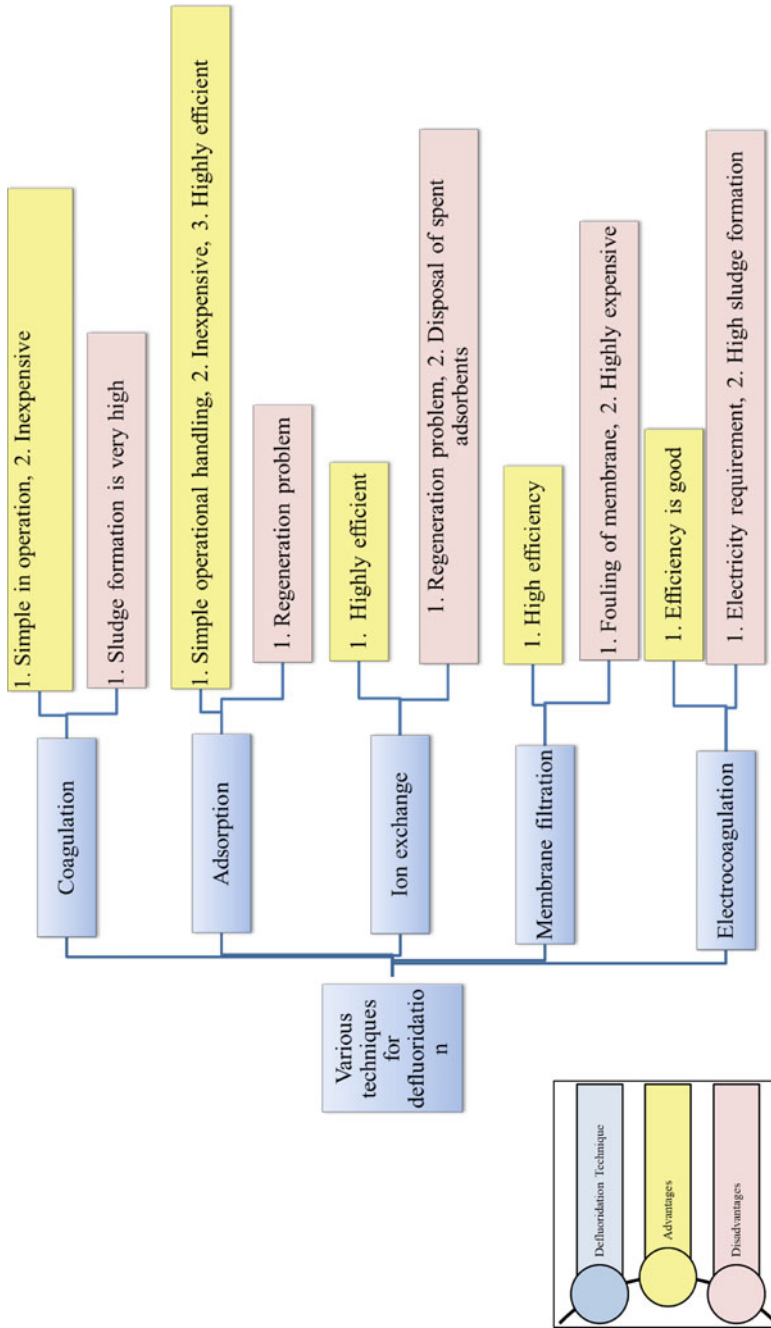


Fig. 2 Various defluoridation techniques with their advantages and disadvantage



The reason behind this is the chemical structure of graphene that has 2 basal planes of one layer of graphene as adsorbent unlike the inaccessible inside walls of carbon nanotubes. Graphene-based adsorbents could be easily manufactured by chemically exfoliating graphene in the absence of any complicated equipment. The developed graphene-based adsorbents also do not need any further purification process.

## 2 Adsorbents Used for Fluoride Removal

Adsorption technique has some interesting features like easy operational handling and lesser time consuming and is sustainable in terms of efficiency and reasonability [12]. An efficient adsorbent should have the characteristics including high affinity towards fluoride ion, inexpensive nature, and high regenerability. Various adsorbents have been tested to find the fluoride adsorbing capacity and have been described in Table 1 [3, 33, 50].

### 2.1 Calcium-Based Adsorbents

It could be observed from Table 1 that calcium has a significant affinity towards fluoride ion, and much research has been done towards this. Calcium-based adsorbent materials are inexpensive in nature, and in addition to this, calcium does not harm the human body in any other way. Although, one of the negative impacts of using calcium-based adsorbents is the increased hardness in treated water. Prabhu and Meenakshi [52] conducted batch study for adsorption of fluoride by using hydroxyapatite after modifying with cation-based surfactant (Muthu Prabhu). It was observed that the highest removal of approximately 9.4 mg/g at 50 mg/L adsorbent dosage was there. Various adsorption isotherms including Freundlich, Langmuir, and D-R models fitted well with the experimental data. The adsorption kinetics fitted well for pseudo-2nd-order kinetics. The adsorption reaction was found to be feasible and endothermic because the change in Gibbs free energy was negative, and the enthalpy change was positive, respectively. Husain and Jha [31] observed the adsorption behaviour for fluoride ion by using marble slurry as adsorbent [30]. The maximum fluoride removal of 58% was observed for 15 g dosage adsorbent dosage and initial fluoride concentration of 5 mg/L. The optimum pH range and contact time for fluoride adsorption were observed to be between 6 and 8 and 2 h, respectively. The spent adsorbent was utilized in the construction of bricks, tiles, road, etc. [22] applied phosphoric acid modified limestone for fluoride removal, and the adsorption capacity increased from 0.39 to 1 mg/g. The used adsorbent was also regenerated by scrubbing with lime of sodium hydroxide. The major adsorption mechanism included formation of calcium fluoride precipitate followed by adsorption.

**Table 1** Calcium-based adsorbents for fluoride removal

S. No	Adsorbent	Initial fluoride capacity (mg/L)	Fluoride adsorption capacity (mg/g)	Equilibrium isotherm/thermodynamic nature/kinetics	Reference
1	Cationic surfactant modified hydroxyapatite calcium-based adsorbent	10	9.369	Freundlich, Langmuir and D-R isotherms/spontaneous-endermic/pseudo-second-order and intraparticle diffusion kinetic models	[52]
2	Marble slurry	5	0.193	–	[32]
3	Dilute phosphoric acid to the with mixing of limestone	10	1.1	–	[22]
4	Ca-deficient hydroxyapatite (d-HAp)	–	26.11	Langmuir/-pseudo-second-order	[42]
5	Hydroxyapatite	–	–	Freundlich/-pseudo-second-order	[35]
6	Nanosized hydroxyapatite	50	1.438	Freundlich/spontaneous-endermic/ pseudo-second-order	[71]
7	Dicalcium phosphate dihydrate (DCPD)	10	26.37	–	[47]
8	Lacunar hydroxyapatite (L-HAp)	10	18.96	–	[47]
9	Calcite	19.82	40.65	Langmuir/-/	[25]
10	Crushed limestone	10	–	–	[55]

## 2.2 Aluminium-Based Adsorbents

Amongst the several adsorbents, Al-based adsorbents are found to be highly efficient for fluoride removal. The reason behind this is the high attraction of fluoride ion towards Al adsorption sites. Although, the major drawback of using Al-based adsorbents is the residual Al that is left in the treated water after defluoridation (Table 2). Magnesium oxide modified alumina has been investigated for fluoride removal, and it was observed that the adsorption capacity was 5.6 mg/g within the pH range of 6.3–7.3 with the contact time of 140 min [56]. In one study,  $\text{Al}(\text{OH})_3$  and  $\text{Al}(\text{OH})_3$  with double layers were synthesized [16]. The operating temperature for adsorption process was also studied along with the impact of other ions including sulphate, citrate, and metals on the fluoride adsorption capability of the developed adsorbent. The major conclusion that could be drawn was that elevated temperature had an adverse effect on fluoride adsorbing capacity.

## 2.3 Natural Adsorbents

Adsorbents derived from natural substances including plants, natural polymers, and polysaccharides have been synthesized and tested for fluoride removal [61]. Modification of such natural material has also been done to improve the fluoride removal capacity. Bone charcoal which is carbonized animal bone comes under the category of natural adsorbent and has been proved to be a capable adsorbent for fluoride removal. The details have been summarized in Table 3. The developed adsorbent is also cost effective [70]. Regeneration of the spent adsorbent was also performed using NaOH and a backwashing cycle. Bone char is composed of carbon matrix and supports a porous hydroxyapatite structure. The presence of calcium phosphate hydroxide is responsible for fluoride ion adsorption.

## 2.4 Carbon-Based Adsorbents

Several adsorbents based on carbon substances have been developed to purify drinking water regarding removal of fluoride ion. Some of the developed carbon-based adsorbents have been described in Table 4 in terms of their fluoride removal capacity. The main carbon-based adsorbents include activated carbon, graphene oxide, and carbon nanotubes, and they have abundant functional groups on the surface and high specific surface area. Activated carbon is widely applied due to its high porous nature, substantial surface area, and compliant surface chemistry [13, 14]. Activated carbon adsorbents have also been modified with help of different metal hydroxides to increase the surface area and amplify the interactions with fluoride ion [41, 53]. In addition to this, carbon nanotubes have some exceptional characteristics

**Table 2** Al-based adsorbents for fluoride removal

S. No	Adsorbent	Initial fluoride capacity (mg/L)	Fluoride adsorption capacity (mg/g)	Equilibrium isotherm/thermodynamic nature/kinetics	Reference
1	MgO/ $\gamma$ -Al <sub>2</sub> O <sub>3</sub> nano-composite	20	5.6	Langmuir/-/pseudo-II-order kinetics	[56]
2	Aluminium hydroxide AIOOH-25	100	20	Langmuir/-/-	[16]
3	Iron(III)-aluminium(III) mixed oxide	25	17.73	Langmuir/spontaneous-endergonic/pseudo-II-order	[8]
4	Acidic alumina	15	8.4	Langmuir/spontaneous-endergonic/pseudo-II-order	[23]
5	Activated alumina	12	0.788	–	[28]
6	Granular activated alumina	180	8.32	Langmuir/-/-	[15]
7	Metal impregnated alumina	100	4.684	Freundlich isotherm/-/pseudo-second-order	[34]
8	Aluminium hydroxide-loaded zeolite synthesized from coal fly ash	50	18.12	Langmuir isotherm/-/pseudo-II-order	[11]
9	Powdered activated alumina	10	0.98	Freundlich/-/pseudo-II-order	[65]
10	Granular polymer-aggglomerated alumina	10	0.7	Freundlich/-/pseudo-II-order	[65]

**Table 3** Natural adsorbents for fluoride removal

S. No	Adsorbent	Initial fluoride capacity (mg/L)	Fluoride adsorption capacity (mg/g)	Equilibrium isotherm/thermodynamic nature/kinetics	Reference
1	Bivalve shells	12	27.31	Langmuir/spontaneous-exothermic/pseudo-II-order	[29]
2	Neem powder	4	0.165	–	[13]
3	Rice husk powder	4	2.54	–	[13]
4	Coconut husk	4	3.24	–	[13]
5	Coconut shell charcoal	4	2.55	–	[13]
6	Neem stem charcoal	4	3.64	–	[13]
7	Diatomite treated with aluminium hydroxide	10	1.67	Langmuir/pseudo-II-order	[5]
8	Natural clay	100	0.448	Freundlich/spontaneous-endothemic/pseudo-II-order	[54]
9	Cow dung carbon	8	15	Freundlich/spontaneous-exothermic/pseudo-II-order	[59]
10	Citron peel	10	1.79	Langmuir/-/-	[67]
11	Karanj	10	1.96	Langmuir/-/-	[67]
12	Paarijaat	10	1.74	Langmuir/-/-	[67]
13	Neem	10	1.64	Langmuir/-/-	[67]
14	Rice husk	10	1.84	Langmuir/-/-	[67]
15	Tulsi	10	1.96	Langmuir/-/-	[67]

and also have some reactive functional groups with 1D structure [40, 43]. Also, their structure could easily be controlled and enhanced.

### 3 Graphene-Based Adsorbents Used for Fluoride Removal

Some of the primary graphene-based adsorbents include graphene oxide and reduced graphene oxide. They are the emerging carbon allotropes [6]. Graphene has a 2D matrix having 1–10 layered carbon atoms with  $sp^2$  hybridization in 6 membered rings. Moreover, graphene oxide has some additional structures of oxygen-based functional groups including hydroxyl, alkoxy, carbonyl, and carboxylic acid. Hence, this adds to the major drawback to the structure of graphene of having different kinds of defects in the structure of graphene [72]. On the contrary, the structure with so many defects provides the opportunities of various other applications to graphene oxide. Due to the presence of electron rich  $\pi$  arrangement in graphene and electron rich oxygen matrix, the structure of graphene oxide gets an added advantage. Graphene-based adsorbents have reported to have a surface area of 2630  $m^2/g$ , and graphene oxide adsorbents have an surface area of 2418  $m^2/g$ . Therefore, graphene oxide proves to be remarkable adsorbents for solving water treatment problems.

In recent times, graphene oxide has been applied in various water treating problems. Although, graphene oxide adsorbents have some drawbacks of having insufficient adsorption capacity, instable in water solution, and their regenerability is quite low. A promising solution to this drawback is the amendment of the surface of graphene oxide. Various researches have been carried out in which graphene-based materials are been doped with elements like aluminium, manganese, iron, magnesium, etc. Various methods for preparing graphene-based adsorbents have been described in Table 5.

#### 3.1 Graphene Oxide/Alumina Nano-composite

Xu et al. [73] modified graphene oxide using aluminium oxide with the process of hydrothermal reactions that have been summarized in Table 6. It has been reported that the effect of varying pH of the water solution was very low on the developed adsorbent, and this observation suggested that this alumina modified graphene oxide adsorbents can be applied for treating the solutions with varying pH. In addition to this, the adsorbent dose would also be low because of the ability of performing good in varying range of pH [73].

Barathi et al. [7] synthesized graphene-based adsorbent by modifying it with aluminium oxy-hydroxide with the help of chemical precipitation technique. The synthesized adsorbent provided proper environment for the interaction of aluminium ions with various functional groups of graphene oxide [7].

**Table 4** Carbon-based adsorbents for fluoride removal

S. No	Adsorbent	Initial fluoride capacity (mg/L)	Fluoride adsorption capacity (mg/g)	Equilibrium isotherm/thermodynamic nature/kinetics	Reference
1	Chicken bone char (CBC)	20	3.56	–	Kikuchi [38]
2	KMnO <sub>4</sub> modified activated carbons	20	15.9	Langmuir and Freundlich isotherm/spontaneous-exothermic/pseudo-II-order	[14]
3	Carbonaceous material	26	2.84	Langmuir–Freundlich/-/pseudo-II-order	[53]
4	Activated carbon prepared from palmyrah	1	0.305	Freundlich isotherm/-/pseudo-II-order	[63]
5	Active carbon derived from barks of Vitex negundo plant	12	1.15	Langmuir/spontaneous-endothemic/pseudo-II-order	[66]
6	Waste carbon slurry	15	4.861	Langmuir/Spontaneous-endothemic/pseudo-II-order	[27]
7	Carbon nanotube supported alumina	6	9.6	Freundlich/-/–	[43]
8	Hydroxyapatite decorated with carbon nanotube	–	11.05	Freundlich/spontaneous-endothemic/pseudo-II-order	[68]
9	Aligned carbon nanotubes	15	4.5	Freundlich/-/–	[40]

**Table 5** Synthesis methods for various graphene-based adsorbents

S. No	Type of graphene-based adsorbent	Methods of preparation	References
1	Zirconium chloride graphene supported on activated carbon matrix	Facile liquid phase exfoliation followed with impregnating and evaporating technique	[48]
2	Graphene oxide-alumina nano-composites	Hydrothermal method	[74]
3	Al <sub>2</sub> (SO <sub>4</sub> ) <sub>3</sub> -graphene hydrogel	Precipitation of basic Al <sub>2</sub> (SO <sub>4</sub> ) <sub>3</sub> in graphene hydrogel	[10]
4	B-FeOOH graphene oxide (GO)	Hydrolysis of GO and FeCl <sub>3</sub>	[45]
5	Fe-Al oxide nanoparticles anchored on graphene oxide	Chemical co-precipitation method	[44]
6	FeO <sub>4</sub> /Fe functionalized graphene nano-sheets based on pyrolysis of <i>sargassum</i> granules	Pyrolysis of seaweed granule	[64]
7	FeOOH/GO	In situ hydrolysis	[39]
8	Graphene oxide incorporated on Fe-Al mixed oxide	Chemical precipitation method	[36]
9	MgO-MgFe <sub>2</sub> O <sub>4</sub>	Hydrothermal method	[62]
10	Al-La oxides incorporated on graphene oxide	Co-precipitation method	[26]

Karkar et al. [36] developed graphene oxide adsorbent by modifying it with iron-aluminium mixed oxide [36].

Guan et al. [24] also synthesized alumina modified graphene oxide-based adsorbents, and the developed adsorbent was found to have an increment in surface area [24]. The matrix of the developed adsorbent provided proper interaction hydroxyl and carboxyl because of the formation of hydrogen bonds between them.

### 3.2 Graphene Oxide/Eggshell Adsorbent

It has been reported that due to the presence of calcium content in the eggshell structure, this makes them a suitable choice for the removal of fluoride ion. One more advantage is the strong affinity of calcium towards fluoride ion that makes it explored by different researchers. Nor et al. [57] investigated the combination of graphene oxide and eggshells as adsorbent, and it was observed that the highest adsorption was 56 mg/g at the operating temperature of 25 °C with the initial fluoride concentration of 25 mg/L [57]. In addition to this, the adsorbent dose was also quite low with the value of 0.05 g/L.



**Table 6** Graphene-based adsorbents for fluoride removal

S. No.	Adsorbent	Surface area ( $m^2/g$ )	Fluoride adsorption capacity (mg/g)	Isotherm	Kinetics	Thermodynamic nature	Reference
1	Graphene oxide (GO) and $\gamma$ - $Al_2O_3$ ( $\gamma$ -alumina)	326.22	4.68	Freundlich	Pseudo-second-order	Spontaneous and endothermic	[73]
2	Graphene oxide–aluminium oxy-hydroxide	–	18.10	Langmuir	Pseudo-II-order	Spontaneous and endothermic	[7]
3	Graphene oxide (GO)-incorporated iron-aluminium mixed oxide (HIAGO) composite	–	7.5	Langmuir	Pseudo-II-order	Spontaneous and endothermic	[36]
4	Graphene oxide with eggshells	–	56	Langmuir	Pseudo-II-order	Spontaneous and exothermic	[57]
5	FeOOH/GO composites	255.24	19.82	Freundlich	Pseudo-II-order	–	[39]
6	Graphene oxide anchored sand (ZIGCS) functionalized by Zr(IV)	–	6	Langmuir	Pseudo-II-order	Spontaneous and endothermic	[58]

### 3.3 Graphene Oxide/Iron Oxide Nano-composites

Kuang et al. [39] developed two graphene-based adsorbents by modifying with Goethite and rice like Akaganeite by using in situ hydrolysis technique and performed a comparison on their adsorption capacity. The effect of induction of crystalline matrix by was studied [39]. Sodium acetate is a chief organic ligand in water and soil. It was observed that the sodium acetate affects the iron hydroxide structure in a great way and ultimately affects the fluoride adsorption mechanism and capacity [44, 45].

Mura et al. [51] applied potassium ferrate oxide for the modification of graphene oxide [51]. The presence of ferrate makes it a capable, inexpensive, and green substitute for the treatment of water. It could also be observed from the literature that the developed adsorbents proved to be the most effective adsorbents for fluoride removal.

Chen et al. [9] modified graphene oxide using iron oxy-hydroxide for the fluoride removal [9]. The developed adsorbents were in the range of nano-metres.

## 4 Conclusions

In the recent times, the concern towards the toxic effects of fluoride on human well-being increased because of high intake of fluoride that leads to some serious health issues including skeletal and dental fluorosis, respiratory problems, etc. Therefore, large number of techniques has been developed to deal with this problem, and adsorption process is amongst the widely applied technology for fluoride adsorption. The adsorbent used for fluoride removal should be cost effective and simple in operation and easily regenerative. Graphene-based adsorbents have been investigated nowadays to fulfil the requirement of desired adsorbent for defluoridation. The current study reviews the various adsorbents and their limitations and also mentions the various advantages of graphene including large surface area and high mobility charge carriers, etc. It has also been suggested that graphene-based adsorbents could be a good alternative for the conventional adsorbents used for defluoridation.

## References

1. Agarwal, M., Dubey, S., Gupta, A.B.: Coagulation process for fluoride removal by comparative evaluation of Alum and PACl coagulants with subsequent membrane microfiltration. *Int. J. Environ. Technol. Manage.* **20**(3–4), 200–224 (2017)
2. Agarwal, M., Dubey, S., Bisht, R.: Synthesis and characterization of nZVI grafted alumina and its application for fluoride removal from drinking water: equilibrium and kinetics study 1–12 (2018)
3. Agarwal, M., Kumari, P., Dubey, S., Gupta, R.: Adsorption behavior of azo dyes on carbon nanotubes grown on alumina: process optimization, kinetics, and equilibrium study **145**(2), 1–16 (2019)

4. Aggeborn, L., Öhman, M.: The effects of fluoride in drinking water. *J. Polit. Econ.* **129**(2), 465–491 (2021)
5. Akafu, T., Chimdi, A., Gomoro, K.: Removal of fluoride from drinking water by sorption using diatomite modified with aluminum hydroxide (2019)
6. Ali, I., Basheer, A.A., Mbianda, X.Y., Burakov, A., Galunin, E., Burakova, I., Mkrtchyan, E., Tkachev, A., Grachev, V.: Graphene based adsorbents for remediation of noxious pollutants from wastewater. *Environ. Int.* **127**, 60–180 (2019)
7. Barathi, M., Krishna Kumar, A.S., Kumar, C.U., Rajesh, N.: Graphene oxide-aluminium oxyhydroxide interaction and its application for the effective adsorption of fluoride. *RSC Adv.* **4**(96), 53711–53721 (2014)
8. Biswas, K., Saha, S.K., Ghosh, U.C.: Adsorption of fluoride from aqueous solution by a synthetic iron(III)-aluminum(III) mixed oxide. *Ind. Eng. Chem. Res.* **46**(16), 5346–5356 (2007)
9. Chen, X., Zeng, Y., Chen, Z., Wang, S., Xin, C., Wang, L., Shi, C., Lu, L., Zhang, C.: Synthesis and electrochemical property of FeOOH/graphene oxide composites. *Front. Chem.* **8**, 1–8 (2020)
10. Chen, Y., Zhang, Q., Chen, L., Bai, H., Li, L.: Basic aluminum sulfate@graphene hydrogel composites: preparation and application for removal of fluoride. *J. Mater. Chem. A* **1**(42), 13101–13110 (2013)
11. Chen, J., Yang, R., Zhang, Z., Wu, D.: Removal of fluoride from water using aluminum hydroxide-loaded zeolite synthesized from coal fly ash. *J. Hazard. Mater.* **421**, 126817 (2022)
12. Chufa, B.M., Gonfa, B.A., Anshebo, T.Y.: Graphene oxide nanoadsorbent for the removal of fluoride ion from groundwater: adsorbent performance and adsorption mechanism. *J. Nanotechnol.* (2022)
13. Chukka, N.D.K., Nagajothi, P.G., Natrayan, L., Reddy, Y.B.S., Veeman, D., Patil, P.P., Thanappan, S.: Investigation on efficient removal of fluoride from ground water using activated carbon adsorbents. *Adsorpt. Sci. Technol.* (2022)
14. Daifullah, A.A.M., Yakout, S.M., Elreefy, S.A.: Adsorption of fluoride in aqueous solutions using KMnO<sub>4</sub>-modified activated carbon derived from steam pyrolysis of rice straw. *J. Hazard. Mater.* **147**(1–2), 633–643 (2007)
15. Dan, D., Wenming, D., Anguo, C., Shuming, L.I.U., Xu, Z.: Isotherm equation study of F adsorbed from water solution by. *Chin. J. Chem. Eng. Chem. Ind. Eng. Soc. China (CIESC) Chem. Ind. Press (CIP)* **19**(4), 581–585 (2011)
16. Du, J., Sabatini, D.A., Butler, E.C.: Synthesis, characterization, and evaluation of simple aluminum-based adsorbents for fluoride removal from drinking water. *Chemosphere* **101**, 21–27 (2014)
17. Dubey, S., Agarwal, M., Gupta, A.B.: A study on the characterisation of the species formed during fluoride removal through coagulation. *Interdiscip. Environ. Rev.* **18**(2), 143–154 (2017)
18. Dubey, S., Agarwal, M., Gupta, A.B.: Recent developments in defluoridation of drinking water in India. In: Singh, V.P., Yadav, S., Yadava, R.N. (eds.) *Environmental Pollution*, pp. 310–322. Springer International Publishing (2018)
19. Dubey, S., Agrawal, M., Gupta, A.B.: Advances in coagulation technique for treatment of fluoride-contaminated water: a critical review. *Rev. Chem. Eng.* **35**(2), 1–29 (2018)
20. Dubey, S., Agarwal, M., Gupta, A.B.: Experimental investigation of Al-F species formation and transformation during coagulation for fluoride removal using alum and PACl. *J. Mol. Liq.* **266**, 349–360 (2018a)
21. Dubey, S., Agarwal, M., Gupta, A.B.: Fluoride removal using Alum and PACl in batch and continuous mode with subsequent microfiltration 302017 (2021)
22. Gogoi, S., Nath, S.K., Bordoloi, S., Dutta, R.K.: Fluoride removal from groundwater by limestone treatment in presence of phosphoric acid. *J. Environ. Manage.* **152**, 132–139 (2015)
23. Goswami, A., Purkait, M.K.: The defluoridation of water by acidic alumina. *Chem. Eng. Res. Des.* 1–9 (2012)
24. Guan, C., Lv, X., Han, Z., Chen, C., Xu, Z., Liu, Q.: The adsorption enhancement of graphene for fluorine and chlorine from water. *Appl. Surf. Sci.* **516**(932), 146157 (2020)

25. Gunawan, E.K., Warmadewanthi, Liu, J.C.: Removal of phosphate and fluoride from opto-electronic wastewater by calcite. *Int. J. Environ. Technol. Manage.* **12**(2–4), 308–321 (2012)
26. Guo, Y., Xing, X., Shang, Y., Gao, B., Zhang, L., Yue, Q., Qian, L., Wang, Z.: Multiple bimetallic (Al-La or Fe-La) hydroxides embedded in cellulose/graphene hybrids for uptake of fluoride with phosphate surroundings. *J. Hazard. Mater.* **379** (2019)
27. Gupta, V.K., Ali, I., Kumar, V.: Defluoridation of wastewaters using waste carbon slurry. *Water Res.* **41**, 3307–3316 (2007)
28. Gupta, A.B., George, S., Mondal, P.: Effect on activated alumina fluoride removal capacity in presence of chloride 2–5 (2014)
29. Hashemkhani, M., Ghalhari, M.R., Bashardoust, P.: Fluoride removal from aqueous solution via environmentally friendly adsorbent derived from seashell. *Sci. Rep.* **0123456789**, 1–13 (2022)
30. Husain, M., Chavan, F., Abhale, B.: Use of maize husk fly ash as an adsorbent for removal of fluoride from water. *Int. Res. J. Eng. Technol. (IRJET)* **2**(7), 393–401 (2014)
31. Husain, J., Jha, R.C.: Fluoride distribution and occurrence of fluorosis in central Rajasthan and alternative low cost defluoridation technique by the use of marble slurry. *World water week, Stockholm*, 5–11, September (2010)
32. Hussain, I., Arif, M., Hussain, J.: Fluoride contamination in drinking water in rural habitations of Central Rajasthan, India. *Environ. Monit. Assess.* **184**(8), 5151–5158 (2012)
33. Jagtap, S., Yenkie, M.K., Labhsetwar, N., Rayalu, S.: Fluoride in drinking water and defluoridation of water. *Chem. Rev.* **112**(4), 2454–2466 (2012)
34. Jain, S., Bansiwala, A., Biniwale, R.B., Milmlle, S., Das, S., Tiwari, S., Siluvai, P.: Enhancing adsorption of nitrate using metal impregnated alumina. *J. Environ. Chem. Eng.* (2015)
35. Jiménez-Reyes, M., Solache-Ríos, M.: Sorption behavior of fluoride ions from aqueous solutions by hydroxyapatite. *J. Hazard. Mater.* **180**(1–3), 297–302 (2010)
36. Karkar, S., Debnath, S., De, P., Parashar, K., Pillay, K., Sasikumar, P., Ghosh, U.C.: Preparation, characterization and evaluation of fluoride adsorption efficiency from water of iron-aluminium oxide-graphene oxide composite material. *Chem. Eng. J.* **306**, 269–279 (2016)
37. Kashyap, S.J., Sankannavar, R., Madhu, G.M.: Fluoride sources, toxicity and fluorosis management techniques—a brief review. *J. Hazard. Mater. Lett.* **2**, 100033 (2021)
38. Kikuchi, M., Arioka, Y., Tafu, M., Irie, M.: Changes in fluoride removal ability of chicken bone char with changes in calcination time. *Int. J. Ceram. Eng. Sci.* **2**(2), 83–91 (2020)
39. Kuang, L., Liu, Y., Fu, D., Zhao, Y.: FeOOH-graphene oxide nanocomposites for fluoride removal from water: acetate mediated nano FeOOH growth and adsorption mechanism. *J. Colloid Interface Sci.* **490**, 259–269 (2017)
40. Li, Y.H., Wang, S., Zhang, X., Wei, J., Xu, C., Luan, Z., Wu, D.: Adsorption of fluoride from water by aligned carbon nanotubes. *Mater. Res. Bull.* **38**(3), 469–476 (2003)
41. Li, Y., Zhang, C., Jiang, Y., Wang, T.J.: Electrically enhanced adsorption and green regeneration for fluoride removal using Ti(OH)<sub>4</sub>-loaded activated carbon electrodes. *Chemosphere* **200**, 554–560 (2018)
42. Li, L., Zhu, Z., Qiu, Y.L., Zhang, H., Zhao, J.F.: Adsorption of fluoride ions on a Ca-deficient hydroxyapatite. *Huan Jing ke Xue = Huanjing Kexue* **31**(6), 1554–1559 (2010)
43. Li, Y.H., Wang, S., Zhang, X., Wei, J., Xu, C., Luan, Z., Wu, D., Wei, B., Wang, S., Zhang, X., Wei, J., Xu, C., Luan, Z., Wu, D., Wei, B.: Removal of fluoride from water by carbon nanotube supported alumina. *Environ. Technol.* **3330** (2003b)
44. Liu, L., Cui, Z., Ma, Q., Cui, W., Zhang, X.: One-step synthesis of magnetic iron-aluminum oxide/graphene oxide nanoparticles as a selective adsorbent for fluoride removal from aqueous solution. *RSC Adv.* **6**(13), 10783–10791 (2016)
45. Liu, Y., Lv, J., Jin, W., Zhao, Y.: Defluoridation by rice spike-like akaganeite anchored graphene oxide. *RSC Adv. Roy. Soc. Chem.* **6**(14), 11240–11249 (2016)
46. Majumdar, K.K.: Prevalence of fluorosis and pattern of domestic filters use in two fluoride endemic blocks of West Bengal, India. *J. Compr. Health* **3**(1), 17–30 (2015)

47. Manzola, A.S., Laouali, M.S., Ben Amor, M.: A comparative study of the defluoridation efficiency of synthetic dicalcium phosphate dihydrate (DCPD) and lacunar hydroxyapatite (L-HAP): an application of synthetic solution and Koundoumawa field water. *Afr. J. Environ. Sci. Technol.* **9**(2), 111–125 (2015)
48. Marin, P., Módenes, A.N., Bergamasco, R., Paraíso, P.R., Hamoudi, S.: Synthesis, characterization and application of ZrCl<sub>4</sub>-graphene composite supported on activated carbon for efficient removal of fluoride to obtain drinking water. *Water Air Soil Pollut.* **227**(12) (2016)
49. Mondal, P., George, S.: A review on adsorbents used for defluoridation of drinking water. *Rev. Environ. Sci. Biotechnol.* **14**(2), 195–210 (2014)
50. Mumtaz, N., Pandey, G., Labhasetwar, P.K.: Global fluoride occurrence, available technologies for fluoride removal and electrolytic defluoridation: a review. *Crit. Rev. Environ. Sci. Technol.* (2015)
51. Mura, S., Jiang, Y., Vassalini, I., Gianoncelli, A., Alessandri, I., Granozzi, G., Calvillo, L., Senes, N., Enzo, S., Innocenzi, P., Malfatti, L.: Graphene oxide/iron oxide nanocomposites for water remediation. *ACS Appl. Nano Mater.* **1**(12), 6724–6732 (2018)
52. Muthu Prabhu, S., Meenakshi, S.: Synthesis of surface coated hydroxyapatite powders for fluoride removal from aqueous solution. *Powder Technol.* **268**(1), 306–315 (2014)
53. Márquez-Mendoza, S.S., Jiménez-Reyes, M., Solache-Ríos, M., Gutiérrez-Segura, E.: Fluoride removal from aqueous solutions by a carbonaceous material from pyrolysis of sewage. *Water Air Soil Pollut.* **223**(5), 1959–1971 (2012)
54. Nabbou, N., Belhachemi, M., Boumelik, M.: Removal of fluoride from groundwater using natural clay (kaolinite): optimization of adsorption conditions. *Comptes Rendus—Chimie* **22**(2–3), 105–112 (2019)
55. Nath, S.K., Dutta, R.K.: Fluoride removal from water using crushed limestone. *Indian J. Chem. Technol.* **17**(2), 120–125 (2010)
56. Nazari, M., Halladj, R.: Adsorptive removal of fluoride ions from aqueous solution by using sonochemically synthesized nanomagnesia/alumina adsorbents: an experimental and modeling study. *J. Taiwan Inst. Chem. Eng.* **45**(5), 2518–2525 (2014)
57. Nor, N.M., Kamil, N.H.N., Mansor, A.I., Maarof, H.I.: Adsorption analysis of fluoride removal using graphene oxide/eggshell adsorbent. *Indonesian J. Chem.* **20**(3), 579–586 (2020)
58. Prathibha, C., Biswas, A., Chunduri, L.A.A., Reddy, S.K., Loganathan, P., Kalaruban, M., Venkataramanah, K.: Zr(IV) functionalized graphene oxide anchored sand as potential and economic adsorbent for fluoride removal from water. *Diamond Relat. Mater.* **109**, 108081 (2020)
59. Rajkumar, S., Murugesu, S., Sivasankar, V., Chaabane, T.: Low-cost fluoride adsorbents prepared from a renewable biowaste: syntheses, characterization and modeling studies. *Arab. J. Chem.* **12**(8), 3004–3017 (2019)
60. Ravi Kiran, E., Vijaya, K.: A study on epidemiology of fluorosis in a village of Nalgonda district, Andhra Pradesh. *Nat. J. Res. Com. Med* **1**(3), 123–127 (2012)
61. Reddy, K., Reddy, N., Niharika, P., Reddy, M., Reddy, H., Daneswari, V.: Defluoridation of water using natural adsorbents. *Int. J. Pedodontic Rehabil.* **2**(2), 51 (2017)
62. Sahoo, S.K., Hota, G.: Surface functionalization of GO with MgO/MgFe<sub>2</sub>O<sub>4</sub> binary oxides: a novel magnetic nanoadsorbent for removal of fluoride ions. *J. Environ. Chem. Eng.* **6**(2), 2918–2931 (2018)
63. Senewirathna, D.S.G.D., Thuraisingam, S., Prabagar, S., Prabagar, J.: Current research in green and sustainable chemistry fluoride removal in drinking water using activated carbon prepared from palmyrah (*Borassus fl abellifer*) nut shells. *Curr. Res. Green Sustain. Chem.* **5**, 100304 (2022)
64. Sharma, M., Mondal, D., Singh, N., Upadhyay, K., Rawat, A., Devkar, R.V., Sequeira, R.A., Prasad, K.: Seaweed-derived nontoxic functionalized graphene sheets as sustainable materials for the efficient removal of fluoride from high fluoride containing drinking water. *Sustain. Chem. Eng.* **5**(4), 3488–3498 (2017)
65. Sivasankari, C., Mahadevan, M., Aeulanatham, A.: Comparative study of powdered activated alumina with granular polymer-agglomerated alumina in fluoride removal from drinking water. *Asian J. Chem.* **22**(6), 4663–4670 (2010)

66. Suneetha, M., Sundar, B.S., Ravindhranath, K.: Removal of fluoride from polluted waters using active carbon derived from barks of *Vitex negundo* plant, 1–19 (2015)
67. Tamrakar, S., Verma, R., Sar, S.K., Verma, C.: Cost effective natural adsorbents for the removal of fluoride: a green approach **12**(2), 455–463 (2019)
68. Tang, Y., Guan, X., Su, T., Gao, N., Wang, J.: Fluoride adsorption onto activated alumina: modeling the effects of pH and some competing ions. *Colloids Surf. A* **337**(1–3), 33–38 (2009)
69. Tolkou, A.K., Manousi, N., Zachariadis, G.A., Katsoyiannis, I.A., Deliyanni, E.A.: Recently developed adsorbing materials for fluoride removal from water and fluoride analytical determination techniques: a review. *Sustainability (Switzerland)* **13**(13) (2021)
70. Vardhan, C.M.V., Karthikeyan, J.: Removal of fluoride from water using low-cost materials. In: Fifteenth International Water Technology Conference, IWTC-15 2011, vol. I(2), pp. 1–14. Alexandria, Egypt (2011)
71. Wang, Y., Chen, N., Wei, W., Cui, J., Wei, Z.: Enhanced adsorption of fluoride from aqueous solution onto nanosized hydroxyapatite by low-molecular-weight organic acids. *Desalination* **276**(1–3), 161–168 (2011)
72. Wang, Y., Pan, C., Chu, W., Vipin, A. K., Sun, L.: Environmental remediation applications of carbon nanotubes and graphene oxide: adsorption and catalysis. *Nanomaterials* **9**(3) (2019)
73. Xu, N., Li, S., Li, W., Liu, Z.: Removal of fluoride by graphene oxide/alumina nanocomposite: adsorbent preparation, characterization, adsorption performance and mechanisms. *ChemistrySelect* **5**(6), 1818–1828 (2020)
74. Xu, L., Wang, J.: The application of graphene-based materials for the removal of heavy metals and radionuclides from water and wastewater. *Crit. Rev. Environ. Sci. Technol.* **47**(12), 1042–1105 (2017)

# Design and Analysis of Fractal-Based THz Antenna with Co-Axial Feeding Technique for Wireless Applications



K. Vasu Babu, Gorre Naga Jyothi Sree, Kumutha Duraisamy, Devi Priya Vanarajan, and Sudipta Das

**Abstract** This research article proposed a co-axial feeding technique fractal shape radiator designed for THz regime. The designed radiator has compact structure of  $565 \times 400 \mu\text{m}$  with co-axial feeding of  $220 \mu\text{m}$ . The structure is resonating at 3.6 THz for the area of application regions like high-security devices, biologic information extraction, environmental monitoring and sensing. The antenna ranges an impedance bandwidth (3.57–3.68 THz) of 110 GHz which offers  $-10$  dB within the resonant frequency. The radiator exhibits a gain 7.2 dBi with efficiency of 87% at the resonant frequency and its  $S_{11}$  as  $-47.02$  dB. These parameters make the current structure an excellent design for high-frequency-band regions in terahertz detectors.

**Keywords** THz antenna · Fractal design structure · E-field · H-field · VSWR

## 1 Introduction

The transmission of wireless data has surged an exponential data rate, and the current researchers are looking for radio frequency-related bands which can accommodate increasing the needs of cellular data users. The requirements to meet connectivity and capacity growing must be utilized and developed wireless infrastructure. Research

---

K. V. Babu (✉) · G. N. J. Sree

BVRIT Hyderabad College of Engineering for Women, Bachupally, Hyderabad, India  
e-mail: [vasubabuece@gmail.com](mailto:vasubabuece@gmail.com)

K. Duraisamy

Department of Biomedical Engineering, Karpaga Vinayaga College of Engineering and Technology, Chengalpattu, Tamilnadu, India  
e-mail: [skvijaykumu@gmail.com](mailto:skvijaykumu@gmail.com)

D. P. Vanarajan

Department of EEE, Karpaga Vinayaga College of Engineering and Technology, Chengalpattu, Tamilnadu, India

S. Das

Department of Electronics and Communication Engineering, IMPS College of Engineering and Technology, Malda, West Bengal, India

community development fulfills the high-speed data requirement for the transmission of wireless devices, and frequency range of THz is considered the crucial step. For any design of THz communications, antennas become critical part and for the designing part of the system which become the great deal of expertise. In paper [1] designed high input resistance Yagi-uda graphene design, for the tunable band THz communications designed plasmonic patch radiator using graphene material [2], using guided surface waves and dyadic green's function modeled using graphene using graphene [3], using trigonometric tapered leaves designed plant shaped radiator for THz regime [4], a wide-band tree shaped micro scaled design with graphene material for THz region [5], for the body centric regions designed wearable and flexible graphene THz antennas [6], inverted structure slots of L & ohm designed a patch radiator [7], for the biological matter designed EM interaction of THz design [8], a micro-sized fractal wide-band system based on CMA optimized and designed using graphene as patch material [9], for the region of super wide-band structure designed a hexagonal fractal structure in the THz region [10], using half-circular compact radiator for wireless systems designed [11], using graphene as patched load for reconfigurable characteristics enhancing the gain improvement by considered the metamaterial radome structure at THz region [12], for UWB systems with DGS structure reducing inherent interference designed [13] and designed UWB system reduce the interference among the radiator structure [14]. The major objective of the current work is to address the issues like narrow bandwidth and miniaturization at frequency of the lower band of THz communication systems. The novelty of the current structure is simple antenna configuration, good radiation efficiency, miniaturization dimensions and good operating bandwidth.

## 2 Geometrical Configuration of THz Antenna

The design of THz structure and its parameters are shown in Fig. 1. The proposed design structure is obtained by cutting the slots in the form of a fractal structure using the substrate of polyimide with thickness 45  $\mu\text{m}$ . Silver material is employed for ground plane configuration, and graphene material is used as a patch on front plane of the design on substrate. The size of related structure employed as  $565 \times 400 \mu\text{m}$  which provides a bandwidth of 110 GHz for  $S_{11} \leq -10.0 \text{ dB}$ . Ensuring the maximum transfer of input power related to antenna provides effective radiations through 50 ohms SMA connector. Table 1 represents the major geometrical parameters. The simulation and design are performed by using CST MW studio. The fractal-based design structure resonant frequency is obtained by using the relation [10] by Eq. (1). The value of  $\epsilon_{\text{eff}}$  is 1.8 obtained from Eq. (2). After calculation, desired response value is 3.6 THz from Eq. (1).

$$f_r = \frac{16.5}{(a + j - i)\sqrt{\epsilon_{\text{eff}}}} \quad (1)$$



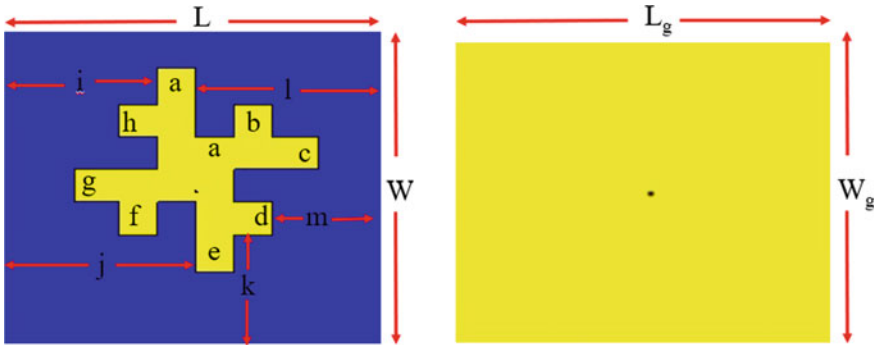


Fig. 1 Geometry of proposed antenna system

Table 1 Parameters in  $\mu\text{m}$

Symbol	$L$	$W$	$a$	$b$	$c$	$d$	$e$	$f$	$g$
Value	565	400	30	30	40	30	65	30	30
Symbol	$h$	$i$	$j$	$k$	$l$	$m$	$L_g$	$W_g$	$\epsilon_r$
Value	30	200	203.5	180	250	90	565	400	3.5

where  $a = 30 \mu\text{m}$ ,  $j-i = 3.5 \mu\text{m}$  and  $\epsilon_r = 3.5$

$$\epsilon_{eff} = \frac{\epsilon_r + 1}{2} \tag{2}$$

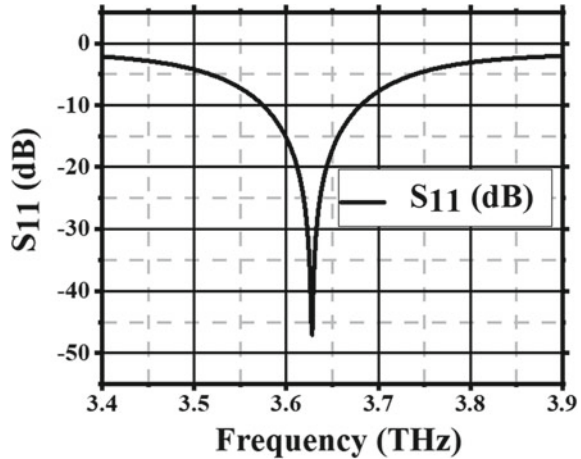
### 3 Design Results Analysis

The fractal designed structure is a combination of number of rectangular and circular slots which provides the reflection characteristics shown in Fig. 2. It operates a single band ranging from 3.57 to 3.68 THz of 110 GHz at 3.6 THz. Figure 3 can be observed an improvement of impedance offering the desired value of VSWR at the operating frequency. The impact of the current design is also investigated in terms of radiation characteristics related to radiation efficiency and gain. Figure 4 shows the impedance variations in terms of real and imaginary parts which is nearly zero and negative impedance. Figure 5 shows the frequency versus gain and efficiency. The variations of gain and efficiencies are varied according to the varying of frequency of variation. It can be identified that as frequency increases the gain of the antenna increases at one particular frequency and then decreases in terms of both gain and efficiency. Figure 6 indicates that the E-field distribution at the fractal region represents the maximum field distributed uniformly in all directions of the region with horizontal direction. Figure 7 indicates the H-field distribution at the fractal region represents

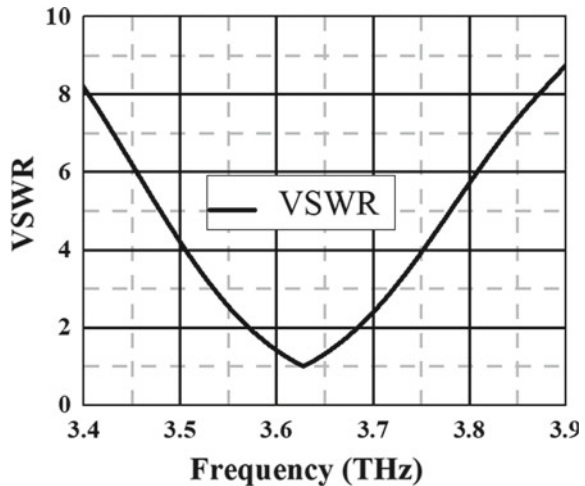
the maximum field distributed uniformly in all directions of the region with vertical direction.

Figure 8 indicates the currents of surface distribution at the fractal region represent that the maximum field is distributed uniformly in all directions of the designed structure. The maximum currents are identified in the central region of the fractal structure that produces high amount current created inside the antenna on front plane and also produces the current in similar fashion in ground structure. Figure 9 displays the far-field radiation patterns at 3.62 THz.

**Fig. 2** Reflection characteristics of THz designed radiator



**Fig. 3** Frequency versus VSWR characteristics



**Fig. 4** Impedance related to real and imaginary parts

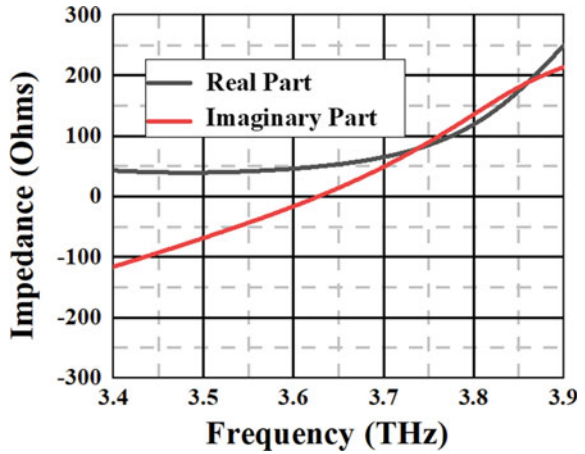
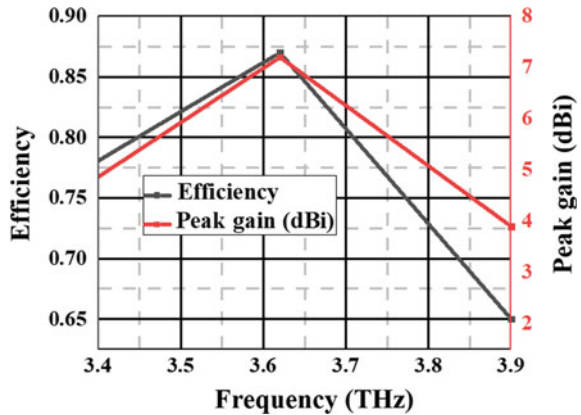


**Fig. 5** Frequency versus peak gain and efficiency



## 4 Conclusions

In this article designed, a fractal structure antenna with the help of polyimide substrate for the regions of biomedical imaging, material characterization and image system of video rating. The designed structure in the region of THz regime with compact, wide-band and more efficient. The fractal structure results a resonance characteristic of 110 GHz (3.57 –3.68 THz) with –10.0 Db bandwidth. The design suggested radiator provides the efficiency of 87%, and peak gain of 7.2 dBi has been achieved.

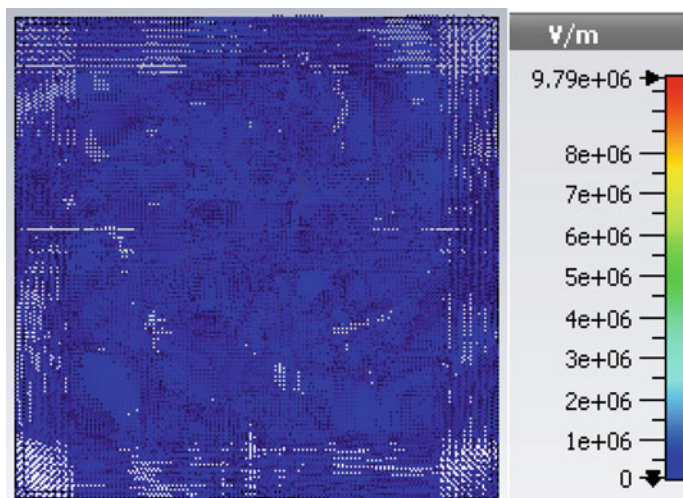


**Fig. 6** E-field distribution representation

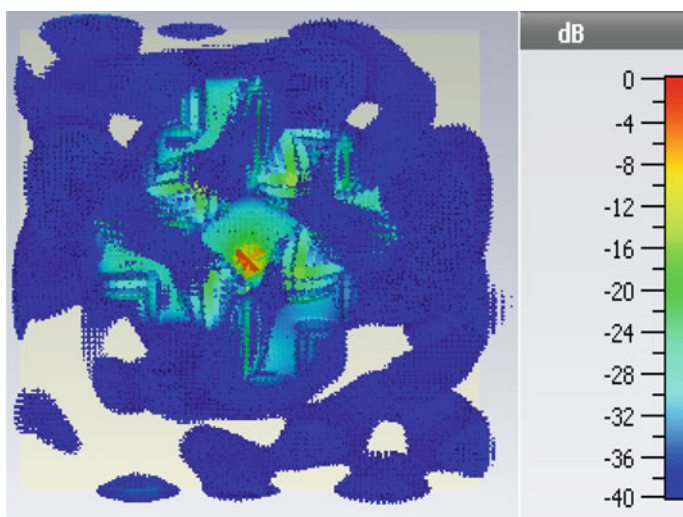


**Fig. 7** H-field distribution representation

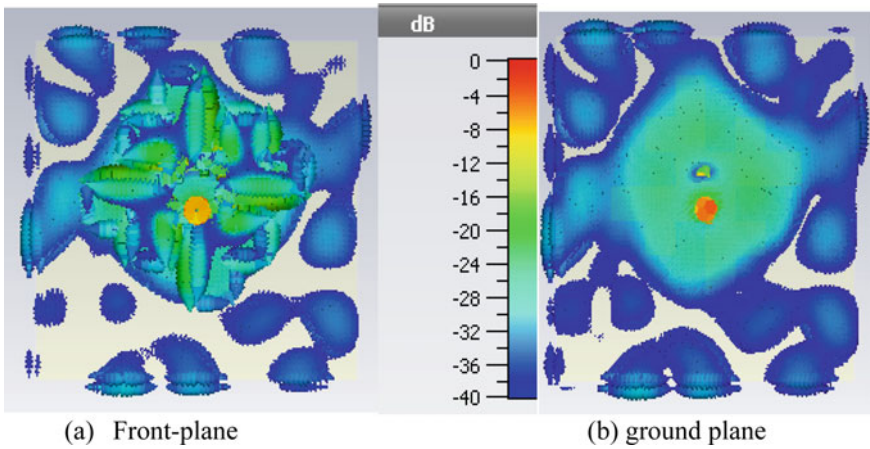


Fig. 8 Surface current distribution representation

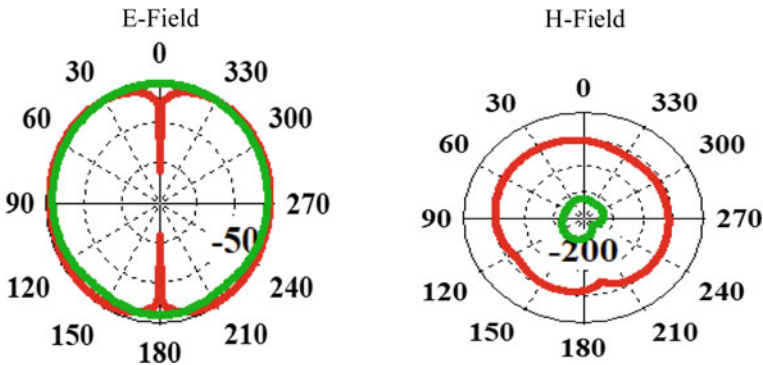


Fig. 9 Far-field radiation patterns of E-plane and H-plane

## References

1. Han, K., et al.: Terahertz Yagi-Uda antenna for high input resistance. *J. Infrared Millimeter Terahertz Waves* **31**(4), 441–454 (2010)
2. Naghdehforushha, S.A., Moradi, G.: Plasmonic patch antenna based on graphene with tunable terahertz band communications. *Optik* **158**, 617–622 (2018)
3. Hanson, G.W.: Dyadic Green’s functions and guided surface waves for a surface conductivity model of graphene. *J. Appl. Phys.* **103**(6), 064302 (2008)
4. Keshwala, U., Rawat, S., Ray, K.: Plant shaped antenna with trigonometric half sine tapered leaves for THz applications. *Optik* **223**, 165648 (2020)
5. Vasu Babu, K., et al.: A micro-scaled graphene-based tree-shaped wideband printed MIMO antenna for terahertz applications. *J. Computational Electron.* 1–15 (2022)
6. Abohmra, A. et al.: Flexible and wearable graphene-based terahertz antenna for body-centric applications. In: 2019 Second International Workshop on Mobile Terahertz Systems (IWMTS). IEEE (2019)

7. Babu, K.V., Anuradha, B.: Design of inverted L-shape and ohm symbol inserted MIMO antenna to reduce the mutual coupling. *AEU-Int. J. Electron. Commun.* **105**, 42–53 (2019)
8. Son, J.-H.: Terahertz electromagnetic interactions with biological matter and their applications. *J. Appl. Phys.* **105**(10), 102033 (2009)
9. Babu, K.V., et al.: Design and optimization of micro-sized wideband fractal MIMO antenna based on characteristic analysis of graphene for terahertz applications. *Optical Quantum Electron.* **54**(5), 1–20 (2022)
10. Singhal, S.: Hexagonal fractal antenna for super wideband terahertz applications. *Optik* **206**, 163615 (2020)
11. Babu, K.V., et al.: Compact dual-band design and analysis of half-circular U-shape MIMO radiator for wireless applications. *Microsys. Technol.* 1–14 (2022)
12. Seyedsharbaty, M.M., Sadeghzadeh, R.A.: Antenna gain enhancement by using metamaterial radome at THz band with reconfigurable characteristics based on graphene load. *Opt. Quant. Electron.* **49**(6), 1–13 (2017)
13. Babu, K.V., Anuradha, B.: Design of MIMO antenna to interference inherent for ultra-wide band systems using defected ground structure. *Microwave Opt. Technol. Lett.* **61**(12), 2698–2708 (2019)
14. Babu, K.V., Anuradha, B.: Design of UWB MIMO antenna to reduce the mutual coupling using defected ground structure. *Wireless Pers. Commun.* **118**(4), 3469–3484 (2021)

# Application of Graphene, Its Derivatives, and Their Nanocomposites



Rahul Kumar Sinha and Navjot Kaur Kanwal

**Abstract** The scientific and engineering community has become interested in graphene, on the ground of its distinctive bidimensional structure and superior physical, electrochemical, electrical, chemical, and optical qualities. The purpose of this chapter is to represent a prospective use of graphene in the fields of life science, medicine, forensic science, etc., basically in diagnostics for illnesses, near-infrared photothermal therapy, and scans to detect cancer. Now, graphene is being used in high-performing gadgets that produce and reserve energy, water purification and in biomedical areas for precise biosensing through graphene-quenched fluorescence and mass spectrometry using laser ionization and desorption on graphene. In forensic science, graphene is of intense interest. Drugs, including amphetamine, nitrazepam, and diazepam, that are relevant to forensics can be detected and quantified using graphene nanoparticles as a fluorescence sensor. In forensic electrochemistry, electrochemically reduced graphene oxide (ERGO) can be used to identify cocaine paracetamol, caffeine, and levamisole.

**Keywords** Graphene · Graphene oxide · Nanomedicine · Biomolecules · Drug delivery · Biofunctionalization · Forensic drugs · Imaging · Nanoforensics

## 1 Introduction

The scientific and engineering community has become interested in graphene, on the ground of its distinctive bidimensional structure and superior physical, electrochemical, electrical, chemical, and optical qualities. Recently, the popularity of graphene and its derivatives has increased as a global research hotspot in both the research society and industry. The purpose of this chapter is to represent a prospective use

---

R. K. Sinha (✉) · N. K. Kanwal  
Department of Criminology and Forensic Science, Dr. Harisingh Gour Vishwavidyalaya, Sagar,  
MP, India  
e-mail: [rahulkr.sinha36@gmail.com](mailto:rahulkr.sinha36@gmail.com)

N. K. Kanwal  
e-mail: [nkkanwal@dhsu.edu.in](mailto:nkkanwal@dhsu.edu.in)

of graphene in the fields of life science, medicine, forensic science, etc., basically in diagnostics for illnesses, near-infrared photothermal therapy, and scans to detect cancer and Alzheimer's disease.

Due to the arrival of graphene-quenched fluorescence and mass spectrometry using laser ionization and desorption supported by graphene, graphene's physical and chemical properties have now made it an ideal material for producing high-performance energy and storing it as well as biomedical applications for precise biosensing. There are several applications of graphene in biomedical fields, including drug delivery, antibiotic substances, and biocompatible support concerned with cell culture, imaging, and biological sensing.

Graphene is a great substance for oil and gas exploration, production, drilling and transportation, pipeline corrosion prevention, etc., on the ground of its distinguishable electrical, optical, thermal, and mechanical characteristics.

Additionally, this chapter explores the modern developments in the delivery of drugs using graphene, including its oxide, particularly graphene oxide functionalization and graphene oxide cytotoxicity.

## 2 Graphene Derivatives

The recent advancement of graphene's various forms or derivatives has also attracted researchers' attention for future utilization in broad fields, including medical and nanobiotechnology [1].

### 2.1 Graphene Oxide

Graphene basically oxidized to produce graphene oxide (GO), which has a single layer of monomers that functions as oxygen like hydroxyl and carboxyl group [2] and has become a crucial additive and performance-enhancing material. Graphene oxide (GO) has exposed some exceptional physicochemical characteristics like small size, extensive surface area, attractive electronic attributes, and uncommon stability in 2D structure, among others [3, 4] as desquamated graphene (from graphite) is hydrophobic in nature. Graphene's additional functions increase the distance between molecular layers and make the substance hydrophilic, making it easily dispersible in water. On account of this, graphene oxide (GO) achieves outstanding processability in water, surfacing functionality, amphiphilicity, and the ability to quench fluorescent light [5]. Figure 1 shows the sequential production of graphene oxide from graphene. Most GO is produced by the Hummers technique [6], which involves chemically treating graphite with a potassium permanganate solution through oxidation in hydrogen tetraoxosulfate (IV) acid [7].



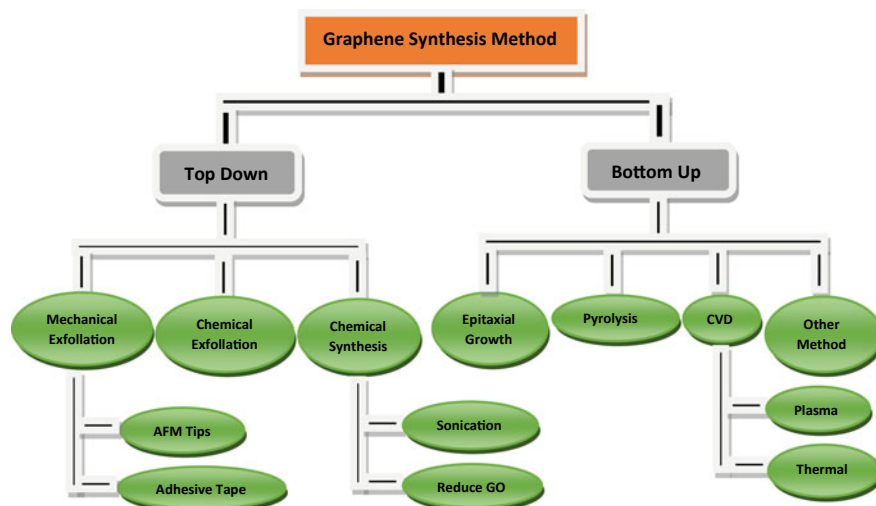


Fig. 1 Systematic illustration of graphene oxide production from graphene

## 2.2 *Reduced Graphene Oxide*

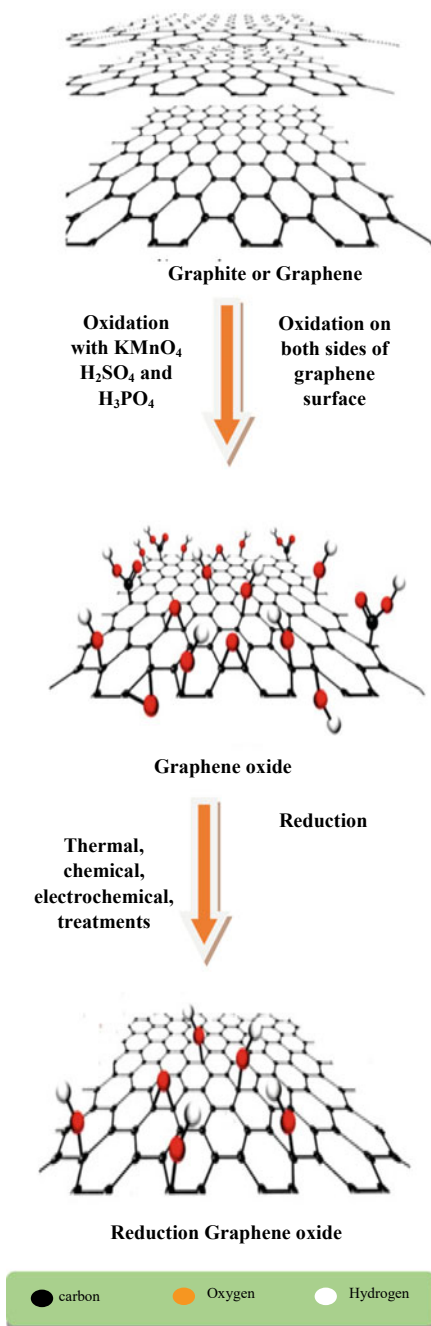
Reduced graphene oxide (rGO) is a fabrication of graphene from graphene oxide (GO), which uses chemical, thermal, electrochemical, or any other practical means to lower the oxygen ( $O^2$ ) content.

The research on this specific derivative has developed into a crucial study area due to synthesis by utilizing affordable graphite as a main component. Additionally, it has incredible water-heating characteristics and the ability to conceive stable colloids in aqueous solution to make it easier for solution processes to assemble macroscopic structures. These aspects extend their application in biomedical, biosensors, bioimaging, etc. The honeycomb hexagon lattice distortion is enhanced by reducing graphene oxide and becomes more electrically conductive [2, 8]. The carbon–oxygen ratios and chemical contents of reduced graphene oxide are essentially affected by different reducing agents (rGO). Figure 2 systematically depicting the transformation of graphene oxide into reduced graphene oxide (GO). Reduced graphene oxide (rGO) is particularly intriguing for biological applications because of the affordability and controllability of the oxygen functional group.

## 2.3 *Graphane*

A completely hydrogenated graphene derivative with CH composition is called graphane. Hybridization causes changes that turn conducting graphene into dielectric

**Fig. 2** Systematically depicting the transformation of graphene oxide into reduced graphene oxide (GO)



graphene and create bandgap in graphane, advancing hydrogen fuel and graphene-based nanoelectronics [9, 10]. The calculation of binding energy has shown that the binding energy of graphane is superior to benzene, acetylene, and any other form of hydrocarbons [1], making graphene the most stable type of hydrocarbon, and making its potential use in biotechnology. Graphene was exposed to plasma of cold hydrogen, diluted with argon at minimum temperature and pressure for its reversible synthesis. In this process, graphene generally becomes totally hydrogenated graphane with intermediate structures that are partly hydrogenated, and this causes progressive changes in the material's electrical characteristics. It is therefore predicted that imperfect graphene hydrogenation in controlled form can provide materials of desired properties.

## 2.4 Graphone

Graphone is one of the derivatives of graphene that is semihydrogenated. This derivative has a 50% hydrogenated graphene sheet structure with the chemical formula  $C_2H$ . Carbon sheet, experiencing only one side of hydrogen atom bonding, produced a combination of hybridized carbon atoms with  $sp^2$  and  $sp^3$ . In a study, the geometrical pattern of graphone has been revealed as a zigzag form [11, 12].

## 2.5 Graphene-Based Film

There are huge applications of self-supporting film material in industrial fields, which use as an energy storage material, an adhesive layer, a layer of protection, and for chemical adsorption. It is possible to create graphene film materials with macroscopic two-dimensional (2D) structures using the desired features of graphene and its microscopic two-dimensional (2D) structure [13]. High toughness and high-strength macroscopically two-dimensional (2D) graphene materials can be created by making graphene material more compact and by improving the way the layers interact, which can be applied to thin films. Graphene-based films have high-performance behavior for reducing friction as a lubrication system and excellent transferability with promising futures in engineering applications.

## 3 Application in Electronics

Graphene oxide is used in electronic devices for electronic fabrication as starting material. Graphene-effect transistors (GFETs) and field-effect transistors (FETs) are two graphene-based electronic devices [14]. FETs consist graphene oxide in reduced form and have been used as biological and chemical sensors [15–17]. Functionalized

reduced graphene oxides (rGOs) used as semiconductors in FETs have been utilized for detecting avidin [18], catecholamine hormone molecules [19], and DNA. An electrified glucose sensor is made of graphene oxide that has been functionalized with glucose oxidase mounted on an electrode [20]. The vast area where it is anticipated that, after being deposited on any substrate, graphene oxide (GO) would be used to create transparent conductive films. The usage of these coatings is possible in chemical sensors, touch screens, LCDs, solar cells, and electronics. GO/rGO is also utilized as a transparent electrode in LEDs.

## 4 Energy Storage Applications

GO and rGO have extremely large surfaces and good conductivity; because of this, these materials are used in energy storage devices as electrode materials in things like batteries, fuel cells, solar cells, and capacitors having double-layered [21, 22]. Graphene is frequently utilized as an anode in Li-ion batteries with a capacity of roughly 1000 mAh g<sup>-1</sup>, which are almost three times greater as compared to graphite electrodes. Graphene also provides longer-lasting batteries with good cycle stability and faster recharge time. Graphene is also used for wearable electronics such as solid-state supercapacitor-printed devices [23]. In the future, hybrid cars may be able to store hydrogen fuel because of GO's ability to store hydrogen.

## 5 Water Purification

Since the 1960s, researchers have been concentrating on graphite oxide for water desalination [24]. In 2011, some scientists used graphene oxide to accomplish the same goal by leveraging the fundamentals of reverse osmosis. [25]. In their initial study of the classical molecular dynamics of graphene, Tanugi and Grossman discovered that graphene membranes permit water to move through a membrane at a high rate, i.e., up to 100 L cm<sup>-2</sup> per day than reverse osmosis diffusive membranes [26], but its narrow mono- or bilayer capillaries retain some larger ions. Nanoporous membranes of graphene can be applied for water desalination and filtration with an efficiency, ranging from 33 to 100%. The effectiveness of graphene membranes totally depends on the pore size, chemical composition, and the pressure applied to the membranes. Graphene membranes can reject about 97% of seawater's NaCl.

Graphene oxide membranes have some difficulties in certain water treatment techniques. The graphene oxide (GO) interlayer spacing can increase in dry and hydrated conditions from 7.76 to 17.63 [27]. The sizes of the hydrated ions in typical salts are smaller than this value for hydration, which leads to inadequate salt rejection by the GO membranes.

The GO membrane was created by physically confining the GO nanosheets and embedding them in epoxy that maintains an interlayer spacing of 9.8–6.4 at different

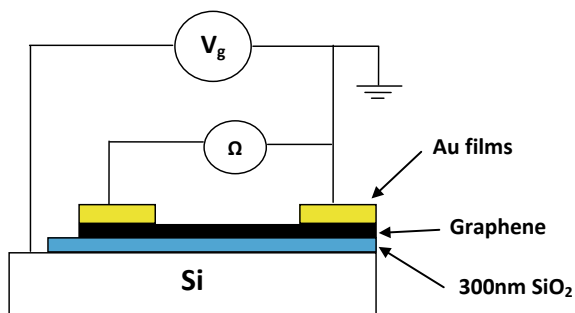
relative humidities. The salts utilized via the membrane with defined interlayer distances demonstrated remarkably low penetration with this controlled spacing. However, the movement of water was only marginally impacted [28].

## 6 Biosensor Application

Recent theoretical and experimental study results have shown that monolayer graphene is suitable for various molecular detection, from gases to biomolecules [29, 30]. Due to the exchange of charges between the graphene and the molecules that are adsorbed, the chemical reaction is anticipated to be caused by graphene. As molecules adhere to graphene's surface, the transfer of charges using graphene as a donor or acceptor, depending on the absorption site, causes changes in the Fermi level of graphene, carrier density, and resistance to electricity. Figure 3 demonstrates a typical graphene FET device schematic for sensing gas molecules. As GO/rGO has fluorescent properties that could be used for biosensing applications for detecting biologically relevant molecules, even to aid in the early diagnosis of disease and the search for cancer treatments. Electronic doping techniques and electrodeposition methods are used to alter graphene sheets to develop biosensors. Its exceptional qualities, including its electrical, thermal, optical, and surface-to-volume ratio, lead to the invention of more precise biosensors [31]. Glucose biosensors are developed using graphene placed on polyethylenimine-functionalized ionic liquid (PFIL). An effective method for creating biosensors with strong stability and sensitivity to enzymes at a reasonable cost is graphene on PFIL [32]. Graphene oxide has been extensively employed in fluorescent-based biosensors to detect proteins and DNA, enabling more accurate HIV diagnosis. The sensitivity of the biosensors depends on the interaction of DNA with carbon [33]. Graphene oxide is currently employed in biosensors as a fluorescence-suppressing agent that utilizes the effect of the fluorescence resonance energy transfer (FRET). Some studies used enhanced folic acid GO for the purpose of identifying breast cancer cells and cervical carcinoma of the human being.

Various examples of graphene-based biosensors are real-time optical biosensors without labels, manufactured by substances having graphene [34]. A surface plasmon

**Fig. 3** Graphene FET gas sensor device



resonance biosensor (SPR), which is used in environmental monitoring and medical diagnostics, is an example of an optical biosensor. Due to its carbon ring structure with hexagons, graphene serves as a superior biomolecule adsorbing layer and enhances the effectivity of surface plasmon resonance biosensors.

## 7 Biomedical Applications

A promising material for biological uses is graphene oxide, which is chemically exfoliated from oxidized graphite. Due to its superior water processing capacity, it has two different affinities, surface-enhanced Raman scattering (SERS) and a decrease of fluorescence intensity capacity. Additionally, graphene with a high surface area made by chemical vapor deposition, its hydrophobicity, and flexibility allow this substance to play a crucial part in cell differentiation and proliferation. Numerous biomedical applications of GO/rGO were investigated, focusing on cancer therapy, biological imaging, and drug delivery [35]. Figure 4 depicting the application of graphene and its derivative in the medical and non-medical field.

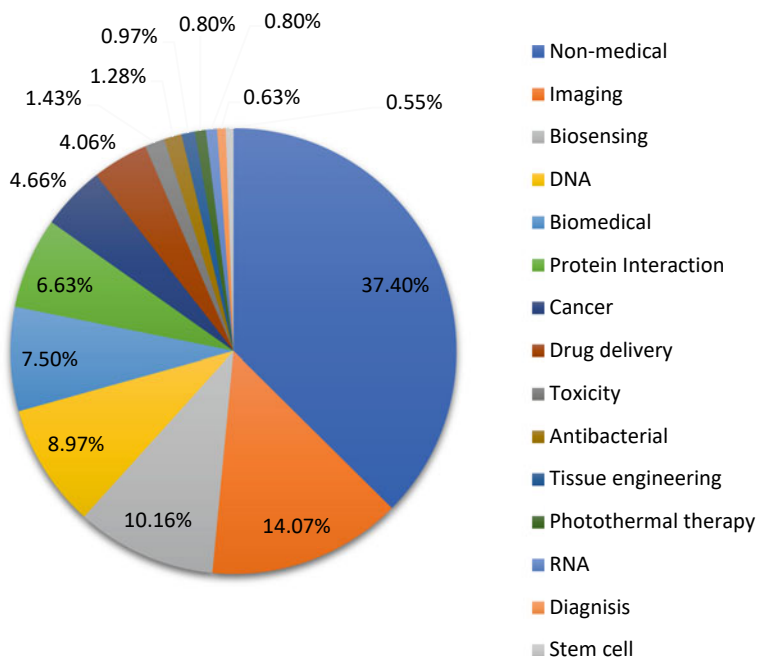


**Fig. 4** Chart depicting the application of graphene and its derivative in the medical and non-medical application

## 7.1 Gene Delivery

Surface modifier of GO sheet, polyethylenimine (PEI) has extensive usage for gene delivery into cells [36]. In a study, it was revealed that linear and branched GO conjugates with PEI62 were more efficient at transfecting and were less toxic than PEI/pDNA complexes.

## 7.2 Drug Delivery

The biomedical industry extensively uses graphene and its derivatives, particularly in medication delivery systems. When employed as an anticancer treatment, magnetite combined with graphene oxide (GO) and the chemical doxorubicin hydrochloride (DXR) adsorbed onto the system kills cancer cells by directing it to a specific site.

GO is supposed to be more effective than many other anticancer medications since it solely targets tumors, has little toxicity, and spares healthy cells [37]. Targeted administration of cancer medicines using specialized nGO has been demonstrated in various applications. Currently, functionalized GO with chitosan complex was created and used to deliver antineoplastic drugs [38]. The researcher has utilized polyethylene glycol functionalized nano-GO (nGO) with SN38, a surface-adsorbed derivative of camptothecin, for the drug's serum-soluble and water-soluble sources [39]. Studies have revealed that nGO-PEG-SN38 has three orders of magnitude more effective than SN38 prodrug, approved by the FDA and irinotecan at lowering the cell feasibility of the human colorectal cancer (CRC) cell line HTC-116. In DMSO, it was found that nGOPEGSN38 was similar to SN38 [39] (Table 1).

## 7.3 Graphene-Based Nanosystem in Bioimaging and Tissue Engineering

Recent research has shown that nanocarriers based on graphene can be useful in the fields of bioimaging as well as in tissue engineering [40]. Materials based on graphene have been potentially utilized for regenerative medicine, wound repair, stem cell, and tissue engineering [41]. Graphene has tremendous flexibility, strength, and potential to maintain and operate various functions on flat surfaces. Due to these specific mechanical properties, it can be successfully applied as an additional component of biodegradable films, hydrogels, electrospun fibers, etc.

Studies found that compared to chitosan, GO-chitosan hydrogel scaffolds maintain their size and shape in physiological and severe pH levels. Hence, it provides excellent mechanical properties as well as a lower degradation rate. The use of materials based on graphene for wound healing in both mice and rabbits revealed that these outstanding materials have the potential to heal injuries completely and fastly.

**Table 1** Applications of graphene-based nanosystem for drug and gene delivery

Graphene composites	Drug/Gene cargo	Highlights of the study
NGO-PEG-RB-DOX	DOX	An antibody targeting CD20 was used to release drug [53]
NGO-SS-PEG-DOX	DOX	GO composites release DOX rapidly into HeLa cells at tumor relevant glutathione concentrations [54]
DOX-GO-CHI-FA	DOX	DOX is released faster in acidic environments due to pH-sensitive drug release [55]
Gelatin-GS-DOX	DOX	An imaging and delivery system for DOX based on gelatin-functionalized graphene [56]
GO-sulfonic acid	DOX and CPT	For the first time, GO was successfully used to co-deliver multiple drugs with significantly increased toxicity in MCF-7 cells than CPT or DOX alone [57]
FeCo-GC-DOX	DOX	FeCo-GC nanocomposite-based photothermally enhanced drug delivery with improved distribution at high temperatures made possible by NIR laser irradiation [58]
PNIPAM-GS-CPT	CPT	The use of PNIPAM for temperature-sensitive drugs [59]
NGO-PEG-SN38	SN38 (CPT analog)	Delivery of an anticancer medication with greater potency and effectiveness than CPT that is water-insoluble [39]
Chitosan-GO	Ibuprofen, 5FU and pDNA delivery	Controlled release of various chemicals from GO comprised of chitosan, along with the compacting of pDNA with the complex, showed acceptable in vitro transfection efficiency [60, 61]
PEG-GO	Ce6 photosensitizer	PEG-GO-Ce6 is utilized for photodynamic therapy [62]
PEG-BPEI-rGO	Gene delivery	Delivering genes under photothermal control with improved gene transfection efficiency [63]
PEI-Go	Gene delivery	Reduced toxicity and improved transfection efficiency are two benefits of PEI functionalization with GO [64–66]

(continued)



**Table 1** (continued)

Graphene composites	Drug/Gene cargo	Highlights of the study
PEG-GO	Protein ribonuclease A and protein kinase A	Protein distribution inside cells without enzymatic hydrolysis or biological function loss [35]
Ti-GO-BMP2	BMP2 protein	In in vivo mice experiments, GO-coated Ti surfaces demonstrate efficacy as a therapeutic protein BMP2 carrier, resulting in increased variations in human MSCS and strong new bone production [67]

Along with wound healing, graphene-based materials have extended their usage for musculoskeletal tissue engineering [42] and stem cell engineering [43–46] (Table 2). Prokaryotic cell division is prevented by free electrons in graphene, whereas eukaryotic cell division is unaffected.

## 8 Forensic Application

Graphene is thought to be the best matter for sensors. It has demand due to low-cost, high bioabsorbable properties, and eco-friendly. Simultaneously, it has the property of dispersing in an aqueous solution with excellent stability. Recently, research-based graphene chemical sensors have found increased application. According to earlier studies, graphene-based sensors could be used to detect various medicines or series of drugs chemically [47, 48]. A project of the Research Institutes of Sweden AB (RISE) in collaboration with the National Forensic Centre (NFC) illustrates that amphetamine sensors use graphene quantum dots (GQDs) as a quick and affordable analytical technique. Based on these findings, GQDs for amphetamine detection mechanism, selective detection potential, and related sensitivity are further explored.

In forensic science, mainly the technologies used for drug detection are chromatographic techniques such as TLC, HPTLC, GC, and HPLC. However, these instruments are very expensive and often require a longer detection time to complete a process with accurate measurement. Irrespective of these techniques GQDs can be used as a simple, safe, portable, and pre-detection tool which can reduce instrument and laboratory costs as well as greatly shorten the testing time [49].

Fluorescent GQDs as nanosensors were used by Majid and his colleagues to characterize methamphetamine and morphine [50]. They used XRD, fluorescence spectroscopy, and UV–vis spectroscopy to detect its optical properties, microstructure, and energy band structure. Graphene quantum dots (GQDs) are also used as fluorescent sensing probes to determine methamphetamine and morphine.

Francis along with his team applied separate and simultaneous voltammetry in order to detect N-acetyl-p-aminophenol (APAP) and dopamine (DA) and invented a

**Table 2** Bioimaging and tissue engineering applications of graphene-based materials, along with findings of the study

Graphene and its composites	Application	Key findings of the study
GO-IONP-PEG	MRI	An MRI tumor imaging contrast agent based on graphene has been demonstrated for the first time in mice. As a result of using the carrier, the images showed a high degree of contrast and clarity [68]
NGS-PEG-Cy7	Tumor treatment and imaging	Cy7 dye-labeled complexes added up at tumor sites in mice, facilitate easy tumor localization to identify. After 24 h of injection, these tumor sites had been laser-irradiated, showing complete cell destruction [69]
GO-PEG-FA/Gd/DOX and GO-FA	Drug delivery and imaging	Treatment and diagnosis of hepatocarcinoma using multifunctional nanocomposites [70]
GO-G4-Fe-Cy5	Cellular imaging	MCF-7 cells successfully internalized GO-G4-Fe-Cy5 nanosystems that showed bright, stable fluorescence [71]
G/GO-CHI	Bone tissue engineering	GO-chitosan hydrogel scaffolds and graphene-reinforced chitosan composite films boosted cell proliferation and calcium phosphate deposition while having no harmful effects on L929 cells [72]
Graphene-CHI-PVA	Wound healing	Due to graphene's ability to limit prokaryotic cell multiplication, nanofibrous scaffolds made by electrospinning CHI-PVA with graphene facilitated full wound repair in both mice and rabbits at a considerable rate [73]
Graphene-diazodium salt	Biosensors	Streptavidin in solution can be detected by graphene biotinylation using the functionality of diazodium salts [74]
PL-PEG-NH2-GO	Circulating tumor cells (CTC) capture	Using a PLPEG-NH2-GO gold surface with a nanocomposite design, circulating tumor cells were collected at low blood concentration levels with great sensitivity [75]

(continued)

**Table 2** (continued)

Graphene and its composites	Application	Key findings of the study
Graphene amyloid composite	Shape memory, enzyme sensing	Adjustable physical, mechanical, and electrical qualities were made possible by the alternative graphene amyloid protein layer. And it has been used for its reversible shape memory effect in water and enzyme-sensing capabilities [76]

single-sex sensor [51]. The developed sensor is fabricated by dip-coating (GNPs)-Nafion (Naf) nanocomposites made of graphene nanosheets onto screen-printed electrodes (SPE). The sensor has the potential to simultaneously analyze dopamine and N-acetyl-p-aminophenol (APAP) by differential pulse voltammetry, and in their mixture, the sensor shows specific detection with excellent sensitivity.

According to a study, square-wave voltammetric detection was used to detect cocaine (COC), levamisole (LEV), caffeine (CAF), and paracetamol (PAR) using electrodes modified by electrochemically reducing graphene oxide. ERGO-modified electrode experiences a single voltammetric scan and during the detection process, may distinguish four substances with at least a twofold increase in current and adequate peak resolution compared to the unmodified electrode. Additionally, electrode fouling is eliminated when CAF and LEV are oxidized. An actual COC sample was used to assess the levels of paracetamol (PAR) and caffeine (CAF), and satisfactory recovery findings were achieved with values of 85 and 103%, respectively [52].

**Acknowledgements** None to declare

**Funding** No funding organization is involved in the drafting of this manuscript.

**Competing Interests** The authors declare no potential competing interest.

## References

1. Inagaki, M., Kang, F.: Graphene derivatives: graphane, fluorographene, graphene oxide, graphyne and graphdiyne. *J. Mater. Chem. A* **2**, 13193–13206 (2014)
2. Mao, S., Pu, H., Chen, J.: Graphene oxide and its reduction: modeling and experimental progress. *RSC Adv.* **2**, 2643–2662 (2012)
3. Dreyer, D.R., Park, S., Bielawski, C.W., Ruoff, R.S.: The chemistry of graphene oxide. *Chem. Soc Rev.* **39**, 228–240 (2010)
4. Nanda, S.S., Papaefthymiou, G.C., Yi, D.K.: Functionalization of graphene oxide and its biomedical applications. *Crit. Rev. Solid State Mater. Sci.* **40**, 291–315 (2015)

5. Yang, K., Feng, L., Shi, X., Zhuang, L.: Nanographene in biomedicine: theranostic applications. *Chem. Soc. Rev.* **42**, 530–547 (2013)
6. Marcano, D.C., Kosynkin, D.V., Berlin, J.M., Sinitskii, A., Sun, Z., Slesarev, A., Alemany, L.B., Lu, W., Tour, J.M.: Improved synthesis of graphene oxide. *ACS Nano* **4**, 4806–4814 (2010)
7. Hummers, J., Offeman, R.E.: Preparation of graphitic oxide. *J. Am. Chem. Soc.* **80**, 1339 (1958)
8. Priyadarsini, S., Mohanty, S., Mukherjee, S., Basu, S., Mishra, M.: Graphene and graphene oxide as nanomaterials for medicine and biology application. *J. Nanostruct. Chem.* **8**, 123–137 (2018)
9. Sofo, J., Chaudhari, A., Barber, G.: Graphane: a two-dimensional hydrocarbon. *Phys. Rev. B.* **75**, 153401 (2007)
10. Boukhvalov, D.W., Katsnelson, M.I., Lichtenstein, A.I.: Hydrogen on graphene: electronic structure, total energy, structural distortions and magnetism from first-principles calculations. *Phys. Rev. B.* **77**, 035427 (2008)
11. Peng, Q., Dearden, A.K., Chen, X.J., Huang, C., Wen, X., De, S.: Peculiar pressure effect on poisson ratio of graphone as a strain damper. *Nanoscale* **7**, 9975–9979 (2015)
12. Pujari, B.S., Gusarov, S., Brett, M., Kovalenko, A.: Single-side-hydrogenated graphene: density functional theory predictions. *Phys. Rev. B.* **84**, 041402 (2011)
13. Sun, J., Du, S.: Application of graphene derivatives and their nanocomposites in tribology and lubrication: a review. *RSC Adv.* **9**, 40642 (2019)
14. Wang, S., Ang, P.K., Wang, Z., Tang, A.L.L., Thong, J.T.L., Loh, K.P.: High mobility, printable, and solution-processed graphene electronics. *Nano Lett.* **10**, 92 (2010)
15. Lu, G., Park, S., Yu, K., Ruoff, R.S., Ocola, L.E., Rosenmann, D., Chen, J.: Toward practical gas sensing with highly reduced graphene oxide: a new signal processing method to circumvent run-to-run and device-to-device variations. *ACS Nano* **5**, 1154–1164 (2011)
16. Chen, K., Lu, G., Chang, J., Mao, S., Yu, K., Cui, S., Chen, J.: Hg(II) ion detection using thermally reduced graphene oxide decorated with functionalized gold nanoparticles. *Anal. Chem.* **84**, 4057–4062 (2012)
17. He, Q., Wu, S., Yin, Z., Zhang, H.: Graphene-based electronic sensors. *Chem. Sci.* **3**, 1764–1772 (2012)
18. He, Q., Wu, S., Gao, S., Cao, X., Yin, Z., Li, H., Chen, P., Zhang, H.: Transparent, flexible, all-reduced graphene oxide thin film transistors. *ACS Nano* **5**, 5038–5044 (2011)
19. He, Q., Sudibya, H.G., Yin, Z., Wu, S., Li, H., Boey, F., Huang, W., Chen, P., Zhang, H.: Centimeter-long and large-scale micropatterns of reduced graphene oxide films: fabrication and sensing applications. *ACS Nano* **4**, 3201–3208 (2010)
20. Liu, Y., Yu, D., Zeng, C., Miao, Z., Dai, L.: Biocompatible graphene oxide-based glucose biosensors. *Langmuir* **26**, 6158 (2010)
21. Zhu, Y., Murali, S., Stoller, M.D., Velamakanni, A., Piner, R.D., Ruoff, R.S.: Microwave assisted exfoliation and reduction of graphite oxide for ultracapacitors. *Carbon* **48**, 2118–2122 (2010)
22. Zhu, Y., Murali, S., Cai, W., Li, X., Suk, J.W., Potts, J.R., Ruoff, R.S.: Graphene and graphene oxide: synthesis, properties, and applications. *Adv. Mater.* **22**(35), 3906–3924 (2010)
23. Abdelkader, A.M., Karim, N., Valles, C., Afroj, S., Novoselov, K.S., Yeates, S.G.: Ultralexible and robust graphene supercapacitors printed on textiles for wearable electronics applications. *Astrophys. Data Syst.* **4**(3), 035016 (2017)
24. Bober, E.S.: Final Report on Reverse Osmosis Membranes Containing Graphitic Oxide. U.S. Department of the Interior, p. 116 (1970)
25. Gao, W., Majumder, M., Alemany, L.B., Narayanan, T.N., Ibarra, M.A., Pradhan, B.K.: Engineered graphite oxide materials for application in water purification. *ACS Appl. Mater. Interfaces* **3**(6), 1821–1826 (2011)
26. Cohen-Tanugi, D., Grossman, J.C.: Water desalination across nano porous graphene. *Nano Lett.* **12**(7), 3602–3608 (2012)
27. Tansel, B.: Significance of thermodynamic and physical characteristics on permeation of ions during membrane separation: hydrated radius, hydration free energy and viscous effects. *Separ. Purif. Technol.* **86**, 119–126 (2012)

28. Abraham, J., Vasu, K.S., Williams, C.D., Gopinadhan, K., Su, Y., Cherian, C.T., Dix, J., Prestat, E., Haigh, S.J., Grigorieva, I.V., Carbone, P., Geim, A.K., Nair, R.R.: Tunable sieving of ions using graphene oxide membranes. *N Nano*. **12**(6), 546 (2017)
29. Schedin, F., Geim, A., Morozov, S., Hill, E., Blake, P., Katsnelson, M., Novoselov, K.: *Nat. Mater.* **6**, 652 (2007)
30. Tang, L., Wang, Y., Li, Y., Feng, H., Lu, J., Li, J.: *Adv. Funct. Mater.* **19**, 2782 (2009)
31. Morales-Narv'aez, E., Merkoçi, A.: Graphene oxide as an optical biosensing platform. **24**(25), 3298–3308 (2012)
32. Cui, R., Han, Z., Pan, J., Abdel-Halim, E.S.: Direct electrochemistry of glucose oxidase and biosensing for glucose based on helical carbon nanotubes modified magnetic electrodes. *Electrochim. Acta* **58**(1), 179–183 (2011)
33. Tang, Z., Wu, H., Cort, J.R., Buchko, G.W., Zhang, Y., Shao, Y., Aksay, I.A., Liu, J., Lin, Y.: Constraint of DNA on functionalized graphene improves its biostability and specificity. *Small*. **6**(11), 1205–1209 (2010)
34. Yang, K., Zhang, S., Zhang, G., Sun, X., Lee, S., Liu, Z.: Graphene in mice: ultrahigh in vivo tumor uptake and efficient photothermal therapy. *Nano Lett.* **10**(9), 3318–3323 (2010)
35. Shen, A.J., Li, D.L., Cai, X.J., Dong, C.Y., Dong, H.Q., Wen, H.Y., Dai, G.H., Wang, P.J., Li, Y.Y.: Multifunctional nanocomposite based on graphene oxide for in vitro hepatocarcinoma diagnosis and treatment. *J. Biomed. Mater. Res. Part A* **100**, 2499–2506 (2012)
36. Feng, L.Z., Zhang, S., Liu, Z.: Graphene-based gene transfection. *Nanoscale* **3**, 1252–1257 (2011)
37. Yang, X., Wang, Y., Huang, X., Ma, Y., Huang, Y., Yang, R., Duan, H., Chen, Y.: Multifunctionalized graphene oxide based anticancer drug-carrier with dual-targeting function and pH-sensitivity. *J. Mater. Chem.* **21**, 3448–3454 (2011)
38. Bao, H.Q., Pan, Y.Z., Ping, Y., Sahoo, N. G., Wu, T., Li, L., Li, J., Gan, L.H.: Chitosan functionalized graphene oxide as a nanocarrier for drug and gene delivery. **7**, 1569–1578 (2011)
39. Liu, Z., Robinson, J.T., Sun, X., Dai, H.: PEGylated nano-graphene oxide for delivery of water-insoluble cancer drugs. *J. Am. Chem. Soc.* **130**, 10876–10877 (2008)
40. Mahmoudi, M., Sant, S., Wang, B., Laurent, S., Sen, T.: Superparamagnetic iron oxide nanoparticles (SPIONs): development, surface modification and applications in chemotherapy. *Adv. Drug Deliv. Rev.* **63**, 24–46 (2011)
41. Sant, S., Hancock, M.J., Donnelly, J.P., Iyer, D., Khademhosseini, A.: Biomimetic gradient hydrogels for tissue engineering. *Can J. Chem. Eng.* **88**, 899–911 (2010)
42. Ku, S.H., Park, C.B.: Myoblast differentiation on graphene oxide. *Biomaterials* **34**, 2017–2023 (2013)
43. Nayak, T.R., Andersen, H., Makam, V.S., Khaw, C., Bae, S., Xu, X., Ee, R., Ahn, J., Hong, B.H., Pastorin, G., Ozyilmaz, B.: Graphene for controlled and accelerated osteogenic differentiation of human mesenchymal stem cells. *ACS Nano* **5**, 4670–4678 (2011)
44. Lee, W.C., Lim, C.H.Y., Shi, H., Tang, L.A., Wang, Y., Lim, C.T., Loh, K.P.: Origin of enhanced stem cell growth and differentiation on graphene and graphene oxide. *ACS Nano* **5**, 7334–7341 (2011)
45. Wang, Y., Lee, W.C., Manga, K.K., Ang, P.K., Lu, J., Liu, Y.P., Lim, C.T., Loh, K.P.: Fluorinated Graphene for Promoting neuroinduction of stem cells. *Adv. Mater. Weinheim* **24**, 4285–4290 (2012)
46. Chen, G.Y., Pang, D.P., Hwang, S.M., Tuan, H.Y., Hu, Y.C.: A graphene-based platform for induced pluripotent stem cells culture and differentiation. *Biomaterials* **33**, 418–427 (2012)
47. Karlsson, M., Strandqvist, C., Jussi, J., Öberg, O., Petermann, I., Elmlund, L., Dunne, S., Fu, Y., Wang, Q.: Chemical sensors generated on wafer-scale epitaxial graphene for application to front-line drug detection. *Sensors* **19**(10), 2214 (2019)
48. Ülle-Linda, T.: Characterization of graphene-based sensors for forensic applications: Evaluating suitability of graphene-based resistive sensor for detection of amphetamine. Master thesis at Royal Institute of Technology, pp. 789, TRITA-EECS-EX (2019)

49. MA, X.: The Use of Graphene Quantum Dots as Detection Elements in Nanomaterials-Based Sensors for Forensic Applications. Degree Project in Engineering Physics, Stockholm, Sweden (2021)
50. Masteri-Farahani, M., Askari, F.: Design and photophysical insights on graphene quantum dots for use as nanosensor in differentiating methamphetamine and morphine in solution. *Spectrochim. Acta Part A Mol. Biomol. Spectrosc.* **206**, 448–453 (2019)
51. Krampa, F.D., Aniweh, Y., Kanyong, P., Awandare, G.A.: Graphene nanoplatelet-based sensor for the detection of dopamine and N-acetyl-aminophenol in urine. *Arab. J. Chem.* **13**(1), 3218–3225 (2020)
52. Rocha, D., Dornellas, R., Nossol, E., Richter, E., Silva, S., Santana, M., Munoz, R.: Electrochemically Reduced Graphene Oxide for Forensic Electrochemistry: Detection of Cocaine and its Adulterants Paracetamol, Caffeine and Levamisole, p. 29. *Electroanalysis* (2017)
53. Sun, X., Liu, Z., Welscher, K., Robinson, J.T., Goodwin, A., Zaric, S., Dai, H.: Nano-graphene oxide for cellular imaging and drug delivery. *Nano Res.* **1**, 203–212 (2008)
54. Wen, H., Dong, C., Dong, H., Shen, A., Xia, W., Cai, X., Song, Y., Li, X., Li, Y., Shi, D.: Engineered redox-responsive PEG detachment mechanism in PEGylated nano-graphene oxide for intracellular drug delivery. *Small* **8**, 760–769 (2012)
55. Depan, D., Girase, B., Shah, J., Misra, R.: Structure–process–property relationship of the polar graphene oxide-mediated cellular response and stimulated growth of osteoblasts on hybrid chitosan network structure nanocomposite scaffolds. *Acta Biomater.* **7**, 3432–3445 (2011)
56. Liu, Z., Robinson, J.T., Tabakman, S.M., Yang, K., Dai, H.: Carbon materials for drug delivery and cancer therapy. *Mater. Today* **14**, 316–323 (2011)
57. Zhang, L., Xia, J., Zhao, Q., Liu, L., Zhang, Z.: Functional graphene oxide as a nanocarrier for controlled loading and targeted delivery of mixed anticancer drugs. *Small* **6**, 537–544 (2010)
58. Sherlock, S.P., Tabakman, S.M., Xie, L., Dai, H.: Photothermally enhanced drug delivery by ultrasmall multifunctional FeCo/graphitic shell nanocrystals. *ACS Nano* **5**, 1505–1512 (2011)
59. Pan, Y., Bao, H., Sahoo, N.G., Wu, T., Li, L.: Water-soluble poly (N-isopropyl acrylamide)–graphene sheets synthesized via click chemistry for drug delivery. *Adv Funct. Mater.* **21**, 2754–2763 (2011)
60. Rana, V.K., Choi, M.C., Kong, J.Y., Kim, G.Y., Kim, M.J., Kim, S.H., Mishra, S., Singh, R.P., Ha, C.S.: Synthesis and drug-delivery behavior of chitosan-functionalized graphene oxide hybrid nanosheets. *Macromol. Mater. Eng.* **296**, 131–140 (2011)
61. Kodali, V.K., Scrimgeour, J., Kim, S., Hankinson, J.H., Carroll, K.M., Berger, C., Curtis, J.E.: Nonperturbative chemical modification of graphene for protein micropatterning. *Langmuir* **27**, 863–865 (2011)
62. Tian, B., Wang, C., Zhang, S., Feng, L., Liu, Z.: Photothermally enhanced photodynamic therapy delivered by nano-graphene oxide. *ACS Nano* **5**, 7000–7009 (2011)
63. Kim, H., Kim, W.J.: Photothermally controlled gene delivery by reduced graphene oxide–polyethylenimine nanocomposite. *Small* **10**, 117–126 (2014)
64. Chen, W., Yi, P., Zhang, Y., Zhang, L., Deng, Z., Zhang, Z.: Composites of aminodextran-coated  $\text{Fe}_3\text{O}_4$  nanoparticles and graphene oxide for cellular magnetic resonance imaging. *ACS Appl. Mater. Interfaces* **3**, 4085–4091 (2011)
65. Feng, L., Liu, Z.: Graphene in biomedicine: opportunities and challenges. *Nanomedicine* **6**, 317–324 (2011)
66. Kim, H., Namgung, R., Singha, K., Oh, I., Kim, W.J.: Graphene oxide–polyethylenimine-nanoconstruct as a gene delivery vector and bioimaging tool. *Bioconjug. Chem.* **22**, 2558–2567 (2011)
67. La, W., Park, S., Yoon, H., Jeong, G., Lee, T., Bhang, S.H., Han, J.Y., Char, K., Kim, B.: Delivery of a therapeutic protein for bone regeneration from a substrate coated with graphene oxide. *Small* **9**, 4051–4060 (2013)
68. Ma, X., Tao, H., Yang, K., Feng, L., Cheng, L., Shi, X., Li, Y., Guo, L., Liu, Z.: A functionalized graphene oxide-iron oxide nanocomposite for magnetically targeted drug delivery, photothermal therapy, and magnetic resonance imaging. *Nano Res.* **5**, 199–212 (2012)

69. Yang, K., Zhang, S., Zhang, G., Sun, X., Lee, S., Liu, Z.: Graphene in mice: ultrahigh in vivo tumor uptake and efficient photothermal therapy. *Nano Lett.* **10**, 3318–3323 (2010)
70. Huang, P., Xu, C., Lin, J., Wang, C., Wang, X., Zhang, C., Zhou, X., Guo, S., Cui, D.: Folic acid-conjugated graphene oxide loaded with photosensitizers for targeting photodynamic therapy. *Theranostics*. **1**, 240 (2011)
71. Wate, P.S., Banerjee, S.S., Jalota-Badhwar, A., Mascarenhas, R.R., Zope, K.R., Khandare, J., Misra, R.: Cellular imaging using biocompatible dendrimer-functionalized graphene oxide-based fluorescent probe anchored with magnetic nanoparticles. *Nanotechnology* **23**, 415101 (2012)
72. Fan, H., Wang, L., Zhao, K., Li, N., Shi, Z., Ge, Z., Jin, Z.: Fabrication, mechanical properties, and biocompatibility of graphene-reinforced chitosan composites. *Biomacromol* **11**, 2345–2351 (2010)
73. Lu, B., Li, T., Zhao, H., Li, X., Gao, C., Zhang, S., Xie, E.: Graphene-based composite materials beneficial to wound healing. *Nanoscale* **4**, 2978 (2012)
74. Li, N., Zhang, Q., Gao, S., Song, Q., Huang, R., Wang, L., Liu, L., Dai, J., Tang, M., Cheng, G.: Three-dimensional graphene foam as a biocompatible and conductive scaffold for neural stem cells. *Sci. Rep.* **3**, 604 (2013)
75. Yoon, H.J., Kim, T.H., Zhang, Z., Azizi, E., Pham, T.M., Paoletti, C., Lin, J., Ramnath, N., Wicha, M.S., Hayes, D.F.: Sensitive capture of circulating tumour cells by functionalized graphene oxide nanosheets. *Nat. Nanotech.* **8**, 735 (2013)
76. Li, C., Adamcik, J., Mezzenga, R.: Biodegradable nanocomposites of amyloid fibrils and graphene with shape memory and enzyme-sensing properties. *Nat. Nanotech.* **7**, 421–427 (2012)